CURSO ORGANIZADO EN COLABORACION DE LA ORGANIZACION LATINOAMERICANA DE ENERGIA Y CON EL APOYO DE LA COMISION FEDERAL DE ELECTRICIDAD Y EL INSTITUTO DE INVESTIGACIONES ELECTRICAS.

"INGENIERIA DE YACIMIENTOS GEOTERMICOS"
TEMA: PRUEBAS DE PRESION

INSTRUCTOR: DR. FERNANDO SAMANIEGO V.

MARZO 1984.

SPE

SPE 7480

WELL TESTING IN TWO-PHASE GEOTHERMAL WELLS

by Alain C. Gringarten, Member SPE-AIME, B.R.G.M.

ABSTRACT

This paper deals with the possibility of using usual oil well transient pressure testing methods in hot water wells when flashing occurs in the wellbore. Multiple rate analysis techniques have been successfully applied to available data on a well drilled by B.R.G.M. in the former French Territory of Afars and Issas. Practical recommendations concerning such tests are also included.

INTRODUCTION

Well established pressure transient analysis techniques are routinely used in oil and gas wells for the determination of reservoir parameters[1,2]. In recent years, improvements in these techniques have allowed a better understanding of complex reservoir and well behavior, as in the presence of skin, wellbore storage[3], or fractures[4].

Only recently have these methods been applied to geothermal systems. For a number of years, geothermal well testing was based on empirical methods[5], that, although useful for estimating geothermal field production potential, gave limited knowledge on the reservoir itself.

Pressure transient techniques have been applied successfully in vapor dominated geothermal reservoirs[6,7]. It was found that gas well analysis methods apply to steam wells and that wellhead measurements were generally adequate for analysis, thus eliminating the need for downhole instrumentation.

In water dominated systems, on the contrary, transient well testing can be far more complex, depending upon whether two-phase flow develops with flashing in the wellbore or in the formation. Usual oil well methods have already been shown to apply when no flashing develops[8]. On the other hand, they apparently cannot be used when flashing occurs in the formation[9]. Very little information was available until recently on the case of hot water wells in which flashing occurs at some depth in the wellbore. This is mainly due to the difficulty of bottom hole data gathering, that often results in mechanical damage of the measuring devices because of the high temperatures involved, and of the high production rates of boiling geothermal fluids.

A two rate flow test, conducted on one well in the Cerro Prieto field was recently presented by Rivera and Ramey[10]. The data were satisfactorily interpreted by means of models suggested by Russel[11], Selim[12], and Odeh and Jones[13,14].

To the author's knowledge, no other example of transient test in a two-phase well has been published in the literature. Unpublished data, however, were available from a well drilled in 1975 by B.R.G.M. in the French Territory of Afars and Issas (now Republic of Djibouti).

Analysis of these data, which include pressure build-up as well as two rate flow tests is presented hereafter.

ASAL WELL

The Asal rift, located 80 km west of Djibouti, is one of the active "rifts-in rift" structures of the Afar depression, a transition between the Gulf of Aden and the Red Sea ridges.

Attention was drawn to this zone because of the presence of a graben structure, and of geochemical particularities of various hot springs. Two wells were drilled on the S-W margin of the rift, at locations chosen mainly from geological considerations. The first hole (Asal 1) reached a hot water geothermal reservoir, the second, one kilometer away, was dry.

Both wells found, from top to bottom, a recent basaltic series, then a thick rhyolitic volcanic series, and finally an old tectonic, tilted, basaltic series, where the reservoir is located. The first well was drilled to a depth of 1130 m, where heavy mud losses occured, while the second well reached 1550 m. An important normal fault appears to separate the two wells.

A schematic of Asal 1 wellhead is presented in figure 1. The well could be produced either vertically through a 6" tube, or horizontally

References and illustrations at end of paper.

through a calibrated pipe. Four sizes were available (namely, 6", 4", 2" and 1") which were used to control the well flow rate. In addition, a 2" stainless steel tubing was lowered into the wellbore to a depth of 650 m, for wireline temperature and pressure measurements with bourdon-tube type gauges. As the well could not initially start by itself, the same tubing was used for inducing it into production by air lift. The initial water level in the well was at an approximate depth of 200 m below the well head.

The flow rate history of ASAL 1 well is presented on figure 2. After completion, the well was produced through a 6" outlet for 6 days in preparation for a build-up test for obtaining reservoir parameters (flow period # 1). Mechanical problems, however, were encountered with the stuffing box on the lubricator attached to the 2" stainless steel tubing, and these required the closing of the well for about 9 hours in order to retrieve the measuring devices (flow period # 2). During this unplanned pressure build-up, temperature and pressure could only be measured at the wellhead and are shown on figure 3.

It can be noticed on figure 3 that the wellhead temperature drops suddenly after 400 minutes. This apparently corresponds to steam condensation in the wellbore and defines the time limit after which the well has to be induced into production.

The well was again started by air-lift and flown through the 6" outlet for approximately 4 days (flow period # 3) before being shut-in for 20 hrs (flow period # 4). In order to obtain the well characteristic curve relating wellhead pressure and mass-flow rate, the well was again started by air-lift, flown for 43 hours with a 4" outlet (flow period # 5), shut-in for 3 hours (flow period # 6), and open again with the 6" outlet. Because of the short 4" pressure build-up duration, the well was able to start by itself. After about 3 hours of 6" production (flow period # 7), the 6" outlet was changed into a 2" outlet; the well was then produced for 3 days (flow period # 8), shut-in for 7 hours (flow period # 9), open again with the 6" outlet (flow period # 10) which was changed into a 1" outlet after 3 hours (flow period # 11). During this final test, there was evidence that the flow could not be sustained, and no build-up was attempted.

Although the primary objective of these last tests was to obtain the well characteristic curve, bottomhole measurements were taken throughout the duration of most individual flow period, in order to check the results of the second 6" build-up test. Temperature and pressure measurements were also performed at various depths in the wellbore, and are shown on figures 4 and 5, respectively. They indicate a reservoir temperature of 253°C, and show the presence of a flashing front at approximately 870 m with the 6" outlet, 850 m with the 4" outlet and 700 m with the 2" outlet.

TYPE - CURVE ANALYSIS

Asal 1 bottomhole pressure data that were available for flow periods 4, 6, 7, 8, 9, 10 and 11 are shown on the log-log plot of figure 6. For each individual flow period, the difference between the bottomhole pressure during the test and that at the beginning of the test is plotted versus the time since the beginning of that test.

Although no unique quantitative estimate of the reservoir parameters can be deduced from figure 6, important quantitative information can be obtained.

By comparing the log-log plot of figure 6 with the skin and storage type curves published in ref. 3, it becomes apparent that none of the 6" flowing tests had been run long enough for the radial flow logarithmic approximation to apply. On the other hand, that approximation does apply to the 2" flowing test, which had a much longer duration, and to the various build-up tests.

The comparison also suggests that the early time behavior of the well is of the changing wellbore storage type, going from liquid level controlled storage to compressibility controlled storage when flashing or condensation occurs.

Figure 6 further indicates that the radial flow logarithmic approximation applies sooner for build-up than for drawdown tests. This is somewhat opposite to what is generally observed in single phase wells, and may be due to the two-phase nature of the flow.

Another comment regarding figure 6 is that, although a dry well had been drilled one kilometer away from ASAL 1, no impermeable boundary is apparent on the log-log plot.

Figure 6 was also used to estimate the mass flow rates under reservoir conditions during the various flow periods.

As no separator was available, these were first deduced from James' lip pressure method[3] : James observed that, as a fairly large flow of steam or steam-water mixture was expanded along a pipe to the atmosphere, the pressure at the extreme end (lip) of the pipe was greater than the atmospheric pressure, and proportional to the mass flowing, and the enthalpy, as in the following formula :

$$\frac{G\,E^{1.102}}{P_L^{0.96}} = 11\,400. \qquad (1)$$

where G is the mass velocity (in lb/sq ft.sec), E is the stagnation enthalpy (in Btu/lb, at reservoir conditions), and P_L the critical lip pressure (in psi absolute).

James's formula was transformed for the present study into a more convenient system of units to yield :

$$w = 692.33\, P_L^{0.96}\, E^{-1.102}\, d^2 \qquad (2)$$

where w is expressed in tons/hr*, P_L in bars*, and d in inches.

Data for mass flow rate calculations are summarized in Table 1. The enthalpy value used in Eq. 1 was that for pure water, although the geothermal fluid salinity was of the order of 200,000 ppm. Enthalpy values for highly saline brines are not readily available in the literature.

As indicated in Table 1, the lip pressure was uniquely defined only with the 6" outlet, corresponding to a rate of approximately 83 t/hr. With the 4" and 2" outlets, on the contrary, the

* Metric units are used throughout this paper : 1 ton = 10^3 kg; 1 bar = 10^5 Pa

lip pressure was oscillating between two extreme values, because of the slug nature of the flow, and only a range of rate values could be obtained by applying James' formula (71 - 83 t/hr and 40 - 54 t/hr, respectively). According to James [16], such pulsations could have been eliminated by using a glycerine-damped pressure gauge with a needle valve. By throttling the valve, the lip pressure stabilizes at the correct value, between the two extreme ones.

However, by comparing the relative position of the different curves on figure 6, it appears that the rates with the 4" and 2" outlets were more likely 71 and 23 t/hr, respectively. In the same way, the rate with the 1" outlet seems to be equal to 11 t/hr.

MULTIPLE RATE ANALYSIS

Quantitative analysis of Asal 1 bottomhole pressure data was performed with a variable drawdown model, similar to that proposed by Odeh and Jones [17]. The well was considered as having been produced at different flow rates, $q_1, q_2, \ldots q_n$. Assuming the radial flow logarithmic approximation valid for each one of the flow periods, the bottomhole well pressure during the n^{th} test is equal to :

$$P_{wf_n} = P_i - \frac{q_n \nu\mu}{4\pi kh} \left\{ \sum_{j=1}^{n} \frac{q_j - q_{j-1}}{q_n} \ln (t_n - t_{j-1}) \right.$$

$$\left. + \ln \frac{k}{\phi\mu c r_w^2} + 0.80907 + 2S \right\} \qquad (3)$$

in Darcy units.

With geothermal metric units, Eq. (3) becomes :

$$P_{wf_n} =$$

$$- 0.228 \frac{\nu\mu}{kh} \sum_{j=1}^{n} (w_j - w_{j-1}) \ln 60 (t_n - t_{j-1})$$

$$+ p_i - 0.228 \frac{w_n \nu\mu}{kh} (\ln \frac{k}{\phi\mu c r_w^2} - 8.434 + 2S) \quad (4)$$

In Eq.(4), k is expressed in darcy, t in minutes, and r_w in meters.

Therefore, by graphing p_{wf} versus $\Sigma (w_j - w_{j-1}) \ln 60 (t_n - t_{j-1})$ in cartesian coordinates, one should obtain a straight line, the slope of which is equal to :

$$m = - 0.228 \frac{\nu\mu}{kh} \qquad (5)$$

This slope is independant of the flow rate. The intercept of the straight line can be used to calculate the skin, if p_i and ϕ are known. In the case of a build-up test ($w_n = 0$), the intercept is equal to the initial pressure p_i.

Build-up test analysis

A plot of p_{wf} during the second 6" build-up test (flow period # 4), versus the multiple rate function, (expressed in tons/hr), is shown on figure 7.

A straight line of slope m = 3.6 10^{-3} is clearly evident on figure 7. Substituting m = 3.6 10^{-3} into Eq. (5) and taking ν= 1.25 10^{-3} m /kg and μ = 0,2 cp yields :

$$kh = 15,9 \text{ Dm.}$$

(μ = 0,2 cp was obtained by extrapolating published viscosity curves[1] to a temperature of 253°C and a salinity of 200,000 ppm).

The calculated initial pressure is 76,6 bars, which compares reasonably well with the value of 77,4 bars measured before the test.

It can be observed in figure 7 that data points for build-up times greater than 6 hours deviate from the straight line. This is a consequence of the condensation effect already noticed on figure 3 during the first 6" build-up (flow period # 2).

The early time deviation (for build-up times less than 20 minutes) is caused by wellbore storage effects.

In the same way, analysis of the 4" build-up test (flow period # 6) yields a kh value of 15,0 Dm and a p_i value of 76,4 bars (figure 8).

kh and p_i from the 2" build-up (flow period # 9) are equal to 16,8 Dm and 77,2 bars, respectively (figure 9).

Flowing test analysis

A plot of p_{wf} versus the multiple rate function for the two 6" flowing tests (flow periods # 7 and 10) is shown on figure 10. The slope for the first one (# 7) is equal to 7,2 10^{-3}, which yields kh = 8 Dm, while that for the second one (# 10) is equal to 10,2 10^{-3} (kh = 5,6 Dm). As expected from figure 6, these kh values are much lower than those obtained before, and are not correct. On the other hand, the analysis shown on figure 11 of the 2" flowing test (flow period # 0) yields a slope equal to 3,5 10^{-3}, corresponding to kh = 16,3 Dm, which is consistent with the results of the build-up test analyses.

The sudden increase in bottom hole pressure indicated on figure 11 is likely to be caused by a decrease in the flow rate. The same phenomena appears on figure 12, in the analysis of the 1" flowing test (flow period # 11), during which the well was not able to sustain the flow : the last recorded pressure is roughly equal to the initial pressure. All the other pressure points fall on a straight line, whose slope is equal to 3,2 10^{-3}. The corresponding kh is equal to 17,8 Dm, which agrees well with the build-up tests results.

SKIN EVALUATION

It is not possible to obtain the skin factor directly from the multiple rate analysis plot, because of insufficient reservoir information. The skin factor, however, can be evaluated from a type curve match, with a dimensionless pressure given by :

$$P_D = \frac{kh}{0.228} \frac{\Delta P}{w_{n-1} \nu\mu} = \frac{\Delta P}{2 w_{n-1} m} \qquad (6)$$

for a build-up test, or

$$P_D = \frac{kh}{0.228} \frac{\Delta P}{(w_n - w_{n-1}) \nu\mu} = \frac{\Delta P}{2(w_n - w_{n-1}) m} \qquad (7)$$

for a flowing test.

The type curve match is shown on figure 13, and indicates a skin approximately equal to 25. This high skin value is probably due to rocks plugging the bottom of the hole : although the well was drilled to 1130 m, the pressure gauge could only be lowered to a depth of approximately 1050 m. This would also explain why, although the formation is known to be fractured, no fracture controlled flow period is apparent on the log-log plot of figure 6.

CONCLUSIONS

The following conclusions can be reached from the present study :

1. Two phase geothermal well testing can be carried out with standard bourdon-tube type instruments for extended periods of time at temperatures as high as 253°C and salt content of the order of 200,000 ppm.
2. Usual multiple rate techniques can be used in two phase geothermal wells for obtaining reservoir characteristics from bottom hole transient pressure data. Type curve matching also provides useful qualitative and quantitative reservoir information.
3. Early time bottom hole pressure appear to be wellbore storage controlled. There are indications that wellbore storage changes from liquid level type to compressibility type, as a consequence of water flashing or steam condensing in the wellbore. These wellbore storage effects appear to last longer in drawdown and double-rate tests than in build-up tests (200 mn compared to 20 mn for the well Asal 1 studied in this paper). This has to be taken into account when planning such tests.
4. When the well is not artesian, there is no practical avantage of running long build-up tests, because of the effects of steam condensation in the wellbore (6 hours was the practical limit in the case of well Asal 1).

NOMENCLATURE

c	=	total fluid compressibility, bar-1
E	=	enthalpy, kcal/kg
h	=	formation net thickness, m
k	=	permeability , darcy
m	=	slope of straight line
n	=	constant rate intervals
p	=	pressure, bar
q	=	volumetric flow rate, m^3/hr
r	=	wellbore radius, m
S_w	=	skin factor
t	=	producing time, min
w	=	mass flow rate, t/hr
μ	=	viscosity, cp
v	=	specific volume, m^3/kg
φ	=	porosity, fraction

Subscripts

i	=	initial condition
j	=	constant rate interval
w	=	wellbore or water
wf	=	flowing conditions at well bottom

ACKNOWLEDGEMENT

The work reported in this study was supported in part by the Commission of the European Communities (Contract 081-76 EGF, Geothermal Energy Program). The author is grateful to the Commission of the European Communities and to the management of the Bureau de Recherches Géologiques et Minières for permission to publish this paper.

REFERENCES

1. Matthews, C.S., and Russell, D.G. : "Pressure build-up and flow tests in wells" Monograph series, Society of Petroleum Engineers of AIME, Dallas,(1967), Volume 1.
2. Earlougher, R.C. : "Advances in well test analysis" Monograph series, Society of Petroleum Engineers of AIME, Dallas, (1977), Volume 5.
3. Agarwal, R.G.,Al-Hussainy, R.and Ramey, H.J., Jr: "An investigation of wellbore storage and skin in transient liquid flow - I: analytic treatment", Soc. of Pet. Eng. J, Sept. 1970, 279.
4. Gringarten, A.C., Ramey; H.J., Jr and Raghavan: "Applied pressure analysis for fractured wells" Pet. Tech., July 1975, 887.
5. James, R. : "Factors controlling borehole performance"U.N. Symposium on the Development and Utilization of Geothermal Resources, Pisa Proceedings (Geothermics, Spec.Iss.2) V.2 pt.2 p 1502.
6. Ramey, H.J., Jr and Gringarten A.C. : "Effect of high volume vertical fractures on geothermal steam well behavior", Proceedings, 2nd U.N. Symposium on the Development and use of geothermal resources, San Francisco , California (USA), May 20-29, 1975, V.3, p. 1759.
7. Barelli, A., Manetti, G., Celati, R, and NERI, G. : "Build-up and back-pressure tests on italian geothermal wells", Proceedings, 2nd U.N. Symposium on the Development and use of geothermal resources, San Francisco, California (USA), May 20-29, 1977, V.3, p.1537.
8. Witherspoon, P.A., Narasimhan, T.N. and Mc Edwards, D.G. : "Results of interference tests from two geothermal reservoirs", SPE paper 6052 51st Annual Fall Meeting, New Orleans, Oct.3-6, 1976.
9. Gulati, M.S. : "Pressure and temperature build-up in geothermal wells" Proceedings, Stanford geothermal workshop, Stanford University, Dec. 15-17, 1975.
10. Rivera, J.R. and Ramey, H.J., Jr : "Application of two-rate flow tests to the determination of geothermal reservoir parameters", SPE paper 6887, 52nd Annual Fall Meeting of SPE, Denver, Oct. 9-12, 1977.
11. Russell, D.G. : "Determination of formation characteristics by two-rate flow tests", J. Pet. Tech., Dec. 1962, 1349.

12. Odeh, A.S. and Jones, L.G. : "Two-rate flow test, variable rate case", J. Pet. Tech., Janv. 1974, 93.

13. Selim, M.A. : "A modification of the two-rate flow method for determination of reservoir parameters", J. Institute of Petroleum, V. 53, N°527, Nov. 1967, 343.

14. Odeh, A.S. and Jones, L.G. : "Pressure drawdown analysis, variable rate case", J. Pet. Tech., Aug. 1965, 960.

15. James, R. : "Alternative methods of determining enthalpy and mass flow" Proceedings, U.N. Conference on new sources of energy, Rome, 1961.

16. James, R. : "Private communication" Orléans (France), Nov. 1977.

TABLE 1

MASS FLOW RATE MEASUREMENTS

OUTLET DIAMETER (inch)	LIP PRESSURE (bar)	ABSOLUTE LIP PRESSURE (bar)	CALCULATED MASS FLOW RATE t/hr (from JAMES' formula)	ESTIMATED MASS FLOW RATE t/hr
6"	0.5	1.5	83	83
4"	2-2.5	3-3.5	71 - 83	71
2"	6-8.5	7.9.5	40 - 54	23
1"	not available			11

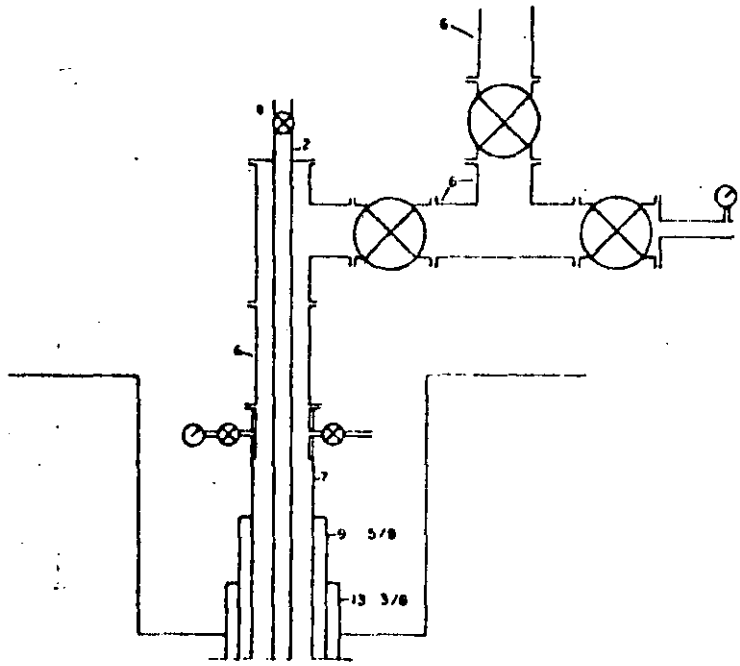

Fig. 1 - Schematic of ASAL 1 well.

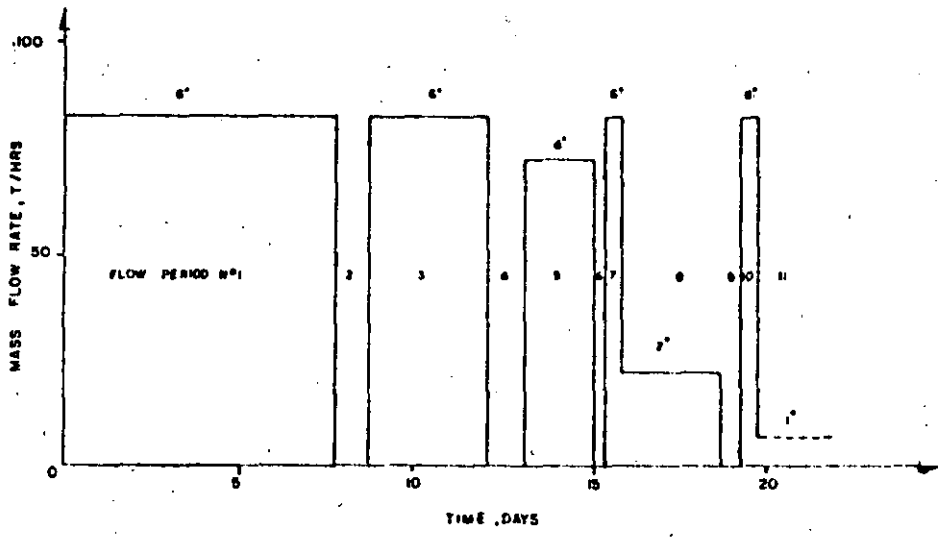

Fig. 2 - Mass flow rate changes during ASAL 1 tests.

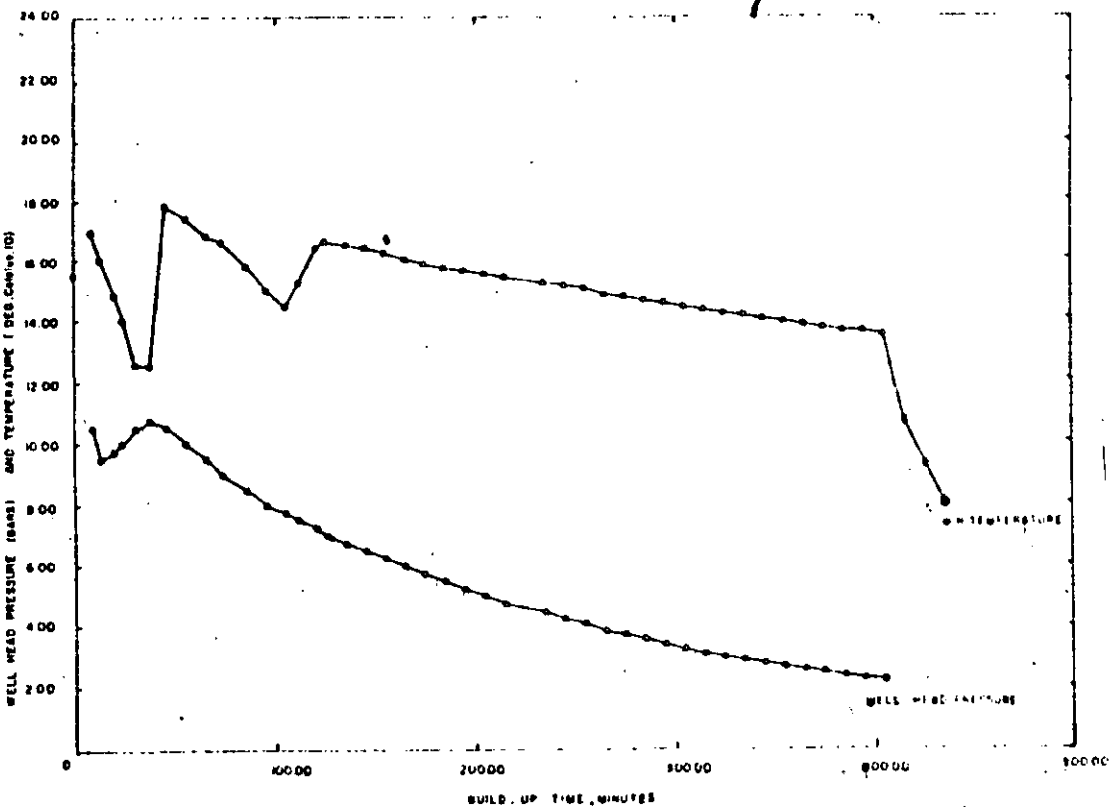

Fig. 3 - ASAL 1 pressure build-up test (6" outlet, flow period #2).

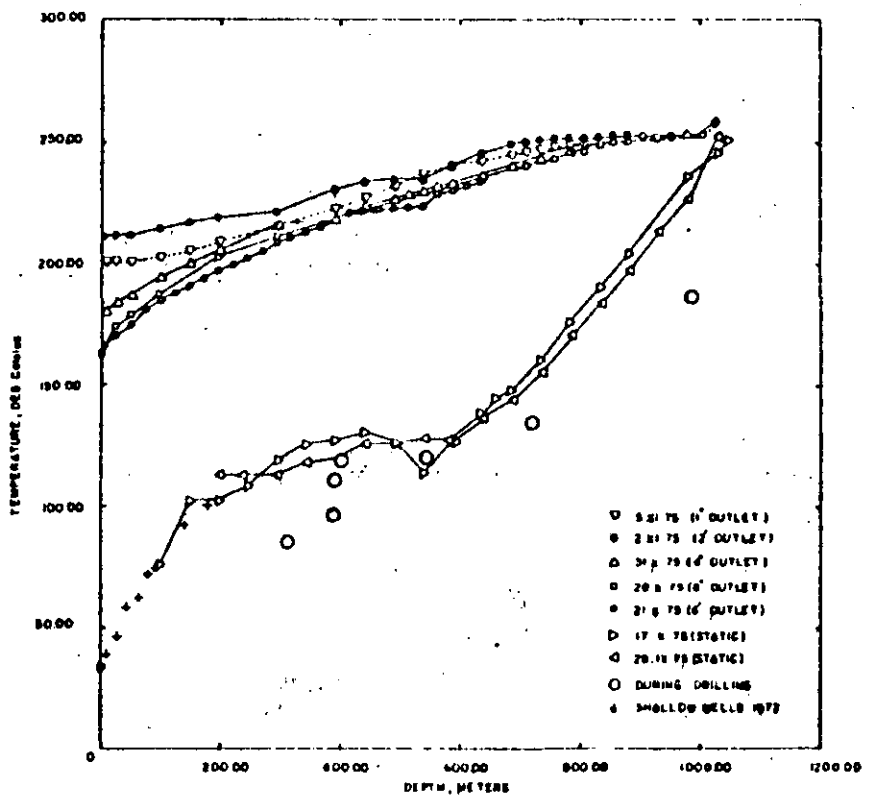

Fig. 4 - Temperature profiles in well ASAL 1.

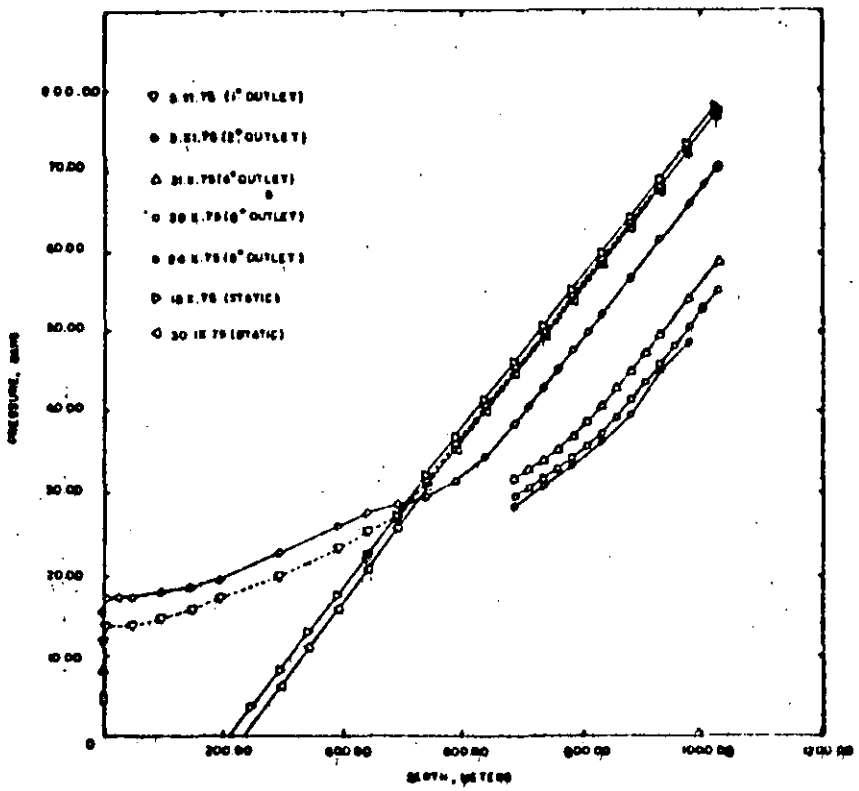

Fig. 5 - Pressure profiles in well ASAL 1.

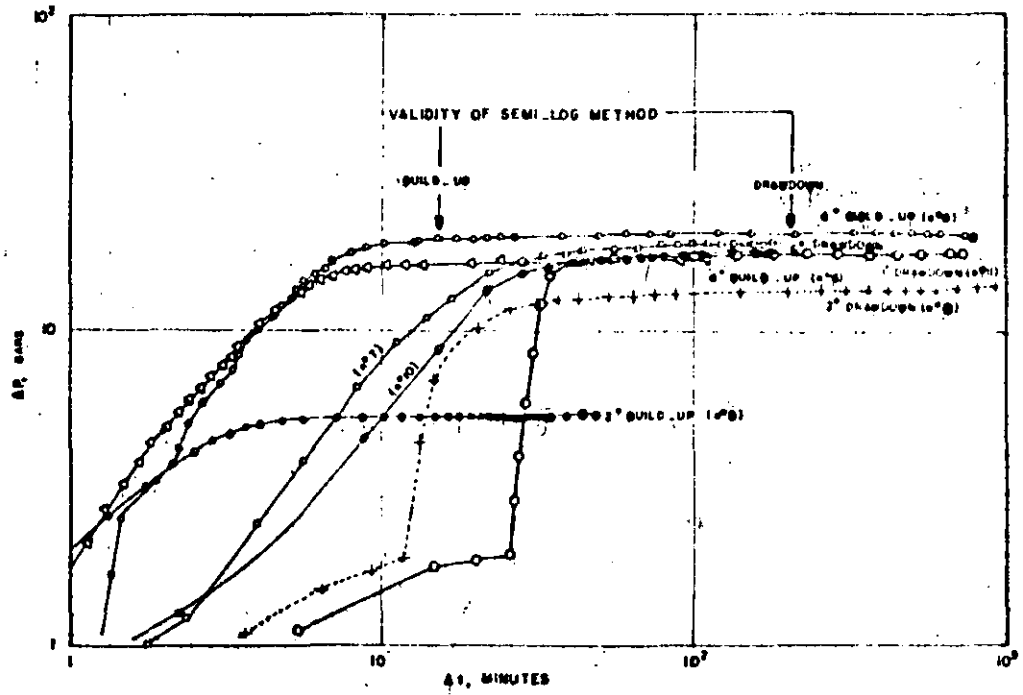

Fig. 6 - ASAL 1 pressure tests.

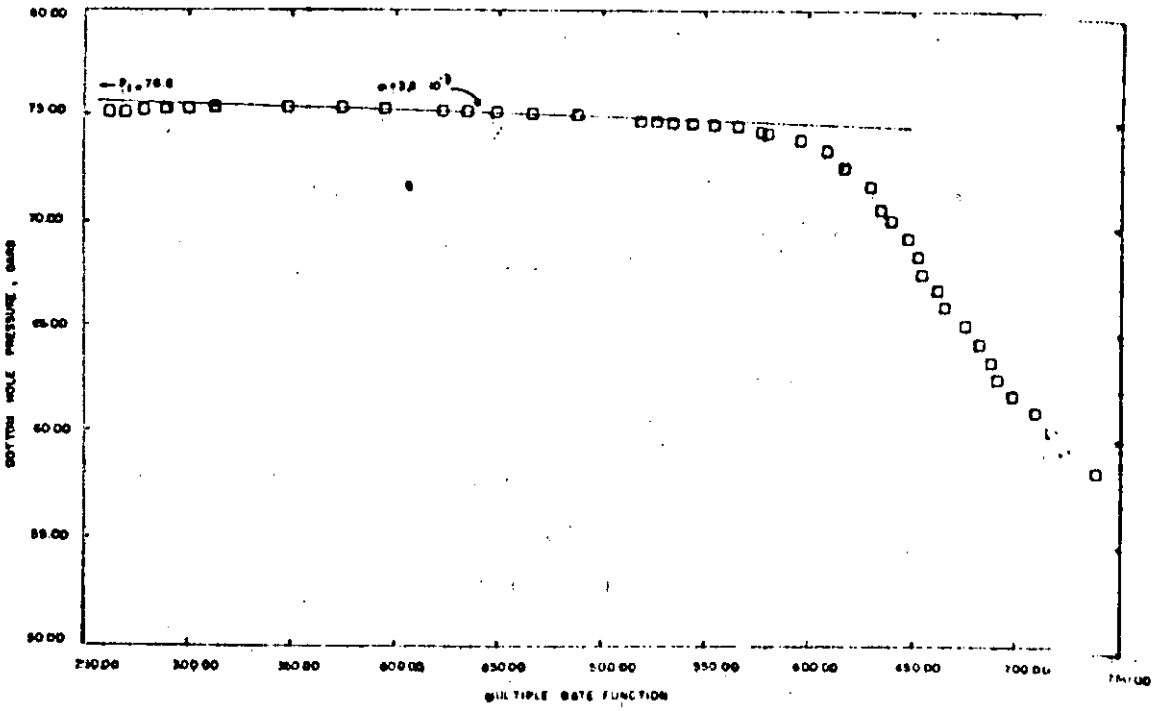

Fig. 7 - ASAL 1 pressure build-up test (6" outlet, flow period #4).

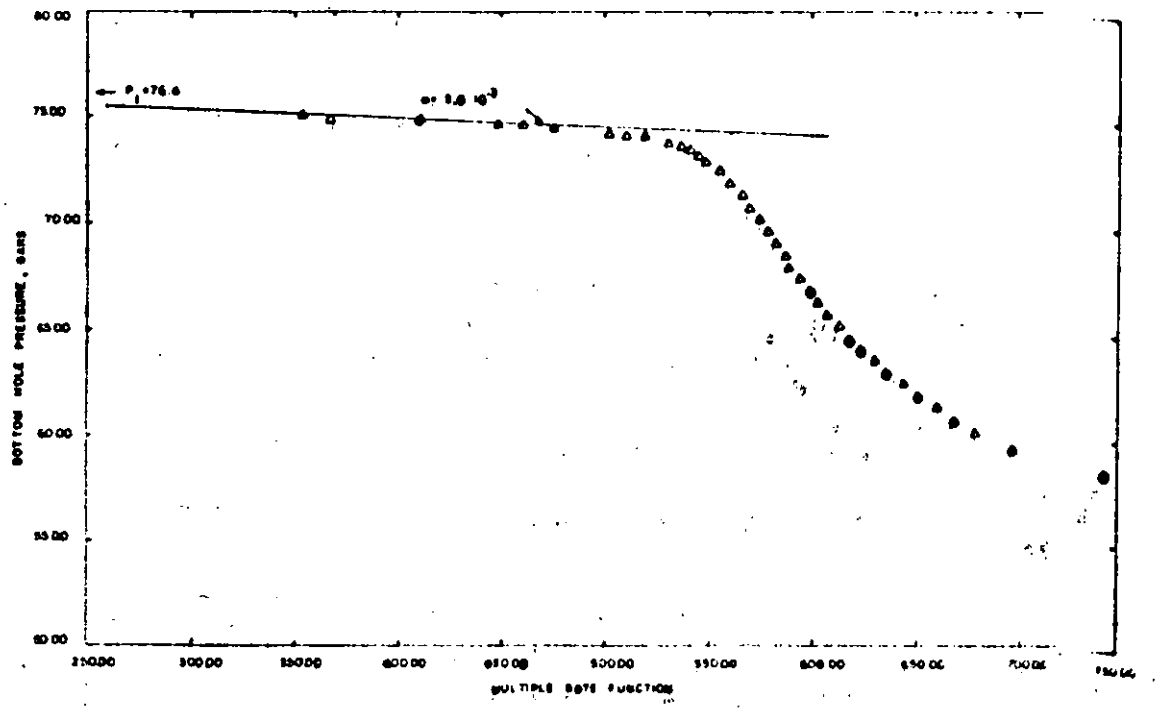

Fig. 8 - ASAL 1 pressure build-up test (4" outlet, flow period #6).

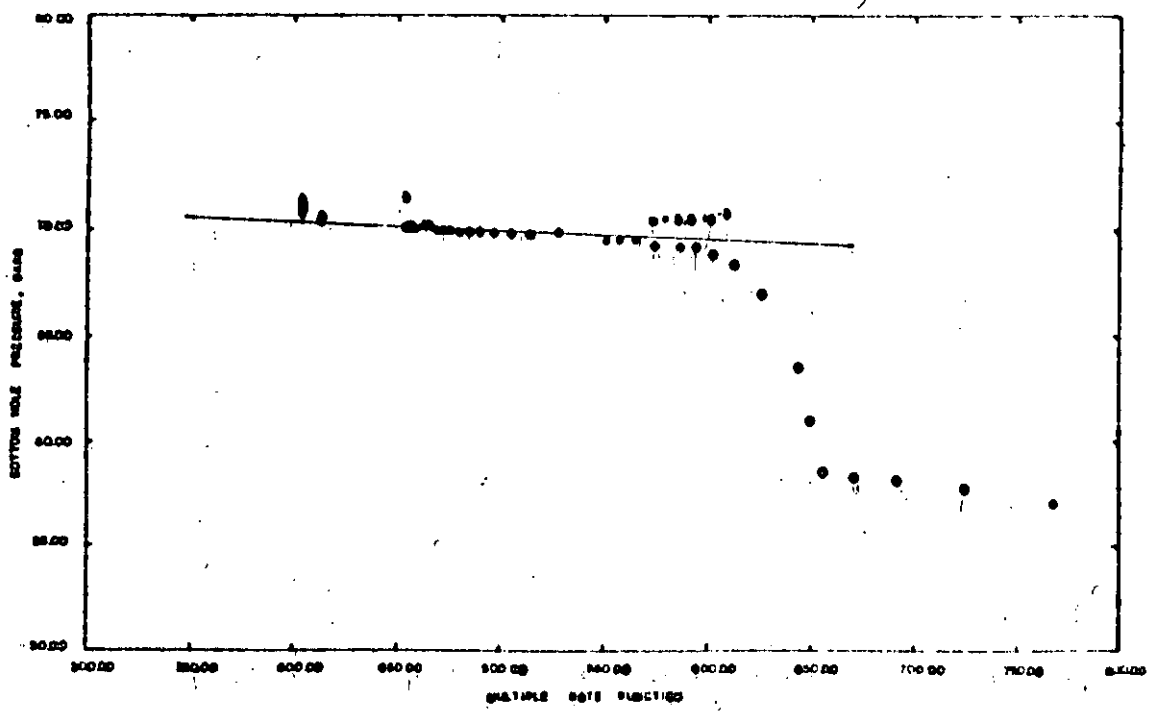

Fig. 11 - ASAL 1 pressure flowing test (2" outlet, flow period #8).

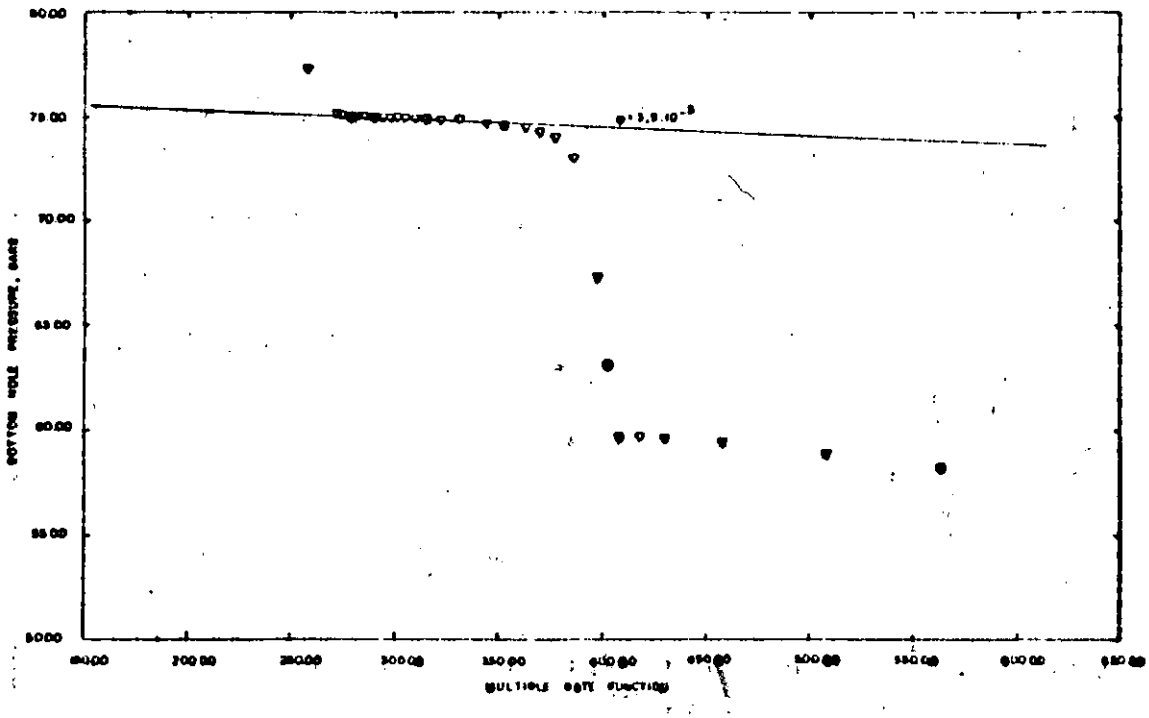

Fig. 12 - ASAL 1 pressure flowing test (1" outlet, flow period #11).

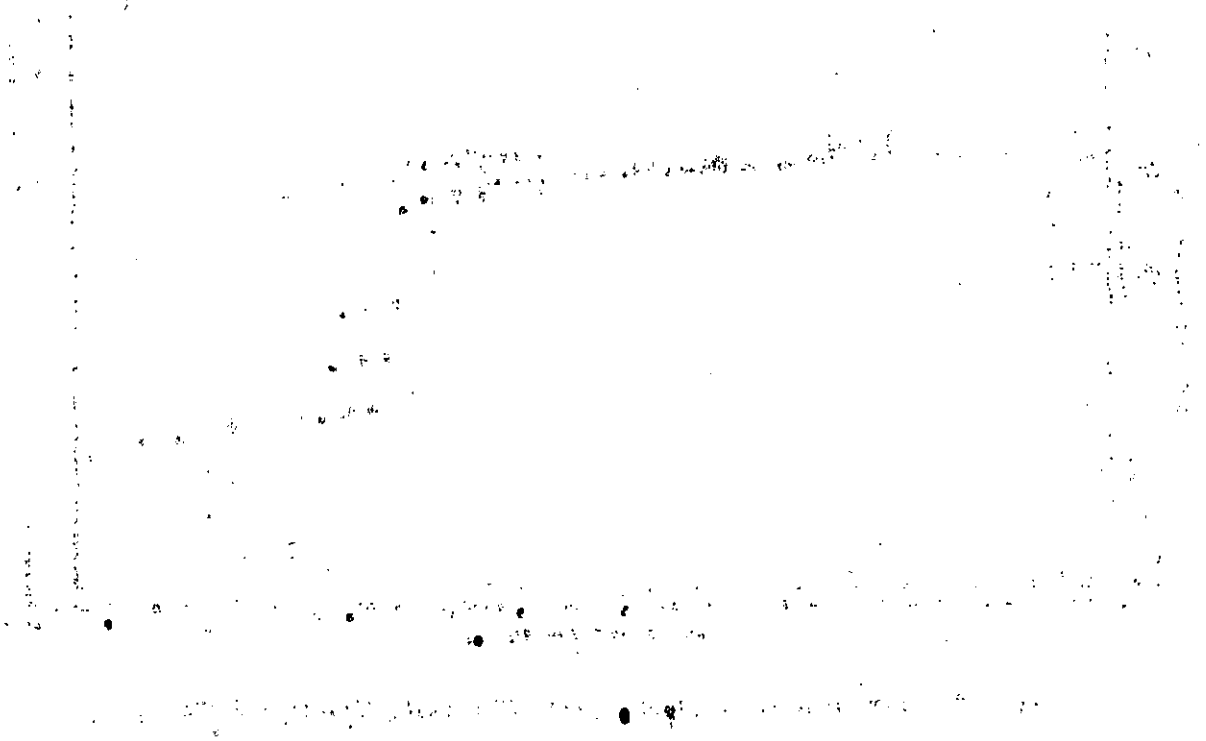

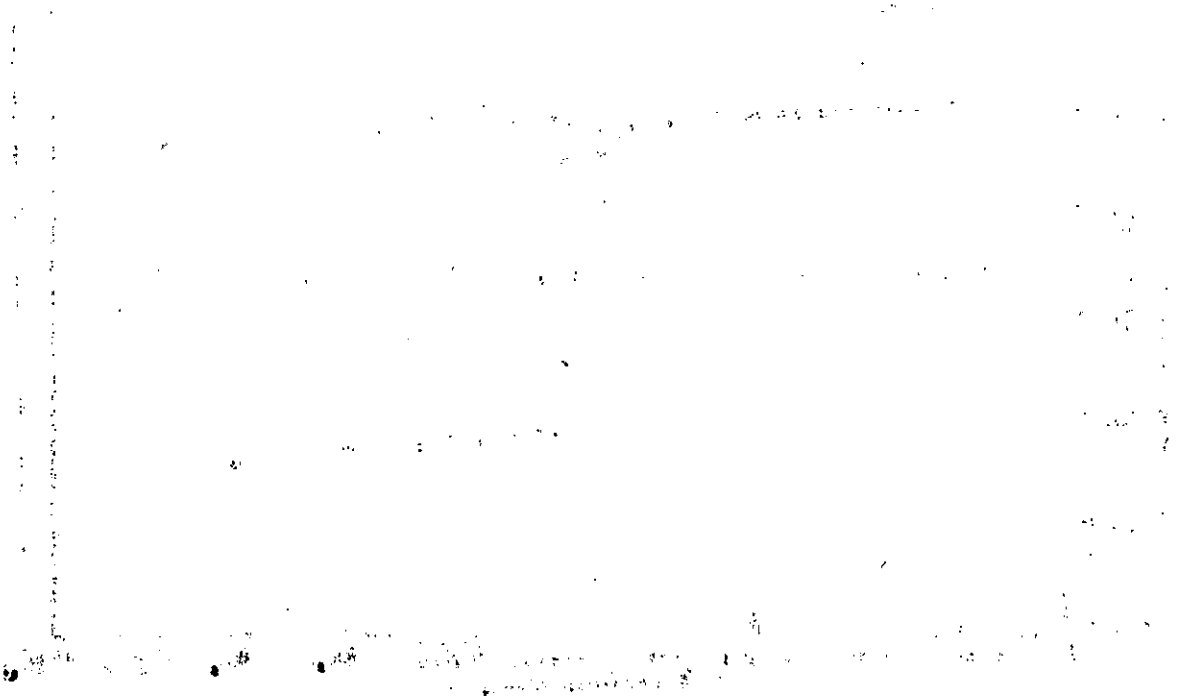

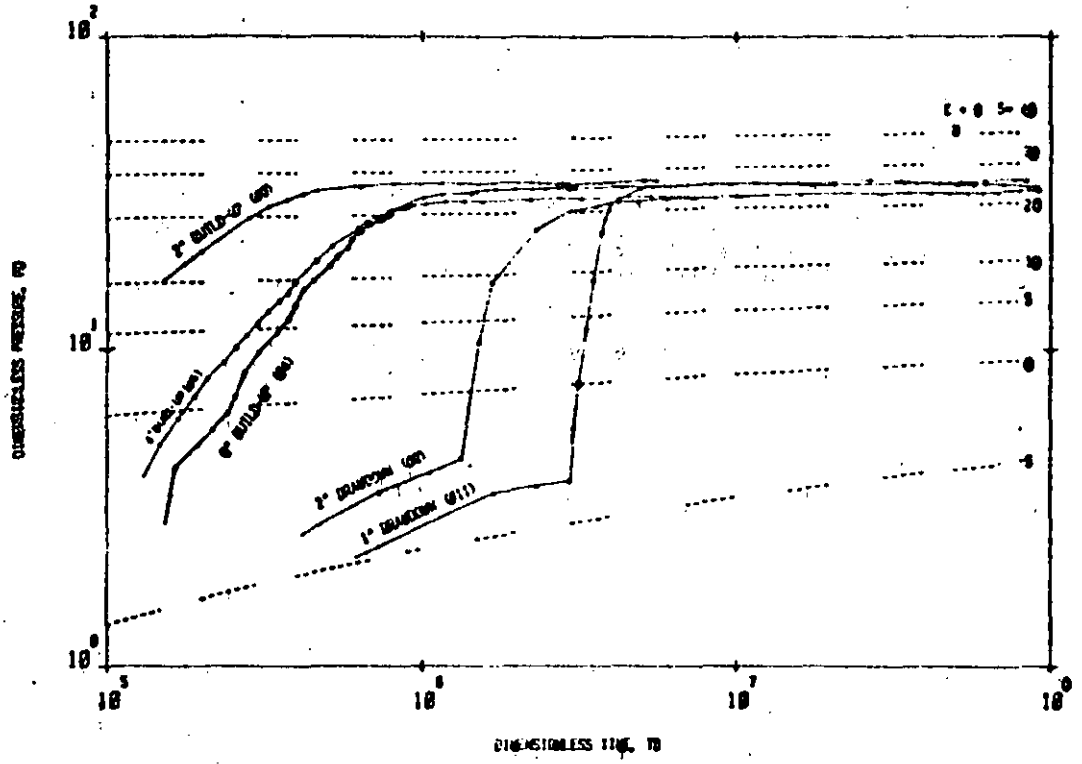

Fig. 13 - Type curve matching with skin and storage type curves (ref.3).

Wellbore Storage Effects in Geothermal Wells

Constance W. Miller, Lawrence Berkeley Laboratory

Abstract

The early-time response in the well testing of a homogeneous reservoir customarily is expected to give a unit slope when the logarithm of pressure is plotted vs. the logarithm of time. It is shown that this response is a special case and that another non-dimensional parameter must be defined to describe the set of curves that could take place for each value of the wellbore storage coefficient C_D. In addition, the effect of temperature changes along the bore is shown to increase the time when wellbore storage is important.

Introduction

The petroleum industry's technique of assessing oil and gas reservoirs by well testing has been extended to the geothermal field by a number of workers.[1-3] However, at least two important differences between a geothermal field and an oil or gas field must be considered in analyzing geothermal well test data. First, the kh/μ value of a geothermal field is usually much larger than that of an oil or gas field because the reservoir thickness h is greater in a geothermal field and the viscosity μ is smaller (k is the permeability). Second, heat loss in the wellbore, which can be ignored in oil and gas fields, is significant in geothermal bores.

The concept of wellbore storage – which has been considered quite extensively[4,5] and refined in such detailed studies as those of Agarwal *et al.*,[6] Wattenberger and Ramey,[7] and Ramey[8] – usually is treated as a boundary condition on the reservoir flow. The boundary condition used is

$$q_{sf} = q_s + C\frac{dp_w}{dt}, \quad \ldots\ldots\ldots\ldots\ldots\ldots\ldots (1)$$

where dp_w/dt is the flowing pressure change with time in the wellbore. However, dp_w/dt is not necessarily independent of position in the well. When dp_w/dt is dependent on the measurement point, a plot of $\log(p_{sf})$ vs. $\log(t)$ will not result in a unit slope at early times. This study will consider wellbore storage by looking at the flow in the well itself while treating the reservoir as simple homogeneous radial flow into the well.

Heat loss from the well and temperature changes along the bore also have been ignored because oil and gas fields can be treated as isothermal. Heat transfer from the well and heating of the fluid in the well is usually a very slow process. When very long times are considered, these temperature effects can become important. Once the early transient behavior is over and a semilog straight line of p_{sf} vs. $\log(t)$ is expected in the pseudosteady region, temperature changes in the well can alter the slope of that line so that the slope would no longer be $q\mu/4\pi kh$. The duration and importance of any temperature changes will be considered.

A numerical model of transient two-phase flow in the wellbore with heat and mass transfer has been developed. It is used to investigate (1) the early-time interaction of the well flow with that of the reservoir and (2) the longer-time effect of temperature changes on the well test data.

Concept of Wellbore Storage

Wellbore storage is the capacity of the well to absorb or supply any part of a mass flow rate change out of a well/reservoir system. For a change in flow rate at the surface of the well, the sandface mass flow rate usually is expressed as

$$w_{sf} = w_s + \rho c V\frac{dp_w}{dt}. \quad \ldots\ldots\ldots\ldots\ldots\ldots\ldots (2)$$

At time $t = 0^+$, when the surface mass flow rate is

0197-7520/80/0012-8203$00.25

increased, the change in the sandface rate is zero and the well is supplying all of the increase in flow rate. As the pressure in the well drops, the reservoir begins to supply part of the increased flow. The sandface rate steadily increases and approaches the surface flow rate as the well supplies less and less of the additional flow. The rate of increase in the sandface flow depends on the reservoir properties.

Because the change in w_{sf} is initially zero, it is assumed that the initial slope of the dp_w/dt curve gives the storativity of the well and that when p_w and t are plotted on a log-log scale, a unit slope will result. Such a plot is measured only, though, if p_w is some average pressure in the well, because $\rho cV(dp_w/dt)$ actually should be written as

$$\frac{1}{L}\int_0^L \rho cV\frac{dp_w}{dt}dx.$$

However, it would be difficult to determine an appropriate average pressure, and it is the downhole pressure that is used in the analysis of well test data. If the downhole pressure is measured, dp_{sf}/dt must be zero at $t=0^+$ because there is a finite time for changes made at wellhead to arrive downhole. If one plots the downhole pressure vs. time on a log-log scale, a unit slope is not necessarily seen. It is of interest to determine what should be measured downhole and if this early transient effect can be correlated with a nondimensional factor.

Eq. 2 can be nondimensionalized:

$$\frac{w_{sf}}{w_s}=1-C_D\frac{dp_D}{dt_D}, \quad \ldots\ldots\ldots\ldots\ldots\ldots (3)$$

where

$$p_D=2\pi(kh/\mu)(\rho_{sf}/w_s)p_w,$$

$$t_D=kt/\phi\mu c_R r_w^2,$$

and

$$C_D=\rho cV/\rho_{sf}2\pi\phi c_R h r_w^2.$$

The determination of ρcV for a two-phase or flashed system will be discussed. Also, the nondimensionalization was done using the sandface density explicitly instead of using a formation volume factor. Generally, p_D is plotted vs. t_D on a log-log scale for different wellbore storage factors C_D. However, as stated above, these plots are generated by assuming that the fluid in the well is mixed thoroughly, meaning that dp_w/dt is not a function of position in the well, even an isothermal well. Before one can assume that this uniformly mixed condition is valid, the wave nature of the original disturbance at wellhead must be damped out. When dp_w/dt is a function of position in the well, Eq. 2 and, therefore, Eq. 3 are not valid because of the question of what pressure should be used for p_w. Nevertheless, once the initial transient effects in the well have died out and dp_w/dt is no longer a function of position, Eqs. 2 and 3 should be valid for the isothermal case, provided one uses $\int_0^L \rho c(V/L)dx$ in the expression for C_D. The approach of the true behavior to that given by Eq. 3, however, can occur during or after the period when the unit slope is expected. Although Eq. 3 will not be valid as written at the very early times, it will be shown that the downhole pressure vs. time data can be correlated using another nondimensional parameter for the cases considered here – i.e., a single-phase reservoir, with the fluid single phase, two phase, or flashing in the bore. The expected drawdown curve will be described by the C_D factor as well as this additional parameter. The derivation of this parameter is made by neglecting the change in fluid head which occurs when the fluid is not isothermal. The calculation will show that the effect of the fluid head change is a longer-term effect, and neglecting it will not alter significantly the initial plot of p_{sf} vs. t.

To achieve a given surface mass flow rate, the pressure at wellhead must be decreased by Δp. This pressure drop, then, propagates down the well and interacts with the reservoir. If the reservoir can supply only a small percentage of the surface flow for that pressure drop Δp, the well will continue to supply most of the fluid until the well pressure has dropped further. Because the sandface flow rate is given by $2\pi r(kh/\mu)\rho\partial p/\partial r$ for a single-phase reservoir, the ability of the reservoir to deliver its fluid depends on the value of kh/μ. When kh/μ is relatively low, the nonuniformity of dp_w/dt in the well is damped out before the reservoir can supply any significant portion of the surface flow. Because w_{sf} is still negligible when dp_w/dt is no longer a function of position, a unit slope will be measured if p_{sf} is plotted vs. t on a log-log scale. This condition is true when an oil reservoir is tested. A typical kh value is 600 md-ft (1.8×10^{-13} m^3), and for a viscosity of 1 cp (1×10^{-3} Pa·s), kh/μ is about 600 md-ft/cp (1.8×10^{-10} m^3/Pa·s). However, there are cases when the reservoir can supply a significant portion of the surface flow rate before dp_w/dt is uniform in the well. In geothermal reservoirs, kh can be large [e.g., 30,000 to 90,000 md-ft (9×10^{-12} to 2.7×10^{-11} m^3] and μ is low [0.1 cp at 572°F (1×10^{-4} Pa·s at 300°C)]. Because of the large value of kh/μ, the reservoir is capable of supplying a much greater quantity of fluid for the original pressure drop Δp. The initial sandface flow from the reservoir when the pressure pulse arrives downhole can even be equal to or greater than the desired sandface flow rate. The nondimensional parameter used to correlate the data is the ratio of the surface mass flow rate that results from the initial pressure drop made at wellhead to the reservoir flow rate that can be achieved for the same Δp. This parameter is written as

$$w_D=\frac{w_s}{(w_{sf})_i},$$

where $(w_{sf})_i$ is defined as the initial flow from the reservoir for the sudden drop in pressure Δp at the sandface. However, $(w_{sf})_i$ will be estimated, and it is this estimate that will be used in determining w_D. The initial flow from the well is just the surface flow rate because all the fluid is initially from the well.

One calculates the pressure drop Δp given this latter condition.

To derive w_D in terms of the fluid properties and reservoir conditions, several assumptions were made.

1. The velocity of the fluid from the reservoir is described by $(k/\mu)\partial p/\partial r$, so the reservoir is single phase. The ability of w_D to correlate the early-time data of a two-phase reservoir has not been done because of the difficulty of obtaining similarity solutions for two-phase flow in the reservoir itself.

2. The compressibility of the fluid in the well is not a strong function of position. A nonflashing two-phase flow is not necessarily ruled out here. However, the assumption does seem to preclude a flashing well. The extension of the derivation to include the flashing system is considered later.

3. The flow in the well is isentropic. The effect of change in the fluid head in the well, therefore, will be ignored in this initial derivation. This effect depends on a much longer time and is considered in the next section. It will be shown in the calculations that the change in fluid head will have a small effect on these initial pressure curves.

4. The pressure pulse at wellhead travels as a step change. Friction effects will smear the front out, but the pulse interaction takes place over the entire height of the reservoir, and it is assumed that the smearing effect takes place over a smaller distance than this height.

5. No skin effect is considered.

For a step change in surface mass flow rate, all of the mass is taken initially from the bore. As it is usually the surface flow rate that is assumed to be kept constant during a well test, the surface flow rate will be prescribed, and the initial pressure pulse needed to achieve this flow rate is calculated. Given this pressure change, the initial flow from the reservoir is determined.

When all the mass is taken from the well, the decrease in mass in the well must equal the total mass out or

$$(\Delta\rho)\pi r_w^2\Delta x=\rho q\Delta t, \quad \ldots\ldots\ldots\ldots\ldots\ldots (4)$$

where Δx is the distance down the well from which the mass is taken. This distance is just the distance the signal has propagated. Assuming the flow is isentropic (an approximation), Eq. 4 can be rewritten as

$$(\Delta\rho)\frac{\Delta x}{\Delta t}=\left(\frac{\partial\rho}{dp}\right)_s\Delta p\frac{\Delta x}{\Delta t}=\frac{\rho q}{\pi r_w^2},$$

or

$$\Delta p=\left(\frac{\partial\rho}{\partial p}\right)_s^{-1}\frac{\rho q}{\pi r_w^2}\frac{\Delta t}{\Delta x}.$$

The disturbance travels at the local speed of sound, a, so

$$(\Delta x/\Delta t)=a=(\partial p/\partial\rho)_s^{1/2}, \quad \ldots\ldots\ldots\ldots (5a)$$

and

$$\Delta p=\left(\frac{\partial\rho}{\partial p}\right)_s^{-1/2}\frac{\rho q}{\pi r_w^2}. \quad \ldots\ldots\ldots\ldots\ldots (5b)$$

The sandface flow at any time is

$$w_{sf}=2\pi r_w\frac{kh}{\mu}\rho_{sf}\frac{\partial p}{\partial r}. \quad \ldots\ldots\ldots\ldots\ldots (6)$$

Now the initial sandface flow is estimated by describing $\partial p/\partial r$ as $\Delta p/r_w$ (the initial pressure drop in the well divided by the radius of the well), so $(w_{sf})_i$ is obtained from Eq. 6:

$$(w_{sf})_i=2\pi\frac{kh}{\mu}\rho_{sf}\left(\frac{\partial\rho}{\partial p}\right)_s^{-1/2}\frac{\rho q}{\pi r_w^2}. \quad \ldots\ldots\ldots\ldots (7)$$

Since $\rho q=w_s$, one can obtain the nondimensional parameter w_D using the estimate for $(w_{sf})_i$:

$$w_D=\frac{w_s}{(w_{sf})_i}=\frac{\mu}{kh}\frac{r_w^2}{2}\frac{1}{\rho_{sf}}\left(\frac{\partial\rho}{\partial p}\right)_s^{1/2}. \quad \ldots\ldots\ldots\ldots (8)$$

The storage coefficient C_D represents the ratio of the ability of the well to store fluid to that of the reservoir, while the nondimensional parameter w_D represents the ratio of the ability of the well to give up its fluid to that of the reservoir. We see that this latter quantity depends on the value of kh/μ of the reservoir and on the rate of signal propagation in the well. The reservoir may have a large storage capacity but, because of a low permeability-thickness factor and high viscosity, it may not be able to deliver the fluid very rapidly. Transient changes in the well would die out before the reservoir could deliver any significant portion of the flow rate. However, for the same storage coefficient, the value of kh/μ could be large enough that the reservoir could deliver large quantities of fluid while the transient changes in the well were still important. The very early-time data will be different in these two cases, although C_D would be the same. To describe this early-time data completely, one needs to use both the storage coefficient and the nondimensional parameter w_D.

We now extend this discussion to include a two-phase or flashing system. First, it is necessary to define C_D in these cases and then to consider whether w_D still can be used to correlate the early-time data. The storage coefficient is defined in the petroleum literature by assuming dp_w/dt is not a function of position. The same approach will be used here. Therefore, although the plot of p_D vs. t_D will deviate at early times from those developed in the literature, these plots must approach the expected curves at later times when dp_w/dt is not a function of position. Eq. 2 actually should be written as

$$w_{sf}=w_s-\int_0^L A\left(\frac{\partial\rho}{\partial p}\right)_s\frac{\partial p}{\partial t}dx, \quad \ldots\ldots\ldots\ldots (9)$$

If the equation is nondimensionalized and if one looks at the case where $\partial p_w/\partial t$ is not a function of x,

$$\frac{w_{sf}}{w_s}=1-\frac{A}{2\pi r_w^2\phi c_R h}\frac{dp_D}{dt_D}\frac{1}{\rho_{sf}}\int_0^L\left(\frac{\partial\rho}{\partial p}\right)_s dx, \quad \ldots\ldots\ldots\ldots (10)$$

so

$$C_D=\frac{AL}{2\pi r_w^2\phi c_R h}\frac{1}{\rho_{sf}}\left(\overline{\frac{\partial\rho}{\partial p}}\right)_s,$$

and

$$\frac{\overline{\partial\rho}}{dp_s} = \frac{1}{L}\int_0^L (1-\alpha)\left(\frac{\partial\rho}{\partial p}\right)_1 + \alpha\left(\frac{\partial\rho}{\partial p}\right)_2 dx, \quad \ldots\ldots(11)$$

where α is a function of x. For a single-phase system, $\alpha=0$.

It is now necessary to determine if w_D still can be used to correlate the early-time data for the two-phase or flashing case. In the preceding derivation, it was assumed that $(\partial\rho/\partial p)_s$ was not a function of x. If the flow is two-phase, but not flashing, α usually is not a strong function of position. Therefore, as long as the flow can be described by $v=-(k/\mu)\partial p/\partial r$, none of the assumptions made are violated and w_D is appropriate. When the fluid is flashing, however, α is a strong function of position, especially where the fluid starts to flash.

The value of $(\partial\rho/\partial p)_s$ in the flashed region is on the order of 4.2×10^{-2} lbm/cu ft-psi (10^{-4} kg/m$^3\cdot$Pa) and in the single-phase region it is about 4.2×10^{-4} lbm/cu ft-psi (10^{-6} kg/m$^3\cdot$Pa). Such a change cannot be ignored. The derivation of w_D depends on the storage capacity of the well and the speed of signal propagation. The time for the signal to propagate in the single-phase region is about an order of magnitude smaller than in the two-phase region. Also, the storativity of the well in the single-phase region is two orders of magnitude less than in the flashed region. The changes in the well are controlled entirely by the two-phase region. When the signal arrives at the two-phase boundary in the well, it essentially can be assumed to be at the reservoir boundary, meaning that the single-phase region acts merely as a connection between the two-phase region and the reservoir. The signal is propagated instantaneously over that region. Then in the derivation of w_D, the single-phase region can be neglected and the average value of $(\partial\rho/\partial p)_s$ will be that of the flashed region. In this region, $(\partial\rho/\partial p)_s$ will be a weak function of position again, so the derivation for w_D is still appropriate.

Using w_D and C_D, it will be shown that the downhole pressure can be correlated even when the well transients are important. A numerical program is used to derive the nondimensional plots. It will be seen that in all cases, the p_D vs. t_D plot (where p_D is the nondimensionalized downhole pressure) will approach the nondimensional plots derived in petroleum literature.

Transient Flow in Wellbore

Several papers in the literature have dealt with flow in a geothermal well.[9-12] However, all these papers assume steady-state flow—i.e., $\partial p_w/\partial t=0$ and the mass into the well equals the mass out of it. Obviously these models cannot consider the effect of the interaction of a pressure wave propagating down the well into the reservoir, and they cannot be used to describe the flow when wellbore storage is important. Steady-state models can be used to obtain wellhead conditions when the downhole pressure is approximately constant and when wellbore storage is over. The intent of this work, though, is to consider the very early-time data, so a transient model of the flow is necessary.

To investigate the nonuniform changes in the well in detail, a numerical model to simulate compressible transient flow in a wellbore has been developed. The model is capable of handling single-phase as well as two-phase flow with mass transfer (e.g., steam/water flow) and includes the heat transfer between the ground and the well. The one-dimensional equations of mass, momentum, and energy in the well are solved, as well as a radial Darcy flow equation for a homogeneous single-phase reservoir. The equations are

$$\frac{\partial\rho}{\partial t}+\frac{\partial}{\partial x}(\rho v)=0, \quad \ldots\ldots(12)$$

$$\frac{\partial}{\partial t}(\rho v)+\frac{\partial}{\partial x}(\rho v^2)+\frac{\partial p}{\partial x}+\rho g+\frac{f\rho v^2}{4r_w}=0, \quad \ldots(13)$$

and

$$\frac{\partial}{\partial t}(\rho E)+\frac{\partial}{\partial x}(\rho E v)-\frac{2U}{r_w}(T_f-T_w)+p\frac{\partial v}{\partial x}=0 \quad \ldots\ldots(14)$$

in the well and

$$\frac{\partial p}{\partial t}=-\frac{k}{\phi c_R\mu}\left(\frac{\partial^2 p}{\partial r^2}+\frac{1}{r}\frac{\partial p}{\partial r}\right) \quad \ldots\ldots(15)$$

in the reservoir.

An equation of state is used to relate density to pressure and energy. A more complete description of the numerical model is given in the Appendix. For the initial calculations presented here, a constant friction factor was used and no slip was assumed. Many interesting and meaningful transient results are possible without going into a more elaborate description of the friction and slip. The program is used to investigate the initial transient nature of the wellbore and to determine the duration of temperature changes. The inclusion of slip will not alter significantly the effects being considered here. Initially the behavior of dp_{wf}/dt will be investigated, with no heat loss assumed, to show how consideration of the transient changes in the well will alter the curves developed in the petroleum literature. The effect of temperature changes will be considered in the following section.

Adiabatic Flow

Using the developed numerical model, calculations were performed to generate the deviation of the drawdown (or buildup) curve from the unit slope for different values of w_D and C_D. The calculations were done for $C'_D=25$ and 100 [the C'_D factor is calculated using $(\partial\rho/\partial p)_E$ instead of $(\partial\rho/\partial p)_s$] with $w_D=0.1$, 1.0, and 10.0. For all calculations, the length of the well was 6,561.7 ft (2000 m) and the radius was 0.0323 in. (0.082 cm). The mass flow rate per unit area out was kept constant at 102.4 lbm/sq ft-s (500 kg/m$^2\cdot$s). No heat loss was assumed. The downhole pressure was adjusted to obtain flashing or

TABLE 1 – DIMENSIONAL VALUES USED FOR GENERATING NONDIMENSIONAL WELLBORE STORAGE PLOTS

w_D	C_D	kh (m³)	μ (Pa·s)	ϕch (m/Pa)	Downhole Pressure (Pa)	Downhole Temperature (°C)
10.0	25	6.4×10^{-14}	0.2×10^{-3}	0.32×10^{-7}	2.9×10^{7}	200
1.0	25	6.4×10^{-13}	0.2×10^{-3}	0.32×10^{-7}	2.9×10^{7}	200
0.1	25	6.4×10^{-12}	0.2×10^{-3}	0.32×10^{-7}	2.9×10^{7}	200
10.0	100	4×10^{-13}	0.9×10^{-4}	0.53×10^{-6}	2×10^{7}	320
1.0	100	4×10^{-12}	0.9×10^{-4}	0.53×10^{-6}	2×10^{7}	320
0.1	100	4×10^{-11}	0.9×10^{-4}	0.53×10^{-6}	2×10^{7}	320

17

no flashing. The reservoir parameters used for the calculations are given in Table 1. The results are shown in Figs. 1A and 1B. Each plot included the analytical solution for both a wellbore storage curve derived by assuming (dp_D/dt_D) is not a function of position in the well and the $C_D=0$ curve. The particular analytical solution chosen for comparison is for a value close to that of the numerical calculations. The small difference between the C_D used for the numerical calculations and the C_D of the analytical curve is discussed later. The $C_D=0$ curve is just the Theis curve. The general behavior of the transient flow in the well can be described using these figures.

In Fig. 1A, liquid water was assumed to flow under a positive head to generate the curves for the different values of w_D. The average value of $(\partial\rho/\partial p)_E$ in the well was 3.0×10^{-4} lbm/cu ft-psi (7×10^{-7} kg/m³·Pa), and the C_D factor for this plot is 25. Included in the figure are points calculated for a flashed system where the average value of $(\partial\rho/\partial p)_E$ is 1.7×10^{-2} lbm/cu ft-psi (4×10^{-5} kg/m³·Pa). Fig. 1B and some points in Fig. 1A are for calculations that assume that the water is flashing about 1,640 ft (500 m) down the well but still flowing under a positive head. A friction factor of 0.04 was used for all calculations except for one case in Fig. 1B. To generate the different curves, kh, μ, and ϕch were varied. The arrival time of the initial pulse downhole is the same if the average compressibility is not changed. However, the time has been nondimensionalized by $(k/\mu c\phi r_w^2)t$, so the nondimensionalized arrival time will be different when the reservoir parameters are varied.

The first case to consider is $w_D>1$, illustrated in the figures by $w_D=10$. The fluid in the well may not be very compressible, but because the reservoir is even less responsive, the well must continue to supply the surface flow rate long after the initial pressure arrives downhole. For Δp_i, the flow from the reservoir is significantly less than the surface flow rate. Actually, this case serves as a check on the numerical calculations. There always will be some initial delay, but this delay is a very small portion of the initial curve. Once the pressure disturbance arrives downhole, the pressure change with time there increases abruptly. After the downhole pressure drops to what it would be at this time, if the well had responded uniformly, the $\log p_D$ vs. $\log t_D$ curve follows a unit slope. In both figures the unit slope is calculated for the $w_D=10$ case, as expected. As

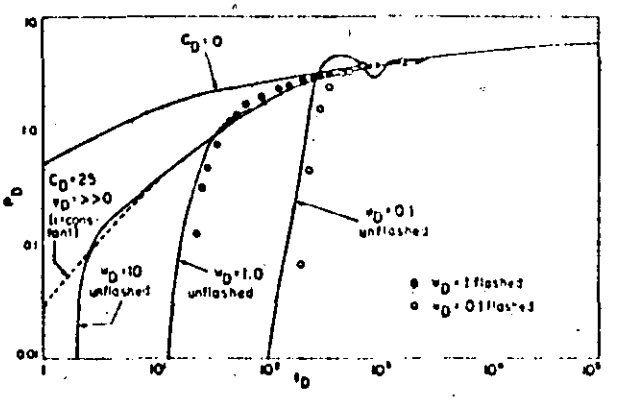

Fig. 1A – Nondimensional plot of sandface pressure vs. time for $C_D=25$ and $w_D=0.1$ to 10.

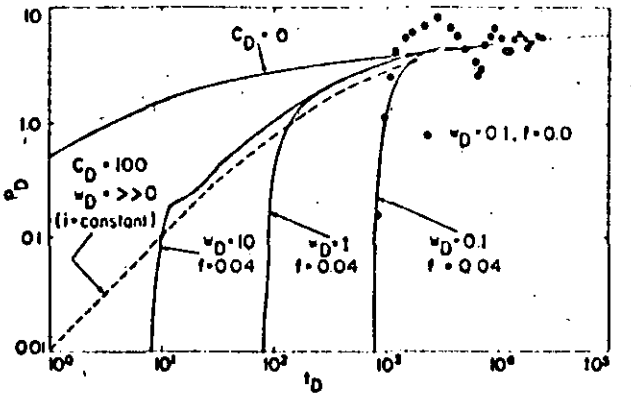

Fig. 1B – Nondimensional plot of sandface pressure vs. time for $C_D=100$ and $w_D=0.1$ to 10.

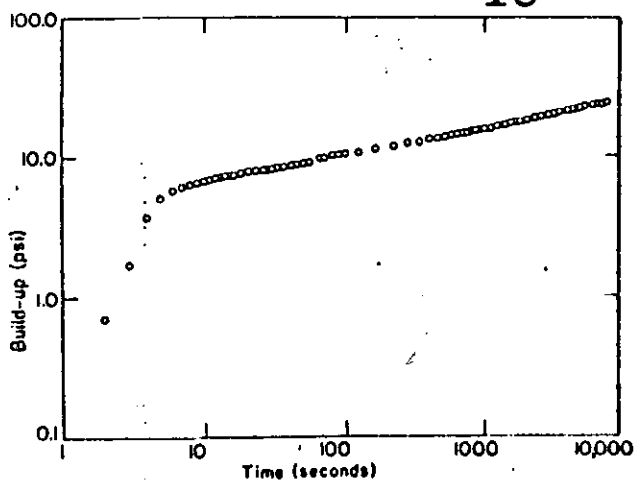

Fig. 2 – Buildup data from the geothermal Well RRGE2 at Raft River.[13]

noted, included on each plot is the analytic solution for the wellbore storage curve when $dp_w/dt \neq \text{fn}(x)$. In Fig. 1A the C_D should be calculated with $(\partial\rho/\partial p)_s$, while the estimation of C_D for the calculations was done here using $(\partial\rho/\partial p)_E$. Only $(\partial\rho/\partial p)_E$ could be calculated in the numerical solution because the steam tables were fit with polynomials and $\rho = \text{fn}(P,s)$ was not included. The error in the estimation for C_D is less in the single-phase case because the difference between these two derivatives is negligible. As the fluid flashes more, $(\partial\rho/\partial p)_s$ and $(\partial\rho/\partial p)_E$ start to differ. For the single-phase case plotted in Fig. 1A, the calculations fall on the analytical solution for the $w_D = 10$ case. In Fig. 1B (the two-phase case), the calculations fall on a unit slope corresponding to a C_D that is slightly less than the plotted analytical curve for $C_D = 100$, as expected.

When $w_D = 1$, the pressure drop needed to achieve a step change in flow rate at the surface is close to the pressure drop needed to obtain this same flow rate from the reservoir. The pressure change with time is initially zero, but once the disturbance reaches downhole, it rises abruptly until it reaches the expected drawdown curve. Since $w_{sf})_i = w_s$, this occurs after the expected wellbore storage curve is almost over. The plot is shown in the figures by $w_D = 1$. The actual value of $(w_{sf})_i$ when $w_D = 1$ is less than w_s. In the derivation, $(\partial p/\partial r)_i$ was estimated as $\Delta p_i/r_w$. The actual value of $(\partial p/\partial r)_i$ at the reservoir is always less than this, so that $(w_{sf})_i < w_s$ when $w_D = 1$. The error in estimating $(\partial p/\partial r)_i$ as $\Delta p_i/r_w$ is just the same percent for all cases, so w_D still can be used to correlate the early-time behavior.

The third interesting case is when $w_D < 1$. When the given pressure drop arrives downhole, the reservoir will be so responsive that it can supply more fluid than the well could for the same pressure drop. This situation produces an oscillation illustrated in Fig. 1A by $w_D = 0.1$. The pressure drop is so large that the reservoir supplies more fluid than is being taken out at the surface. The pressure in the well will be increased, and this increase will propagate back up the well. The interaction between the reservoir and the well produces the oscillation which slowly dies out. For the liquid-filled well in Fig. 1A, the time of the oscillations is a couple of seconds. However, the large oscillations seen in Fig. 1A for $w_D = 0.1$ are not observed in Fig. 1B, where a flashed system was used for the calculations. The oscillations have been damped out by friction effects. The friction term is dependent on the flow velocity squared. Thus, for the same mass flow rate, there will be more dampening in the flashed system than in the unflashed, because the velocity is greater. One can see the influence of the friction factor in Fig. 1B, where one calculation was done with $f = 0$ in the case $w_D = 0.1$. The effect of the friction factor decreases as w_D increases.

A lack of one-to-one slope at early times has been observed in the field. Fig. 2 plots data obtained from a field test of a liquid-filled well at the Raft River geothermal project.[13] The data were taken with a Hewlett-Packard pressure gauge, capable of providing readings every second with a resolution of 0.01 psi (0.07 kPa). The well was flowing and then was shut in. Any error in the initial buildup because of temperature effects on the instrument should not be important as the instrument already had been heated. (The fluid was flowing under a positive head before it was shut in.) When the data were analyzed, the lack of the unit slope was observed but no explanation was given. The signal that the well was shut in takes about 1 to 2 seconds to arrive downhole. The pressure then builds up very quickly and approaches the curve that would exist if the well behaved uniformly. Using the measured properties of the reservoir [$\phi ch = 8.9 \times 10^{-2}$ ft/psi (4×10^{-6} m/Pa), $kh = 49{,}940$ md-ft (1.5×10^{-11} m^3), $\mu = 0.2$ cp (2×10^{-4} Pa·s)], the wellbore storage coefficient is 0.35 and $w_D = 0.2$. For this low value of w_D one should see oscillations in the p_D vs. t_D curve. However, these oscillations are damped out if the flow rate change is less than a step function. For the case plotted in Fig. 2, it probably would be hard to achieve a step-rate change because the typical time needed to close a valve is longer than the required time for a pressure signal to propagate to the bottom of the well. Even without a step-rate change in flow rate, the plot is still not a unit slope, emphasizing even more that the unit slope is only a special case when the reservoir is less responsive than the well.

A plot of the pressure pulse as it propagates into the well and interacts with the reservoir gives more insight into the well/reservoir interaction. Figs. 3A, 3B, and 3C plot the pressure distribution in the well as a function of time for a drawdown test and for different values of w_D. The first two calculations are done with water throughout the well, and the third case is for water that has flashed about 1,640 ft (500 m) down the well.

For the cases in Figs. 3A and 3B, the propagation of the signal is the same until the pulse arrives at the formation/well boundary. Then the pressure distributions in the well will start to differ. The value of kh/μ is greater in Fig. 3A than in 3B, so w_D will be

...ot in Fig. 3A, the changes of pressure with time ... have been plotted in a nondimensional ... Fig. 3A has been split into three successive ... to illustrate the oscillations in the well as a ... of time. Fig. 3B is only one graph because ... change with time quickly becomes ... To illustrate that there is no difference in ... propagation of the pressure pulse, the first ... of Fig. 3A and the graph of Fig. 3B have been ... so that the dimensional units coincide. Once ... arrives at the reservoir, the two cases start ... In Fig. 3A, the reservoir supplies more fluid ... being taken out at the surface, and an increase ... travels up the bore, canceling out part of ... pressure decrease. This pulse produces an ... in pressure that is too large in the well. When ... in pressure arrives at the surface, the ... must decrease again to sustain the flow rate. ... a pressure oscillation in the well that slowly ... out. In Fig. 3B, the reservoir has a relatively low ... of kh/μ. Even when the initial pressure drop ... downhole, the reservoir cannot supply very ... fluid. The pressure must continue to drop in ... well, and dp_w/dt will be a very weak function of ... in the well.

In Fig. 3C, the signal propagation is different ... there is a boundary between the two-phase ... and the liquid. The boundary tends to distort ... signal pressure pulse because most of the pulse ... from the boundary while a small portion ... transmitted. This is how the single-phase region ... be seen as just a connection between the two- ... region and the reservoir. The pressure pulse ... with the liquid interface is essentially the ... with the reservoir boundary except for ... damping. The pulse then oscillates in the two- ... region. The propagation of the signal is ... slow in the two-phase region – about 230 to ... ft/s (70 to 150 m/s).

The sound speed is low in a two-phase region ... of the lower density and high com- ...ility. However, once the pulse reaches the ..., the signal is propagated about 10 times faster ... the compressibility is lower. Because of this ... in propagation speed, the changes in the ... are relatively uniform. For larger values of ... the pressure will drop faster in the liquid region ... the pressure change in the well will become more ... more quickly. For $w_D > 1$ the pressure drop ... be closer to Fig. 3B, even though there is a two- ... region.

The question still is whether w_D can be used as a ...dimensional parameter to describe this in- ...tion when different fluids are used in the well – ... if C_D and w_D are kept the same while the fluid ...ditions in the well and the reservoir properties are ...ged, will the same curve be generated? It might ... thought that changes in the two-phase region ... never be correlated by a term w_D that was ...ed by assuming no abrupt changes in the initial ...sure pulse. However, when the fluid flashes, the ...ing region dominates the effects in the well and ... essentially can ignore the single-phase region. ... two-phase region then acts almost as a single-

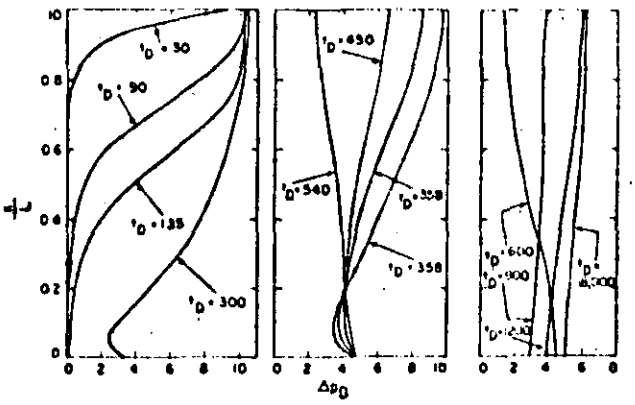

Fig. 3A – Pressure profile in a well as a function of time ($w_D = 0.1$, $C_D = 25$, and fluid is not flashing).

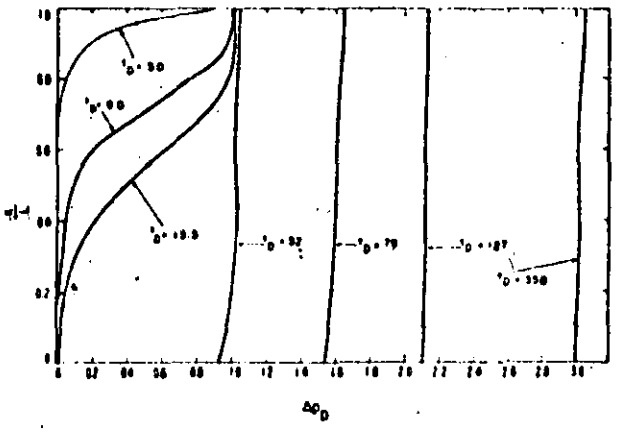

Fig. 3B – Pressure profile in a well as a function of time ($w_D = 1.0$, $C_D = 25$, and fluid is not flashing).

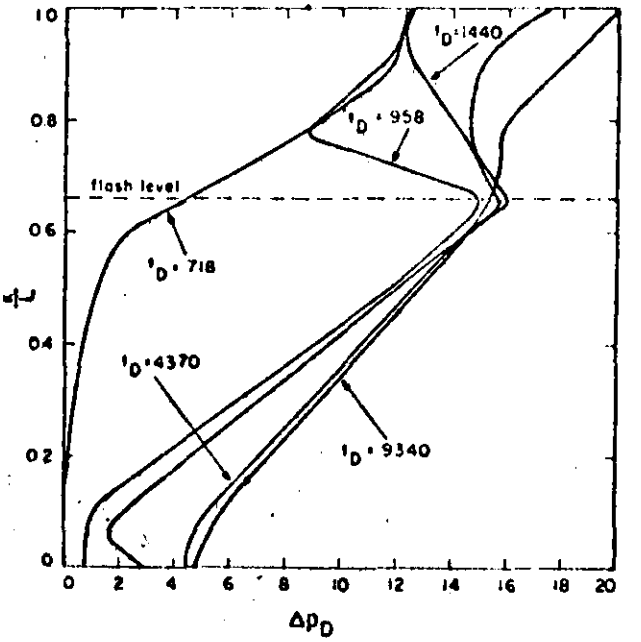

Fig. 3C – Pressure profile in a well as a function of time ($w_D = 0.1$, $C_D = 100$, and fluid is flashing in the bore).

TABLE 2 – DIMENSIONAL VALUES USED FOR CALCULATING DRAWDOWN IN WELLBORE FOR DIFFERENT AVERAGE COMPRESSIBILITIES IN THE BORE

Conditions	kh (m^3)	ϕch (m/Pa)	μ (Pa·s)	$(\partial\rho/\partial p)_t$ ($kg/m^3 \cdot Pa$)
Unflashed	6.4×10^{-13}	8.0×10^{-9}	2×10^{-4}	$7.0 \times 10^{-}$
Unflashed	4.5×10^{-13}	2.3×10^{-8}	9×10^{-5}	$1.4 \times 10^{-}$
Flashed	4.0×10^{-12}	5.0×10^{-7}	9×10^{-5}	$4.0 \times 10^{-}$

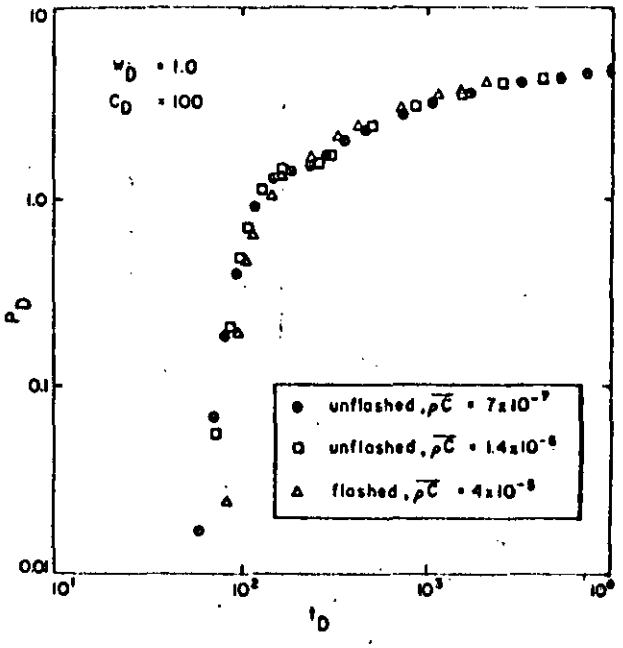

Fig. 4 – Nondimensional plot of sandface pressure vs. time for different average compressibilities in the well but for the same values of C_D and w_D.

phase case with a large compressibility, and the parameter w_D then can be used to correlate the initial behavior.

If the fluid in the well is not varied, but μ, k, and h are changed such that kh/μ remains constant, the generated curve is the same. The calculation depends on kh/μ, and if this is not varied, the interaction of the well and reservoir will not change. (There is a very slight difference in the calculations as h is varied, but the size of the change is too small to be of any use.) A more interesting case is if the fluid properties in the well are varied but the reservoir properties are adjusted to give the same w_D and C_D. Under these circumstances, will the same curve be generated? Fig. 4 shows this comparison when $C_D = 100$ and $w_D = 1.0$. Two calculations are for a liquid-filled well and the third is for a flashed system. The reservoir values used are given in Table 2.

It is a little hard to contrive a case where w_D and C_D will be the same when the average compressibility in the well varies as much as it does between these two cases. Some of the reservoir properties used may be a little extreme. However, one can see that there is excellent agreement between the three different cases. Again, the constant friction factor of 0.04 was used. The other properties of the well are the same as those used for the calculations done for Fig. 1. The agreement is especially good when $w_D > 1$. As w_D decreases, pressure changes in the well become more nonuniform and the assumptions used in deriving w_D become less valid. Oscillations can occur in some cases, and the size of the oscillations depend on the friction factor. Because friction losses are more significant in a flashing system, the p_D vs. the t_D curve for this latter case will start to deviate at early times from the single-phase case that has the same values of w_D and C_D. Oscillations would occur in a single-phase case but would be damped out for the two-phase case. This situation exists when $w_D << 1$. However, from the very rough analysis used to estimate it, w_D can describe the flow for both two- and single-phase flow over a wide range of cases.

Heat Loss Effects

The change in energy of the reservoir fluid while flowing through the wellbore is due both to the heating of the fluid in the bore and to heat loss out of the bore. The effect of this energy loss is to change the fluid head in the well and to increase the time when wellbore storage is important. The heating of the fluid in the bore is important when a well has not been flowing. A geothermal temperature gradient will exist down the bore. When the well starts to flow, the temperature of the fluid in the bore increases and the fluid head in the bore decreases. Because of this decrease, the wellhead pressure increases, although the downhole pressure is decreasing. The downhole pressure itself is not affected significantly by this fluid head because it is the properties of the reservoir that control the flow from the reservoir and not the properties of the fluid in the well. The effect of any energy change is to alter the rate at which the sandface flow rate approaches the surface flow rate – i.e., wellbore storage is increased. The density of the fluid is affected significantly by changes in energy, and the duration of transient energy effects is much longer than transient pressure changes. However, the time when wellbore storage should be over when the flow is not isothermal is not obvious from the plots. The rate of the energy change can be slow enough so that one can obtain a straight line on a plot of p_D vs. $\log(t_D)$ but with just a slightly increased slope resulting in a smaller estimate for kh.

Fig. 5 illustrates the effect of fluid heating in the bore on the transient downhole pressure. Plotted in the figure is the nondimensional downhole pressure vs. the nondimensional time for both an initially

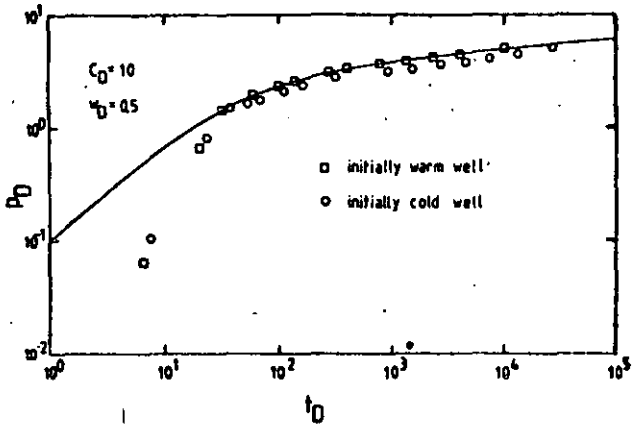

Fig. 5 – Transient sandface pressure for an isothermal well and for a well that initially has a temperature gradient along the bore.

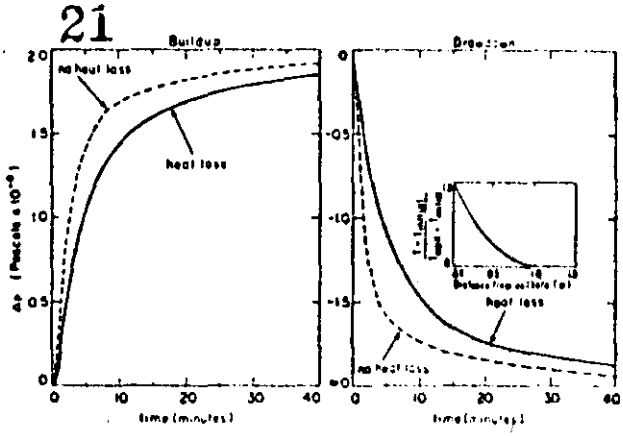

Fig. 6 – Effect of heat loss on a buildup and a drawdown test.

warm well (the flow is isothermal) and an initially cold well [the temperature in the well before flowing is linear from 68°F (20°C) at the wellhead to 392°F (200°C) downhole]. One can see that there is little difference in the initial drawdown for the two cases (w_D still could be used to correlate this early drawdown data), but that at later times the plots start to differ. At much later times, when the flow in the initially cold well becomes isothermal, the plots must coincide again. For the isothermal case, wellbore storage depends only on the changes in density because of pressure changes. When the downhole pressure is not changing significantly with time, the sandface flow rate will be approximately equal to the surface flow rate and wellbore storage will be over. Changes in the energy have a much longer time effect. Wellbore storage will be important until $\partial E/\partial t = 0$ throughout the well. For a well that is initially at the geothermal gradient, a minimum time for $\partial E/\partial t \approx 0$ is the transit time for a fluid particle in the well. For a flow of 800 gal/min (5.05×10^{-2} m^3/s) in a liquid-filled well of 5,905 ft (1800 m) with a radius of 0.295 ft (0.09 m), this transit time is approximately 15 minutes. Any heat loss to the surrounding rock will increase the time until $\partial E/\partial t \approx 0$. The duration of wellbore storage based on pressure changes alone would be only 38 seconds for the cases plotted in Fig. 5.

In most cases when testing a well, the well will be flowed until the change at wellhead steadies out; then flow tests will be started. However, even in this situation the heat loss of the fluid in the bore will change because of the increase or decrease in the fluid transit time in the well. As stated previously, the effect of the heat loss is a slight alteration of the p_D vs. t_D plot. If one ignored it completely and analyzed the downhole data with methods developed in the petroleum literature, the value of kh calculated would be too small. The numerical model of the transient behavior of the fluid in the well has been used to model the flow with heat transfer. The temperature change in the rock surrounding the wellbore was assumed to be radial only and was calculated using

$$\frac{\partial T}{\partial t} = \alpha\left(\frac{\partial^2 T}{\partial r^2} + \frac{1}{r}\frac{\partial T}{\partial r}\right). \quad \ldots\ldots\ldots\ldots\ldots\ldots (16)$$

Heat transfer is especially important in two-phase geothermal wells because of the large temperature changes that occur along the bore. Fig. 6 is a plot of p_{sf} vs. t for a buildup and a subsequent drawdown test. To simulate the heat loss from the well, a temperature gradient from ambient to the reservoir temperature was assumed far from the well and a small temperature buildup was used near the bore. A nondimensional representative temperature profile is given by the insert in Fig. 6. It is assumed that the well has been flowing so that the initial heating of the well has been completed. In the figure, the plots on the left (labeled buildup) show Δp vs. time during buildup with and without heat loss. The calculations had the well flowing 12 hours before the buildup test calculation was begun. The plots on the right (labeled drawdown) show the same for the subsequent drawdown test. The fluid flowed into the well from a simple, homogeneous reservoir with a kh value of 22,272 md-ft (6.7×10^{-12} m^3). The heat transfer coefficient used between the fluid and the wellbore was specified as a function of flow rate and density. For turbulent flow in a pipe, $N_{Nu} \approx 0.023 N_{Re}^{0.8}$ ($N_{Pr} = 1$), and $U = 0.023 \times (\rho v)^{0.8}/\mu^{0.8} D^{0.2}$ (Ref. 14). In the two-phase region, the heat transfer coefficient was averaged between the steam and liqiud. However, the heat transfer is controlled by the properties of the rock and any error in the heat transfer coefficient U will be negligible. The rock properties used for the heat loss calculations were a thermal conductivity of 1.04 BTU/hr-ft-°F (1.8° W/m·°C) and a thermal diffusivity of 1.08×10^{-5} sq ft/s (1×10^{-6} m^2/s).

It can be seen from the figure that the heat transfer causes the pressure to change initially at a slower rate

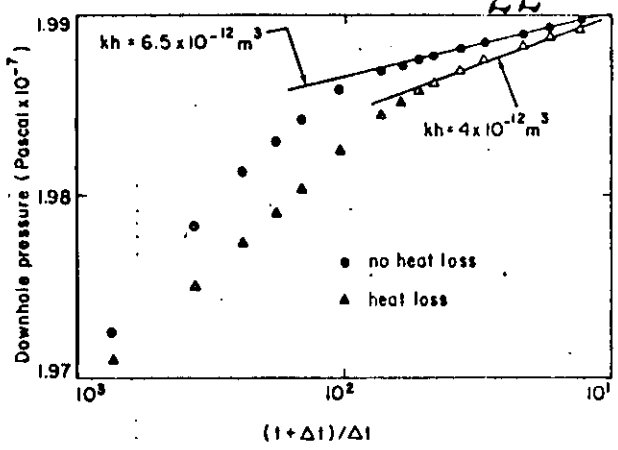

Fig. 7 – Effect of heat loss on a buildup curve shown on a semilog plot of p vs. t.

for both the buildup and the drawdown tests. The deviation between the two cases is smaller initially. It increases and then will decrease when $\partial E/\partial t \approx 0$. During a buildup test, the enthalpy of the exiting fluid decreases because of the increased time that the fluid is in the well. As the enthalpy decreases, the fluid can condense or compress more for the same pressure, so more fluid flows into the well with a smaller pressure rise. In a drawdown, the enthalpy of the fluid increases in time and the density will decrease. For the same pressure, more fluid will exit the well, so the initial drawdown pressure is less. As the enthalpy change steadies out, the drawdown (or buildup) curve with heat loss must approach the curve without heat loss. Enthalpy changes from acceleration or deceleration are not important in the pseudosteady region because these changes already have taken place. It is only the changes from heat loss that affect the slope of the p_D vs. t_D curve in this region.

Fig. 7 shows the error in the kh value if the test is analyzed assuming heat loss is not important. The figure is a plot of p vs. $\log[(t+\Delta t)/\Delta t]$ for the buildup test where $t = 12$ hours. Assuming that $kh = q\mu/4\pi m$, where m is the slope of the straight-line portion, then the kh obtained is about 21,608 md-ft (6.5×10^{-12}m^3) in the buildup. Although not plotted, the analysis gives 22,938 md-ft (6.9×10^{-3}m^3) in the drawdown for no heat loss. The actual value used was 22,272 md-ft (6.7×10^{-12}m^3). However, if the same analysis is used when heat loss is important, different values for kh are obtained – i.e., 13,297 md-ft (4×10^{-12}m^3) in the buildup and 17,619 md-ft (5.3×10^{-12}m^3) in the drawdown. The longer the test is run, the less significant the heat loss is, as shown by the approach of the two slopes toward one another at later times. The straight-line semilog plot shown in Fig. 7 is seen after about 10 minutes when heat loss is zero and after 20 minutes when heat loss is present.

Conclusions

The early-time response of a unit slope when $\log(p_{sf})$ is plotted vs. $\log(t)$ is a special case; actually there are a whole series of curves for each value of C_D, a series that can be defined by the nondimensional time w_D. An expression for w_D was determined that is applicable when the compressibility in the well is relatively constant. Even in two-phase wells, where the compressibility changes by orders of magnitudes, w_D still can be used to correlate the flow because the two-phase region dominates and the compressibility is approximated as constant in the two-phase region. In addition, it has been shown that the temperature changes will increase the time when wellbore storage is important, and if this increase is ignored, one still can obtain a straight line on a plot of p_{sf} vs. $\log(t)$ but the slope of that line will be larger than $q\mu/4\pi kh$.

Nomenclature

A = area of wellbore
c = isentropic compressibility, $(1/\rho)(\partial\rho/\partial p)_s$
c_r = compressibility of reservoir
C = wellbore storage, $\rho cV/\rho_{sf}$
C_D = wellbore storage coefficient, $(\partial\rho/\partial p)_s V/\rho_{sf}2\pi\phi c_R h r_w^2$
C'_D = $(\partial\rho/\partial p)_E V/\rho_{sf}2\pi\phi c_R h r_w^2$
D = diameter of well
E = specific energy
f = friction factor
g = gravity
h = reservoir thickness
i = specific enthalpy
k = permeability
L = depth of wellbore
N_{Nu} = Nusselt number
N_{Pr} = Prandtl number
N_{Re} = Reynolds number
p = pressure
p_D = nondimensional downhole pressure, $2\pi(kh/\mu)(\rho_{sf}/w_s)p_w$
Δp_i = initial pressure drop in well
q = volume flow rate
r_w = radius of wellbore
s = specific entropy
t = time
t_D = nondimensional time $(k/\mu\phi c_R r_w^2)t$
T_r = temperature in rock surrounding the wellbore
T_w = temperature of fluid in wellbore
U = heat transfer coefficient
v = velocity
V = volume
w = mass flow rate
w_D = nondimensional parameter $w_s/(w_{sf})_i$
$(w_{sf})_i$ = initial change in sandface mass flow rate
α = thermal diffusivity
ϕ = porosity
ρ = density
μ = absolute viscosity

Subscripts
i = initial
s = surface
sf = sandface
w = well

Acknowledgment

This work was supported by the Div. of Geothermal Energy, U.S. DOE, under Contract No. W-7405-ENG-48.

References

1. Rivera-R., J. and Ramey, H.J. Jr.: "Application of Two Rate Flow Tests to the Determination of Geothermal Reservoir Parameters," paper SPE 6887 presented at the SPE 52nd Annual Technical Conference and Exhibition, Denver, Oct. 9-12, 1977.
2. Gringarten, A.C.: "Well Testing in Two-Phase Geothermal Wells," paper SPE 7480 presented at the SPE 53rd Annual Technical Conference and Exhibition, Houston, Oct. 1-3, 1978.
3. Kihara, D., Chen, B., Yuen, P., and Takahashi, P.: "Summary of Results of HGP-A Well Testing," *Proc.*, Third Workshop, Geothermal Reservoir Engineering, Stanford U., Stanford, CA (1977).
4. van Everdingen, A.F. and Hurst, W.: "The Application of the Laplace Transformation to Flow Problems," *Trans.*, AIME (1949) 186, 305-324.
5. Earlougher, R.C. Jr.: *Advances in Well Test Analysis*, Monograph Series, Society of Petroleum Engineers, Dallas (1977) 5.
6. Agarwal, R.G., Al-Hussainy, R., and Ramey, H.J. Jr.: "An Investigation of Wellbore Storage and Skin Effect in Unsteady Liquid Flow: I. Analytical Treatment," *Soc. Pet. Eng. J.* (Sept. 1970) 279-290; *Trans.*, AIME, 249.
7. Wattenbarger, R.A. and Ramey, H.J. Jr.: "An Investigation of Wellbore Storage and Skin Effect in Unsteady Liquid Flow: II. Finite Difference Treatment," *Soc. Pet. Eng. J.* (Sept. 1970) 291-297; *Trans.*, AIME, 249.
8. Ramey, H.J. Jr.: "Short-Time Well Test Data Interpretation in the Presence of Skin Effect and Wellbore Storage," *J. Pet. Tech.* (Jan. 1970) 97-104; *Trans.*, AIME, 249.
9. Nathenson, M.: "Flashing Flow in Hot-Water Geothermal Wells," *J. Research*, USGS (1974) 2, No. 6, 743-751.
10. Gould, T.L.: "Vertical Two-Phase Steam-Water Flow in Geothermal Wells," *J. Pet. Tech.* (Aug. 1974) 26, 833-842.
11. Sugiura, T. and Farouq Ali, S.M.: "A Comprehensive Wellbore Steam-Water Flow Model for Steam Injection and Geothermal Applications," paper SPE 7966 presented at the SPE California Regional Meeting, Ventura, April 18-20, 1979.
12. Garg, S.K. and Pritchett, J.W.: "Two Phase Flow in Geopressured Geothermal Wells," *Energy Conversion* (1976) 18, 45-51.
13. Narasimhan, T.N. and Witherspoon, P.A.: "Reservoir Evaluation Tests on RRGE 1 and RRGE 2, Raft River Geothermal Project, Idaho," Report No. LBL-5958, Lawrence Berkeley Laboratory, Berkeley, CA (1977).
14. Holman, J.P.: *Heat Transfer*, McGraw-Hill Book Co. Inc., New York City (1977) 203-207.
15. Harlow, F.H. and Welch, J.E.: "Numerical Calculation of Time-Dependent Viscous Incompressible Flow," *Phys. Fluids* (1965) 8, 2182.

APPENDIX

A numerical model of transient two-phase flow was used to study wellbore flow. A brief outline of the model and its limiting assumptions is given here.

Flow in the well is described by equations for continuity, momentum, and energy (Eqs. 12 through 14). An equation of state also is needed to relate the state variables p, e, and ρ:

$$d\rho = \frac{1}{\rho}\left(\frac{\partial \rho}{\partial E}\right)_p (\rho dE) + \left(\frac{\partial \rho}{\partial p}\right)_E dp. \quad \ldots\ldots (A\text{-}1)$$

Equilibrium was assumed, so the equation of state was based on the thermodynamic steam/water tables. The friction losses have been written as a friction factor f times $\frac{1}{2}(\rho v^2/r_w)$. For these calculations, the slip between the phases was assumed to be zero and the friction factor was kept constant. Although both slip and friction effects can be important and should be included accurately, they will not alter the physical phenomena being discussed in this paper.

The method of the numerical model is to combine all four equations (Eqs. 12 through 14 and A-1) to obtain an expression for the new pressure. The pressure is solved implicitly. Once the new pressure is known, the value of ρdE is obtained from Eq. 14, and the density can be evaluated using Eq. A-1. Given the new density, the velocity is evaluated using the continuity equation, and the energy is obtained from knowing ρ and ρdE. The state variables are defined at node points, while the velocity is calculated at half-node points. The method used is similar to the pressure method developed for incompressible fluids by Harlow and Welch,[15] except that compressibility has been included.

The finite difference of the continuity equation is

$$\frac{\rho_j^{\ell+1} - \rho_j^{\ell}}{\Delta t} = -\frac{(\rho v)_{j+\frac{1}{2}}^{\ell+1} - (\rho v)_{j-\frac{1}{2}}^{\ell+1}}{\Delta t}, \quad \ldots\ldots (A\text{-}2)$$

where j denotes the node points and ℓ denotes the time level. The equation is written in an implicit fashion to eliminate time-step restrictions. The expression for $(\rho v)^{\ell+1}$ can be obtained from the momentum equation. The finite difference form of the momentum equation is

$$\frac{(\rho v)_{j+\frac{1}{2}}^{\ell+1} - (\rho v)_{j+\frac{1}{2}}^{\ell}}{\Delta t} = -\frac{(\rho v^2)_{j+\frac{1}{2}}^{\ell} - (\rho v^2)_{j-\frac{1}{2}}^{\ell}}{\Delta x}$$

$$-\rho_{j+\frac{1}{2}} g - f\left(\frac{\rho v_j^2}{4 r_w}\right)^{\ell}. \quad \ldots\ldots (A\text{-}3)$$

The pressure term is evaulated implicitly to reduce the time restriction imposed by the small compressibility of the fluid, while the advection effects are treated explicitly. If the pressure term were evaluated explicitly, the time restriction would be limited by the propagation of the pressure signal over the finite space difference, approximately $\Delta t < \Delta x/(\partial p/\partial \rho)_s^{\frac{1}{2}}$ or $\Delta t < \Delta x \div 3{,}937$ ft/s (1200 m/s) for a liquid. However, the restrictions on the advection are only the order of $\Delta x/v$ where v is the fluid velocity.

The energy equation is finite-differenced as

$$\rho_j\left(\frac{E_j^{\ell+1} - E_j^{\ell}}{\Delta t}\right) = -p_j^{\ell+1}\frac{v_{j+\frac{1}{2}}^{\ell} - v_{j-\frac{1}{2}}^{\ell}}{\Delta x}$$

$$+2U\frac{T_r - T_w}{r_w} - \frac{(\rho v E)_j^{\ell} - (\rho v E)_{j-1}^{\ell}}{\Delta x}. \quad (A\text{-}4)$$

Upwind differencing is used for the advection form.

The expression for flow advection must be altered when the flow is not in the positive direction. The method of solution is to rewrite the density in terms of E and p:

$$\Delta\rho = \frac{1}{\rho}\left(\frac{\partial\rho}{\partial E}\right)(\rho\Delta E) + \left(\frac{\partial\rho}{\partial p}\right)\Delta p. \quad \ldots\ldots\ldots (A\text{-}5)$$

to obtain $(\rho\Delta E)$ from Eq. A-4 and to use Eq. A-5 in the continuity of Eq. A-1. Eqs. A-1 and A-2 then are combined and an expression for the unknown pressure p is determined. The resultant equation is

$$\begin{aligned}
&-(2+r)p_j^{\ell+1} + p_{j+1}^{\ell+1} + p^{j+1} \\
&= -rp_j^{\ell} + \frac{\Delta x}{\Delta t}\left(\rho v_{j+\frac{1}{2}} - \rho v_{j-\frac{1}{2}}\right)^{\ell} \\
&\quad -\left(\rho_{j+\frac{1}{2}} - \rho_{j-\frac{1}{2}}\right)^{\ell} g\Delta x - \left(\rho_{j+\frac{1}{2}} v_{j+\frac{1}{2}}^2\right. \\
&\quad \left. -2\rho_{j-\frac{1}{2}} v_{j-\frac{1}{2}}^2 + \rho_{j-3/2} v_{j-3/2}^2\right)^{\ell} \\
&\quad -f\left(\rho_{j+\frac{1}{2}} v_{j+\frac{1}{2}}^2 - \rho_{j-\frac{1}{2}} v_{j-\frac{1}{2}}^2\right)^{\ell} \frac{\Delta x}{4r_w} \\
&\quad -\left(\frac{\Delta x}{\Delta t}\right)^2\left(\frac{1}{\rho}\frac{\partial\rho}{\partial E}\right)\rho_j\left(E_j^{\ell+1} - E_j^{\ell}\right),
\end{aligned}$$

where

$$r = \left(\frac{\Delta x}{\Delta t}\right)^2\left(\frac{\Delta\rho}{\partial p}\right)_E.$$

The expression for $E_j^{\ell+1} - E_j^{\ell}$ is obtained from Eq. A-4.

The pressure in the reservoir and the temperature change around the bore are solved using a finite difference of the radial diffusion equation. A grid was generated by using a logarithmic transformation. The pressure was kept constant 4,921 ft (1500 m) from the well while the temperature was maintained at the initial geothermal gradient 19.6 ft (6 m) from the well. The finite difference of the radial diffusion equation used was

$$\frac{p_j^{\ell+1} - p_j^{\ell}}{\Delta t} = \frac{k}{\mu\phi c}\,\frac{2}{(r_{j+1} - r_{j-1})}$$
$$\cdot\left[r_{j+\frac{1}{2}}\left(\frac{p_{j+1} - p_j}{r_{j+1} - r_j}\right) - r_{j-\frac{1}{2}}\left(\frac{p_j - p_{j-1}}{r_j - r_{j-1}}\right)\right].$$

SI Metric Conversion Factors

cp	×	1.0* E−03	=	Pa·s
cu ft	×	2.831 685 E−02	=	m^3
°F		(F−32)/1.8	=	C
ft	×	3.048* E−01	=	m
lbm	×	4.535 924 E−01	=	kg
psi	×	6.894 757 E+00	=	kPa

*Conversion factor is exact.

SPEJ

Original manuscript received in Society of Petroleum Engineers office July 2, 1979. Paper accepted for publication April 4, 1980. Revised manuscript received Sept. 14, 1980. Paper (SPE 8203) first presented at the SPE 54th Annual Technical Conference and Exhibition, held in Las Vegas, Sept. 23-26, 1979.

SPE
Society of Petroleum Engineers of AIME

SPE 8231

A PARALLELEPIPED MODEL TO ANALIZE THE PRESSURE BEHAVIOR OF GEOTHERMAL STEAM WELLS PENETRATING VERTICAL FRACTURES

by Heber Cinco-Ley, Member SPE-AIME, W.E. Brigham, M. Economides, F.G. Miller, and H.J. Ramey Jr., Stanford Univ.; A. Barelli and G. Manetti, ENEL

ABSTRACT

Reservoir geometry is often the basis for development of models used to analyze field transient pressure data. The presence of a deep horizontal steam-water interface or boiling front first gave rise to the idea of a constant pressure boundary. Faults suggest vertical no-flow boundaries, and impermeable rocks overlying the steam zone indicate a no-flow cap.

In the past, parallelepiped models have been used to analyze the results of predesigned buildup and well interference tests. The model described herein is of more general use, and can be used to analyze long-term pressure-production well data. In this study, it is applied to analyze pressure data of a drawdown test for a geothermal reservoir.

As in earlier models, the boiling front is assumed to be a constant fluid-pressure boundary, and the sides --as well as the top--are assumed to be impermeable boundaries. Equations of reservoir pressure behavior are derived using Green's functions and source functions. Graphs describing dimensionless pressure as a function of time and various reservoir parameters are provided. Partially penetrating fractures common to many geothermal well systems are considered in the development of the model.

INTRODUCTION

Many geothermal areas are characterized by reservoirs whose dimensions are controlled by sealing faults or low permeability boundaries. Some of these reservoirs produce steam diluted with small quantities of noncondensable gases. There is often evidence of boiling water at a considerable distance from the producing horizon (presumably lying below the steam cap). In addition, the transient pressure behavior of these wells sometimes indicates they intersect large, high conductivity fractures. These are natural fractures; no hydraulic fracturing has been done in any of these wells.

This general description leads naturally to a model in the shape of a parallelepiped with closed boundaries on five sides and a constant pressure boundary on the bottom. The fracture intersecting the well can be simulated as a rectangular-shaped source or sink. Such a system was described by Atkinson et al.[1] for a limited set of geometric conditions which approximated the producing system in the Travale area, in Italy. Because of the success of this approach, personnel at Stanford University and at ENEL, in Pisa, have developed general programs for generating long-term pressure-production forecasts for a variety of parallelepiped conditions and well-fracture geometries. This approach appears to be generally useful, for many geothermal systems worldwide will have fault-controlled geometry of the type described here.

References and illustrations at end of paper

The purpose of this work is to determine which unique characteristics of such systems can be identified. This, in turn, will lead to greater confidence in predictions of the long-range producing characteristics of these systems.

DESCRIPTION OF THE MODEL

Let us consider a well intersected by a vertical fracture in a parallelepiped reservoir, as shown in Fig. 1. The system is bounded laterally by vertical impermeable planes; the top of the reservoir is a horizontal no-flow boundary, and underlying the reservoir there is a constant pressure plane.

The general assumptions for this model are as follows:

1) The well produces at a constant flowrate in an anisotropic, homogeneous reservoir of constant properties (k and ϕ are independent of pressure and temperature).

2) The reservoir contains a slightly compressible fluid of constant viscosity, μ, and compressibility, c. Although this assumption is not valid, there is considerable evidence that it is a good approximation for gaseous systems when the $m(p)$ function is used.

3) There are small pressure gradients and negligible gravity effects in the reservoir.

4) Well fluid production is via a vertical fracture which partially penetrates the reservoir. The top of the fracture can be located at any elevation and the fracture can extend to any depth.

5) The initial pressure, p_i, is the same throughout the reservoir.

Although the fracture can be located anywhere in the reservoir and the reservoir dimensions can be chosen arbitrarily (the Barelli and Manetti model), the only cases studied in this paper are those in which the fracture is located in the center of a parallelepiped reservoir of square horizontal cross-section, with the fracture oriented parallel to two of the vertical boundaries (Fig. 2).

As shown by Gringarten and Ramey, the pressure drop in a reservoir with any boundary conditions can be expressed as:

$$\Delta p = \frac{1}{\phi c_t} \int_0^t S(x,y,z,\tau)\, d\tau \qquad (1)$$

where $S(x,y,z,\ )$ represents the source function for the particular reservoir-well system. The term S depends on both the geometry and the boundary conditions of the system. The appendix shows the derivation of the source function for the parallelepiped model considered in this study.

The dimensionless pressure drop at any point in the reservoir can be given by either of the two following equations:

$$p_D(x_D,y_D,x_D,x_{De},y_{De},h_D,h_{fD},z_{fD},t_{Dxf})$$

$$= \frac{\sqrt{\pi}}{8} \frac{h_D}{h_{fD}} \int_o^{t_{Dxf}} \frac{1}{\sqrt{\pi}} \cdot \left\{ \sum_{n=-\infty}^{\infty} e^{-\frac{(y_D-2ny_{De})^2}{4\tau}} \right\} \left\{ \sum_{n=-\infty}^{\infty} \left[\text{erf} \frac{x_D-2nx_{De}+1}{2\sqrt{\tau}} + \text{erf} \frac{x_{fD}-2nx_{De}-1}{2\sqrt{\tau}} \right] \right\}$$

$$\left\{ \sum_{n=-\infty}^{\infty} \left[- \text{erf} \frac{z_D + \frac{h_{fD}}{2} + z_{fD} + 4nh_D}{2\sqrt{\tau}} - \text{erf} \frac{-z_D + \frac{h_{fD}}{2} - z_{fD} - 4nh_D}{2\sqrt{\tau}} + \text{erf} \frac{z_D - \frac{h_{fD}}{2} - z_{fD} + 4nh_D}{2\sqrt{\tau}} \right.\right.$$

$$+ \text{erf} \frac{\frac{h_{fD}}{2} - z_D + z_{fD} - 4nh_D}{2\sqrt{\tau}} + \text{erf} \frac{z_D + \frac{h_{fD}}{2} + z_{fD} + 4nh_D - 2h_D}{2\sqrt{\tau}}$$

$$+ \text{erf} \frac{-t_D + \frac{hf_D}{2} - z_{fD} - 4nh_D + 2h_D}{2\sqrt{\tau}} - \text{erf} \frac{z_D + \frac{hf_D}{2} - 2h_D - z_{fD} + 4nh_D}{2\sqrt{\tau}}$$

$$\left.\left. - \text{erf} \frac{\frac{hf_D}{2} - z_D + 2h_D + z_{fD} - 4nh_D}{2\sqrt{\tau}} \right] \right\} d\tau \qquad (2)$$

Or, alternatively:

$$p_D(x_D,y_D,z_D,x_{De},y_{De},h_D,h_{fD},z_{fD},t_D) = \frac{4h_D}{h_{fD}y_{De}x_{De}} \cdot \int_o^{t_{Dxf}} \left[1 + 2 \sum_{n+1}^{\infty} e^{-\frac{n^2\pi^2\tau}{y_{De}^2}} \cos \frac{n\pi y_D}{y_{De}} \right] \left[1 + \frac{2x_{De}}{\pi} \sum_{n=1}^{\infty} e^{-\frac{n^2\pi^2\tau}{x_{De}^2}} \cos \frac{n\pi x_D}{x_{De}} \sin \frac{n\pi}{x_{De}} \right]$$

$$\left[\sum_{n=1}^{\infty} \frac{e^{-\frac{(2n-1)^2\pi^2\tau}{4h_D^2}}}{(2n-1)} \sin \frac{(2n-1)\pi h_{fD}}{4h_D} \right] \sin \frac{(2n-1)\pi z_{fD}}{2h_D} \sin \frac{(2n-1)\pi z_D}{2h_D} \, d\tau \qquad (3)$$

where the dimensionless terms in the equations are defined as follows:

$$p_D = 1.291\times10^{-2}\ \frac{M\sqrt{k_x k_y}\ h\ (p_i^2 - p_{wf}^2)}{ZTq\mu}$$

$$t_{Dxf} = 0.3604\ \frac{k_x t}{\phi\mu c_t x_f^2}$$

$$x_D = \frac{x}{x_f}\ ;\ y_D = \frac{y}{x_f}\sqrt{\frac{k_x}{k_y}}\ ,\ x_D = \frac{z}{x_f}\sqrt{\frac{k_x}{k_y}}$$

$$x_{De} = \frac{x_e}{x_f}\ ;\ y_{De} = \frac{y_e}{x_f}\sqrt{\frac{k_x}{k_y}}\ ;\ h_D = \frac{h}{x_f}\sqrt{\frac{k_x}{k_z}}$$

$$h_{fD} = \frac{h_f}{x_f}\sqrt{\frac{k_x}{k_z}} \text{ and } z_{fD} = \frac{z_f}{x_f}\sqrt{\frac{k_x}{k_z}} \qquad (4)$$

Although Eqs. 2 and 3 are equivalent, Eq. 2 is the better for calculations of dimensionless pressure drop at small values of time, and Eq. 3 better for large values of time. These solutions obtained are valid for both anisotropic and isotropic reservoirs according to Eq. 4.

Wellbore Pressure Behavior

A computer program was written to calculate the pressure drop at any point in the system, at any dimensionless time, $t_{D_{xf}}$. Several runs were made by considering different values of dimensionless formation thickness, h_D, fracture penetration ratio, x_e/x_f, and dimensionless fracture height, h_f/x_f. The dimensionless formation thickness varies from 2 to 20, the fracture penetration goes from 2 to 10, and the fracture height is assumed to be unity.

Figures 3 through 6 show a log-log graph of p_D/h_D versus $t_{D_{xf}}$ for the cases mentioned above. The wellbore pressure was calculated at the locations recommended by Cinco et al.[4] for the case of a partially penetrating well (i.e., $y_D = 0$, $x_D = 0.732$, and $z_D = z_{f_D} - 0.232$).

All cases exhibit a unique cone-half straight line for small values of time. This behavior is caused by the linear flow behavior in the vicinity of the fracture. The equation for wellbore pressure during this early time period can be derived from Eq. 2 by using the short-time approximation of the error functions.

$$p_D(t_{D_{xf}}) = \sqrt{\pi t_{D_{xf}}}\ h_D$$

for $t_{D_{xf}} \leq 0.016$*

*According to Gringarten et al.[4]

At large values of time, the wellbore pressure drop stabilizes indicating steady-state flow in the system. Figure 7 presents the stabilized value of pressure drop as a function of both fracture penetration x_e/x_f and dimensionless formation thickness.

Figures 3 through 5 show that over a large region of the graph the curves for pressure response at a fractured well in a parallelepiped reservoir are similar in slope to the infinite conductivity vertical fracture solution for an infinite reservoir.

Figure 8 is a graph of dimensionless wellbore pressure versus the logarithm of dimensionless time. This graph clearly indicates that these systems do not exhibit the characteristic semilog straight line portion of the pressure versus log time relationship arising from conventional methods of analysis for radial flow.

The fracture penetration ratio has a strong effect on the transient pressure behavior in a parallelepiped reservoir, as shown by Fig. 9. A higher penetration produces a higher pressure drop, because of a smaller porous volume in the system.

Figure 3 shows that when the fracture penetration ratio is high, type-curve analysis methods can be applied to determine the dimensionless formation thickness and the characteristics of the formation and fracture. However, in a case for a low-fracture penetration ratio (Fig. 6), type-curve analysis may not give a unique answer for dimensionless formation thickness because the curves for different cases are too close together to give a good match.

The effect of dimensionless formation thickness on pressure behavior is shown in Figs. 3 through 6. Pressure response for a thick formation is high because the effect of the constant pressure boundary occurs late in dimensionless time.

As mentioned, a large portion of the curves for different cases are similar in shape during early and intermediate time, to the infinite conductivity vertical fracture solution. However, these solutions will provide completely different results from type-curve analysis. When analyzing pressure data for a fractured well in a parallelepiped reservoir, the infinite conductivity solution gives large estimates of permeability as well as low estimates for fracture length.

Although in this work only drawdown solutions are presented, they can be extended to produce both buildup and multiflow rate solutions by using the principle of superposition.

EXAMPLE OF APPLICATION

Flowing wellhead pressure was measured in a dry-steam well during a period of two years. The flowing bottomhole pressure and additional well and reservoir information are given in Table 1.

Figure shows a log-log graph of pressure squared difference versus flow time. The pressure data on this figure show the characteristic features of the behavior of a fractured well in a parallelepiped reservoir: early data approach a one-half slope straight line, and the late portion of the

pressure data seems to reach a stabilized value. Figure 11 also shows the application of the type-curve matching technique for this case. The following match points are obtained:

$$(p_i^2-p_{wf}^2) = 10^2 \quad [K_g/cm^2]^2 \; ; \; p_D/h_D = 0.3$$

$$t = 1 \text{ day} \; ; \; t_{Dx_f} = 0.26$$

and

$$h_D = 10$$

From Table 1 and the definition of dimensionless pressure drop:

$$p_D = \left(\frac{p_D}{h_D}\right) \cdot h_D = 0.3 \times 10 = 3$$

$$.3 = \frac{1.291\times10^{-2}(18)(k_xk_y)^{1/2}\; x_f\sqrt{\frac{k_z}{k_x}}\; (10^2)}{(0.85)(553)(205)(0.019)}$$

$$\therefore (k_zk_y)^{1/2}x_f = 23.63 \text{ darcy-meters}$$

From the definition of dimensionless time:

$$0.26 = \frac{0.3604(k_x)(1)\times24}{(0.16)(0.019)(0.01)x_f^2}$$

$$\therefore \frac{k_x}{x_f^2} = 9.138\times10^{-7} \text{ darcy/m}^2$$

Evidently,

$$k_xk_yk_z = [(k_zk_y)^{1/2}x_f]^2 \left(\frac{k_x}{x_f^2}\right) = (23.63)^2\,(9.138\times10^{-7})$$

$$= 5.1\times10^{-4} \text{ darcy}^3$$

$$\sqrt{k_xk_yk_z} = 0.0799 \text{ darcy}$$

If $k_x = k_y = k_z = k$,

$$k = 0.0799 \text{ darcy}$$

$$x_f = 295 \text{ meters}$$

and

$$h = 2950 \text{ meters}$$

CONCLUSIONS

From the analysis of the results obtained in this work, the following conclusions may be drawn:

1) The pressure behavior of a fractured well in a parallelepiped reservoir exhibits several flow periods.

2) Initially, a linear flow dominates the behavior of the system.

3) At later times, side boundary effects are felt through an increasing rate of pressure decline.

4) At large values of time, steady-state flow is established; as a consequency, the wellbore pressure remains constant.

5) Type-curve analysis can be applied to determine the constant pressure boundary depth whenever the fracture penetration is high.

6) Although the early and intermediate time behavior of infinite conductivity vertical fracture solutions is similar to the behavior of a fractured well in a parallelepiped reservoir, results from type-curve analysis for both cases are different.

7) The parallelepiped model seems to be adequate for dry steam reservoirs with a water steam surface.

NOMENCLATURE

c = isothermal compressibility, cm^2/Kg

h = formation thickness, m

h_f = fracture height, m

k = permeability, darcies

M = molecular weight, gr/gr mole

p = pressure, Kg/cm^2

p_i = initial pressure, Kg/cm^2

p_{wf} = flowing bottomhole pressure, Kg/cm^2

q = mass flowrate, ton/hr

S = source function

t = time, hrs

T = reservoir temperature, °K

x = distance in x-direction, m

x_f = half-fracture length, m

x_e = boundary location in x-direction, m

y = distance in y-direction, m

y_e = boundary location in y-direction, m

z = distance in z-direction, m

z_f = elevation of midpoint of fracture, m

Z_i = gas deviation factor, dimensionless

μ = viscosity, cp

ϕ = porosity, fraction

Subscripts

D = dimensionless

e = external

f = fracture

i = initial

w = wellbore

t = total

Special Functions

$$\mathrm{erf}(x) = \frac{2}{\sqrt{\pi}} \int_0^x e^{-\eta^2} d\eta$$

ACKNOWLEDGEMENT

This work was developed under Contract ENEL 1673600 through the Department of Energy.

REFERENCES

1. Atkinson, P., Barelli, A., Brigham, W.E., Celati, R., Manetti, G., Miller, F.G., Neri, G., and Ramey, H.J., Jr.: "Well Testing in Travale-Radicondoli Field," Proc., ENEL-ERDA Workshop, Larderello, Italy, Sept. 12-16, 1977, 1-75.

2. Al-Hussainy, R., Ramey, H.J., Jr., and Crawford, P.B.: "The Flow of Real Gases Through Porous Media," J. Pet. Tech. (May 1966), 624-636; Trans., AIME ( )___, 232.

3. Gringarten, A.C., and Ramey, H.J., Jr.: "The Use of Source and Green's Functions in Solving Unsteady Flow Problems in Reservoirs," Soc. Pet. Eng. J. (Oct. 1973), 285-296; Trans., AIME (255.

4. Cinco-Ley, H., Ramey, H.J., Jr., and Miller, F.G.: "Unsteady-State Pressure Distribution Created by a Well with an Inclined Fracture," Paper SPE 5591, presented at the 50th Annual Fall Meeting, SPE of AIME, Dallas, Texas, Sept. 28-Oct. 1, 1975.

5. Gringarten, A.C., Ramey, H.J., Jr., and Raghavan, R.: "Pressure Analysis for Fractured Wells," Paper SPE 4051, presented at the 47th Annual Fall Meeting, SPE of AIME, San Antonio, Texas, Oct. 8-11, 1972.

TABLE 1

DRAWDOWN TEST DATA

Flowrate, q, Ton/hr	205	Porosity, ϕ, fraction	0.16
Viscosity, μ, cp	0.019	Reservoir temperature, T, °K	553
Gas deviation factor, Z	0.85	Molecular weight, M, lb/lb-mole	18
Compressibility, ct, $(Kg/cm^2)^{-1}$	0.01	Initial pressure, p_i, Kg/cm^2	55

t (days)	$(p_i^2-p_{wf}^2)(Kg/cm^2)^2$	t (days)	$(p_i^2-p_{wf}^2)(Kg/cm^2)^2$
1	188	90	788
2	228	100	828
3	253	120	871
4	271	140	927
5	287	160	982
6	305	180	1032
7	318	200	1066
8	330	240	1134
9	343	280	1174
10	352	320	1205
15	401	360	1233
20	441	400	1254
25	478	440	1263
30	503	480	1279
35	534	520	1288
40	562	560	1297
45	587	600	1304
50	618	640	1307
60	664	680	1310
80	747	720	1310

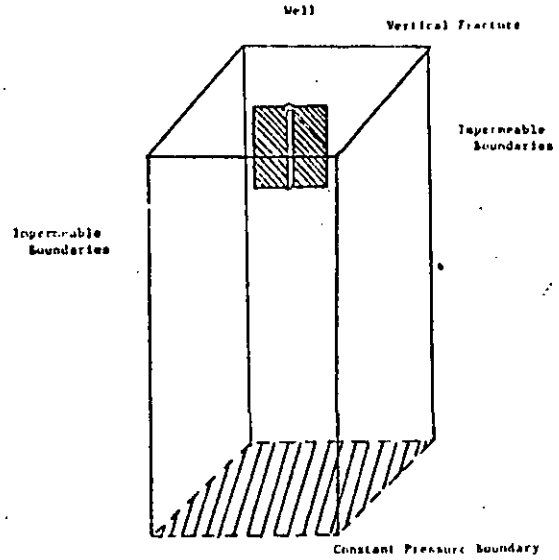

Fig. 1 - Fractured well in a parallelepiped reservoir.

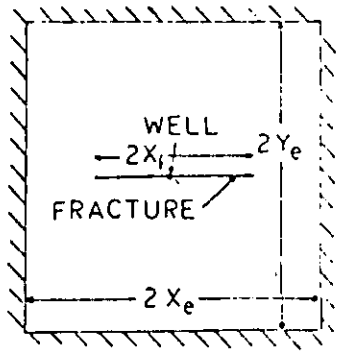

Fig. 2 - Fractured well in the center of a square parallelelpiped reservoir.

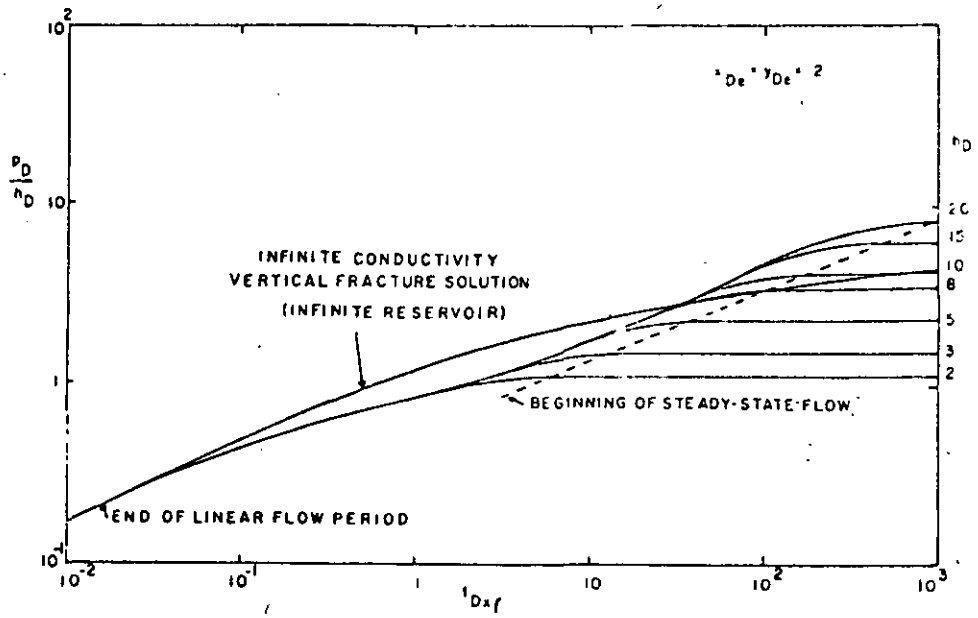

Fig. 3 - Log p_D/h_D vs log t_{Dx_f} for a fractured well in a parallelepiped reservoir ($x_e/x_f = 2$).

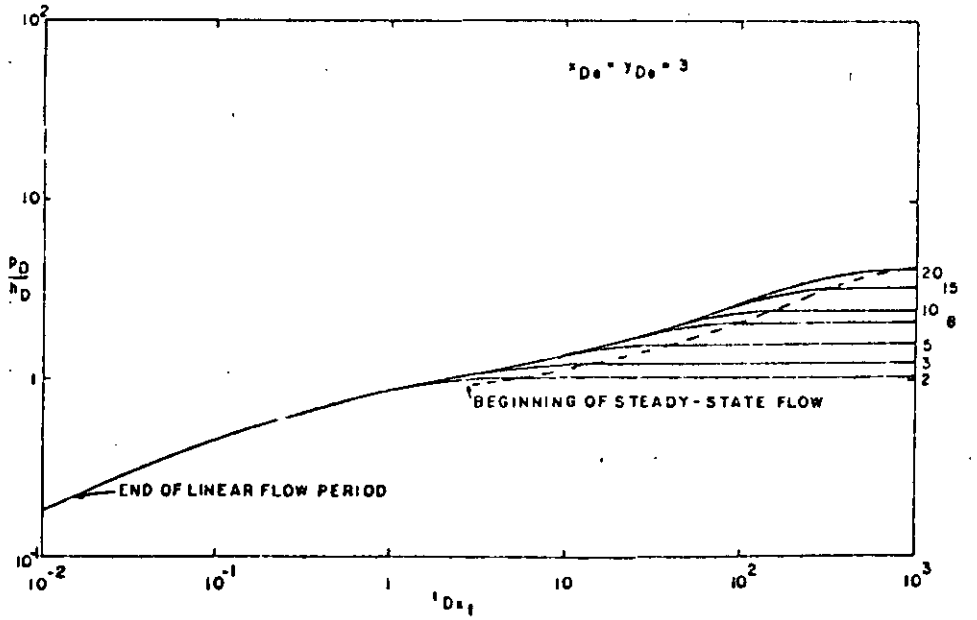

Fig. 4 - Log p_D/h_D vs log t_{Dx_f} for a fractured well in a parallelepiped reservoir ($x_e/x_f = 3$).

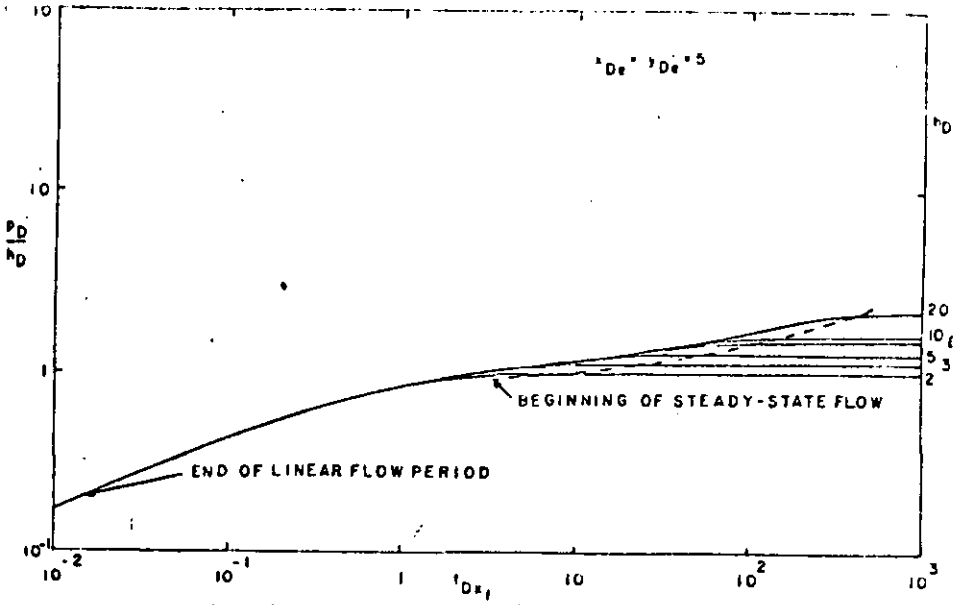

Fig. 5 – Log p_D/h_D vs log t_{Dx_f} for a fractured well in a parallelepiped reservoir (x_e/x_f = 5).

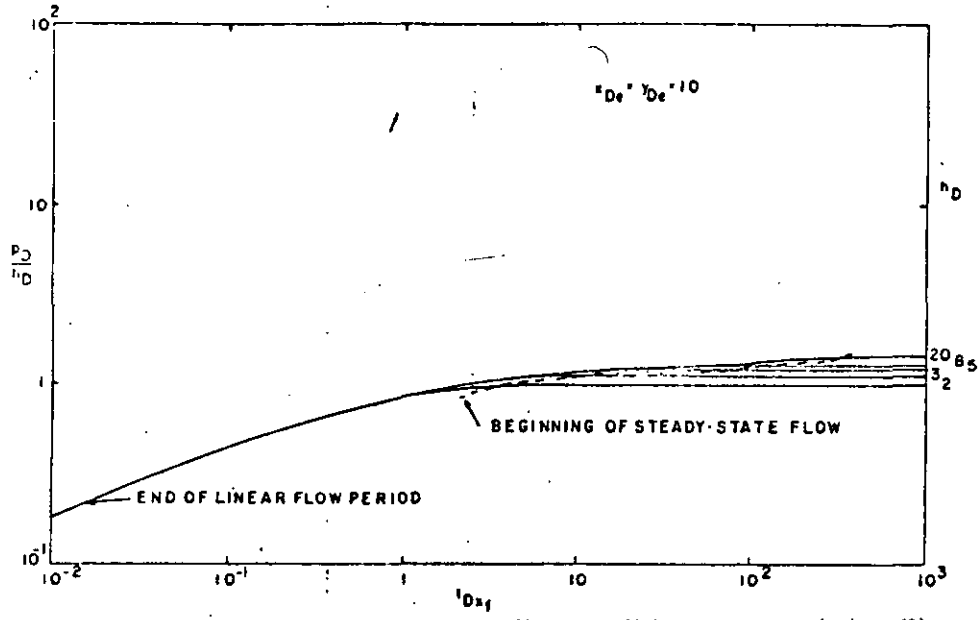

Fig. 6 – Log p_D/h_D vs log t_{Dx_f} for a fractured well in a parallelepiped reservoir (x_e/x_f = 10).

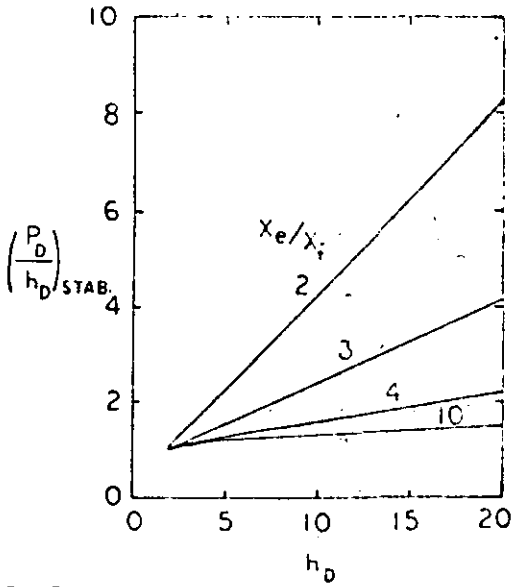

Fig. 7 – Stabilized value of (p_D/h_D) vs h_D as a function of x_e/x_f.

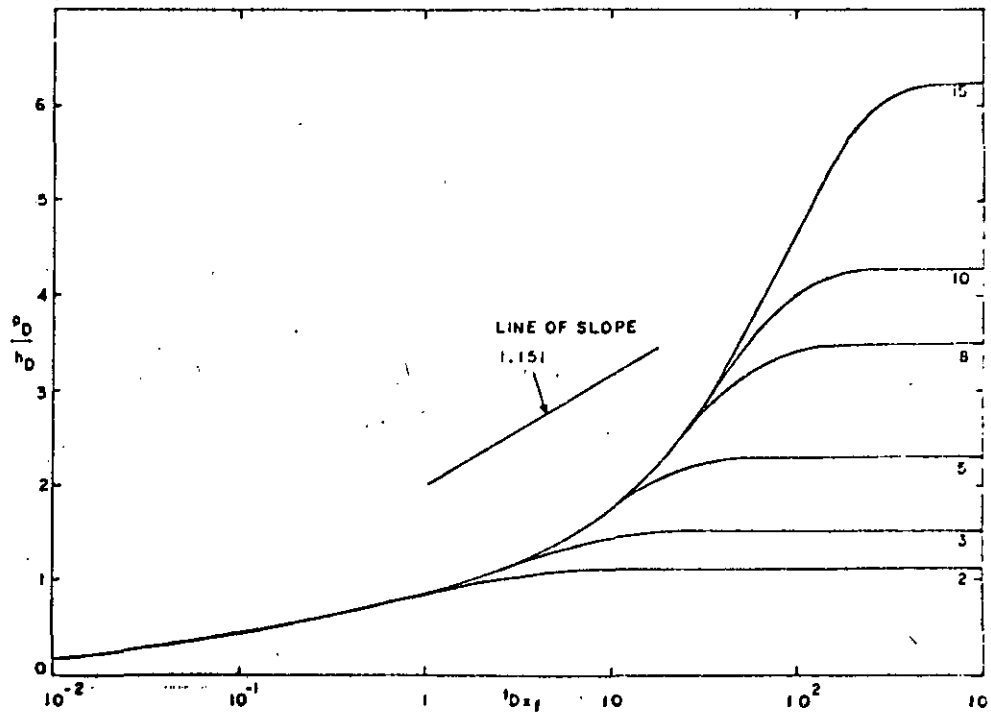

Fig. 8 – p_D/h_D vs log t_{Dx_f} for a fractured well in a parallelepiped reservoir (x_e/x_f = 2).

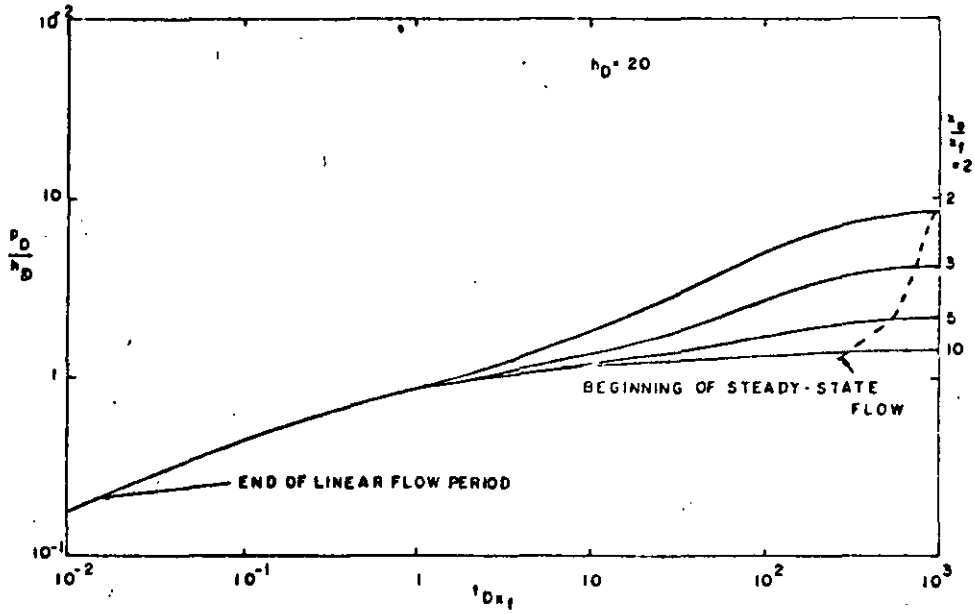

Fig. 9 - Log p_D/h_D vs t_{Dx_f} for a fractured well in a parallelepiped reservoir (h_D = 20).

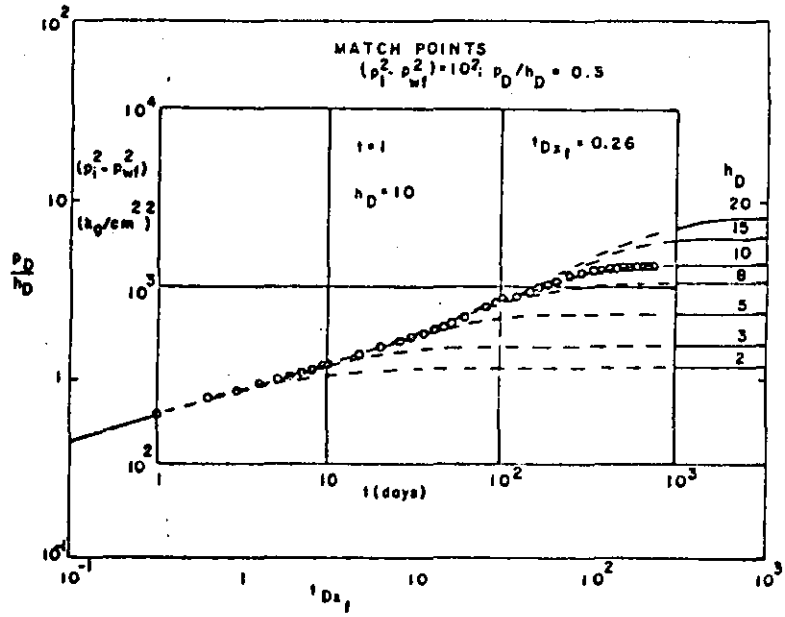

Fig. 10 - Type-curve matching for example 1.

FSV

33

Pressure Transient Analysis for Geothermal Wells

HENRY J. RAMEY, JR.
Stanford University, Stanford, California 94305, USA

ABSTRACT

Throughout the geothermal literature, concern has been expressed many times about the potential effect of precipitation of solids at the wellbore face, throughout the drainage region of a geothermal well, and about the periphery of a geothermal reservoir as cold recharge fluid contacts the warmer geothermal fluids. Many field observations indicate such concern. For example, it is well known that steam wells in Larderello, Italy, decline in rate during production, and have an active life of about 12 years. Similar declines in production rate are often observed in the production histories of gas and oil wells. For this reason, the specialty of pressure transient analysis has been developed to aid determination of the reason for such rate decline. In addition to precipitation or plugging of the porous media near the well face, other reasons for decline in producing rates include a decrease in the formation pressure and low initial formation permeability. A review of the history of pressure transient analysis and applications to geothermal wells are presented in this paper.

INTRODUCTION

Throughout the geothermal literature, much concern has been expressed regarding potential precipitation of solids at the wellbore face, throughout the drainage volume of a geothermal well, or at the periphery of the drainage volume where recharging cold fluid meets the hot geothermal reservoir. The potential damage to the productivity of a geothermal well, not to mention the reservoir proper, is the main reason for such concern. Similar concern for decline in productivity or for low producing rates of gas and oil wells, has been evident in the petroleum literature of the United States almost from the time of the drilling of the Drake well in Pennsylvania in 1859. Within ten years of that time patents aimed at improving the producing characteristics of oil wells began to appear.

The most powerful tool available to the petroleum engineer for diagnosing well conditions is pressure transient analysis. The purposes of pressure-transient analysis include the following: (1) determination of the condition of the well, that is, whether the sand face at the wellbore is damaged or has been stimulated; (2) the quantitative value of the permeability in the drainage volume of the well; (3) the mean formation pressure; and (4) quantitative information concerning the shape and size of the drainage volume and its porosity. Quantitative information on the preceding four items obviously would furnish answers to questions such as: is the low productivity of a given well due to plugging of the well, low formation permeability, or a low driving force and/or formation capacity available for moving fluid into the well? This information would provide a sound basis for decisions involving costly stimulation of a well, or perhaps other operating procedures.

Quantitative tools have been available for performing such tasks since the early 1950's. In view of the potential importance of this information, it is worth considering why it has not been used to much extent to date. There are several reasons, one being a mistaken impression in geothermal circles that oil reservoir engineering can be applied only to closed systems not subject to water recharge. Another reason pertinent to pressure-transient analysis is a widespread belief common in both geothermal and petroleum scientific communities: that the simplifying assumptions common to most analytical solutions are not applicable to real, nonideal reservoirs—particularly fractured reservoirs. This belief is logical, but largely not correct. The common simplifying assumptions of constant rate, constant permeability, and so on, often are found to be sufficient but not necessary for the solutions. Many fractured systems have been found to behave like ideal homogeneous systems with, at most, simple anisotropy.

We now turn to a brief review of the history of the development of pressure-transient analysis to provide a bridge to the current state of this technology.

HISTORY

In the petroleum literature alone more than 300 technical papers have been published on the subject of pressure-transient analysis in the past 45 years. A similar number of publications exists on pump test analysis in the field of ground-water hydrology. This literature has developed because the pressure behavior of a well is easily measured, and is a highly useful quantity. Instruments for measuring maximum pressures in oil wells were developed and used in the United States during the early 1920's (Carter, 1961). These devices included bourdon tube gauges which would record via a stylus mark on a blackened metal sheet, and the measurement of liquid levels in wells utilizing floats or sonic echoes. By 1931 continuously recording instruments, such as the Amerada and Humble and MacDonald gauges, were available (Millikan and Sidwell, 1931).

One of the early applications for bottom-hole pressures in wells was a measurement of the "static" formation pressure. After a well had been closed in for a period of time such as 24 to 72 hours, a bottom-hole pressure measurement was made as an indication of the static formation

pressure. These static measurements indicated the formation pressure in permeable, high-productivity reservoirs. Engineers soon recognized that static pressure measurements depended greatly upon the closed-in time. The lower the permeability, the longer the time required for the pressure in the well to stabilize. This led to the important realization that when a well was closed in, the duration of the pressure build-up was a reflection of the permeability of the reservoir rock around that well. It appears that one of the first determinations of formation permeability for pressure-transient data was published by Moor, Schilthius, and Hurst in 1933. Many papers concerning pressure transients caused by water influx into oil reservoirs began to appear in the following years.

A classic study of pressure-transient analysis involved in the pump testing of water wells was published by Theis in 1935. Among other things, Theis discussed analysis of pressure recovery data. Pressure recovery data are referred to as pressure build-up data in petroleum engineering, and consist of information obtained after a well had produced at a constant rate for a period of time, and was then shut in and its pressures allowed to equalize. Theis suggested a form of graphing and analysis which remains one of the basic techniques employed in petroleum engineering to this day. The method was discovered independently some fifteen years later by Horner. The Theis pressure recovery graph of ground-water hydrology is known as the Horner pressure build-up graph in petroleum engineering. Horner did introduce the important concept of estimating the mean formation pressure which would be obtained in an enclosed reservoir system at an infinite shut-in time.

In 1937, Muskat introduced a graphical method for determining the ultimate static formation pressure from bottom-hole pressure-transient data. It is often said in petroleum engineering that had Morris Muskat had access to a modern digital computer there would be little left to do today.

During the 1940's there were many classic studies. Many important papers appeared as Geological Survey water supply papers. Notable are publications by Wenzel in 1942, and Cooper and Jacob in 1946. Jacob also prepared a classic chapter in the book edited by Rouse, on engineering hydraulics, in 1950. Because the readership of this paper is apt to be familiar with publications in ground-water hydrology in the geophysical, geological, and civil engineering literatures, the main emphasis in this paper will be on publications in the specific area of petroleum engineering. Also notable in the 1940's was a publication by Elkins in 1946, which presented graphs for interference analysis similar to those used today, and publications by Arps and Smith in 1949 dealing with pressure build-up, and a classic study by Van Everdingen and Hurst in 1949. The Van Everdingen and Hurst study presented applications of the Laplace transformation for solving transient flow problems in reservoirs. The main application stressed was estimation of transient water influx (water recharge) into oil reservoirs. However, the authors did discuss applications to pressure-transient analysis for individual wells during presentation of the material in the late 1940's. It is clear that many researchers were investigating quantitative analysis of pressure transient data in the late 1940's.

WELL TESTING FROM 1950 TO 1966

In 1950, two separate publications appeared which are generally recognized as providing the fundamental basis for modern well test analysis. These included the paper by Horner, and the paper by Miller, Dyes, and Hutchinson. The Miller, Dyes, Hutchinson study indicated that static pressures during pressure build-up should be graphed versus the logarithm of the shut-in time. On the other hand, the Horner study indicated that static build-up pressure should be graphed versus the logarithm of a time ratio involving the sum of the producing time plus the shut-in time, divided by the shut-in time. Both graphs were reported to produce straight lines, the slope of which was inversely proportional to the formation permeability by precisely the same relation. Confusion between the validity of the results of these two methods remains to this date, despite the fact that Ramey and Cobb (1971) showed that the Horner (or Theis) graph was generally the most reliable.

Figure 1 presents a Miller-Dyes-Hutchinson graph for a well in the center of a square whose outer boundary is subject to a full recharge, that is, constant pressure (Ramey, Kumar, and Gulati, 1973). Dimensionless build-up pressures are graphed vs dimensionless shut-in time. The dimensionless producing time prior to shut-in is shown as a parameter. The dimensionless groups are defined as follows:

$$p_{Ds} = \frac{kh(p_i - p_{ws})}{0.4568 r_{sc}\, qB\mu}, \text{ for liquid flow} \qquad (1)$$

$$p_{Ds} = \frac{Mkh(p_i^2 - p_{ws}^2)}{0.2789\, q\mu\, ZT}, \text{ for flow of steam or gas} \qquad (2)$$

$$t_D = \frac{0.3604\, kt}{\phi \mu c_t r_w^2} \qquad (3)$$

$$t_{DA} = \frac{0.3604\, kt}{\phi \mu c_t A} = t_D (r_w^2/A) \qquad (4)$$

Identification of symbols and units is presented in Table 1. A delta symbol before the symbol t for time indicates a period of time Δt after the producing period of time t.

Graphs similar to Figure 1 may be found for many different well drainage shapes, for wells located at almost any position within the shape, and with any combination of closed or recharge boundaries on the shape. See Ramey, Kumar, and

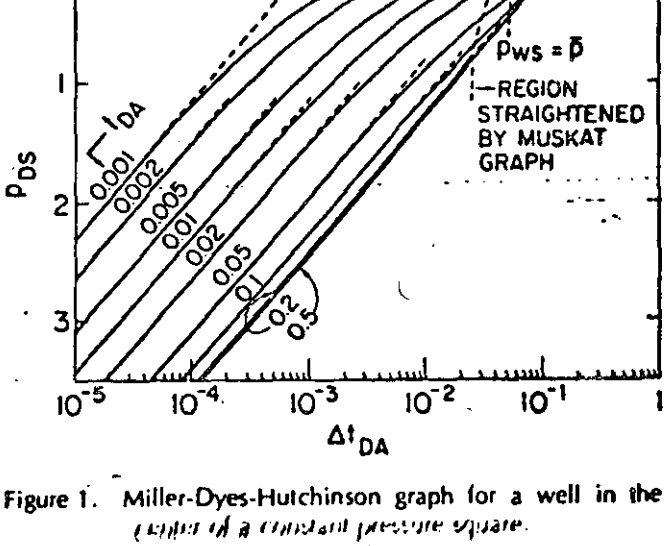

Figure 1. Miller-Dyes-Hutchinson graph for a well in the center of a constant pressure square.

Table 1. Nomenclature.

Symbol	Meaning
k	= effective permeability to flowing phase, darcies
h	= net formation thickness, m
p	= pressure, kg/cm²
v_{sc}	= specific volume at standard conditions, cc/gm
q	= production rate, tons/hr (1000 kg/hr)
B	= formation volume factor, reservoir volumes/std volume
μ	= viscosity of flowing fluid, centipoise
M	= molecular weight, gm/gm-mole
Z	= real gas law deviation factor ($pv = ZnRT$)
n	= gm moles
R	= 84.78 (cu cm-kg/cm²)/(moles-°K)
T	= absolute formation temperature, °K
p_D	= dimensionless pressure
t_D	= dimensionless time
ϕ	= porosity, fraction of bulk volume
c_t	= total system effective isothermal compressibility, (kg/cm²)⁻¹
r	= radial distance from a constant rate well, m
r_w	= well radius, m
A	= drainage area, m²
t	= time, hr
m	= slope of semi-log graph, (kg/cm²)/log cycle for liquid; (kg/cm²)²/log cycle for gases
s	= skin effect, dimensionless
Δp_{skin}	= see Eq. 10
FE	= flow efficiency, see Eq. 11
p^*	= Horner's false pressure at $(t + \Delta t)/\Delta t = 1$
C_D	= dimensionless storage constant, see Eqs. 13 and 14
C	= wellbore storage, tons/(kg/cm²) See Eq. 13
C'	= wellbore storage, tons/(kg/cm²)² See Eq. 14
x_e	= half length of side of square enclosing a vertically fractured well, see Fig. 11, m
x_f	= vertical fracture length from center of well to tip of fracture, m
r_f	= horizontal fracture radius, m
$\bar{p}$	= volumetric average pressure within drainage region resulting from constant-rate production for a time t
r_D	= dimensionless radius, r/r_w
c_g	= isothermal compressibility of gas, (kg/cm²)⁻¹
Subscripts	
w	= bottom hole, well
t	= surface
s	= static (zero surface production rate)
f	= flowing
r	= radial dimension
z	= vertical dimension
D	= dimensionless
f	= fracture
A	= based on drainage area A
i	= initial
1 hr	= at one hour on semi-log straight line or its extension

Gulati, 1973. The parallel straight lines in the lower left-hand portion of Figure 1 possess a slope inversely proportional to the effective permeability to the flowing phase, or to the total mobility (k/μ) for all phases flowing in the case of multiphase flow (Matthews and Russell, 1967). The relationship between the slope and the permeability is:

$$k = 0.5258 \frac{v_{sc}\, qB\mu}{mh}, \text{ for liquids} \qquad (5)$$

$$k = 0.3210 \frac{q\mu ZT}{mhM}, \text{ for steam or gases} \qquad (6)$$

The slope m has units of pressure per log cycle for liquids, and pressure squared per log cycle for steam. Figure 1 may also be used to find both the mean pressure $\bar{p}$ and the recharge pressure p_i.

Figure 2 is a general Horner graph for a well in the center of a constant pressure square (full recharge). An infinitely long shut-in would cause a time ratio of unity, and a dimensionless buildup pressure p_{Ds} of zero because the well would return to the initial pressure p_i on the recharge boundary. The parallel lines on the lower right-hand portion of Figure 2 bear the same relationship between slope and permeability as given previously by Eqs. (5) and (6). The build-up lines appear to move to the right as producing time prior to shut-in increases. The static pressure within the drainage region at the shut-in time can also be found from the dashed line.

Figure 3 presents a Horner-type graph for a well in a closed square—a depletion case. One distinct difference from the previous figure is that the lines appear to move downwards, rather than to the right. This behavior is a characteristic difference between closed and water-drive shapes which often can be identified from a series of pressure transient tests run with longer producing times prior

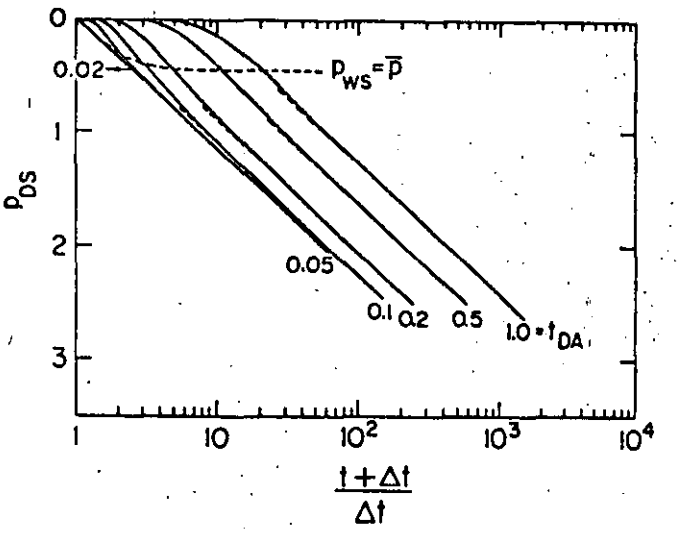

Figure 2. Horner graph for a well in the center of a constant-pressure square.

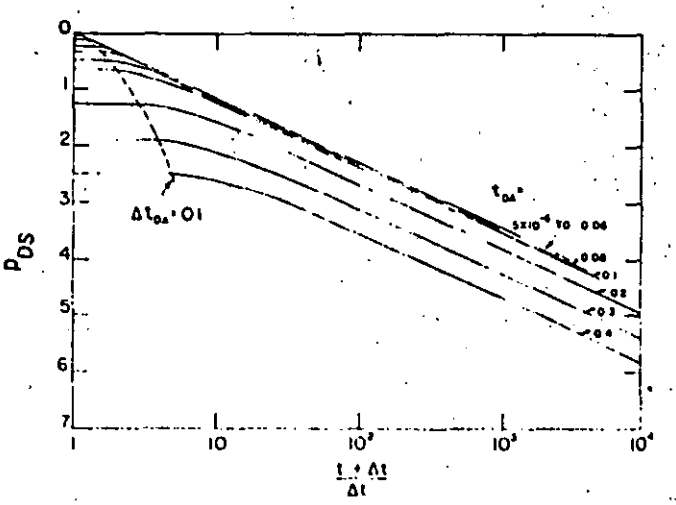

Figure 3. Horner graph for a well in the center of a closed square.

Another important use of Figures 2 and 3 is estimation of the porosity. If the initial pressure p_i is known, field values of p_{DS} can be calculated from:

$$p_{DS} = \frac{p_i - p_{ws}}{0.87m} \quad (7)$$

Because the time ratio for the field data and the dimensionless time ratios are the same, field data can be graphed on either Figures 2 or 3 (or other appropriate figures for other shapes) and the value of the dimensionless producing time, t_{DA}, read as a parameter. From Eq. (4), $\phi c_t A$ can be calculated because k should be known from the slope of the normal build-up graph. In the event that the thickness, h, is not known, then $\phi c_t hA$ may be calculated—the reservoir pore volume-compressibility product.

Figure 4 presents a Muskat graph for the case of a well in the center of a constant-pressure square. The slopes of the parallel straight lines are related to the porosity of the system, while the pressure intercepts may be related to the effective permeability of the flowing phase. This interesting build-up graph can often be prepared with very little knowledge of reservoir conditions. However it should be used with care with full knowledge of the pitfalls involved in the graph. The same can be said of all of the common build-up graphs. Recent studies show it is possible to investigate each type of graph thoroughly by empirical methods and to clearly define the regions of usefulness of each graph (Ramey and Cobb, 1971; Kumar and Ramey, 1974).

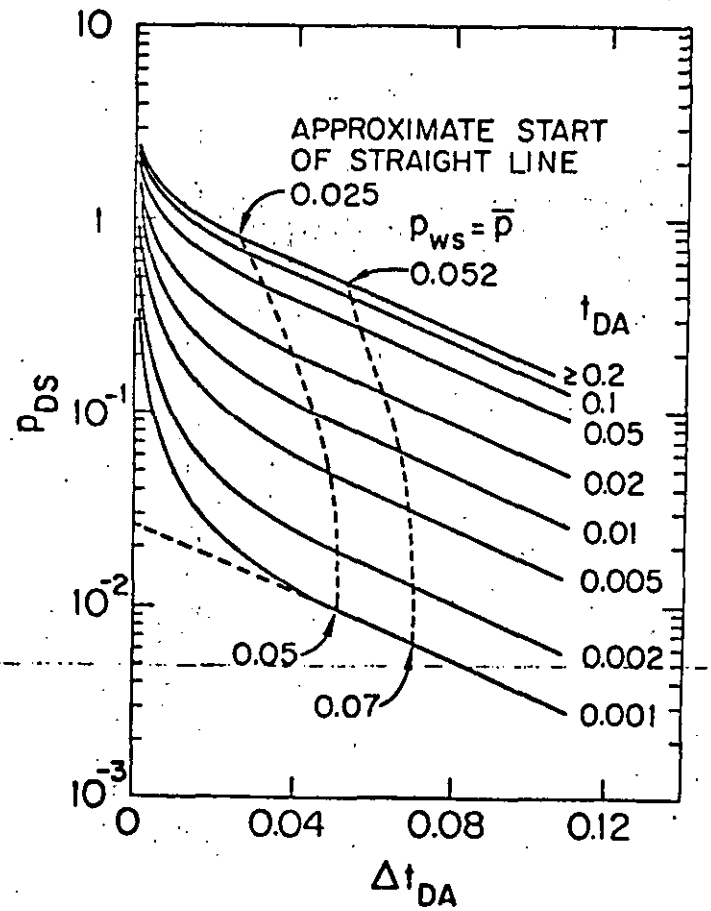

Figure 4. Muskat graph for a well in the center of a constant-pressure square.

The preceding methods have been applied to geothermal well data with success (Ramey, 1970; Ramey and Gringarten, 1975; and Barelli et al., 1975). Figure 5 presents a Horner build-up graph for a geothermal steam well at The Geysers. The proper semi-log straight line is shown by the solid line. Table 2 presents other pertinent data for this transient test. Unfortunately, all well tests do not look like Figure 5. Sometimes there is a complete absence of a straight line, such as shown in Figure 6 for a test in the Geysers. Table 3 presents other information for this well test. Fortunately, new methods are now available to aid selection of the proper straight line, as will be discussed in a later section.

In the 15-year period from 1950 through 1965, many important basic papers in pressure-transient analysis appeared in the petroleum engineering literature. Notable are publications by Van Everdingen (1953) and Hurst (1953), concerning the concept of the skin effect and the quantitative effect of wellbore damage on the performance of a well; the classic study by Matthews, Brons, and Hazebroek in 1954, concerning determination of mean pressure for closed reservoir systems; Perrine's review of pressure build-up analysis in 1956, which presented the first sound analysis of multiphase-flow pressure-transient analysis; and in 1959, Martin presented the theoretical foundation for Perrine's method for multiphase flow.

Let us consider just a few of these findings in more detail. The Van Everdingen-Hurst skin effect or skin factor concept is particularly important to geothermal well

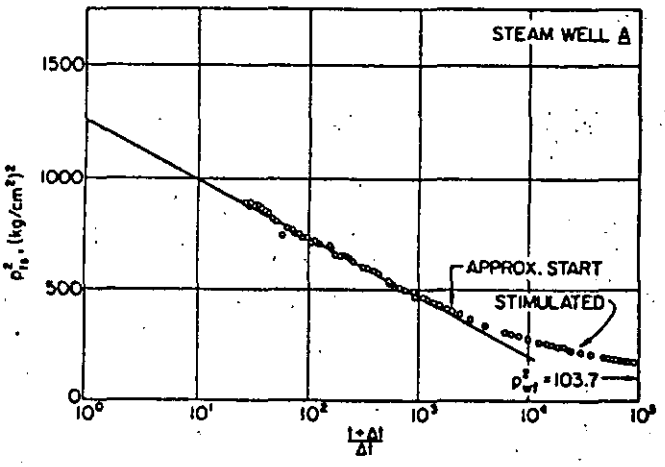

Figure 5. Horner buildup graph for Geysers Steam Well A.

Table 2. Pressure buildup data for Steam Well A.

Symbol	Value
q	= 26 tons/hr
t	= 12 240 hr
r_w	= 0.122 m
μ	= 0.0226 centipoise
c_g	= 0.032 (kg/cm²)⁻¹
Z	= 0.84
T	= 515°K
M	= 18 gm/gm mole
m	= 262 (kg/cm²)²/log cycle
p_{1hr}^2	= 260
p_{wf}^2	= 103.7
p^{*2}	= 1245

Total depth is 663 m; open hole below 110 m.

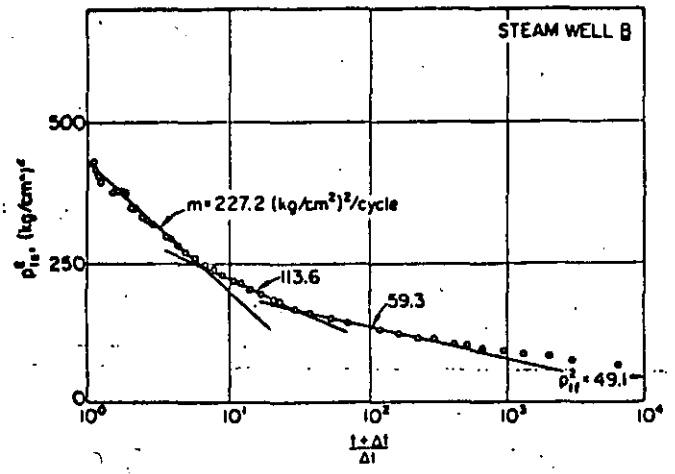

Figure 6. Horner buildup graph for Geysers Steam Well B.

testing. These investigators said that they had found that producing pressures generally did exhibit semi-log straight lines, but they appeared to be displaced. They reasoned that some resistance to flow existed at the sand face, and that it could be handled by adding a dimensionless pressure drop across a skin at the well face:

$$\frac{kh(p_i - p_{wf})}{0.4568 v_{sc} q B \mu} = p_{Dw} + s \qquad (8)$$

Eq. (8) applies for liquid flow, and a similar expression may be written for steam flow by using the form of Eq. (2). The skin effect, s, can be found by combining the flowing pressure p_{wf} at the instant of shut-in and a pressure obtained from the semi-log straight line during build-up at one hour of shut-in time, p_{1hr}. This pressure must be read on the straight line or its extension. The proper relationship for gas flow is:

$$s = 1.151 \left[\frac{p_{1hr}^2 - p_{wf}^2}{m} - \log_{10} \frac{k}{\phi \mu c_t r_w^2} + 0.0387 \right] \qquad (9)$$

The pressure drop (loss) caused by the skin effect is

$$\Delta p_{skin} = 0.87\, ms \qquad (10)$$

The pressure drop across the skin is usually used to compute the flow-efficiency of the well, FE:

$$FE = \frac{p^* - p_{wf} - \Delta p_{skin}}{p^* - p_{wf}} \qquad (11)$$

37

Table 3. Pressure buildup data for Steam Well B.

Symbol	Value
q	= 26.7 tons/hr
t	= 540 hr
r_w	= 0.122 m
μ	= 0.02 centipoise
c_g	= compressibility of steam, 0.054 (kg/cm²)⁻¹
Z	= 0.884
T	= 489°K
M	= 18 gm/gm mole
m	= 59.3 (kg/cm²)²/log cycle
p_{1hr}^2	= 93 (kg/cm²)²
p_w^2	= 49.1
p^{*2}	= 434.7
p_i	= 21.4 kg/cm²

Total depth is 261.5 m; open hole below 109.7 m.

For liquid flow, Eq. (9) is slightly modified: the pressures are not squared.

The dimensionless skin effect has the following interpretation. The value of s will be positive if the well is damaged, zero if neither damaged nor stimulated, and negative if the well is stimulated. The flow efficiency is the ratio of the actual flow rate per unit pressure drop (productivity index) to an ideal flow rate per unit pressure drop neglecting the pressure loss across the skin.

The effect of the skin can be seen in the early portion of a pressure build-up test. If a well is stimulated and has a negative skin effect, the early portion of the build-up will appear as shown for the Steam Well A case on Figure 5. The build-up pressures will approach the semi-log straight line from above. If a well is damaged, build-up pressures will approach the semi-log straight line from below as indicated in the right-hand portion of Figure 7 for Steam Well C case. Another important phenomenon can cause a build-up to have the same early shape as the damaged curve for Figure 7. This effect is known variously as wellbore storage, annulus unloading, and afterflow. The cause of the effect is that the sand-face fluid flow rate does not respond instantaneously to changes caused at the wellhead. If a well is suddenly opened at a constant rate, the first production results from expansion or depletion of wellbore fluids (annulus unloading). If a well is suddenly shut in at the surface, fluid continues to pass through the sand face at the bottom hole as if nothing had happened (afterflow). Both effects are a result of the wellbore storage volume. Because the wellbore storage effect causes the same appearance as a damaged wellbore in the early build-up data, it is possible to mistake a storage effect for wellbore damage. An example of such an effect for a steam well was presented by Ramey (1970) and reanalyzed by Ramey and Gringarten (1975) at this same symposium.

Many phenomena cause the appearance of skin effects. Examples are partial penetration of the formation, cementing casing in place and gun perforating, bore inclination from the vertical, hydraulic fracturing, acidization, boiling or gas evolution from produced liquids, condensation of liquids from produced gases, and inertial (non-Darcy) flow effects at high velocities, to name a few. These are often termed

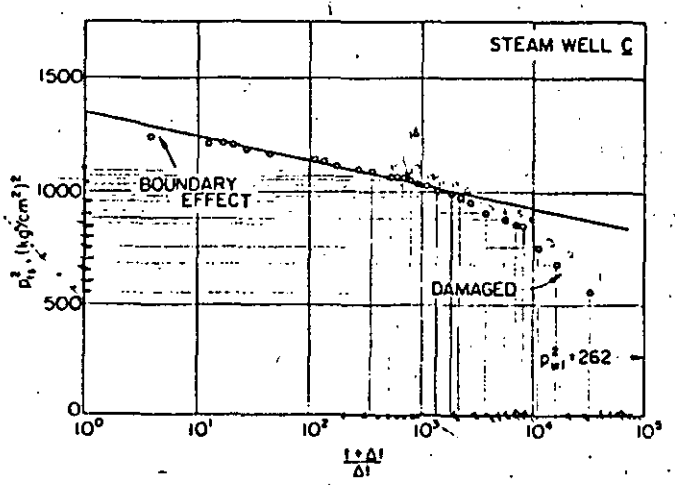

Figure 7. Horner buildup graph for Geysers Steam Well C.

Pseudo-skin effects. Many published studies are available which can be used to estimate the order of magnitude of such pseudo-skin effects (Brons and Marting, 1961; Harris, 1966; Ramey, 1965; Gringarten, Ramey, and Raghavan, 1975).

Let us now consider the classic study by Matthews, Brons, and Hazebroek in 1954. One important contribution was a generalization of Horner's method for determination of the ultimate static formation pressure from a build-up to include many rectangular shapes with wells in various positions within the shape. They presented figures similar to that of Figure 8. Figure 8 applies to the case of a well in the center of a constant pressure square. Horner suggested extending the semi-log straight line to a time ratio of unity, and calling this extrapolated pressure a "false" pressure p^*. Figure 8 presents a method for correcting the false pressure p^* to either p_i or $\bar{p}$ for the constant pressure square case. Another important contribution of the Matthews, Brons, and Hazebroek study was a method for dividing closed reservoirs into per-well drainage shapes. Ramey, Kumar, and Gulati (1973) presented a monograph dealing with the recharged reservoir shapes. Matthews, Brons, and Hazebroek provided the basis for this study by pointing out the usefulness of superposition of infinite arrays of wells. Figure 9 shows one such array. It contains the answer to two important problems: fluid reinjection, and generation of constant-pressure outer boundaries.

We now turn to consideration of other important studies in the 1950's. A number of important papers began to appear in the early 1950's in the area of transient flow of ideal gases through a porous medium. In regard to practical applications, the papers by Aronofsky and Jenkins (1953), Bruce (1953), and Tracy (1956), are important. Both the Aronofsky and Jenkins, and Bruce et al. studies were aimed at the same problems, that is, the transient flow of ideal gases through porous media. Each study produced a classic result. The Aronofsky and Jenkins study is notable because of the introduction of the concept of the transient drainage radius for flow of gases. The Bruce, et al. study is notable for introduction of the concept of alternating direction implicit finite difference calculations. It is clear that one study or the other would have been stopped had both groups been functioning within the same research laboratory.

The Aronofsky and Jenkins work inspired a number of

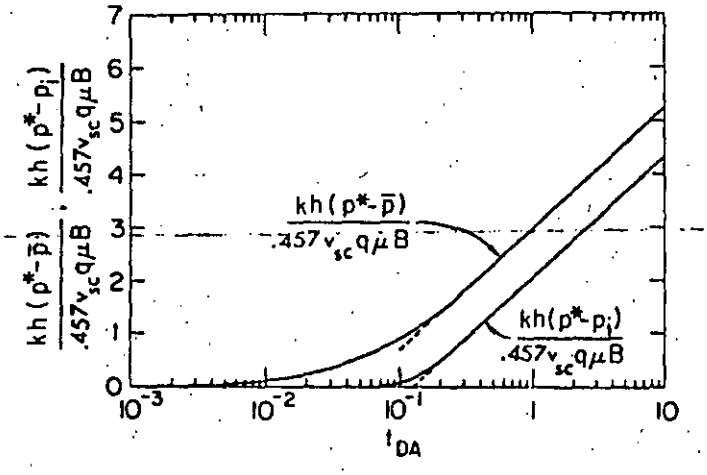

Figure 8. Matthews-Brons-Hazebroek graph for a well in the center of a constant-pressure square.

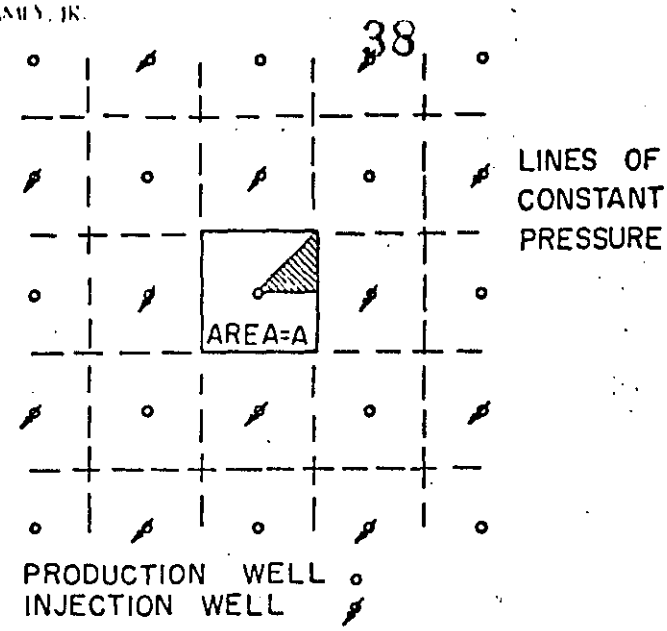

Figure 9. Infinite array to generate a well in the center of a constant pressure square, or a developed five-spot injection production pattern.

studies of the effect of pressure variation of fluid and rock properties. See Al-Hussainy, Ramey, and Crawford (1966). A "real gas potential" was introduced which coupled fluid viscosity and density variation with pressure with stress-sensitive permeability. This concept has also been tested for liquid flow successfully. It appears that dependence of fluid and rock properties on pressure can usually be handled practically.

By the mid-1960's, the details of well test analysis apparently were thoroughly investigated. This led the Society of Petroleum Engineers of the AIME to commission the preparation of a monograph on the subject, "Pressure Build-Up and Flow Tests in Wells," by Matthews and Russell. The result was published in 1966. To underscore the importance of this subject, the Society of Petroleum Engineers also commissioned the production of a Reprint Series Manual No. 9 titled, "Pressure Analysis Methods." The Matthews and Russell monograph was the first in a series of monographs intended to aid a program of self-education by members of the Society of Petroleum Engineers.

MODERN PRESSURE ANALYSIS

A study of wellbore storage (Ramey, 1965) and the skin effect began to bear interesting fruit by the end of the decade (Ramey, 1970; Agarwal, Al-Hussainy, and Ramey, 1970). A renewed interest in using log-log type curves to study the early pressure data prior to the onset of the usual semi-log straight line led to a number of important findings. Figure 10 is a log-log type curve for pressures measured in a well produced at constant rate with a skin effect. The unit slope straight lines emanating from the lower left portion of the graph represent pressures controlled altogether by wellbore storage. In effect, there is no flow through the sand face during times when the unit slope is evident. Then there is a transition to the flat, zero wellbore storage lines passing across the graph. When the transition lines reach the flat portion, the correct semi-log straight line starts for these cases, because the flat lines are semi-log straight for

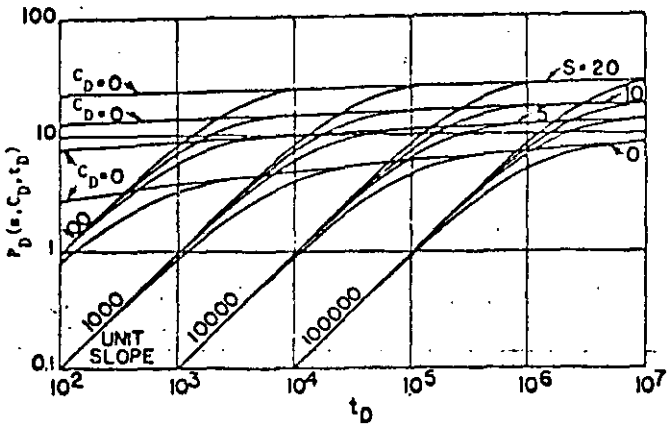

Figure 10. p_D vs t_D for a well with storage and a skin effect.

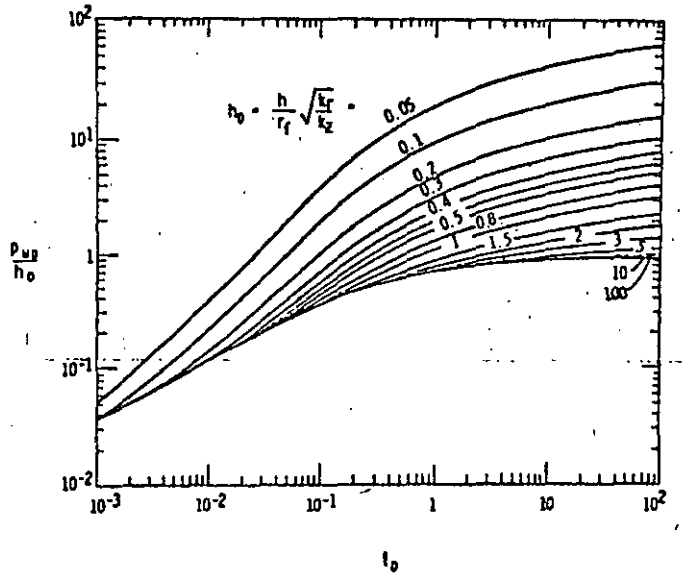

Figure 12. p_{wD}/h_D vs t_{Dt} for a constant-flux, circular horizontal fracture in the center of the interval.

times of about 5. The time of start of the semi-log straight line can be expressed (Ramey, Kumar, and Gulati, 1973):

$$t_D = C_D(60 + 3.5\,s) \tag{12}$$

where:

$$C_D = \frac{C\,B\,v_{sc}}{2\pi\phi h c_t r_w^2}, \text{ for liquids} \tag{13}$$

$$C_D = \frac{27\,C'ZT}{M\phi\,h c_t r_w^2}, \text{ for gases.} \tag{14}$$

In the 1970 study, it was recommended that type-curve matching be used to obtain permeability and skin effect by means of Figure 10. This is now believed to be a very crude procedure. Type-curve matching can be used approximately at any position on Figure 10 to determine where the correct semi-log straight line begins. This procedure plus general diagnostic uses make Figure 10 a very useful type curve.

One result of this study was that it became apparent that it would be necessary to specify the physical nature of the skin effect for pressures prior to the onset of the semi-log straight line. An acidized well with an annular zone of high permeability near the well could have the same negative skin effect as a fractured well with a large, vertical fracture. But it was likely that these two cases would not have the same early time behavior. Likewise, it was not likely that wells with the same skin effect, but vertical or horizontal fractures, would exhibit the same early time behavior. To answer these speculations, studies of annular skin regions (Wattenbarger and Ramey, 1970), and fractured wells (Gringarten, Ramey, and Raghavan, 1974) were made. Figures 11 and 12 present log-log type curves for vertical and horizontal fractures.

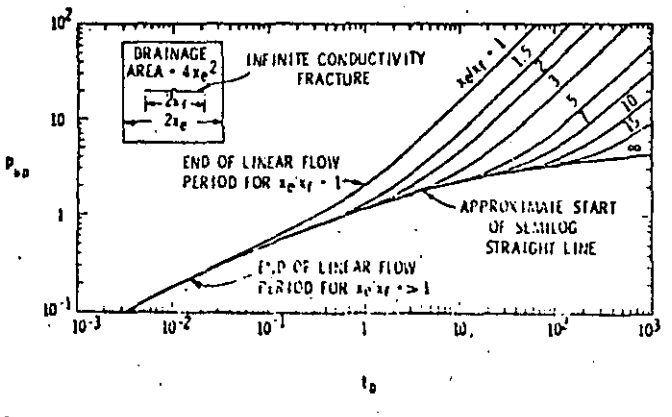

Figure 11. p_{wD} vs t_{Dt} for an infinite-conductivity vertical fracture in the center of a closed square or in an infinitely large reservoir.

Figure 11 presents the producing pressures for a well with a vertical fracture in the center of a closed square, or in an infinitely large reservoir. It is a simple matter to place the fractured well in almost any position within any sort of drainage shape. The left-hand side of this curve is a straight line of slope 1/2. This period represents linear flow normal to the surface of the fracture. Later, the fracture behaves like a circular well with a radius half the distance from the center to the top of the fracture, $x_f/2$. This sort of log-log type curve reveals the presence of fractures and can be used in matching whether a semi-log straight line can be found or not. Permeability may be found from the pressure match (Ramey and Gringarten, 1975), the fracture length x_f from the time match, and the drainage area, or a minimum estimate of the drainage area may be found from the parameter x_e/x_f.

Figure 12 presents a log-log type curve for a single horizontal fracture located at the center of the interval. The left-hand portion of the lowest line on the graph is also linear and of slope 1/2. This represents vertical flow normal to the fracture surface. Because there is a vertical flow component, it is necessary to specify both the radial and vertical permeabilities. Pressure behavior of horizontal fractures does behave similarly. The dimensionless time for the horizontal fracture is based upon the radius of the fracture, r_f.

Figure 13 presents a log-log type curve for the build-up data of Steam Well A (see Fig. 5). Almost two log cycles of half-slope line are evident. One important use of such a graph is to locate the start of the correct semi-log straight line. Wattenbarger and Ramey (1970) noticed that the start of the semi-log straight line corresponded roughly to a

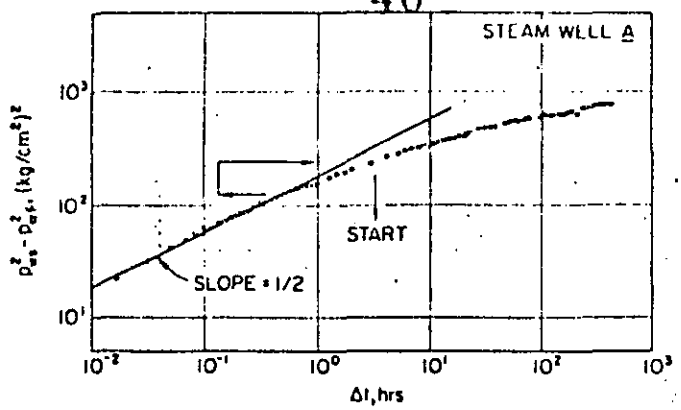

Figure 13. Log-log type curve for pressure buildup for Geysers Steam Well A.

Table 4. Pressure buildup data for Steam Well C.

Symbol		Value
q	=	102.3 tons/hr
t	=	55.2 hr
r_w	=	0.122 m
μ	=	0.0225 cps
c_g	=	0.037 $(kg/cm^2)^{-1}$
Z	=	0.84
T	=	515°K
M	=	18 gm/gm mole
m	=	210 $(kg/cm^2)^2$/log cycle
p_{1hr}^2	=	1047 $(kg/cm^2)^2$
p_{wf}^2	=	262
p^{*2}	=	1333
$\bar{p}^2$	=	1260 (after 15 months shut in)

Total depth 1120 m; open hole below 155 m.

pressure difference about twice that at the top of the half-slope log-log line. This rule, the double-delta-p rule, is shown by the arrows on Figure 13. This can be used to select the proper straight line when several are indicated as shown on Figure 6.

The wellbore storage type curve has been in use for 10 years, the fracture type curves for 4 years. Extensive field experience has been gained in gas and oil reservoirs and in several geothermal reservoirs. They provide a most powerful diagnostic device. It has been possible to unravel strange behavior of different fractured systems. One natural gas reservoir was found to have fracture porosity only. Hydraulic fracturing produced only propped, high-conductivity storage volume, not a single planar fracture. In other fractured systems, widely spaced trending fractures were evident in pressures measured in a producing well, but apparently caused only simple anisotropy in interference testing. This offers much hope for simple interference testing in geothermal systems. By interference testing is meant the sort of test wherein one well is producing and the resulting pressure drop is measured in a distant well. The result may be type curve matched with some appropriate solution such as the continuous line source solution shown on Figure 14 (also known as Lord Kelvin's point source, the Theis solution, and so on).

CONCLUDING REMARKS

In the preceding, I have focused on the positive aspects of pressure-transient analysis. The result may be misleading.

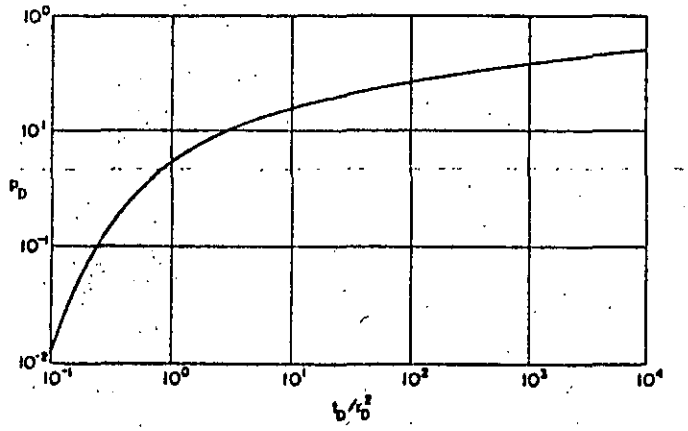

Figure 14. p_D vs t_D/r_D^2 for the continuous line source solution (Theis solution).

Pressure-transient analysis may not always be practical. One common problem in both oil and geothermal reservoirs may be called the thick sand problem. For thick sands, the product of permeability-thickness may be so great that the semi-log straight line has a negligible or undetectable value at practical producing rates. This likelihood is evident from Eqs. (5) or (6). Even in this case, important results may be obtained by an experienced, sophisticated analyst under fortunate circumstances.

Another problem is that geothermal reservoirs may require solutions not yet available. The presence of a boiling liquid interface in a vapor-dominated system would be evident as a constant-pressure interface. This interface would be horizontal, rather than vertical as is assumed in most of the available solutions. Generally, production of new solutions is not difficult, and usually does not require large amounts of computer time. Analytical solutions are usually much better than finite-difference solutions for short-time results.

Finally, it can be said that many of the models available are certainly adequate for the geothermal field data inspected to date. It can be said that results appear reasonable. It is certain that continued work in this area will lead to development of valid models which can be used to analyze pressure-time data from geothermal reservoirs and produce information not available from any other source. One important weapon in this study will be the development of new pressure- and temperature-sensing tools. Several new pressure-measuring devices are currently being used in oil wells to measure pressures to almost 7×10^{-5} kg/cm². It is certain that similar instruments will become available for geothermal applications in the near future. What is impossible today will be easy tomorrow.

REFERENCES CITED

Agarwal, R. G., Al-Hussainy, R., and Ramey, H. J., Jr., 1970, An investigation of wellbore storage and skin effect in unsteady liquid flow—1. Analytical treatment: Soc. Petroleum Engineers Jour. (September), p. 279.

Al-Hussainy, R., Ramey, H. J., Jr., and Crawford, P., 1966, The flow of real gases through porous media: Jour. Petroleum Technology, v. 18, no. 5, p. 645.

Aronofsky, J., and Jenkins, R., 1953, Unsteady radial flow of gas through porous media: Jour. Applied Mechanics, v. 20, p. 210.

Arps, J. J., and Smith, A. E., 1949, Practical use of bottom hole pressure buildup curves: Reprint paper no. 851-23-I, Tulsa, Oklahoma meeting, API.

Barelli, A., Celati, R., Manetti, G., and Neri, G., Buildup and back-pressure tests on Italian geothermal wells: Second UN Symposium on the Development and Use of Geothermal Resources, San Francisco, Proceedings, Lawrence Berkeley Lab., Univ. of California.

Brons, F., and Marting, V. E., 1961, The effect of restricted fluid entry on well productivity: Jour. Petroleum Technology (February), p. 172.

Bruce, G. H., Peaceman, D. W., Rachford, H. H., and Rice, J. D., 1953, Calculations of unsteady state gas flow through porous media: AIME, Trans., v. 198, p. 79.

Carter, D. V., 1961, History of petroleum engineering: API.

Cooper, H. H., Jr., and Jacob, C. E., 1946, A generalized graphical method for evaluating formation constants and summarizing well field history: Am. Geophys. Union Trans., v. 27, p. 526.

Earlougher, R. C., Jr., Ramey, H. J., Jr., Miller, F. G., and Mueller, T. D., 1968, Pressure distributions in rectangular reservoirs: Jour. Petroleum Technology, v. 20, no. 2, p. 199.

Elkins, L. F., 1946, Reservoir performance and well spacing—silica arbuckle pool, Kansas: Drill. and Prod. Prac., API, p. 109.

Gringarten, A. C., and Ramey, H. J., Jr., 1974, Unsteady state pressure distributions created by a well with a single horizontal fracture, partial penetration, or restricted entry: Soc. Petroleum Engineers Jour. (August), SPE 3819, p. 413.

Gringarten, A. C., Ramey, H. J., Jr., and Raghavan, R., 1974, Unsteady state pressure distributions created by a well with a single infinite conductivity vertical fracture: Soc. Petroleum Engineers Jour. (August), p. 347.

——, 1975, Pressure analysis for fractured wells: Jour. Petroleum Technology (July).

Harris, M. H., 1966, The effect of perforating on well productivity: Jour. Petroleum Technology (April), p. 518.

Horner, D. R., 1950, Pressure buildup in wells: Third World Petroleum Congress, Proc., Leiden, E. J. Brill, v. 2, p. 503.

Houpeurt, A., 1953, Etude analogique de l'ecoulement radial circulaire transitoire des gas dans les milieux poreux: Revue IFP, v. 8, p. 129.

Hurst, W., 1953, Establishment of the skin effect and its impediment to fluid flow into a wellbore: Petroleum Engineering (October), v. 25, p. B-6.

Jacob, C. E., 1940, Flow of water in elastic artesian aquifers: AGU Trans, v. 2, p. 574.

——, 1950, chapter, *in* Rouse, H., ed., Engineering hydraulics, Proceedings of the Fourth Hydraulics Conference, Iowa Institute of Hydraulics Research, June, 1949: New York, John Wiley & Sons.

Kumar, A., and Ramey, H. J., 1974, Well test analysis for a well in a constant pressure square: Soc. Petroleum Engineers Jour. (April), p. 107.

Martin, J. C., 1959, Simplified equations of flow in gas drive reservoirs and the theoretical foundation of multiphase pressure buildup analyses: AIME Trans., v. 216, p. 309.

Matthews, C. S., and Russell, D. G., 1967, Pressure buildup and flow in wells, Henry L. Doherty Series Monographs, Vol. 1: Dallas, Henry L. Doherty Memorial Fund of AIME.

Miller, C. C., Dyes, A. B., and Hutchinson, C. A., Jr., 1950, The estimation of permeability and reservoir pressure from bottom hole pressure buildup characteristics: AIME Trans., v. 189, p. 91.

Millikan, C. V., and Sidwell, C. V., 1931, Bottom hole pressures in oil wells: AIME Trans., v. 92, p. 194.

Moore, T. V., Schilthius, R. J., and Hurst, W., 1933, The determination of permeability from field data: Proc., API Bulletin 211, p. 4.

Muskat, M., 1937, The use of data on the buildup of bottom hole pressures: AIME Trans., v. 123, p. 44.

Perrine, R. L., 1956, Analysis of pressure buildup curves: Drill. and Prod. Prac., API, p. 482.

Ramey, H. J., Jr., 1965, Non-darcy flow and wellbore storage effects in pressure build-up and drawdown of gas wells: Jour. Petroleum Technology (February), p. 223.

——, 1970, Short-time well test data interpretation in the presence of skin effect and wellbore storage: Jour. Petroleum Technology (January), p. 97.

Ramey, H. J., Jr., and Cobb, W. M., 1971, A general pressure buildup theory for a well in a closed drainage area: Jour. Petroleum Technology (December), p. 1493.

Ramey, H. J., Jr., and Gringarten, A. C., May, 1975, Effect of high-volume vertical fractures on geothermal steam well behavior: Second Symposium on the Development and Use of Geothermal Resources, San Francisco, Proceedings, Lawrence Berkeley Lab., Univ. of California.

Ramey, H. J., Jr., Kumar, A., and Gulati, M., 1973, Gas well test analysis under water drive conditions: AGA, Arlington, Virginia.

SPE Reprint Series No. 9, 1967, Pressure analysis methods: Dallas, SPE of AIME.

Theis, C. V., 1935, The relationship between the lowering of piezometric surface and rate and duration of discharge of wells using ground water storage: AGU Trans., v. 2, p. 519.

Tracy, G. W., 1956, Why gas wells have low productivity: Oil and Gas Jour. (August), p. 84.

Van Everdingen, A. F., 1953, The skin effect and its influence on the productive capacity of a well: AIME Trans., v. 198, p. 171.

Van Everdingen, A. F., and Hurst, W., 1949, The application of the Laplace transformation to flow problems in reservoirs: AIME Trans., v. 186, p. 305.

Wattenbarger, R. A., and Ramey, H. J., Jr., 1970, An investigation of wellbore storage and skin effect in unsteady liquid flow—2: Soc. Petroleum Engineers Jour. (September), p. 291.

Wenzel, L. K., 1942, Methods of determining permeability of water bearing materials with special reference to discharging well methods: U.S. Geological Survey, W.S.P., p. 887.

FSV

SPE

Society of Petroleum Engineers of AIME

SPE 7963

WELL TEST ANALYSIS OF HGP-A

by B.H. Chen, D.H. Kihara, A. Seki,
and P.C. Yuen, U. of Hawaii

ABSTRACT

Since the successful initial flashing on July 2, 1976, HGP-A has undergone five flash discharge tests with the longest one lasting 42 days. Production records including wellhead pressure and temperature, production rate and steam quality were kept for drawdown analysis. After two of the discharge tests, Kuster pressure bombs were lowered to the bottom repeatedly to record pressure data for buildup analysis.

Initial analyses of the drawdown and buildup tests indicate that the Kapoho Geothermal Reservoir, where HGP-A is located, seems to be in a tight formation with possible severe mud damage in the well. The reservoir also appears to be a liquid-dominated system but with two-phase flow during the discharge of HGP-A. Evidence of this claim will be presented in this paper.

The pressure drawdown and buildup analyses were performed with the traditional single-phase petroleum reservoir engineering techniques modified when necessary.

INTRODUCTION

The experimental well, HGP-A, drilled under the auspices of the Hawaii Geothermal Project, is located on the island of Hawaii near the eastern rift of Kilauea volcano. Drilling was completed to a depth of 6450 feet (1966 m) in April 1976. The well is cased to 2230 feet (680 m) below the wellhead, which is approximately 600 feet (183 m) above sea level. A slotted liner is placed from the end of the casing to bottomhole. Cuttings and core samples obtained during drilling indicate that the region is composed of volcanic basalt with a profile that contains open fracture zones separated by relatively impermeable layers.[1]

References and illustrations at end of paper.

The well has undergone five flash discharge tests since an initial flashing on July 2, 1976. Figure 1 is a sketch of the equipment and instrumentation for the discharge tests. As shown, the method involves basically the James technique[2] for measuring total mass flow with twin cyclone separators for separation of steam and water. A 90° V-notch weir is used to measure the liquid flow rate, permitting steam quality and specific enthalpy to be calculated. A recovery tube is mounted on the wellhead to permit temperature and pressure profiles to be obtained and water samples to be gathered during quiescent and discharge periods.

Since the temperature of the reservoir in general exceeds 300°C (572°F) with a maximum recorded temperature of 358°C (676°F), no electronic equipment can survive the extreme conditions downhole. Therefore, Kuster Amerada RPG-3 Type subsurface recording temperature and pressure gauges were selected to provide all temperature and pressure measurements downhole.

DOWNHOLE FLOW CHARACTERISTICS

During January and March 1977, the flow tests consisted of a series of discharges in which the flow was throttled by placing orifice plates of various sizes in the discharge line. The results are summarized in Table 1. Pressure and temperature profiles taken during the throttled flow tests are shown in Figures 2 and 3. These profiles indicate that the fluid in the wellbore is at saturation conditions with a mixture of liquid and vapor flowing up to the wellhead. Since the steam quality at the wellhead is high and no steam/water interface is found in the wellbore, the conclusion is that flashing occurs in the formation rather than in the wellbore.

Examination of Figure 2 shows that the pressure profiles are essentially three constant slope lines meeting at the junction of the casing and the slotted liner and at approximately 4300 feet (1311 m). These constant pressure gradient

lines indicate that the major production zones may be near the bottomhole and in the vicinity of 4300 feet (1311 m).

ESSURE TRANSIENT TESTS

While data sufficient to assess a producible geothermal field can be obtained only from a number of properly-spaced wells, some limited reservoir information can be obtained from a single geothermal well by utilizing the theory developed for oil and gas fields.[3] These standard petroleum engineering techniques, however, assume single phase flow, while the flow in HGP-A is definitely two-phase, so that caution is required in interpreting the results of these analyses.

PRESSURE DRAWDOWN ANALYSIS

Wellhead pressure vs. time plotted on log-log scales for type-curve matching and on semi-log scales for a pressure drawdown analysis are shown in Figures 4 and 5, respectively. The initial pressure was obtained from Figure 6. These data can be used in a pressure drawdown analysis to obtain information about the geothermal reservoir and the following observations can be made:

1. The analysis is based on a constant production rate during the discharge, and this condition was impossible to achieve. In order to apply the theory, a normalized pressure was obtained by dividing the measured pressure by the concomitant production rate.

2. There was some overpressure at the wellhead prior to the start of the test. Consequently, opening the valve took some effort and about 2 to 3 minutes were needed to open the valve completely. Thus there is an uncertainty of that amount in the determination of zero time.

3. The theory is for bottomhole pressure whereas the data in Figures 4 and 5 are for wellhead pressure. Thus the assumption must be made that wellhead pressure is proportional to downhole pressure and the proportionality factor remains constant throughout the test.

Within these restrictions and assumptions, some information can be obtained. To normalize the pressure with respect to production the pressure relation can be written as:

$$\frac{p_i - p_{wf}}{q} = \frac{162.6\mu B}{kh}\left(\log_{10} t + \log_{10}\frac{k}{\phi\mu C_t r_w^2} - 3.23 + 0.87s\right) \quad (1)$$

The left side of equation (1) is a linear function of $\log_{10}t$ so that a plot of $\frac{p_i - p_{wf}}{q}$ vs. $\log_{10}t$ will yield a straight line with a slope, m, psi/bbl/day/cycle, where

$$|m| = \frac{162.6\mu B}{kh} \quad (2)$$

and this equation can be used to calculate the permeability-thickness, kh.

Equation (1) can also be used to calculate the skin effect factor, s. Letting p_{1hr} be the value of p_{wf} for t=1 hour on the correct semi-log straight line, equation (1) can be rearranged to yield

$$s = 1.15\left(\frac{\frac{p_i - p_{1hr}}{q}}{|m|} - \log_{10}\frac{k}{\phi\mu C_t r_w^2} + 3.23\right) \quad (3)$$

By using (3), the pressure drop due to the skin effect can be calculated from

$$\frac{\Delta p_s}{q} = 0.87\,|m|s \quad (4)$$

and the flow efficiency

$$FE = \frac{\frac{p_i - p_{wf} - \Delta p_s}{q}}{\frac{p_i - p_{wf}}{q}} \quad (5)$$

With the assumptions made previously, a log-log type-curve plot of $\frac{p_i - p_{wf}}{q}$ vs. t for the drawdown test is shown in Figure 4. The two unit-slope lines shown verify the existence of wellbore storage effects. From the end of the second straight line, it appears that the semi-log straight line or the radial flow period started at about 10 hours after the test was begun.

Figure 5 is a semi-log graph of $\frac{p_i - p_{wf}}{q}$ vs. $\log_{10}t$. An analysis of the plotted data shows that the permeability thickness

$$kh = \frac{162.6(24\text{ hr/day})(0.09\text{ cp})(1.5\text{ res bbl/std bbl})}{(350\text{ lb/bbl})(1.11\times10^{-3}\text{ psi/lb/hr/cycle})}$$

$$kh = 1356\text{ md-ft}\ \left(0.408\mu m^2 - m\right)$$

and if the thickness of the producing layer is assumed to be h = 1000 ft (305 m) then the permeability

$$k = 1.4\text{ md}\ \left(1.38\times10^{-3}\mu m^2\right)$$

The skin effect factor

$$s = 1.15\left[\frac{5.23\times10^{-3}}{1.11\times10^{-3}} - \log_{10}\frac{1.4}{(0.03)(0.09)\left(8\times10^{-6}\right)\left(\frac{8.755}{24}\right)^2} + 3.23\right]$$

$$= -0.86$$

The small negative skin effect factor suggests that skin damage is not present. Therefore, the flow efficiency of the well is approximately 1, or the well is discharging as much as it is able to produce.

Figure 7 shows the total mass flow rate vs. time in the drawdown test. Note that the flow rate did not change significantly after the initial five or six hours of flow. However if we neglect the fact that the flow is not constant and plot the wellhead pressure vs. time as in Figure 8 we would have obtained a slope

$$|m| = 11 \text{ psi/cycle } (76 \text{ kPa/cycle})$$

Assuming q = 86.00 Klb/hr (10.8 kg/s), one would have obtained

$$kh = \frac{162.6(86{,}000 \text{ lb/hr})(24 \text{ hr/day})}{(350 \text{ lb/bbl})} \cdot \frac{(0.09 \text{ cp})(1.5 \text{ res bbl/std bbl})}{(11 \text{ psi/cycle})}$$

$$= 11{,}200 \text{ md-ft } (3.37\mu m^2 - m)$$

which is one order of magnitude greater than the normalized value.

PRESSURE BUILDUP ANALYSIS

Following the December discharge, a pressure buildup test was conducted, with bottomhole pressure being measured using two Kuster KPG pressure elements and recorders in tandem to ensure that pressure data were acquired in spite of equipment malfunction because of the high temperature. Figure 9 is a log-log type curve of the difference between bottomhole pressures during static (no flow) and flow conditions. It shows two distinct wellbore storage effects; the top of the second wellbore storage interval is indicated by the arrow A. Arrow B indicates the onset of the radial flow period, roughly 70 hours after the well is shut in. From these curves, the product of permeability and production zone thickness (kh) is calculated to be approximately 880 millidarcy-feet ($0.265\mu m^2$ - m), with the pressure drop across the mud-damaged skin of the well being 560 psi (3861 kPa).

Bottomhole pressure measurements made after HGP-A was shut in following the January test produced data and plots similar to those for the December test. However, close examination of the data shows that two consecutive straight-line approximations may be made to the Horner plot (Figure 10). Interpretation of this occurrence is that there are at least two different production layers in the wellbore with different kh values. The same effect is also present in the December data, but until it was reproduced in the January test, little credence was given to it. The results of these analyses are summarized in Table 2.

DISCUSSION

From the above analyses, it appears that the Kapoho Geothermal Reservoir, where HGP-A is located, has a fairly tight formation with a permeability thickness of approximately 1000 millidarcy-feet ($0.301\mu m^2$ - m). During production, the HGP-A wellbore contains steam and water at saturation and flashing appears to occur in the formation. There are possibly two production layers, one at bottomhole and another at approximately 4300 ft (1311 m) from the wellhead. The buildup analyses show that HGP-A may have severe skin damage.

As stated before, one cannot obtain the characteristics of the Kapoho Geothermal Reservoir with only one producing well. Thus the above conclusions are preliminary and present the best estimates at this time. It is also evident that pressure buildup analyses are more reliable than the pressure drawdown analyses.

ACKNOWLEDGMENTS

The results reported were obtained with support from the U.S. Energy Research and Development Administration, the U.S. Department of Energy, the State of Hawaii, and the County of Hawaii.

Special thanks are due to Dr. Henry J. Ramey, Jr., who has encouraged us in conducting the tests and analyses.

NOMENCLATURE

P_i = initial pressure, psi (kPa)
P_{wf} = flowing pressure, psi (kPa)
P_{wh} = wellhead pressure, psi (kPa)
P_{ws} = shut in pressure, psi (kPa)
q = production rate, std bbl/day (m^3/day)
μ = viscosity, cp (Pa·s)
B = formation volume factor, res vol/std vol
k = permeability, md (μm^2)
h = formation thickness, ft (m)
t = time, hr (hr)
ϕ = fractional porosity
C_t = total system effective isothermal compressibility, psi^{-1} (kPa^{-1})
r_w = well radius, ft (m)
s = skin effect factor

REFERENCES

1. Kingston, Reynolds, Thom and Allardice, Ltd.: "Hawaii Geothermal Project Well Completion Report, HGP-A", (September 1976).

2. James, R.: "Measurement of Steam-Water Mixtures Discharging at the Speed of Sound to the Atmosphere", New Zealand Engineering, October 1966, pp. 437-441.

3. Ramey, H.J., Jr.: "Practical Use of Modern Well Test Analysis", presented at the 46th Annual California Regional Meeting of the Society of Petroleum Engineering of AIME (April 1976).

TABLE 1

PRELIMINARY THROTTLED FLOW DATA

Orifice Size (Inches)	(mm)	Total Mass Flow Rate (Klb/hr)	(kg/s)	Steam Flow Rate (Klb/hr)	(kg/s)	Steam Quality (%)	Wellhead Pressure (psig)	(kPa)	Wellhead Temp. (°F)	(°C)
8	(203)	101	(12.7)	64	(8.1)	64	51	(352)	295	(164)
6	(152)	99	(12.5)	65	(8.2)	66	54	(372)	300	(167)
4	(102)	93	(11.7)	57	(7.2)	64	100	(689)	338	(188)
3	(76)	89	(11.2)	54	(6.8)	60	165	(1138)	372	(207)
2-1/2	(64)	84	(10.6)	48	(6.1)	57	237	(1634)	401	(223)
2	(51)	81	(10.2)	43	(5.4)	53	293	(2020)	419	(233)
1-3/4	(45)	76	(9.6)	39	(4.9)	52	375	(2585)	439	(244)

TABLE 2

COMPARISON OF PRESSURE DRAWDOWN AND BUILDUP TESTS

	Constant Production Drawdown	December Buildup One Layer	December Buildup Two Layer	January Buildup Two Layer
Permeability thickness, kh, md-ft (μm^2 - m)	1356 (0.408)	880 (0.265)	1553 (0.467)	1089 (0.328)
Apparent skin factor, s	-0.86	4.3	14.8	4.3
Pressure drop across skin, psi (kPa)	---	561 (3868)	1098 (7570)	575 (3964)
Flow efficiency	1	0.65	0.38	0.60

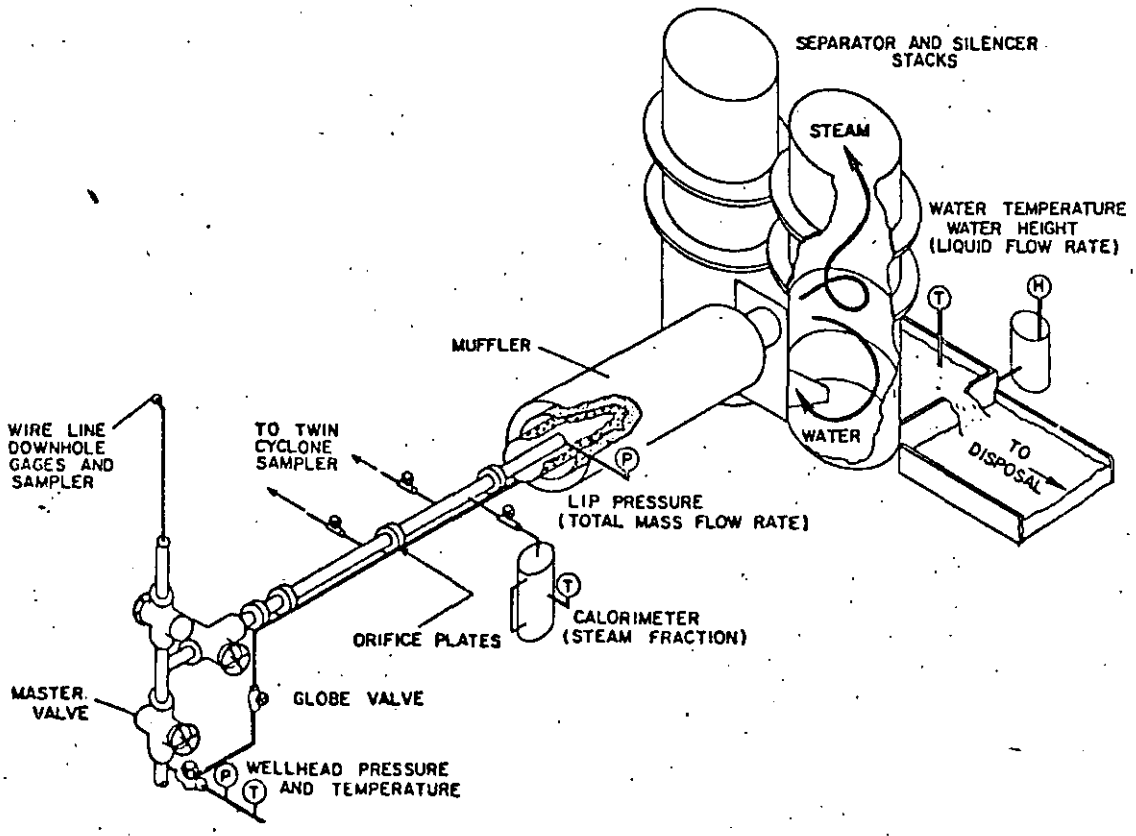

Fig. 1 - Flow test equipment and instrumentation.

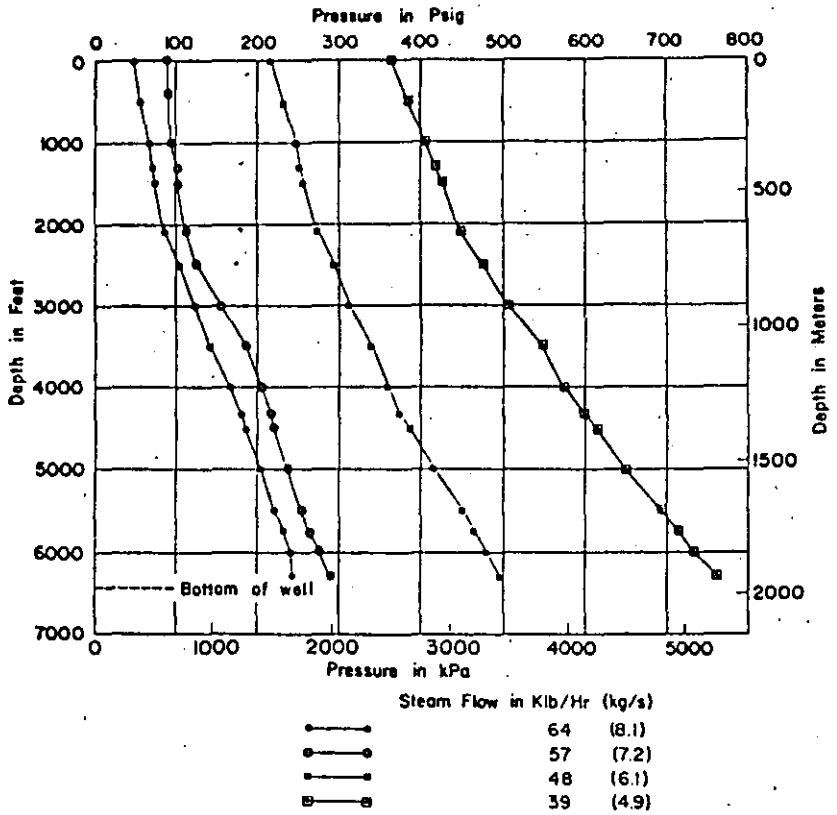

Fig. 2 - Pressure profiles for HGP-A.

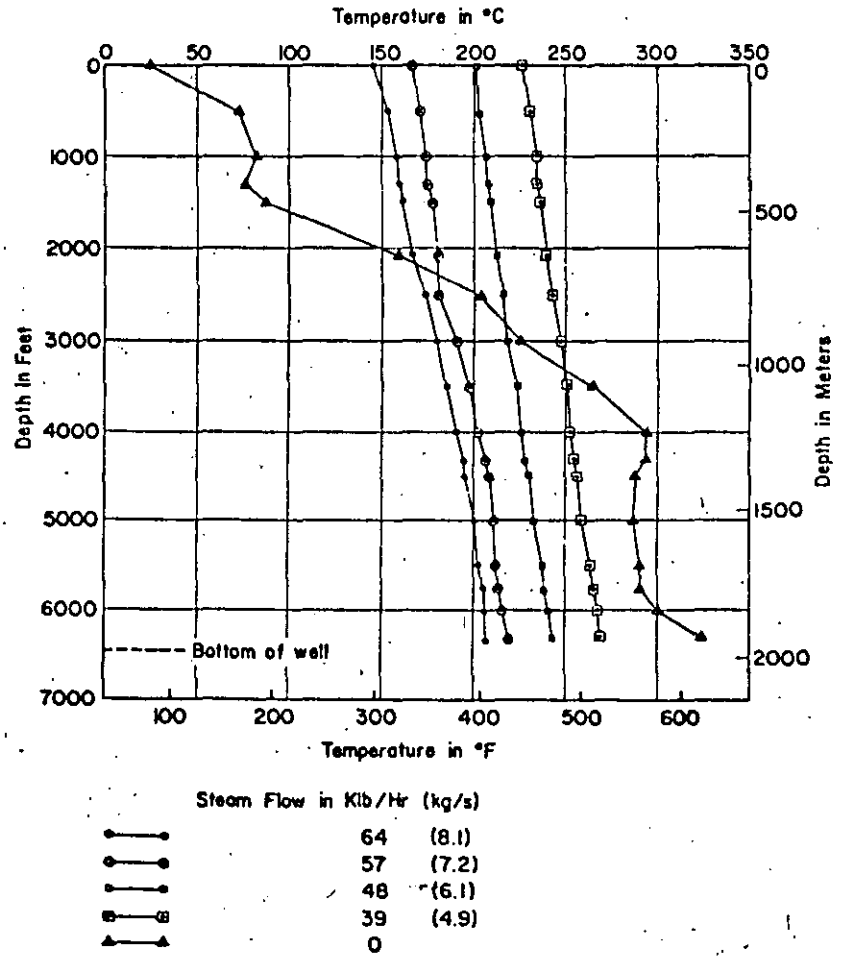

Fig. 3 - Temperature profiles for HGP-A.

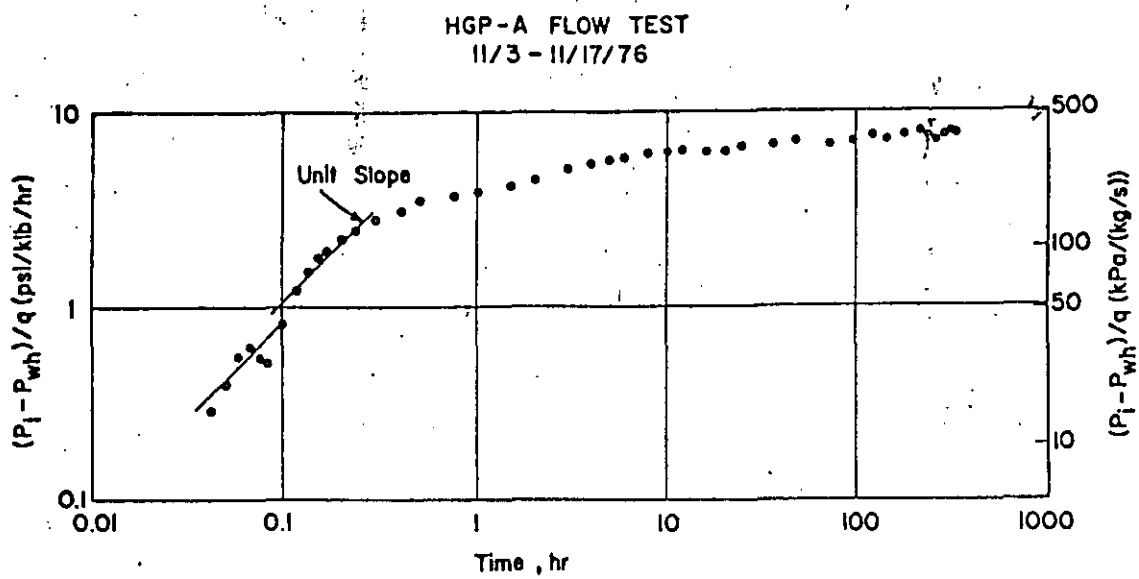

Fig. 4 - Log-log plot of November 1976 discharge test data.

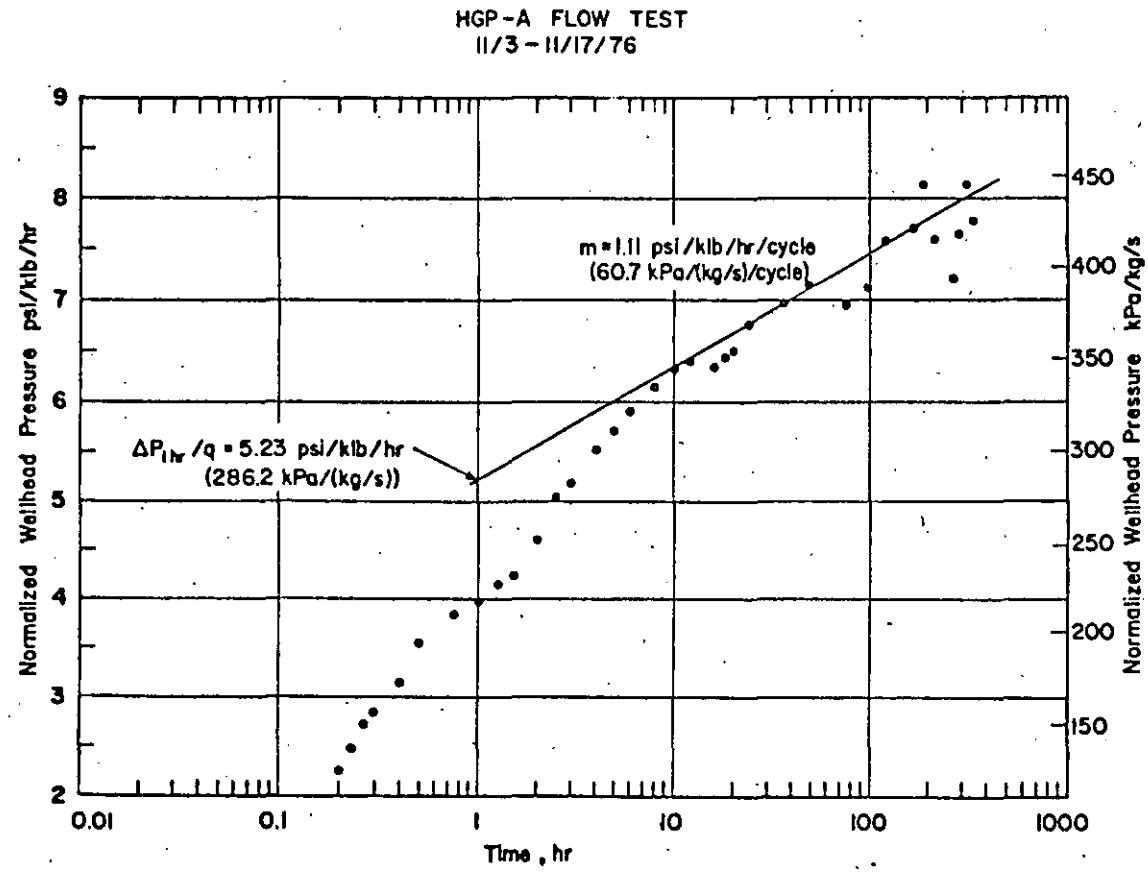

Fig. 5 - Semi-log plot of November 1976 discharge test data.

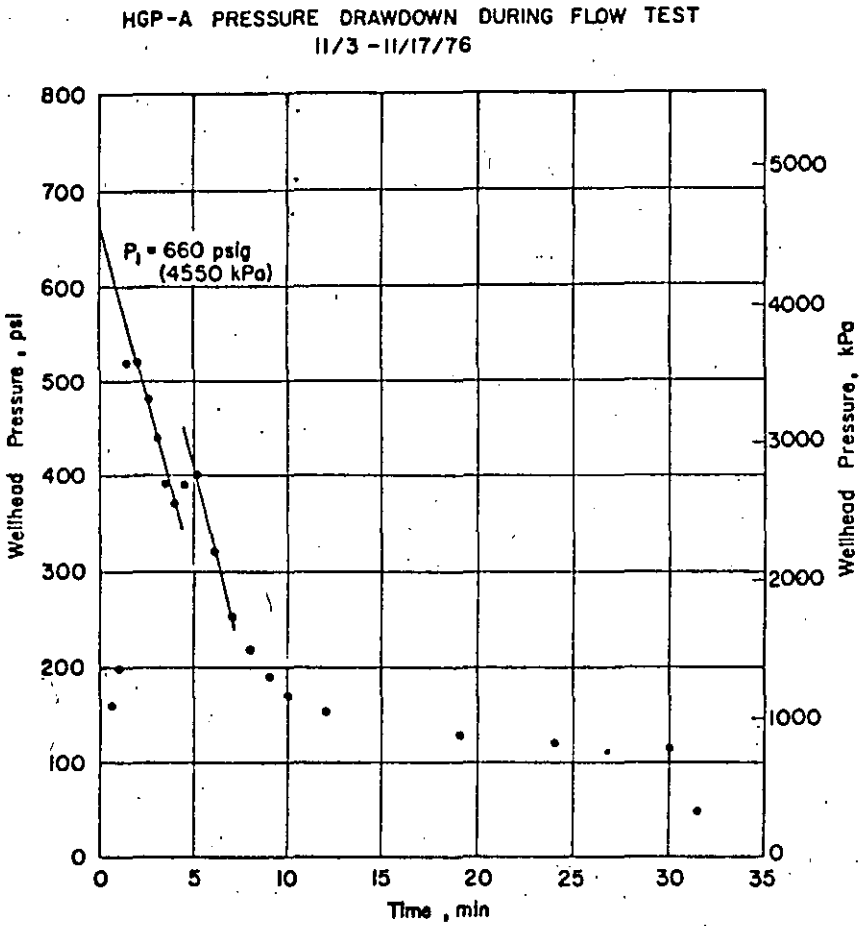

Fig. 6 - Linear plot of initial data for November 1976 discharge test.

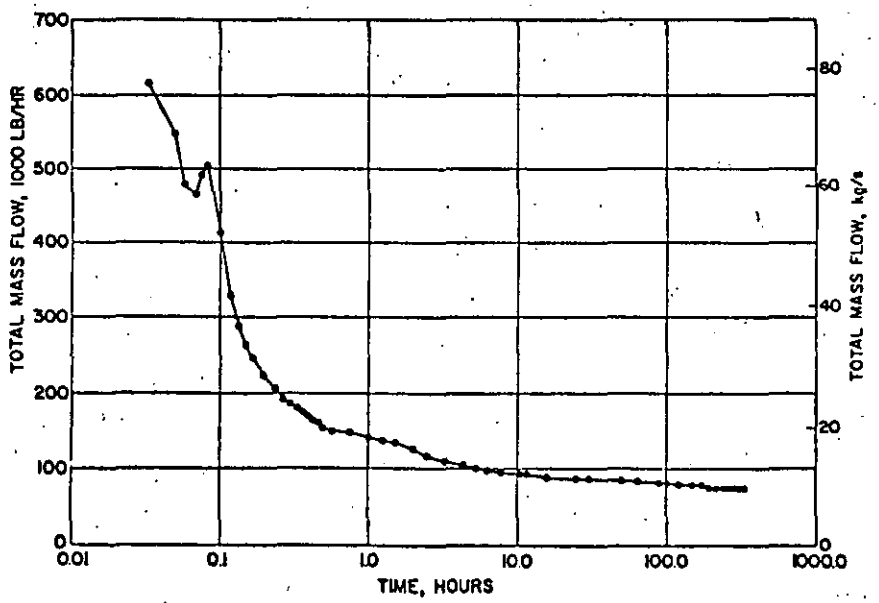

Fig. 7 - Total mass flow as a function of time.

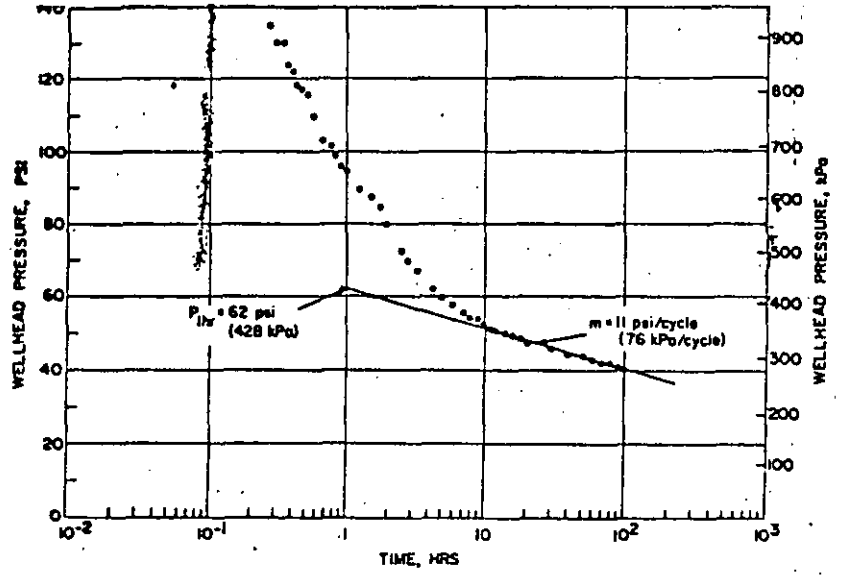

Fig. 8 - Wellhead pressure as a function of time.

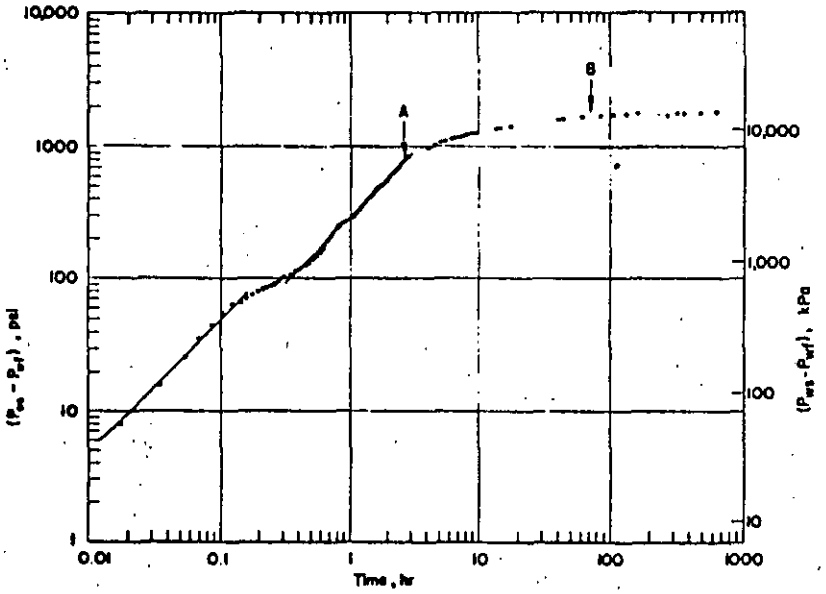

Fig. 9 - Log-log plot of December 1976 buildup test data.

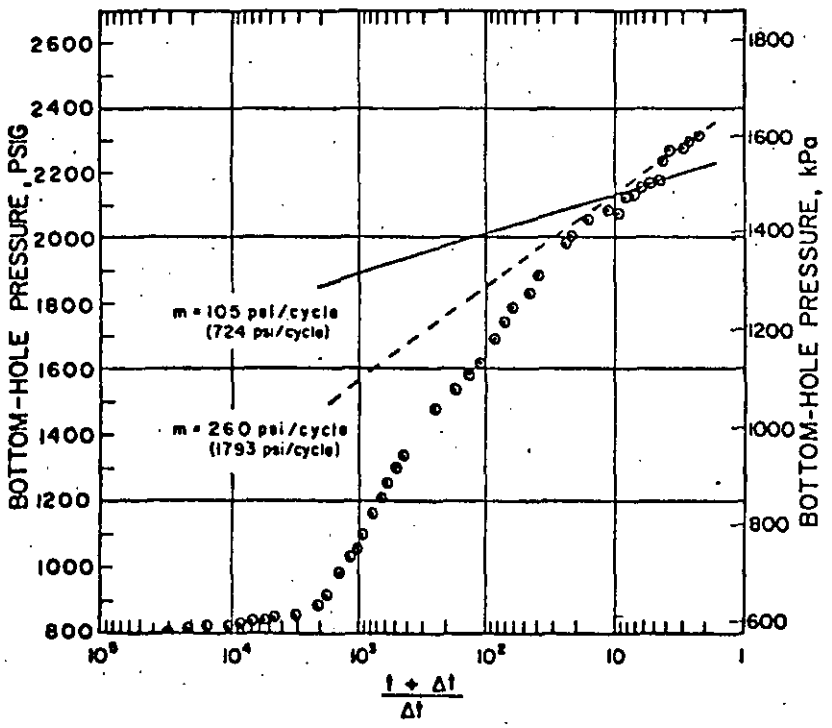

Fig. 10 - Semi-log plot of January/February 1977 buildup test data.

SPE
Society of Petroleum Engineers of AIME

PE 7479

PRESSURE TRANSIENT ANALYSIS FOR TWO-PHASE (LIQUID WATER/STEAM) GEOTHERMAL RESERVOIRS

by S. K. Garg, Systems, Science and Software

This paper was presented at the 53rd Annual Fall Technical Conference and Exhibition of the Society of Petroleum Engineers of AIME, held in Houston, Texas, Oct. 1-3, 1978. The material is subject to correction by the author. Permission to copy is restricted to an abstract of not more than 300 words. Write: 6200 N. Central Expy., Dallas, Texas 75206.

ABSTRACT

A new diffusivity equation for two-phase (liquid water/steam) flow in geothermal reservoirs is derived. The geothermal reservoir may either be initially two-phase or may evolve into a two-phase system during production. Solutions of the diffusivity equation for a continuous line source are presented; the solutions imply that the plot of bottomhole pressure versus $\log_{10}t$ (t = time) should be a straight line. The slope of the straight line is inversely proportional to the total kinematic mobility (defined in the text). Comparison of the theory with a limited number of computer simulated drawdown histories shows excellent agreement.

INTRODUCTION

In petroleum engineering and groundwater hydrology, well tests are routinely conducted to diagnose the well's condition and to estimate formation properties. Analysis of well test data may be made to yield quantitative information regarding (1) formation permeability, storativity and porosity, (2) the presence of barriers and leaky boundaries, (3) the condition of the well (i.e., damaged or stimulated), (4) the presence of major fractures close to the well, and (5) the mean formation pressure. Well testing procedures (and the quality of information obtained) depend on the age of the well. During temporary completion, testing involves producing the reservoir using a temporary plumbing system (e.g., Drill Stem Testing); and the estimates obtained for the formation parameters are not very accurate. After completion, testing is usually performed in the hydraulic mode. In hydraulic testing, one or more wells are produced at controlled rates and changes in pressure within the producing well itself or nearby observation wells (interference tests) are monitored.

A major concern of well testing is the interpretation of pressure transient data. Much of the existing literature (see Matthews and Russell[1] and Ramey[2] for reviews) deals with isothermal single-phase (water/oil) and isothermal two-phase (oil with gas in solution, free gas) systems. There is, in general, a lack of a methodology for the analysis of nonisothermal reservoir systems, either single or two-phase (liquid water/steam). Geothermal reservoirs commonly involve nonisothermal two-phase (water/steam) flow during well testing. In this paper, we present a theoretical framework for analyzing multiphase pressure transient data in geothermal systems.

References and illustrations at end of paper.

TWO-PHASE (LIQUID WATER/STEAM) FLOW IN GEOTHERMAL SYSTEMS

We consider a fully penetrating well located in an infinite reservoir of thickness H. We will neglect any variations in either formation or fluid properties in the vertical direction (this is a common assumption in pressure transient analysis). The geothermal system may either be two-phase prior to production, or may evolve into a two-phase system as a result of fluid production. In the latter case, a boiling front will propagate outwards from the wellbore. The boiling front may be treated as a constant pressure boundary (p=saturation pressure corresponding to the local reservoir temperature).

For the sake of simplicity, let us consider a reservoir which is initially two-phase everywhere. Furthermore, it is convenient to assume that the pressure (and hence temperature) is uniform throughout the system. In radial geometry, the pressure response is governed by the following diffusivity equation (see Appendix for a derivation of equation (1)):

$$\frac{\partial p}{\partial t} - \frac{(k/\nu)_T}{\phi \rho\, C_T}\left[\frac{1}{r}\frac{\partial p}{\partial r} + \frac{\partial^2 p}{\partial r^2}\right] = 0 \quad \ldots\ldots \quad (1)$$

We are interested in solutions of equation (1) for the case of flow into a centrally located well at a constant mass rate of production M. Mathematically, we have at $r = r_w$

$$r \left.\frac{\partial p}{\partial r}\right|_{r=r_w} = - \frac{M}{2\pi H\, (k/\nu)_T} \quad \ldots\ldots \quad (2)$$

For the sake of mathematical convenience, the boundary condition at $r=r_w$ is replaced by the "line source"

approximation, i.e.,

$$\lim_{r\to 0} r\frac{\partial p}{\partial r} = -\frac{M}{2\pi H}(k/\nu)_T \quad \ldots\ldots\ldots \quad (3)$$

The "line source" boundary condition yields identical results (from a practical viewpoint) with those obtained with the original condition.[1,3] We also require that initially (t=0) the reservoir is at a uniform pressure p_i, and that at r=∞ (for all t) we have

$$\lim_{r\to\infty} p(r,t) = p_i \quad \ldots\ldots\ldots\ldots\ldots \quad (4)$$

The solution for equation (1) subject to the boundary conditions (3) and (4) can be written as follows[4]

$$p(r,t) = p_i + \frac{M}{4\pi H\,(k/\nu)_T}\,Ei\left\{-\frac{r^2}{4t}\frac{\phi\rho\,C_T}{(k/\nu)_T}\right\} . \quad (5)$$

Equation (5) implies that the pressure at the wellbottom $p_w(t)$ is

$$p_w(t) = p_i + \frac{M}{4\pi H\,(k/\nu)_T}\,Ei\left[-\frac{r_w^2}{4t}\frac{\phi\rho\,C_T}{(k/\nu)_T}\right] . \quad (6)$$

For $[4t\,(k/\nu)_T/\phi r_w^2\,\rho\,C_T] > 100$, equation (6) yields the approximate solution:[1]

$$p_w(t) = p_i - \frac{1.15\,M}{2\pi H\,(k/\nu)_T}\left\{\log_{10}\left[\frac{t\,(k/\nu)_T}{\phi r_w^2\rho\,C_T}\right] + 0.351\right\} \quad \ldots\ldots\ldots\ldots \quad (7)$$

Equation (7) implies that a plot of p_w versus $\log_{10}t$ should be a straight line. Let m be the slope of this straight line; then we have

$$(k/\nu)_T = \frac{1.15\,M}{2\pi H\,m} \quad \ldots\ldots\ldots\ldots \quad (8)$$

Substituting from equation (8) into equation (7), we obtain for compressibility C_T

$$\frac{1}{C_T} = \frac{\phi r_w^2\rho}{t(k/\nu)_T}\,\text{Antilog}_{10}\left[\frac{p_i - p_w(t)}{m} - 0.351\right] . \quad (9)$$

PROPAGATING FLASH-FRONT

Theoretical considerations for the case when a flash front propagates into an initially single-phase reservoir are much more complex than those outlined above for the purely two-phase case. In this instance, the reservoir is two-phase for r < R (R = R(t) denotes the location of the flash-front) and is single phase for r > R. The flow behavior in these two regimes is governed by

$$\frac{\partial p_j}{\partial t} - \left[\frac{(k/\nu)_T}{\phi\rho\,C_T}\right]_j \frac{1}{r}\frac{\partial}{\partial r}\left[r\frac{\partial p_j}{\partial r}\right] = 0 \quad \ldots\ldots \quad (10)$$

where j=1 and 2 denote the two-phase and single-phase regions, respectively. The definitions for the various quantities in equation (10) for the two-phase region (j=1) have already been given. In the single-phase region (j=2), we have:

$$[(k/\nu)_T]_2 = k\rho_\ell/\mu_\ell$$

$$\rho_2 = \rho_\ell$$

$$(C_T)_2 = ((1-\phi)/\phi)\,C_m + C_f$$

Note that with the above definitions, equation (10) (in the single-phase region) reduces to the usual diffusivity equation for the isothermal flow of a liquid of small and constant compressibility.

We will assume that the reservoir is initially at a uniform pressure p_i and temperature T_i. We will, furthermore, require the fluid flow to be isothermal in the single-phase region (r > R); in practice, this implies no severe restriction as temperature changes in single-phase flow are usually very small. The boundary conditions at the wellbore and at infinity are:

$$\lim_{r\to 0} r\frac{\partial p_1}{\partial r} = -\frac{M}{2\pi H\,[(k/\nu)_T]_1} \quad \ldots\ldots\ldots \quad (11a)$$

$$\lim_{r\to\infty} p_2(r,t) = p_i \quad \ldots\ldots\ldots \quad (11b)$$

In addition to the boundary conditions (11), we need to satisfy continuity conditions on mass flow and pressure at the flash-front (r=R). Mathematically, we have at r=R:

$$\left[(k/\nu)_T\frac{\partial p}{\partial r}\right]_1 = \left[(k/\nu)_T\frac{\partial p}{\partial r}\right]_2 \quad \ldots\ldots\ldots \quad (12a)$$

$$p_1 = p_2 = p_s(T_i) \quad \ldots\ldots\ldots \quad (12b)$$

To develop a solution for equations (10) subject to the boundary conditions (11) and (12), we note that these equations are similar to the equations for melting and freezing with cylindrical symmetry presented by Carslaw and Jaeger.[4] The solution for the present case can, therefore, be obtained by following the general approach of Carslaw and Jaeger. We have thus:

$$0 < r < R: \quad p = p_s + \frac{M}{4\pi H\,[(k/\nu)_T]_1}\left[Ei\left(-\frac{r^2}{4t}\left[\frac{\phi\rho\,C_T}{(k/\nu)_T}\right]_1\right) - Ei\,(-\lambda^2)\right] \quad \ldots\ldots \quad (13a)$$

$$r > R: \quad p = p_i + \frac{p_s - p_i}{Ei\left(-\lambda^2\left[(k/\nu)_T/\phi\rho C_T\right]_1/\left[(k/\nu)_T/\phi\rho C_T\right]_2\right)} \times Ei\left(-\frac{r^2}{4t}\left[\frac{\phi\rho\,C_T}{(k/\nu)_T}\right]_2\right) \quad \ldots\ldots\ldots \quad (13b)$$

where

$$R = 2\lambda \left[\left\{ \frac{(k/\nu)_T}{\phi\rho\, C_T} \right\}_1 t \right]^{1/2} \quad \ldots\ldots\ldots \quad (13c)$$

and λ is the root of

$$[(k/\nu)_T]_2 \frac{p_s - p_i}{Ei\left(-\lambda^2 \left\{(k/\nu)_T/\phi\rho C_T\right\}_1 / \left\{(k/\nu)_T/\phi\rho C_T\right\}_2\right)} \times \exp\left(-\lambda^2 \left\{(k/\nu)_T/\phi\rho C_T\right\}_1 / \left\{(k/\nu)_T/\phi\rho C_T\right\}_2\right) = \frac{M}{4\pi H} \exp(-\lambda^2) \quad \ldots\ldots\ldots \quad (13d)$$

Equation (13a) yields the following expression for well-bottom pressure $p_w(t)$

$$p_w(t) = p_s + \frac{M}{4\pi H [(k/\nu)_T]_1} \left[Ei\left(-\frac{r_w^2}{4t} \left[\frac{\phi\rho\, C_T}{(k/\nu)_T} \right]_1 \right) - Ei(-\lambda^2) \right] \quad \ldots\ldots\ldots\ldots \quad (14)$$

For $4t\,[(k/\nu)_T]_1/r_w^2[\phi\rho C_T]_1 > 100$, equation (14) can be approximated as follows:

$$p_w(t) = p_s - \frac{M\, Ei(-\lambda^2)}{4\pi H [(k/\nu)_T]_1} - \frac{1.15\, M}{2\pi H [(k/\nu)_T]_1} \left\{ \log_{10}\left[t \frac{[(k/\nu)_T]_1}{r_w^2 (\phi\rho C_T)_1} \right] + 0.351 \right\} \quad \ldots\ldots\ldots\ldots\ldots\ldots \quad (15)$$

Equation (15), like equation (7), implies that a plot of p_w versus $\log_{10} t$ should be a straight line and that $[(k/\nu)_T]_1$ is given by equation (8).

NUMERICAL RESULTS

In order to test the validity of the preceding theory, the Systems, Science and Software (S^3) reservoir simulator MUSHRM[5] was exercised in one-dimensional radial configuration to generate a series of drawdown histories. All of the cases described below were simulated using a 50 zone ($\Delta r_1 = \Delta r_2 = \ldots = \Delta r_{11} = 1$m (3.281 feet); $\Delta r_{12} = 1.2\,\Delta r_{11}$, $\Delta r_{13} = 1.2\,\Delta r_{12}$, ..., $\Delta r_{50} = 1.2\,\Delta r_{49}$) radial grid.

The reservoir rock is assumed to be a sandstone with the following properties (unless otherwise indicated):

$\rho_R = 2.65\ 10^3$ kg/m^3 (165.4 lbm/ft^3)

$\phi = 0.2$

$C_m = 0$ MPa^{-1} (0 psi^{-1})

$K_R = 5.25$ W/m.K (3.03 Btu/h.ft^2.°F/ft)

$C_R = 1$ kJ/kg.K (0.239 Btu/lbm °F)

$k = 0.1\ \mu m^2$ ($\sim$ 0.1 darcy)

$S_{\ell r} = 0.3$

$S_{gr} = 0.05$.

Relative permeabilities R_ℓ and R_g are represented by the Corey equations and the mixture (rock-liquid-vapor) thermal conductivity is approximated by Budiansky's formula.[5] The mass withdrawal rate is assumed to be 0.14 kg/s.m (0.094 lbm/s.ft.).

In the numerical examples discussed here, the effect of mass withdrawal is represented by a volumetric sink term in the well-block (radial extent r = 0 to $r = \Delta r_1$). For purposes of comparison with the analytical results presented earlier, it is necessary to define an equivalent radius r_w at which the calculated well-block pressure is equal to the actual flowing pressure due to a continuous line source/sink.

In the numerical simulation of reservoir behavior, it is often necessary to employ well-blocks (i.e., a grid block containing a well) with dimensions much larger than the wellbore radius. Naturally, the pressure calculated for the well-block will be, in general, different from the actual flowing bottomhole pressure. Van Poolen, et al.[6] stated that the calculated pressure for a well-block should be the average pressure in the portion of the reservoir represented by the block. Assuming steady-state single-phase flow in the well-block (but not in the reservoir as a whole), this implies that the calculated well-block pressure should be equal to the actual flowing pressure at a radius r_w,

$$\ell n \frac{r_w}{r_0} = \frac{R^2\, \ell n\,(R/r_0)}{R^2 - r_0^2} - \frac{1}{2} \quad \ldots\ldots\ldots \quad (16a)$$

where r_0 is the actual well radius and R is the radius of the grid block. For $R \gg r_0$, equation (16a) simplifies to

$$r_w = R \exp(-1/2) \quad \ldots\ldots\ldots\ldots \quad (16b)$$

$$\sim 0.6065\ R$$

Equations (16a) and (16b), strictly speaking, hold only for a well located in the center of a radial grid block. For rectangular grid blocks (with dimensions Δx, Δy), equation (16b) is usually replaced by the following expression

$$\frac{r_w}{\sqrt{\Delta x\, \Delta y}} = \frac{0.6065}{\sqrt{\pi}} \quad \ldots\ldots\ldots\ldots \quad (17)$$

Assuming $\Delta x = \Delta y$, equation (17) yields

$\frac{r_w}{\Delta x} = 0.342$.

Peaceman[7] examined the grid pressures obtained in the numerical solution of steady incompressible single-phase flow into a single well located in the center of a square grid block ($\Delta x = \Delta y$) and concluded that the well-block pressure should be equal to the actual flowing pressure at a radius of 0.2 Δx (and not at the radius given by equation (17)).

In an attempt to evaluate the significance of Peaceman's results for numerical simulation, Garg, et al.[8] analyzed the numerical solution of steady incompressible single-phase flow into a single well located in both radial and rectangular grid blocks. It is found that the equivalent radius depends, among other things, on the shape of the grid block (radial or rectangular) and the type of mesh (uniform or stretch) employed. Thus, for example, use of uniform radial mesh yields $r_w/R \simeq 0.5615$ in the limit $N \to \infty$; where N denotes the number of grid blocks.

Garg, et al.[8] also compared the numerical solution for transient, slightly compressible (water) single-phase flow into a single well with the line-source solution for the diffusivity equation (see, e.g., Matthews and Russell[1]). It was concluded that the equivalent radius (i.e., the radius at which the actual flowing pressure is equal to the calculated well-block pressure) is approximated by 0.56 R. In this work, we will, therefore, assume that r_w in transient single-phase flow (and also approximately in transient two-phase flow) is given by 0.56 R.

Figures 2-5 show five examples for the case when the reservoir initially boiling everywhere was produced at a constant rate. As can be seen, the drawdown data closely fit a straight line; furthermore, the values of $(k/\nu)_T$ computed from the slope of the straight line are in excellent agreement with the actual values in the well-blocks (see Tables 1-5 for the actual values). Note that the actual values (Tables 1-5) vary over a range; this variation is the result of slow changes (except at very early times not considered in drawing the straight line) in steam saturation in the computational well-block as a result of continued production. Figure 3 (drawdown history c) and Table 3 present an especially interesting case; in this case the liquid, initially immobile, becomes mobile for $t > \sim 2\ 10^5$s due to condensation in the well-block. The condensation is caused by a drop in pressure (and hence temperature); in drawing the straight line the pressure data for $t > \sim 2\ 10^5$s was ignored. If the computation had been carried for times sufficiently greater than $t > 2\ 10^5$s, one would see another straight line segment (with a different slope).

Table 6 compares the compressibility C_T values inferred from the slope of the straight line and equation (9) with the actual values. The agreement is quite good for Cases b, c and d. In Cases a and e, the inferred values are quite a bit larger than the actual values; this disagreement is not really surprising in view of the extremely large changes in $(k/\nu)_T$ t very early times (see Tables 1 and 5). Large values of $(k/\nu)_T$ at very early times lead to relatively small pressure drops compared to those implied by the straight line. Stated somewhat differently, at early times, equation (7) with constant $(k/\nu)_T$ cannot be used to calculate the well-block pressure in Cases a and e.

Figures 6 and 7 show two additional drawdown histories generated by MUSHRM. In these examples, the reservoir was initially single-phase (liquid) everywhere. In the case shown in Figure 6, a flash-front starts propagating outward from the wellbore at $t \sim 0$; it takes, however a finite time for conditions to stabilize in the two-phase region. For $t > 5\ 10^3$s the data lie on a straight line; and the kinematic mobility calculated from the slope of this straight line agrees quite well with the actual range of values. Figure 7 presents a more interesting case; in this instance the liquid water does not start flashing at the instant the production starts. Thus, we have a short time of single-phase flow followed by a propagating flash-front. The two-phase part of the drawdown curve has a relatively long flat part; this part of the curve is associated with boiling only in the computational well-block. Since the flow behavior in the two-phase region is primarily governed by the location of the flash-front, it follows that a failure to adequately resolve the location of the flash-front in numerical simulations (as it happens when the two-phase flow is restricted to one or two computational zones) would lead to physically meaningless results. In other words, the flat part of the curve in Figure 7 is a purely numerical phenomenon and has no physical significance. A straight line is again seen to fit the late-time data; once again the computed value of $(k/\nu)_T$ is in good agreement with the actual range of values. We have also examined the numerical solutions (Figures 6 and 7) for flash-front velocities; the flash-front position, as a function of time is given by (within numerical precision) $R(t) = A\ t^{1/2}$ where A is constant. The latter observation is in agreement with equation (13c).

CONCLUDING REMARKS

The analytical solutions for two-phase flow discussed in the preceding sections provide a potentially powerful tool for the analysis of pressure transient data from multiphase geothermal systems. Determination of the total kinematic mobility only requires the measurement of mass flow rate M and the bottomhole pressures p_w. The mass flow rate M can be measured at the well-head provided there is no loss of the produced fluid to the non-producing formations as the fluid travels through the wellbore to the well-head. Practical techniques exist for measuring the needed variables. It should be noted that the present analysis does not require separate measurements for liquid and vapor phase mass flow rates. Such data, if available, may be combined with the analysis of the preceding sections to yield additional information regarding relative permeabilities, etc.

NOMENCLATURE

C_f = isothermal liquid compressibility

C_m = formation compressibility

C_R = heat capacity of the rock matrix

C_T = total compressibility, equation (A.12b)

h = enthalpy of liquid/vapor mixture

$= (1-Q)\ h_\ell + Q\ h_g$

$h_\ell (h_g)$ = liquid (vapor) enthalpy

$h_{g\ell}$ = heat of vaporization = $h_g - h_\ell$

h_R = enthalpy of rock matrix

H = formation thickness

k = absolute permeability

K_R = thermal conductivity of the rock grain

m = slope of p_w versus $\log_{10} t$ straight line

M = mass production rate

p = pressure

p_i = initial reservoir pressure

$p_s(T_i)$ = saturation pressure at $T = T_i$

p_w = well-bottom pressure

Q = steam quality = $S \rho_g/\rho$

r = radius

r_w = wellbore radius

$R(t)$ = instantaneous position of the flash-front

$R_\ell(R_g)$ = relative liquid (vapor) permeability

S = vapor volume fraction

$S_{\ell r}(S_{gr})$ = residual liquid (vapor) saturation

t = time

$(k/\nu)_g$ = kinematic mobility for the vapor = $k R_g \rho_g/\mu_g$

$(k/\nu)_\ell$ = kinematic mobility for the liquid = $k R_\ell \rho_\ell/\mu_\ell$

$(k/\nu)_T$ = total kinematic mobility = $(k/\nu)_\ell + (k/\nu)_g$

$\mu_\ell(\mu_g)$ = liquid (vapor) dynamic viscosity

ρ = mixture (liquid and vapor) density = $(1-S)\rho_\ell + S\rho_g$

$\rho_\ell(\rho_g)$ = liquid (vapor) density

ρ_R = rock grain density

ϕ = porosity

ACKNOWLEDGMENTS

This work was performed under Systems, Science and Software IR&D research project No. 93102-06. I would like to thank my colleagues Dr. T. R. Blake, Mr. J. W. Pritchett, Dr. M. H. Rice and Dr. T. D. Riney for many helpful discussions.

REFERENCES

1. Matthews, C. S. and Russell, D. G.: Pressure Buildup and Flow Tests in Wells, Society of Petroleum Engineers of AIME, Monograph No. 1, Dallas, Texas (1967).

2. Ramey, H. J., Jr.: "Pressure Transient Analysis for Geothermal Wells", Proceedings Second United Nations Symposium on the Development and Use of Geothermal Resources, San Francisco, California, Volume 3 (May 1975), 1749-1757.

3. Mueller, T. D. and Witherspoon, P. A.: "Pressure Interference Effects within Reservoirs and Aquifers", Journal of Petroleum Technology (April 1965), 471-474.

4. Carslaw, H. S. and Jaeger, J. C.: Conduction of Heat in Solids, Oxford University Press, London, 2nd Edition (1959), 294-296.

5. Garg, S. K., Pritchett, J. W., Rice, M. H. and Riney, T. D.: "U.S. Gulf Coast Geopressured Geothermal Reservoir Simulation", Systems, Science and Software, La Jolla, California, Report SSS-R-77-3147 (1977).

6. Van Poolen, H. K., Breitenbach, E. A. and Thurnau, D. H.: "Treatment of Individual Wells and Grids in Reservoir Modeling", Journal of Petroleum Technology (December 1968), 341-346.

7. Peaceman, D. W.: "Interpretation of Well-Block Pressures in Numerical Reservoir Simulation", paper SPE 6893 presented at Society of Petroleum Engineers 52nd Annual Fall Meeting, Denver, Colorado, October 9-12, 1977.

8. Garg, S. K., Pritchett, J. W., Brownell, D. H., Jr. and Riney, T. D.: "U.S. Gulf Coast Geopressured Geothermal Reservoir Simulation - Year 2", Systems, Science and Software, La Jolla, California, Report SSS-R-78-3639 (1978).

9. Donaldson, I. G.: "The Flow of Steam Water Mixtures through Permeable Beds: A Simple Simulation of a Natural Undisturbed Hydrothermal Region", New Zealand Journal of Science, Volume 11 (1968), 3-23.

10. Mercer, J. W., Jr., Faust, C. and Pinder, G. F.: "Geothermal Reservoir Simulation", Proceedings NSF/RANN Conference on Research for the Development of Geothermal Energy Resources, Jet Propulsion Laboratory/California Institute of Technology, Pasadena, California (1974), 256-267.

11. Brownell, D. H., Jr., Garg, S. K. and Pritchett, J. W.: "Governing Equations for Geothermal Reservoirs", Water Resources Research, Volume 13 (1977), 929-934.

12. Garg, S. K. and Pritchett, J. W.: "On Pressure-Work, Viscous Dissipation and the Energy Balance Relation for Geothermal Reservoirs", Advances in Water Resources, Volume 1 (1977), 41-47.

13. Moench, A. F. and Atkinson, P. G.: "Transient Pressure Analysis in Geothermal Steam Reservoirs with an Immobile Vaporizing Liquid Phase - Summary Report", Proceedings Third Stanford Workshop on Geothermal Reservoir Engineering, Stanford, California (1977), 64-69.

APPENDIX: DERIVATION OF DIFFUSIVITY EQUATION FOR TWO-PHASE (LIQUID WATER/STEAM) FLOW IN POROUS MEDIA

The balance equations for two-phase flow in porous media have previously been discussed by Donaldson,[9] Mercer, et al.,[10] Brownell, et al.[11] and Garg and Pritchett.[12] For the present application, the most general form of the balance laws will not be required. In particular, we will assume that (1) the rock porosity depends only upon the fluid pressure, (2) the rock matrix, the liquid and the vapor are in local thermal equilibrium and that heat conduction is negligible, (3) the liquid and the vapor are in local pressure equilibrium such that the capillary pressure is negligible, and (4) the fluid flow is governed by Darcy's law. The second assumption implies that we need consider only the mixture (rock, liquid, vapor) energy balance.

With these assumptions, the balance equations for mass and energy in radial geometry can be written as follows[12]

Mass (Liquid and Vapor)

$$\frac{\partial}{\partial t}(\phi\rho) - \frac{1}{r}\frac{\partial}{\partial r} r\left[(k/\nu)_T \frac{\partial p}{\partial r}\right] = 0 \quad \ldots \quad (A.1)$$

Energy (Rock, Liquid and Vapor)

$$\frac{\partial}{\partial t}[(1-\phi)\rho_R h_R + \phi\rho h - \phi p] - \frac{1}{r}\frac{\partial}{\partial r}\left\{r[(k/\nu)_\ell h_\ell + (k/\nu)_g h_g]\frac{\partial p}{\partial r}\right\} = 0 \quad \ldots \quad (A.2)$$

The first term in equation (A.1) can be expanded and rewritten in the following form:

$$\frac{\partial}{\partial t}(\phi\rho) = \rho\frac{\partial\phi}{\partial t} + \phi\left[\left(\frac{\partial\rho}{\partial p}\right)_h \frac{\partial p}{\partial t} + \left(\frac{\partial\rho}{\partial h}\right)_p \frac{\partial h}{\partial t}\right]$$

On noting that[5]

$$\frac{\partial\phi}{\partial t} = (1-\phi)\, C_m \frac{\partial p}{\partial t} \quad \ldots \quad (A.3)$$

we obtain

$$\frac{\partial(\phi\rho)}{\partial t} = \phi\rho\left\{\left(\frac{1-\phi}{\phi}\right) C_m \frac{\partial p}{\partial t} + \frac{1}{\rho}\left(\frac{\partial\rho}{\partial p}\right)_h \frac{\partial p}{\partial t} + \frac{1}{\rho}\left(\frac{\partial\rho}{\partial h}\right)_p \frac{\partial h}{\partial t}\right\} \quad \ldots \quad (A.4)$$

We will now proceed to express $\partial h/\partial t$ in terms of $\partial h/\partial r$, $\partial p/\partial t$ and $\partial p/\partial r$.

For geothermal applications, it will suffice to assume that

$$h_R = c_R T \quad \ldots \quad (A.5a)$$

where T is the common local temperature of the rock matrix and the pore fluids. Under the steam dome (i.e., two-phase regime), temperature T is a unique function of fluid pressure p.

$$T = T(p) \quad \ldots \quad (A.5b)$$

Combining equations (A.5a) and (A.5b) and differentiating w.r.t. t, we have

$$\frac{\partial h_R}{\partial t} = c_R \frac{dT}{dp}\frac{\partial p}{\partial t} \quad \ldots \quad (A.6)$$

Substituting for $\partial/\partial t\,(\phi\rho)$ from equation (A.1), for $\partial\phi/\partial t$ from equation (A.3), and for $\partial h_R/\partial t$ from equation (A.6) into equation (A.2), we obtain:

$$\left\{-(1-\phi)\, C_m\rho_R h_R + (1-\phi)\,\rho_R c_R \frac{dT}{dp} - \phi - (1-\phi)\, C_m p\right\} \times \frac{\partial p}{\partial t} + \phi\rho\frac{\partial h}{\partial t} = \left[(k/\nu)_\ell h_\ell + (k/\nu)_g h_g - (k/\nu)_T h\right]\frac{1}{r}\frac{\partial}{\partial r}\left(r\frac{\partial p}{\partial r}\right) + \frac{\partial p}{\partial r}\left\{\frac{\partial}{\partial r}[(k/\nu)_\ell h_\ell + (k/\nu)_g h_g - (k/\nu)_T h] + (k/\nu)_T\frac{\partial h}{\partial r}\right\} \quad \ldots \quad (A.7)$$

We next note that in practical geothermal applications, the last two terms in the brackets on the left hand side of equation (A.7) (ϕ and $(1-\phi)\, C_m p$) are liable to be negligible compared to the first two terms. Also, we have

$$h_\ell - h = -Qh_{g\ell}$$
$$h_g - h = (1-Q)h_{g\ell} \quad \ldots \quad (A.8)$$

Substitution of equation (A.8) in equation (A.7) yields:

$$\phi\rho\frac{\partial h}{\partial t} = (1-\phi)\rho_R h_R\left[C_m - \frac{1}{T}\frac{dT}{dp}\right]\frac{\partial p}{\partial t} + h_{g\ell}\,(k/\nu)_T\left[\frac{(k/\nu)_g}{(k/\nu)_T} - Q\right]\frac{1}{r}\frac{\partial}{\partial r}\left(r\frac{\partial p}{\partial r}\right) + \frac{\partial p}{\partial r}\left\{\frac{\partial}{\partial r}\left[h_{g\ell}\,(k/\nu)_T\left(\frac{(k/\nu)_g}{(k/\nu)_T} - Q\right)\right] + (k/\nu)_T\frac{\partial h}{\partial r}\right\} \quad \ldots \quad (A.9)$$

Combining equations (A.1), (A.4) and (A.9) we obtain:

$$\phi\rho\left\{\left(\frac{1-\phi}{\phi}\right) C_m + \frac{1}{\rho}\left(\frac{\partial\rho}{\partial p}\right)_h + \frac{1}{\rho^2}\left(\frac{\partial\rho}{\partial h}\right)_p \left(\frac{1-\phi}{\phi}\right)\rho_R h_R \left[C_m - \frac{1}{T}\frac{dT}{dp}\right]\right\}\frac{\partial p}{\partial t} - (k/\nu)_T\left[1 - \frac{1}{\rho}\left(\frac{\partial\rho}{\partial h}\right)_p h_{g\ell}\left\{\frac{(k/\nu)_g}{(k/\nu)_T} - Q\right\}\right]\frac{1}{r}\frac{\partial}{\partial r}\left(r\frac{\partial p}{\partial r}\right) + \frac{\partial p}{\partial r}\left\{-\frac{\partial}{\partial r}(k/\nu)_T + \frac{1}{\rho}\left(\frac{\partial\rho}{\partial h}\right)_p (k/\nu)_T\frac{\partial h}{\partial r} + \frac{1}{\rho}\left(\frac{\partial\rho}{\partial h}\right)_p \frac{\partial}{\partial r}\left[h_{g\ell}(k/\nu)_T\left(\frac{(k/\nu)_g}{(k/\nu)_T} - Q\right)\right]\right\} = 0 \quad \ldots\ldots\ldots \quad (A.10)$$

An examination of the numerical solution for equations (A.1) and (A.2) with a constant rate of mass production (e.g., Cases 1-5 discussed elsewhere in this paper) reveals the following important points:

1. The total kinematic mobility $(k/\nu)_T$ increases with increasing distance r from the wellbore.

2. In the vicinity of the wellbore, we have

$$(k/\nu)_T\left[1 - \frac{1}{\rho}\left(\frac{\partial\rho}{\partial h}\right)_p h_{g\ell}\left\{\frac{(k/\nu)_g}{(k/\nu)_T} - Q\right\}\right]\frac{1}{r}\frac{\partial}{\partial r}\left(r\frac{\partial p}{\partial r}\right) \gg \left|\frac{\partial p}{\partial r}\left\{-\frac{\partial}{\partial r}(k/\nu)_T + \frac{1}{\rho}\left(\frac{\partial\rho}{\partial h}\right)_p (k/\nu)_T\frac{\partial h}{\partial r} + \frac{1}{\rho}\left(\frac{\partial\rho}{\partial h}\right)_p \frac{\partial}{\partial r}\left[h_{g\ell}(k/\nu)_T\left(\frac{(k/\nu)_g}{(k/\nu)_T} - Q\right)\right]\right\}\right| \quad \ldots\ldots\ldots \quad (A.11)$$

This strong inequality does not, however, hold for radial distances greater than a few borehole radii.

3. Both the radial terms in equations (A.10) are maximum (in an absolute sense) near the wellbore, and fall off rapidly with increasing radial distance r.

4. The radial terms in equation (A.10) are of opposite signs.

We now replace equation (A.10) by the following diffusivity equation:

$$\phi\rho\, C_T\frac{\partial p}{\partial t} - (k/\nu)_T\frac{1}{r}\frac{\partial}{\partial r}\left(r\frac{\partial p}{\partial r}\right) = 0 \quad \ldots \quad (A.12a)$$

where

$$C_T = \left\{\frac{(1-\phi)}{\phi} C_m + \frac{1}{\rho}\left(\frac{\partial\rho}{\partial p}\right)_h + \frac{(1-\phi)}{\phi}\frac{1}{\rho^2}\left(\frac{\partial\rho}{\partial h}\right)_p \rho_R h_R\left[C_m - \frac{1}{T}\frac{dT}{dp}\right]\right\} \Big/ \left\{1 - \frac{1}{\rho}\left(\frac{\partial\rho}{\partial h}\right)_p h_{g\ell}[(k/\nu)_g/(k/\nu)_T - Q]\right\} \quad (A.12b)$$

Note that $(k/\nu)_T$ in equation (A.12a) represents the value of the total kinematic mobility in the vicinity of the borehole. The approximations involved in deriving equation (A.12a) (i.e., (1) neglecting the second radial term in equation (A.10) and (2) replacing $(k/\nu)_T$ by its value near the wellbore) are strictly speaking valid only in the immediate neighborhood of the borehole. Even though equation (A.12a) is not expected to apply at large radii, its use should not cause large errors in the computed response since pressures change only very slowly at large radial distances from the borehole.

The diffusivity equation (A.12a) forms the basis for our analysis of two-phase flow in geothermal systems. Unlike in single-phase isothermal flow, the total compressibility C_T in two-phase flow (c.f., equation (A.12b)) has no simple interpretation; consequently its determination from well-tests, in the absence of data regarding rock thermomechanical properties and detailed knowledge regarding the thermodynamic state of the produced fluid, may have only limited practical utility.

We shall now briefly consider a geothermal steam reservoir with an immobile vaporizing liquid phase in the pores. In this case, we have

$$(k/\nu)_\ell = 0,\ (k/\nu)_T = (k/\nu)_g = k_g\rho_g/\mu_g \quad . \quad (A.13)$$

where $k_g = kR_g$. Substituting from equation (A.13) into equation (A.12) and rearranging terms, we obtain:

$$\frac{\partial p}{\partial t} - \frac{k_g}{\phi\,\mu_g\,C_T'}\frac{1}{r}\frac{\partial}{\partial r}\left(r\frac{\partial p}{\partial r}\right) = 0 \quad \ldots\ldots \quad (A.14)$$

where

$$C_T' = \frac{\rho\, C_T}{\rho_g} \quad \ldots\ldots\ldots \quad (A.15a)$$

$$C_T = \left\{\frac{(1-\phi)}{\phi} C_m + \frac{1}{\rho}\left(\frac{\partial\rho}{\partial p}\right)_h + \frac{(1-\phi)}{\phi}\frac{1}{\rho^2}\left(\frac{\partial\rho}{\partial h}\right)_p \rho_R h_R\left[C_m - \frac{1}{T}\frac{dT}{dp}\right]\right\} \Big/ \left\{1 - \frac{1}{\rho}\left(\frac{\partial\rho}{\partial h}\right)_p h_{g\ell}(1-Q)\right\} \quad (A.15b)$$

We note that equation (A.14) is identical (albeit with a different definition for the total compressibility) to the diffusivity equation for isothermal single-phase reservoir systems; this fact provides the fundamental justification for the application of classical single-

phase procedures to determine the steam-phase permeability of a geothermal steam reservoir with an immobile vaporizing liquid phase (see, e.g., Moench and Atkinson[13]).

57

TABLE 1

ACTUAL $(k/\nu)_i$ ($i = \ell, g, T$) AND VAPOR SATURATION (S) VALUES

IN THE WELL-BLOCK FOR SIMULATED DRAWDOWN HISTORY (a)

Time s		Vapor Saturation (S)	$10^8\ (k/\nu)_\ell$ s	$10^8\ (k/\nu)_g$ s	$10^8\ (k/\nu)_T$ s
0		0.050	79.85	0	79.85
0.576	10^4	0.163	37.26	0.22	37.48
0.1296	10^5	0.169	35.43	0.26	35.69
0.3456	10^5	0.175	34.00	0.29	34.29
0.7056	10^5	0.178	33.12	0.31	33.43
0.14256	10^6	0.181	32.36	0.33	32.69
0.35856	10^6	0.185	31.52	0.36	31.88
0.71856	10^6	0.187	30.96	0.37	31.33
0.100656	10^7	0.188	30.69	0.38	31.07

TABLE 2

ACTUAL $(k/\nu)_i$ ($i = \ell, g, T$) AND VAPOR SATURATION (S) VALUES

IN THE WELL-BLOCK FOR SIMULATED DRAWDOWN HISTORY (b)

Time s		Vapor Saturation (S)	$10^8\ (k/\nu)_\ell$ s	$10^8\ (k/\nu)_g$ s	$10^8\ (k/\nu)_T$ s
0		0.350	6.71	3.48	10.19
0.504	10^4	0.400	3.59	4.90	8.49
0.1224	10^5	0.402	3.49	4.90	8.39
0.3384	10^5	0.404	3.41	4.88	8.29
0.6984	10^5	0.404	3.39	4.84	8.23
0.14184	10^6	0.405	3.37	4.79	8.16
0.35784	10^6	0.405	3.34	4.74	8.08
0.71784	10^6	0.406	3.30	4.71	8.01
0.100584	10^7	0.406	3.29	4.69	7.98

TABLE 3

ACTUAL $(k/\nu)_i$ (i = ℓ, g, T) AND VAPOR SATURATION (S) VALUES IN THE WELL-BLOCK FOR SIMULATED DRAWDOWN HISTORY (c)

Time s	Vapor Saturation (S)	10^8 $(k/\nu)_\ell$ s	10^8 $(k/\nu)_g$ s	10^8 $(k/\nu)_T$ s
0	0.702	0	23.02	23.02
0.432 10^4	0.731	0	22.26	22.26
0.1152 10^5	0.734	0	22.13	22.13
0.3312 10^5	0.734	0	21.99	21.99
0.6912 10^5	0.729	0	21.89	21.89
0.14112 10^6	0.714	0	21.80	21.80
0.35712 10^6	0.662*	0*	19.12*	19.12*
0.71712 10^6	0.624	0.02	16.58	16.60
0.100512 10^7	0.623	0.02	16.53	16.55

*Liquid slightly mobile

TABLE 4

ACTUAL $(k/\nu)_i$ (i = ℓ, g, T) AND VAPOR SATURATION (S) VALUES IN THE WELL-BLOCK FOR SIMULATED DRAWDOWN HISTORY (d)

Time s	Vapor Saturation (S)	10^8 $(k/\nu)_\ell$ s	10^8 $(k/\nu)_g$ s	10^8 $(k/\nu)_T$ s
0	0.160	35.38	0.10	35.48
0.720 10^4	0.298	10.84	0.96	11.80
0.144 10^5	0.301	10.47	0.97	11.44
0.360 10^5	0.305	10.02	0.99	11.01
0.720 10^5	0.308	9.68	1.01	10.69
0.144 10^6	0.309	9.58	1.00	10.58
0.360 10^6	0.312	9.27	1.00	10.27
0.720 10^6	0.314	9.00	1.01	10.01
0.1008 10^7	0.315	8.87	1.01	9.88

TABLE 5

ACTUAL $(k/\nu)_f$ (f = ℓ, g, T) AND VAPOR SATURATION (S) VALUES IN THE WELL-BLOCK FOR SIMULATED DRAWDOWN HISTORY (e)

Time s		Vapor Saturation (S)	10^8 $(k/\nu)_\ell$ s	10^8 $(k/\nu)_g$ s	10^8 $(k/\nu)_T$ s
0		0.050	74.49	0	74.49
0.720	10^4	0.236	19.21	0.45	19.66
0.144	10^5	0.241	18.50	0.47	18.97
0.360	10^5	0.246	17.62	0.50	18.12
0.720	10^5	0.250	16.94	0.53	17.47
0.144	10^6	0.254	16.42	0.54	16.96
0.360	10^6	0.256	16.01	0.56	16.57
0.720	10^6	0.259	15.56	0.57	16.13
0.1008	10^7	0.261	15.35	0.60	15.93

TABLE 6

COMPARISON OF ACTUAL (C_{Tact}) AND INFERRED (C_{Tinf}) COMPRESSIBILITIES

Drawdown Case	Time s		C_{Tact} MPa^{-1} $(10^{-2}psi^{-1})$	C_{Tinf} MPa^{-1} $(10^{-2}psi^{-1})$	C_{Tinf}/C_{Tact}
a	0.14256	10^6	1.80 (1.24)	6.83 (4.70)	3.79
b	0.14184	10^6	0.286 (0.197)	0.305 (0.211)	1.07
c	0.6912	10^5	0.309 (0.213)	0.399 (0.275)	1.29
d	0.144	10^6	1.99 (1.37)	2.91 (2.00)	1.46
e	0.144	10^6	3.75 (2.59)	8.79 (6.06)	2.34

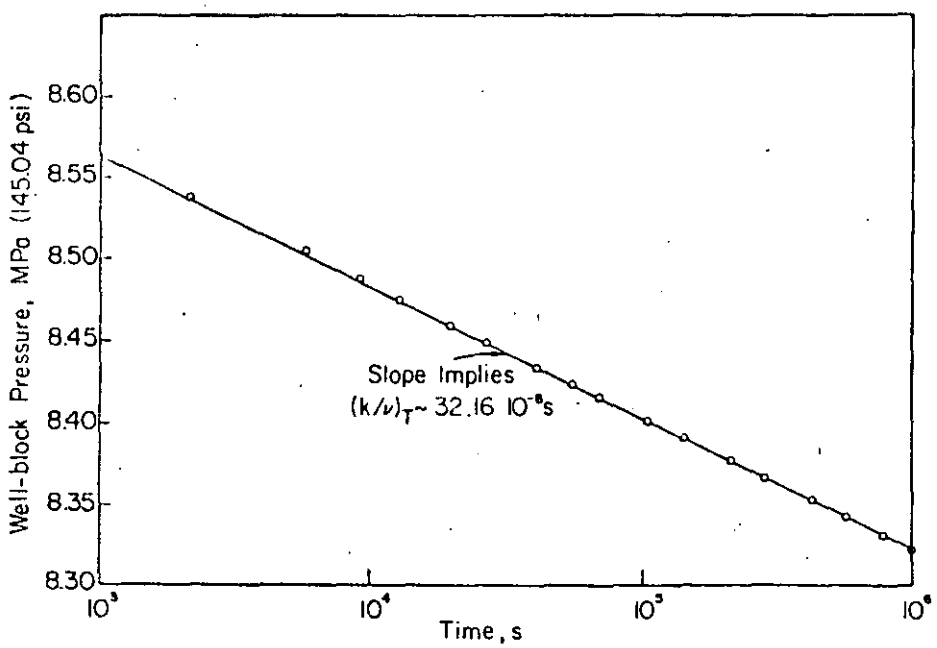

FIG. 1 - SIMULATED DRAWDOWN HISTORY (A). RESERVOIR IS INITIALLY TWO-PHASE EVERYWHERE (P=8.5991 MPA ~ 1247.2 PSI, S=0.05). SEE TABLE 1 FOR ACTUAL $(K/\nu)_T$ VALUES.

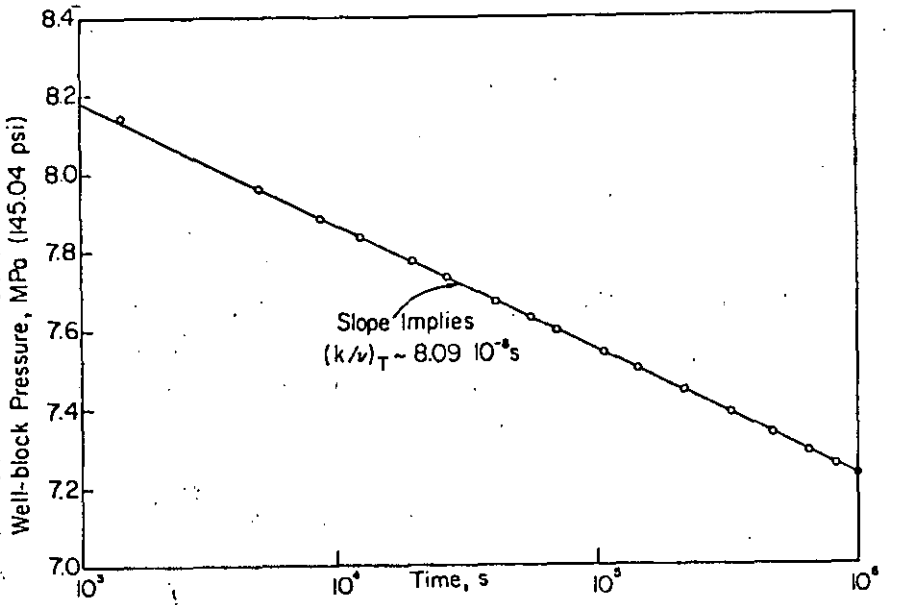

FIG. 2 - SIMULATED DRAWDOWN HISTORY (B). RESERVOIR IS INITIALLY TWO-PHASE EVERYWHERE (P=8.5991 MPA ~ 1247.2 PSI, S=0.35). SEE TABLE 2 FOR ACTUAL $(K/\nu)_T$ VALUES.

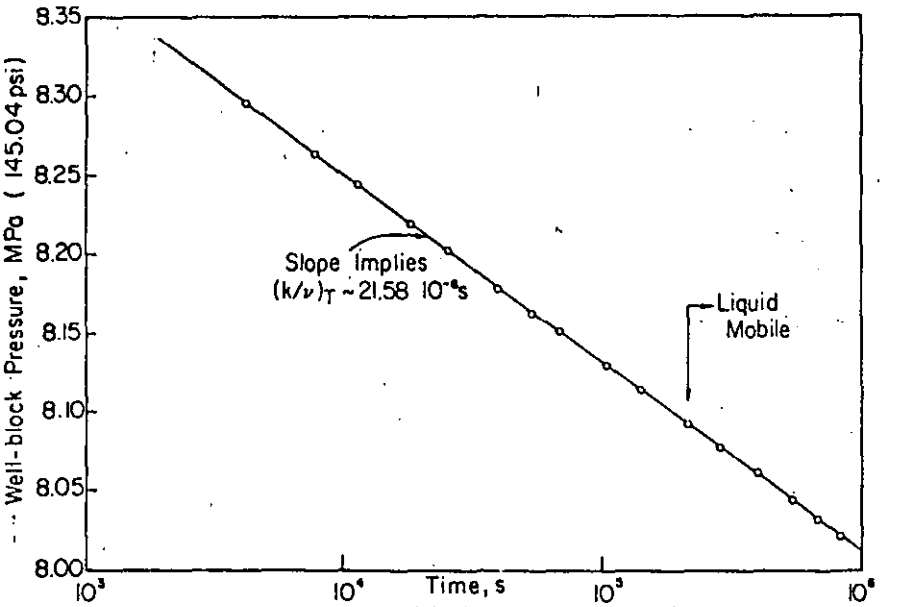

FIG. 3 - SIMULATED DRAWDOWN HISTORY (C). RESERVOIR IS INITIALLY TWO-PHSE EVERYWHERE (P=8.5991 MPA ~ 1247.2 PSI, S=0.7015). SEE TABLE 3 FOR ACTUAL $(K/\nu)_T$ VALUES

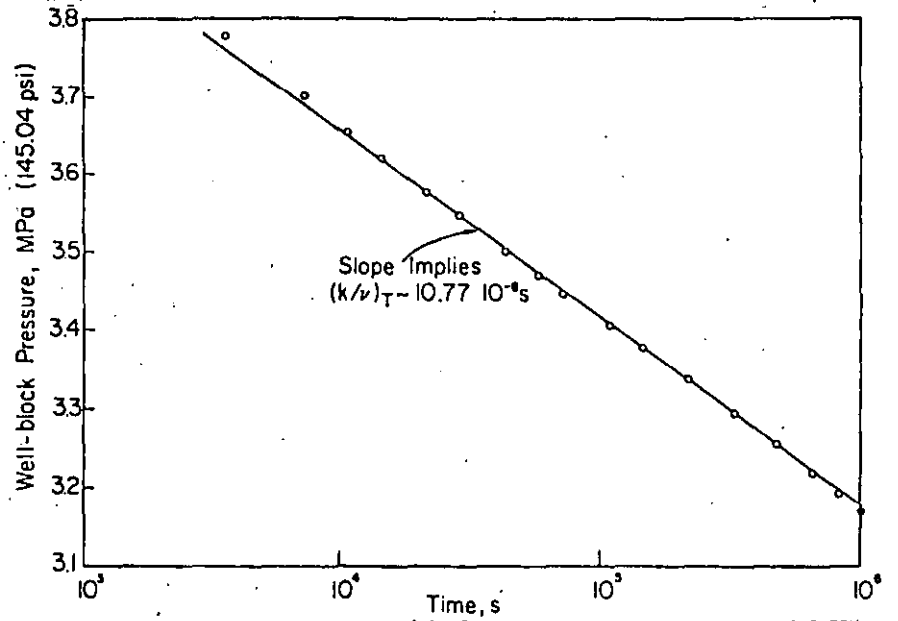

FIG. 4 - SIMULATED DRAWDOWN HISTORY (D). RESERVOIR IS INITIALLY TWO-PHASE EVERYWHERE (P=3.9808 MPA ~ 577.4 PSI, S=0.1604). SEE TABLE 4 FOR ACTUAL $(K/\nu)_T$ VALUES.

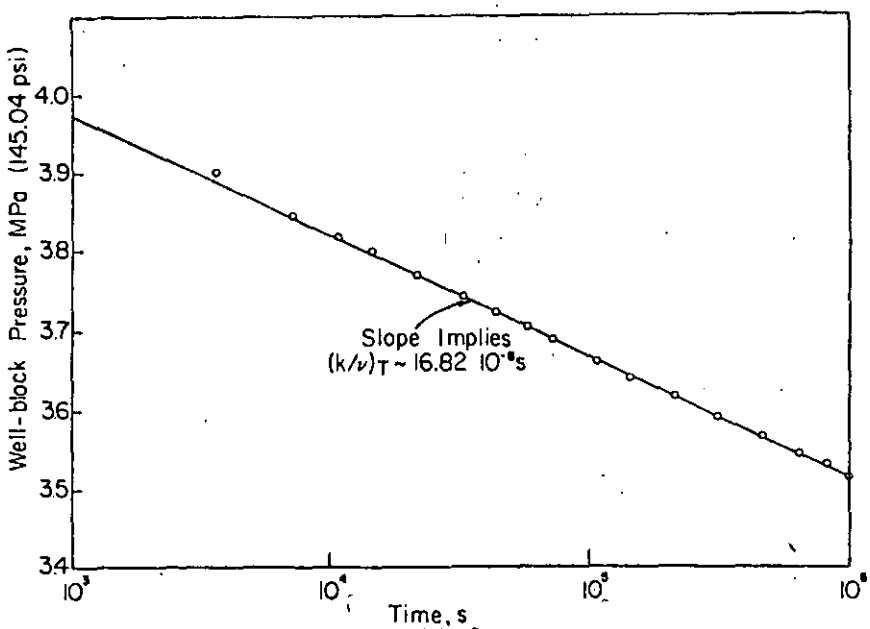

FIG. 5 - SIMULATED DRAWDOWN HISTORY (E). RESERVOIR IS INITIALLY TWO-PHASE EVERYWHERE (P=3,9808 MPA ~ 577.4 PSI, S=0.0.05). SEE TABLE 5 FOR ACTUAL $(K/\nu)_T$ VALUES.

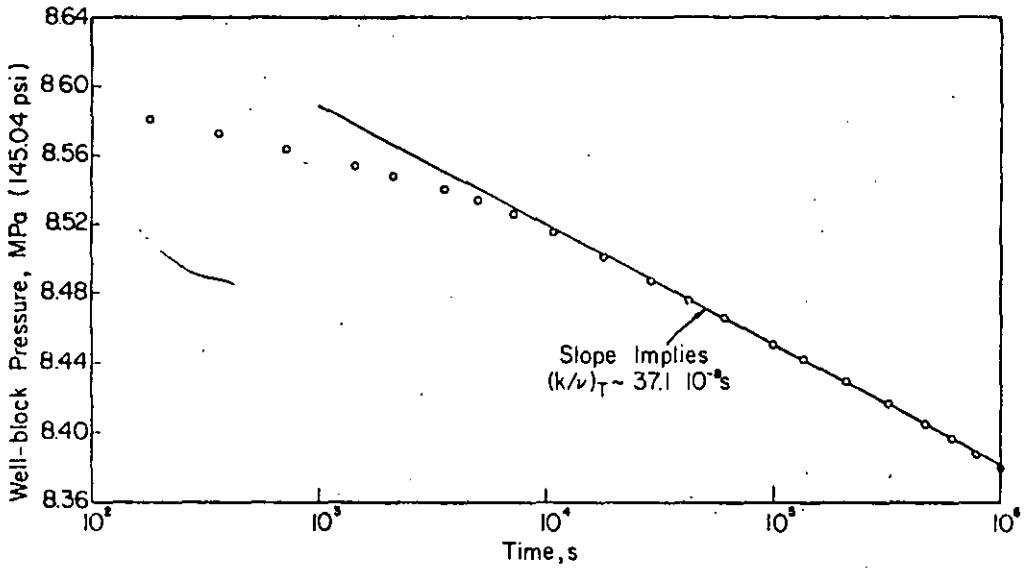

FIG. 6 - SIMULATED DRAWDOWN HISTORY (F). RESERVOIR IS INITIALLY SINGLE-PHASE (LIQUID) EVERYWHERE (P=8.62 MPA ~ 1250.2 PSI, T=573.15K=572°F). ACTUAL RANGE OF $(K/\nu)_T$ VALUES FOR POINTS LYING ON THE STRAIGHT LINE IF (36.1-42.3) 10^{-8}s.

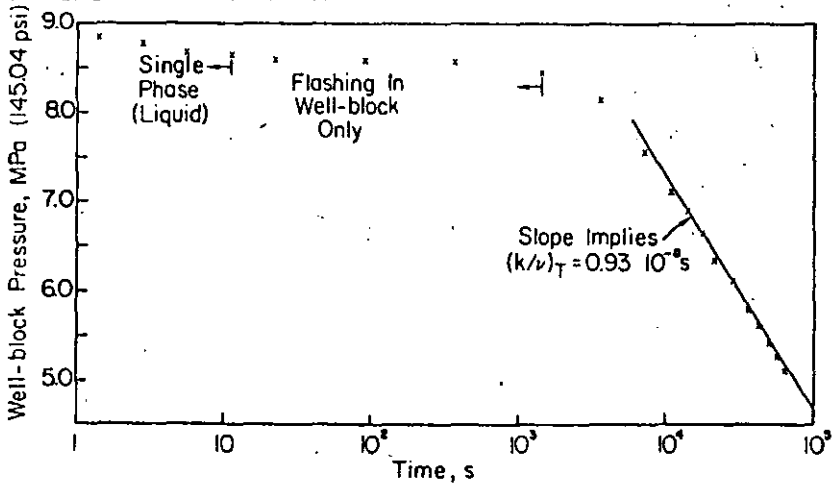

FIG. 7 - SIMULATED DRAWDOWN HISTORY (G). RESERVOIR IS INITIALLY SINGLE-PHASE EVERYEVERYWHERE (P=9.000 MPA ~ 1305.3 PSI, T = 573. 15K=572°F). ABSOLUTE PERMEABILITY K FOR THIS CASE IS 0.01 μm^2 (~ 0.01 DARCY) AND THE ACTUAL RANGE OF $(K/\nu)_T$ VALUES FOR POINTS LYING ON THE STRAIGHT LINE IS (0.93-1.15) 10^{-8}s.

SPE
Society of Petroleum Engineers of AIME

SPE 6887

APPLICATION OF TWO-RATE FLOW TESTS TO THE DETERMINATION OF GEOTHERMAL RESERVOIR PARAMETERS

by Jesus Rivera-R., Member SPE-AIME, Comisión Federal de Electricidad, and Henry J. Ramey, Jr., Member SPE-AIME, Stanford U.

This paper was presented at the 52nd Annual Fall Technical Conference and Exhibition of the Society of Petroleum Engineers of AIME, held in Denver, Colorado, Oct. 9-12, 1977. The material is subject to correction by the author. Permission to copy is restricted to an abstract of not more than 300 words. Write: 6200 N. Central Expy, Dallas, Texas 75206.

ABSTRACT

This paper deals with the application of well-established pressure transient analysis techniques to the determination of geothermal reservoir parameters. Among the pressure transient techniques available, those concerned with two-rate flow testing were chosen. A two-rate test may permit obtaining data while reducing interruption of power generation. Two-rate techniques have been applied successfully to both oil and gas reservoirs; however, no data have been published to date--to the authors' knowledge--on the application of this method to liquid-dominated geothermal reservoirs. Data from one test run on a well in the Cerro Prieto Geothermal Field are shown. The field data were interpreted by means of four different models. Three of the models produced results that agreed with each other, the fourth one produced data scatter.

INTRODUCTION

The Cerro Prieto Geothermal Field is located about 30 kilometers south of Mexicali, Baja California. As shown in Figure 1, this field is situated at the southern end of the Salton-Mexicali trough, which includes other thermal anomalies of great interest, such as Heber and East Mesa. The reservoir is a liquid-dominated system having a cap rock made of impervious plastic clays. This cap acts as a seal, keeping the hot water trapped and preventing the dissipation of heat to the surface. Figure 2 shows a schematic geological cross section of the reservoir drawn in an East-West direction.[1] The permeable layers consist of alternating shale and sandstone layers resting on a highly fractured granitic basement. Basement rocks were encountered in one of the wells at a depth of approximately 2500 meters. The thickness of the cap rock varies, according to the location of the wells, from 700 up to almost 1000 meters in the portion of the field already drilled.

The first exploratory well in the area was drilled in 1961, and in 1964, four more exploratory wells were drilled. After an extensive field-test program, the Comisión Federal de Electricidad started the construction of a 75-MW geothermal power plant in 1968. The plant was located in the Mexicali valley and named for the Cerro Prieto volcano. This plant started commercial operation in April 1973, and has been in operation since that date. The turbines operate on steam from 14 wells. The geothermal fluid is obtained as a water-vapor mixture, because flashing takes place at some depth inside the wellbore. The separated hot brine is disposed of in an evaporation pond; however, plans are being made to evaluate the feasibility of reinjecting at least part of the spent liquid.

Although well testing and pressure transient analysis techniques have been widely applied by petroleum engineers to gas and oil reservoirs (to find mean formation pressure, skin factor, and average permeability and porosity), the application of the same techniques to geothermal reservoirs encounters problems that are not commonly found in petroleum applications. In hot-water wells,[3] two-phase flow and heat transfer influence the pressure response when the wells are shut-in. In addition to this, gathering of the data is difficult because of the high temperatures involved. Bottom-hole temperatures in the range of 300 to 320 °C are common in the Cerro Prieto Field. Until recently, there were no bottom-hole pressure measuring devices that could withstand such temperatures for more than three hours. Another problem is mechanical damage due to extreme buffeting by the high production rates of boiling geothermal fluids. Rates in excess of 24,000 B/D are common.

Considering these facts, it was decided that the best choice for obtaining pressure-time data by means of standard bourdon-tube type pressure bombs would be short-time duration drawdown tests. These tests could be run by changing the flow rate to some predetermined value after the well was stabilized at a given constant rate for some time. This type of test is known in petroleum technology as a "two-rate" flow test. It was first proposed by Russell[4] in 1962. Further improvements in this technique were introduced by Selim[5] and Odeh and Jones.[6] Two-rate flow tests had been applied extensively in both gas

References and illustrations at end of paper.

and oil reservoirs; however, no data have been published to date on an application of this technique to liquid-dominated geothermal reservoirs to the authors' knowledge. The three techniques mentioned above were used for interpretation of the data; additionally, the data were analyzed as a variable-rate drawdown case according to the Odeh and Jones[7] method.

TWO-RATE FLOW TEST

In preparation for the test, the well was stabilized for a period of approximately 48 hours at a constant rate of 111 tons/hour. The flow rate was measured several times during this stabilization period. A pressure bomb was lowered into the well, measuring the bottom-hole pressure for approximately 20 minutes prior to the rate change, in order to have a dependable value for the flowing pressure prior to the change in rate.

The producing rate was changed to a value of 66.1 tons/hour. A record as continuous as possible was kept of water and steam production, and changes in wellhead pressure.

Figure 3 shows the mass-flow rate and bottom-hole pressure during the test. After stabilized conditions were evident from wellhead measurements, the flow rate was increased to a value as close to the initial flow rate as possible, following the procedure suggested by Selim.[5]

INTERPRETATION OF THE DATA

The data obtained from this test were interpreted by means of the models suggested by Russell,[4] Selim[5] and Odeh and Jones (two-rate tests[6] and drawdown variable rate[7]). The results obtained from the application of these models are as follows.

Russell's[4] Model

The interpretation equation as presented by Russell[4] is as follows:

$$p_{wf} = p_i - \frac{162.6q_2B\mu}{kh}\left(\log\frac{k}{\phi\mu cr_w^2} - 3.23 + 0.87\,s\right) - \frac{162.6q_1B\mu}{kh}\left(\log\frac{t+\Delta t'}{\Delta t'} + \frac{q_2}{q_1}\log\Delta t'\right) \quad (1)$$

Equation 1 is in standard oil field units. The nomenclature is presented at the end of the paper. Changing these units into metric geothermal units and expressing the flow rates in terms of mass rates, Eq. 1 can be written as:

$$p_{wf} = p_i - 527.4\frac{w_2\nu_{sc}B\mu}{kh}\left(\log\frac{k}{\phi\mu cr_w^2} + 0.891 + 0.87\,s\right) - 527.4\frac{w_1\nu_{sc}B\mu}{kh}\left(\log\frac{t+\Delta t'}{\Delta t'} + \frac{w_2}{w_1}\log\Delta t'\right) \quad (2)$$

From Eq. 2 it is evident that by graphing p_{wf} vs. $\left(\log\left(\frac{t+\Delta t'}{\Delta t'}\right) + \frac{w_2}{w_1}\log\Delta t'\right)$ a straight line should be obtained whose slope is given by:

$$m_R = 527.4\frac{w_1\nu_{sc}B\mu}{kh} \quad (3)$$

Figure 4 shows the result of graphing the data according to Eq. 2. The kh is obtained as 1,946 md-m, and the skin factor as -5.28. The details of the calculations are shown in the appendix.

The equation for the skin factor in geothermal units is given by the following expression:

$$s = 1.151\left(\frac{w_1}{w_1-w_2}\frac{p_{1hr}-p_{wf}}{m_R} - \log\frac{k}{\phi\mu cr_w^2} - 0.891\right) \quad (4)$$

The average reservoir pressure in the volume drained by the well was obtained by means of the Matthews, et al.,[8] method.

SELIM MODIFICATION[5] OF RUSSELL'S MODEL

Selim observed that the results obtained from a two-rate test were sensitive to the slope of the straight line drawn according to the method proposed by Russell. He suggested modification of the method by returning the well to the producing rate it had prior to the test once the well had reached stable conditions. The pressures and flow rates should be measured until new stabilized conditions are reached.

The equation originally proposed by Selim is:[5]

$$p_{wf} = p_i - \frac{162.6q_3B\mu}{kh}\left(\log\frac{k}{\phi\mu cr_w^2} - 3.23 + 0.87\,s\right) - \frac{162.6q_2B\mu}{kh}\left(\log\left[\frac{(\frac{q_1}{q_2})t+\Delta t'+\Delta t''}{\Delta t''}\right] + \frac{q_3}{q_2}\log\Delta t''\right) \quad (5)$$

Equation 5 is expressed in standard oilfield units. Changing these units into metric geothermal units and expressing the flow rates in terms of mass, this equation can be expressed as:

$$p_{wf} = p_i - 527.4\frac{w_2\nu_{sc}B\mu}{kh}\left(\log\frac{k}{\phi\mu cr_w^2} + 0.891 + 0.87\,s\right) - 527.4\frac{w_2\nu_{sc}B\mu}{kh}\left(\log\frac{(\frac{w_1}{w_2})t+\Delta t'+\Delta t''}{\Delta t''} + \frac{w_3}{w_2}\log\Delta t''\right) \quad (6)$$

From Eq. 6 it is evident that graphing p_{wf} vs. $\left(\log\left[\frac{(\frac{w_1}{w_2})t+\Delta t'+\Delta t''}{\Delta t''}\right]+\frac{w_3}{w_2}\log \Delta t''\right)$ a straight line is obtained whose slope is

$$m_S = \frac{527.4\, w_2 \nu_{sc} B\mu}{kh} \qquad (7)$$

Figure 5 shows the graph obtained by plotting the data according to Eq. 6.

Selim[5] showed that the slope calculated by means of Russell's method and that calculated using the modification he suggested should hold the following relationship:

$$\frac{m_R}{m_S} = \frac{w_1}{w_2} \qquad (8)$$

Equation 8 represents an additional constraint that the straight line portions of Eqs. 2 and 6 must satisfy. It can be used to select the appropriate straight line portion in the event that several straight sections are present due to scatter of the field data. Three straight line segments are evident in Fig. 5. The one labelled number 2 satisfies Eq. 8 and was considered to be the correct one. Results were kh was 1,905 md-m. Details of the calculations are included in the appendix.

ODEH AND JONES[7] VARIABLE DRAWDOWN MODEL

The field data obtained during the transient conditions after the change in rate were analyzed as a variable drawdown case having w_1 and w_2 as the initial and final flow rates. The result of this analysis is shown in Fig. 6 and the calculations are included in the appendix. The kh product obtained from this method was 1,990 md-m and agreed well with those determined by the methods mentioned before. The interpretation equation in oilfield units given in the original paper is as follows:

$$\frac{p_i - p_{wf}}{q_n} = \frac{162.6B\mu}{kh}\left(\sum_{i=0}^{n-1}\frac{\Delta q_i}{q_n}\log (t_n - t_i) - 3.228 + 0.87\, s + \log\frac{k}{\phi\mu c r_w^2}\right) \qquad (9)$$

Writing this equation in metric geothermal units and expressing the flow rate in terms of mass, this equation can be written as follows:

$$\frac{p_i - p_{wf}}{w_n} = 527.4\,\frac{\nu_{sc} B\mu}{kh}\left(\sum_{i=0}^{n-1}\frac{\Delta w_i}{w_n}\log (t_n - t_i) + 0.8926 + 0.87s + \log\frac{k}{\phi\mu c r_w^2}\right) \qquad (10)$$

Therefore, by graphing

$$(p_i - p_{wf}) \text{ vs. } \sum_{i=0}^{n-1}\frac{\Delta w_i}{w_n}\log (t_n - t_i),$$

a straight line is obtained whose slope is given by the following equation:

$$m_{OJV} = 527.4\,\frac{\nu_{sc} B\mu}{kh} \qquad (11)$$

ODEH AND JONES[6] TWO-RATE MODEL

This method is similar to the one described before, except that it includes second differences of the flow rates as shown by Eq. 13 below. The field data were analyzed according to Eq. 12 below. Figure 7 shows the graph obtained by plotting the data according to Eq. 14. Scatter of the data points is observed, making it very difficult to find a proper straight line. Fitting a straight line to the data points by means of linear regression produced a kh product of 2,860 md-m, much higher than that obtained with the models described before. The calculations are included in the appendix.

The original equation[7] in oilfield units is as follows:

$$\frac{p_{wf}|_{t} - p_{wf}|_{t=0}}{\Delta q_n} = \frac{162.6B\mu}{kh}\left(\frac{1}{\Delta q_n}\sum_{i=0}^{n-1}\Delta\Delta q_i \log (t_n - t_i) + \log\frac{k}{\phi\mu c r_w^2} - 3.23 + 0.87\, s\right) \qquad (12)$$

where:

$$\left.\begin{aligned} \Delta q_i &= q_o - q_i \\ \Delta\Delta q_i &= \Delta q_{i+1} - \Delta q_i \\ \Delta q_o &= 0 \\ \Delta q_n &= q_o - q_n \end{aligned}\right| \qquad (13)$$

Expressing Eq. 12 in metric geothermal units and using mass-flow rate instead of volumetric-flow rate, this equation can be written as follows:

$$\frac{p_{wf}|_{t} - p_{wf}|_{t=0}}{w_n} = 527.4\,\frac{\nu_{sc} B\mu}{kh}\left(\frac{1}{\Delta w_n}\sum_{i=0}^{n-1}\Delta\Delta w_i \log (t_n - t_i) + \log\frac{k}{\phi\mu c r_w^2} + 0.87s + 0.891\right) \qquad (14)$$

where

$$\left.\begin{aligned} \Delta w_i &= w_o - w_i \\ \Delta\Delta w_i &= \Delta w_{i+1} - \Delta w_i \\ \Delta w_o &= 0 \\ \Delta w_n &= w_o - w_i \end{aligned}\right| \qquad (15)$$

Graphing:

$$\frac{P_{wf}|_t - P_{wf}|_{t=0}}{\Delta w_n} \text{ vs. } \frac{1}{\Delta w_n}\sum_{i=0}^{n-1} \Delta\Delta w_i \log (t_n - t_i) ,$$

a straight line is obtained whose slope is given by:

$$m_{OJT} = 527.4 \frac{\nu_{sc} B \mu}{kh} \qquad (16)$$

CONCLUSIONS

The equations reported to describe two-rate flow tests have been converted to metric geothermal form and used to analyze a test for a geothermal well which produces a boiling brine. The interpretive equations are presented and an example calculation made for each of four methods. Good agreement was obtained from the application of the models of Russell,[4] Selim,[5] and Odeh and Jones drawdown variable-rate case.[7] However, scatter of the data was observed when the two-rate Odeh and Jones[6] technique was used. Other conclusions reached include the following.

1. Two-rate flow tests can be used for calculating basic geothermal reservoir parameters.

2. Russell's model and the modification by Selim seem to produce better results than the technique proposed by Odeh and Jones.[6] However, the Odeh and Jones variable-rate method[7] gave results comparable to those of Russell and Selim.

3. Two-rate flow tests for geothermal wells can be carried out with standard bourdon-tube type pressure instruments at temperatures as high as 315°C. One reason for this result is that it appears possible to conduct a test in a period of time as short as 3 hours. It is not known whether this is a general observation, and the main criterion of success used herein was reasonableness of the results. However, the interpretive equations and example calculations should be useful for two-rate tests of any duration.

NOMENCLATURE

B = brine formation volume factor, (volume, reservoir conditions/volume, standard conditions)
c_t = total fluid compressibility, $(Kg/cm^2)^{-1}$
h = formation net thickness, m
k = permeability, md
m = slope of a straight line
n = constant rate intervals in Odeh and Jones model
p = pressure, Kg/cm^2
p_i = initial pressure, Kg/cm^2
p_{wf} = flowing bottom-hole pressure, Kg/cm^2
p_{1hr} = flowing bottom-hole pressure 1 hr after the rate change, Kg/cm^2
q = volumetric flow rate, bbl/day
r_w = wellbore radius, cm
s = skin factor, dimensionless
t = producing time to instant of rate change, hrs
t' = producing time measured from first rate change, hrs
t'' = producing time measured from second rate change, hr
v = specific volume, cm^3/gr
w = mass flow rate, ton/hr
y = correlation parameter in Odeh and Jones method

GREEK SYMBOLS

μ = viscosity, cp
ν = specific volume, cm^3/gr
ϕ = porosity, fraction

SUBSCRIPTS

1 = conditions prior to rate change
2 = conditions after first rate change
3 = conditions after second change
i = initial condition
OJT = refers to Odeh and Jones two-rate model
OJV = refers to Odeh and Jones variable drawdown model
M = Matthews
R = refers to Russell's model
S = refers to Selim's model
sc = standard conditions
w = wellbore
wf = flowing conditions

ACKNOWLEDGEMENT

The authors wish to thank the Comisión Federal de Electricidad for permission to publish the field data presented in this paper. The assistance received from Ing. Hector Alonso E. and Ing. Jorge Guiza L. is also acknowledged.

REFERENCES

1. "Cerro Prieto - Underground Power," Comisión Federal de Electricidad Pamphlet (1971).

2. Ramey, H.J., Jr.: "Pressure Transient Analysis for Geothermal Wells," Second United Nations Symposium on the Use and Development of Geothermal Energy, San Francisco, Ca., May 20-29, 1975.

3. Gulati, M.S.: "Pressure and Temperature Build-Up in Geothermal Wells," Stanford Geothermal Workshop, Stanford University, Dec. 15-17, 1975.

4. Russell, D.G.: "Determination of Formation Characteristics by Two-Rate Flow Tests," J. Pet. Tech., December 1962, pp. 1347-1355.

5. Selim, M.A.: "A Modification of the Two-Rate Flow Method for Determination of Reservoir

Parameters," J. Institute of Petroleum, v. 53, no. 527, November 1967, pp. 343-352.

6. Odeh, A.S., and Jones, L.G.: "Two-Rate Flow Test, Variable Rate Case," J. Pet. Tech., January 1974, pp. 93-99.

7. Odeh, A.S., and Jones, L.G.: "Pressure Drawdown Analysis, Variable Rate-Case," J. Pet. Tech., August 1965, pp. 960-964.

8. Matthews, C.S., Brons, F., and Hazebroek, P.: "A Method for Determination of Average Pressure in a Bounded Reservoir," Trans. AIME, v. 201, 1952, pp. 182-191.

APPENDIX - TWO-RATE FLOW CALCULATIONS

The test data are shown on Fig. 1 and a listing is given in Table 1. The data were interpreted by four methods. A brief description of the interpretation follows.

Russell's[4] Model

From Fig. 4, a straight line of slope - 3.719 is obtained. According to Eq. 3 in the text:

$$3.719 = 527.4 \frac{w_1 \nu_{sc} B\mu}{kh}$$

$$kh = \frac{527.4\, w_1 \nu_{sc} B\mu}{3.719}$$

$$kh = \frac{527.4\ (111)\ (1.043)\ (1.185)\ (0.1017)}{3.719}$$

$$= 1{,}946 \text{ md-m}$$

The skin factor is obtained from Eq. 4:

$$s = 1.151 \left[\frac{111}{111-66.1} \frac{60.5-54.9}{3.719} - \log\left(\frac{36}{(0.20)(0.1017)(119\times10^{-6})(0.27)} \right) - 0.891 \right]$$

$$s = 5.28$$

Selim's[5] Model

From Fig. 5, three straight lines are obtained whose slopes are as follows:

$$m_{S1} = -5.5$$
$$m_{S2} = -2.3$$
$$m_{S3} = -2.0$$

According to the restriction imposed by Eq. 8 in the text, the ratios for the straight line portions are:

$$\frac{m_R}{m_{S1}} = \frac{3.719}{5.5} = 0.68$$

$$\frac{m_R}{m_{S2}} = \frac{3.719}{2.3} = 1.62$$

$$\frac{m_R}{m_{S3}} = \frac{3.719}{2.0} = 2.0$$

The ratio of the flow rates is:

$$\frac{w_1}{w_2} = \frac{111}{66.1} = 1.68$$

Therefore, the second straight line portion (the one having a slope of 2.3) is the correct one.

From Eq. 7 in the test:

$$2.3 = 527.4 \frac{w_2 \nu_{sc} B\mu}{kh}$$

$$kh = \frac{527.4\ (66.1)\ (1.043)\ (1.185)\ (0.1017)}{2.3}$$

$$kh = 1{,}905 \text{ md-m}$$

Odeh and Jones[7] Variable Drawdown Model

From Fig. 6, the slope of the straight line is 0.0333.

From Eq. 11 in the text:

$$0.0333 = \frac{527.4\, \nu_{sc} B\mu}{kh}$$

$$kh = \frac{527.4\ (1.043)\ (1.185)\ (0.1017)}{0.0333}$$

$$kh = 1{,}990 \text{ md-m}$$

Odeh and Jones[6] Two-Rate Model

From Fig. 8, the slope of the straight line is 0.0228.

From Eq. 16 in the text:

$$0.0228 = \frac{527.4\, \nu_{sc} B\mu}{kh}$$

$$kh = \frac{527.4\ (1.043)(1.185)(0.1017)}{0.0228} = 2{,}860 \text{ md-m}$$

TABLE 1

TWO-RATE FLOW TEST DATA

Total Time (min)	Time Ellapsed since Rate Change (min)	Wellhead Pressure psi	Wellhead Pressure kg/cm^2	Bottom-Hole Pressure psi	Bottom-Hole Pressure kg/cm^2	Mass Flow Rate ($\frac{ton}{hr}$)
0		432	30.4	779.9	54.9	111.0
15		432		779.9	54.9	111.0
16	1	432	30.4	779.9	54.9	101.4
18	3	510	35.9	822.2	57.9	86.0
19	4	520	36.6	828.0	58.3	70.2
20	5	528	37.2	830.9	58.5	67.4
21	6	526	37.0	832.4	58.6	67.4
22	7	522	36.8	833.8	58.7	66.1
23	8	520	36.6	835.3	58.8	66.1
24	9	518	36.5	835.3	58.8	66.1
25	10	518	36.5	836.7	58.9	- -
26	11	518	36.5	838.2	59.0	66.1
27	12	518	36.5	838.2	59.0	- -
28	13	518	36.5	838.2	59.0	66.1
29	14	518	36.5	839.7	59.1	- -
30	15	518	56.5	839.7	59.1	- -
31	16	518	36.5	841.1	59.2	- -
32	17	518	56.5	842.6	59.3	66.1
33	18	518	36.5	842.6	59.3	- -
34	19	518	36.5	842.6	59.3	- -
35	20	518	36.5	842.6	59.3	- -
36	21	518	36.5	842.6	59.3	- -
37	22	518		842.6	59.3	67.4
38	23	498	35.1	828.0	58.3	- -
39	24	430	30.3	817.8	57.6	68.6
40	25	428	30.1	810.5	57.1	108.0
41	26	432	30.4	806.1	56.8	113.2
42	27	432	30.4	801.7	56.5	114.7
43	28	432	30.4	800.3	56.4	115.7
44	29	439	30.9	798.8	56.3	114.7
45	30	444	31.3	797.4	56.2	- -
46	31	443	31.2	793.0	55.8	115.3
47	32	442	31.1	787.2	55.4	- -
48	33	442	31.1	785.7	55.3	- -
50	35	- -	- -	784.3	55.2	- -
51	36	- -	- -	784.3	55.2	- -
52	37	- -	- -	784.3	55.2	- -
53	38	- -	- -	784.3	55.2	- -
54	39	- -	- -	784.3	55.2	- -
55	40	436	30.7	784.3	55.2	109.7
59	44	- -	- -	784.3	55.2	111.0
60	45	- -	- -	785.7	55.3	- -

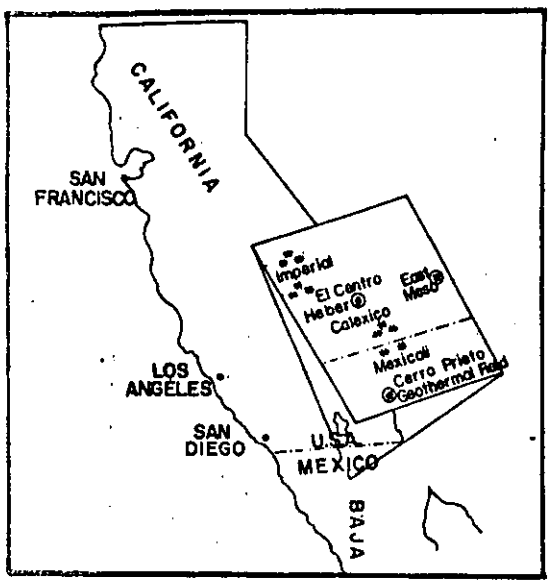

Fig. 1 - Schematic representation of the location of the Gerro Prieto Geothermal Field.

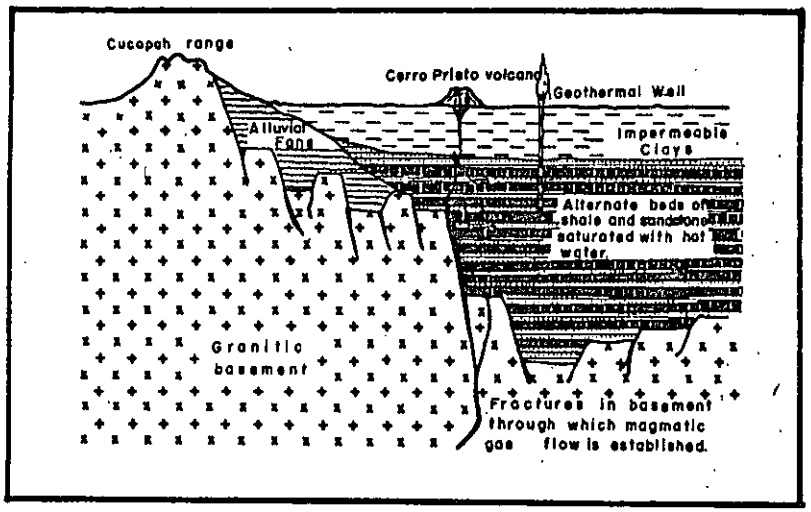

Fig. 2 - Ideal geological cross-section of the Cerro Prieto Reservoir. (After Ref. 1).

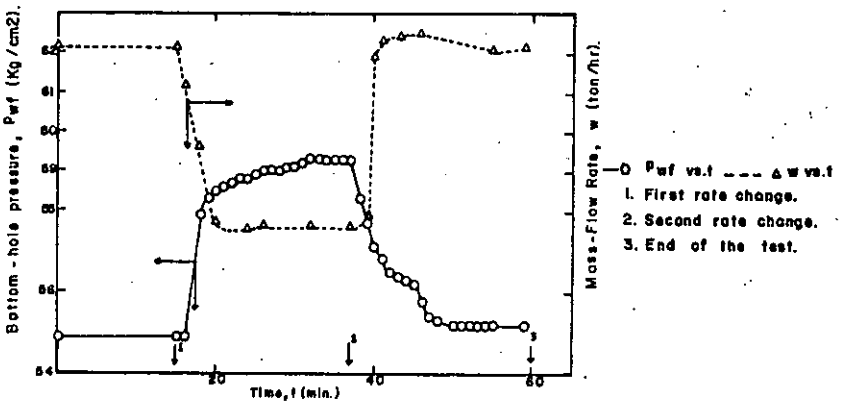

Fig. 3 - The bottom-hole pressure and mass flow rate during the two-rate flow test.

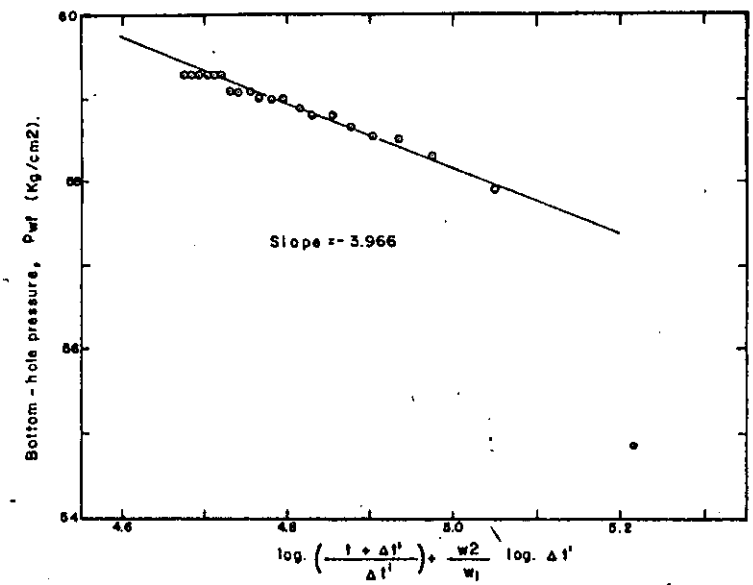

Fig. 4 - Two-rate graph for Russell's-Method.[4]

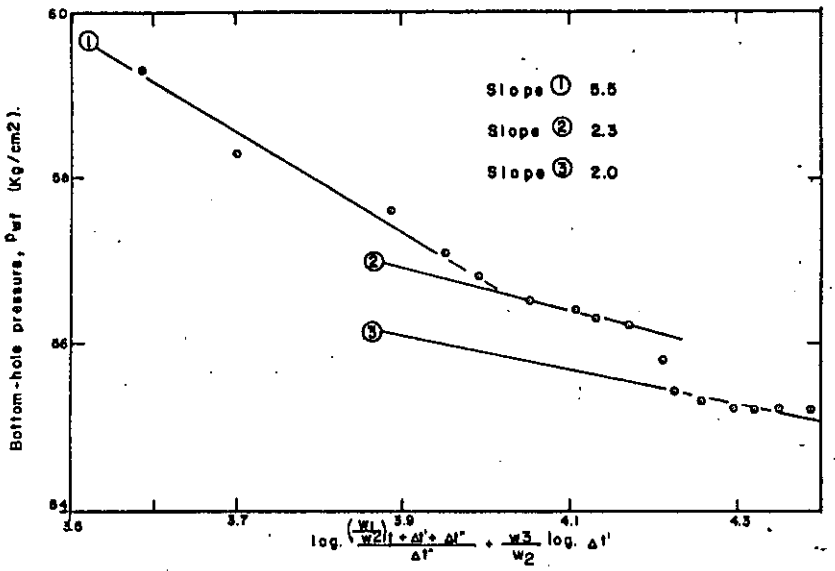

Fig. 5 - Two-rate graph for Selim's[5] Method.

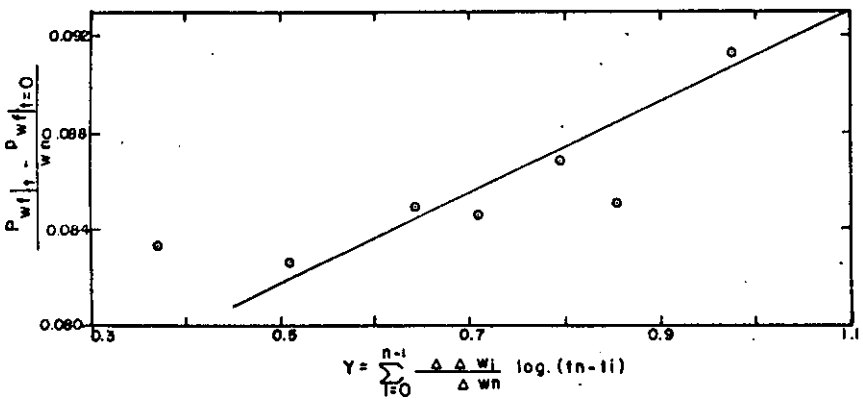

Fig. 6 - Odeh and Jones[7] Variable Drawdown Model.

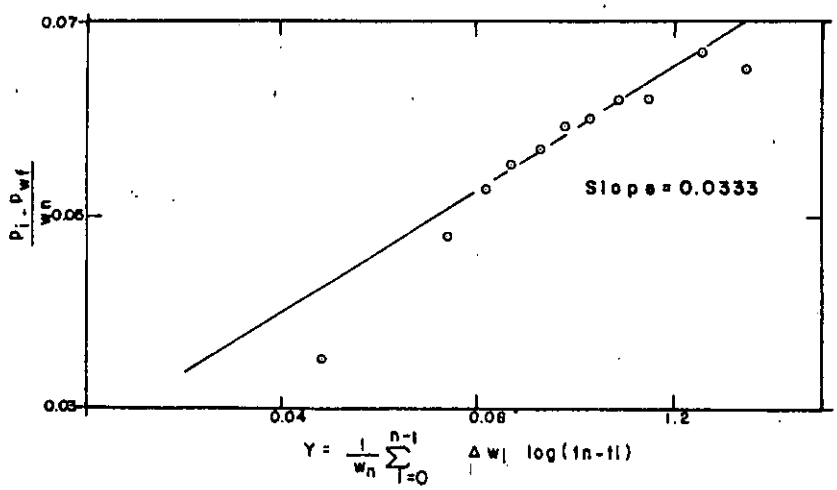

Fig. 7 - Odeh and Jones[6] Two-Rate Model.

Geothermics, Vol. 9, pp. 189–196
Pergamon Press Ltd. 1980. Printed in Great Britain.

70

0375–6505/80/1101–0189 $02.00/0

PRESSURE TRANSIENT TESTING AT CERRO PRIETO GEOTHERMAL FIELD.

J. RIVERA R*., F. SAMANIEGO V†., and R. C. SCHROEDER‡

Comision Federal de Electricidad, Mexicali, Baja California, México, †Instituto de Investigaciones Electricas, México, D.F., México and ‡Lawrence Berkeley Laboratory, Berkeley, CA, U.S.A.

Abstract—The Cerro Prieto geothermal reservoir may be classified as a liquid-dominated system whose initial temperature and pressure conditions place it in the liquid-saturated region. In this field commercial power production began in 1973 and has continued since that date.

Because of the inherent problems in applying pressure build-up tests to wells producing two-phase fluids, it was decided to use variable flow tests of short duration known as two-rate tests. In these tests a variation in the well flow rates can be used to interpret the transient pressure response in order to determine reservoir parameters such as permeability, well-bore damage and mean reservoir pressure in the well drainage area. Some examples will illustrate the application of this technique.

Pressure drawdown tests have been planned in some of the wells in the field. On the other hand, a well interference test has been made in the southern part of the field using M-90, M-91, M-50 and M-51 as production wells and M-101 as an observation well. The interpretation of this test using curve-matching procedures is illustrated.

In the future, several of these tests are planned which will take advantage of the wells being drilled in new areas of the field.

NOMENCLATURE

B	brine formation volume factor, (volume, reservoir conditions/volume, standard conditions).
C_t	total fluid compressibility $(kg/cm^2)^{-1}$
h	formation net thickness, m
k	permeability, md
m	slope of a straight line
p	pressure, kg/cm^2
p_i	initial pressure, kg/cm^2
p_{wf}	flowing bottom-hole pressure, kg/cm^2
p_{1hr}	flowing bottom-hole pressure 1 hr after the rate change, kg/cm^2
q	volumetric flow rate, bbl/day
r	radial distance, m
r_w	wellbore radius, cm
s	skin factor, dimensionless
t	producing time to instant of rate change, h
$\Delta t'$	producing time measured from first rate change, h
V	specific volume, cm^3/g
W	mass flow rate, t/h
μ	viscosity, cp
ϕ	porosity, fraction

Subscripts

D	dimensionless
i	initial condition
M	matching
R	refers to Russell's model
sc	standard conditions
w	wellbore
wf	flowing conditions.

INTRODUCTION

Interference testing is preferred in some instances over single well tests depending on the type of information required (Earlougher 1977). Interference tests provide information about

*Present address: División de Estudios de Post-grade de la Facultad de Ingenieria, UNAM, México 20, D.F., México.

reservoir connectivity, which is important because the number of wells in a reservoir usually increases, causing mutual interference of wells. Another important datum obtained from this test is reservoir porosity, which cannot be obtained from a single-well test (Matthews and Russell, 1967; Ramey *et al.*, 1973).

Modern transient pressure analysis techniques have been basically developed in the fields of petroleum engineering and hydrogeology. Its use on geothermal reservoirs has been shown to be possible (Ramey, 1975; Barelli *et al.*, 1975; Ramey and Gringarten, 1975; Rivera and Ramey, 1977; Witherspoon *et al.*, 1978; Garg, 1978a). Ramey (1975) has presented a summary of transient pressure analysis techniques for geothermal wells. Field examples of pressure buildup tests have been discussed by Barelli *et al.*(1975), and by Ramey and Gringarten (1975); Rivera and Ramey (1977) have presented field results of two-rate flow tests; and Witherspoon *et al.*, (1978) have shown results of interference tests. All of these studies fall in the single phase category. Recently, the two phase flow problem (liquid water and steam) has been addressed by Garg (1978a, 1978b). He discusses a theory for well test analysis of multiphase fluid-flow pressure data.

The purpose of this paper is to present the analysis of an interference test performed in the Cerro Prieto Geothermal Field. Four active production wells (M-50, 51, 90 and 91) and one monitoring well M-101 were involved in this test. In addition, a brief description of the two-rate flow testing efforts carried out at Cerro Prieto is discussed.

GENERAL BACKGROUND

The Cerro Prieto Geothermal Field is located about 30 km south of Mexicali, Baja California. This field is located at the southern end of the Salton-Mexicali trough, which includes other geothermal anomalies such as Heber and East Mesa. It is a liquid-dominated system having a cap rock made of impervious plastic clays. The permeable layers consist of alternating shale and sandstone layers resting on a highly fractured granitic basement.

Comisión Federal de Electricidad started the construction of a 75 MW geothermal power plant in 1968. This plant started commercial operation in April 1973, and has been in operation since that date. The geothermal fluid is obtained as a water – steam mixture, with flashing of the brine taking place at some depth inside the wellbore. The separated hot brine is disposed of in an evaporation pond; however, a project is in progress in order to reinject at least part of the spent liquid (Rivera *et al.*, 1978).

TWO-RATE FLOW TESTS

Among the transient pressure analysis techniques available for obtaining reservoir basic parameters (Earlougher, 1977; Matthews and Russell, 1967; Ramey, 1975) the technique known as 'two-rate flow test' was selected (Rivera and Ramey, 1977). Basically, these tests are performed by changing the flow rate to some predetermined value after the well was stabilized at a given constant rate for some time.

The interpretation equations (Rivera and Ramey, 1977) are as follows:

$$P_{wf} = P_i - 527{\cdot}4\,\frac{W_2\,V_{sc}\,B\,\mu}{kh}\left(\log\frac{k}{\phi\mu\,c_t\,r_w^{\,2}} + 0{\cdot}891 + 0{\cdot}87\,s\right)$$
$$- 527{\cdot}4\,\frac{W_1\,V_{sc}\,B\,\mu}{kh}\left(\log\frac{t+\Delta t'}{\Delta t'} + \frac{W_2}{W_1}\log\Delta t'\right) \qquad (1)$$

From Equation (1) it is evident that by plotting

$$P_{wf} \text{ vs } \log\frac{t+\Delta t'}{\Delta t'} + \frac{W_2}{W_1}\log\Delta t'$$

a straight line should be obtained whose slope is given by:

$$m_R = 527{\cdot}4\,\frac{W_1\,V_{sc}\,B\,\mu}{kh} \qquad (2)$$

The equation for the skin factor is given by the following expression:

$$s = 1{\cdot}151\,\frac{W_1}{W_1 - W_2}\,\frac{P_{1\,hr} - P_{wf}}{m_R} - \log\frac{k}{\phi\mu\,c_t\,r_w^2} - 0{\cdot}891 \qquad (3)$$

Figures 1 and 2 show the results obtained from the application of the two-rate flow technique to wells M-21A and M-25 at Cerro Prieto. In well M-21A a good straight line section was developed; however, in well M-25 no straight line is evident. Most of the tests conducted so far have shown the development of good straight line sections.

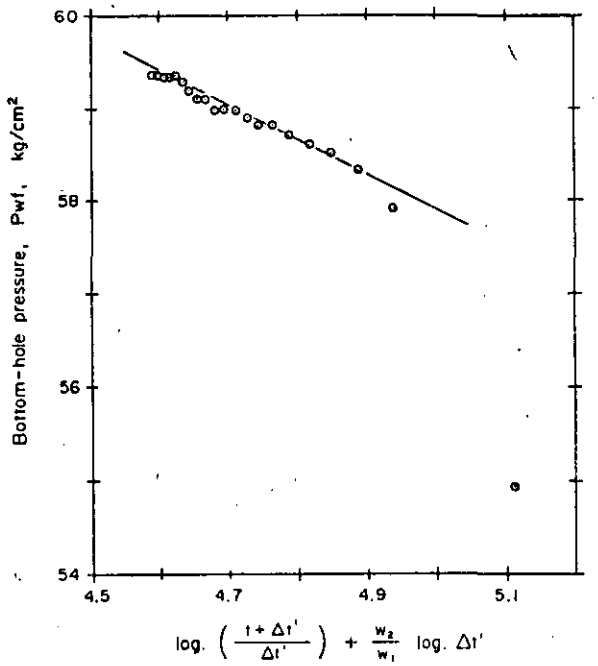

Fig. 1. Two-rate flow test for well M-21A.

INTERFERENCE TEST

An interference test is a multiple-well technique which has the advantage of investigating more reservoir than a single-well test. Because of this fact, it was decided to run an interference test in the southern portion of the Cerro Prieto Geothermal Field. This portion of the field has not as yet been exploited and several wells were already available to carry out this test. Figure 3 shows the location of the wells, and Fig. 4 illustrates both the production history of the active wells (M-50, 51, 90 and 91) and the transient pressure behavior at the observation well (M-101).

The test was performed taking advantage of the fact that the new wells drilled in that portion of the field should be brought into production one at a time. However, this also imposed an extra difficulty in analyzing the data, because of strong variations of flow rates, as can be seen in Fig. 4. This study presents the results of a first attempt to analyze the data obtained from the early part of the test when only well M-91 was flowing. The procedure used was type curve

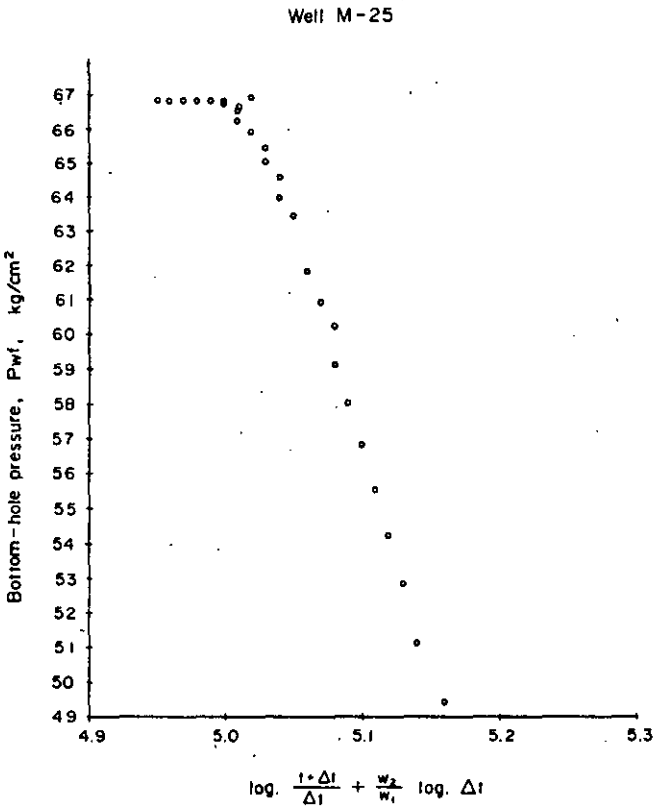

Fig. 2. Two-rate flow test for well M-25.

matching by means of the line source solution. A more rigorous analysis that considers the rate variation is underway. Fig. 5 shows the results obtained from this analysis. The match-point obtained is as follows:

For

$$(\Delta P)_M = 1 \text{ psi}, (P_D)_M = 1{\cdot}8 \times 10^{-2},$$
$$(t)_M = 100 \text{ days}, \left(\frac{t_D}{r_D^2}\right)_M = 0{\cdot}63,$$

where the dimensionless variables are defined as follows:

$$P_D = 1{\cdot}5388 \times 10^{-4} \frac{k\,h\,\Delta P}{W\,V_{sc}\,B\,\mu} \tag{4}$$

$$\frac{t_D}{r_D^2} = 0{\cdot}0008366 \frac{kt}{\phi\,\mu\,c_t\,r^2} \tag{5}$$

Table 1 shows the pressure interference data. Table 2 below shows the values of the variables in equations (4) and (5).

Actually, it is possible to obtain two good matches of the data points with the type curve. The match shown in Fig. 5 was obtained by taking into account the set of drawdown data. On the other hand, it is also possible to obtain a good match by using only those points concerned with the drawdown produced by well M-91 alone. Table 3 below illustrates the results obtained in those cases mentioned before.

74

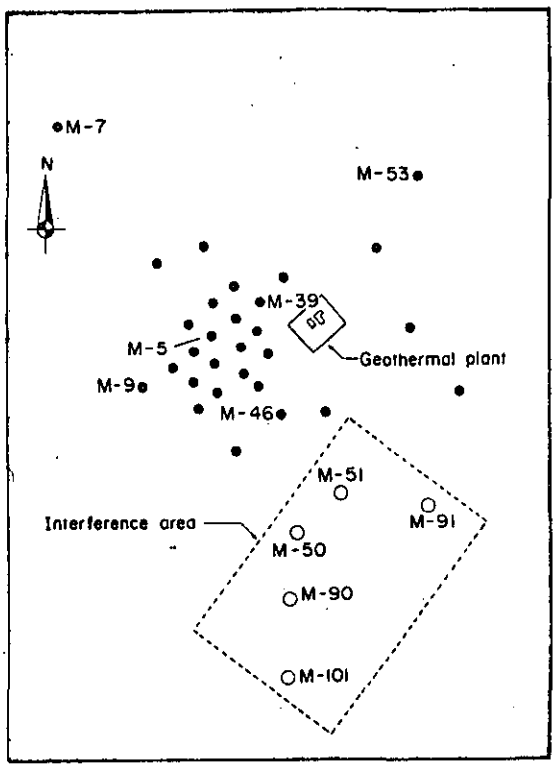

Fig.3. Location of the wells.

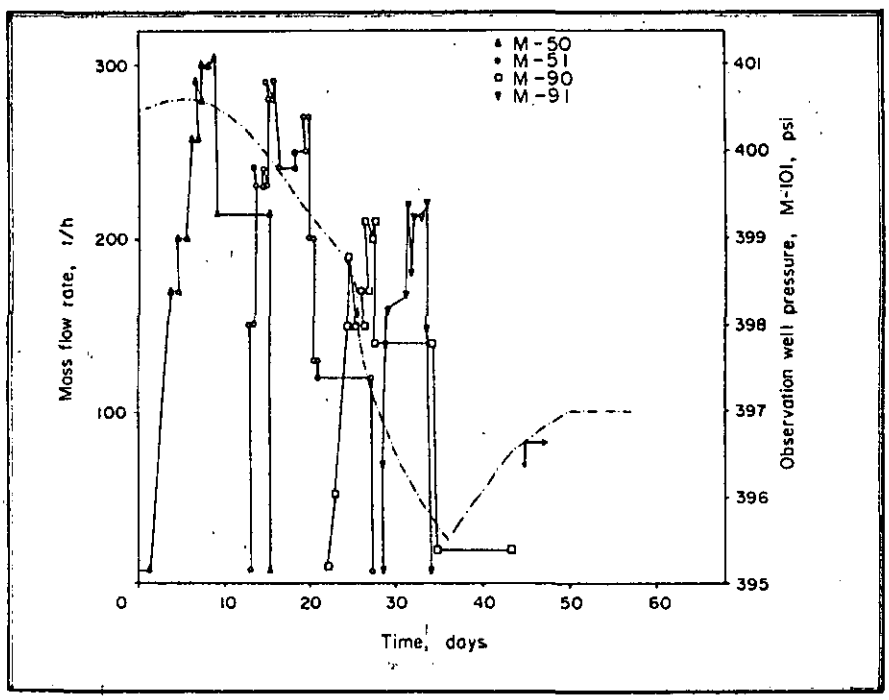

Fig. 4. Active wells production schedule and observation well pressure.

75

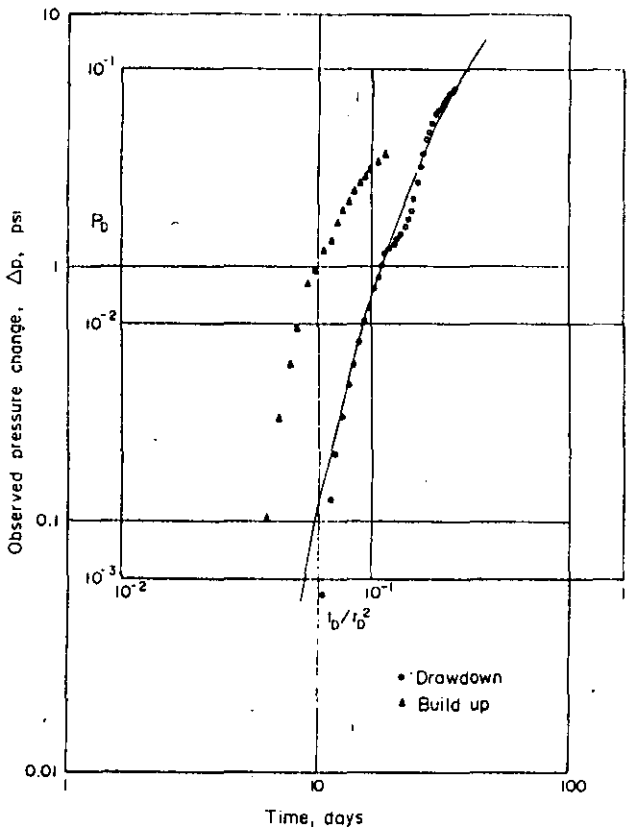

Fig. 5. Type curve match of an interference test, active wells M-90, M-91, M-50, and M-51. Observation well M-101, Cerro Prieto geothermal field.

Table 1. Pressure interference data

Total time (days)	Well pressure at 1000 ft (psi)	Pressure drop (psi)	Total time (days)	Well pressure at 1000 ft (psi)	Pressure drop (psi)
9·72*	400·50	0	27·08	397·40	3·10
10·42	400·45	0·045	27·78	397·15	3·35
11·11	400·38	0·12	28·47¶	396·90	3·60
11·81	400·32	0·18	29·17	396·90	3·90
12·50	400·25	0·25	29·86	396·40	4·10
13·19†	400·17	0·33	30·56	396·25	4·4
13·89	400·10	0·40	31·25	396·10	4·5
14·58	400·00	0·50	31·94	395·95	4·55
15·28	399·90	0·60	32·64	395·85	4·65
15·97‡	399·82	0·68	33·33	395·75	4·75
16·67	399·70	0·80	34·03	395·65	4·85
17·36	399·62	0·88	34·72	395·55	4·95
18·06	399·52	0·98	35·42	395·50	5·00
18·75	399·40	1·10	36·11	395·55	4·95
19·44	399·35	1·15	36·81	395·70	4·80
20·14	399·32	1·18	37·50	395·80	4·70
20·83	399·25	1·25	38·19	395·90	4·60
21·53§	399·20	1·30	38·89	396·00	4·50
22·22	399·10	1·40	39·58	396·10	4·40
22·92	399·00	1·50	40·28	396·20	4·30
23·61	398·90	1·60	40·97	396·25	4·25
24·31	398·70	1·80	41·67	396·35	4·15
25·00	398·40	2·10	42·36	396·45	4·05
25·69	398·10	2·40	43·06	396·55	3·95
26·39	397·75	2·75	43·75	396·60	3·90

* Well M-91 producing. All others shut-in.
† Well M-51 starts production.
‡ Well M-91 shut-in.
§ Well M-90 starts production.
¶ Well M-50 starts production.

Table 2. Values used in calculations of capacity (kh) and storativity ($\phi c_t h$).

w = Average flow rate = 185·3 (t/h)
V_{sc} = 1·043 (cm³/g)
B = 1·185 (res. vol/st. vol)
μ = 0·1017 cp
r = 1550 m

76

Table 3. Summary of results obtained from match points.

Data points matched	(kh) (md - m)	($\phi c_t h$) (m/(kg/cm²))	* k(md)	†ϕ%
All drawdown	38684	0·0210	38	18
Only well M91	53728	0·01946	54	16
Average	46206	0·0203	46	17

* In calculating k and ϕ a net pay thickness of 1000 m was assumed; well log data should be considered in order to determine a more realistic value of h.
† A value of 119×10^{-6} (kg/cm²)$^{-1}$ was considered for c_t.

A more rigorous mathematical analysis of the data which takes into account superposition in time of the influence of the four active wells, as well as the closest row of producing wells from that part of the field on exploitation is in progress.

CONCLUSIONS AND RECOMMENDATIONS

The main purpose of this study has been to present the results of the analysis of two-rate flow tests and a preliminary analysis of an interference test performed in the Cerro Prieto Geothermal Field. From the results of this study the following points can be drawn.

1. Two-rate flow tests seem to be an adequate and quick technique for obtaining reservoir parameters in the drainage area of a well. It is necessary to take into account the total fluid mobility when two-phase flow is taking place.
2. It is convenient to plan in advance a more adequate schedule of production for the active wells involved in an interference test, in order to provide a convenient way to analyze the results obtained from the pressure response at the observation well.
3. From the results obtained, it is evident that the portion of the reservoir studied in the interference test is a very complex, probably highly fractured, structure.
4. Since presence of fractures could be inferred from both well electrical logs correlation and interference response, it seems convenient to take this fact into account in the interpretation of the pressure response data.
5. The results of the interference test presented in this work are only preliminary; a more comprehensive and rigorous analysis is underway.

REFERENCES

Barelli, A., Manetti, G., Celati, R., and Neri, G. (1975). Buildup and back pressure tests on Italian geothermal wells. *Proc. 2nd U.N. Symposium Development and Use of Geothermal Resources, San Francisco*, 3, 1537 – 1546.

Earlougher, R. C., Jr. (1977) *Advances in Well Test Analysis*, Monograph Series, Society of Petroleum Engineers of AIME, Dallas, 5.

Garg, S. K. (1978a). Pressure transient analysis for two-phase geothermal reservoirs. *Geothermal Resources Council, Trans.* 2, 203 – 206.

Garg, S. K. (1978b). Pressure transient analysis for two-phase (liquid water/steam) geothermal reservoirs. Paper SPE 7479, to be presented at the *53rd. Annual Fall Technical Conference*, Houston, TX., 1 – 4 Oct.

Matthews, C. S, and Russell, D. G. (1967). *Pressure Buildup and Flow Test in Wells*, Monograph Series, Society of Petroleum Engineers of AIME, Dallas, 1.

Ramey, H. J., Jr. (1975). Pressure transient analysis for geothermal wells. *Proc. 2nd U.N. Symposium Development and Use of Geothermal Resources, San Francisco*, 3, 1749 – 1757.

Ramey, H. J., Jr. and Gringarten, A. G. (1975). Effect of high-volume vertical fractures on geothermal steam well behavior. *Proc. 2nd U.N. Symposium Development and Use of Geothermal Resources, San Francisco*, 3, 1759 – 1762.

Ramey, H. J., Jr., Kumar, A. and Gulati, M. S. (1973). *Gas Well Test Analysis Under Water-Drive Conditions*, AGA, Arlington, Va.

Rivera, R. J., Mercado, G. S., and Tsang, C. F. (1978). Preliminary studies of reinjection of the produced brine at Cerro Prieto Geothermal Field. *Joint CFE/DOE Cooperative Program Symposium San Diego, CA*.

Rivera, R. J., and Ramey, H. J., Jr. (1977). Application of two-rate flow tests to the determination of geothermal reservoir parameters. Paper SPE 6887. Presented at the *52nd Annual Fall Technical Conference and Exhibition of SPE*, Denver, CO., 9–12 October.

Witherspoon, P. A., Narasimham, T. N. and McEdwards, D. G. (1978). Results of interferences tests from two geothermal reservoirs. *J. Pet. Tech.* **30**, 10–16.

SPE
Society of Petroleum Engineers of AIME

SPE 8348

WELL TESTING AT LOS AZUFRES GEOTHERMAL FIELD

by Jesus Rivera-R., Comision Federal de Electricidad; and
Mehmet Saltuklaroglu, ELC, Electroconsult, Members SPE-AIME

This paper was presented at the 54th Annual Fall Technical Conference and Exhibition of the Society of Petroleum Engineers of AIME, held in Las Vegas, Nevada, September 23-26, 1979. The material is subject to correction by the author. Permission to copy is restricted to an abstract of not more than 300 words. Write 6200 N. Central Expy., Dallas, Texas 75206.

ABSTRACT

It is important to determine reservoir characteristics as early in the life of the reservoir as possible. This paper presents a summary of the efforts made by Comision Federal de Electricidad to evaluate Los Azufres field by means of the implementation of standard pressure transient analysis techniques to geothermal reservoirs. Among these techniques, constant injection, falloff, multiple-rate injection, build-up, drawdown, two-rate and variable rate tests have been applied. Discussion is presented on constant injection, falloff, two-rate and variable rate testing. Interference testing is now being conducted on a small portion of the field.

INTRODUCTION

After the discovery of a geothermal field has been confirmed by successfully drilling one or more wells, the reservoir engineer has to obtain as much information out of them as possible. This information is needed in order to perform a proper evaluation of the field, before the utility company can proceed with the construction of an electric power generating facility.

Among those geothermal fields undergoing exploration in Mexico, Los Azufres is the one in the most advanced stage of exploration. This geothermal field is located some 300 kilometers southwest of Mexico City, in the state of Michoacan in Central Mexico. As shown in Figure 1, this field is situated on the E-W oriented neo-volcanic axis. It is a highly fractured system, located on neo-quaternary volcanic deposits overlying a basement which is believed to be made of limestone. The lower part of the igneous deposits is constituted by microgranular andesites which are overlaid at places by ryolites and pyroclastics.

References and illustrations at end of paper.

There are many thermal manifestations and alteration zones around the field which are related to tectonic activity and are located near faults and fracture zones. To date, 8 wells have been drilled in the field, 6 of them are for production and 2 injectors. Three more wells are on the drilling stage and 6 additional wells are schedulled to be drilled during 1979, Figure 2 illustrates the main faults and the location of the wells.

The wells so far drilled in this area are sited near the known major faults. The reason behind this may of selecting locations is that because of the tightness of igneous rocks, the main production is thought to come through fractures. The deepest well is 2450 m and the shallowest is 960 m deep.

Los Azufres field is under the last stage of the feasibility study, which has been carried out in order to determine the optimum size of turbines to be installed for electricity generation. This field has been divided into several possible producing areas called "modules" around the main fracture zones. This areas will be developed independently from each other. Thus, reference will be made in the text to Laguna Verde Module, Agua Fria Module and Tejamaniles Module, among them the latter is under intensive drilling development (See Fig. 2).

Figure 3 shows a typical temperature survey and well completion of this field. Wells are drilled using low density bentonitic mud from surface up to the top of the reservoir and with water from that depth downwards.

Los Azufres reservoir is a liquid-dominated system having a steam cap located on the Tejamaniles Module, in the zone of well A-6, whose productivity test showed a 99 percent steam. Figure 4 illustrates a

cross-section going from well A-10 up to well A-11 drawn on a SE-NW direction through the field. This section shows a correlation of the production zone based upon calculated static bottom-hole temperatures whose range is from 270 to about 298°C.

WELL TESTING PROGRAM

As it was stated before, standard pressure transient analysis techniques adapted to geothermal systems have proven to be of great help to evaluate wells at Los Azufres field. Among those techniques published in the literature, pressure build-up, drawdown, two-rate and variable rate flow, injection and interference testing have been applied in this field.

INJECTION TESTING

The possibility of obtaining commercial production from igneous rocks is to encounter secondary permeability, which in Los Azufres is represented by highly fractured volcanic rock. An index of these permeable zones observed in drilling the well is to have lost of drilling fluid circulation. If this lost is big enough and the static bottom-hole temperature is within commercial ranges (greater than 230°C), a short-term injection test is performed.

Injection tests[1,2,3] are carried out as a part of completion procedures in this field by using standard bottom-hole pressure bombs. The main purpose of these tests is to obtain early information about the well and reservoir parameters, which could be helpful in selecting the most appropriate zone for completion of the well; in addition they can be used in order to predict future well performance. These type of tests have been found easier and quicker to perform than drawdown and build-up tests and the results obtained from them are judged to be reasonably good.

Within the several types of tests available in the literature, those known as injection, multiple-rate injection and falloff tests have been employed in this field. Results obtained from typical injection and falloff tests are described below. For more detailed description of these tests the reader should refer to Reference 3.

Several temperature surveys are carried out in order to determine temperature distribution before any injection test is performed. Injection rates commonly used in this field are 4528, 10870 and 13580 bbl/day. The usual procedure is to run an injection test at any of the rates mentioned above for a period of 3 to 4 hours, recording changes in bottom-hole pressure by means of a standard bourdon-tube type pressure bomb. Immediately after injection stops, the falloff period is recorded in order to obtain enough data to check the results obtained from the analysis of injection data.

When results obtained from analysis of constant rate injection and falloff data are not conclusive, two-rate injection tests have been conducted. However, it has been observed that in those wells applied, dispersion of the data is present, making the interpretion difficult.

Interpretation of injection and falloff data is made by applying well-known pressure transient analysis techniques already reported in the literature[1,2,3]. Results of a test conducted in well A-2 are shown in Figs. 5 thru 8.

First, a log-log plot of bottom-hole pressure difference versus either injection or shut-in time is tried in order to determine the duration of wellbore storage effects. Then by using the type-curve procedure, a match is obtained between field data and published type curves[2,4]. Dimensionless pressure and time are according to the usual definition[1]:

$$p_D = \frac{kh}{141.2q\mu B}\,\Delta p \qquad (1)$$

$$t_D = \frac{0.0002637kt}{\phi\mu\, c_t r_w^2} \qquad (2)$$

Figs. 5 and 6 show the match obtained by fitting the data obtained in an injection and falloff test to the type-curves published by Agarval et al[2]. Data of these test are shown in Table 1. Calculations of reservoir parameters are included in the Appendix. It has been observed that sometimes it is difficult to obtain a unique match. In these cases, an estimation of C_D has been made in order to reduce uncertainty in the match.

From experience of application of injection tests in this field[3], it has been observed that in a log-log plot the transition period between the section of slope 1 and the start of the semilog straight line is very short in undamaged wells as that shown in Figs. 5 and 6; meanwhile, in damaged wells it can be very long (it usually takes about 2 1/2 to 3 hours).

After the correct start of the semilog straight line has been determined, analysis of the data by these methods is performed. Figs. 7 and 8 show data from injection and falloff tests respectively. Techniques for this type of analysis are well known and the basic equations are as follows[1]:

For a constant rate injection test, the bottom-hole injection pressure is given by the following equation:

$$p_{wf} = p_{1hr} + m \log t \qquad (3)$$

and the skin factor is as follows:

$$s = 1.1513\left[\frac{p_{1hr}-p_i}{m} - \log\left(\frac{k}{\phi\mu c_t r_w^2}\right) + 3.2275\right] \quad (4)$$

where:

$$p_{1hr} = p_i + m\left[\log\left(\frac{k}{\phi\mu c_t r_w^2}\right) - 3.2275 + 0.86859s\right] \quad (5)$$

$$m = \frac{-162.6qB\mu}{kh} \quad (6)$$

For a falloff test following a constant injection period, the bottom-hole pressure is given by the following equation:

$$p_{ws} = p^* - m\log\left(\frac{t_p + \Delta t}{\Delta t}\right) \quad (7)$$

A plot of p_{ws} vs $\log\left(\frac{t_p + \Delta t}{\Delta t}\right)$ should show a straight line whose slope m is given by the following expression:

$$m = \frac{162.6qB\mu}{kh} \quad (8)$$

and the skin factor is given by the following equation:

$$s = 1.1513\left[\frac{p_{1hr}-p_{wf}(\Delta t=0)}{m} - \log\left(\frac{k}{\phi\mu c t r_w^2}\right) + 3.2275\right] \quad (9)$$

Calculation of these tests are illustrated in the Appendix, Table 2 shows a comparison of the results obtained by using both type-curve and standard semilog techniques. As it can be observed from this table, results from both methods are in good agreement. Generally speaking, results obtained from semilog methods should be prefered to those obtained from graphical procedures.

MULTIPLE RATE TESTS.

After the wells have produced some time, multiple-rate production tests [5,6] have been applied to check values of (kh/μ) obtained by means of injection and falloff tests. Thus far, the application of these techniques have proven to be successfull. For well A-2, the value of (kh/μ) obtained from a multiple-rate test is 86910 md-ft, which is in the range of those reported in table 2.

Application of two-rate flow tests[5] to wells with low (kh/μ) values, producing fluid in a two-phase flow regime from the bottom of the hole up to the surface, have shown scatter of the data, making the interpretation very uncertain.

INTERFERENCE TESTING

Interference testing is underway in a portion of the field known as Tejamaniles Module (See Fig. 2). Wells A-2, A-6, A-7 and A-8 are involved in this test. Basic information is expected to be obtained which will help in selecting well spacing and the most convenient well grid orientation in this zone.

CONCLUSIONS

From results of tests described in this paper, the following conclusions can be reached:

1.- Constant rate, injection tests falloff tests have proven to be successful in obtaining geothermal reservoir parameters in Los Azufres Field.

2.- Short term injection tests seem to be adecuate in providing a quick and reasonable good estimate of basic parameters in geothermal reservoirs located on igneous rocks, whose main production takes place through fractures.

3.- Standard pressure transient analysis techniques seem to find application in liquid-dominated geothermal systems similar to Los Azufres Field.

NOMENCLATURE

- B = brine formation volume factor, (volume, reservoir conditions/volume, standard conditions).
- C_D = dimensionless wellbore storage coefficient.
- c_t = Total compressibility, $(psi)^{-1}$
- h = formation net thickness, ft.
- k = permeability, md.
- m = slope of a straight line.
- p = pressure, psi.
- p_i = initial pressure, psi.
- p_{wf} = flowing bottom-hole pressure, psi.
- p_{1hr} = flowing bottom-hole pressure al 1hr, psi.
- p_{ws} = static bottom-hole pressure, psi.
- p_D = dimensionless pressure.
- q = volumetric flow rate, bbl/day.
- r_w = wellbore radius, ft.
- s = skin factor, dimensionless.
- t = time, hrs.
- t_p = injection time, hrs.
- Δt = shut-in time, hrs.

GREEK SYMBOLS

- μ = viscosity, cp.
- ϕ = porosity, fraction.

ACKNOWLEDGEMENTS

The authors wish to thank the Comision Federal de Electricidad for permission to publish the field data presented in this paper. The assistance received from Ing. Alfonso Aragon-Aguilar in processing the data and helpful discussions with Dr. Fernando Samaniego-Verduzco are also acknowledged.

REFERENCES

1. Earlougher, R.C., Jr.: Advances in Well Test Analysis, Society of Petroleum Engineers of AIME Monograph Volume 5. The Society, New York (1977).

2. Agarval, R.G., Al-Hussainy, R., and Ramey, H.J.,Jr.: "An Investigation of Wellbore Storage and Skin Effect in Unsteady-Liquid Flow": I Analytical Treatment, Soc. Pet. Eng. Jour. (Sept., 1970) 279-290.

3. Saltuklaroglu, M., and Rivera-R.,J.: "Injection Testing in Geothermal Wells", Proceedings, Fourth Workshop on geothermal Reservoir Engineering, Stanford, C.A. (Dec. 13-15, 1978) 176-187.

4. Earlougher, R.C.,Jr. and Kersch, K.M.: "Analysis of Short Time Transient Test Data by Type-Curve Matching", J. Pet. Tech. (July 1974) 793-800.

5. Odeh, A.S. and Jones, L.G.: "Pressure Drawdown Analysis, Variable-Rate Case", J. Pet. Tech. (Aug. 1965) 960-964.

6. Rivera-R, J., and Ramey, H.J.,Jr.: "Application of two-Rate Flow Tests to the Determination of Geothermal Reservoir Parameters", paper SPE 6887 presented at SPE-AIME. 52nd Annual Technical Conference, Denver, Colorado, Oct. 9-12, 1977.

APPENDIX - RESERVOIR PARAMETERS CALCULATIONS.

INJECTIVITY TESTS.

A. Injection test.

a). Type-curve procedure.
From Fig. 5, the match point is as follows:
For $(t)_M$=100 min, $(t_D)_M$=8.4x10^4, s= -2
For $(\Delta p)_M$=10 psi, $(p_D)_M$=1.28
From eq.(1) in the text:

$$\frac{kh}{\mu} = 141.2\ qB\ \frac{(pn)M}{(\Delta p)_M} = 141.2(4528)(1)\frac{1.28}{10}$$

$$= 81837\left(\frac{md\text{-}ft}{cp}\right)$$

From eq.(2) in the text:

$$\phi c_t h = \frac{0.0002637}{r^2_w}\ \frac{kh}{\mu}\ \frac{(\Delta t)M}{(t_D)M} =$$

$$= \frac{0.0002637}{(0.463)^2}\ (81837)\ \frac{1,667}{8.4x10^4}$$

$$= 1.99x10^{-3}\ (ft/psi)$$

b). Semilog analysis.
From Fig. 7 : m = 6.96 psi/cycle.
From eq.(6) in the text:

$$\frac{kh}{\mu} = \frac{162.6qB}{m} = \frac{162.6(4528)(1)}{6.96}$$

$$\frac{kh}{\mu} = 105814\left(\frac{md\text{-}ft}{cp}\right)$$

From eq.(4) in the text:

$$s=1.1513\left\{\frac{838.1-818.5}{6.96} - \log\left[\left(\frac{105814}{1.99x10^{-3}}\right)\left(\frac{1}{0.463^2}\right)\right] + 3.2275\right\} = -2.7$$

From Fig.7 it is evident from the change in slope,that a barrier is located close to the wellbore which is corroborated by geologic evidence (see Figs. 2 and 4). Distance to this barrier is as follows:

$$L = 0.01217\sqrt{\left(\frac{kh}{\mu}\right)\left(\frac{1}{\phi\mu ct}\right)}\,tx = 0.01217$$

$$\sqrt{105814\left(\frac{1}{1.99x10^{-3}}\right)\left(\frac{1}{0.463^2}\right)} = 192\ ft.$$

B. Falloff test.

a). Type - curve procedure.
From Fig. 6, the match point is given by:
For $(t)_M$=100 min; $(t_D)_M$=6.4x10^5, s= -1
For $(\Delta p)_M$=10psi, $(p_D)_M$=1.4
From eq.(1) in the text:

$$\frac{kh}{\mu} = 141.2(4528)(1)\frac{1.4}{10} = 89509\left(\frac{md\text{-}ft}{cp}\right)$$

From eq(2) in the text:

$$\phi c_t h = \frac{0.0002637}{(0.463)^2}(89509)\frac{1.667}{6.4x10^5} = 2.87x10^{-4}\ \left(\frac{ft}{psi}\right)$$

b). Semilog analysis.
From Fig. 8 : m = 7.1 psi/cycle
From eq.(8) in the text:

$$\frac{kh}{\mu} = \frac{162.6(4528)(1)}{7.1} = 103705\frac{(md\text{-}ft)}{cp}$$

From eq.(9) in the text:

$$s=1.1513\left\{\frac{811-849}{7.1} - \log\left[(103705)\left(\frac{1}{2.87x10^{-2}}\right)\left(\frac{1}{0.463^2}\right)\right] + 3.2275\right\} = -1.3$$

Table 1

Data from injection and fallof tests in well A-2. q_{inj}=4528 bbl/day.

INJECTION		FALLOFF	
Time (min)	Pwf (psi)	Time (min)	Pws (psi)
0	818.5	1	848.2
1	825.7	3	847.3
2	827.9	4	832.3
4	830.0	5	827.2
6	831.5	6	821.3
8	832.3	7	819.2
10	833.0	8	819.2
12	833.0	9	819.2
14	833.7	10	817.6
16	833.7	12	817.6
18	835.1	22	815.5
28	837.9	32	813.4
38	840.2	42	812.0
48	840.9	52	811.2
58	841.6	62	809.7
68	843.1	72	809.7
78	845.3	80	809.7
88	846.7		
98	848.2		
108	848.2		
118	848.9		
128	848.9		
138	848.9		
148	847.9		
210	847.9		

Table 2

Summary of results obtained applying Type-curve and semilog techniques. Injection rate =4528 bbl/day.

	$\frac{kh/\mu}{(md\text{-}ft)/cp}$	$\frac{c_t h}{ft/psi}$	s
INJECTION			
Type-curve	81837	1.99×10^{-3}	-2
Semilog	105814		-2.7
FALLOFF			
Type-curve	89509	2.87×10^{-4}	-1
Semilog	103705		-1.3

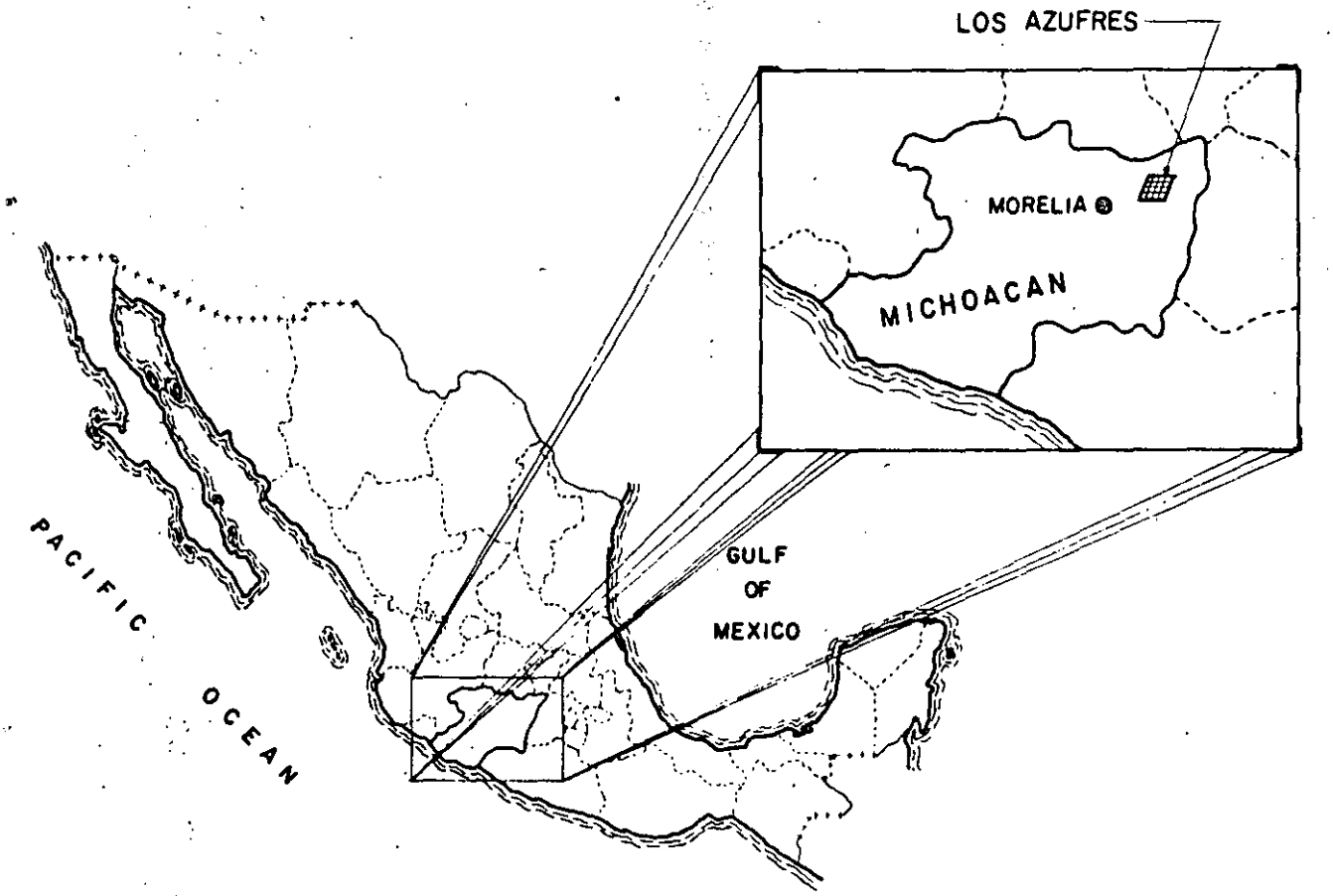

Fig. 1 - Location on Los Azufres geothermal field.

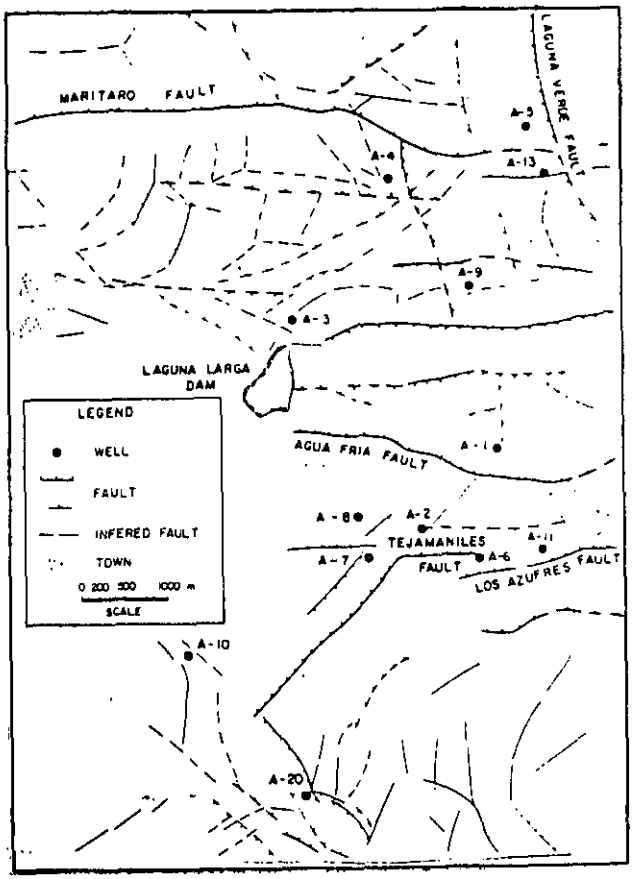

Fig. 2 - Location of wells and main faults.

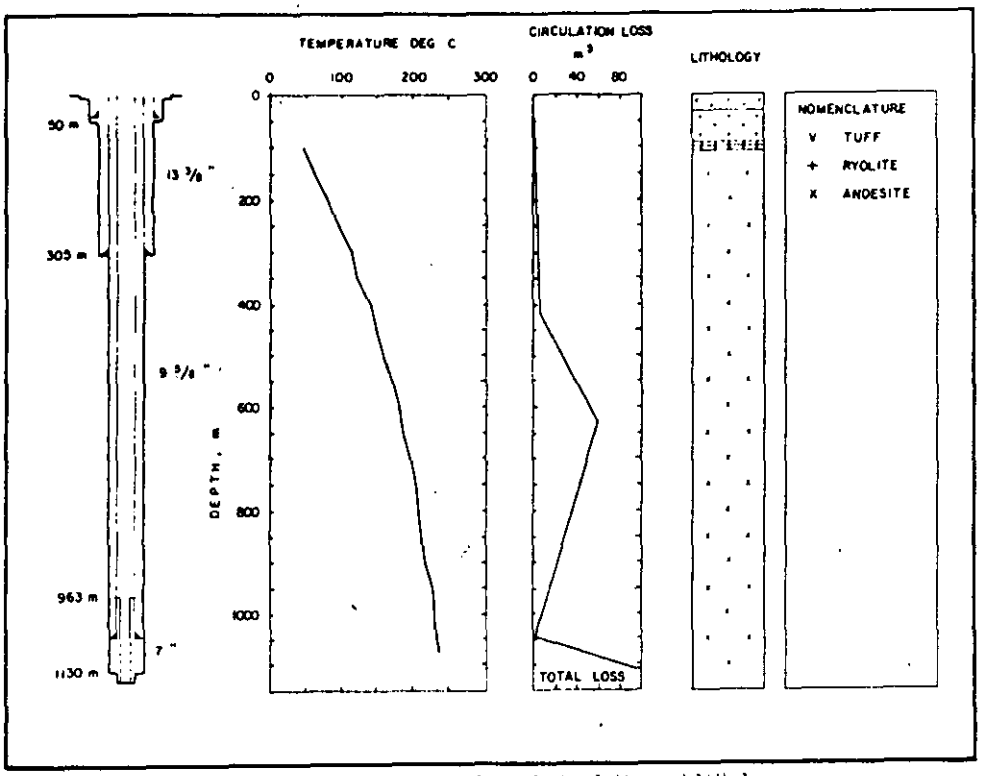

Fig. 3 - Completion, temperature, loss of circulation and lithology of well A-2.

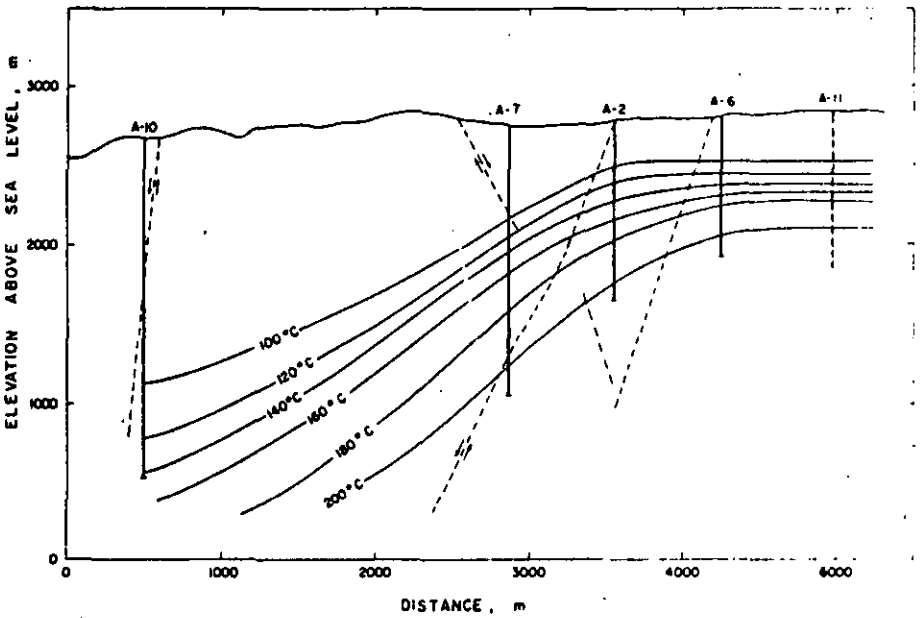

Fig. 4 - Cross-section through the field on a NE-SW direction.

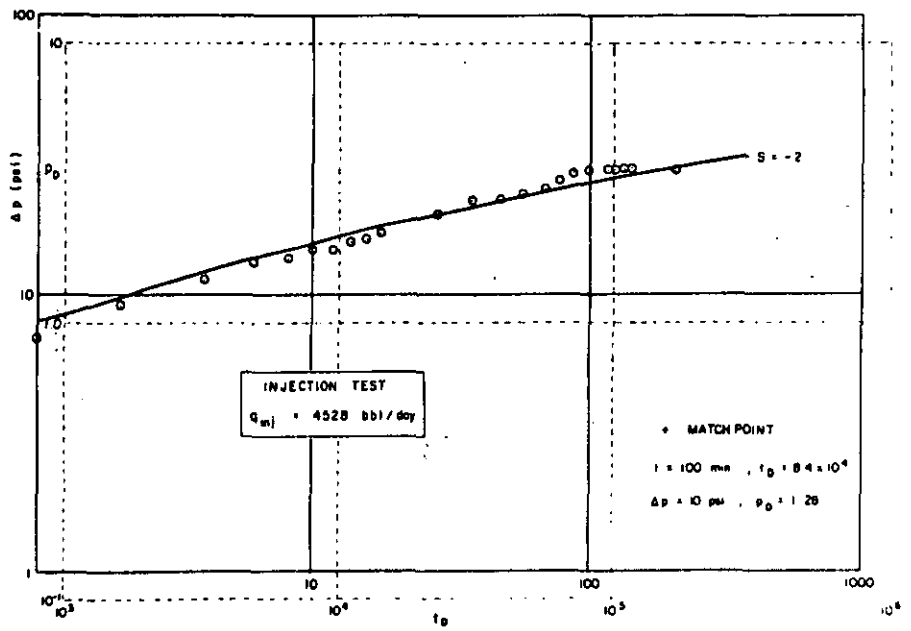

Fig. 5 - Type-curve match of data from an injection test in well A-2. q_{inj}=4528 bbl/day.

CURSO: "INGENIERIA DE YACIMIENTOS GEOTERMICOS"

En colaboración con, OLADE, C.F.E., I.I.E.

Del 13 marzo - 18 mayo

TEMA: PRUEBAS DE PRESION

1.- Bourdet, D, Whittle, TM y Pirard M., Curva Tipo de P_D y (T_D/C_D) P_D Contra TD/CD

DR. FERNANDO SAMANIEGO

13-23 MARZO 1984

WELL WITH WELLBORE STORAGE AND SKIN
INFINITE ACTING RESERVOIR WITH HOMOGENEOUS BEHAVIOR

The use of this type-curve is described in World Oil - May 1983 : A NEW SET OF TYPE CURVES SIMPLIFIES WELL TEST ANALYSIS by D.BOURDET, T.M.WHITTLE, A.A.DOUGLAS, Y.M.PIRARD.

$$C_D = \frac{0.8936\,C}{\phi c_t h r_w^2}$$

$$\frac{t_D}{C_D} = 0.000295\,\frac{kh}{\mu}\,\frac{\Delta t}{C}$$

FOR OIL — $p_D = \frac{kh}{141.2qB\mu}\,\Delta p$

— $\frac{t_D}{C_D}p_D' = \frac{kh}{141.2qB\mu}\,\Delta t.\Delta p'$

FOR GAS — $p_D = \frac{kh}{5.030\ 10^4 q}\,\frac{T_{sc}}{T}\,\frac{2}{p_{sc}}\int_{p_0}^{p_0+\Delta p}\frac{p}{\mu(p)Z(p)}\,dp$

— $\frac{t_D}{C_D}p_D' = \frac{kh}{5.030\ 10^4 q}\,\frac{T_{sc}}{T}\,\frac{2}{p_{sc}}\,\frac{p}{\mu(p)Z(p)}\,\Delta t.\Delta p'$

Schlumberger

DIMENSIONLESS PRESSURE p_D AND PRESSURE DERIVATIVE GROUP $(t_D/C_D)p_D'$

DIMENSIONLESS TIME GROUP t_D/C_D

C_De^{2S}

damaged well

non-damaged well

acidized well

APPROXIMATE END OF UNIT SLOPE LOG-LOG STRAIGHT LINE

CURSO: "INGENIERIA DE YACIMIENTOS GEOTERMICOS"

En colaboración con la OLADE, C.F.E., I.I.E.

Del 13 Marxo - 18 Mayo.

TEMA: PRUEBAS DE PRESION

2.- Economides, M.J. Ogbe, D. Miller, F.G.
Cinco Ley M. y Fehlber E.L.;

"Pressure Buildup Analysis of Geothermal
Steam Wells With a Parallelepiped Model",
J. Pet. Tech. (Abril, 1982,925-929)

DR. FERNANDO SAMANIEGO
13-23 MARZO 1984

Pressure Buildup Analysis of Geothermal Steam Wells With a Parallelepiped Model

Michael J. Economides,* SPE, Stanford U.
David Ogbe, Stanford U.
Frank A. Miller, SPE, Stanford U.
Heber Cinco-Ley, SPE, U. of Mexico
Eric L. Fehlberg, Shell Oil Co.

Summary

Geothermal well testing, a discipline that evolved from conventional oil and gas well testing, often requires special considerations. The geometry of the reservoir and those characteristics frequently found in geothermal systems engendered the idea of a parallelepiped model with interpenetrating fractures. Such geometry can be described mathematically using Green's and source functions. Equations of reservoir pressure behavior then can be developed for both drawdown and buildup tests. Graphs describing dimensionless pressure as a function of time and various reservoir parameters are provided in this paper. The general method used is type-curve matching.

Introduction

There are three major types of geothermal resources: (1) vapor-dominated (dry-steam) such as in The Geysers (CA) or in Tuscany of central Italy, (2) two-phase such as in New Zealand, and (3) hot-water, found in several locations. The most useful, in terms of power production, are the vapor-dominated reservoirs. They are also the most rare.

A number of geothermal reservoirs exhibit transient pressure behavior that indicates large, highly conductive fractures. The size of these reservoirs is controlled by faults and overlying impermeable rocks. A constant-pressure boundary, presumably boiling water, often is observed.

A parallelepiped model conceptually could approximate such a configuration. A model with closed, no-flow boundaries on five sides and a constant-pressure boundary on the bottom was described by Cinco-Ley *et al.*[1] The fracture system was simulated as a rectangular-shaped source.

The concept is limited to vapor-dominated reservoirs. Both geologic evidence and production histories have precluded the use of radial models in both The Geysers and Larderello, Italy. Hence, the parallelepiped model, with the included fracture and subformation boiling front, is intended to analyze pressure transient behavior in dry-steam geothermal wells.

Model Description

The model assumes constant-flow-rate production in an anisotropic, homogeneous reservoir. If the flow rate varies, an influence function such as that described by Economides *et al.*[2] can be used in the subsequent type-curve matching. The reservoir described by the model contains a slightly compressible fluid of constant viscosity μ and compressibility c, an assumption totally inadequate in the case of geothermal steam. Yet the shortcomings can be overcome if the pseudopressure function $m(p)$ is used. The real-gas pseudopressure was discussed by Al-Hussainy and Ramey.[3] All of these assumptions normally are used in geothermal well testing, irrespective of the model. Although the solution can be modified to incorporate fracture(s) anywhere in the reservoir, a vertical, partially penetrating fracture has been used. The fracture is in the center of a parallelepiped reservoir of square horizontal cross section.

From source and Green's functions, as presented by Gringarten and Ramey,[4] an expression for dimensionless pressure drop at any point in the reservoir was developed:

$$p_D(x_D, y_D, z_D, x_{De}, y_{De}, h'_D, h_{fD}, z_{fD}, t_{Dxf})$$

$$= \frac{\sqrt{\pi}}{8} \frac{h_D}{h_{fD}} \int_0^{t_{Dxf}} \frac{1}{\sqrt{\pi}}$$

*Now with U of Alaska.

0149-2136/82/0004-8886$00.25

$$\cdot\left[\sum_{n=-\infty}^{\infty} e^{-(y_D-2ny_{De})^2/4\tau}\right]$$

$$\cdot\left[\sum_{n=-\infty}^{\infty}\left(\operatorname{erf}\frac{x_D-2nx_{De}+1}{2\sqrt{\tau}}\right.\right.$$

$$\left.\left.+\operatorname{erf}\frac{x_{fD}-2nx_{De}-1}{2\sqrt{\tau}}\right)\right]\cdot$$

$$\cdot\left[\sum_{n=-\infty}^{\infty}\left(-\operatorname{erf}\frac{z_D+\frac{h_{fD}}{2}+z_{fD}+4nh_D}{2\sqrt{\tau}}\right.\right.$$

$$-\operatorname{erf}\frac{-z_D+\frac{h_{fD}}{2}-z_{fD}-4nh_D}{2\sqrt{\tau}}$$

$$+\operatorname{erf}\frac{z_D-\frac{h_{fD}}{2}-z_{fD}+4nh_D}{2\sqrt{\tau}}$$

$$+\operatorname{erf}\frac{\frac{h_{fD}}{2}-z_D+z_{fD}-4nh_D}{2\sqrt{\tau}}$$

$$+\operatorname{erf}\frac{z_D+\frac{h_{fD}}{2}+z_{fD}+4nh_D-2h_D}{2\sqrt{\tau}}$$

$$+\operatorname{erf}\frac{-z_D+\frac{h_{fD}}{2}-z_{fD}-4nh_D+2h_D}{2\sqrt{\tau}}$$

$$-\operatorname{erf}\frac{z_D+\frac{h_{fD}}{2}-2h_D-z_{fD}+4nh_D}{2\sqrt{\tau}}$$

$$\left.\left.-\operatorname{erf}\frac{\frac{h_{fD}}{2}-z_D+2h_D+z_{fD}-4nh_D}{2\sqrt{\tau}}\right)\right]d\tau \quad \ldots\ldots (1)$$

or alternatively

$$p_D(x_D,y_D,z_D,x_{De},y_{De},h_D,h_{fD},z_{fD},t_D)=\frac{4h_D}{h_{fd}y_{De}x_{De}}$$

$$\cdot\int_0^{t_{Dxf}}\left(1+2\sum_{n=1}^{\infty} e^{-n^2\pi^2\tau/y_{De}^2}\cos\frac{n\pi y_D}{y_{De}}\right)$$

$$\cdot\left(1+\frac{2x_{De}}{\pi}\sum_{n=1}^{\infty} e^{-n^2\pi^2\tau/x_{De}^2}\right.$$

$$\left.\cdot\cos\frac{n\pi x_D}{x_{De}}\sin\frac{n\pi x_{fD}}{x_{De}}\right)$$

$$\cdot\left[\sum_{n=1}^{\infty}\frac{e^{-(2n-1)^2\pi^2\tau/4h_D^2}}{(2n-1)}\sin\frac{(2n-1)\pi h_{fD}}{4h_D}\right.$$

$$\left.\cdot\sin\frac{(2n-1)\pi z_{fD}}{2h_D}\sin\frac{(2n-1)\pi z_D}{2h_D}\right]d\tau, \quad \ldots\ldots (2)$$

where the dimensionless terms in the equations are defined as follows.

$$p_D=1.291\times10^{-2}\frac{M\sqrt{k_xk_y}h(p_i^2-p_{wf}^2)}{ZTq\mu} \quad (3a)$$

$$t_{Dxf}=0.3604\frac{k_xt}{\phi\mu c_tx_f^2}. \quad \ldots\ldots (3b)$$

$$x_D=\frac{x}{x_f}. \quad \ldots\ldots (3c)$$

$$y_D=\frac{y}{x_f}\sqrt{\frac{k_x}{k_y}}. \quad \ldots\ldots (3d)$$

$$z_D=\frac{z}{x_f}\sqrt{\frac{k_x}{k_y}}. \quad \ldots\ldots (3e)$$

$$x_{De}=\frac{x_e}{x_f}. \quad \ldots\ldots (3f)$$

$$y_{De}=\frac{y_e}{x_f}\sqrt{\frac{k_x}{k_y}}. \quad \ldots\ldots (3g)$$

$$h_D=\frac{h}{x_f}\sqrt{\frac{k_x}{k_z}}. \quad \ldots\ldots (3h)$$

$$h_{fD}=\frac{h_f}{x_f}\sqrt{\frac{k_x}{k_z}}. \quad \ldots\ldots (3i)$$

$$z_{fD}=\frac{z_f}{x_f}\sqrt{\frac{k_x}{k_z}}. \quad \ldots\ldots (3j)$$

Eq. 1 was found better for calculating dimensionless pressure drop at small values of time, while Eq. 2 was

better at larger values of time. Using these equations, Cinco-Ley *et al.*[1] developed a number of solutions of drawdown testing for different values of x_D with the dimensionless thickness h_D as a parameter.

By the principle of superposition, type curves were developed for pressure buildup testing. The principle of superposition has been used extensively in pressure transient analysis, both in the simulation of closed boundaries through the use of image wells (superposition in space) and, more importantly, in the calculation of the pressure response following shut-ins or flow-rate fluctuations (superposition in time).

The superposition principle as applied here can be expressed as follows.

$$P_D(t_{pD}+\Delta t_D)_{\text{observed}} = p_D(t_{pD}+\Delta t_D)_{\text{drawdown}} - P_D(\Delta t_D)_{\text{buildup}}. \quad \ldots\ldots(4)$$

The equation denotes that the observed dimensionless pressure drop (and its proportional real pressure drop) is equal to the pressure drop caused by drawdown, presumed to continue following shut-in, minus the pressure drop evaluated at Δt.

From the solution for drawdown from Eqs. 1 and 2, solutions for buildup may be developed from Eq. 4.

The solutions are significantly more numerous than those for drawdown since the duration of flowing time before shut-in presents an additional and significant parameter. Of all parameters considered, the fracture penetration x_{De} had the least effect on the pressure response. To avoid the presentation of a great number of type curves, only those with $x_{De}=2$ are published here. Figs. 1 through 5 show a log-log graph of p_D/h_D vs. t_{Dxf} with the production t_{pD} as a parameter. The curves are for a dimensionless fracture penetration ratio of 2:1, while the values of the dimensionless formation thickness vary from 2:1 to 20:1.

Example

Pressure buildup data were recorded for a steam well (Well D-7) in Shell Oil Co.'s leases in The Geysers. Shut-in bottomhole pressures were calculated, and a plot of log $(p^2_{ws}-p^2_{wf})$ [measured in $(\text{kg/cm}^2)^2$] vs. time appears in Fig. 6. A type-curve match with one of the curves developed for this work obtains the following points.

$p^2_{ws}-p^2_{wf}=1150\ (\text{kg/cm}^2)^2$.

$p_D/h_D=4.1$.

$\Delta t=10^{-1}$ hours.

$\Delta t_{Dxf}=5.5$.

$t_p=7.5$ hours.

$t_{pD}=400$.

Pertinent reservoir parameters appear in Table 1.

TABLE 1—WELL D-7 RESERVOIR DATA

Flow rate q, ton/h	52.5
Viscosity μ (average), cp	0.0165
Gas deviation factor z	0.87
Compressibility c_t, kg/cm²	0.046
Porosity (estimated)	0.05
Reservoir temperature T, K	494
Molecular weight M	18
Flowing pressure p_{wf}, kg/cm²	3.6

From the definition of dimensionless pressure,

$$4.1=\frac{1.291\times10^{-2}(18)(k_xk_y)^{1/2}x_f\sqrt{\frac{k_z}{k_x}}(1150)}{(0.87)\ (494)\ (52.5)\ (0.0165)}$$

$$\therefore (k_xk_y)^{1/2}x_f=5.71\ \text{darcy-m}. \quad \ldots\ldots(5)$$

From the definition of dimensionless time,

$$5.5=\frac{0.3604\ k_x(0.1)}{(0.05)\ (0.0165)\ (0.046)\ x_f^2}$$

$$\therefore \frac{k_x}{x_f^2}=5.79\times10^{-3}\ \text{darcy/m}^2. \quad \ldots\ldots(6)$$

From Eqs. 5 and 6,

$$k_xk_yk_z=0.189\ \text{darcy}^3. \quad \ldots\ldots(7)$$

With $k_x/x_f^2=5.79\times10^{-3}$ and $t_p=7.5$ hours, we can calculate $t_{pD}=412$, which agrees well with the obtained match.

The practical result so far is that important reservoir parameters, such as the directional permeabilities and the length of the fracture, have been related through simple relationships. The permeabilities refer to the matrix, and full anisotropy is allowed by the results of Eqs. 5, 6, and 7. If isotropy were assumed and, hence, $k=k_x=k_y=k_z$, then $k=0.574$ darcy (from Eq. 7) and $x_f=99$ m (from Eq. 6). Finally, the length of the reservoir is 198 m, since $x_D=2$ and $x_D=x/x_f$.

All these findings are significant, since not only the permeability but also the areal extent of the reservoir were calculated. The longevity of the field, future drilling programs, and location of future wells are related directly to the reservoir permeability and the extent of the drainage area of the tested well.

Geothermal formations have been known to exhibit anisotropy. In the case of Well D-7, a study on anisotropy can be done.

From the definition of the dimensionless thickness,

$$h_D=\frac{h}{x_f}\sqrt{\frac{k_x}{k_z}},$$

and since $h_D=10$, a graph such as the one in Fig. 7 can be constructed.

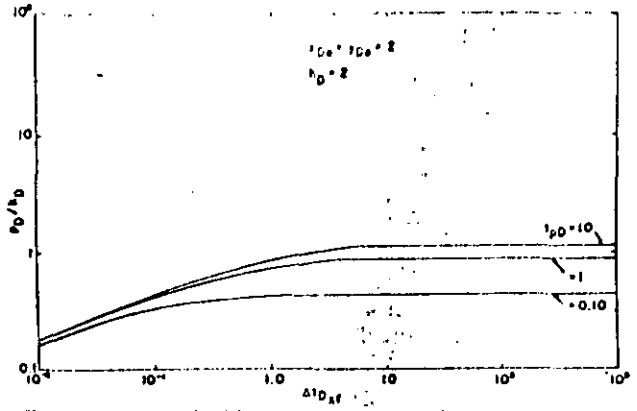

Fig. 1—Pressure buildup type curve of a fractured well in a parallelepiped reservoir ($h_D = 2$).

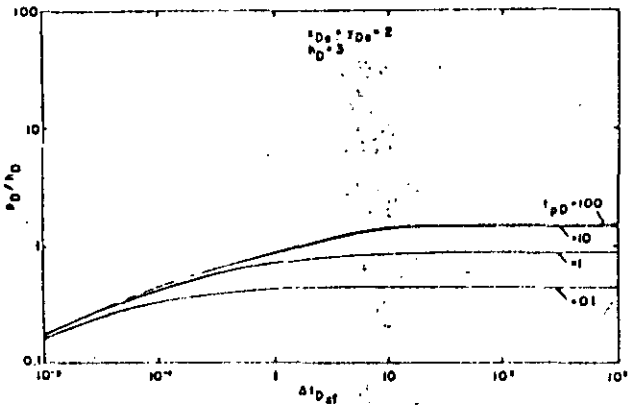

Fig. 2—Pressure buildup type curve of a fractured well in a parallelepiped reservoir ($h_D = 3$).

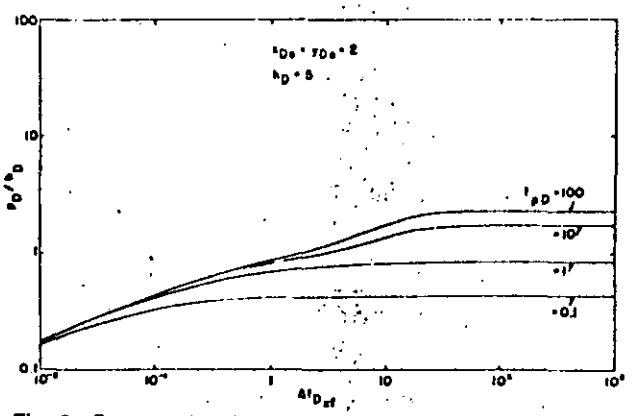

Fig. 3—Pressure buildup type curve of a fractured well in a parallelepiped reservoir ($h_D = 5$).

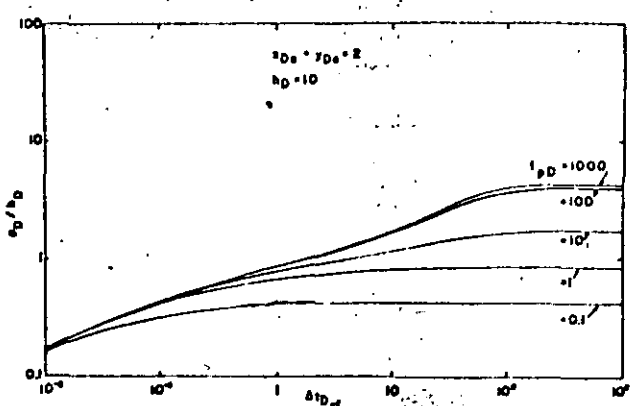

Fig. 4—Pressure buildup type curve of a fractured well in a parallelepiped reservoir ($h_D = 10$).

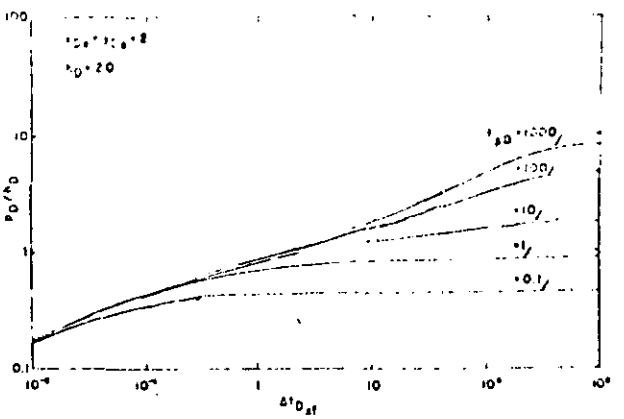

Fig. 5—Pressure buildup type curve of a fractured well in a parallelepiped reservoir ($h_D = 20$).

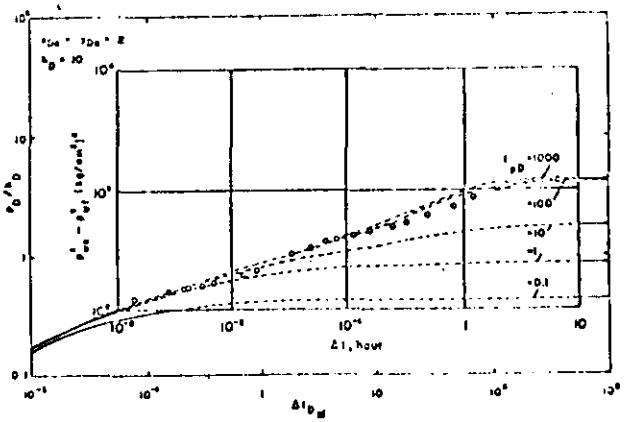

Fig. 6—Type-curve matching for the example.

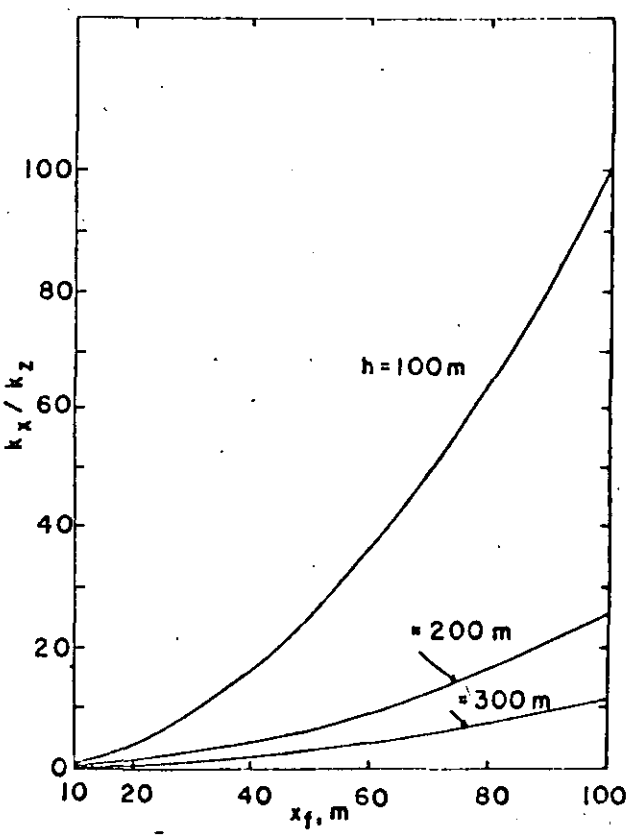

Fig. 7—Ratio of horizontal to vertical permeability as a function of reservoir thickness and fracture length (Shell D-7).

One can assume a reasonable x_f and h, obtain the k_x/k_z ratio, and, using Eqs. 5 and 6, calculate all permeabilities. Then, Eq. 7 can be used as a check. The results of this calculation are x_f=20 m, h=300 m, k_x=2.32 darcies, k_z=5.21 darcies, and k_y=0.0156 darcy.

The calculation can be repeated for any set of fracture lengths and reservoir thicknesses. Geologic evidence and future drilling programs actually may limit the iteration to just the reservoir thickness since the fracture may be measured.

Conclusions

1. The parallelepiped model seems to be a reasonable interpretation of dry-steam reservoir behavior.
2. Buildup and drawdown data can be analyzed with the model, although the analysis is more cumbersome with buildup data because of the presence of an additional parameter, t_p.
3. The method provides significant information otherwise unavailable from such established techniques as Horner.
4. Shell's Well D-7 appears to be analyzed adequately by use of the parallelepiped model.

Nomenclature

c = isothermal compressibility, cm²/kg (psi⁻¹)
h = formation thickness, m (ft)
h_f = fracture height, m (ft)
k = permeability, darcy
$m(p)$ = real gas pseudopressure
M = molecular weight, g/gmol
p = pressure, kg/cm² (lbm/sq in.)
p_i = initial pressure, kg/cm² (lbm/sq in.)
p_{wf} = flowing bottomhole pressure, kg/cm² (lbm/sq in.)
q = mass flow rate, ton/h (lbm/hr)
S = source function
t = time, hours
t_p = production time before shut-in, hours
Δt = time since shut-in, hours
T = reservoir temperature, K
x = distance in x direction, m (ft)
x_e = boundary location in x direction, m (ft)
x_f = half-fracture length, m (ft)
y = distance in y direction, m (ft)
y_e = boundary location in y direction, m (ft)
z = distance in z direction, m (ft)
z_f = elevation of fracture midpoint, m (ft)
Z_i = gas deviation factor, dimensionless
μ = viscosity, mPa·s (cp)
ϕ = porosity, fraction

Subscripts

D = dimensionless
e = external
f = fracture
i = initial
p = production
w = wellbore

Acknowledgments

This work was part of Project 3 of the U.S. DOE/Italian ENEL Agreement on Cooperative Research and Development in Geothermal Energy. We thank our sponsoring agencies for the funding that made this research possible. We also express our gratitude to the management of Shell Oil Co. for permission to publish field data.

References

1. Cinco-Ley, H., Brigham, W.E., Economides, M.J., Miller, F.G., Ramey, H.J. Jr., Barelli, A., and Manetti, G.: "A Parallelepiped Model to Analyze the Pressure Behavior of Geothermal Steam Wells Penetrating Vertical Fractures," paper SPE 8231 presented at the SPE 54th Annual Technical Conference and Exhibition, Las Vegas, Sept. 23-26, 1979.
2. Economides, M.J., Brigham, W.E., Cinco-Ley, H., Miller, F.G., Ramey, H.J. Jr., Barelli, A., and Manetti, G.: "Influence Functions and Their Application to Geothermal Well Testing," *Trans.*, Geothermal Resources Council (1979) 3, 177-180.
3. Al-Hussainy, R., Ramey, H.J. Jr., and Crawford, P.B.: "The Flow of Real Gases Through Porous Media," *J. Pet. Tech.* (May 1966) 624-636; *Trans.*, AIME, 237.
4. Gringarten, A.C. and Ramey, H.J. Jr.: "The Use of Source and Green's Functions in Solving Unsteady Flow Problems in Reservoirs," *Soc. Pet. Eng. J.* (Oct. 1973) 285-296; *Trans.*, AIME, 255.

SI Metric Conversion Factors

cp	× 1.0*	E+00	=	mPa·s
ft	× 3.048*	E-01	=	m
lbm	× 4.535 924	E-01	=	kg
sq ft	× 9.290 304*	E-02	=	m²
sq in.	× 6.451 6*	E+00	=	cm²
ton	× 9.071 847	E-01	=	Mg

*Conversion factor is exact.

JPT

Original manuscript received in Society of Petroleum Engineers office Feb. 25, 1980. Paper accepted for publication Sept. 2, 1981. Revised manuscript received Feb. 1, 1982. Paper (SPE 8886) first presented at the SPE 50th California Regional Meeting held in Bakersfield April 9-11, 1980.

CURSO: "INGENIERIA DE YACIMIENTOS GEOTERMICOS"

En colaboración con la OLADE, C.F.E., I.I.E.

Del 13 Marzo - 18 de mayo

TEMA: PRUEBAS DE PRESION

3.- Grant. M.A., Bixley, P.E. y Donaldson, I G. "Internal Flows in Geothermal Wells; Their identification and effect on the wellbore temperatura and pressure profiles" Soc. Pet. Eng. J. (Feb. 1983), 168-176.

DR. FERNANDO SAMANIEGO

13-23 Marzo 1984

Internal Flows in Geothermal Wells: Their Identification and Effect on the Wellbore Temperature and Pressure Profiles

Malcom A. Grant, SPE, New Zealand Dept. of Scientific & Industrial Research
Paul F. Bixley, New Zealand Ministry of Works & Development
Ian G. Donaldson, New Zealand Dept. of Scientific & Industrial Research

Abstract

Geothermal wells exhibit a variety of internal flow effects caused by the flow of water, steam, or both between distinct permeable zones tapped by the well. These internal flow effects are described and it is shown how they may be recognized from downhole pressure and temperature profiles.

Pressure transients measured at depths other than that of the well's primary permeable zone can be corrupted by such flows. The effects of such flows on injection and discharge transients are discussed.

Introduction

Two types of flow can occur in wells in geothermal reservoirs: (1) interzonal flow in which fluid enters the well at one depth, flows up or down the wellbore, and exits at a second depth, and (2) internal convection in which fluid circulates within the wellbore. The first is more common.

A geothermal wellbore is a long, vertical or near-vertical pipe penetrating a reservoir of heated fluid. Most geothermal reservoirs consist of fractured rocks, and a well draws its fluid supply from one or a few fractures (also called "permeable zones," "aquifers," "productive horizons," or "feedpoints"). Normally no attempt is made to isolate individual feedpoints from one another, so multiple feeds are often exposed to the well over a vertical distance of 3,000 to 6,000 ft (1000 to 2000 m).

0197-7520/83/0021-0317$00.25

Over the depth of open hole the well is exposed to the reservoir, which may contain waters of different temperatures or steam/water mixtures. In addition, the reservoir pressure distribution is not static[1] because the natural throughflow of the reservoir causes a nonstatic distribution of fluid. In Wairakei, New Zealand, the pre-exploitation vertical pressure gradient was, for example, about 7% above hydrostatic (for the temperatures involved).[1]

The very high permeabilities encountered in good geothermal wells [permeability-thickness of the order of 3 to 300 darcy-ft (1 to 100 darcy·m)][2] mean that comparatively small pressure differences from buoyancy effects or from the nonstatic reservoir profile may cause substantial flows within a wellbore. If a well has more than one significant feedpoint, it is impossible for it to attain both thermal and pressure equilibrium with the reservoir, and fluid will flow between the permeable zones. Such flow up or down the wellbore distorts temperature profiles, so measured downhole data reflect not reservoir temperatures but the physics of heat and mass transfer within the wellbore. Pressure profiles measured downhole likewise reflect not the reservoir pressure profile but the fluid column occupying the wellbore.

In the absence of these strong interzonal flow effects, the fluid-filled wellbore still represents an effective means of vertical heat transport by convective circulation within it. Internal flow up or down the wellbore or convection within the wellbore are by far the dominant features influencing measurements in geothermal wells

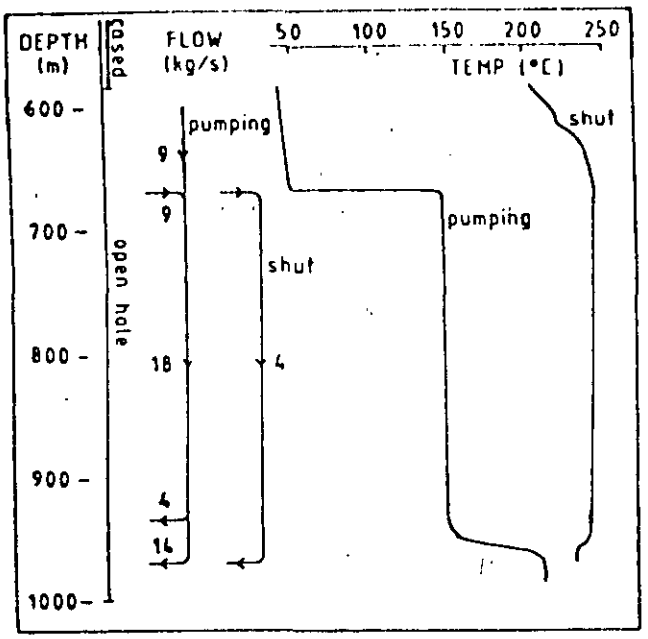

Fig. 1—Temperature and flow logs for Well NG9 at Ngawha, New Zealand (adapted from Ref. 23).

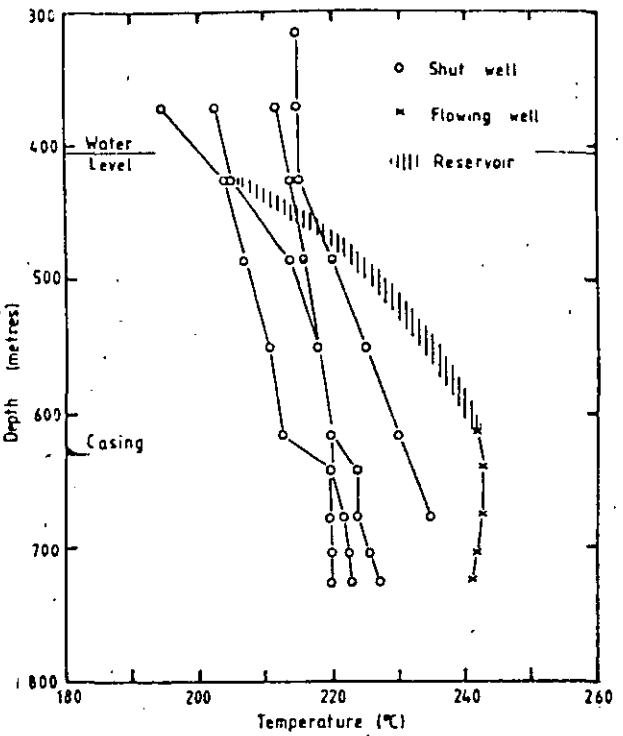

Fig. 2—Downhole temperatures measured in Well WK47, Wairakei, 1968-69.

in New Zealand. For this reason, downhole profiles require careful interpretation.[2-7] It is a rare well that, throughout the length of open hole, reaches a convincing static equilibrium with reservoir temperatures.

We now consider the different types of internal flows and the measurements that identify them. Unless otherwise specified, the discussion refers only to unexploited, liquid-dominated reservoirs. It also is assumed that the reservoir is fractured, although the same wellbore effects have been observed at Cerro Prieto, Mexico.[8] The flows concerned range from small (up to a few pound-mass per second), which only affect the fluid profiles in the wellbore itself, to very large [more than 200 lbm/sec (100 kg/s)], which may form a significant part of the mass transfer within the reservoir.

Downflow in the Wellbore

Most easily recognized is the downflow of liquid water in the wellbore. With the well shut in, water enters at an upper feedpoint, descends the wellbore, and is injected back into the reservoir at a lower permeable zone. The temperature profile within the section of the wellbore involved is controlled by wellbore heat transfer to the downflowing water.[9] Geothermal wells, in reservoirs permeable enough to be exploitable, have high flow rates by petroleum well standards. It is possible for the downflow to be so large that temperature is (essentially) isothermal in the interzonal flow section of the well. In the shut-in well, this temperature will be close to that of the water entering at the main feedpoint. It need not be a low temperature. In many situations it is little different from temperatures found in deeper feedpoints in the same or other wells in the reservoir.

Fig. 1 shows an example, Well NG9 in Ngawha, New Zealand, in which both temperature and flow rate have been measured in the wellbore. Here, with the well shut in, isothermal conditions are found over the 2,200- to 3,200-ft (670- to 970-m) section of the wellbore. The measured downflow in this section is 9 lbm/sec (4 kg/s). Also shown in this figure is a temperature profile measured during cold-water injection into the same well. The wellbore is not filled with the cold injection water. At the upper feedpoint, hot water still enters the well, and it is the mixture that flows down to the lower permeable zones. There are wells in New Zealand in which such a downflow always has been present, and consequently reservoir temperatures are unknown beneath the inflow point. The problem is prevalent in the Ngawha field, and Well NG9 (Fig. 1) recently was worked over with a double completion to obtain "clean" temperatures and production from its lower zone.

In some wells it is possible to use the downflow regime to determine the reservoir pressure at the main feed zone. The inflow to the well from this feed must depend on the reservoir/well pressure difference at the feed level. By comparing simultaneous pressure and temperature profiles measured at different rates of injection of water into the well, it is possible to determine the pressure at the feed level at which no inflow occurs. This must be the reservoir pressure at this level.

The well with a small downflow is more difficult to recognize. In this case, wellbore heat transfer results in a nonzero temperature gradient in the downflowing water. Such minor downflows often can be recognized only by comparison of shut-in with discharging temperature profiles. The downflowing water cools the well when it is shut in. Fig. 2 shows an example from Wairakei—an exploited field—where this effect is now common. Some measured static downhole profiles in Well WK47 are shown under shut-in and discharge conditions. The latter

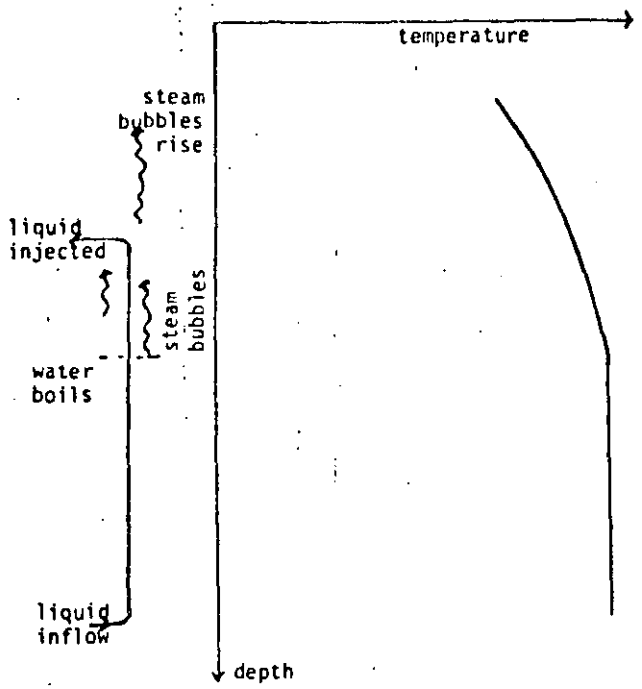

Fig. 3—Temperature and flow profiles in a wellbore for upflow with boiling.

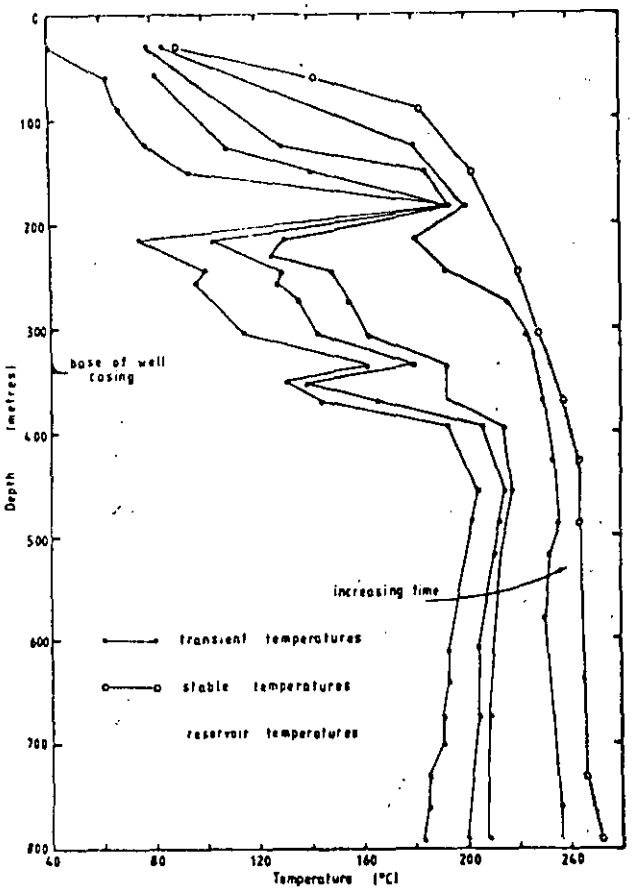

Fig. 4—Warm-up and stable temperature profiles in Well WK24, Wairakei.

curve ties in with reservoir temperatures established by use of data from different wells in the neighborhood that are (in part) uncorrupted by internal flow effects. These discharge temperatures are higher than the shut-in ones, indicating water of higher temperature entering the well, presumably from the deeper feedpoint.

Upflow in the Wellbore

An upflow of liquid water in the wellbore has characteristics similar to those of a downflow. Thus it may not be possible to distinguish an upflow from a downflow with shut-in temperature profiles alone. If downhole flows cannot be measured directly, temperature measurement during injection can be used to clarify the situation.[2]

A different effect is introduced if the rising water boils as it ascends the wellbore. Liquid water enters at the lower feedpoint and rises up the wellbore until it boils. From that level up, steam bubbles move up with the water. Provided that the upflow is small, the pressure gradient remains near hydrostatic. At the upper permeable zone, water is injected into the formation. The steam bubbles upward into the casing, heating the water in this section of the well and causing a small downflow of condensate. Residual gas in the steam accumulates within the casing. This mechanism creates the very high wellhead pressures from gas that can occur even in reservoirs of low gas content. The upper part of the well acts as a distillation plant. The gas column sometimes extends down to the shallowest feedpoint, where there is then a sharp change in fluid density, as indicated by downhole pressure.

The flow and temperature profiles that might be expected in the wellbore in this case are shown in Fig. 3. If the upflow is large enough, isothermal conditions will apply in the liquid-filled interzonal-flow section of the wellbore. Above the boiling level, however, saturation conditions must apply, and the temperature thus will decrease as the fluid moves up the well.

The stable downhole temperature profiles measured in many wells are of this form. In Fig. 4, the stable temperature profile for Well WK24 at Wairakei is shown, along with other profiles obtained during warm-up and the reservoir temperature profile that these warm-up curves imply (by extrapolation at different levels). [The higher temperatures at 2,000 ft (600 m) derive from other data.] The final temperature profile in the shut-in well is smooth, featuring approximately isothermal conditions at depth and boiling point conditions at shallower levels. The cooler temperatures of the reservoir above 1,300 ft (400 m) are obscured totally because of the flow-established conditions in the well. The contrast between reservoir and wellbore temperatures also is found when comparisons are made between temperatures measured during drilling (i.e., stable bottomhole temperatures) and in the completed hole—e.g., at Wairakei Well WK10[5] and at Yellowstone Well Y-4.[10]

If the fluid entering the well is boiling, the isothermal

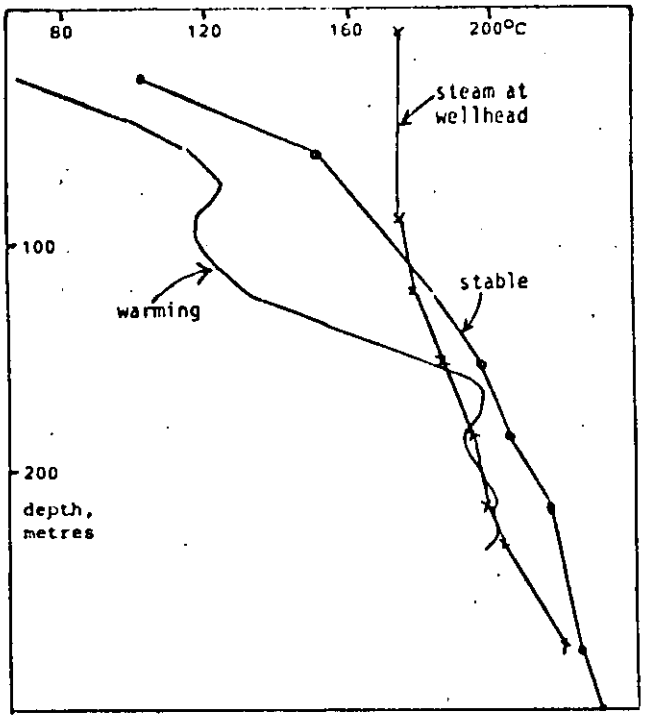

Fig. 5—Temperature profiles measured in Well WK21, Wairakei, in 1953 showing conditions during and at the end of warm-up and after steam buildup at the wellhead.

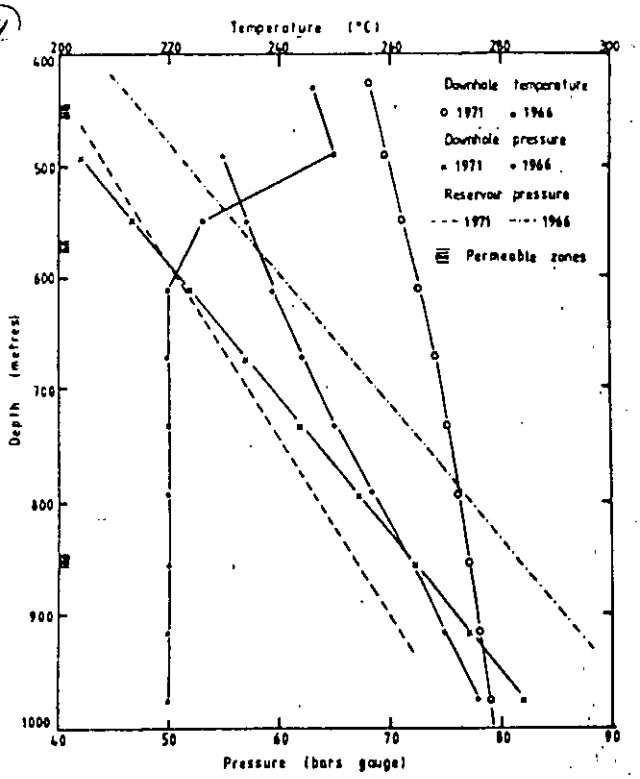

Fig. 6—Downhole and reservoir profiles in Well BR2 in Broadlands under upflow conditions (before production testing in 1966) and downflow conditions (at the end of the production test in 1971).

section of the temperature profile is absent. In this case the well has a boiling-point profile—it appears to contain a column of water at boiling point. An example, for Well WK21 at Wairakei, is illustrated in Fig. 5. This well initially warmed to the boiling-point profile illustrated. Separation of the steam and water in the well casing ultimately resulted in the second profile (marked "steam at wellhead") shown. The timing of measurements thus also may play a role in interpretation.

More vigorous upflow in the wellbore can result in the steam/water flow being in the slug rather than in the bubble regime. In this event, the wellbore contains a steam/water mixture (recognized by a low-density fluid column) rather than the bubbles-in-water mixture (with a fluid column of approximately liquid water density) associated with lower rates of upflow. This type of wellbore flow has been called "internal discharge" because of the high rate of discharge into the higher permeable zones. Fig. 6 shows the downhole temperature and pressure profiles in Well BR 2 at Broadlands and the reservoir pressure profile in the vicinity of this well in 1966 when it was in an internal discharge mode. By 1971, drawdown in this reservoir, because of extensive test discharge of wells in this field, had resulted in the inversion of this flow. The later well and reservoir pressures and well temperatures are plotted for comparison.

Another well that shows an internal discharge is Well Y-13 at Yellowstone. There, staged measurements show the contrast between the reservoir and downhole pressure profiles.[10] Because the internal discharge permits greater differences between reservoir and downhole pressure gradient (a result of the lower density of the fluid in the well), flow rates are greater than for liquid flows.

In all these situations, the upflow in the well controls the downhole temperature profile. The only opportunity to observe reservoir temperatures is thus during warm-up, before the upflow becomes established.

Correlation of Downhole and Reservoir Pressures

In a single well with one dominant feedpoint, downhole pressure approximates reservoir pressure at the depth of the feedpoint only. Comparison of pressures in different wells permits construction of a reservoir pressure profile.[1] Comparing this profile with the profile in a well indicates where flow into or out of the well may occur.

In a region of a reservoir where fluid is rising, the vertical pressure gradient must be superhydrostatic. In outflow or downflow regions it is hydrostatic or subhydrostatic. Correspondingly, the pressure gradient disposes wells to internal upflows and downflows, respectively (the vertical pressure gradient in the wellbore must be close to hydrostatic in most cases), with possible complications from changes in liquid density with temperature. Thus, in an unexploited reservoir, we would expect wells to exhibit upflows in the region where the natural upflow occurs, and downflows in peripheral or outflow regions of the reservoir. At Wairakei and Broadlands, nearly all early productive wells showed upflows.

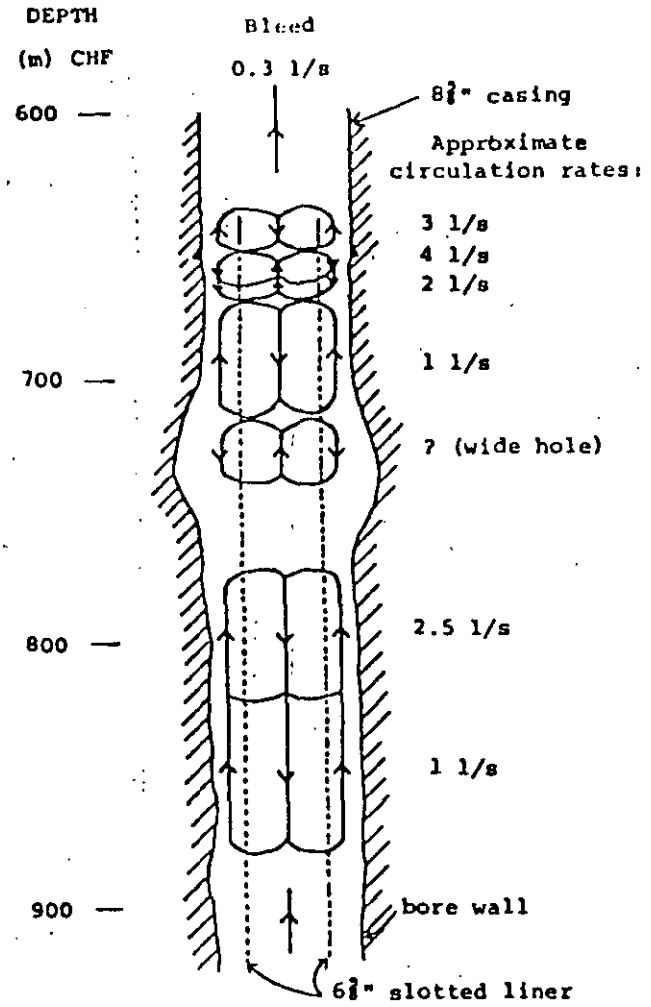

Fig. 7—Convection cells observed in Well KA27, Kawerau (after Ref. 13).

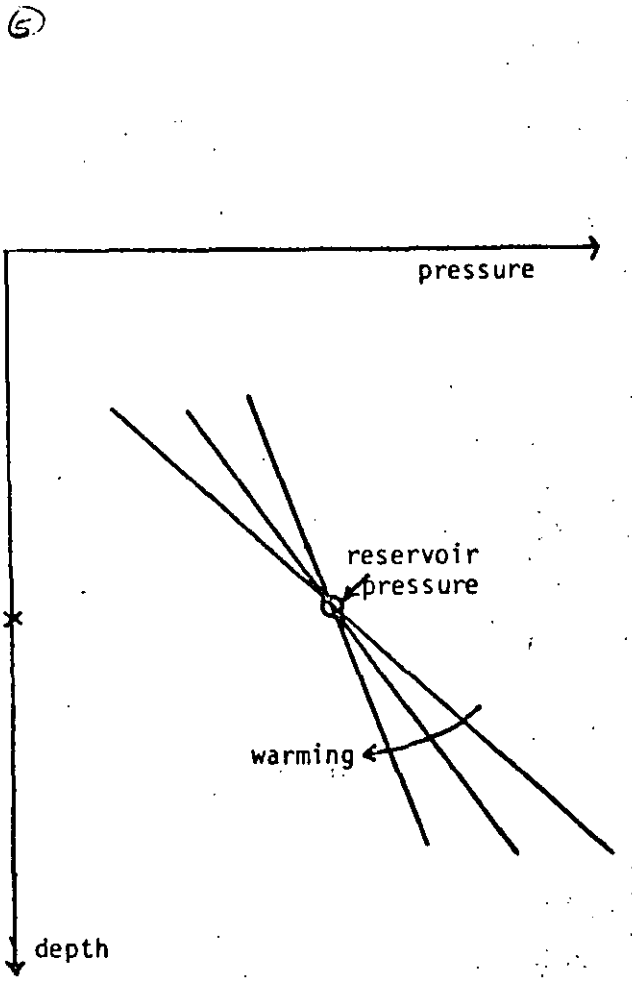

Fig. 8—Definition of a pressure pivot at the feedpoint during well warm-up (differences from hydrostatic are exaggerated).

Exploitation will alter the pressure distribution in the reservoir, and internal flow can change. This can create marked changes in downhole pressure and temperature, which reflect not changes in reservoir values but changes in the internal flow in the well. Fig. 6 (discussed earlier) shows the effects from a reversal of flow in Well BR2 at Broadlands that have been brought about by exploitation.

Given sufficient downhole data, it is possible to estimate quantitatively the magnitude of internal flows, together with the reservoir pressure and injectivity/productivity of each permeable zone.[11,12] For a well with a substantial internal flow, such an analysis is the only way to estimate the undisturbed reservoir pressure at each feed zone.

Although most internal flows are small and consequently difficult to identify, some are not. Analyses have found substantial internal discharges in several wells in different New Zealand fields. The internal discharge in Well BR28 at Broadlands has, for example, been estimated at about 200,000 lbm/hr (30 kg/s). Direct measurements by spinner of large flows also have been carried out. Downflows at Ngawha are typically up to 80,000 lbm/hr (10 kg/s).[13] At Wairakei, with a disturbed reservoir pressure profile, a downflow of 650,000 lbm/hr (80 kg/s) was measured in Well WK107.[14]

Convection Cells

Convection cells have been identified with a flowmeter in injection wells and in shut-in wells.[13] They appear to be influenced strongly by the geometry of the drilled hole and of the liner,[15] and they probably are controlled to a degree in sections of the well where the hole is larger than gauge. A convection cell often will terminate at a break in geometry or at a feed zone. An extreme case is illustrated in Fig. 7. This convection cell pattern was observed in Well KA27 at Kawerau. The solid and slotted casing sections are indicated, along with an estimate of the shape of the actual drilled hole.

Identification of Permeable Zones

For the discussion of transient analysis, it is important to be able to identify the location of the major feed of the well—i.e., at what depth the well intersects the dominant permeability. Permeable zones in a well can be recognized by drilling losses/entries; petrology (hydrothermal alteration); a zone cooled by injection; an endpoint of in-

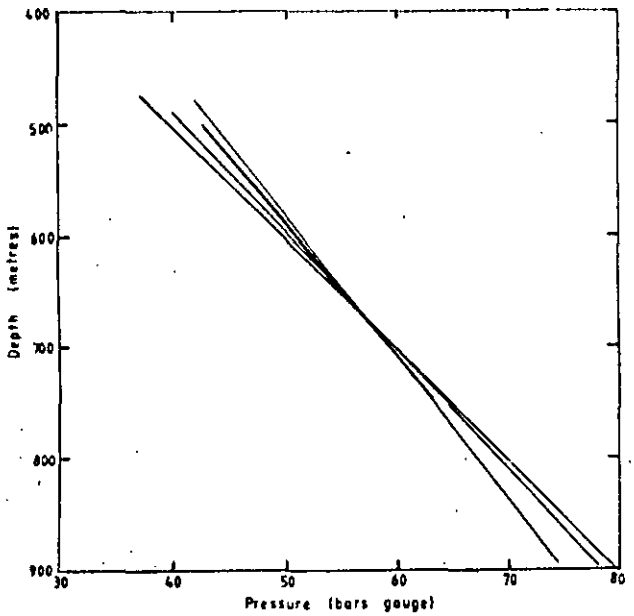

Fig. 9—Pressure profiles measured during warm-up in Well KA16, Kawerau, in 1981. Temperature curves for this well indicate permeability at the pivot depth [– 2100 ft (– 650 m)].

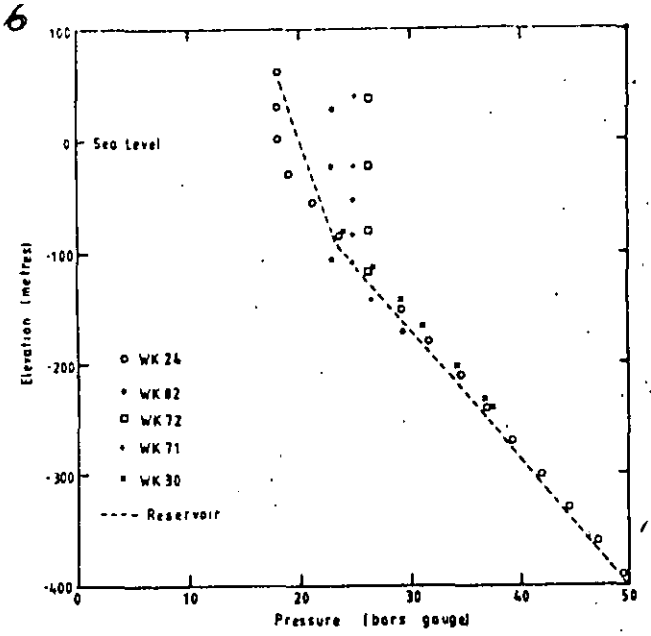

Fig. 10—Downhole and reservoir temperatures for a group of Wairakei wells.

terzonal flow during warm-up; a zone warming abnormally rapidly; flowmeter logs, if available; and the level of phase change.[2,5,6]

Sometimes one zone clearly dominates; at other times it may be difficult to decide. A method that can identify the dominant zone conclusively, if it produces a unique result, is the pressure pivot. This is illustrated in general terms in Fig. 8 and for a specific well, Well KA16 at Kawerau, in Fig. 9. After drilling and any subsequent cold-water injection, the wellbore contains cold water. Once any transient pressure effects of drilling and injection have died away, the downhole pressure equates to reservoir pressure at or near the dominant feed. In the time span involved for these transients to die out, the water temperature will not have changed. The pressure gradient in the well thus will relate to cold-water hydrostatic. As the well warms, the pressure at the feed will not change. The gradient, however, must reflect the increase in temperature through the associated density decrease. The pressure profiles pivot about the reservoir pressure at the feedpoint, simultaneously identifying the feedpoint and its reservoir pressure. Note that for Well KA16 (Fig. 9), the permeable zone suggested by the pressure pivot has been confirmed by analysis of temperature data. Such confirmation always is sought if appropriate data are available.

If there are two significant feed zones, the pivot appears at a point between them that is a mean of the two depths weighted by their injectivities/productivities. Where there are multiple feeds, intermediate ones may be hidden, and the pivot point may reflect the inflows and outflows of the extreme points alone.

An extreme case of the pressure pivot is in a vapor system.[16-18] Downhole pressure profiles with the well containing cold water, and containing steam, have sharply contrasting gradients. The feedpoint thus can be defined clearly.

Exploited Reservoirs

An exploited reservoir differs from an unexploited one in that the reservoir pressure profile may be far from static, and two-phase mixtures of any steam/water ratio can be produced. Presence of fluids of higher enthalpy can make a reservoir more prone to internal discharge in the wells. Such internal discharges were, for example, quite common in Wairakei wells between 1959 and 1965.[19]

Usually, after some exploitation, a steam zone forms near the top of the reservoir. Correspondingly, wells often adopt a steam-cap profile—the wellbore contains a column of liquid beneath a column of steam. The steam in the well may or may not correspond to a coherent steam column in the reservoir. Fig. 10 shows the stable downhole pressure profiles measured in a group of wells at Wairakei during 1971–74 and the reservoir profile as identified by comparison between many wells.[20] Pressures in the water columns of the wells agree with the reservoir pressures. In the steam zone, agreement is found only at the permeable zones because the steam columns have a markedly lower pressure gradient than does the reservoir.

When a well has a steam cap, it can equilibrate against reservoir pressure at two depths: one in steam and one in water. Within each fluid column in the well, interzonal flow can occur.

Pressure Transients

The theory of pressure-transient analysis is based on flow in a horizontal aquifer and on the pressure changes at wellface that result from withdrawal from or injection into that aquifer. The pressure change analyzed is the downhole pressure at the well's producing depth. The pressure at some other depth can be used conveniently, provided that there is a constant pressure difference between that depth and the feed depth.

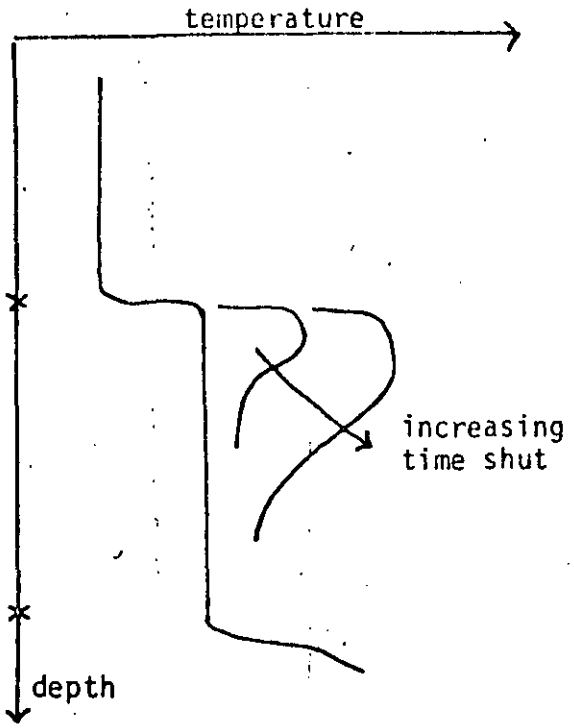

Fig. 11—Downhole temperatures during and after cessation of injection.

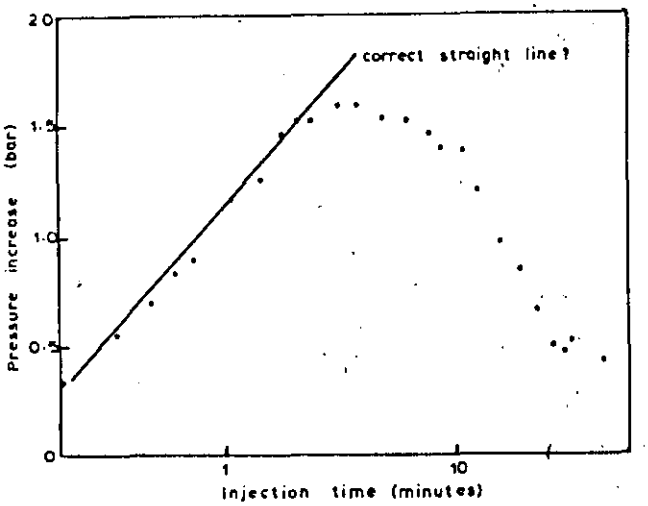

Fig. 12—Falloff of the pressure change during an injection test in Well KA22, Kawerau (after Ref. 23).

Unrecognized flow effects result in a varying pressure difference between other points in the well and the feedpoint. Often this results in a transient measured away from the feedpoint being so peculiar that it must be ignored. Less often, an apparently good result may be accepted as valid when it is not. In all cases, the problem can be recognized if downhole temperature or pressure profiles are measured during, before, or after the transient test to see whether inconsistencies exist. In practice, it is best to avoid such problems in geothermal wells by measuring all transients at the well's primary feed depth. Measurements at other depths, such as bottomhole or casing shoe, can be misleading.

The flow effects on pressure-transient data can be regarded as extreme cases of humping, complemented by thermal effects and multiple entries. With suitable theory,[21,22] analysis may be possible someday.

Different problems and effects may occur in injection and discharge tests. For example, an injection test in a well may prove quite unsatisfactory; in contrast, a discharge test in the same well may provide excellent information. We thus consider these two tests independently.

Injection Tests

Problems with injection tests most commonly are encountered in a well with interzonal flow. Under injection, fluid may enter the well from the formation at the upper feedpoint, and mixed water of intermediate temperature may flow down the well. At a change of injection rate, the inflow rate also will change (and will continue to change). Water of different temperature begins to fill the wellbore beneath the upper feed (Fig. 11), and a water column of a density that changes with time plays a role in setting the pressure. If one zone has a much larger permeability, the pressure at that level will be set by the injection conditions. A good transient should be obtained at that depth. If both inflow and outflow zones are of comparable permeability, it may not be possible to get any meaningful result.

Now it will be assumed that one zone does have a much higher permeability, so that a good transient can be measured at that depth. At the wrong depth, the pressure transient measured typically shows an initial correct response, but this is followed by a reversal and oscillations. Fig. 12 shows a transient measured in Well KA22 at Kawerau.[23] Here a straight line fits the first few minutes of data, but then the pressure change decreases. It can be shown that there is a period of time in any well over which the interzonal flow effects are negligible. If a semilog straight line develops during this period, it gives the correct result. This period, however, can be as short as 1 minute.

A discharge test in Well KA22 gave no problems, because during discharge and recovery the wellbore at all times contains a column of 482°F (250°C) water between the two feed zones.

The interzonal flow problem under injection typically causes humping or oscillatory response. At times this can be so severe that the first measurable response is a pressure change of the wrong sign.[2,24] This problem also may be recognized from downhole temperature profiles showing interzonal flow during injection, in the well as it warms up, or when it is fully warmed up.

Discharge Tests

Problems under discharge also arise from varying densities, but here they are associated with flashing in the

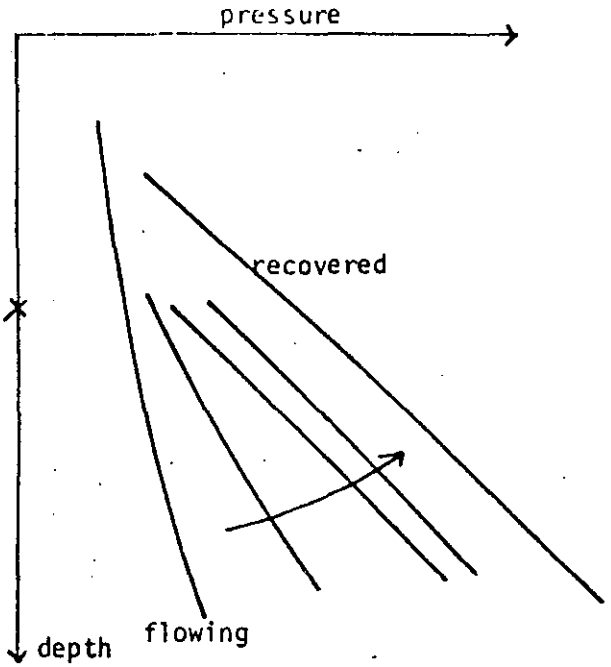

Fig. 13—Downhole pressure profiles during recovery after a discharge test, illustrating the effect of collapse of two-phase conditions in the wellbore.

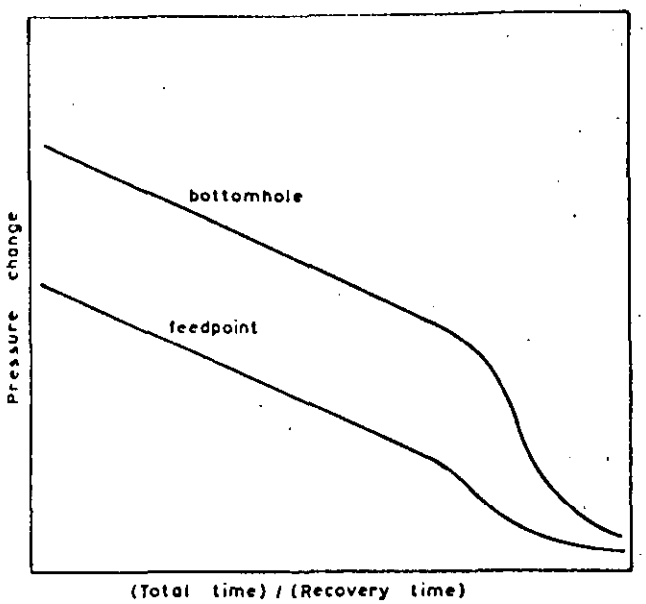

Fig. 14—A Horner plot of pressure recovery at bottomhole and at the feedpoint in a well.

wellbore. Fig. 13 shows a simple illustration of how the pressure may change in such a well upon shut-in. The well, during discharge, has a two-phase column in the wellbore. The primary feed is above bottomhole, although some fluid must enter lower down to maintain the flashing column. Upon shut-in, a two-phase column persists for some period in the well.[25] Then, however, it collapses to form a water column with steam (or gas) above. From that time on, the pressure difference from bottomhole to feedpoint will be constant. The misleading pressures at the wrong level occur this time in the early period. Fig. 14 shows a Horner plot of pressure recovery in a well at feedpoint and at bottomhole. Late-time semilog slopes must agree, so both histories give the same permeability-thickness. The pressure change after, say, 1 hour is larger at bottomhole than at feedpoint, so the bottomhole data overestimate skin.

A less common problem occurs in wells with an internal discharge. In these, a two-phase column is always present. Pressure changes at bottomhole are always larger than at feedpoint, approximately by a constant ratio. In this case both permeability-thickness and storativity (porosity/compressibility/thickness) will be underestimated.

Setting the gauge in the well at levels below that of the primary feed for a discharge transient thus risks underestimating reservoir permeability. The problem is recognized by checking pressure profiles (or carrying out calculations) for two-phase fluid in the wellbore.

Conclusions

Internal flows in wellbores in geothermal reservoirs do exist and need to be recognized. Careful analyses of downhole pressure and temperature data can give information about these flows and about reservoir characteristics relating to the permeable zones tapped by the well. In many situations, such analyses are the only means of obtaining information regarding these reservoir characteristics.

Changing density of the fluid in the wellbore during pressure-transient tests (both injection and discharge) resulting from internal flows in the wellbore and/or variation in the two-phase nature of the fluid can result in misleading or meaningless test data. Most problems in such testing can be overcome by ensuring that the pressure transients are measured at the well's primary feed level.

Acknowledgments

Paul F. Bixley thanks the Commissioner of Works, New Zealand, for permission to publish this paper. We thank the Ministry of Works and Development, New Zealand, for supplying the data used.

References

1. Donaldson, I.G., Grant, M.A., and Bixley, P.F.: "Nonstatic Reservoirs: the Natural State of the Geothermal Reservoir," *J. Pet. Tech.* (Jan. 1983) 189-94.
2. Grant, M.A., Donaldson, I.G., and Bixley, P.F.: *Geothermal Reservoir Engineering*, Academic Press Inc., New York City (1982).
3. Bolton, R.S.: "The Behavior of the Wairakei Geothermal Field During Exploitation," *Geothermics*, Special Issue (1970) 2, 1426-39.
4. Wainwright, D.K.: "Subsurface and Output Measurements on Geothermal bores in New Zealand," *Geothermics*, Special Issue (1970) 1, 764-67.
5. Grant, M.A.: "Interpretation of Downhole Measurements in Geothermal Wells," Report 88, Applied Mathematics Div., Dept. of Scientific & Industrial Research, New Zealand (1979).

6. Stefansson, V. and Steingrimsson, B.: "Geothermal Logging," Report OS8017-JHD09, Natl. Energy Authority, Reykjavik, Iceland (1980).
7. Grant, M.A.: "Interpretation of Downhole Measurements at Baca," *Proc.*, Stanford U. Fifth Workshop Geothermal Reservoir Engineering, H.J. Ramey Jr. and P. Kruger (eds.), Report SGP-TR-40, Palo Alto, CA (1979) 261-68.
8. Castaneda, O.M. and Horne, R.N.: "Location of Production Zones with Pressure Gradient Logging," *Trans.*, Geothermal Resources Council, Houston (1981) 5, 275-78.
9. Ramey, H.J. Jr.: "Wellbore Heat Transmission," *J. Pet. Tech.* (April 1962) 427-35; *Trans.*, AIME, 225.
10. White, E.D. *et al.*: "Physical Results of Research Drilling in Thermal Areas of Yellowstone National Park, Wyoming," Prof. Paper 892, USGS (1975).
11. Bixley, P.F. and Grant, M.A.: "Evaluation of Pressure-Temperature Profiles in Wells with Multiple Feed Points," *Proc.*, The New Zealand Geothermal Workshop, Auckland (1981) 121-24.
12. Grant, M.A.: "Ngawha Geothermal Hydrology," *The Ngawha Geothermal Area*, DSIR Geothermal Report 7, Dept. of Scientific & Industrial Research, New Zealand (1981) 60-68.
13. Syms, M.C. and Syms, P.H.: "Water Flow and Temperature Logs from Wells in the Ngawha, Kawerau and Tauhara Geothermal Fields, 1978," Report 175, Geophysics Div., Dept. of Scientific & Industrial Research, New Zealand (1981).
14. Syms, M.C. and Bixley, P.F.: "The Interpretation and Application of Flowmeter Logs in Geothermal Bores," *Proc.*, The New Zealand Geothermal Workshop, Auckland (1979) 50-55.
15. Allis, R.G. and James, T.: "A Natural-Convection Promoter for Geothermal Wells," *Trans.*, Geothermal Resources Council, Salt Lake City (1980) 4, 409-12.
16. Celati, R. *et al.*: "Study of Water Levels in Larderello Region Geothermal Wells for Reconstruction of Reservoir Pressure Trend," *Geothermics* (1977) 6, 183-98.
17. Dench, N.D.: "Interpretation of Fluid Pressure Measurements in Geothermal Wells," *Proc.*, The New Zealand Geothermal Workshop, Auckland (1980) 55-60.
18. Grant, M.A.: "The Effect of Cold Water Entry in a Liquid-Dominated Geothermal Reservoir," *Water Resources Research* (1981) 17, No. 4, 1033-43.
19. Grant, M.A.: "On the Existence of Two Phase Fluid in Good Communication with Liquid Water," *Proc.*, Stanford U. Sixth Workshop Geothermal Reservoir Engineering, Report SGP-TR-50, Palo Alto, CA (1980) 28-33.
20. Grant, M.A. and Horne, R.N.: "The Initial State and Response to Exploitation of Wairakei Geothermal Field," *Trans.*, Geothermal Resources Council, Salt Lake City (1980) 4, 333-36.
21. Fair, W.B.J.: "Pressure Buildup Analysis with Wellbore Phase Redistribution," *Soc. Pet. Eng. J.* (April 1981) 259-70.
22. Chu, W.C. and Raghavan, R.: "The Effect of Noncommunicating Layers on Interference Test Data," *J. Pet. Tech.* (Feb. 1981) 370-82.
23. Grant, M.A., Bixley, P.F., and Syms, M.: "Instability in Well Performance," *Trans.*, Geothermal Resources Council, Reno, NV (1979) 3, 275-78.
24. Horne, R.N., Grant, M.A., and Gale, R.O.: "Results of Well-Testing in the Broadlands Geothermal Field," *Proc.*, Stanford U. Fourth Workshop Geothermal Reservoir Engineering, Report SGP-TR-30, Palo Alto, CA (1978) 139-45.
25. Miller, C.W.: "Wellbore Storage Effects in Geothermal Wells," *Soc. Pet. Eng. J.* (Dec. 1980) 555-66.

SI Metric Conversion Factors

bar	× 1.0*	E+00	=	kPa
ft	× 3.048*	E−01	=	m
°F	(°F−32)/1.8		=	°C
in.	× 2.54*	E+00	=	cm
lbm	× 4.535 924	E−01	=	kg
L	× 1.0*	E+00	=	dm^3

*Conversion factor is exact

SPEJ

Original manuscript received in Society of Petroleum Engineers office July 13, 1981. Paper accepted for publication May 19, 1982. Revised manuscript received Oct. 29, 1982. Paper (SPE 10317) first presented at the 1981 SPE Annual Technical Conference and Exhibition held in San Antonio Oct. 5-7.

CURSO: "INGENIERIA DE YACIMIENTOS GEOTERMICOS"

En colaboración con la OLADE, C.F.E., I.I.E.

Del 13 marzo - 18 mayo

TEMA: PRUEBAS DE PRESION

4.- Grant. Donaldson y Bixley, Pags. 160-192, 234-241, 276-311

DR. FERNANDO SAMANIEGO

13-23 MARZO 1984.

Chapter 7

Quantifying Reservoir Properties

7.1. INTRODUCTION

In Chapter 2 we dealt with the conceptualization of the geothermal reservoir and the qualitative inferences that can be made from the natural state of the field. In this chapter we go a stage further and treat the large-scale measurements that can be made to quantify additional reservoir parameters. This ideally leads to a reservoir model that may serve as a basis for projections of future performance of the reservoir under exploitation. We would like such predictions to contain sufficient detail to include, possibly, even the changes in mass flow, enthalpy, and wellhead pressure of each well and the changes taking place in various parts of the reservoir that control the surface performance. In practice, such detail and precision is unlikely since some reservoir properties cannot be determined prior to actual exploitation. Recharge, the rate of influx of make-up fluid to the reservoir, is probably the most important such property.

For this discussion it is assumed that sufficient single well tests and analyses have been done throughout the reservoir to define the properties of the well and the neighboring reservoir. Here we discuss the measurement and estimation of the reservoir properties on a more extensive scale. Such properties can only be determined using data from many wells, either as a unit to get field scale information or intercomparatively to assess local and regional inhomogeneities. We depend primarily on two types of tests: those based on the sustained discharge of a group of wells, and those seeking interference effects between groups of wells. In both cases the intent is to disturb the reservoir over some substantial area and thereby determine some *average* reservoir properties for that section of the reservoir.

A prolonged and substantial *discharge* from several wells is intended to remove sufficient fluid to make a measurable change in that zone of the reservoir. The change that takes place may show up any anomalous reservoir behavior as well as indicating general trends. A standard *interference test*, utilizing sufficiently precise instrumentation to allow measurement of small pressure changes, can give us transmissivity and storativity over

a large area. Again, anomalous areas and inhomogeneities can be noted. Chemical and other changes in discharge from wells affected by reinjection provide an alternative type of "interference" test. Injection of tracers is another means of seeking interconnections between injectors and production wells.

Many factors will affect the type of test that may be carried out and/or the information that may be obtained. Environmental restraints, for example, may preclude long-term discharge tests in many areas. Field drawdown data may not become available until the surface plant has been in operation for some years.

The nature of the reservoir and its surroundings is also important. For example, contrast a homogeneously permeable low-temperature (liquid) reservoir with a fractured high-temperature (two-phase) one. In the former the liquid state of the fluid means that pressure changes are transmitted over long distances in short times, and because of the homogeneous nature of the reservoir the measured properties can be related unambiguously to the reservoir rock. Such a field can be well defined by a thorough program of pressure tests on single wells supplemented with some selected interference tests. In the two-phase reservoir any pressure changes move out slowly, making it almost impossible to measure permeability on any field or zonal scale. Even when the pressure change information is available the fractured nature of the system limits its usefulness. There may be no clear indication of the thickness of any aquifer in a transmissivity evaluation. In this situation a sustained well discharge is the only test that can indicate the long-term changes in well performance, i.e., we cannot predict, we can only measure.

The nature of the reservoir can also determine the time scale necessary for any test. A well near a boundary, for example, cannot show the presence of that boundary unless the test runs long enough for the pressure change to propagate out to the boundary and back to the well. Nor can any recharge effects be seen unless measurements are made over times on the order of the characteristic time τ of the reservoir (see Sections 3.4 and 7.4.3). A large flow rate is not a substitute for a long time. The time period is essential for the data to exist; the size of the flow rate merely controls the magnitude of any change.

Geothermal reservoirs are, in general, complex, and complexity must mean uncertainties in our conceptualizations of these reservoirs and our interpretations of the measurement data. Even with these uncertainties useful results may still be obtained. If recharge, for example, is unknown, a worst case may be assumed—that of no recharge. Any recharge to the reservoir must then mean a lesser drawdown. It may not be possible to predict pressure and enthalpy changes in a two-phase field. One can,

however, predict which wells (the shallow feeding ones) will go dry if a steam zone does form. No good theory of a fractured reservoir currently exists. Tracer tests provide a way to detect in a short time any fast return from injection wells.

7.2. INFERENCE FROM FLUID DISTRIBUTION

7.2.1. Introduction

In almost all decisions regarding reservoir behavior, it is convenient to assume some specific property as being representative: a mean pressure or temperature, for example, or a mean chloride content. For changes in such field properties local variations may not be that important—lumped parameter models are then successful.

In actual reservoirs there will be a marked variation in some properties over the field, and these properties will generally not change as a unit. The amount and rate of change will vary with position in both the vertical and horizontal directions. Having collected reservoir data (pressure, temperature, chemistry, permeability), the first task is to correlate or plot it against relevant variables (distance, depth, time). From such plots it should be clear what controls the distribution of observed results. For example, Figure 7.1 demonstrates that depth is essentially the only parameter controlling pressure at Kawerau. In other fields areal variation is important. Not only pressure changes are important: temperatures, or enthalpy if two-phase conditions occur, are equally so. In gassy fields gas content can be traced with time or position or by changes in chloride or silica content. Examples of all of these occur in the fields discussed in Chapter 8.

The parameter most sensitive to any alteration in flow and to exploitation in general is pressure. In an unexploited reservoir the vertical pressure gradient is normally close to that of a static column of water or steam at the reservoir temperature. Horizontal pressure gradients are normally small. Once the field is exploited this pressure pattern may change markedly, and it is this change that we look for in our interference and long-term reservoir tests.

The changes in vertical pressure distribution at Wairakei are shown in Figure 8.16 as is an idealization of the pressure and fluid distribution into vapor- and liquid-dominated zones after a transition period. The Broadlands example illustrated the development of subhydrostatic gradients in the reservoir. In each case, by correlating data between wells we are able to simplify the data into a single pressure–depth profile for the reservoir at each time.

Fluid chemistry and temperatures in liquid regions respond much more slowly to flow changes than does pressure. Chemical changes, being fluid tagged, only show up when the different fluid reaches the production or test wells. Temperature changes may be even slower, since the movement of heat between rock and fluid buffers the effect. Chemical changes are of greatest importance in situations where the entry of cold water or return of reinjected water is possible. Tracer tests are a variant in which the reservoir is tested for preferential return between production and injection wells.

7.2.2. Kawerau: Upflow

Both the uniform upflow and BPD models are idealizations in that to apply either, both horizontal and structural effects in the reservoir must be unimportant or ignored. Few real systems are that neat. In particular, the uniform upflow model may be applicable only partly in some systems and not at all in others.

Kawerau, New Zealand, may be approximated overall with the uniform upflow model, although lateral flow is also present. Here we describe the

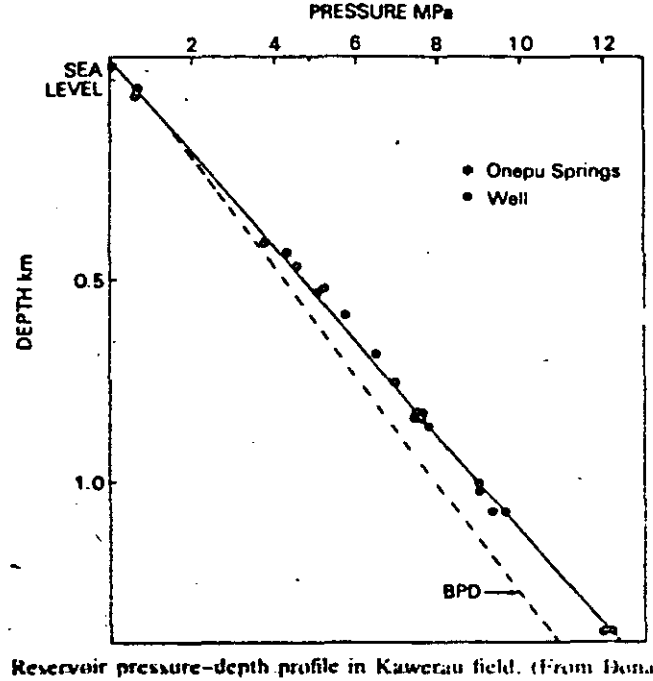

Fig. 7.1. Reservoir pressure–depth profile in Kawerau field. (From Donaldson *et al.*, 1981; copyright © SPE-AIME.)

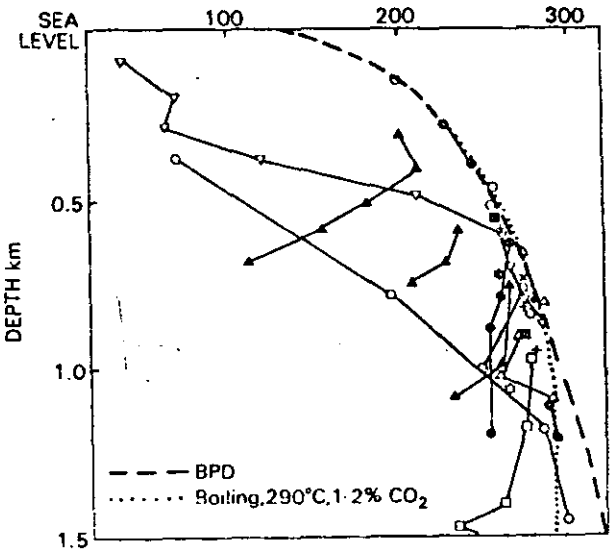

Fig. 7.2. Reservoir temperatures at Kawerau. (Ministry of Works and Development, New Zealand, 1981; personal communication.)

fluid profile in the Kawerau reservoir and the implications that can be drawn from this and the associated pressure profile.

The pressure and temperature profiles for Kawerau are illustrated in Figs. 7.1 and 7.2, respectively. This field has been exploited at a low level since the mid-1950s, but there have been no detectable, systematic changes in pressure (Dench, 1962; Smith, 1970; Donaldson and Grant, 1981a). The illustrated pressure profile therefore represents both the current field state and its undisturbed condition. The temperatures are interpreted reservoir temperatures from measurements in wells before substantial discharge.

The pressure profile is also well defined, since wells of an unusually wide range of depth have been drilled. Pressures at feedpoints of these wells have then been used to build up these profiles. The pressures exceed a hydrostatic column at BPD by 7%.

From the excess pressure gradient it is possible to calculate the vertical permeability k_v by application of Darcy's law. The natural discharge of the field was given by Thompson (1962) as 20–70 MW. At the deep temperature of 290°C this is $W = 15$–55 kg/s of water. If the area of upflow is A, and assuming $k_{rw} \approx 1$,

$$W = \frac{k_v A}{\nu}\left(\frac{dP}{dz} - \rho_w g\right) = \frac{k_v A}{\nu}(0.07\ \rho_w g),$$

which gives $k_v A = (3.5 - 12)$ md-km^2. The field area is 6–8 km^2, so that the vertical permeability is estimated as 1 millidarcy, with an uncertainty of a factor of 2.

In this field the difference between the actual pressure (and temperature) profile and BPD gives us information. It is to be noted that here the excess pressure showing in the profile is due to a fairly uniform excess pressure gradient rather than to any fixed absolute pressure difference. At all depths the pressure exceeds hydrostatic, the absolute excess increasing as we go deeper. This excess pressure must therefore be due to the resistance of the reservoir to the upward mass movement at all levels. There is no indication of any specific capping or higher resistance layer.

The absence of any capping structure at Kawerau has been proposed as a reason for this reservoir's history of cold water intrusion into producing wells. The water is apparently surface groundwater, making it tempting to associate the inflow with the absence of an obvious structural restraint such as a capping layer. It must be noted that Wairakei had nearly identical initial pressures to Kawerau and is also regarded as having no cap. Even with the significant drawdown that has occurred in Wairakei, proportionately much less cold inflow has been observed there.

The temperature distribution in the Kawerau reservoir falls significantly below BPD and hence further below saturation for actual pressures. In addition to the BPD curve Fig. 7.2 also shows the boiling temperature, assuming that the upflow consists, at depth, of water at 290°C containing 1.2% carbon dioxide (using the method of Appendix 2). Discharges from deeper feeding wells have a similar amount of gas. It can be seen that maximum temperatures are close to this revised boiling curve. (The lower temperature and the gas content increase the water density above BPD and so would decrease the excess pressure gradient and increase k_v.) Discharge enthalpies of newly drilled wells are sometimes at that for downhole liquid and sometimes higher, with excess enthalpy being more common and larger in shallow wells.

Thus, the fluid distribution in the high-temperature parts of Kawerau is close to that of a uniform vertical upflow of water and carbon dioxide.

7.2.3. Vapor System

An estimate of vertical permeability in one part of a vapor system has been given by Hite and Fehlberg (1976). Figure 7.3 shows the temperature profiles obtained during the drilling of two wells into part of The Geysers. In both there is a linear increase in temperature with depth through the caprock and a much lesser increase below. Using the upper temperature gradient and available thermal conductivities, Hite and Fehlberg esti-

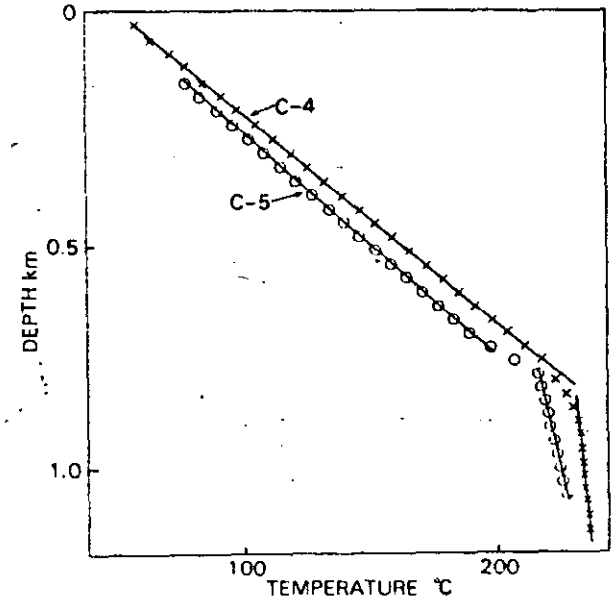

Fig. 7.3. Temperature profiles in two wells at The Geysers, before encountering production. (From Hite and Fehlberg, 1976.)

mated the vertical heat flux through the caprock. They then assumed this to be the convective heat flux up through the steam zone due to the upflow of steam and downflow of (an equal mass of) condensate. From the necessary mass flows and available pressure data they were able to estimate the probable vertical permeabilities. For the two wells, both drilled in an unproductive part of the reservoir, they obtained values of 0.2 md and 0.5 md, respectively.

7.3. INTERFERENCE TESTING

As we have pointed out, there are two ways of testing the behavior of a significant section of a geothermal reservoir. One is to watch for the long-term changes that may occur while the reservoir as a whole is being exploited. The other is to attempt to measure the effect of discharge of a single well, or group of wells, on some other neighboring (observation) wells. Both are, in effect, interference tests in that withdrawal of fluid from some wells affects pressures in others. In practice, the term "interference test" is primarily applied to the latter situation, and for groundwater and oil and gas reservoirs the theory and methods for analysis of the test data are readily available. This is probably the most important test

available for defining the properties of a reservoir over an extensive distance.

In an interference test we measure the drawdown at an observation well (or an array of observation wells) caused by the discharge of other wells tapping the reservoir. Thus, the time-changing drawdown at the observation well due to some specific production pattern (areal as well as time) is experimentally known. The result could be extrapolated if that were of specific value. More valuable is the information that we can extract from this data about the reservoir in the area between the production and observation wells.

If the test gives results that conform to those for a homogeneous aquifer, i.e., if the drawdown in the observation well follows the line-source solution, a transmissivity and storativity may be determined for the aquifer. The transmissivity may be interpreted as a representative aquifer value. The storativity $S = \phi c_t h$ may be further interpreted: assuming that the aquifer is confined and contains only liquid water, $c_t = c_w$—a value that may be obtained directly from a table of water properties. The porosity–thickness ϕh of the water-filled aquifer that was disturbed by the interference test can then be obtained. The test demonstrates the existence of as much water as fills the thickness ϕh of an aquifer of known transmissivity. If the transmissivity is high enough the ability to produce this water has been demonstrated. A fluid reserve has been proven and the test has shown both its existence and the fact that we may extract it.

This fluid reserve estimation has been carried over directly from petroleum and groundwater applications. Its use in geothermal reservoirs can be risky. The major problem is the dependence of the storativity on the compressibility of the fluid. Because the compressibility of liquid water is so small, even a small amount of vapor in the aquifer will result in a much greater storativity (Bodvarsson, 1979). Such boiling fluid need not be apparent at the production depth, it need only be somewhere in the aquifer. For this reason a large storativity in a high-temperature reservoir should not be immediately interpreted as meaning a thick high-porosity aquifer. The possibility of contact with more compressible fluid should always be considered. One example of difficulty in interpreting storativity is the Svartsengi reservoir in Iceland, discussed later in Section 7.6.

Naturally, in many situations the test will not give a drawdown curve that matches the solution for the homogeneous aquifer. As in petroleum and groundwater reservoirs, the drawdown in the observation wells may indicate that the reservoir is laterally bounded. Some observation wells may respond strongly, whereas others do so only to a lesser degree or not at all. In these cases we learn other things about the reservoir structure, such as its boundaries, its heterogeneous nature, and the extent of the permeable region tapped in that particular test.

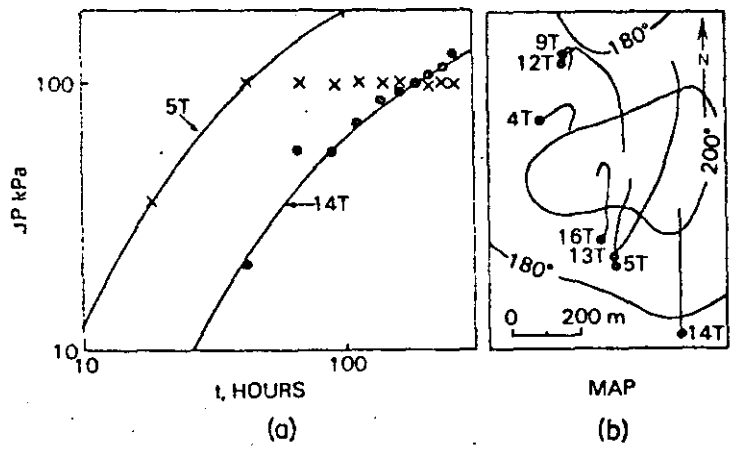

Fig. 7.4. Chingshui interference test. (a) Type curve matches to interference observations in two wells. (b) Field map. (Both from Chang and Ramey, 1979.)

7.3.1. Chingshui Geothermal Field, Taiwan

Chingshui geothermal field on the island of Taiwan has been described by Chiang *et al.* (1979) and Lee *et al.* (1981). Well tests carried out in the area have been discussed by Shen and Chang (1979) and Chiang and Chang (1979). We shall discuss here the comprehensive interference test described by Chang and Ramey (1979).

Figure 7.4b shows the locations of the wells in the field and the isotherms at 1500 m depth. The low temperatures at this depth (measured in water-filled wells) indicate single-phase fluid. For the interference test, well 16T was flowed at a nearly steady rate of 22 kg/s and wellhead pressures were observed on six other wells. On one of these a pressure rise was recorded due to failure of a gas release pipeline. At the others falls in pressure of 80–120 kPa were observed. The transient drawdowns were matched to the Theis solution, the data giving some good and some poor fits (Fig. 7.4a). The results of these matches are listed in Table 7.1. The five observations give permeability thicknesses of 2.5–8.8 d-m, i.e., within a factor of 4. This is generally regarded as good agreement for a geothermal reservoir test. (Tests on a single well, described by Shen and Chang (1979), give kh = 3.2–5.4 d-m, in the same range as the interference test.

To obtain the porosity-thickness values a fluid compressibility of 1.5×10^{-9} Pa^{-1} was used. The values of porosity-thickness obtained, 60–200 m, (excluding the poor results from 5T) suggest an extensive aquifer.

TABLE 7.1
RESULTS OF CHINGSHUI INTERFERENCE TEST[a]

	Well				
Matchpoint	4	5	9	12	14
P_D (at ΔP = 70 kPa)	0.90	0.26	0.80	0.90	0.44
t_D/r_D^2 (at t = 100 hr)	1.20	1.55	1.07	1.67	0.70
Distance (m)	300	65	300	200	250
kh (d-m)	8.8	2.5	7.8	8.8	4.3
ϕh (m)	160	790	60	120	200

[a] From Chang and Ramey (1979.)

7.3.2. Baca, New Mexico

Baca geothermal field is located in the Valles Caldera in New Mexico. Another part of this same caldera—one virtually impermeable to water at depth—is being used for the Hot-Dry-Rock geothermal experiment. That section of the caldera at Baca contains a liquid-dominated reservoir at temperatures of 250°C and above (Dondanville, 1978; Atkinson, 1980; Grant and Garg, 1981). The interference test discussed here is described by Hartz (1976). Prior to that test, individual wells had been tested and these had shown permeability-thicknesses in the range 0.7–2.7 d-m. The aim of the interference test was to determine reservoir transmissivity and storativity and to prove or disprove the continuity of the reservoir fracture system.

The field layout is illustrated in Fig. 7.5b. Wells Baca-6, 11, and 13 were used as producers; Baca-5A, 12, and 14 as injectors; and Baca-4, 10, 15, and 16 as observation wells. Calculations made before the test, using the aquifer properties determined from the single well tests, indicated that a measurable response should occur within 90 days. The test ran for 300 days.

Pressures were measured weekly in observation wells using conventional Kuster gauges. Stops of 30–60 min at observation depths were used to ensure equilibrium between tool and well. The same instrument was used for repeat measurements. Only Baca-10 showed a response; the other three observations wells exhibited no measurable pressure trend.

The pressure trend in Baca-10 (Fig. 7.5a) was initially obscured by the scatter in the data. Considerable improvement was achieved by the installation of a gas purge pressure monitor. The quality of the two data periods

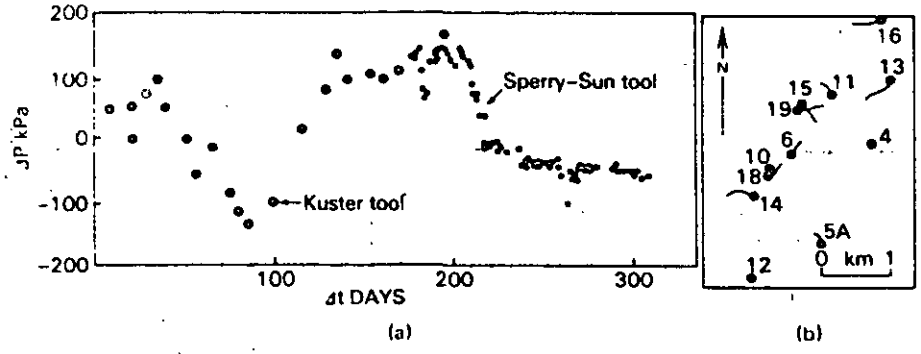

Fig. 7.5. Baca interference test. (a) Response of Baca-10. (From Hartz, 1976.) (b) Field map. (From Atkinson, 1980.)

indicates the importance of being able to measure the response in an interference test. The early data indicates that a response exists; the later data, with its finer detail, makes possible a much more extensive interpretation of the results. The response of Baca-10 was matched using a homogeneous confined liquid aquifer model with all production and injection wells in that aquifer. Using liquid water viscosity and compressibility, a permeability thickness of 1.8 d-m and a porosity thickness of 27 m were obtained. These values are of the same order as those obtained in the single well tests. This model was not consistent with the nonresponse of the other observation wells.

7.3.3. Brady's Hot Springs, Nevada

In the Baca reservoir test described above, the aim was to determine continuity of permeability as well as the reservoir parameters. The test at Brady's Hot Springs in Nevada, described by Rudisill (1978), had the same purpose. It was made to obtain information to assist in siting a disposal well.

This liquid reservoir has temperatures reaching about 160°C. Hot water is produced for direct use. The layout of the test wells is shown in Fig. 7.6b, and a section showing the interpreted structure is shown in Fig. 7.6a. B-8 is the producer. Pressure effects propagated out quickly to both B-4 (about 150 m) and B-1 (about 400 m) but took much longer to reach B-3 (about 220 m, located roughly halfway between B-1 and B-4). This illustrates the inhomogeneous nature of geothermal reservoirs as indicated in such tests.

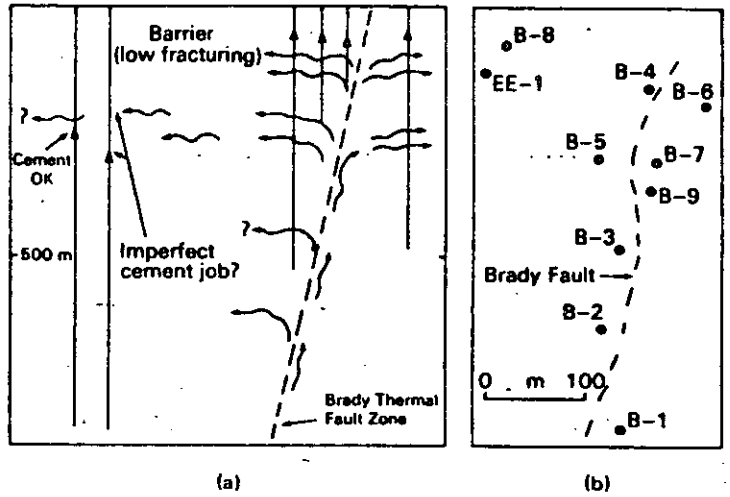

Fig. 7.6. Brady's Hot Springs interference test. (a) Conceptual model of reservoir as indicated by interference. (b) Field map. (Both from Rudisill, 1978.)

It was intended to use well EE-1 as an injection well. This well was drilled about 500 m deeper than B-8 and, although it was only 43 m away, the hope was that there would be no interconnection. On test, however, EE-1 showed interference with B-8, apparently through a shallow casing break and some perforations. The risk of a fluid return was considered too high and alternative waste fluid disposal arrangements were made.

7.3.4. Broadlands Interference Tests

A considerable number of interference tests have been carried out at Broadlands, New Zealand. For a map of the western borefield, showing all affected wells, see Fig. 6.1. Results of the tests are shown in Table 7.2. The response of BR2 to BR8, described in Section 6.3.2, used repeat Kuster gauge measurements. All other tests used water level measurements in wells containing stable water columns. One test used the water level in Ohaki Pool, the main natural discharge vent.

The results fall into two groups. The group of wells around BR13 and 23 all gives very consistent results. One of these tests is shown in Fig. A1.1. These wells all feed at depths of 800–1000 m, and reservoir fluid at the time of the test was liquid water. (Discharge enthalpies were sometimes above liquid water at larger flow rates.) The second group reflects the interference between shallow-feeding wells. The tests (see Fig. A1.18 for an example) show two-phase transmission, and all show very high trans-

TABLE 7.2
BROADLANDS INTERFERENCE TESTS[a]

Observation well	Producing well	kh/ν (10^{-4} sec · m)	kh (d-m)	ϕch (10^{-6} m/Pa)	Comments
Ohaki Pool	BR3	2.2	60	90	H_t = 1440 kJ/kg, T = 260°
BR2	BR8	0.4	15	35	See Chapter 6
BR33	BR8	17	200	4	Viscosity of 260° water used
BR33	BR11	21–25	300	170	Viscosity of 260° water used
BR23	BR13	8.7	120	0.31	Barrier shown
BR23	BR19	5.8	80	0.56	1980
BR23	BR19	11–15	150–200	0.5	1977
BR23	BR13	Injection	95	0.28	Barrier
BR23	BR13	65	90	0.08	
BR23	BR20	8.0	110	0.20	
BR34	BR23	3.3	45	0.30	
BR34	BR31	3–5	45–65	0.9–1.0	Possible barrier

[a] BR2, 8, and 11 feed at about 450 m, BR33 at 330 m, and Ohaki Pool at 200 m. The other wells all feed at 800–1000 m depth. All tests but one are responses to discharge. Fracture relative permeabilities were used for two-phase tests.

missivities. Some boundaries are also indicated. Individual well tests generally indicate much lower transmissivities. This could be interpreted as showing damage in the wells. Alternately, the lower transmissivities could indicate that the interference reflects the largest fractures in the reservoir, whereas well tests reflect the fracture actually intersected by a well. Thus, the testing indicates the presence of an aquifer of very high permeability, with possible permeability restrictions near some wells and at field margins.

The performance of the field under exploitation, discussed in Section 8.7, conformed partly to this pattern. The pressure–depth plots show considerable horizontal uniformity, confirming the high permeability. Recharge is very poor, indicating that high permeability must be bounded everywhere around the field. Since the amount of recharge is determined by the poorer external permeability, these tests do not give any guide to field recharge under exploitation. Individual wells varied greatly in performance; some (for example, BR23) ran down rapidly, which is inconsistent with a well feeding from a highly permeable aquifer, with or without skin

at the well. The interference test thus serves as a partial predictor of reservoir performance under exploitation.

7.3.5. Summary

The preceding examples give some idea of the types of results that may be obtained from interference tests in liquid conditions, where a pressure signal can propagate over substantial distances in a short time. Broadlands shows an example of the response in a two-phase reservoir. It is seen that the time scales are quite different. A lack of response in the time scale expected for a liquid system does not necessarily indicate a lack of connective permeability; it could indicate some two-phase conditions.

The basic results obtained from these interference tests are transmissivity, storativity, and the pattern of continuity in the reservoir. Transmissivity is usually converted immediately to permeability-thickness by multiplying by the water viscosity at some appropriate temperature. In productive reservoirs kh values of 10 d-m or more are usually obtained, and some in excess of 100 d-m have been reported. If values much below 10 d-m are obtained in interference tests, the ability to deliver fluid to the wells may be a restraint on development (Bodvarsson *et al.*, 1980).

Storativity can be converted to porosity-thickness by dividing by liquid water compressibility. This porosity-thickness is a value that can then be checked for consistency with anticipated aquifer thickness or reservoir depth. A high value of porosity-thickness may indicate the presence of some vapor in the system rather than a very thick aquifer. For this reason unless the reservoir temperatures are low and liquid conditions thus guaranteed, it is often preferable to stay with storativity and not convert it to a porosity-thickness that may be incorrect.

Some measure of reservoir continuity is obviously obtained from an interference test, although difficulties arise if some vapor is present. Nonetheless, the tests do indicate connections, barriers, and boundaries. If the wells are not all drilled and cased to similar depths or into one hydrologic stratum, the tests can also indicate interconnections between aquifers in the reservoir. Care must be taken to check that any connection found is not within the wells themselves, either through casing breaks or through external channeling.

7.4. LONG-TERM RESERVOIR TESTS

The only way to find out just how any particular complex reservoir will behave under exploitation is actually to exploit it. The discharge associated with the exploitation will disturb the reservoir. This disturbance will,

in turn, permit determination of the reservoir parameters required, in the detail appropriate to that reservoir and that mode of exploitation. This approach is the one that has been used with currently exploited fields, and discussions and models of the well-known fields show up regularly in the literature. In Chapter 8 we discuss these better-known fields that have a long history of exploitation. Here we consider some examples of more limited testing, where, although some results have been obtained, the interpretation may be incomplete or only some parameter values can be defined.

7.4.1. Kamojang, Indonesia

Well KMJ-11 was the first deep well drilled into the Kamojang reservoir. The reservoir is vapor dominated (Hochstein, 1976; Grant, 1979a) and the steam produced is slightly wet. A short-term discharge test of KMJ-11 gave a permeability thickness of about 35 d-m.

To test long-term behavior, the well was discharged for 450 days at a constant wellhead pressure of 800 kPa. Figure 7.7 shows the flow rate for part of this time, corrected for the minor fluctuations in wellhead pressure using the slope of the most recent output test measurements. It is seen that the flow rate declines over the period of observation. The flow rate decline that would be expected if the well tapped an aquifer of kh = 35 d-m is plotted on the figure for comparison. Within the limits of measurement scatter, these curves are comparable.

It is of interest to determine the volume of the adjacent reservoir affected by this 450-day discharge. In terms of the field parameters this

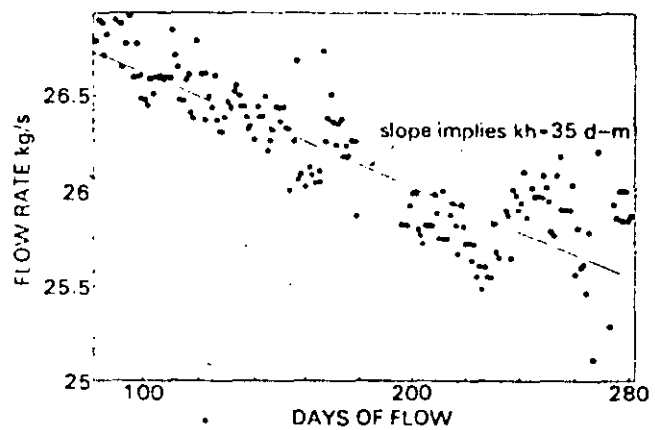

Fig. 7.7. Rundown of well KMJ-11, Kamojang. (Reproduced by permission of the Governments of Indonesia and New Zealand/Geothermal Energy NZ Ltd.)

volume is

$$V = \pi r^2 h, \tag{7.1}$$

where the diffusion radius is

$$r = (\kappa t)^{1/2}, \quad \kappa = k/\phi\mu c_t, \tag{7.2}$$

so

$$V = \pi k h t/\phi\mu c_t. \tag{7.3}$$

For vapor-dominated conditions, and the temperatures involved, these parameters may be specified:

$$\mu_t = 17 \times 10^{-6}\ \text{Pa} \cdot \text{s};$$

$$\phi c_t = 1.1 \times 10^{-6}\ \text{Pa}^{-1};$$

$$kh = 5\ \text{d-m} = 3.5 \times 10^{-11}\ \text{m}^3.$$

For the test

$$t = 450\ \text{days} = 3.9 \times 10^7\ \text{s}.$$

Thus

$$V = \pi(3.5 \times 10^{-11})(3.9 \times 10^7)/(17 \times 10^{-6})(0.11 \times 10^{-5})\ \text{m}^3$$

$$= 0.2\ \text{km}^3.$$

This is not a very large volume. If a layer thickness of, say, 300 m is assumed it implies a cylinder of radius 450 m. Unless channeling is significant and other wells thus tap the same unit, no interference with any other well is to be expected, and the test will not glean any information about reservoir structure at greater distance. Because of the two-phase fluid in the reservoir, pressure propagation is inherently slow, even in this high permeability example. One could not, for example, use pressure tests here as in a liquid water system to detect reservoir boundaries. We can only wait and monitor production and pressures on an even longer time scale, i.e., during actual exploitation and operation of the surface plant that will be associated with this field.

7.4.2. Momotombo, Nicaragua

In view of the inability of the extended discharge at Kamojang to define the reservoir, one might ask just what such a test might achieve. A test at Momotombo in Nicaragua is a good example of its usefulness.

The Momotombo reservoir is liquid dominated. Wells have penetrated a region of upflow where temperatures increase with depth and an eastern

outflow region with temperature reversals (Dykstra and Adams, 1978; Lopez *et al.*, 1980).

The productive capacity of the wells was initially assessed by short-period testing, i.e., discharges of up to 30 days. Later it was decided to run a longer well discharge (Lopez and Eckstein, 1980). Over this discharge period of 6 months, a clear pattern emerged: wells in the upflow zone ran down moderately; wells to the east of this zone ran down more; wells to the far east experienced extreme declines in flow. Examples of each are illustrated in Fig. 7.8. In addition to the flow decline, all well discharges increased in dryness.

The rundown here has been explained as being due to the inward advance of cooler (external) water and consequent silica deposition that sealed off further recharge. The important result is the discovery of the rundown, which indicates that only part of the reservoir will sustain production for power generation, at least if exploitation is carried out as is currently planned. This conclusion could not be drawn from the short-term test data.

7.4.3. Broadlands

Broadlands, New Zealand, is interesting in that wells tapping this reservoir were discharged long-term and then shut in for an equivalently long period. The reservoir thus sustained both a drawdown and a recovery. An analysis of the data shows that in this double test we can get some field results not easily obtained otherwise.

The simplest possible model that can be applied to a reservoir to simulate such drawdown and recovery is the basic model of Section 3.4,

$$W = \alpha_r P + \mathcal{S}_M \frac{dP}{dt}. \tag{7.4}$$

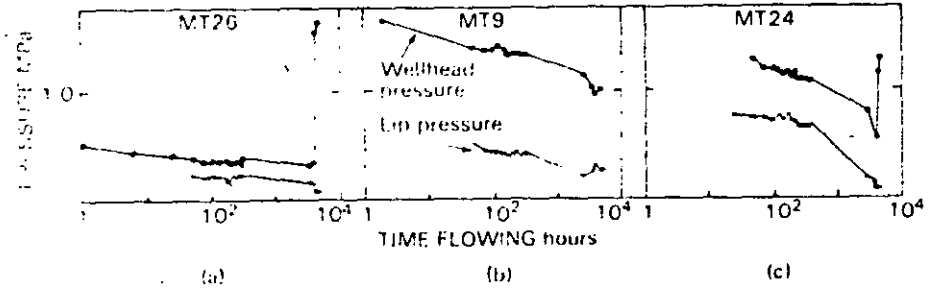

Fig. 7.8. Rundown of three wells in different parts of Momotombo field. (a) MT-26 in the upflow zone, (b) MT-9 on the outflow, (c) MT-24 at extreme end of outflow. (All from Lopez and Eckstein, 1980.)

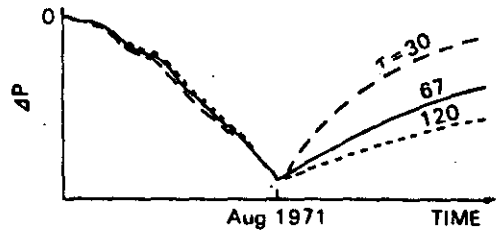

Fig. 7.9. Parameter variation of simple model fitted to pressure history of Broadlands reservoir. (From Marshall, 1975; personal communication.)

The ratio $\tau = \mathcal{S}_M/\alpha_r$ is a time constant for the model. In seeking a best fit for the Broadlands data this ratio was varied (keeping maximum drawdown constant) and the results plotted. These curves are shown in Fig. 7.9. It will be noted that for the values chosen there is little difference in the curves over the drawdown time period (D. C. Marshall, 1975; personal communication). The curves can only be distinguished during the recovery. Basically the recharge is low and the drawdown approximates to the drawdown that would occur if there were no recharge. The storage constant $\mathcal{S}_M$ is determined during this phase of the test.

In contrast, with no withdrawal and no other input of fluid the recharge controls the rate of recovery. The time constant τ is thus defined by this phase.

It should be noted that, with longer-term withdrawal and greater drawdown, the recharge begins to play a more significant role. Ultimately the various drawdown curves would therefore separate and a best time constant could then be estimated. The best fit has a value $\tau = 6$ years. Observations over only 3 years cannot define τ.

7.4.4. Tongonan

We now return to Tongonan, a high-temperature reservoir containing a two-phase zone. For such a reservoir it is desirable to estimate not only the future mass flow from a well but also the future enthalpy. Both will change with time, and knowledge of both is needed for proper surface plant design. From experience in other fields we know that the enthalpy is most likely to increase with time and with flow rate, but we have no *a priori* idea of how fast or how far. We also know that with exploitation a steam zone may form at the top of the two-phase zone and shallow wells may go dry. Again, we have little knowledge as to how big this zone will be or how quickly it may form.

To discover just how the enthalpy of a particular well may change there is therefore no good alternative to an actual trial discharge for some extended time. Such a discharge will not give any information about the

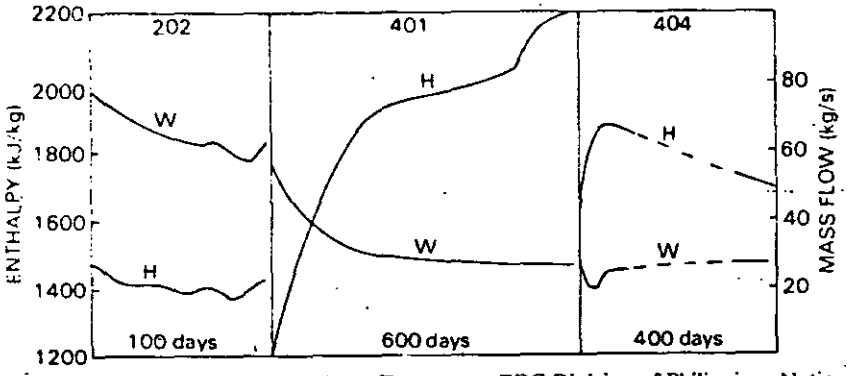

Fig. 7.10. Rundown of three wells at Tongonan. (EDC Division of Philippines National Oil Company/Kingston Reynolds Thom and Allardice, New Zealand, 1981; personal communication.)

possible future steam zone (a major and extended field discharge would be needed for that), but it can indicate the well's own local characteristics. We are attempting to define the local reservoir physics where they cannot yet be predicted.

Figure 7.10 shows the discharge history of several wells. Well 202 shows a low-enthalpy well—enthalpy remains constant and mass flow declines. Well 401 shows a normal two-phase well—enthalpy rises and mass flow falls with time. Well 404 shows anomalous behavior—enthalpy falls with time. Such anomalous wells represent a deviation from the trend expected for wells tapping a fluid-charged layer with homogeneous characteristics. Possible explanations are thermal stress cracking, thermal contraction (Stefansson and Steingrimsson, 1980b), presence of two zones in the well, and entry of cooler water from outside the area. The last could be serious and so comprise a warning of a potential problem.

For the very long term, i.e., under full exploitation conditions, these trends can be taken only as indicators. Anomalous wells may or may not be used, depending on output characteristics, their locations, and the explanations of the anomalous behavior. An average trend may be assessed for likely production wells and this should at least give basic information for plant design.

7.5. OTHER TESTS

7.5.1. The Use of Tracers

The heterogeneous and fractured nature of many geothermal reservoirs creates problems for the practical engineer and also for the theorist, for example, in his attempts to predict reservoir behavior from well and

interference tests. In many reservoirs we deliberately drill for faults, for best production. In others we seek sites for injection wells that are both permeable and yet somewhat isolated from the main production zone. We want to get rid of the waste water and we would like the benefit of some pressure maintenance, but we do not want cooling of production wells.

One testing tool that proves useful in such fractured and heterogeneous systems is the chemical or isotopic tracer (Vetter, 1978). Some of these tracers are natural, i.e., they already occur in the fluid in some part of the system and the changes in them from one zone to another may be relevant. These changes may give some sort of time scale for the movement of fluid from one location to another, or they may indicate a mixing of fluids from different zones or the dilution of thermal waters with cold groundwaters. For example, the low chloride content of cool groundwater surrounding a geothermal reservoir may ultimately be the tracer that indicates that recharge water is reaching the production zone.

Natural tracers that tag water directly could be of particular interest. These are the hydrogen and oxygen isotopes: tritium, deuterium, and oxygen-18. The increased tritium in meteoric waters resulting from the atomic bomb tests at Bikini Atoll has been used as a time marker for some hydrologic studies. The presence of tritium in well discharges, as at Larderello (D'Amore *et al.*, 1977), shows recharge of recent groundwater. Natural tracers have been used at Krafla to indicate the velocity of the natural flow (Stefansson, 1981).

Introduced tracers are the most common means of tracking inhomogeneities in the reservoir. Such tracer studies have become an essential part of the testing procedure when reinjection into a fractured reservoir is contemplated. As a tool the introduced tracer indicates, and in some respects evaluates, a basic physical property of the reservoir: the preferential nature of the permeability. It should be pointed out, however, that if the reservoir is sufficiently heterogeneous for marked connections to show in some places, a poor connection elsewhere in that reservoir does not necessarily mean (unless there is other supporting evidence) that the tracer is not getting out to that area quickly. A pertinent flow channel may be only meters away from the observation well and yet may not connect with it. Consequently, a tracer test in an injector may only be assumed to give information relating to connections with existing wells, not to projected ones in the same area.

7.5.2. Tracer Tests at Wairakei

Three wells at Wairakei (WK80, WK101, and WK107) have developed cool downflows. Natural reinjection takes place as steam-heated groundwaters enter these wells at a shallow feedpoint, flow down, and are in-

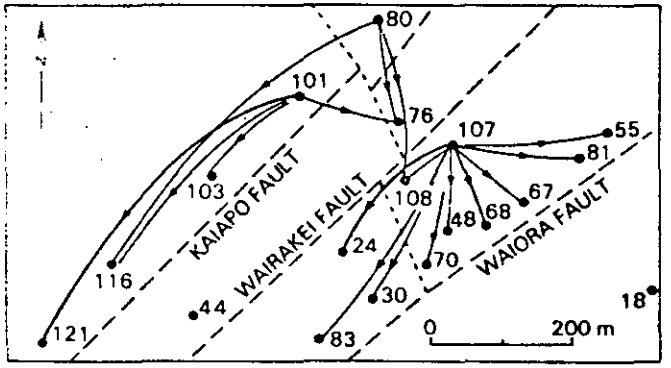

Fig. 7.11. Isotope tracer tests at Wairakei. (From McCabe *et al.*, 1981.)

jected into the reservoir at greater depth. To determine where this water was going, radioactive tracer was released into the downflowing water (McCabe *et al.*, 1981). Figure 7.11 shows the results. The pattern of tracer flow shows strong preferential return. In the test at WK107, returns to WK24 and WK48 were followed by a fairly uniform return to all wells sampled along the Waiora Fault. The tests at WK80 and WK101 show a strong orientation of flow along the Kaiapo fault, and all show a general trend of flow to the southwest. In each test less than 10% of the tracer was recovered, so it is not known where most of the injected water went.

If the medium were homogeneous, no return at all would have occurred. A chemical front should advance less than 50 m from any well over the 30 day detection period of the tracer. Thus, the observed returns indicate strong preferential flow paths within the reservoir. There was also some vertical structure to the returns—the tracer was traveling downward.

This pattern of preferential flow paths and marked heterogeneity contrasts with the uniformity of the drawdown and the general uniformity of Wairakei behavior. In some respects the Wairakei reservoir behaves like a homogeneous medium; in others it does not.

7.5.3. The Partial Shutdown of Wairakei, 1968–1969

Although a long-term disturbance in a reservoir is needed in order to determine some parameters, such as the recharge, a sudden change in some field characteristic can also given information. A good example of such a change was the partial shutdown of the Wairakei field in 1968. At that time a temporary surplus of base generation capacity meant that about two-thirds of the production wells at Wairakei could be shut down

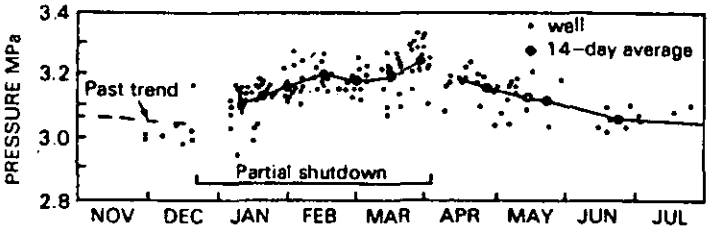

Fig. 7.12. Recovery of average reservoir pressure at Wairakei during partial shutdown in 1968. (Ministry of Works and Development, New Zealand, 1981; personal communication.)

for 3 months. The shutdown was not fully representative of average field response as it was the high enthalpy wells that were kept on flow. All available wells were monitored for changes in pressure and other measurable properties. Figure 7.12 shows pressure observations made in the period around the shutdown. These measurements were made in wells throughout the reservoir, and are all adjusted to standard Wairakei pressure level. There is an observable recovery in the field pressure. Some outlying wells also showed fast responses to the shutdown, whereas others did not produce any observable response.

In absolute terms the field pressure increased at the rate of about 470 kPa/yr during the shutdown. Allowing for the prior falling trend, this is a change of about 570 kPa/yr, with a mass discharge reduction from 1.9 t/s to 0.8 t/s, i.e., 1.1 t/s.

If we assume that the pressure change is controlled only by the change in mass flow and ignore the enthalpy changes, this test gives us the reservoir storage coefficient

$$\mathcal{S}_M = (1.1 \text{ t/s})/[(4.7 \times 10^5 \text{ Pa})/(3 \times 10^7 \text{ s})] = 70 \text{ t/Pa}.$$

Note that from this data alone, only $\mathcal{S}_M$ can be computed. A similar test could be carried out on a new field by simultaneously opening a large number of wells. In essence such a test is carried out when the first power plant is commissioned.

In terms of the simple model of Section 3.4, we have determined one of the two parameters needed to estimate reservoir performance. In the case of this particular test the other parameter can also be found by using the prior history of the field. Before the test the reservoir pressure was falling at the rate of 100 kPa/yr and the mass withdrawal rate was 1.9 t/s. We use the storage coefficient just computed and assume that it applies to the total withdrawal. (Note that the enthalpy is different from that of the partial shutdown withdrawal.) This rate of fall then implies a net mass loss of 0.2 t/s from the reservoir, and it can therefore be assumed that the

remainder of the discharge, i.e., 1.7 t/s, was being replaced in the reservoir. The recharge at the time of the test (1968) must have been this 1.7 t/s.

At that time the pressure drop in the reservoir was 2.1 MPa from its initial value. Assuming that this recharge is proportional to the pressure drop, the recharge coefficient is

$$\alpha_r = (1700 \text{ kg/s})/(2.1 \text{ MPa}) = 810 \text{ kg/MPa} \cdot \text{s}.$$

When compared to the values obtained by analysis of field history (Table 8.2), these figures show that the 3-month test produced results for α_r and $\mathcal{S}_M$ that are about 135% and 50%, respectively, of the historical results—a good match by geothermal standards. The discrepancy is probably due to real differences in short-term and long-term behavior.

7.6. SVARTSENGI, ICELAND

We have chosen Svartsengi in Iceland as an example of a reservoir testing project from which definitive results were obtained. Although there are some problems in interpretation of some of the parameter values obtained, these interpretations are not important for the particular aspects of field behavior being considered. The analyses are therefore valid for their purposes.

The geothermal field of Svartsengi has been described by Thorhallson (1979) and Georgsson (1981). It is located on the Reykjanes Peninsula, along an earthquake zone. In that region geothermal areas are associated with surface fissure zones. Energy from the Svartsengi reservoir is used for district heating and cogeneration of electricity. The reservoir history discussed below was described in detail by Kjaran *et al.* (1979), and our commentary is adapted from their paper, and Kjaran (1981; personal communication).

A model of the natural flow in the earthquake zone is illustrated in Fig. 7.13a. The fluid tapped in wells at Svartsengi is a brine, apparently derived from a mixture of seawater and fresh water concentrated by boiling, and it is at a temperature of about 240°C in the reservoir. The hydrology of the Reykjanes Peninsula, including Svartsengi, is modeled conceptually. A regional flow of fresh water from Lake Kleifarvatn to the sea mixes with intrusions of seawater while gaining heat as it moves through the system. There is some loss of steam to surface activity. The estimated heat input into the Svartsengi reservoir is 300 MW (thermal).

In 1979 five wells had been drilled in Svartsengi; of these, two are in production and one is used as an observation well. This well, H-5, re-

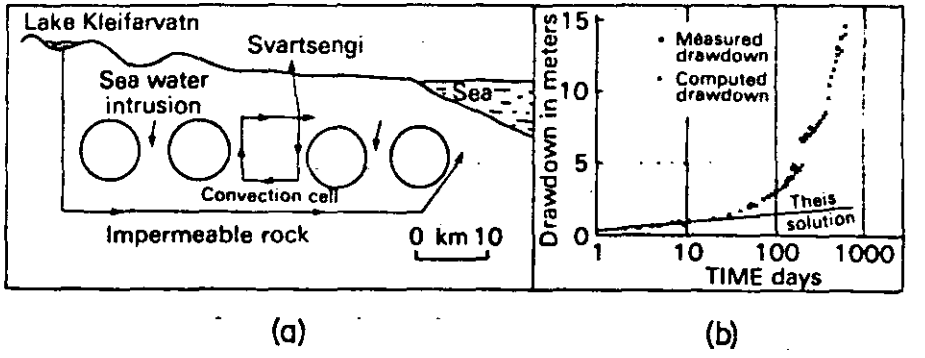

Fig. 7.13. Svartsengi field. (a) Regional flow on the Reykjanes peninsula. (b) Drawdown in observation well H-5, on semilog plot. (Both from Kjaran *et al.*, 1979.)

sponds to the two producers and also to barometric pressure. The barometric efficiency of 75% implies a storativity of 3.0×10^{-7} m/Pa.

The response of H-5 to the first 750 days of production is shown in Fig. 7.13b. For an initial period this drawdown is approximately linear with log(time). A transmissivity of 170 d-m and a storativity of 1.5×10^{-6} m/Pa is obtained from this relationship.

The drawdown later deviates from this log-linear form and ultimately approaches an almost linear pressure–time trend. This has been modeled as a system contained within a semi-infinite trench, with impermeable walls, but one end of the trench at great distance. A model of this form has been used to match the entire pressure history. In this model the "box" is bounded by impermeable walls defined by earthquake activity. With these bounds the average storativity is reduced to about the value suggested by the barometric efficiency. This average reflects the stiffer wall structures.

In the analysis by Kjaran *et al.* (1979) this model is used to determine future pressure drawdown. The future performance of the wells may be estimated from this expected future drawdown. Because the wells are subject to deposition where there is flashing in the wellbore, the future pressures are also used to predict likely future scaling depths. On the basis of this analysis it has been decided to increase the well casing depths and the casing size in any further wells drilled.

This model of the reservoir as a liquid-charged box with a specified transmissivity and storativity is almost ideal for predictive purposes. It is simple and easy to understand physically, and it matches the reservoir behavior with a minimum number of parameters. It is interesting to note that it [illegible]escribe all aspects of the reservoir. For their analysis Kjar[illegible].9) utilize the storativity of 1.5×10^{-6} m/Pa with obvious good[illegible]his storativity is difficult to interpret. It implies either

an unconfined aquifer of 1.2% porosity or a confined one of porosity-thickness 1 km, and both cases are difficult to explain. The surface discharge of steam, coupled with chemical evidence of boiling and two-phase fluid encountered in one shallow-feeding well, suggests the existence of two-phase fluid in the reservoir above the 240°C water. As previously indicated, this would drive up the storativity value. These conceptual problems do not influence the predictions made.

7.7 RAFT RIVER

Raft River in Idaho is a low temperature field with maximum temperature of about 145°C that is being developed for a 5 MW binary power station (Millar, 1979). The testing of the wells and reservoir is described by Allman *et al.* (1979) and Spencer and Callan (1980). There are seven deep (1100–2000 m) wells—four producers and three injectors. In addition there are a number of monitor wells up to 400 m deep and irrigation wells up to 100 m deep.

The deep wells are open to the sedimentary Salt Lake Formation, and five penetrate underlying quartz monzonite. Shallow wells in the area penetrate unconfined aquifers, whereas deeper wells find confined aquifers with increasing overpressure (up to 1 MPa in some of the production wells). Since some shallow wells are hot and nearly all show chemical and thermal evidence of upward leakage, there is some leakage between aquifers. Figure 7.14a shows a model of the natural state of this field, indicating upwelling from depth of two chemically distinct waters that mix with each other and with groundwater (Allen *et al.*, 1979).

Extensive tests have been carried out on the wells in order to determine the drawdown in production wells, the wellhead pressure in injection wells, and hence the pump requirements, at given flow rates, for both. These tests are also used to estimate temperature changes and the effect of development on shallow aquifers.

Interference tests give $kh \approx 70$ d-m, whereas single-well tests give kh values of 5–20 d-m (Kunze, 1977; Ahmed *et al.*, 1979; Hanson, 1980a). There is a complex distribution of permeability (Allman *et al.*, 1979) which means that long-term behavior does not fit simple analytical models (such as pressure buildup in a uniform infinite aquifer). Figure 7.14b shows the buildup of wellhead pressure in RRGI-6. Experience has shown that a semilog straight line usually develops after about 10 hours. The contrast between single-well and interference tests also shows the presence of additional structure. Long-term injection has shown further changes: injectivity increased with time and wellhead pressure fell. Consequently, the shorter-term transient tests did not predict later well performance (L. L. Mink, 1981; personal communication).

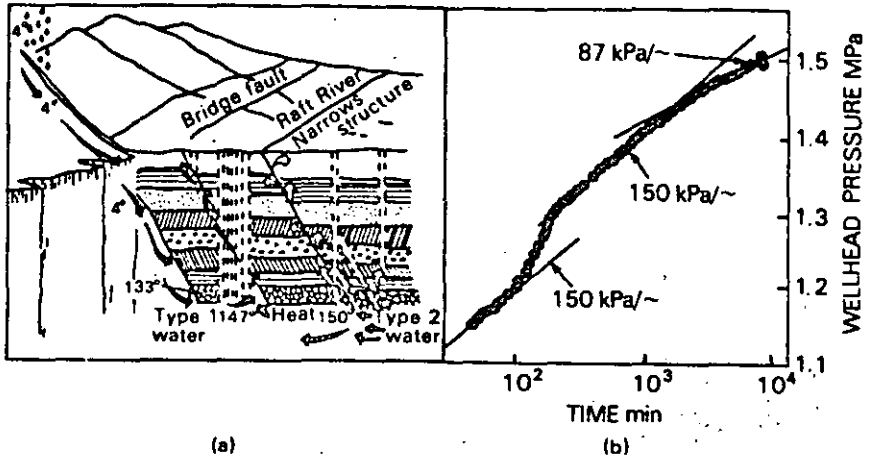

Fig. 7.14. Raft River low-temperature field. (a) Natural flow pattern. (From Allen *et al.*, 1979.) (b) Buildup of wellhead pressure during injection into RRGI-6 (From Allman *et al.*, 1979.)

Detailed interpretation of downhole and other data has defined the nature of the permeability. Temperature changes during warmup define producing zones (Kunze, 1977; Stoker *et al.*, 1977). From analysis of barometric and tidal effects, the porosity of the producing formation has been found to be low (≤5%) in RRGE-1, 2, and 3, but high (14–24%) in wells 4, 6, and 7. The first three wells penetrate the Bridge Fault or the Narrows Structure, and the low porosity confirms production from fractured crystalline rock. The latter three wells produce from the Salt Lake Formation, and the high porosity is consistent with core samples (Hanson, 1980b).

In measuring pressure transients it has been found that results are easily biased by temperature changes in the wellbore. A change of 0.35 K/hr is sufficient to affect pressure data collected at wellhead or bottomhole (Allman *et al.*, 1979). In consequence, it is necessary to flow a well at a low rate for a week before a discharge test in order to warm it up.

The management of the injection wells has been the object of some study. It is desired to avoid thermal degradation of production water or chemical degradation of irrigation water by injecting into an aquifer that does not rapidly communicate with either the producing wells or shallow wells. Injection wells RRGI-6 and 7 are intermediate depth (1180 m). Here, formation temperature is too low for production. Interference tests

between the deep wells and shallow monitor wells show a variety of responses (Skiba *et al.*, 1981; Petty and Spencer, 1981). Observations in the shallow wells are affected by the pumping of irrigation wells and seasonal groundwater changes. Some monitor wells show only these effects, whereas two show direct connection to the deep producers. It is expected that production will lower water levels in shallow wells in this area. One monitor well responds rapidly to injection, and a pressure-sensitive vertical fracture is hypothesized.

Spencer and Goldman (1980) describe a numerical model in which a layered reservoir has some near-vertical zones of high permeability. The model fits the observed response of the shallow wells to the deeper injection and production wells. Simulations using this model indicate that long-term operation of the field will contaminate groundwater, and alternative disposal sites are being sought.

The testing of the reservoir at Raft River is strikingly similar to high-temperature fields as regards some of the problems that confront the analyst: thermal effects in the wells, vertical communication, and the difficulty of characterizing the permeability distribution.

7.8 EAST MESA

7.8.1. Introduction

One purpose of our attempts to quantify conceptual models on a reservoir scale is to develop a reservoir model that may give us some idea as to how that reservoir may behave once exploitation is underway. Most geothermal reservoirs are inherently complex and may not behave in so simple a manner. The reservoir at East Mesa in California appears to be one of the less complicated examples. It also has the advantage of having been thoroughly tested and is therefore an appropriate reservoir for illustrating projection of the behavior of a real field under exploitation. Since no production has yet taken place, the predictions are all theoretical, but both distributed-parameter and lumped-parameter simulations have been carried out.

A clay cap overlies a reservoir of sand and interbedded shales that contains water at temperatures of up to 200°C. Figure 7.15a shows a plan view of the field and 7.15b, shows a section through the field. A domed thermal structure is present. The surface heat flow shows a similar maximum over the dome. The center of the dome corresponds to the intersection of faults.

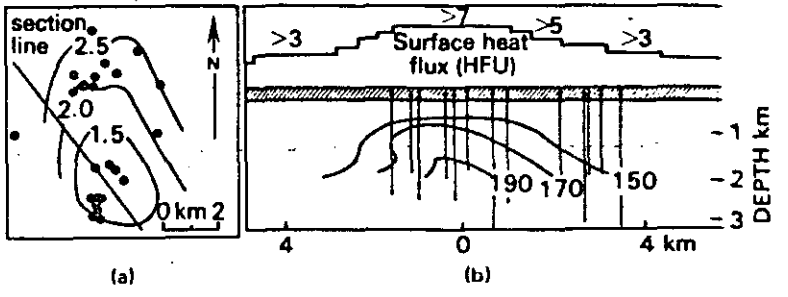

Fig. 7.15. East Mesa field. (a) Plan view, with contours showing depth in kilometers to the 170°C isotherm. (After Morris and Campbell, 1981; copyright © SPE-AIME.) (b) Section through the reservoir along line shown on (a). (From Riney *et al.*, 1980b.)

7.8.2 Reservoir Parameters

Several wells have been drilled, and rock properties such as net sand thickness, porosity, and (air) permeability have been obtained from core samples. Values of these properties for a selection of wells, both potential producers and injectors, are given in Table 7.3 for one depth interval (Morris and Campbell, 1981).

Numerous well and interference tests have also been performed. Values of kh/μ obtained range from 2×10^{-8} to 7.5×10^{-8} m³/Pa · s, equivalent (for water at 160°C) to a permeability-thickness of 3–12 d-m. A distinct trend in permeability is present, with higher values to the north of the field. Considerable inhomogeneity is present (McEdwards *et al.*, 1978).

From the interpretation of this well and other data, a clear picture emerges of a reservoir that is confined above and below, of reasonably

TABLE 7.3

EAST MESA RESERVOIR PROPERTIES, 1680–2130 m[a]

	Well							
	16–29	16–30	38–30	56–30	58–30	78–30RD	74–30	18–28
Sand thickness (m)	317	290	341	309	281	386	309	267
Porosity	0.16	0.16	0.21	0.17	0.13	0.21	0.18	0.17
k (air) (md)	41	63	353	64	11	69	145	470

[a] From Morris and Campbell, 1981; copyright © SPE-AIME.

homogeneous permeability on the reservoir scale, and charged with liquid water. Vertical permeability in the sandstone aquifer is limited by the presence of shale breaks, but these are not continuous and some vertical permeability must remain. The shale layers are also thin and so are assumed to remain in thermal equilibrium with the sandstone and the water in it. On the gross scale the medium is thus assumed to be homogeneous.

7.8.3. The Natural State

Two independent simulations of the natural state have been made: by Goyal and Kassoy (1978), Kassoy and Goyal (1979), and Riney *et al.* (1979, 1980a,b). Both simulations employ a similar conceptual model. Figure 7.16a shows the model of Riney *et al.*, including the system extending to the mantle and the subregion that is the reservoir.

Figure 7.16b shows the reservoir model of Kassoy and Goyal. A permeable layer lies between the impermeable cap and the basement layer. The latter is also taken to be impermeable except for the fault permeability where hot water rises from greater depth. Fluid flow is up the fault and out along the aquifer. Heat is convected with the fluid into and out along the aquifer and is lost by conduction through the cap to the surface, producing the surface heat flow anomaly. The Kassoy and Goyal model is a two-dimensional vertical section that qualitatively reproduces the pressure and temperatures found. With this simple model it was possible to explore the sensitivity of the thermal pattern to reservoir parameters.

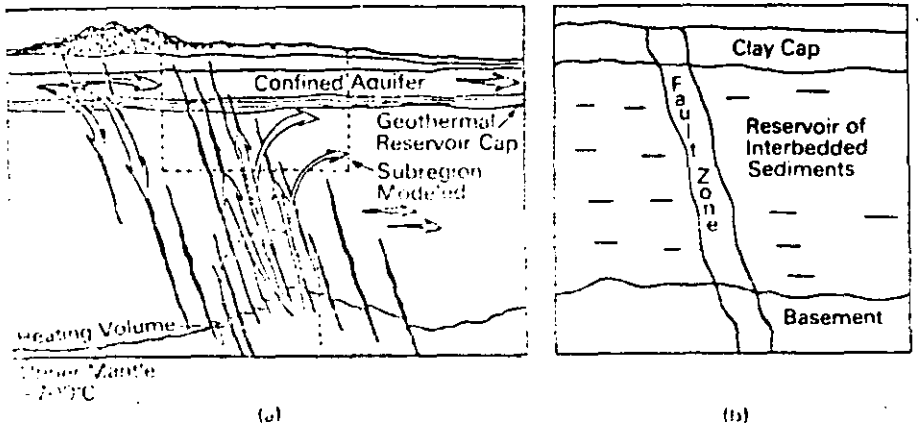

Fig. 7.16. Conceptual models of East Mesa. (a) Large-scale model of Riney *et al.* (1980b). (b) Reservoir model of Kassoy and Goyal (1979).

Riney *et al.* (1979) described an axisymmetric model that was later expanded to the three-dimensional model of Riney *et al.* (1980a,b). The upflow is localized along a narrow zone. Using horizontal permeabilities found from well tests and allowing other parameters to vary, Riney *et al.* (1980b) produced a good match to the surface heat flux and to the isothermal cross-section. The vertical permeability was found to be 0.25–0.5 md, more than an order of magnitude smaller than the horizontal permeability.

Both models of the natural state assume that it is steady, and good agreement with the thermal pattern is found. There are, however, strong variations in salinity not consistent with these models, so that it has been argued that the system is changing (Hoagland and Elders, 1977). The chemical data provides reservoir information not readily apparent in pressure or temperature data.

7.8.4. Distributed-Parameter Simulation of Exploitation

If we ignore any possible changes in inflow from depth, the only changes that can be stimulated by exploitation are changes in flow, both in distribution and in rate, and in temperature in (and around) the sandstone–shale aquifer. It should be noted that the temperature changes follow the flow changes as colder water is pulled into the reservoir. Changes in both flow and temperature have been evaluated using a three-dimensional numerical simulation of the reservoir by Morris and Campbell (1981).

Figure 7.17 shows a section of the simulation model, with the assigned properties in one node. The small-scale inhomogeneities found in the testing are ignored in this larger-scale study. Since the permeabilities obtained from the well tests are less than those measured in the core samples, core values are scaled by a constant factor to match the well-test values more closely.

The aquifer in which the geothermal fluid is found continues out beyond the hot boundaries. The options for the modeler are either to extend the

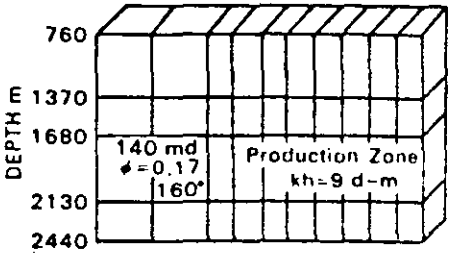

Fig. 7.17. Section of East Mesa numerical simulation model of Morris and Campbell (1981). (Copyright © SPE-AIME.)

model further out into the cold region (in which event he may still need to include a source for additional cold water) or to cut the model off at some appropriate point near the boundary of the hot reservoir and allow some form of pressure-drop-stimulated influx. Morris and Campbell (1981) took the latter option and allowed an influx over their boundaries proportional to the drop in pressure from its initial value at these boundaries.

Under production the wells in this reservoir will be pumped. Each production well is limited to a drawdown of 3.5 MPa or a discharge of 88 kg/s. Injection wells may have wellhead pressure up to 2.8 MPa and/or a flow up to 190 kg/s. For the simulation the total production was kept at a level that would maintain a power plant generating 64 MW.

The general results of the simulation are shown in Fig. 7.18. The temperature of the water produced gradually falls. To maintain the level of power generation, increased fluid production and additional wells are required. The fall in production temperature is one of the important outputs of this simulation; the other is the reservoir pressure, which shows whether or not flow can be maintained from the wells. The initial well location plan assumed only peripheral injectors, resulting in too great a fall in the production zone. Interior injectors were subsequently added.

Other parameter variations were considered. It was assumed, for example, that there was no hydrologic connection between the reservoir and the surrounding colder section of the aquifer. In this event the temperatures fall more rapidly because the reinjected water is colder than that in the surrounding zone. The vertical permeability was also changed. At 20% or less than the horizontal the peripheral shallow injection could no

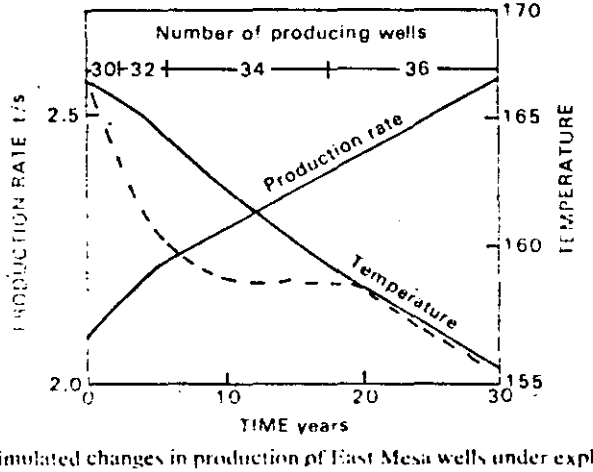

Fig. 7.18. Simulated changes in production of East Mesa wells under exploitation, from Morris and Campbell (1981). Dashed line, results of the lumped-parameter model of Castanier *et al.* (1980). (Copyright © SPE-AIME.)

longer maintain production pressure, indicating that the peripheral injectors would need to be deepened and/or more internal injectors used. The more intensive use of internal injectors, utilizing the "five-spot" pattern of alternating producers and injectors commonly employed in oil production, resulted in a severe fall in production temperature.

Detailed models of this nature can provide much information. However, in order to establish such models and ensure that the results are meaningful requires a large amount of high-quality data. In this case (East Mesa simulation) the engineers obtained not only information about changes in production temperature and reservoir pressure but also an insight into the effects of different sitings of the injection wells. Some of the general information may be obtainable with the simpler field-scale lumped-parameter models. These are much cheaper and quicker to run than a full distributed-parameter model, but they are also much more limited in the information they can produce.

7.8.5. Lumped-Parameter Model

For the East Mesa reservoir a three-zone lumped-parameter model was developed by Castanier *et al.* (1980). There is no allowance for vertical effects in the aquifer. A central zone contains all producers and internal injectors, and the fluid in this zone is assumed to be well mixed. Outside the central zone is an intermediate zone with a radial temperature distribution, and beyond that is an outer zone corresponding to the external aquifer. This outer zone is assumed to remain at a constant temperature. As the fluid moves in from the outer zone through the intermediate zone, the temperatures are swept in with it. Pressures are computed at each well using solutions for a wellface pressure and average pressure in the inner zone.

The results of this lumped-parameter analysis are plotted on Fig. 7.18, with the results from the distributed-parameter study by Morris and Campbell (1981) given for comparison. The initial temperature decline is faster in the lumped-parameter study due to the assumed mixing in the central zone.

In these two analyses of the East Mesa reservoir an energy reserve or a recovery factor has not been specifically determined. These could have been estimated from the reservoir data and analyses, but a decision was made to go directly to the next stage and attempt to predict how the reservoir may behave under actual exploitation conditions, i.e., while maintaining an electric power production of 64 MW. Unfortunately, no production history is available with which to check or improve the model. However, since the reservoir is reasonably homogeneous, bounded above

and below, and water charged, similarity to groundwater systems provides considerable tested experience to draw on. The appropriate reserve estimate for a geothermal reservoir is further discussed by Morris and Campbell (1981).

7.9. SUMMARY

The tests described in this chapter complete the information that may be gathered prior to exploitation. Local properties of the reservoir and reservoir fluid have been obtained from individual well tests. Analysis or modeling of the natural flow in the field or system containing the reservoir provides some reservoir-scale parameters (such as vertical permeability).

Extensive (in both time and distance) testing of the reservoir yields additional properties. Most important of the tests is the interference test, which, if successful, measures transmissivity and storativity over an area of the reservoir and provides possible information about connectedness of the permeable zones encountered by different wells. Even with such thorough measurement it can be difficult to characterize a reservoir by a single constant permeability because of discrepancies between single-well and interference tests, and the improvement in injectivity often observed in long-term and high-rate injection.

Massive discharge can yield the storage coefficient of the entire reservoir. Prolonged discharge of individual wells, particularly in two-phase reservoirs, shows the type of behavior characteristic of long-term flow and gives a guide to the physical mechanisms important in the reservoir—boiling, dilution and cold sweep, drainage, or decompression. Still not determined, in most cases, is the extent of recharge of deeper fluid, or groundwater, to be expected under exploitation.

Chapter 8

Long-Term Behavior: The Observed Response of Fields to Exploitation

8.1. INTRODUCTION

In this chapter we review the changes that have occurred in exploited geothermal fields, as reported in the literature, and the interpretations now placed upon these changes. The ultimate test of any approach to explaining geothermal reservoir behavior is comparison with observation. The behavior observed in these fields provides a guide to what may occur elsewhere.

Nine fields are described: two are vapor dominated (Larderello and The Geysers), two are low-temperature fields (Reykjavik and Selfoss), and the remainder are high-temperature, liquid-dominated fields (Wairakei, Cerro Prieto, Broadlands, Kawerau, and Ahuachapan). In all cases there is sufficient history of exploitation to define the character of the reservoir's response to exploitation. A considerable variety of physical mechanisms is presented in these nine fields. Seven show substantial recharge (The Geysers and Broadlands do not). In four of the seven the recharge is identified as being cold, at least in part. The reservoir storage mechanism, where identified, is either two-phase expansion or drainage of a free surface. Single-phase flow is present near some, many, or all wells in each field, but apparently in no case does the response of the reservoir reflect the expansion of a single phase within sealed boundaries.

Given the variety of response present in these nine fields, it is likely that this list is not a complete survey of possible modes of behavior of geothermal fields. Many more fields are now under exploration and development around the world, and these will add substantially to the experience of exploitation in the next decade.

An additional seven power stations on six fields have not been described here for lack of published information. These are the stations at Pauzhetsk, Kamchatka, U.S.S.R., and the six Japanese stations (Otake, Matsukawa, Onuma, Onikobe, Hatchobaru, and Kakkonda). A moderate amount of information is available about the Japanese plants. Of this the

Chapter 9

Field Monitoring and Management

9.1. INTRODUCTION

Management of a geothermal field entails making decisions between possible courses of action. Such decisions are based on an estimate of or belief about the results expected. There are large decisions (i.e., What size station?) and small decisions (i.e., Does a well need remedial work?).

In many practical cases the uncertainties about a geothermal field's future behavior are so large that any estimate is a guess, although some guesses will be better than others. This particularly applies to the most important choice of all; the design of the power plant. Although the possible cost of each choice can be estimated and the criteria for choice clearly identified, an accurate balance of costs and benefits is not possible. The issues must therefore be discussed in qualitative terms.

After a station has been producing over some period, realistic estimates can be made of the value of incremental changes in field exploitation, e.g., adding an additional plant or adapting an existing plant. In these cases true management is possible.

The existence of a production history makes analysis of the field much simpler. Many properties of the reservoir that can be only subjects of conjecture in the development stages are demonstrated directly once production has started. Some pleasant or unpleasant surprises may appear, and their implications will be considered. Given all this, the opportunities to manage—to exercise a choice of action—can be analyzed far more clearly and accurately.

The possible management choices that may arise are as follows:

1. Whether or not to expand generation
2. Where to site infill wells as the field runs down
3. Which wells to leave idle if there is a surplus
4. Whether or not to shut some wells that are proving deleterious (i.e., close injectors).
5. Whether or not to modify station, well, or pipeline design for economic reasons.

In addition to these decisions, more work must be put into monitoring the performance of the wells and of the surface equipment. This is necessary in order to detect irregularities that may signal the need for repair work, or to measure the trend of declining performance and so anticipate the need for additional wells, or a reduction in wellhead pressure. Numerous problems can occur in the operation of a geothermal project, and regular monitoring is needed to ensure that they do not get out of hand.

9.2. MEASUREMENTS

9.2.1. Well Performance

The most basic monitoring requirement is a record of the flow of each well. The variables to be recorded are mass flow, enthalpy, and wellhead pressure. These variables may be modified as appropriate. If the flows are dry steam or single-phase liquid, temperature rather than enthalpy is recorded. If a downhole pump is used, pressure at the pump or pumping power consumption would replace wellhead pressure.

Chemical samples should be taken at convenient intervals and vapor- and liquid-phase chemistry recorded. It is normally more convenient to record the gas content and solute content of separated steam and water flows than to compute these as fractions of total flows. In addition, if fluid samples are taken from steam or water flows, the results should be reported as such. When total flow values are computed, an erroneous enthalpy will result in an erroneous total value. It is a better practice to report results in a form that is not subject to such external errors.

For each well a history should be kept in a convenient form (usually a graph) that shows changes with time. Any abnormality should be investigated. The first step in an investigation should be to check recent measurements.

9.2.2. Downhole Profiles

Wells should be shut at convenient intervals to measure downhole pressure and temperature profiles. Soon after the start of major production such measurements should be made every month or every few months. Later the frequency can be decreased to once every year or two. The frequency of measurement should be adapted to the rate at which the reservoir is changing. Roughly, the measurements should be made at equal intervals of change in downhole pressure and temperature. Such profiles are less important in a vapor-dominated field since there is less detail to observe downhole.

If the monitoring of the well's production shows any abnormal change, downhole profiles should be run to check possible causes. Caliper or go-devil (drift gauge, sinker bar) runs should be made if there is any doubt

about the casing or if the well appears to be blocked. If fluid of abnormal chemistry is present in the discharge, downhole chemical samples may be required. If temperature profiles indicate a possible flow in the well, a spinner (flowmeter) run is indicated. A new output test should also be considered if a well's performance has changed substantially.

Most fields normally have some nonproductive wells that make convenient monitor holes. When such wells are available, downhole data should be recorded more frequently, and whenever possible a continuous pressure record should be obtained. Such a record may be obtained conveniently by placing a float in a well that stands open to atmosphere and has a water level. Specially drilled monitor holes may also be useful. For example, the possibility of vertical inflow of cold water can best be checked by using wells that feed from different depths. Pressure changes in shallow wells show the extent to which deeper pressure changes propagate upward.

In addition to the physical task of continued measurement and recording, the intellectual task of updating concepts or models of the field is also required. At times this can be difficult. Perhaps the easiest method is to develop predictions or projections using model or analysis. The validity of that model or analysis can be verified later.

9.2.3. Geophysical Measurements

As part of monitoring the changes under exploitation repeat gravity surveys at intervals of several years are very useful in defining the extent of fluid recharge or depletion in the reservoir. At Wairakei, Broadlands, and The Geysers such surveys have provided a strong constraint on reservoir models.

Repeat resistivity surveys may detect changes in chloride content, or the development of a steam zone. Base leveling surveys should be made very early in development, and repeat surveys for determining vertical and horizontal deformation should be made at a frequency that is dependent on the rate of subsidence and the importance of its effects. Changes in the natural activity should be measured as indicators of the interaction of the reservoir with near-surface aquifers.

9.3. CHANGES IN WELL PERFORMANCE

The regular monitoring of well performance gives a record of the mass flow and discharge enthalpy of each well. We shall now discuss some of the types of abnormality that may appear. The list is not exhaustive.

9.3.1. Normal Behavior

First, for background, we shall examine "normal" behavior—the history of a well in a simple depleting reservoir, with no casing break, deposition, or other mechanical problem. If the reservoir is vapor dominated or liquid, there will be little change in enthalpy. Under such circumstances the mass flow at constant wellhead pressure or constant throttle should decline smoothly with time as reservoir pressure falls.

Abnormal behavior appears as a change in mass flow, a change in enthalpy, or both. A change in enthalpy normally signals a change in reservoir fluid. It may also indicate that the well has become partly blocked and taps a different part of the reservoir. Normally, mass flow also changes with changing enthalpy. This is due to the change in (flowing) pressure drop in the well. A change in mass flow (beyond that caused by pressure drop) without a change in enthalpy generally indicates mechanical problems in the well, such as a casing break, liner collapse, or deposition.

9.3.2. Scaling

Figure 9.1 shows the history of well M-9 at Cerro Prieto (Dominguez, 1978; Bermejo *et al.*, 1978, 1980). Mass flow has decreased without large change in enthalpy; since other wells in the field have not declined pressure changes are not responsible. The decline in the well's ability to deliver fluid indicates that the well is becoming blocked, and the progressive nature of the decline indicates that deposition rather than a collapse is responsible. The increasing decline in flow as flow approaches zero is characteristic of deposition. Well M-9 was restored to production by workover, but the deposition continued. (For another example of the effects of deposition, see the discussion of BR2, in Chapter 6.) Normally, scale is deposited in the well and performance can be restored by a workover. Deposition in formation is not a reported problem in producing wells.

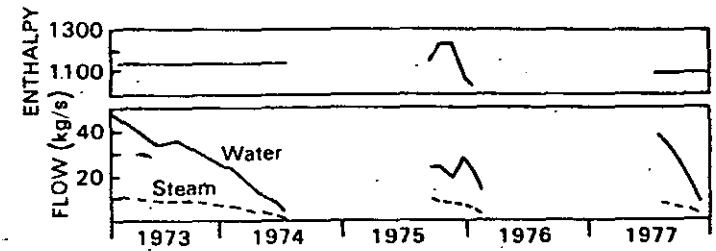

Fig. 9.1. Repeated scaling in well M-9, Cerro Prieto. (From Bermejo *et al.*, 1980.)

The tendency for scale to be deposited is quite variable between fields and between wells in the same field, depending on the fluid chemistry. Affected wells may need to be cleaned every few months or every few years; other wells in the field may remain totally unaffected.

9.3.3. Changes in Enthalpy

If a liquid-dominated reservoir at or near boiling point is exploited, falling pressures will cause more boiling. The higher steam fraction in the reservoir will result in higher discharge enthalpies in producing wells. The changes in discharge enthalpy reflect the manner in which boiling fluid is present in the reservoir.

In Chapter 6 we used BR2 to illustrate the rise and fall of discharge enthalpy in a reservoir that is nearly all two phase. Figure 9.2 shows the changes in three wells at Wairakei. The reservoir, which was initially liquid dominated, underwent considerable boiling and by 1961–1962 had formed a steam zone (see Chapter 8 for more detail). The enthalpy of a deep-feeding well is shown by WK27. The discharge enthalpy is very stable and remains at the enthalpy of liquid water at the well's feedpoint. An exception was a period of excess enthalpy around 1960 when reservoir pressures were falling rapidly, resulting in increased boiling.

In contrast WK9 is a shallow-feeding well and shows the development of a dry steam discharge. The earliest discharge was at an enthalpy a little above liquid water. After 1970 the discharge was nearly dry steam. In between, the enthalpy rose with considerable variability. This intermediate period was prolonged in WK9. In most other wells that went dry, the process took only a few years.

WK4/1 and 4/2 are shallow peripheral wells located close to each other. Individually they are erratic in performance, but taken together their performance has varied smoothly with time. Their discharge enthalpy rose as boiling increases in the reservoir, and a steam zone formed. But

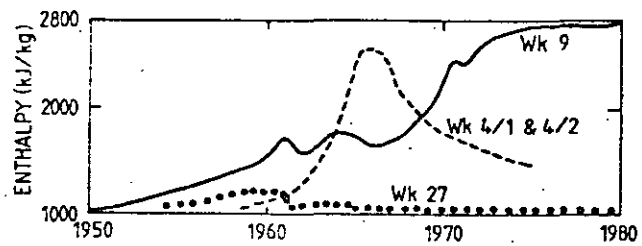

Fig. 9.2. Enthalpy changes in three Wairakei wells. (From Ministry of Works and Development, New Zealand, 1981; personal communication.)

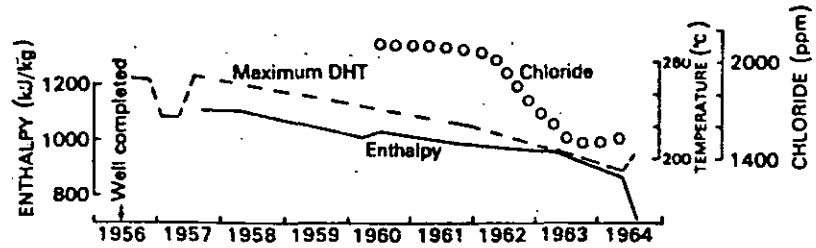

Fig. 9.3. Chemical and physical changes in well WK31, Wairakei. (From Glover, 1977, and Ministry of Works and Development, New Zealand, 1981; personal communication.)

enthalpy later fell again, although the wells' common feed zone lies within the steam zone. The fall in enthalpy is abnormal since such shallow wells normally go dry. It is interpreted as reflecting groundwater entry.

9.3.4. Cold Water Entry

Figure 9.3 shows the history of well WK31 at Wairakei. Discharge enthalpy and chloride content fell with time, as did maximum discharging pressure, reflecting the fall in enthalpy. By 1964 enthalpy had fallen too low to sustain discharge and the well failed and was cemented. The falling enthalpy and chloride content indicate increasing dilution of the discharge by cold water. The downhole profiles show that a shallow feed, originally hot, had started to discharge colder water into the well. (For another example see KA8, Section 8.8.)

9.4. DECLINE CURVES AND TREND ANALYSES

9.4.1. Introduction

If none of the effects of the previous section occur, the mass flow of a well declines smoothly as exploitation reduces reservoir pressures. One means of predicting future mass flow is simply to treat the past history as a time series. It may then be fitted to a convenient formula, which in turn is used for extrapolation. No reservoir model enters such an argument: the trend of past performance is fitted and extrapolated, no matter whether the data concern mass flow of a geothermal well, population of the earth, or sunspot frequency.

This technique can be very effective. The best predictions of future performance derive from such methods, even if they are no more than extrapolating a decline of so many percent per year. However, the technique is limited by the lack of a theoretical model basis. It cannot predict

the effect of a change in management practice, outside of past variation. The flow of one well can be extrapolated only as long as the control of other interfering wells does not change. For example, if another power station is added, the trend with time is likely to change.

9.4.2. Decline Curves

The name "decline curves" is given to a standard set of curves that show mass flow against time. Chierici (1964) found that Larderello wells could be fitted to the formula

$$W = W_0 t^{-n}, \tag{9.1}$$

where t is the time the well has been flowing. A standard set of curves is available in the petroleum literature (Fetkovich, 1980). They take the form

$$a = -\frac{1}{W}\frac{dW}{dt} = KW^b, \tag{9.2}$$

where a is the fractional decline. This results in a standard set of curves plotting flow rate against time on log–log scale, with b having different values. Of greatest importance is the case in which $b = 0$ (exponential decline):

$$W = W_0 e^{-at}. \tag{9.3}$$

The standard decline curves can be used in a number of ways. Future discharge and the total cumulative discharge at abandonment (the fluid reserve producible by the well) can be projected by matching a discharge history to one of the curves. A more immediate use is to match for a certain period of time so that deviations in later performance can be identified as indicating possible mechanical problems in the well (Rivera, 1978).

Zais and Bodvarsson (1980a,b) fitted a substantial number of well histories from Wairakei, Cerro Prieto, Larderello, and The Geysers to decline curves. In general the fits obtained were not good, and the value of this technique thus appears limited. Figure 9.4a shows a fit to one well at Larderello. The best fits obtained were to exponential declines. Rather than using type curves, exponential decline is more conveniently represented by plotting flow rate on a logarithmic scale and time on a linear scale, as is commonly done for petroleum wells. Figure 9.4b shows such a plot of the flow of two wells at The Geysers.

Dykstra (1981) found that an average production well at The Geysers best fitted to harmonic decline ($b = 1$ in Eq. 9.2), or

$$W = W_0/(1 + t/\tau) \tag{9.4}$$

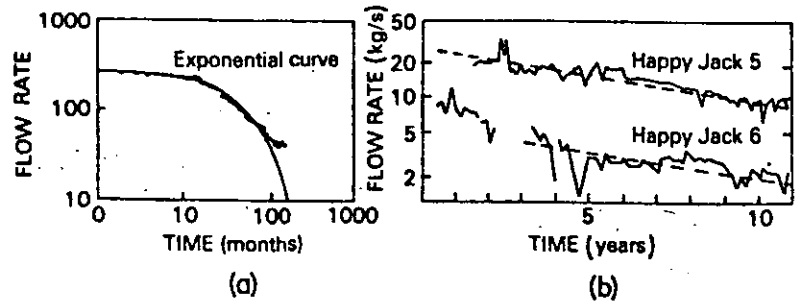

Fig. 9.4. Decline in flow of steam wells. (a) Larderello 82, fitted to log–log type curve. (From Zais and Bodvarsson, 1980b.) (b) Semilog plot of the decline of two steam wells at The Geysers. Dashed lines indicate a decline rate of 9% per year. (After Dykstra, 1980.)

where τ is a time constant.

9.4.3. Wainwright's Wairakei Model

Wainwright (1970) made extensive projections of future behavior of wells at Wairakei using curve-fitting techniques. The wells were divided into three groups: water fed, two phase, and steam producers. Future flow from the wells was estimated from a projection of future pressures. Two pressures were used: the deep liquid pressure at standard elevation, and a steam zone pressure. The change in deep pressure was fitted by trial and error to a formula

$$P_0 - P = \frac{\mathcal{W}}{t - t_0}\frac{a\mathcal{W}}{1 + a\mathcal{W}}, \tag{9.5}$$

where $\mathcal{W}$ is the cumulative discharge since time t_0 and a is a fitted constant. Steam zone pressure was defined as the shut-in wellhead pressure of those wells with steam cap profiles. This pressure was extrapolated linearly at the then-current decline rate of 70 kPa/yr. Flow of steam wells was estimated using a form of the deliverability equation (5.20) and a similar but more complex form for water-fed wells. Two-phase wells were treated as combined water-fed and steam wells. Empirical constants in the deliverability formulas and Eq. (9.4) were fitted to past history. Figure 9.5 shows the projections and what has since occurred.

The projections were used to design a major modification of the surface plant that added 30 MW of generation. Wainwright's model illustrates the strengths and weaknesses of trend-curve analysis. The weakness is the lack of a physical model behind the analysis. No allowance can be made for any change in the character of the reservoir such as cold water entry, that was not present in the fitted period. The strengths of this technique

Another problem is that the maximum subsidence is not linearly related to the deep pressure drop. Figure 10.9 shows subsidence at benchmark A-97, a convenient reference point. Although there is initially a linear relation, the rate of subsidence increases with time. Interpreting the subsidence as simple compaction (Pritchett *et al.*, 1976), the elastic moduli of the rock must decrease with time by a factor of more than 10.

Because of the difficulty in explaining the subsidence at Wairakei as simple compaction of the reservoir rock, it has been proposed that the maximum subsidence area may be the result of a different mechanism, although the field-wide subsidence would represent normal elastic behavior. Pritchett *et al.* (1980b) suggest that aseismic slippage along existing faults is responsible. They also observe that until 1963 an area at the southern boundary was also rapidly subsiding. Recent work (Allis, 1982; Ministry of Works and Development 1982; personal communications) indicates that most of the subsidence occurs in shallow unconsolidated breccia above the main production depths. Casing damage indicates compression at these depths; and the amount of subsidence correlates in space and time with pressure changes in the steam zone.

10.5. CONCLUSION

In this chapter we have briefly surveyed three main problems that are of concern to reservoir engineers and developers at present. These are by no means the only problem areas, nor are any or all of them likely to be important or even present in any specific field. Also, the problems are not necessarily insuperable. All are under study. Perhaps the main feature of the measurements and analyses to date is the extreme variability of what may occur in different geothermal reservoirs or within one reservoir. This variability of likely behavior—a characteristic feature of all aspects of geothermal reservoir engineering—is one of the elements that keep the field alive, challenging, and exciting for all who are involved with it.

Appendix 1

Pressure Transient Analysis

A1.1. INTRODUCTION

In this appendix we review the theory of pressure transient analysis and its application to geothermal wells. The theory has been developed in great detail in the groundwater literature beginning with the work of Theis (1935). Groundwater techniques were applied sporadically in the 1950s in various geothermal fields. The first systematic use was in the early 1960s, in the analysis of the results of a field discharge at Pauzhetsk, Kamchatka, U.S.S.R. (Sugrobov, 1970).

Pressure transient theory is also developed in the petroleum literature. The petroleum and groundwater disciplines have developed almost independently, and they employ different notation to develop similar or identical results. We here follow the petroleum development, in common with most other geothermal literature. For a survey of groundwater techniques, see Walton (1970). A comprehensive exposition of petroleum techniques is given by Matthews and Russell (1967) and Earlougher (1977). Examples of applications to vapor-dominated systems are given by Barelli *et al.* (1976), Ramey (1976a), and Strobel (1976).

We shall describe these techniques only briefly and concentrate instead on examples of their application in geothermal wells and on the many practical problems that can confuse or obscure pressure measurements.

It should be noted that pressure transient analysis has not been proven in geothermal practice in the sense that predictions from well tests have been made and validated by subsequent experience. The frequent observation that kh from interference tests exceeds that of single-well tests indicates that some problems remain.

A1.2. BASIC SOLUTION

A1.2.1. Line Source Solution

The basic aquifer model for pressure transients is of a well that fully penetrates an aquifer of uniform and homogeneous permeability. The fluid is uniform and of constant compressibility. Flow to the well is hori-

zontal and radial. Pressures at the middepth of the aquifer represent the depth-averaged behavior. At any other depth, pressures differ by a constant amount, so that at all depths pressures change by equal amounts. The equation for pressure change, ignoring matrix compressibility, has been derived in Eq. (3.27).

If the reservoir rock has significant compressibility compared to the fluid, the expression ϕc must be replaced throughout by $c_m + \phi c$. This expression is the total compressibility of the rock–fluid combination. Rock compressibility is usually ignored but may be significant if the reservoir fluid is (compressed) liquid. The compressibility c is often replaced by c_t, the total compressibility of the aquifer resulting from all mechanisms.

If an aquifer is initially at rest and at time $t = 0$ a well begins discharge at rate q (m³/s) or $W = \rho_1 q$ (kg/s), the solution is given by Eqs. (3.29–3.31). If the well radius is known, it is then possible in principle to identify two parameters: kh/μ (the transmissivity) and ϕch (the storativity). Note that only these combinations are identified, not the separate parameters k, h, μ, ϕ, c. Here arises one of the distinctive problems of geothermal well tests. A groundwater or petroleum aquifer is clearly defined geologically: thickness is known, porosity and permeability may be measured by tests on cores, viscosity and fluid compressibility are similarly available from lab tests or tabulated values. It is seldom clear what the thickness of a geothermal aquifer is. A fracture intersects the well at a narrow interval, but through this the well presumably draws on a much greater thickness of fractured rock. The depth over which production has been found in a reservoir may be known, but permeable fractures might extend to considerably greater depth. Thus, the thickness is not known *a priori* but must be found. Similarly, the porosity is vague. It could be total porosity or just the porosity in and near the fractures. Fluid properties can at times be unclear if there is doubt as to whether single-phase or two-phase fluid is present. This last uncertainty can in principle be removed by better enthalpy measurement and knowledge of relative permeabilities. Because so much is unknown, it is important to be clear and to report clearly which parameter groups are actually measured by a particular test. Usually the transmissivity is of greatest interest since it controls the ability of the reservoir to deliver fluid.

A1.2.2. Semilog Analysis

The exponential integral E_1 has, for small x (long time), the asymptotic form (following Section 3.3)

$$E_1(x) \sim -\ln x - \gamma = -2.303 \log_{10} x - \gamma, \tag{A1.1}$$

where $\gamma = 0.57721$ is Euler's constant. Then

$$-\Delta P = P_0 - P = \frac{q\mu}{4\pi kh}\left[2.303 \log_{10}\left(\frac{4kt}{\phi\mu c r^2}\right) - 0.5722\right] \tag{A1.2}$$

$$= m\left[\log_{10} t + \log_{10}\left(\frac{4k}{\phi\mu c r^2}\right) - 0.5772\right], \tag{A1.3}$$

where

$$m = \frac{2.303 q\mu}{4\pi kh}, \tag{A1.4}$$

is measured as pressure change per log cycle, and this unit is written as Pa/~ and r is the radius of observation.

Thus when pressure change is plotted against time on semilogarithmic scale, an asymptotic straight line should be obtained. This line is characterized by two numbers: its slope m, and the value at some particular time t. When the slope m is identified, the transmissivity can be found:

$$\frac{kh}{\mu} = \frac{2.303 q}{4\pi m}, \tag{A1.5}$$

assuming that a volume flow is specified. In geothermal wells it is usually more convenient to specify the mass flow W. Then Wv is substituted for $q\mu$ and Equation (A1.5) is replaced by

$$\frac{kh}{\nu} = \frac{2.303 W}{4\pi m}. \tag{A1.6}$$

Using the value of the drawdown ΔP at some time t, (A1.3) gives

$$\frac{\Delta P}{m} = -\log_{10}\left[\left(\frac{4kh}{\mu}\right)\frac{1}{\phi ch}\cdot\frac{t}{r^2}\right] + 0.251 \tag{A1.7}$$

or

$$\phi ch = 2.25\left(\frac{kh}{\mu}\right)\left(\frac{t}{r^2}\right)10^{(-\Delta P/m)}. \tag{A1.8}$$

A1.2.3. Example: Interference BR19–BR23

Figure A1.1 shows an example, from an interference test at Broadlands, of such an analysis. Wells BR19 and BR23 communicate (in 1980) through 270–280°C liquid water. At this temperature $\mu_w = 99$ μPa · s. BR19 discharged at a flow of 64 kg/s = 0.084 m³/s. The pressure change at BR23 is measured as a water level change. The slope of the

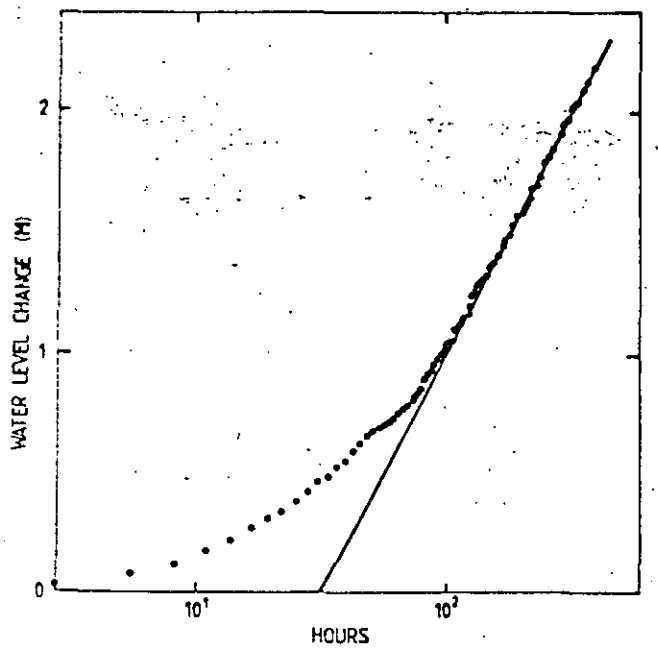

Fig. A1.1. Interference between BR19 and BR23, Broadlands, as measured with float recorder. (From Ministry of Works and Development, New Zealand, 1981, personal communication.)

semilog straight line is 1.98 m/~. The water at the top of the well is cold, so that 1.98 m ≈ 19.5 kPa. Then

$$\frac{kh}{\mu} = \frac{(2.303)(0.084)}{4\pi(19.5 \times 10^3)} = 7.9 \times 10^{-7}\ \text{m}^3/\text{Pa} \cdot \text{s}$$

$$kh = 7.8 \times 10^{-11}\ \text{m}^3 = 80\ \text{d-m}.$$

Alternatively, the calculation could have been made using the mass flow of 64 kg/s, and kinematic viscosity $\nu = 0.132 \times 10^{-6}$ m²/s:

$$\frac{kh}{\nu} = \frac{(2.303)(64)}{4\pi(19.5 \times 10^3)} = 6.0 \times 10^{-4}\ \text{m} \cdot \text{s}.$$

Storativity can be evaluated using any point on the straight line. It is conventional in petroleum analyses to use $t = 1$ h. In this example the straight line intersects $\Delta P = 0$ at $t = 11$ h $= 39600$ sec. Evaluating there, with interwell distance $r = 350$ m,

$$\phi ch = 2.25(7.9 \times 10^{-7})\left(\frac{39600}{350^2}\right) = 5.7 \times 10^{-7}\ \text{m/Pa}.$$

Using the compressibility of liquid water $c_w = 1.9 \times 10^{-9}\ \text{Pa}^{-1}$ gives $\phi h = 300$ m, which may or may not be physically realistic.

As an example we used an interference test to avoid problems with skin (see Section A1.3.2). The radius r in Eqs. (A1.2), (A1.3), (A1.7), (A1.8) is the radial distance of the observation point from the origin $r = 0$. For an interference test this is the interwell distance.

Instead of the graphic semilog analysis, the data can also be matched by a simple regression (with the parameters—transmissivity and storativity—fitted) to the exponential integral solution.

A1.2.4. Superposition

Since pressure transient equation is linear, solutions can be superimposed. The most useful case is when a well is shut after producing for a period at constant rate. The solution is a sum of the pressure changes caused by the flow increase at discharge start and the decrease at shut-in:

$$\Delta P = -\frac{q\mu}{4\pi kh} E_1\left(\frac{\phi\mu cr^2}{4k(t + \Delta t)}\right) + \frac{q\mu}{4\pi kh} E_1\left(\frac{\phi\mu cr^2}{4k\Delta t}\right), \tag{A1.9}$$

where t is the time flowing and Δt is the time shut. If the asymptotic form (A1.1) is valid for both E_1s,

$$\Delta P = -\frac{(2.303)q\mu}{4\pi kh} \log_{10}\left(\frac{t + \Delta t}{\Delta t}\right). \tag{A1.10}$$

A plot of ΔP against $(t + \Delta t)/\Delta t$ on semilog scale is known as a "Horner plot," and $\theta = (t + \Delta t)/\Delta t$ is sometimes called the "Horner time."

The drawdown caused by several wells can also be superimposed. In addition some types of barriers or other reservoir discontinuities can be represented by image wells, whose drawdown is superimposed upon that of real wells.

Figure A1.2 shows a well and an adjacent plane boundary. Three types of boundary can arise: an impermeable boundary, a constant-pressure boundary, and a free surface. An impermeable boundary is one across which there is no flow. The effect of the boundary is equivalent to that of

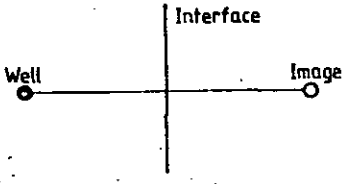

Fig. A1.2. Image well created by plane interface in reservoir.

an image well with the same flow as the real well in a medium of infinite extent. A constant-pressure boundary could be produced by a fault or some other feature of much greater permeability than the reservoir near the well. This is equivalent to an image well of opposite sign. Finally, if the source well withdraws fluid from beneath an aquifer with a free surface, this is equivalent to two images—one at the image point, and a double image of opposite sign that moves away at constant velocity (Zais and Bodvarsson, 1980a,b.)

A1.2.5. Dimensionless Variables

The pressure change in a test depends on the particular flow rates, permeability, and other parameters. These parameters can be absorbed into the definition of pressure and time to define dimensionless variables:

$$P_D = \frac{2\pi kh}{q\mu}\,\Delta P, \tag{A1.11}$$

$$t_D = \frac{kt}{\phi\mu c r_w^2}. \tag{A1.12}$$

Then the drawdown equation is

$$P_D = P_D(t_D) = \tfrac{1}{2}E_1(4t_D). \tag{A1.13}$$

The function P_D is defined independently of the flow rate, transmissivity, or storativity. It does depend on the reservoir geometry. The dimensionless variables P_D, t_D, are principally of use in more complex situations, where correspondingly more complex forms of drawdown can be represented in a standard format.

The asymptotic (long-time) form of the dimensionless pressure for a well in an infinite aquifer is (A1.3):

$$P_D = -(1.151\,\log_{10} t_D - 0.2886). \tag{A1.14}$$

The log slope is 1.151 per cycle, in dimensionless form. The dimensionless time t_D is defined on the basis of the well radius r_w. Other time scales that are dependent on other relevant lengths can be used, but they are denoted by some appropriately varied notation.

A1.2.6. Type-Curve Matching

Given the single function $P_D(t_D)$, the drawdown in an actual situation is related to it by the scaling (A1.11), (A1.12) of the pressure and time variables. Thus if P_D is plotted against t_D on log–log scale, a plot of ΔP against t is obtained by shifting the graph along the time and pressure axes while keeping these axes parallel. To match observed data, one first takes a type-curve and plots the data on the same scale on tracing paper. The tracing paper is then shifted until the points match one of the curves.

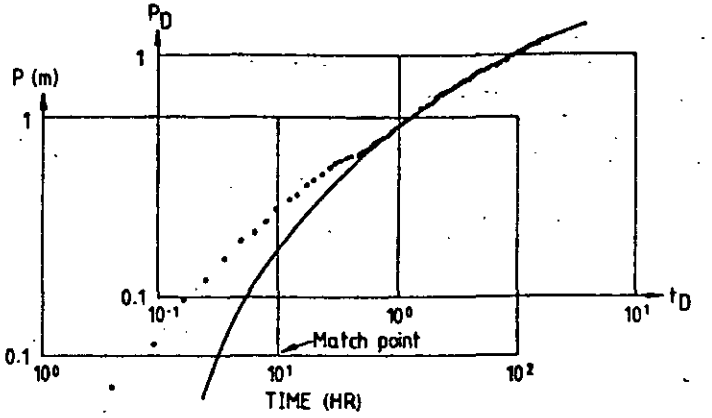

Fig. A1.3. Type-curve match to BR19–BR23 interference. (From Ministry of Works and Development, New Zealand, 1981, personal communication.)

Figure A1.3 shows the data of Fig. A1.1 plotted on log–log scale and matched to the line-source solution. The correspondence between the dimensionless and dimensional scales can be evaluated at any match point. The chosen one is $\Delta P = 0.1$ m = 980 Pa, $t = 10$ h, at which it is found that $P_D = 0.057$ and $t_D = 0.265$.

Then, evaluating the definitions of the dimensionless variables,

$$\frac{kh}{\mu} = \frac{P_D}{\Delta P}\cdot\frac{q}{2\pi} = \frac{0.057}{980}\cdot\frac{0.084}{2\pi} = 7.8\times10^{-7}\ \text{m}^3/\text{Pa}\cdot\text{s},$$

$$\frac{k}{\phi\mu c} = \frac{t_D r^2}{t} = \frac{(0.265)(350)^2}{39600} = 0.9\ \text{m}^2/\text{s},$$

and

$$\phi ch = \left(\frac{kh}{\mu}\right)\Big/\left(\frac{k}{\phi\mu c}\right) = 8.7\times10^{-7}\ \text{m/Pa}.$$

Compared to the semilog analysis, we find a nearly identical value of transmissivity (and hence of kh) and a 50% larger storativity. When both semilog and log–log analyses are possible, the semilog results are generally preferable. The log–log analysis in this particular case yields some additional information: it shows that the data for less than 20 hours deviates from the later data—a fact not apparent in the semilog plot.

A1.2.7. Productivity

Following the line-source solution (Eqs. A1.2)–(A1.4), pressure changes increasingly slowly with time as time increase, so that a quasi-steady state is reached. In this state the drawdown is related to the flow rate by the productivity J:

$$W = J(P_0 - P). \tag{A1.15}$$

Comparing with Eqs. (A1.2–A1.4),

$$\frac{1}{J} = \frac{\nu}{4\pi kh}\left[2.303 \log_{10}\left(\frac{4kt}{\phi\mu c r_w^2}\right) - 0.5772\right]. \tag{A1.16}$$

An alternative expression is obtained if there is a distant radius r_0 at which pressure is held constant. Then flow does ultimately stabilize, with

$$\frac{1}{J} = \frac{2.303\nu}{4\pi kh} \log_{10}\left(\frac{r_0}{r_w}\right). \tag{A1.17}$$

For large values of t or of r_0/r_w, the expression for J is not very sensitive to t or r_0. Then Eq. (A1.16) or (A1.17) can be used to obtain a rough estimate of permeability. A similar expression is used for injection, defining injectivity I.

A1.3. WELLBORE STORAGE AND SKIN

Two simple effects that can occur in or near a well may affect pressure changes measured in the well. These are wellbore storage and skin.

Wellbore storage is wellbore's capacity to store fluid. With an increase in pressure, more fluid is stored. Thus, if a well is shut at wellhead some flow will continue into the wellbore. The flow in the porous medium does not stop instantaneously, but tapers off.

Skin refers to the possibility, that immediately adjacent to the well, there exists a region of different permeability—most often caused by side-effects of drilling. This is idealized as a resistance (possibly negative) concentrated at the wellface.

A1.3.1. Wellbore Storage

Wellbore storage is defined in terms of a coefficient

$$C = \frac{\Delta V}{\Delta P}, \tag{A1.18}$$

where ΔV is the change in fluid volume, at wellbore conditions, for pressure change ΔP. A dimensionless coefficient C_D can be defined. In most groundwater and petroleum wells filled with liquid, if the wellbore volume is V, and the compressibility of the fluid in the wellbore is c, $C = Vc$. However, in geothermal wells a different effect controls wellbore storage. After shut-in, fluid continues to enter the well. The wellbore cools during discharge because downhole pressure is lower. As pressure recovers, the wellbore and adjacent rock reheats, and steam to supply this heat condenses in the well. This results in much more fluid storage than would be achieved by simple compression (Barelli *et al.*, 1976). The wellbore storage coefficient cannot be interpreted literally to give a wellbore volume. Wellbore storage, basically a "nuisance effect", affects the form of pressure transients and must be recognized to avoid our being misled.

A1.3.2. Skin

Skin is defined as an additional pressure drop ΔP_{skin} at wellface:

$$\Delta P_{skin} = \frac{q\mu}{2\pi kh} \cdot s, \tag{A1.19}$$

where s is dimensionless. This is added to the pressure drop caused by flow in the homogeneous medium away from the wellbore, so that the drawdown equation becomes

$$\Delta P = \frac{q\mu}{4\pi kh}\left[E_1\left(\frac{\phi\mu c r^2}{4kt}\right) + 2s\right] \tag{A1.20}$$

or, in dimensionless terms,

$$\frac{2\pi kh}{q\mu}\Delta P = P_D(t)_D + s. \tag{A1.21}$$

The presence of skin does not alter the evaluation of transmissivity in semilog analysis. It does affect storativity. Equation (A1.8) must now be written

$$\phi che^{-2s} = (2.25)\left(\frac{kh}{\mu}\right)\left(\frac{t}{r_w^2}\right)10^{(-\Delta P/m)} \tag{A1.22}$$

$$s = 1.151\left[\frac{\Delta P}{m} - \log_{10}\left(\frac{kt}{\phi\mu c r_w^2}\right) + 0.251\right]. \tag{A1.23}$$

In Equations (A1.21)–(A1.23) ΔP is the difference between the pressure at time t and that before the flow change, i.e., if the transient is for drawdown it is $P_0 - P$; if for buildup $\Delta P = P - P_{wf}$, where P_{wf} is the flowing pressure immediately before shut-in.

In petroleum or groundwater, ϕ, h, and c are known from geologic structure, coring, and fluid samples. Then skin can be evaluated unambiguously through Eq. (A1.23). In geothermal wells none of these may be known. Equation (A1.22) groups the unknowns together, since it is this single combination that is measured. The range of uncertainty of ϕh is such that a very large positive or negative value of s can still be detected.

Skin can be more clearly identified by type-curve matching. In place of the single curve $P_D(t_D)$ corresponding to the line source solution, a family of curves is generated for different C_D and s. Such curves are calculated by Agarwal *et al.* (1970), and Earlougher and Kersch (1974). Figure A1.4 shows a match to one such curve.

It is the skin that is of greatest interest. If a positive skin is obtained, flow of fluid to the well is obstructed, perhaps by drilling mud or cuttings, and there is the hope that larger flows might be obtained by changing drilling practice. In the case of the well in Fig. A1.4, it was concluded that the flow would have been doubled if the skin were absent (Saltuklaroglu and Rivera, 1978).

The type-curves are also of use in refining the use of semilog plots. The early data in any test are influenced by storage and skin, or other possible factors, and it is possible that an apparent semilog straight line may not be correct. If a spurious early semilog straight line is present in addition to a true later one, the method of Garcia-Rivera and Raghavan (1979) can be used in place of log–log matching to analyze the semilog curve. The initial slope on the log–log plots with storage present is always unity. The semi-

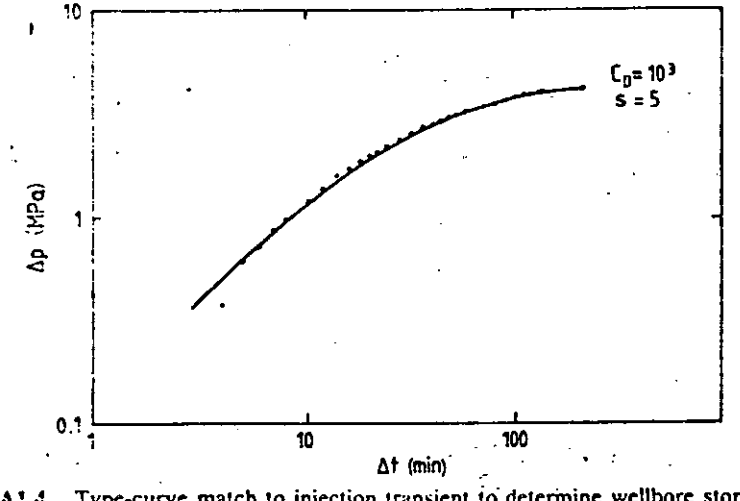

Fig. A1.4. Type-curve match to injection transient to determine wellbore storage and skin. (From Saltuklaroglu and Rivera, 1978.)

log straight line begins 1.5 cycles after this unit slope ceases, and this identifies the correct straight line.

The use of type-curves suffers from the defect that the curves are very similar, so that any match is imprecise (Barelli *et al.*, 1976; Ramey, 1976b). For this reason semilog analysis is preferable if possible. Alternately, semilog analysis to obtain transmissivity may be combined with log–log matching to obtain skin. Note that Eqs. (A1.20)–(A1.23) with skin present apply only to drawdown at the producing well. The pressure drop due to skin occurs only at wellface. For an interference test the original form without skin applies.

Skin may be caused by permeability impairment near the well. At high flow rates the pressure drop near the well may increase more rapidly with flow rate. This can occur if flow ceases to be laminar and becomes turbulent. Then a pressure drop near the well, proportional to the square of the flow rate, can be added to the normal pressure drop. This can be detected if pressure transients at different flow rates show an apparent skin that increases with flow rate.

A1.4. INJECTION

So far, the analysis has been for discharge. Since injection is, in principle, the reverse process, the equations are altered only by changing the signs of ΔP and q. Injection is a simple inverse of production if the fluid injected is of the same enthalpy (quality or temperature) as that produced. More commonly the fluid injected is cold water, or water cooler than reservoir temperature. Then the injected water has different viscosity and compressibility from the reservoir fluid.

For short time scales (such as govern pressure tests), Fig. 5.17 shows the fluid distribution in the reservoir in plan view for injection into an aquifer of homogeneous fluid. Near the well is a bank of cold injected water. Beyond that is injected water heated by contact with rock, and beyond that, reservoir fluid. The reservoir fluid "sees" an expanding volume of water at reservoir temperature. In addition, the region of disturbed pressure extends far beyond the region of cold water so that the bulk of the fluid controlling the pressure transient is close to undisturbed reservoir conditions. Thus, the appropriate fluid properties are those of reservoir fluid, not injected fluid. The injected fluid acts as a volume source to the reservoir fluid. With a volume source specified injection testing yields the transmissivity kh/μ and storativity ϕch of the aquifer.

Over longer times other effects can occur if sufficient cold water accumulates to affect pressure gradients or if mixing of the injected cold water

into reservoir fluid occurs. In the latter case thermal effects can then influence pressure changes. The most striking example is injection of cold water into a two-phase reservoir, which can ultimately lower pressures (Grant, 1981a). (See also Section A1.12.)

A1.5. TWO-PHASE FLOW

A1.5.1. Fluid Parameters

A frequent occurrence in geothermal fields is that two phases (steam and water) flow together. This may occur in a liquid-dominated reservoir or in a vapor-dominated reservoir (in which case the water phase may be immobile). The pressure transient techniques remain valid provided that the fluid properties are redefined (see Chapter 3). Compressibility is given by

$$\phi c_t = \frac{\langle \rho C \rangle}{(H_{sw})} \frac{dT_s}{dP} \frac{(\rho_w - \rho_s)}{\rho_w \rho_s}. \tag{A1.24}$$

Fluid viscosity is defined by

$$\frac{1}{x_t} = \frac{k_{rw}}{x_w} + \frac{k_{rs}}{x_s}, \qquad x = \mu, \nu, \tag{A1.25}$$

and density by

$$\frac{1}{\rho_t} = \frac{1}{H_{sw}} \left(\frac{H_t - H_w}{\rho_s} + \frac{H_s - H_t}{\rho_w} \right), \tag{A1.26}$$

where H_t is the enthalpy of the flowing steam–water mixture and all other thermodynamic variables are evaluated at undisturbed reservoir conditions. Equations (A1.25) and (A1.26) also imply $\mu_t = \rho_t \nu_t$.

To compute the viscosities requires knowledge of the relative permeability functions k_{rw} and k_{rs}. They need not be known as functions of saturation but must to be known as functions of each other. The enthalpy H_t is defined as

$$H_t = \left(\frac{H_w k_{rw}}{\nu_w} + \frac{H_s k_{rs}}{\nu_s} \right) \cdot \nu_t, \tag{A1.27}$$

and this can be rearranged to yield

$$\frac{k_{rw}}{k_{rs}} = \frac{\nu_w}{\nu_s} \frac{H_s - H_t}{H_t - H_w} = \frac{\nu_w}{\nu_s} \frac{1 - X}{X}, \tag{A1.28}$$

where $X = (H_t - H_w)/H_{sw}$ is the flash fraction or dryness. If one other

relation between k_{rw} and k_{rs} is known, Eq. (A1.28) yields k_{rw} and k_{rs}, and then Eq. (A1.25) gives μ_t (or ν_t). (See Appendix 3 for a graph of ν_w/ν_s as a function of temperature.) In the absence of such knowledge (the relative permeability functions for fractured media are not presently known), a transient test yields a measurement of kh/μ_t or kh/ν_t, and not kh.

A1.5.2. Relative Permeabilities

For transient analysis it is not necessary to know the saturation. Only the relative permeabilities k_{rw} and k_{rs} are needed to compute the viscosities μ_t and ν_t. Rather than specify both relative permeabilities as functions of saturation, it is more convenient to specify $|k_r| = k_{rw} + k_{rs}$ as a function of k_{rw}/k_{rs}. This relation involves only observable quantities. Then in an application, Eq. (A1.28) gives k_{rw}/k_{rs}. The relative permeabilities are then evaluated from

$$k_{rs} = |k_r|/(1 + k_{rw}/k_{rs}), \qquad k_{rw} = k_{rs} \cdot (k_{rw}/k_{rs}). \tag{A1.29}$$

There is considerable doubt as to the appropriate relative permeabilities for fractured geothermal media. (For further discussion see Section A2.3.2.) Unless otherwise specified, all two-phase transient analyses in this book use the "fracture" relative permeability:

$$|k_r| = 1. \tag{A1.30}$$

Calculations can then be simplified since it can be shown that

$$\nu_t = X\nu_s + (1 - X)\nu_w, \tag{A1.31}$$

and the dynamic viscosity is found from $\mu_t = \rho_t \nu_t$.

A1.5.3. Numerical Approximation for Compressibility

A convenient numerical approximation for Eq. (A1.24) is available:

$$\phi c_t = \langle \rho C \rangle \times (0.42 \times 10^{-5} P^{-1.66}), \tag{A1.32}$$

where c_t is in MPa^{-1}, P in MPa, and $\langle \rho C \rangle$ is in $J/m^3{}^\circ C$. Taking a typical value, $\langle \rho C \rangle = 2.5 \times 10^6$ J/m^3K),

$$\phi c_t = 10.5 P^{-1.66}. \tag{A1.33}$$

If noncondensible gases are present, the two-phase compressibility is decreased. For a liquid-dominated reservoir, Eq. (A1.33) is modified to

$$\frac{1}{c_t} = \frac{\phi}{10.5} P_{sat}^{1.66} + 5 P_g^{-0.21}, \tag{A1.34}$$

where P_{sat} is the steam pressure and P_g gas partial pressure. The gas is

assumed to be carbon dioxide. Effects of gas on viscosity can usually be ignored.

A1.5.4. Example: Tests on KA28

Figure A1.5 shows two examples of two-phase transients measured in well KA28, Kawerau (Grant, 1980b), pressure change on shut-in from injection and from discharge. The semilog plot of the fall-off after injection at a rate of 11.5 ℓ/s = 1.15×10^{-2} m³/s, has a slope of 140 kPa/~. Then

$$\frac{kh}{\mu_t} = \frac{2.303q}{4\pi m} = \frac{(2.303)\,(1.15 \times 10^{-2})}{4\pi(1.4 \times 10^{5})} = 1.5 \times 10^{-8}\ \text{m}^3/\text{Pa} \cdot \text{s}.$$

Evaluating Eq. (A1.22) gives, with well radius $r_w = 0.1$ m,

$$\phi c_t h e^{-2s} = 6.7 \times 10^{-5}\ \text{m/Pa}.$$

These are the results of the test: measurement of transmissivity kh/μ_t and

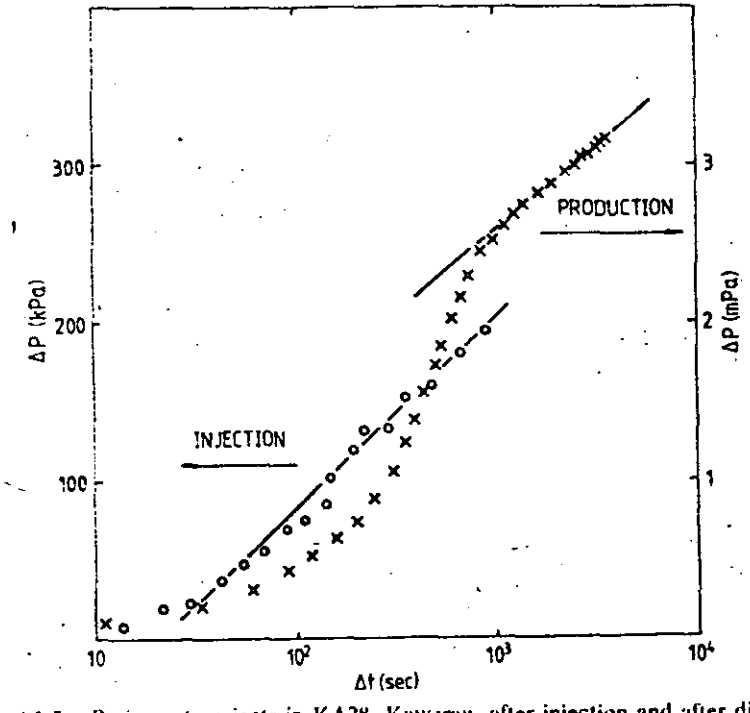

Fig. A1.5. Pressure transients in KA28, Kawerau, after injection and after discharge. (From Grant, 1980b.)

storativity times e^{-2s}. The skin might be better defined by a log–log plot, but a trial shows that the data is not matchable.

To evaluate kh it is necessary to calculate μ_t. Testing subsequent to this injection test shows that the well has a discharge enthalpy of 1200 kJ/kg, drawn from a feed point at 264°C

$$\frac{k_{rw}}{k_{rs}} = \frac{\nu_w}{\nu_s}\frac{h_s - h_t}{h_t - h_w} = \frac{(0.133)}{(0.70)}\frac{(2794 - 1200)}{(1200 - 1155)} = 6.7.$$

Assuming Corey permeabilities gives, from Fig. A2.2, $|k_r| = 0.29$, $k_{rw} = 0.25$, $k_{rs} = 0.04$, and $\mu_t = 220$ μPa · s. Assuming fracture permeabilities, $k_{rw} = 6.7/(1 + 6.7) = 0.87$, and $k_{rs} = 0.13$. Then $\mu_t = 64$ μPa · s, and

$$kh = 3.3\ \text{d-m (Corey)} \qquad = 0.96\ \text{d-m (fracture)}.$$

The compressibility of pure water–steam at 264°C is $\phi c_t = 0.73\ \text{MPa}^{-1}$. A CO_2 partial pressure of 1.28 MPa is present, giving $c_t = 0.22\ \text{MPa}^{-1} = 2.2 \times 10^{-7}\ \text{Pa}^{-1}$. Then $\phi h e^{-2s} = 300$ m.

Because of the present uncertainty about the relative permeabilities, kh cannot be uniquely calculated. Transmissivity kh/μ_t is the result of the injection analysis. Note also the oddity that, because the injection transient measures reservoir fluid behavior, kh cannot be calculated without knowledge of the enthalpy at which the well will later discharge.

In the discharge test a slope of 1 MPa/cycle is obtained. Discharge was at a rate of 37.5 kg/s.

$$\frac{kh}{\nu_t} = \frac{2.303\,W}{4\pi m} = 6.9 \times 10^{-6}\ \text{m} \cdot \text{s}.$$

The density of fluid of enthalpy 1200 kJ/kg at 264°C is given by Eq. (A1.26) as $\rho_t = 430$ kg/m³. Then

$$\frac{kh}{\mu_t} = \frac{1}{\rho_t} \cdot \frac{kh}{\nu_t} = 1.6 \times 10^{-8}\ \text{m}^3/\text{Pa} \cdot \text{s}.$$

kh/ν_t or kh/μ_t is the result of the test. A value for kh still depends on the relative permeabilities.

A1.5.5. Validity of Two-Phase Analysis

The principal practical problem in a two-phase analysis of this form is the value of discharge enthalpy used. In a two-phase reservoir discharge enthalpy normally varies with time and with flow rate. The standard technique of evaluating at undisturbed reservoir conditions (i.e., at conditions distant from the wellface) indicates that it should be the flowing enthalpy of the undisturbed reservoir that is used. This will normally be the dis-

charge enthalpy measured at small flow rates or at small discharge times. With larger drawdown, higher enthalpies may be obtained due to heat transfer from rock near the well (see Section 5.5). In the example of KA28 above, discharge enthalpy varied from 1200 to 1320 kJ/kg. Given the uncertainty about the correct enthalpy to use (and, in consequence, about the flowing density ρ_t), it is best to regard the discharge test as measuring kh/ν_t.

The validity of two-phase transient analysis has been checked, mainly by analysis of simulated data. For vapor-dominated reservoirs, good agreement is obtained both with simulations and with laboratory experiments (Moench and Atkinson, 1978; Herkelrath and Moench, 1980). For reservoirs with both phases mobile, moderately good agreement is obtained with the results of simulations (Garg, 1980; Sorey *et al.*, 1980; Aydelotte, 1980; Garg and Pritchett, 1981).

A1.6. PSEUDOPRESSURE

As a gas flows to a well, pressure may vary sufficiently that the assumption of nearly constant density may not be valid. This problem can be overcome by the definition of a pseudopressure, a modified pressure function (Al-Hussainy *et al.*, 1966).

The equation for (isothermal) flow of a dry gas is

$$\phi c\rho \frac{\partial P}{\partial t} = \nabla \cdot \left(\frac{k}{\nu} \nabla P\right) \tag{A1.35}$$

$$= k\left[\frac{\partial}{\partial P}\left(\frac{1}{\nu}\right)\right](\nabla P)^2 + \frac{k}{\nu}\nabla^2 P. \tag{A1.36}$$

The normal linearization omits the first term on the right-hand side. It can, however, be accommodated by defining the pseudopressure $m(p)$:

$$m(p) = \int \frac{dP}{\nu}. \tag{A1.37}$$

Then Eq. (A1.35) becomes, exactly,

$$\phi\mu c \frac{\partial m}{\partial t} = k\nabla^2 m. \tag{A1.38}$$

There remains nonlinearity in that μ and c are pressure dependent. This is ignored by evaluating these parameters at undisturbed conditions:

$$\left(\frac{\phi\mu c}{k}\right)_0 \frac{\partial m}{\partial t} = \nabla^2 m. \tag{A1.39}$$

This is the linear diffusion equation again. Experience shows that it is valid for large drawdown, whereas a linearized pressure equation is not. A simple justification can be given. Consider a well turned on to discharge. After some time the region near the well is quasi-steady. In this region the equation satisfied is

$$\nabla \cdot \left(\frac{k}{\nu}\nabla P\right) = 0 = \nabla^2 m, \tag{A1.40}$$

so that Eq. (A1.39), in its quasi-steady form, is correct. At distance, the term involving $\partial P/\partial t$ is important, but since drawdown is small there, it is correct to evaluate parameters at an undisturbed state. The pseudopressure approximation is a "uniform approximation"—valid in regions of both large and small drawdown.

It is commonly assumed that the dynamic viscosity μ varies little. Then,

$$m(p) = \int \frac{\rho}{\mu} dP = \frac{1}{\mu}\int \frac{M_s P}{RTZ} dP = \left(\frac{1}{2}\frac{M_s}{\mu RTZ}\right) P^2. \tag{A1.41}$$

The density is proportional to pressure, and this makes the pseudopressure proportional to pressure squared. A dimensionless pseudopressure m_D can be defined and the liquid solutions P_D used in place of m_D,

$$m_D = \frac{\pi khM_s}{W\mu ZRT} P^2. \tag{A1.42}$$

The expression $ZRT/M_s = P/\rho$ is approximately constant for saturated steam at 1.9×10^5 Pa · m³/kg (see Appendix 3).

Expressed in terms of P^2 the line source solution then becomes

$$\Delta P^2 = P_0^2 - P^2 = \left(\frac{W\mu}{2\pi kh}\right)\left(\frac{RTZ}{M_g}\right) E_1\left(\frac{\phi\mu c r^2}{4kt}\right). \tag{A1.43}$$

Note that ΔP^2 is the change in P^2, not $(\Delta P)^2$. Then, if there is a slope of $\mathcal{M}$ on a semilog plot of pressure-squared against time,

$$kh = \left(\frac{W\mu}{2\pi\mathcal{M}}\right)\left(\frac{RTZ}{M_s}\right)(2.303). \tag{A1.44}$$

and

$$\phi che^{-2s} = (2.25)\left(\frac{kh}{\mu}\right)\left(\frac{t}{r^2}\right) 10^{(-\Delta P^2/\mathcal{M})}$$

In geothermal steam wells, flow is usually not isothermal. Temperature follows pressure along the saturation curve. However, Eq. (3.54) for flow of steam with immobile water is identical in form to Eq. (A1.35), using the

two-phase compressibility. The pseudopressure argument remains valid. The definition [Eq. (A1.37)] should be integrated along the saturation curve rather than an isothermal line. An accurate pseudopressure for dry steam is given by Mannon and Atkinson (1977), and one for saturated steam by Grant (1978). Both are close to pressure-squared.

The pseudopressure is used only for wells in vapor-dominated reservoirs. For two-phase flow with both phases mobile, the variation in flowing enthalpy means that it is not possible to define a pseudopressure by simple analogy to Eq. (A1.37).

A1.7. VARIABLE FLOW RATE

A1.7.1. Superposition

It can often be difficult to maintain a constant (mass) flow rate for a geothermal discharge. If there are a series of step changes in flow, the pressure change can be superimposed:

$$\Delta P = \frac{\nu}{4\pi kh} \sum_{t_{Di}} \Delta W_i P_D(t_D - t_{Di}), \tag{A1.45}$$

and a continuous variation can be represented by an integral

$$\Delta P = \frac{\nu}{4\pi kh} \int_0^t P_D(t_D - t'_D) dW'. \tag{A1.46}$$

Given actual observations at varying flow rate, the function P_D must be reconstructed in order to compare it with standard solutions. This can be done numerically (Barelli and Palama, 1980). Superposition can also be calculated through the use of *influence functions* (Zais and Bodvarsson, 1980b). Otherwise, the most common method is to ignore the flow rate variation on the assumption that it is not important. Thus, for example, if the flow is slowly running down, one can attempt to obtain the form of the drawdown for constant flow by plotting $\Delta P/W$ instead of ΔP. This should remove some of the variation caused by nonconstant flow.

A1.7.2. Flow at Constant Pressure

One important case of variable rate is flow at constant pressure. The pressure is held constant (at wellface) and the flow changes. This can arise if a well is in production at constant wellhead pressure and the pressure drop down the hole does not vary much. It can also arise if a well is allowed to blow unrestricted, which, for wells of small mass flow, approximates to lowering downhole pressure to near atmospheric.

If the pressure is changed impulsively, the flow rate changes in a manner that, asymptotically, is of similar form to the line source solution:

$$\frac{1}{q} = \left(\frac{\mu}{4\pi kh}\right)\left(\frac{1}{\Delta P}\right)\left[2.303 \log_{10}\left(\frac{4kh}{\phi\mu c r^2}\right) - 0.5772\right]. \tag{A1.47}$$

Thus, one plots q^{-1} or W^{-1} against time on a semilog graph. If $\mathcal{M}_w$ is the slope of the plot of W^{-1},

$$\frac{kh}{\nu} = \left(\frac{1}{4\pi \mathcal{M}_w}\right)\left(\frac{2.303}{\Delta P}\right), \tag{A1.48}$$

$$\phi c h e^{-2s} = (2.25)\left(\frac{kh}{\mu}\right)\left(\frac{t}{r_w^2}\right) 10^{[(1/\nu)\nu/\mathcal{M}_w]}. \tag{A1.49}$$

Note that Eq. (A1.47) is identical in form to the line source solution. However, the straight line is approached much more slowly.

A1.7.3. Example: KMJ15

Figure (A1.6) shows W^{-1} plotted on semilog scale for the discharge of well KMJ15 at the vapor-dominated Kamojang field, West Java. The well

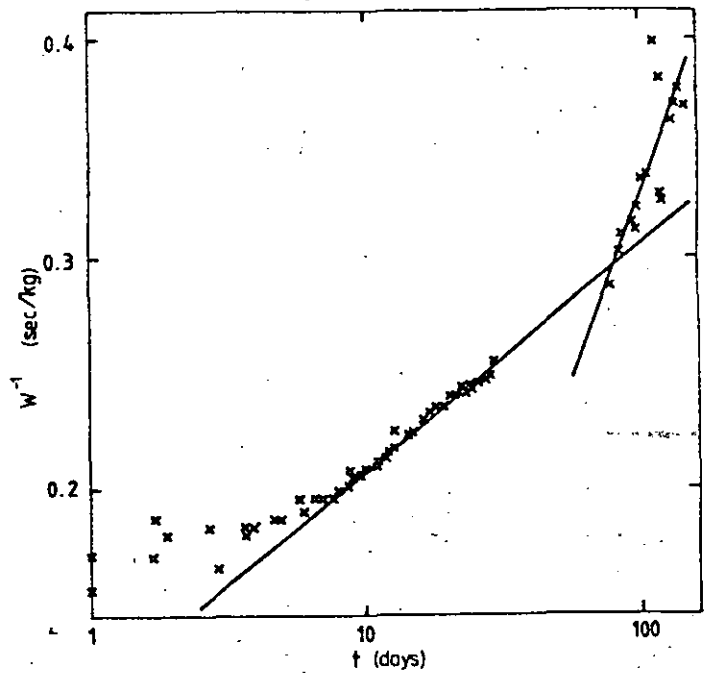

Fig. A1.6. Flow of well KMJ15 at constant pressure. (From Grant, 1979a.)

was flowed at a wellhead pressure of 800 kPa, equivalent to approximately 1 MPa downhole. A well-defined straight line of slope 0.20 (kg/s)$^{-1}$ appears. Note that the straight line is not approached until after nearly 10 days—much longer than for a constant rate test. Reservoir pressure is 3.52 MPa. Combining Eq. (A1.42) and Eq. (A1.48), the semilog straight line gives

$$kh = \left(\frac{\mu}{2\pi}\right)\left(\frac{1}{\mathcal{M}_w}\right)\left(\frac{2.303}{\Delta P^2}\right)\left(\frac{RTZ}{\mathcal{M}_g}\right)$$

$$= \left(\frac{17 \times 10^{-6}}{2\pi}\right)\left(\frac{1}{0.20}\right)\left(\frac{2.303}{[3.52^2 - 1.0^2] \times 10^{12}}\right)(1.9 \times 10^5)$$

$$= 0.52 \text{ d-m},$$

at time 10 days = 1.44×10^5 s, $1/W = 0.41$ s/kg. Then

$$\phi c_t h e^{-2s} = (2.25)\left(\frac{0.52 \times 10^{-12}}{17 \times 10^{-6}}\right)\left(\frac{1.44 \times 10^5}{(0.1)^2}\right)10^{-(0.41/0.20)}$$

$$= 8.8 \times 10^{-3} \text{ m/Pa},$$

for two-phase, $\phi c_t = 10^{-6}$ Pa^{-1}, so $he^{-2s} = 8.8 \times 10^3$ m, implying that the well is stimulated ($s < 0$ for reasonable h). An impermeable boundary is possibly indicated by the doubling of slope after 80 days.

Constant-pressure analysis can also sometimes be applied to the first vertical (clearing) discharge of a well. The abrupt opening and blowing of the well approximates to a step change in downhole pressure. If enthalpy is known or guessed, the change in lip pressure gives the decay of mass flow. Constant-pressure testing and subsequent build-up is described by Ehlig-Economides and Ramey (1981a,b).

A1.8. FRACTURED MEDIA

Two types of pressure transients are specifically directed to the study of fractured media. For a medium that is fractured throughout, characteristic changes occur at a time scale dependent upon block size and other parameters. (See Section 3.7 for more detail.)

Alternatively, if a well penetrates a medium that is homogeneous except for a fracture intersecting the wellbore (as may be produced by fracturing), this produces a distinctive history, best analyzed by type-curves (Gringarten and Ramey, 1975; Cinco-Ley and Samaniego, 1981).

Figure A1.7 shows an example. The data are from a steam well at The Geysers, and so pressure-squared is plotted. The fractured well has a characteristic period of one-half slope during early times on a log–log plot. This reflects the period when flow effects near the plane of the

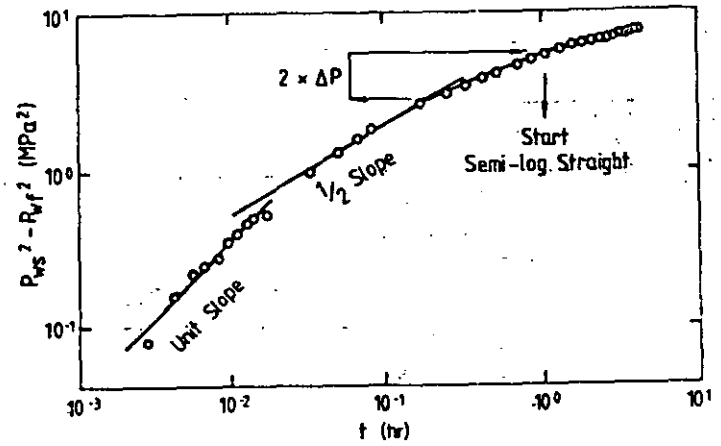

Fig. A1.7. Type-curve match to pressure buildup of a well at The Geysers, showing fractured characteristics. (From Economides and Fehlberg, 1979.)

fracture dominate. There may also a period of unit slope before the half slope, reflecting wellbore storage. The time when the correct straight line for semilog analysis starts is given by the *double* ΔP *rule*. The line starts at a pressure change twice that represented by the end of the half slope straight line (Wattenberger and Ramey, 1969). The rule refers to liquid flow; therefore for steam wells it is twice the value of ΔP^2, not ΔP.

Figure A1.8 shows the semilog Horner plot corresponding to the pre-

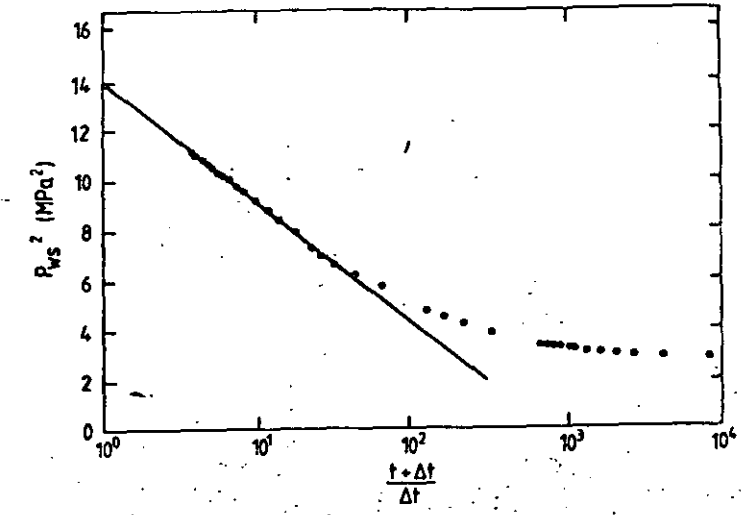

Fig. A1.8. Semilog plot of Fig. A1.7. (From Economides and Fehlberg, 1979.)

vious figure, and the semilog straight line. That the well is stimulated can be recognized from the semilog pot, but its fractured nature cannot.

A1.9. WELLBORE THERMAL AND FLOW EFFECTS

In previous sections we have reviewed briefly pressure transient theory. We now turn to some practical problems involved in the application of this theory to geothermal wells and reservoirs. There are a considerable number of problems peculiar to geothermal wells that do not occur in reservoirs of small vertical extent in which flow is isothermal. These nuisance effects, like wellbore storage, can render transient records useless or misleading. It is necessary to be able to recognize them.

The pressure transient analyzed by theory is the pressure history, at wellface, of a homogeneous medium. Thus, the "true" transient is measured downhole, at the depth where the well responds to reservoir pressure. Which is its principal feed point. It is here, at the well's point of contact with the reservoir, that a pressure gauge should be placed. Placement at any other depth is permissible, provided that the pressure gradient in the well does not change with time.

A1.9.1. Condensation in Steam Wells

Wells in vapor-dominated systems maintain a column of steam in the well, and so it is convenient to measure pressure at wellhead. The pressure recovery at wellhead is a good measure of that downhole provided that the wellbore remains full of steam to the principal feed depth. Sometimes the well will partly fill with condensate during recovery (Strobel, 1976), lowering wellhead pressure. Figure A1.9 shows an example.

A1.9.2. Collapse of Flashing Column in Wellbore

In a liquid-dominated system wellhead pressures are generally not used because a column of fluid in the well can vary between a continuous water column and a low-density two-phase mixture. This variation can also affect transients measured at an inappropriate depth, such as bottomhole. Figure A1.10a shows a buildup after discharge in a hypothetical well. The stable shut profile is a column of water. On flow, a low-density fluid fills the wellbore. The feed point is some distance above bottomhole. When the well is shut there is a period, usually of minutes, during which the two-phase column becomes denser and collapses. After this a column of water

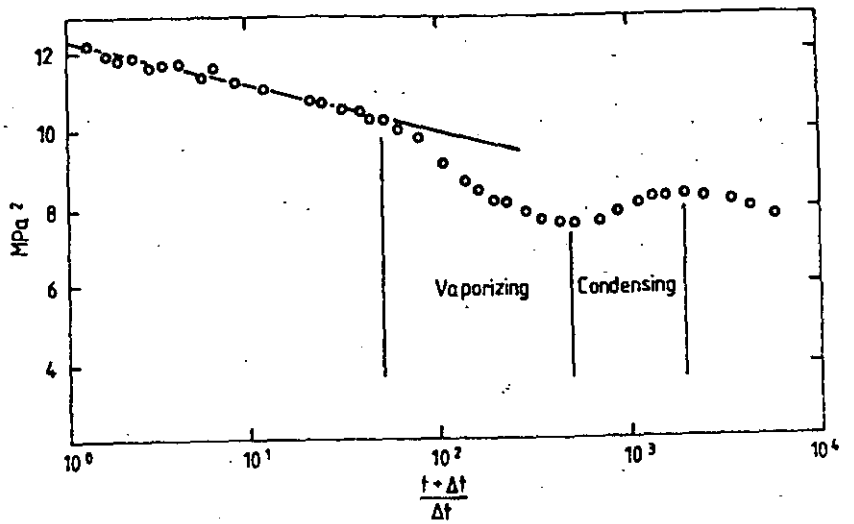

Fig. A1.9. Effect on wellhead pressure buildup of condensation in the wellbore in a steam well at The Geysers. (From Strobel, 1976.)

is present in the wellbore from bottomhole to above the feedpoint. Figure A1.10b shows the pressure recovery measured at bottomhole and at feedpoint. After a continuous water column forms, the pressure difference between feedpoint and bottomhole is constant, and the two records show the same log slope. But the pressure difference was smaller when two-phase fluid occupied the wellbore. Thus, taking pressure at a particular

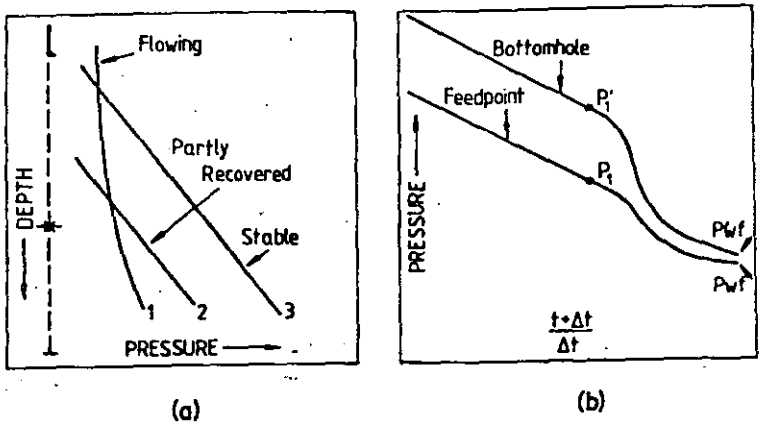

Fig. A1.10. Pressure recovery in a well with flashing fluid present downhole during discharge. (a) Pressure profiles, showing collapse of flashing column: (1) Low-density fluid fills the wellbore, during flow; (2) Configuration at partial recovery; (3) The stable shut profile—a column of water. (b) Recovery at feedpoint and bottomhole. (After Grant *et al.*, 1981b; copyright © SPE-AIME).

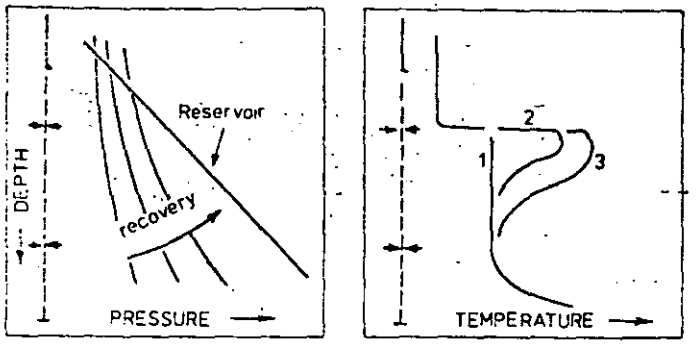

Fig. A1.11. (a) Pressure recovery in a well with internal discharge. (b) Temperature profiles in an injection well with interzonal flow, during and after injection showing (1) the profile under injection, at which time fluid is entering at the upper feed zone; (2) and (3) two subsequent profiles as fluid continues to enter the upper feed zone after injection ceases. (In part after Grant *et al.*, 1981b; copyright © SPE-AIME.)

time, $P - P_{wf}$ at feedpoint is less than $P - P_{wf}$ at bottomhole. Using the bottomhole record gives correct slope and therefore correct kn, but skin is overestimated. Riney and Garg (1981) illustrate the correction of such data by calculating the pressure profiles during discharge and recovery.

A1.9.3. Well with Internal Discharge

Figure A1.11a shows the pressure recovery in a well with an internal discharge. Pressure transients in such a well are complicated by the internal discharge because flow never stops. However, pressure at the principal feedpoint will be closest to reservoir pressure. At any depth beneath this feedpoint pressure rise during recovery is larger, and so a build-up recorded, for example, at bottomhole will underestimate kh by overestimating reservoir pressure change.

A1.9.4. Injection Tests

When pressure transients are measured under injection, the chief hazard arises from interzonal flow. If the gauge is placed at some depth other than opposite the principal feed, a true transient is recorded provided that the wellbore remains filled with water at constant temperature (usually injection temperature). In wells of good permeability this condition is often not met, since internal flow is present. Figure A1.11b shows temperature profiles. The hydrostatic balance between the feed zones and the location of the gauge changes, and a column of water of constant temperature is not present in the well. This situation typically shows up as a pressure transient with rebound or oscillations. An example is KA22 (Fig. 4.8).

A1.9.5. Use of Profiles

In all of these cases the problems with downhole data are caused by fluid of variable density in the wellbore. They can be detected or checked by running pressure or temperature profiles. The interzonal flow problem is shown on a temperature profile by the characteristic step.

A1.9.6. Wellbore Thermal Storage Effects

It has already been mentioned that heating of the wellbore and condensation of steam produce a spuriously large wellbore storage effect (Barelli *et al.*, 1976). Other effects also arise (Miller, 1980a,b). The heating or cooling of the wellbore can change liquid density sufficiently to cause a spurious storage effect that lasts much longer than does simple compression of fluid. In addition, kh/μ for geothermal wells can be so large that downhole pressures change significantly over the time that a pressure pulse takes to ascend the wellbore. During transients the fluid in the well may not be in vertical equilibrium. This can produce pressure transients, plotted log–log, that have initial slope greater than unity, or that oscillate. On standard analysis initial log–log slope cannot exceed unity. In practice it frequently does.

If flashing fluid is present in the wellbore during flow, it persists for some period of time after shutting, producing transient changes in the vertical pressure distribution and corresponding changes in the pressure differences between the feedpoint and the wellhead or bottomhole. The long time before a liquid column forms is caused solely by the transient energy and mass transfer within the wellbore itself.

A1.9.7. Cyclic Discharge

Some wells will not sustain a steady discharge or will do so only over part of their operating range. The well cycles (mass flow, enthalpy, and wellhead pressure) all vary periodically, whereas wellhead valves are at a fixed setting. Such cycling causes problems in well control and measurement interpretation. Sometimes the cycle can be interpreted to provide additional information about reservoir fluid and permeability.

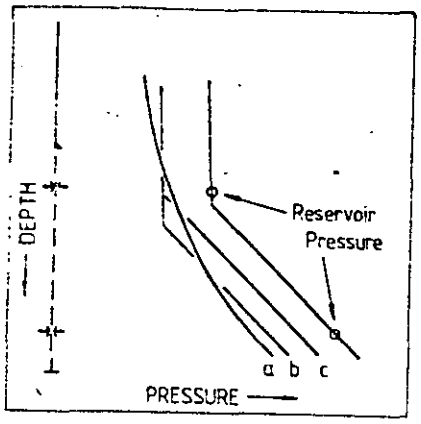

Fig. A1.12. Pressure profiles in cycling well.

Usually, cycling is caused by the presence of two significant feeds, of different enthalpy, to the well. Figure A1.12 illustrates one case, the simplest, in which cycling is normal. The reservoir contains a vapor-dominated zone over a liquid-dominated one, and the well has a steam feed and a liquid feed. Three phases of the cycle are shown. Figure A1.13 shows the pressure and flow history at each feed. In phase (a), both feeds flow. The lower zone draws down, and the two-phase column between the two feeds collapses. Phase (b) follows: steam only is discharged, from the upper feed, but the lower feed recovers and a column of water is present in the wellbore above it. The water level in the well rises until at (c) it is entrained into the steam flow, initiating discharge of the deep feed again. The liquid column flashes, the wellbore unloads, and the cycle continues.

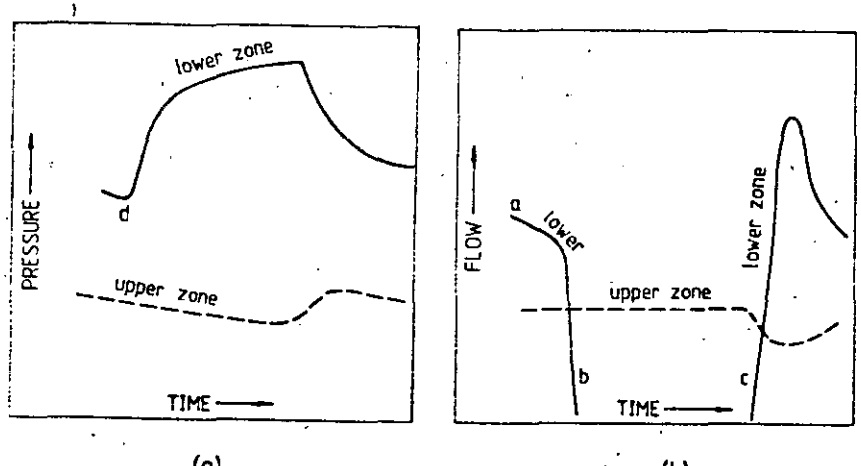

Fig. A1.13. Pressure and flow profiles at upper and lower feeds on cycling well.

The mechanism driving the cycle is the oscillation in pressure gradient in the well between extremes of liquid and low-density two-phase fluid. This couples with oscillatory pressures and flows at each feed. Cycling is possible without the presence of a steam zone, although normally one zone is of high enthalpy. Wells may also cycle when shut, due to repeated initiation and collapse of an internal discharge, and may cycle during recovery from an otherwise stable discharge (see Grant *et al.*, 1979, for some examples).

If the enthalpy of each feed is known, and if the well flow is large enough for mass and energy storage in the wellbore to be ignored, then the measurement of mass flow and enthalpy at wellhead can be converted into flows of each feed. Then permeability of each zone may be estimated. For example, the pressure build-up at the lower zone when it stops flowing (point d) usually gives a semilog straight line initially. Knowledge of the flow gives transmissivity.

Cycling is normally most prevalent on wells of low to moderate permeability. If the permeability is too high, downhole pressures cannot oscillate. Cycling is usually greatest with the well throttled and least with the well opened wide.

A1.9.8. Example of Two-Zone Well Analysis: OW-15

The following analysis, from Pratomo (1980), is reproduced by permission of Kenya Power Company and Geothermal Energy N.Z., Ltd. Well OW-15 is a production well in Olkaria field, Kenya. This field has a steam zone beneath which is a liquid-dominated zone. Wells are cased to the top of the steam zone (Noble and Ojiambo, 1976; McNitt, 1977; Grant and Whittome, 1981). Because of the steam zone, wells normally have a steam cap pressure profile. The steam zone pressure can be measured at wellhead and the liquid-dominated zone pressure is measured downhole.

Wells typically produce from both zones, with the bulk of the permeability in the steam zone. Well OW-15 discharged with two distinctly different characteristics. A discharge of 7.8 kg/s at 2400 kJ/kg, was interpreted as being due to the steam zone alone. Then the lower zone "kicked in," adding 3.6 kg/s at 1440 kJ/kg. The pressure recovery was measured at wellhead and at 1200 m when the well was shut. Slope at wellhead is 980 kPa/cycle and at 1200 m, 2.6 MPa/cycle:

$$\left(\frac{kh}{\nu_t}\right)_{\text{upper zone}} = \frac{(7.8)\,(2.303)}{4\pi\,(9.8 \times 10^5)} = 1.5 \times 10^{-6}\ \text{m} \cdot \text{s},$$

$$\left(\frac{kh}{\nu_t}\right)_{\text{upper zone}} = \frac{(3.6)\,(2.303)}{4\pi\,(2.6 \times 10^6)} = 2.5 \times 10^{-7}\ \text{m} \cdot \text{s}.$$

Using fracture–flow relative permeabilities at an assumed reservoir temperature of 248° gives kh values of 1.1 and 0.075 d-m for upper and lower zone, respectively. For each zone kh was computed using the estimated discharge of that zone alone.

This form of analysis, using data for both zones, is only possible because pressures and flows for both zones can be determined. The pressures in the two zones recover independently because of the steam cap profile—pressure in each zone can change independently, moving the waterlevel in the well. The flows of the two zones were determined through changes in enthalpy and flow corresponding to a sudden change in well performance.

A1.10. BAROMETRIC AND TIDAL EFFECTS; USE OF WATER LEVELS

Changes in barometric pressure, and the strain of the earth's crust of earth tides, apply signals to geothermal reservoirs, producing a pressure response in the reservoir and in any well penetrating it. The pressure changes are not usually detectable with mechanical guages. When pressures are measured with high sensitivity gauges, or when water levels are observed, these effects are visible.

A1.10.1. Tidal Responses

Geothermal reservoirs can exhibit a response to the changes in strain in the rock caused by earth tides. Hanson (1979, 1980a) describes observed responses in wells in the Raft River and Salton Sea fields and interprets the results. The theory of tidal response in an aquifer is described by Bredehoeft (1967), Bodvarsson (1970), and Arditty (1978). The magnitude of tidal pressure responses is less than 1 kPa. Thus, they are normally not large enough to interfere with pressure records collected for other purposes, but they can corrupt interference test results.

The tidal strain in the earth is a superposition of sinusoidal variations with different periods. The main tides have periods of $\frac{1}{4}$, $\frac{1}{2}$, 1, and 16 days. The pressure response in a well to each component depends on its frequency. Consequently, a full analysis of tidal response requires a spectral analysis (by Fourier transform) of the data, unless one frequency clearly dominates.

For a sinusoidal tidal strain of frequency ω, the pressure change in an open well is given by

$$P_w = \frac{\xi b_0}{(c_m + \phi c_t)} \cos\phi \cos(\omega t - \phi), \qquad \text{(A1.50)}$$

where the tidal strain is $b = b_0 \cos(\omega t)$, and $b_0 = 0.49 W_2 / r_E g$, where W_2 is the tidal potential and r_E is the radius of the earth. The phase angle ϕ is defined by

$$\phi = \tan^{-1}(\omega/\beta), \qquad \beta = 2\rho_w g k h/\mu_w r_w^2, \qquad \text{(A1.51)}$$

ξ is a dimensionless constant that is usually assumed to be unity. The form of the response shows that $c_m + \phi c_t$ can be determined from the amplitude of the tidal response.

A1.10.2. Barometric Response

Barometric pressure changes represent a long-period pressure change applied at the surface of the earth. This is transmitted through rock, and a corresponding pressure change occurs in any aquifer containing pore fluid. The change in reservoir pressure is related to the change ΔP_{atm} in atmospheric pressure by the barometric efficiency BE

$$\Delta P = (1 - BE)\, \Delta P_{atm}. \qquad \text{(A1.52)}$$

In a well standing open with a water level that level is controlled by a balance between atmospheric and reservoir pressure. It changes by an amount $\Delta\eta$:

$$\Delta\eta = -(BE/\rho_w g)\Delta P_{atm}. \qquad \text{(A1.54)}$$

The barometric efficiency is given by

$$BE = \phi c_t/(c_m + \phi c_t). \qquad \text{(A1.54)}$$

The barometric efficiency lies between 0 and 1 and approaches 1 for reservoir fluids of high compressibility. Thus, barometric effects are largest in wells feeding from liquid conditions. The pressure changes due to barometric effects may be as large as barometric variations, i.e., on the order of 100 kPa. These variations are large enough to affect interference test data. Figure A1.14 shows barometric noise on an interference test in which water level was recorded at the observation well.

For both tidal and barometric effects the determination of ϕc_t rather than storativity $\phi c_t h$ is extremely useful, in that it gives data not directly available from tests.

A1.10.3. Other Effects

Other external signals have been observed to influence pressures in geothermal fields. Reykjavik shows a response to oceanic tides (Thorsteinsson and Eliasson, 1970) which was explained by assuming that the aquifer extended beneath the sea bed and responded to the changing load of seawater above. Momotombo shows pressure responses to rainfall,

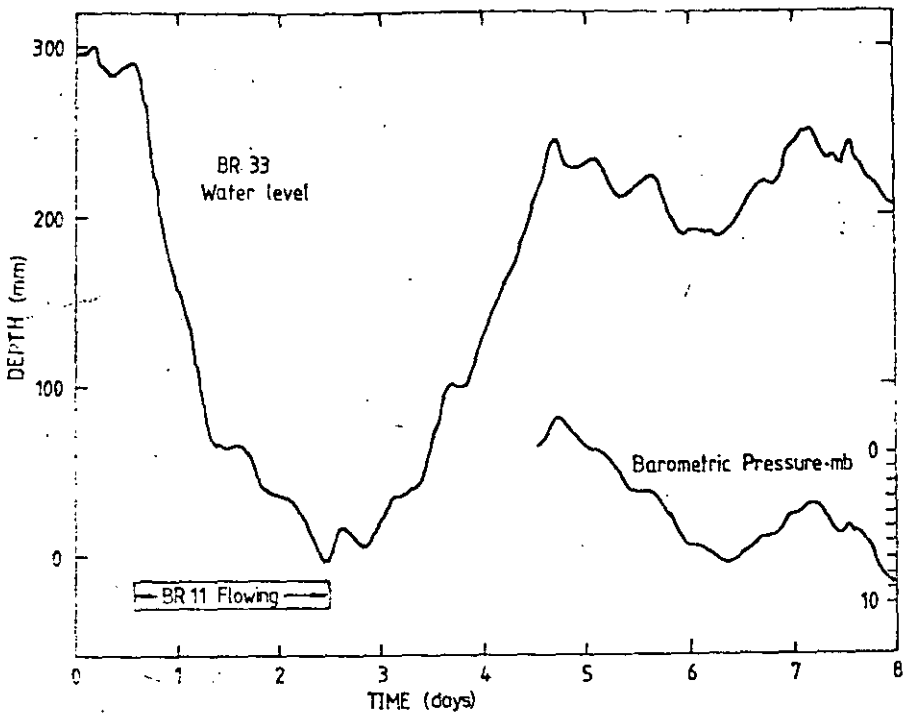

Fig. A1.14. Interference test between BR11 and BR33, Broadlands, using water levels in BR33. Barometric interference is visible. (From Ministry of Works and Development, New Zealand, 1981, personal communication.)

indicating that the reservoir must be open (Dykstra and Adams, 1978). Shallow wells at Matsukawa, up to 400 m deep and reaching 240°C, similarly showed temperature changes correlated with rainfall (Mori, 1970).

All of these responses of a geothermal reservoir to external influence provide information about reservoir properties or about the reservoir's openness to external fluid.

A1.10.4. Contamination of Interference Data

If pressure data is being collected downhole with a high-resolution instrument, or at wellhead in a wellbore full of water, or by measuring the water level in wells that will stand open, barometric and other effects may be present. Most frequently this will arise in interference testing, where small pressure changes are observed. It is then necessary to analyze for barometric effects to eliminate any contamination of the data.

It also commonly happens that the pressure in a well is not static before the test. A drift or trend with time may be present, reflecting residual

pressure changes from past tests. If pressure is observed at wellhead or by float, a drift caused by heating or cooling of the wellbore after previous flow is often present. It is then necessary to make observations before any testing begins to establish the drift of the pressure or water level and the barometric efficiency. Later observations can then be corrected.

A1.11. TEMPERATURE TRANSIENTS

During drilling, and in any subsequent cold water injection, the wellbore is cooled by the flow of water or drilling mud. After this ceases, it warms up (slowly or quickly) to its final temperature. At times it would be desirable to know this final temperature without a long wait.

One approach has been to use a Horner plot. The well is cooled for a time t_p by drilling. Thus, t_p is the time that the formation, at the depth under study, has been exposed to circulating fluid. This would usually be the time since the drill bit passed the particular depth. Then circulation is halted, and the temperature is measured at several times Δt afterward. The data are plotted on a Horner plot and extrapolated to $\Delta t = \infty$, *i.e.*, $(t_p + \Delta t)/\Delta t = 1$ to obtain an estimate of final temperature. For examples see Chiang and Chang (1979).

The validity of the Horner plot is based on the observation that the equation for heat conduction is

$$(\rho C)\frac{\partial T}{\partial t} = K\nabla^2 T, \tag{A1.55}$$

i.e., the diffusion equation, which is of the same form as the pressure transient equation. This governs the cooling and warming of the well provided that conduction is the dominant mechanism of heat transfer. It is not valid at any zone of fluid loss, at any other permeable zone, or if circulation of fluid occurs spontaneously in the wellbore past the depth of observation.

There is an additional problem. The condition imposed at the wellbore during circulation is, approximately, T = constant, rather than (heat flux) = constant. Therefore the temperature recovery is strictly analogous to a pressure recovery after discharge at constant pressure. The Horner plot, in this case, will yield an underestimate of the final temperature. An improved method is given by Roux *et al.* (1979): a Horner plot is made and extrapolated to an apparent final temperature T^*_{ws}. Then the final temperature is computed as

$$T = T^*_{ws} + mT_{DB}(t_{PD}), \tag{A1.56}$$

where m is the slope of the Horner straight line and T_{DB} is a dimensionless correction term, dependent on the dimensionless t_{PD} and on the Horner time $\theta = (t_p + \Delta t)/\Delta t$ (see Fig. A1.15). The term t_{PD} is defined as

$$t_{PD} = \left(\frac{K}{(\rho C) r_w^2}\right) t_p. \qquad \text{(A1.57)}$$

Since rock conductivity and heat capacity is fairly constant, a reasonable average value for $K/(\rho C) r_w^2$ of 0.4 hr^{-1} can be assumed for a well of radius 0.1 m.

Figure A1.16 shows an example from Menzies (1981). The extrapolation yields $T_{ws}^* = 238°C$ and the slope is $m = 194$ K/cycle. The slope is defined at $(t_p + \Delta t)/\Delta t \approx 2.5$. The circulating time is $t_p = 10$ hr, so $t_{PD} = 4$. Then Fig. A1.15 gives $t_{DB} = 0.154$, and $T_i = 283 + (194)(0.154) = 268°$. Later measurement found a downhole temperature of 265°C, but this may have been affected by an internal flow that developed after completion of the well.

Under most circumstances extrapolated temperatures are not accurate to more than 5–10°C. Temperature extrapolation may be the only way of estimating a reservoir temperature in wells where the warmed-up well contains an interzonal flow. If the flow is absent during warm-up, these data can be extrapolated.

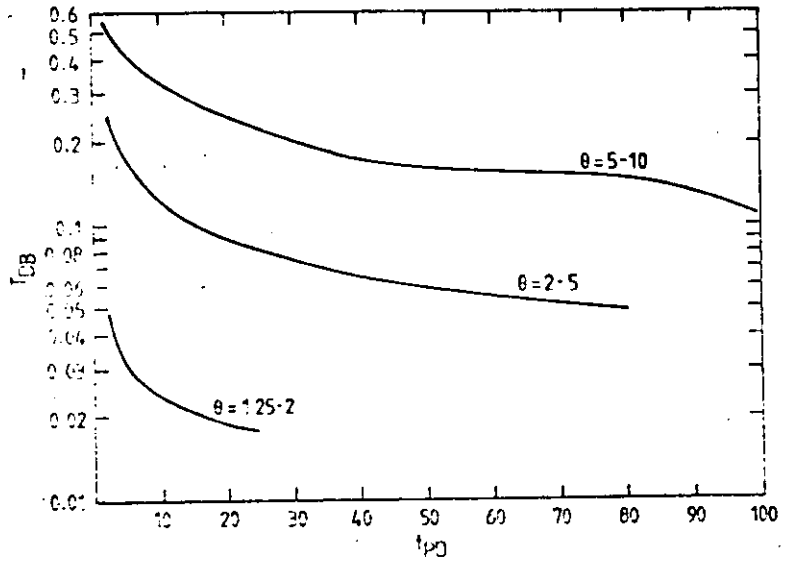

Fig. A1.15. Correction term of Roux *et al.* (1979), for evaluating temperature recovery.

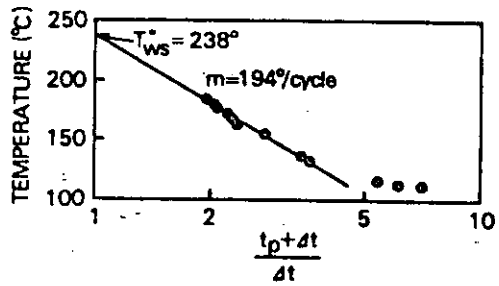

Fig. A1.16. Temperature recovery in well MG-1, Tongonan. (From Menzies, 1981.)

A1.12. CHANGES IN PERMEABILITY

It has been assumed in the discussion so far that the reservoir rock remains constant in its properties and, that all changes are fluid changes. This is not always so. The permeability may change due to fracturing, thermal cracking, thermal expansion or contraction, solid deposition, or dissolution. In each case the changing permeability is monitored by repeat pressure tests. These changes in performance are most commonly associated with injection at high rates or for long times.

A1.12.1. Change with Pressure

Figure A1.17a shows the injection performance of a well from Roosevelt Hot Springs. Wellhead pressure increase is approximately linear with flow rate, up to a critical pressure. Above this, the slope dP/dW decreases. The break in slope is interpreted as the initiation of fracturing. Standard pressure transient analyses cease to be valid above this pressure.

Figure A1.17b shows the stable pressure–flow curve obtained during injection into BR30, Broadlands. The wellhead pressure varies nonlinearly with flow rate. Unlike the previous example, there is no clear parting pressure. Rather, the permeability apparently varies continuously with pressure. Repeat multiple-rate transient tests show that kh is strongly pressure dependent and increases smoothly and rapidly with increasing pressure. There is little change with time or with the temperature of the injected water, and the effect is reversible.

These two examples show permeability changing with pressure—the first a sudden change occurring at a fracturing pressure, and the second a continuous elastic deformation of the reservoir matrix.

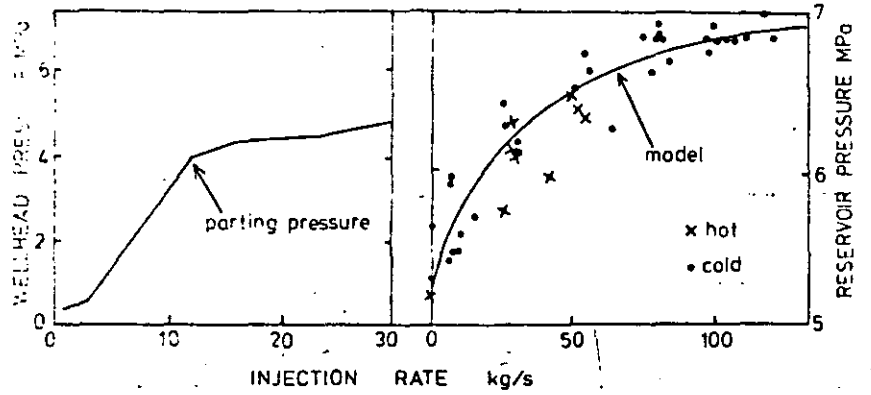

Fig. A1.17. (a) Injection flow rate and wellhead pressure in a well at Roosevelt Hot Springs. (From Allen and Baza, 1980; copyright © SPE-AIME.) (b) Injection flow rate and reservoir pressure in well BR30, Broadlands, and a model based upon pressure transient analyses. (From Ministry of Works and Development, New Zealand, 1981, personal communication.)

A1.12.2. Change with Time

If the injected water is supersaturated with respect to amorphous silica, or any other dissolved component, there may be deposition in the well, at wellface, or in the reservoir (Einarsson *et al.*, 1976; Hayashi *et al.*, 1978). Figure A1.18a shows the decline in performance of an injection well in a liquid-dominated reservoir in California and its restoration by acid treatments. The changing performance of the well was monitored by repeat pressure transient tests (Messer *et al.*, 1978).

More commonly, if the injected water is not supersaturated, injectivity of fractured rock increases with the injecting time (Dobbie and Menzies, [illegible]). Figure A1.18b shows the injectivity measured in a sequence of injection–discharge cycles in well BR23, Broadlands. The injectivity (and productivity) increase during each period of injection and decrease during the period of production. This has been explained as being caused by thermal expansion or contraction accompanied by closing or opening of fractures (A. McNabb, 1980, personal communication.). This example also illustrates another aspect of the same temperature effect. The productivity of the well is found to be less than the injectivity. It was argued above (Sections 5.6 and A1.4) that transmissivity measured with injection tests is that of the hot reservoir fluid. That is, transmissivity or injectivity measured in injection tests is equal to transmissivity or productivity measured in discharge. Often this is so. When it is not so, it is usually the case that injectivity is greater than productivity, despite the lower viscosity of hot water. This implies that the reservoir's permeability is temperature dependent, decreasing with increasing temperature. There is at present no theory describing the variation with temperature of the permeability of fractured rock, but observations such as these indicate that there is sometimes a strong variation.

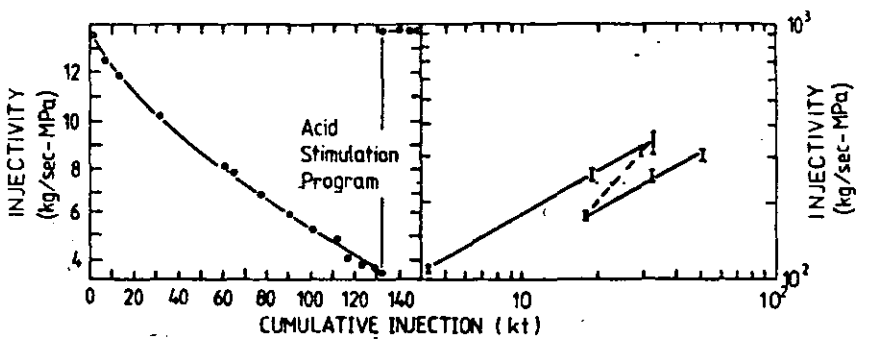

Fig. A1.18. (a) Changes in injection well performance with deposition and acid treatment. (From Messer *et al.*, 1978, copyright © SPE-AIME.) (b) Change of injectivity in BR23 with cumulative injection. Upper line, the first injection series; lower line, second injection series after intervening production. (From Ministry of Works and Development, New Zealand, 1981, personal communication.)

A1.12.3. Stimulation

In the preceding example, injectivity was improved by acid treatment. As with petroleum or groundwater wells, a well with insufficient flow may be improved by stimulation. The available methods are acid treatment and hydraulic fracturing (Howard and Fast, 1970). The latter is more often used.

Geothermal wells in Nigorikawa, Japan, have been stimulated (Katagiri *et al.*, 1980) and the result was an economic success. Two wells at Raft River have been used in stimulation trials. Some improvement was achieved in one and none in the other, but in neither case was the result economic (Republic Geothermal *et al.*, 1980). Similarly, a stimulation trial at Baca improved the ability of a well to flow but did not create a productive well (Verity and Morris, 1981).

Stimulation of geothermal wells is under research at present. To date, it appears that these wells respond to hydraulic fracturing as do any other wells. The major problems are the high flow rates needed in geothermal wells for economic production. At fracturing pressures even a poor well accepts a large amount of fluid, so that very large pumping capacity is required. If additives are used to increase viscosity, these must be able to withstand geothermal temperatures.

CURSO: "INGENIERIA DE YACIMIENTOS GEOTERMICOS"

En colaboración con la OLADE, C.F.E., I.I.E.

del 13 marzo - 18 mayo

TEMA: PRUEBAS DE PRESION

5.- Miller, C.W. y Cols: "Wellbore Effects in the Analysis of two-phase Geothermal Well Tests"

Soc. Pet. Eng. J. (Junio 1982)

309-320

DR. FERNANDO SAMANIEGO

13-23 MARZO 1984

Wellbore Effects in the Analysis of Two-Phase Geothermal Well Tests

Constance W. Miller, Lawrence Berkeley Laboratory
Sally M. Benson, Lawrence Berkeley Laboratory
Michael J. O'Sullivan, Lawrence Berkeley Laboratory
Karsten Pruess, Lawrence Berkeley Laboratory

Abstract

A method of designing and analyzing pressure transient well tests of two-phase (steam/water) reservoirs is given. Wellbore storage is taken into account, and the duration of it is estimated. It is shown that the wellbore flow can dominate the downhole pressure signal completely such that large changes in the downhole pressure that might be expected because of changes in kinematic mobility are not seen. Changes in the flowing enthalpy from the reservoir can interact with the wellbore flow so that a temporary plateau in the downhole transient curve is measured. Application of graphical and nongraphical methods to determine reservoir parameters from drawdown tests is demonstrated.

Introduction

Pressure transient data analysis is the most common method of obtaining estimates of the in-situ reservoir properties and the wellbore condition. Conventional graphical analysis techniques require that, for a constant flowrate well test in an infinite aquifer, a plot of the downhole pressure vs. log time yields a straight line after wellbore storage effects are over. The slope of that line is inversely proportional to the transmissivity (kh/μ) of the reservoir. The extrapolated intercept of this line with the pressure axis at a specified time (1 hour or 1 second depending on the units used) gives the factor $\phi C_t h(r_e^2)$, which is used to calculate the skin value of a well. In this study, the effects of a two-phase steam/water mixture in the reservoir and/or the wellbore on pressure transient data have been investigated.

There have been a number of attempts to extend conventional testing and analysis techniques to two-phase geothermal reservoirs including drawdown analysis by Garg and Pritchett,[1] Garg,[2] Grant,[3] and Moench and Atkinson.[4] Pressure buildup analysis has been investigated by Sorey *et al.*[5] To solve the diffusion equation that governs the pressure change in a two-phase reservoir analytically, it is necessary to make a number of simplifying assumptions. One assumption is that the fluid compressibility in the reservoir is initially uniform and remains uniform throughout the test. With this approach, it can be shown that a straight line on a pressure vs. log time plot will be obtained, the slope being inversely proportional to the total kinematic mobility (k/ν_T).

When conducting a field test it is rarely possible to maintain the uniform saturation distribution in the reservoir required for that type of analysis to be applicable. In addition, the very high compressibility of the two-phase fluid creates wellbore storage of very long duration. Since most of the available instrumentation for hot geothermal wells (>200°C) can withstand geothermal environments for only limited periods, long-duration wellbore storage further complicates data analysis. Thus numerical simulation techniques must be used to study well tests to determine the best method of testing two-phase reservoirs.

This work investigates and defines more thoroughly the well/reservoir system when the reservoir or wellbore is filled with a two-phase fluid. Four examples are considered: (1) a single-phase hot water reservoir connected to a partially two-phase wellbore, (2) a hot water reservoir that becomes two-phase during the test, (3) a two-phase liquid-dominated reservoir, and (4) a two-phase vapor-dominated reservoir. State-of-the-art analysis techniques are applied to pressure transient data after wellbore storage effects have ended. In the first example, a nongraphical method of analysis is discussed, which is applicable at early times when wellbore storage effects still dominate the pressure response.

Note that our analysis has been done for a two-phase homogeneous, nonfractured reservoir. Previous studies of well test methods for two-phase reservoirs[1-5] have been restricted to this case. The purpose of our work is to

0197-7520/82/0006-9922$00.25

determine how transient wellbore flow can alter the well test results and how one could design a well test using these results. Many geothermal reservoirs are predominantly fractured, and a two-phase fractured system can give a very different response from a homogeneous porous reservoir. The study of the reservoir response for a fractured system must be carried out first before the wellbore response can be analyzed—a condition beyond the scope of this paper. However, it can be stated that the transient wellbore flow could mask completely the characteristic response of the fractured medium (as the half-slope expected on a pressure vs. log time plot) just as it is shown to mask changes in a homogeneous two-phase reservoir. This possible transient wellbore interaction with the reservoir response must be considered in the analysis of any pressure transient data.

Approach

To study the pressure transient response of a two-phase geothermal well/reservoir system, a transient wellbore simulator called WELBORE[6] was coupled with a modified version of the reservoir simulator GEOTHNZ.[7] The wellbore model does not assume steady-state flow, in contrast to the numerous wellbore flow models that have been reported in the literature.[8-10] A description of the numerical model is given in Ref. 6 and a brief outline of an earlier version that did not include the slip between the phases is given in Ref. 11. WELBORE solves finite-difference approximations for the following mass, momentum, and energy balance equations.

$$\frac{\partial \rho}{\partial t}+\frac{\partial(\rho v)}{\partial x}=0, \quad \ldots\ldots\ldots\ldots\ldots\ldots\ldots\ldots\ldots\ldots (1)$$

$$\frac{\partial}{\partial t}(\rho v)+\frac{\partial}{\partial x}(S_v\rho_v v_v^2+S_\ell\rho_\ell v_\ell^2)+\rho g+\frac{f\rho v^2}{4r_w}=0, \quad \ldots\ldots\ldots\ldots\ldots\ldots\ldots\ldots\ldots\ldots (2)$$

and

$$\frac{\partial}{\partial t}(\rho E)+\frac{\partial}{\partial x}(S_v\rho_v v_v E_v+S_\ell\rho_\ell v_\ell E_\ell)+p\frac{\partial}{\partial x}(S_v v_v+S_\ell v_\ell)-\frac{u}{2r_w}(T-T_r)=0. \quad \ldots\ldots\ldots (3)$$

The energy equation (Eq. 3) does include kinetic and potential energy. However, the specific energy times the momentum equation has been subtracted out, masking these terms.

The slip between the phases, v_v-v_ℓ, is calculated on the basis of a modified version of that given in Ref. 12. The friction factor is calculated according to Chisholm.[13] For the cases run here, conductive heat loss from the wellbore was ignored ($u=0$).

The version of the program GEOTHNZ used here solves for radial flow only. The equations governing the mass and energy flow in a geothermal reservoir are

$$\frac{\partial}{\partial t}[\phi(S_v\rho_v+S_\ell\rho_\ell)]+\frac{1}{r}\frac{\partial}{\partial r}r(\rho_\ell v_\ell'+\rho_v v_v')=0 \quad \ldots (4)$$

and

$$\frac{\partial}{\partial t}[(1-\phi)\rho_r C_r T+\phi(S_v\rho_v E_v+S_\ell\rho_\ell E_\ell)]+\frac{1}{r}\frac{\partial}{\partial r}r(\rho_\ell H_\ell v_\ell'+\rho_v H_v v_v')=0. \quad \ldots\ldots\ldots\ldots (5)$$

The velocities v_ℓ' and v_v' are calculated with Darcy's law as

$$v_\ell'=-\frac{kk_{r\ell}}{\mu_\ell}\frac{\partial p}{\partial r}, \quad \ldots\ldots\ldots\ldots\ldots\ldots\ldots\ldots\ldots\ldots (6a)$$

$$v_v'=-\frac{kk_{rv}}{\mu_v}\frac{\partial p}{\partial r}. \quad \ldots\ldots\ldots\ldots\ldots\ldots\ldots\ldots\ldots\ldots (6b)$$

For the calculations of the pressure drawdown, the relative permeability functions are assumed to have the form suggested by Corey,[14] where

$$k_{r\ell}=S_\ell^{*4}, \quad \ldots\ldots\ldots\ldots\ldots\ldots\ldots\ldots\ldots\ldots (7a)$$

$$k_{rv}=(1-S_\ell^{*2})(1-S_\ell^{*})^2, \quad \ldots\ldots\ldots\ldots\ldots\ldots\ldots\ldots (7b)$$

and

$$S_\ell^{*}=(S_\ell-S_{\ell r})/(1-S_{\ell r}-S_{vr}), \quad \ldots\ldots\ldots\ldots\ldots\ldots (7c)$$

with $S_{\ell r}=0.3$ and $S_{vr}=0.05$. Finite-difference approximations of Eqs. 4 through 7 are solved assuming that (1) capillary pressure is negligible, (2) fluid and rock are in local thermal equilibrium, and (3) conductive heat transfer is negligible.

In each of the four examples run, the calculations were carried out for a constant rate of mass production at wellhead and for a constant rate of mass production at the sandface (no well transients considered). The pressure transient data was analyzed according to the analysis method given in the following. In addition, the calculated duration of wellbore storage (derivation follows) is verified by comparison with the simulated results.

Design and Analysis of Two-Phase Well Tests

The problem with the analysis of pressure transient data from a two-phase reservoir is that the diffusion equation describing the pressure response in the reservoir is highly nonlinear. When the steam saturation varies in a porous medium, the relative flow of the water and steam phases and the compressibility of the mixture both change. For a two-phase steam/water fluid at 8 MPa, the isenthalpic compressibility is about 5×10^{-7} Pa^{-1} for high liquid saturation, 1×10^{-7} Pa^{-1} for low liquid saturation, but only about 1.3×10^{-9} Pa^{-1} for single-phase compressed liquid at this pressure.

The effective compressibility of a two-phase fluid can be enhanced by a factor of 10 or more in a porous medium because of heat inertia of the rock.[15] Also, the change in the total kinematic viscosity, ν_t, defined as

$$\frac{1}{\nu_t}=\frac{k_{r\ell}}{\nu_\ell}+\frac{k_{rv}}{\nu_v}, \quad \ldots\ldots\ldots\ldots\ldots\ldots\ldots\ldots\ldots\ldots (8)$$

can be large. For relative permeability curves of the Corey type, Eqs. 7a through 7c, and at a pressure of 8 MPa, the total kinematic viscosity varies from 1.3×10^{-7} at $S_v=0$, to 1×10^{-7} at $S_v=0.3$, to 4.6×10^{-7} at $S_v=1$ (using $S_{lr}=0.3$, $S_{vr}=0.05$). At higher pressures the variation can be greater. However, the compressibility and total kinematic viscosity are primarily a function of saturation. Therefore if one can design a test such that the pressure changes occur over a region where the saturation is relatively constant, a reasonable estimate of kh/ν_t may be made.

For a reservoir produced at a constant mass flow rate and assuming small changes in saturation, the pressure response of the system has been shown[2] to be governed by the following linearized diffusion equation.

$$\frac{\partial p}{\partial t}=\frac{(k/\nu_t)}{\phi\rho C_t}\left(\frac{1}{r}\frac{\partial p}{\partial r}+\frac{\partial^2 p}{\partial r^2}\right). \quad \ldots\ldots\ldots\ldots\ldots\ldots(9)$$

When $t>35\phi\rho C_t r_w^{\,2}/(k/\nu_t)$, the solution to this equation is approximated by

$$p_i-p(t)=\frac{w}{4\pi(k/\nu_t)h}\left\{\ln\left[\frac{(k/\nu_t)t}{\phi r_w^{\,2}\rho C_t}\right]+0.809+2s\right\}, \quad \ldots\ldots\ldots\ldots(10)$$

where s is the skin effect. Thus $p(t)$ vs. $\ln t$ will be a straight line, with the slope, m, inversely proportional to the transmissivity of the reservoir:

$$\frac{kh}{\nu_t}=\frac{w}{4\pi m}. \quad \ldots\ldots\ldots\ldots\ldots\ldots\ldots\ldots\ldots\ldots(11)$$

When the skin value, s, is expressed as $\ln(r_w/r_e)$, where r_e is the effective radius of the well, it also can be shown that

$$\phi C_t h r_e^{\,2}=2.24\frac{kh}{\nu_t}e^{+(p_{1s}-p_i)/m}, \quad \ldots\ldots\ldots\ldots(12)$$

where p_{1s} is the pressure at 1 second on the extrapolated semilog straight line given by Eq. 10. (Note that p_{1s} is used here instead of p_{1hr} because slope m is expressed in metric units.)

The linearization of the nonlinear diffusion equation to give Eq. 9 depends on the assumption that the variations in (k/ν_t), in ρ_t and in C_t are small. As stated earlier, these quantities have large variations when the steam saturation changes. When the mass flow rate from the reservoir is increased, the saturation around the bore changes if the fluid is two-phase. However, after a certain amount of time, depending on the initial saturation around the well, the in-place saturation will steady out. It is possible to treat the initial change in steam saturation in the same manner as wellbore storage is treated; i.e., one needs to determine the duration for which these variations persist and to make sure that all the data analysis is performed after the changes no longer affect the data. In the case where such changes do not take place until long after the test has begun, pressure data taken before these changes occur can be analyzed. The problem is to determine at what times $\partial S_v/\partial r\approx0$. Then Eq. 10 can be applied and, from the slope of the straight line on the p vs. log (t) plot, kh/ν_t can be determined

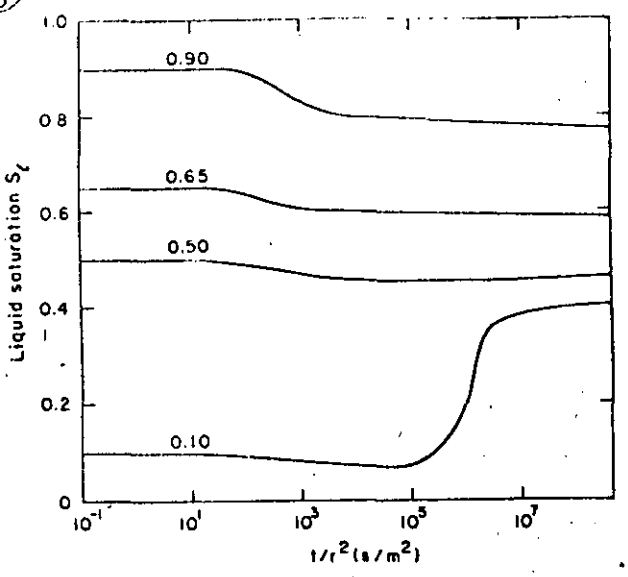

Fig. 1—Liquid saturation response for constant mass production from the reservoir. (Curves are labeled with initial liquid saturations.[16])

(Eq. 11). However, when large saturation changes have occurred during the test, the interpretation of Eq. 12 to give the skin of the well loses its meaning because C_t is a strong function of S and has changed. Therefore, Eq. 12 is valid only for liquid reservoirs.

Using the similarity variable, $\eta=r/\sqrt{t}$, it has been shown[5,16] that

$$\lim_{\eta\to0} H_f/d\eta=0, \quad \ldots\ldots\ldots\ldots\ldots\ldots\ldots\ldots(13)$$

where

$$H_f=\frac{k_{rl}H_l/\nu_l+k_{rv}H_v/\nu_v}{k_{rl}/\nu_l+k_{rv}/\nu_v}. \quad \ldots\ldots\ldots\ldots\ldots(14)$$

This implies that at late times the in-place saturation will approach a constant value because the flowing enthalpy is primarily a function of the relative permeability curves that are in turn a function of S_v. No rigorous derivation has been done to determine when H_f can be assumed constant. However, O'Sullivan[16] calculated S_v as a function of t/r^2 for a number of cases. An example of one of his calculations is given in Fig. 1, where the liquid saturation is plotted as a function of η. For this case, $\phi=0.2$, $k=1\times10^{-13}$ m^2, $p_i=8.6$ MPa, $w=0.14$ kg/s, $\rho_r=2650$ kg/m^3, and $C_r=1.0$ kJ/kg·K. The compressibility of the rock was ignored. For $S_v<0.5$ (or $S_l>0.5$; liquid saturation is plotted in the figure), the saturation changes are complete when $t/r^2\approx10^3$. For high vapor saturations, the changes in saturation do not start until $t/r^2=10^5$ and are not complete until $t/r^2=10^7$. A similar plot was obtained by O'Sullivan for the case where $p_i=3.0$ MPa, $k=2.4\times10^{-13}$ m^2, and the other parameters are approximately the same as above.

It is possible to estimate when S_v will be approximately constant by using the example plotted in Fig. 1. The parameter t/r^2 scales approximately as $k/\phi\nu_t\rho C_t$. However, ρC_t is primarily a function of S_v, and this

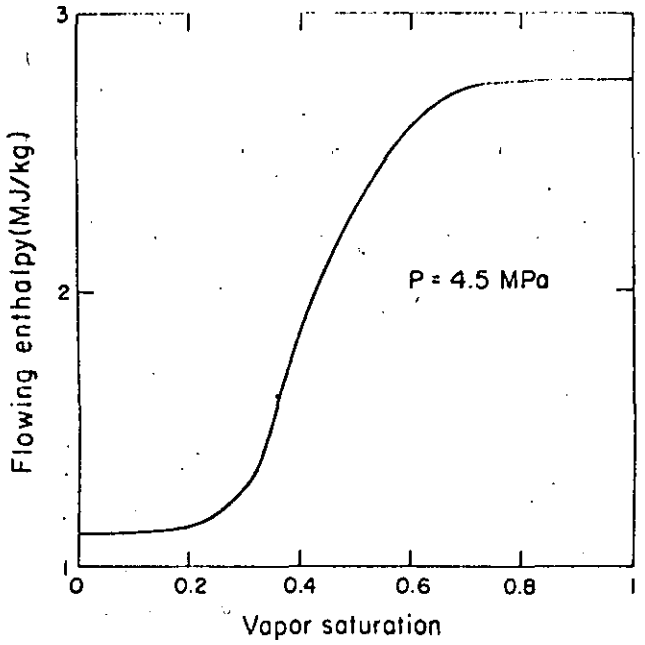

Fig. 2—Enthalpy flowing out of reservoir vs. vapor saturation for Corey-type relative permeability curves with $S_{lr}=0.3$ and $S_{vr}=0.05$.

variation is already taken into account in the solution. The parameter ν_t is a function of the relative permeability curves used and the pressure. Corey relative permeability curves were used in this calculation. Therefore, assuming that these relative permeability curves approximately describe the steam/water flow, it is possible to assume that one obtains the time when $H_f=$ constant by using Fig. 1 and scaling t/r^2 by k/ϕ. Because kh will not be known until after the pressure analysis is done, one must estimate h and, calculating k, check to ensure that the analysis was done for the time when $\partial S_v/\partial r=0$. For a well of radius 0.09 m, a $k/\phi=5\times10^{-13}$ m^2, and a reservoir pressure of 8 MPa, the changes in enthalpy were complete at about 10 seconds for $S_v<0.5$, while for $S_v=0.9$ the changes occurred from 10^3 to 10^5 seconds. For $k/\phi<5\times10^{-13}$, the time of these changes will be longer, and for $k/\phi>5\times10^{-13}$ m^2, the changes will be shorter. Wellbore storage effects, though, can be greater or less than this time for $\partial S_v/\partial r=0$ to hold true.

One method of testing a geothermal reservoir is first to flow the well at a slow steady rate until the saturation around the bore is approximately constant. The initial flowing of the well must be long enough so that pressure changes in the reservoir that occur during the test will penetrate only the region where the enthalpy is approximately constant. Pritchett[17] has defined a radius of investigation as $2\sqrt{Dt}$ where $D=k/\phi C_t\rho\nu_t$. The flow then should be increased (or decreased) to a second constant value. By having the well flowing for a time before the test is begun, it is possible to decrease both the effect of temperature changes in the well during the test and the oscillations that occur when a well is initially opened, and to ensure that $\partial S_v/\partial r\approx0$ around the bore. Now it is possible to perform a buildup test where the well is completely shut-in. However, as pointed out by Sorey *et al.*,[5] the region around the bore becomes saturated with liquid so S_v around the well will not be uniform, and a question arises as to how such data should be analyzed.

The state-of-the-art analysis technique for two-phase well tests has been reviewed by Pritchett.[17] He suggests that a drawdown, a buildup, and an injection test are needed. From the drawdown test the slope of the straight line on the plot of p vs. $\log(t)$ is measured, and from the buildup test the slope of the straight line on the p vs. $\log[(t+\Delta t/\Delta t)]$ is determined. The transmissivity of the reservoir is calculated from the average of these two slopes in Eq. 11 for m. The total kinematic viscosity depends on the saturation around the bore. Pritchett does not give a method of determining the saturation. Instead he suggests that kh be measured independently by an injection test. Then, given kh, the relative permeabilities can be determined from the flowing enthalpy by

$$k_{rl}=\frac{H_v-H_f}{H_v-H_l}\frac{w\nu_l}{4\pi m}\frac{1}{kh} \quad \ldots\ldots\ldots\ldots\ldots\ldots (15a)$$

and

$$k_{rv}=\frac{H_f-H_l}{H_v-H_l}\frac{w\nu_v}{4\pi m}\frac{1}{kh}. \quad \ldots\ldots\ldots\ldots\ldots\ldots (15b)$$

We find several difficulties with this approach. First, many times it is neither possible nor desirable to run an injection test. Secondly, a straight line may be seen on the semilog plot while wellbore storage is still important. For a well 2000 m deep with a radius of 0.09 m, $kh=6\times10^{-12}$ m^3, and with two-phase flow throughout the well, wellbore storage can last on the order of 5 hours. Lastly, the duration of wellbore storage may be orders of magnitude different between a buildup and a drawdown because, in a buildup, the fluid in the well separates out into a liquid and gas phase. The compressibility of a two-phase mixture is usually larger than the compressibility of each phase separately.

Assuming that an injection test cannot be done, the following testing and analysis technique was used in the examples. A drawdown test was simulated in all cases because it is possible to establish a region where $\partial S_v/\partial r\approx0$ around the bore. Both the downhole pressure and the flowing enthalpy must be measured as a function of time. The downhole pressure is plotted as a function of $\log(t)$, and the transmissivity of the reservoir is determined from the slope of the straight line that is plotted on that graph. Given the value of kh/ν_t, the duration of wellbore storage is calculated to determine whether the data used in the analysis were affected by wellbore storage. An estimate of wellbore storage is given in the following. Once the proper kh/ν_t has been found, kh will be determined by calculating ν_t.

The crucial assumption made in this part of the analysis is that we know the relative permeabilities as a function of S_v. The flowing enthalpy permits us to determine the ratio of relative permeabilities for water and steam:

$$\frac{k_{rl}}{k_{rv}}=\frac{\nu_l(H_v-H_f)}{\nu_v(H_f-H_v)}. \quad \ldots\ldots\ldots\ldots\ldots\ldots (16)$$

In writing Eq. 16 it was assumed that $k_{rv} \neq 0$. If the pressure is known, ρ_f, H_f, ρ_s, and H_s will be known. If k_{rl} and k_{rv} are given as a function of S_v, then, knowing H_f, the saturation can be determined. Fig. 2 is a plot of H_f vs. S_v for $p = 4.5$ MPa using k_{rl} and k_{rv} as given by Eqs. 7a through 7c. Since k_{rl} and k_{rv} are known, ν_t can be calculated as well as the absolute permeability thickness, kh.

If the relative permeability functions are not known, two lower estimates can be made for kh. Using Eqs. 15a and 15b, khk_{rl} and khk_{rv} can be computed, both of which will be smaller than kh. However, usually not both k_{rl} and k_{rv} will be much less than one, so the larger of the two quantities khk_{rl} and khk_{rv} will provide an estimate for kh.

For all the cases calculated here, the Corey relative permeability curves were used. In the third example the effect of using other relative permeability curves was investigated. It is recognized that relative permeability curves for steam/water mixtures are not well known. It also is recognized that they may be dependent on the rock type in which a geothermal resource occurs. Our point is that if these relative permeability curves were better known, a plausible methodology for obtaining the in-situ reservoir parameters would be available. It is stressed that more work is necessary to obtain these curves.

Duration of Wellbore Storage

As stated earlier, wellbore storage phenomena in two-phase geothermal well/reservoir systems can last for several hours. The duration of wellbore storage is proportional to both $\rho(\partial\rho/\partial p)_H$ and $(kh/\nu_t)^{-1}$. Because the transmissivity of geothermal reservoirs is usually greater than the transmissivity of oil/gas formations, wellbore storage in liquid-filled reservoirs tends to be shorter than in hydrocarbon reservoirs. However, for two-phase geothermal reservoirs, the compressibility effects of the steam/water mixture in the wellbore are an order of magnitude larger than oil and gas systems because of phase transition effects. In addition, wellbore storage calculations in the petroleum literature neglect energy changes in the well. We define both an isenthalpic and an isobaric wellbore storage term. The wellbore storage phenomenon persists until both of these wellbore storage contributions have become negligibly small.

Wellbore storage is complete when the sandface flow rate is approximately equal to the surface flow rate. For an isothermal well, Ramey[18] determined that when $t_D > 60\,C_D$, the effects of wellbore storage can be neglected. We assume a similar formulation to estimate the isenthalpic wellbore storage time by defining an average isenthalpic compressibility in the wellbore. The isobaric wellbore storage term is determined by calculating when energy changes in the well are over. Heat loss out of the bore is ignored although it can be important.

For a change in mass flow rate at wellhead, the sandface mass flow rate can be calculated by the continuity equation and by integrating it over the length of the well.

$$\int_0^L \frac{\partial \rho}{\partial t} dx = -\int_0^L \frac{\partial}{\partial x}(\rho v) dx = \frac{-w_s + w_{sf}}{A} \quad \ldots\ldots\ldots (17)$$

or

$$w_{sf} = w_s + A\int_0^L \frac{\partial \rho}{\partial t} dx. \quad \ldots\ldots\ldots (18)$$

Changes in density in the well are a function of pressure and energy. If $\partial\rho/\partial t$ is rewritten in terms of p and E, Eq. 18 is written as

$$w_{sf} = w_s + A\int_0^L \rho C_E \frac{\partial p}{\partial t} dx + A\int_0^L \rho\beta \frac{\partial E}{\partial t}\, dx, \quad \ldots\ldots (19)$$

where $C_E = 1/\rho(\partial\rho/\partial p)_E$ and $\beta = 1/\rho(\partial\rho/\partial E)_p$. The durations of energy and pressure changes are estimated separately.

The difference in wellhead and the downhole mass flowrate caused by pressure changes only is

$$w_{sf} = w_s + A\int_0^L \rho C_E \frac{dp}{dt} dx, \quad \ldots\ldots\ldots (20)$$

where C_E and p are functions of x. However, as wellbore storage dies out, dp/dt will be a very weak function of x, and it is possible to rewrite Eq. 20 as

$$w_{sf} = w_s + \frac{dp}{dt} A\int_0^L \rho C_E dx. \quad \ldots\ldots\ldots (21)$$

If the wellbore storage coefficient is defined as

$$\bar{C} = \frac{1}{L}\int_0^L \rho C_E dx = \frac{1}{L}\int_0^L \left(\frac{\partial \rho}{\partial p}\right)_E dx, \quad \ldots\ldots\ldots (22)$$

Eq. 21 can be written (as in the petroleum literature)

$$w_{sf} = w_s + V\bar{C}\frac{dp}{dt}. \quad \ldots\ldots\ldots (23)$$

Defining

$$C_D = \frac{V\bar{C}}{\rho_{sf} 2\pi\phi C_t h r_w^{\,2}}$$

and

$$t_D = \frac{kt}{\rho_{sf}\phi C_t \nu_t r_w^{\,2}},$$

and assuming that the effects of wellbore storage on the downhole pressure changes will be complete when $t_D > 60\,C_D$, then

$$t_H = 60\frac{V\bar{C}}{(2\pi)kh/\nu_t}. \quad \ldots\ldots\ldots (24)$$

The factor kh/ν_t is measured directly from the slope of the p vs. $\log(t)$ plot and, given the steady-state initial conditions in the well, the average value of $(\partial\rho/\partial p)_E$ in it can be determined. Note it is $(\partial\rho/\partial p)_E$ and not

TABLE 1—INITIAL AND DOWNHOLE CONDITIONS AFTER 24 HOURS OF PRODUCTION FOR THE FOUR EXAMPLES

	Example			
	1	2	3	4
p_i, MPa	12.70	11.1	10.0	10.0
p_{24}, MPa	12.34	10.74	8.94	9.26
h_i, MJ/kg	1.400	1.400	1.433	1.700
$(H_t)_{24}$, MJ/kg	1.400	1.400	1.566	2.736
$(S_v)_i$	0	0	0.19	0.78
$(S_v)_{24}$	0	0	0.29	0.70 to 0.82
$(w_s)_i$, kg/s	5	5	5	5
$(w_s)_f$, kg/s	30	30	15	15

$(\partial\rho/\partial p)_E/\rho$ which is averaged in the bore.

There may be some question as to whether one should use $(\partial\rho/\partial p)_E$ or $(\partial\rho/\partial p)_H$ or something else. Garg and Pritchett[1] have shown that $(\partial\rho/\partial p)_E/\rho$ and $(\partial\rho/\partial p)_H/\rho$ can vary by a factor of two at high pressure when the fluid is compressed liquid. However, in the two-phase region no large variations occur, in contrast to what one might expect. It is possible to show that

$$\left(\frac{\partial\rho}{\partial p}\right)_H = \frac{(\partial\rho/\partial p)_E - \frac{1}{\rho}(\partial\rho/\partial E)_p}{1-\frac{p}{\rho}\frac{1}{\rho}\left(\frac{\partial\rho}{\partial E}\right)_p} \quad \ldots\ldots\ldots(25)$$

In the two-phase region $(\partial\rho/\partial p)_E$ is much larger than$[(\partial\rho/\partial E)_p/\rho]$, while in the compressed liquid region these terms are more comparable. Therefore, as an estimate for two-phase wellbore storage, one can use either $(\partial\rho/\partial p)_E$ or $(\partial\rho/\partial p)_H$.

For the changes caused by energy increases or decreases in the well, the continuity equation is

$$w_{sf} = w_s + A\int_0^L \rho\beta\frac{dE}{dt}dx. \quad \ldots\ldots\ldots(26)$$

Wellbore storage caused by energy changes will be complete when $dE/dt \approx 0$. If the heat loss out of the bore is ignored,

$$\rho\frac{\partial E}{\partial t} \approx \rho v\frac{\partial H}{\partial x}. \quad \ldots\ldots\ldots(27)$$

As long as there is a significant change in the flowing enthalpy from the reservoir, wellbore storage effects will persist. However, once H_f is approximately constant, the additional time for the energy changes in the well to steady out is the time for a particle to travel through the wellbore, or L/v_{ave}. This average velocity is defined as

$$v_{ave} = \frac{\int_0^L \rho v\,dx}{\int_0^L \rho\,dx} = \frac{\overline{\rho v}}{\bar{\rho}}. \quad \ldots\ldots\ldots(28)$$

If $\rho v \approx w_s/A$, $v_{ave} \approx w_s/A\bar{\rho}$. However, if ρv is still varying in the well, a more conservative estimate would be to use w_{sf}/A for ρv.

Wellbore storage effects will persist until $t > 60\,V\bar{C}/2\pi(kh/\nu_t)$ or until $t > L/v_{ave}$ after the flowing enthalpy is constant from the reservoir, whichever is greater. In all the following analyses, a check is done to determine whether wellbore storage is over.

Example

To consider the effects of the wellbore flow on the testing of geothermal reservoirs and to consider methods of determining the permeability of such reservoirs, four different examples were considered. (See Table 1 for the initial conditions.) For all the cases run, $k = 3\times10^{-14}$ m^2, $h = 80$ m, $\phi = 0.15$, $C_r = 1.0$ kJ/kg·K, and $\rho_r = 2000$ kg/m^3. The viscosities of the liquid and steam phases were calculated with

$$\mu_l = 2.414\times10^{-5}\left[10^{247.8/(T+133.15)}\right] \text{Pa·s}$$

and

$$\mu_v = (9+0.035T)\times10^{-6}\,\text{Pa·s},$$

respectively.[7]

A drawdown pressure transient test was simulated by first flowing the well/reservoir system for 24 hours at 5 kg/s. (The flowing enthalpy, pressure, and vapor saturations at the sandface after this initial 24 hours also are given in Table 1.) Subsequently the flow rate was increased from 5 to 30 kg/s in the first two examples and from 5 to 15 kg/s in Examples 3 and 4. The drawdown test then was run up to 10 hours. Both a constant flow rate at wellhead and a constant flow rate at the sandface were considered. When the well flow was included, the well was assumed 2000 m deep with a radius of 0.09 m. Both skin effects and heat loss from the wellbore were

TABLE 2—ANALYSIS OF PRESSURE TRANSIENT DATA FOR THE EXAMPLES

	Example					
	1	2a	2b	3a	3b	4
$\rho\bar{C}_h$, s^2/m^2	1.3×10^{-4}	1.1×10^{-4}	1.1×10^{-4}	6.0×10^{-5}	6.0×10^{-5}	8.0×10^{-6}
m, MPa·s	0.10	0.49	0.40	1.70	0.47	0.13
kh/ν_t, milliseconds	2.0×10^{-5}	4.1×10^{-6}	5.0×10^{-6}	4.7×10^{-7}	1.7×10^{-6}	6.0×10^{-6}
t_H, seconds	3200	12 000	11 000	62 000	17 000	650
H_F, MJ/kg	1.40	1.39	1.41	2.03	2.06	2.75
p_{dh}, MPa	10.8	9.3	7.8	6.7	4.5	8.0
S_v	0	0.18	0.26	0.40	0.42	0.7 to 1.0
khk_{rl}, m^3	—	—	1.0×10^{-12}	—	5.6×10^{-13}	4.2×10^{-15}
khk_{rv}, m^3	—	—	1.7×10^{-13}	—	7.7×10^{-13}	2.7×10^{-12}
t_p, seconds	0 to 3600	—	—	—	0 to 3600	2×10^3 to 2×10^5
ν_t, m^2/s^2	1.3×10^{-7}	3.0×10^{-7}	5.6×10^{-7}	1.3×10^{-6}	1.7×10^{-6}	4.9×10^{-7}
kh, m^3	2.6×10^{-12}	1.2×10^{-12}	2.8×10^{-12}	6×10^{-13}	2.9×10^{-12}	2.9×10^{-12}

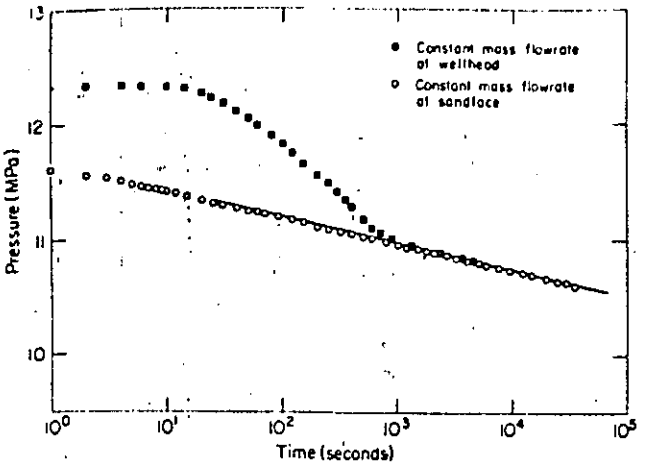

Fig. 3—Pressure drawdown curve for hot water reservoir with flashing in the wellbore.

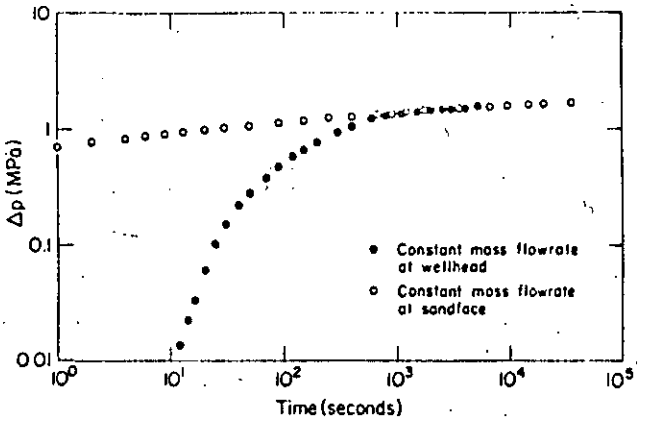

Fig. 4—Log-log plot of pressure drawdown curve for hot water reservoir with flashing in the wellbore.

ignored, although they both can influence well test transient data.

For all the examples, the following method of analysis was applied. Table 2 is a summary of the calculations presented in the following. First the average value of the compressibility density term, ρC_E, was computed at the flowing conditions in the well before the flow rate was increased. Then a straight-line segment on the plot of p_{dh} vs. log(t) was chosen. The regions chosen for analysis are indicated in the figures (Fig. 3 for Example 1, Fig. 6 for Example 2, Fig. 8 for Example 3, and Fig. 10 for Example 4) for each example. Note that two analyses were done for both Examples 2 and 3 to illustrate the error in kh if the wrong straight line is chosen.

Given the measured slope of the straight line, the transmissivity, kh/ν_f and, in turn, the duration of the isenthalpic wellbore storage effect (using Eq. 24 and designated by t_H in Table 2) were calculated. The duration of wellbore storage because of energy changes during the test is best determined by monitoring the flowing enthalpy. However, a very rough estimate can be made by assuming that it persists for a time equal to L/v_{ave} after the enthalpy from the reservoir is constant. A rough estimate of the time when these energy changes are important is given in the table and designated t_p. If the straight-line segment chosen occurs while wellbore storage was still important, the calculation of kh/ν_f should be repeated using the correct line segment.

Now, given the flowing enthalpy, H_f, and downhole pressure at some point along the straight-line segment (given in Table 2), and assuming Cory relative permeability curves when the fluid is two-phase in the reservoir, the vapor saturation around the bore was calculated (Eqs. 7a through 7c, and Eq. 16). Given this S_v, the total kinematic viscosity, ν_f, was computed and, in turn, kh was determined. The computed values for kh were compared with the kh of 2.4×10^{-12} m^3 used in the actual simulation (see Table 2).

Hot Water Reservoir

The first example is a hot water reservoir, where the fluid flashes in the bore during the well test. The downhole transient pressure after the increase in mass flow rate to 30 kg/s is given in Fig. 3. Results for both the constant flow rate at wellhead and at the sandface are plotted. The calculation for kh gave 2.6×10^{-12} m^3 and the isenthalpic wellbore storage lasted 3.2×10^3 seconds (54 minutes). The calculation for the time until energy changes can be neglected is the time for a fluid particle to travel through the bore. Because the fluid flowing from the reservoir remains single phase, the flowing enthalpy at the sandface is constant. In the pressure drawdown simulation, when the flow rate was increased, the wellhead enthalpy decreased initially and then increased back to the initial flowing enthalpy. A conservative estimate for the time is $v\bar{\rho}/(w_{sf})_i$ or 60 minutes in this case ($\bar{\rho}\approx400$ kg/m^3).

Because the analysis for kh was done after the end of wellbore storage, excellent agreement was obtained between the calculated kh (2.6×10^{-12} m^3) and the actual kh (2.4×10^{-12} m^3) used in the simulation.

For this example, it is also possible to calculate $\phi C_t h r_e^2$ because the fluid remains single phase in the reservoir so C_t is not changing drastically during the test. Using the intercept of the straight-line segment with $t=1$ second, $\phi C_t h r_e^2$ was computed as 1×10^{-10} m^3/Pa. The value used for the simulation was 1.45×10^{-10} m^3/Pa. The difference between these numbers occurs because the finite grid used around the wellbore introduces a slight skin effect.

In many cases, because of high flow rate and high temperatures in a geothermal well, it is difficult to keep tools downhole for extended periods of time. Many tests cannot be run for even 1 hour, and, as we see from this case, wellbore storage is not over until 1 hour. To obtain a good estimate of kh, the test would have to be run at least 10 hours. Data from a shorter test can be analyzed only if proper allowance is made for the change of sandface flow rate with time.

If the fluid in the reservoir remains single phase as in this example, the reservoir parameters, kh/μ and $\phi C_t h r_e^2$, can be calculated even when the sandface flow rate is varying, as long as this flow rate is known. It is possible to solve for this sandface flow rate if both the wellhead flow rate and the downhole pressure are measured. However, a transient wellbore simulator must be used for this calculation. It is not possible to use some

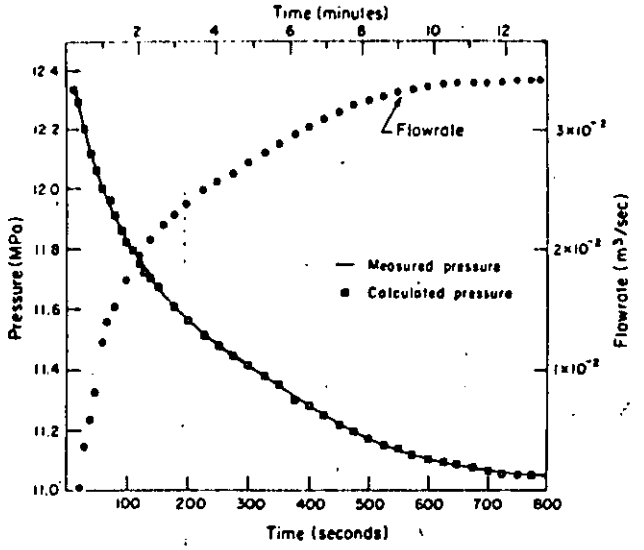

Fig. 5—Sandface flow rate and pressure drawdown for hot water reservoir example. Calculated pressure match using ANALYZE is plotted also.

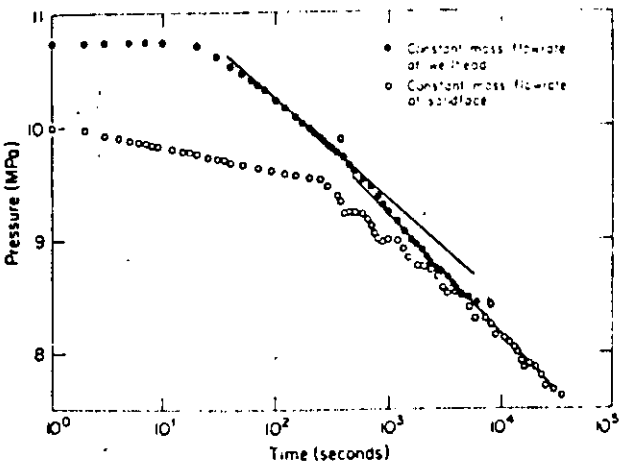

Fig. 6—Pressure drawdown curve for hot water reservoir which flashes during test.

average compressibility in the well and then compute the mass exiting the bore as $\rho C(dp_{dh}/dt)$. No one pressure measurement is characteristic of the average pressure change in the bore. If the transient pressure change in the bore were independent of position, the initial slope of a $\log\Delta p$ vs. $\log(t)$ plot would be unity, as derived in the petroleum literature. Fig. 4 plots $\log\Delta p$ vs. $\log(t)$ for this first case. We see that the initial slope of the plot is greater than one, indicating that the transient pressure changes in the bore are a function of position. The change in pressure made at wellhead takes about 20 seconds to arrive downhole, after which the downhole pressure rises abruptly. (More detailed discussion of this phenomenon is given in Ref. 11.) The pressure response approaches the downhole pressure change expected when dp/dt is not a function of position. The average compressibility of the fluid in the well also is changing during the test. Therefore a transient wellbore flow model must be used to obtain the sandface flow rate.

Using the simulator WELBORE,* the actual sandface flow rate can be calculated. Wellbore effects can be eliminated, allowing reservoir properties to be determined from a variable rate analysis technique. We have done this with a computer program called ANALYZE.*[18] This program performs history matching for pressure transient data of a system of wells in a Theis-type reservoir. It uses a least-squares technique to minimize the difference between a set of measured pressure points and a set of calculated pressure points. The calculated pressure points are generated by varying the transmissivity (kh/μ) and the skin (r_e).

The program is designed for analysis of interference and production tests in single-phase, fluid-saturated hydrothermal reservoirs. It is used to analyze data from just one production well in this case. Given the sandface flow rate for the first 15 minutes (calculated with the wellbore simulator), the sandface flow and the downhole pressure were input to the program. Fig. 5 shows both the actual sandface flow rate and the downhole pressure as a function of time. Included on the figure are the calculated pressures after a best fit was obtained. The best fit gave a $kh/\mu = 2.8\times10^{-8}$ m³/Pa·s and a $\phi C_t h r_e^2 = 7\times10^{-9}$ m³/Pa. (Again, the values used in the simulation were 2.4×10^{-8} m³/Pa·s and 1.45×10^{-9} m³/Pa.) This latter quantity is a good fit considering that it is very sensitive to errors. The result for kh/μ is quite accurate. Note that the pressure data for this first 15 minutes would be useless without a technique for evaluating time-dependent sandface flow due to wellbore storage, because wellbore storage is not over for 60 minutes. The pressure data from 10^2 to 10^3 seconds plots as a fairly straight line. If no data were taken afterward, the subsequent change in slope would not be noticed. If these data were analyzed incorrectly assuming constant sandface flow rate, the kh/μ value obtained would be only 6.5×10^{-9} m³/Pa·s. The value for $\phi C_t h r_e^2$ would be several orders of magnitude off, on the order of 1.4×10^{-7}. Because of the current limit on the time for keeping a tool downhole in a geothermal field, a method for evaluating time-dependent sandface flow rates is of great practical value because it allows good estimates of kh/μ and $\phi C_t h r_e^2$ to be made from short tests.

Hot Water Reservoir With Flashing

In the second example, the initial reservoir pressure was lowered somewhat so that flashing around the well would occur during the well test. The pressure drawdown in this case is given for a constant sandface flow rate and a constant wellhead flow rate in Fig. 6. For the former case, the pressure drawdown follows the single-phase case until the first grid block starts to flash (at about 150 seconds). At 250 seconds, the next block flashes, and the pressure begins to drop at a faster rate because of the decrease in the total kinematic mobility. Small oscillations about the average of drawdown curve occur because of finite space discretization. This is a well-known effect that can be diminished by using a finer grid.

The second case (constant wellhead flow rate) given in

*Available from Natl. Energy Software Center, Argonne, Ill.

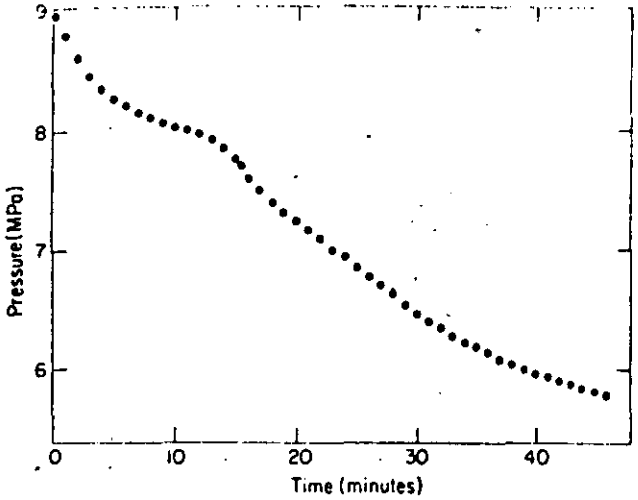

Fig. 7—Linear plot of pressure drawdown curve for liquid-dominated two-phase reservoir.

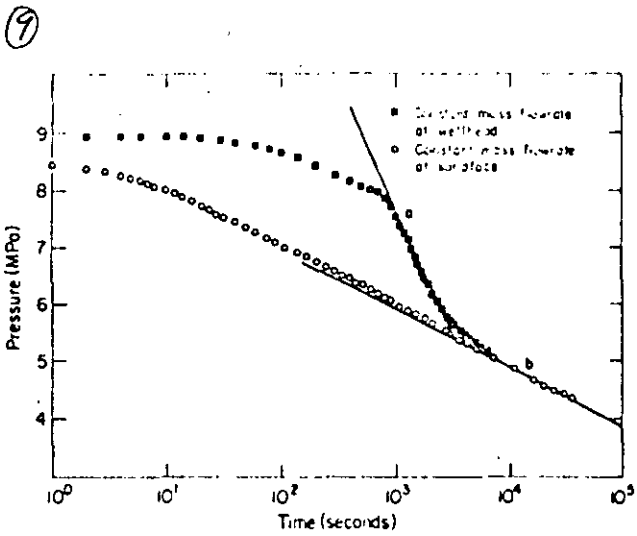

Fig. 8—Semilog plot of pressure drawdown for liquid-dominated two-phase reservoir.

the figure shows that the downhole pressure does not start to drop until after 20 seconds. (The propagation of a disturbance through the compressible two-phase mixture in the wellbore is slow.) For this particular case, a straight line is obtained from 10^2 to 10^4 seconds, and the change in slope of the drawdown curve when the reservoir begins to flash is masked completely. Also, the oscillations that occurred in the calculation with constant sandface flow rate are damped out by the well. (The same grid was used in both cases.) It is not possible to rely on changes in the downhole pressure to predict when flashing begins in the reservoir during a test. Measurements of the flowing enthalpy and downhole pressure are needed to detect flashing in the bore.

For this example, it is very important to determine the duration of wellbore storage. One might be tempted to use the slope of the line from 10^2 to 10^4 seconds (Line "a" in Fig. 6). Although the calculated value of kh/ν_t might not be far off, the determination of kh would be inaccurate, as seen in Table 2.

The flowing enthalpy needed to determine ν_t varies considerably when the fluid first starts to flash in the reservoir. If the test was run for only 1 hour, the calculation for kh gives 1.2×10^{-12} m^3, only half of the actual value used in the simulation. The second analysis for kh in this example given (Line "b" in Fig. 6) in the table shows that a more reasonable value of kh is obtained (2.8×10^{-12} m^3) when the analysis is done after wellbore storage is complete (1.1×10^4 seconds). The calculations for khk_{rl} and khk_{rv} give the lower estimate on kh.

A check must be done to ensure that the energy changes in the bore are negligible. However, because flashing in the reservoir can occur at any time during the test in this case, the best method is to monitor the wellhead enthalpy until it steadies out. No estimate was made for this time for this example.

Liquid-Dominated Two-Phase Reservoir

The third example is a liquid-dominated two-phase reservoir. Before the initial 24 hours' drawdown, the initial steam saturation was 0.19. After the 24 hours, the average saturation around the bore out to approximately 10 m is 0.29. When the flow rate is increased to 15 kg/s, the vapor saturation increases to about 0.4. It is evident from the test that it would be difficult to determine the in-place vapor saturation because the testing itself changes the saturation conditions in the reservoir.

When the flow from the reservoir is increased, the enthalpy from the reservoir increases. However, there is usually a slight delay, depending on the conditions in the reservoir. Therefore, the downhole pressure begins to drop, while the enthalpy of the fluid entering the well remains fairly constant. The sandface flow rate is increasing slowly. However, once the flowing enthalpy begins to increase, the interaction of this flow with the wellbore fluid flow produces a very interesting phenomenon, shown in Fig. 7. The pressure drops until the enthalpy flowing into the well begins to increase. At this point, because the energy in the bore is increasing, the amount of mass that can be taken from the bore increases. Because less mass must come from the reservoir to keep a constant mass at wellhead, the downhole pressure stops dropping and remains on a plateau until the flowing enthalpy from the reservoir steadies out. Subsequently, more fluid must come from the reservoir, so downhole pressure begins to drop again. However, wellbore storage is not necessarily complete because only the energy changes are negligible. It is still necessary to calculate the isenthalpic wellbore storage term.

Again, two analyses were performed for this example, as given in Table 2. In one case, the analysis was done for the time period from 1×10^3 to 3×10^3 seconds (Line "a" in Fig. 8). However, wellbore storage was estimated to last at least 6.2×10^4 seconds with this analysis. The calculated kh gave a very low value (6×10^{-13} m^3). When the second analysis (Line "b" in Fig. 8) was done at the later times, the calculation for kh was closer (2.9×10^{-12} m^3) to that actually used.

The analysis shown in Table 2 was performed with Corey relative permeability curves. The calculation for kh with alternate relative permeability curves also was done for this example. Table 3 summarizes the calculation for the Corey-relative permeability curves with two different irreducible liquid saturations, the straight-line relative permeability curves ($k_{rl}=1-S_v$, $k_{rl}+k_{rv}=1$),

TABLE 3—ANALYSIS OF PRESSURE TRANSIENT DATA FOR CASE 3 USING DIFFERENT RELATIVE PERMEABILITY CURVES

	Cory ($S_{rl}=0.3$)	Cory ($S_{rl}=0.7$)	Straight Line	Grants	Corey and Brooks
S_v	0.42	0.19	0.89	0.53	0.236
k_{rl}	0.034	0.033	0.11	0.12	0.01
k_{rv}	0.26	0.270	0.89	0.88	0.12
$1/\nu_t$	5.9×10^{5}	5.9×10^{5}	1.9×10^{6}	2.0×10^{6}	2.2×10^{5}
kh	2.9×10^{-12}	2.9×10^{-12}	8.75×10^{-13}	3.5×10^{-13}	7.5×10^{-12}

Grant's curves[20] ($k_{rl}=S^{*4}$, where S^* is given by Eq. 7c, $k_{rl}+k_{rv}=1$), and the extrapolated curves[21] of Counsil and Ramey[22] ($k_{rl}=1-S_v/0.3$ for $S_v\le0.3$, otherwise $k_{rl}=0$, $k_{rv}=(S_v-0.2)/0.8$ for $S_v>0.2$, $k_{rv}=0$ for $S_v\le0.2$). We see that different values of the irreducible liquid saturation with the Corey curves do not affect the analysis. Also, both the straight-line permeability curves and Grant's curves give similar results for this case. However, there is a very large difference in the calculation for kh when the different relative permeability curves are assumed. We conclude that for an accurate estimation of kh when injection testing cannot be done, some reasonable estimate of which relative permeability curves apply is important.

A buildup case also was simulated for this example, and the downhole pressure change is plotted in Fig. 9. The pressure change is greater than for the drawdown case because the change in flow rate was from 15 to 0 kg/s, while in the drawdown case it was from 5 to 15 kg/s. Note on this graph that wellbore storage seems to last a much shorter time for buildup than for a drawdown test. When the well is shut in, the steam and liquid phases separate out in the bore. The compressibility of each phase is much less than the compressibility of a well dispersed two-phase mixture, resulting in a longer wellbore storage phenomenon. However, it is difficult to analyze buildup data when the fluid is two-phase in the reservoir because the liquid forms at the bottom of the well and the liquid saturation around the bore is 100%. Small amounts of liquid can flow from the well back into the reservoir during the buildup test. Although the buildup test may seem more desirable, it is very difficult to determine ν_t when S_v around the bore is such a strong function of position.

Vapor-Dominated Two-Phase Reservoir

In the fourth example, an initial steam saturation of 0.78 was assumed. After 24 hours of production, the steam saturation varies between 0.7 and 0.82 around the bore. As indicated earlier (Fig. 1), when the steam saturation is high, changes in enthalpy can occur at very late times. It probably would have been better to initialize this case for a longer time.

Fig. 10 is a plot of the drawdown pressure vs. time, both considering the wellbore flow and neglecting it. At these high initial vapor saturations and using Corey relative permeability curves, only steam flows in the well. The average compressibility in the well is much less than in the other cases. The enthalpic contribution to wellbore storage lasts only 650 seconds and the test need be run for only 1 hour.

Over the time span that kh/ν_t was calculated, H_f is approximately constant, indicating that energy changes in the well/reservoir are not important. However, at about 7×10^3 seconds, the drawdown curve suddenly begins to drop at a greater rate. A check of the flowing enthalpy shows that some liquid is beginning to flow. The liquid saturation around the bore is now greater than the assumed irreducible liquid saturation (0.3 here). Condensation occurs around the bore when the system is initially at a pressure above the maximum steam enthalpy point, as in this case. To analyze the drawdown curve after 7×10^3 seconds, it is necessary to wait until the flowing enthalpy from the reservoir steadies out.

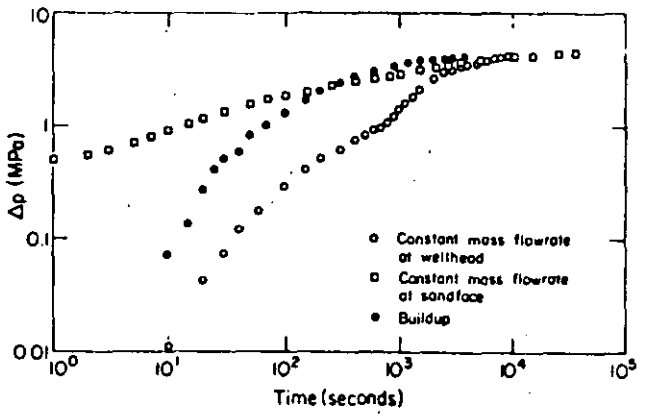

Fig. 9—Log-log plot of pressure drawdown and pressure buildup for liquid-dominated two-phase reservoir.

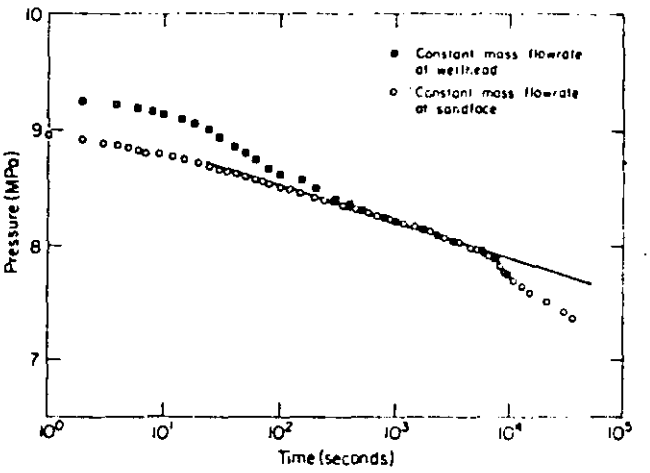

Fig. 10—Pressure drawdown for vapor-dominated two-phase reservoir.

Conclusions

A geothermal reservoir simulator and a transient wellbore model have been coupled to generate a series of drawdown histories for various types of two-phase reservoirs. Estimates of wellbore storage times have been made. Pressure decline curves have been analyzed with analytical methods and with computerized curve-matching for variable flow rates. The following results have been obtained.

1. Wellbore storage effects in two-phase drawdown tests can last for several hours, during which time the pressure response is controlled by the variable sandface flow rate. However, in contrast to oil and gas wells, the sandface flow rate does not always approach the surface flow rate in a monotonic way, producing a temporary plateau in the downhole pressure transient curve.

2. Monitoring the flowing wellhead enthalpy is essential for meaningful results.

3. If the drawdown test is designed appropriately, pressure transients are governed by a linear diffusion equation, and a determination of the total kinematic mobility can be made.

4. A transient wellbore model allows for evaluation of the total kinematic mobility from short time tests, which are dominated by wellbore storage effects.

5. The ratio of relative permeabilities for water and steam, k_{rl} and k_{rv}, can be determined as a function of flowing enthalpy.

6. Absolute permeability/thickness and the in-place vapor saturation around the wellbore during the test can be obtained if the relative permeabilities are known as a function of saturation, or, alternatively:

7. The relative permeability curves can be determined if the absolute permeability and in-place saturation are known.

Nomenclature

A = area of wellbore, sq ft (m^2)
C = isenthalpic compressibility, $(1/\rho)(\partial\rho/\partial p)_H$, psi^{-1} (Pa^{-1})
C_r = heat capacity of rock, Btu/lbm = °F(kJ/kg·K)
C_t = total compressibility of reservoir, psi^{-1} (Pa^{-1})
C_E = compressibility, $(1/\rho)(\partial\rho/\partial p)_E$, psi^{-1} (Pa^{-1})
E = specific energy, Btu/lbm (kJ/kg)
f = friction factor
h = reservoir thickness, ft (m)
H = specific enthalpy, Btu/lbm (kJ/kg)
k = permeability, md (m^2)
k_{rl} = relative permeability of liquid water
k_{rv} = relative permeability of steam
L = length of wellbore, ft (m)
m = slope of straight line segment on p vs. $\log(t)$ plot, psi/sec (mPa/s)
p = pressure, psi (Pa)
r = radial distance, ft (m)
r_e = effective wellbore radius, ft (m)
r_w = wellbore radius, ft (m)
s = skin
S = saturation
S_{lr} = irreducible liquid saturation
S_{vr} = irreducible steam saturation
t = time, seconds
T = temperature, °F (°C)
u = heat transfer coefficient, Btu ft-°F (kJ/m·°C)
v = mass averaged velocity, ft/s (m/s)
v_l = Darcy liquid velocity, ft/s (m/s)
v_v = Darcy steam velocity, ft/s (m/s)
w = mass flow rate, lbm/s (kg/s)
x = axial distance, ft (m)
β = $(1/\rho)(\partial\rho/\partial E)p$, lbm/Btu (kg kJ)
η = $r/\sqrt{t}$
μ = absolute viscosity, cp (Pa·s)
ν = kinematic viscosity, sq ft/s (m^2/s)
ν_t = total kinematic viscosity, sq ft/s (m^2/s)
ρ = density, lbm/cu ft (kg/m^3)
ϕ = porosity

Subscripts

dh = downhole
f = flowing
i = initial
l = liquid
r = rock
sf = sandface
s = surface
v = vapor

Acknowledgments

This work was supported by the Assistant Secretary for Conservation and Renewable Energy, Office of Renewable Technology, Div. of Geothermal and Hydropower Technologies of the U.S. DOE under Contract No. W-7405-ENG-48.

References

1. Garg, S.K., and Pritchett, J.W.: "Pressure Transient Analysis for Hot Water and Two-Phase Geothermal Wells: Some Numerical Results," Systems, Science and Software Report SSS-R-81-4708, La Jolla, CA (1980).
2. Garg, S.K.: "Pressure Transient Analysis for Two-Phase (Water/Steam) Geothermal Reservoirs," *Soc. Pet. Eng. J.* (June 1980) 206-214.
3. Grant, M.A.: "Two-Phase Linear Geothermal Pressure Transients: A Comparison with Single-Phase Transients," *New Zealand J. Sci.* (1978) 21, 355-364.
4. Moench, A.F. and Atkinson, P.G.: "Transient Pressure Analysis in Geothermal Steam Reservoirs with an Immobile Vaporizing Liquid Phase—Summary Report," *Proc.*, Third Stanford U. Workshop on Geothermal Reservoir Engineering, Stanford, CA (1977) 64-69.
5. Sorey, M.L., Grant, M.A., and Bradford, E.: "Nonlinear Effects in Two-Phase Flow to Wells in Geothermal Reservoirs," *Water Resources Research* (Aug. 1980) 16, 767-777.
6. Miller, C.W.: "WELLBORE User's Manual," Lawrence Berkeley Laboratory, LBL 10910, Berkeley, CA (1980).
7. Zyvoloski, G.A., O'Sullivan, M.J., and Krol, D.E.: "Finite Difference Techniques for Modeling Geothermal Reservoirs," *Num. Anal. Meth. Geomech.* (1979) 3, 355-366.
8. Gould, T.L.: "Vertical Two-Phase Steam-Water Flow in Geothermal Wells," *J. Pet. Tech.* (Aug. 1974) 833-842.
9. Nathenson, M.: "Flashing Flow in Hot-Water Geothermal Wells," USGS *J. Research* (1974) 2, 743-751.
10. Farouq Ali, S.M.: "A Comprehensive Wellbore Steam Water Flow Model for Steam Injection and Geothermal Applications,"

Soc. Pet. Eng. J. (Oct. 1981) 527-534.
11. Miller, C.W.: "Wellbore Storage Effects in Geothermal Wells," *Soc. Pet. Eng. J.* (Dec. 1980) 555-565.
12. Orkiszewski, J.: "Predicting Two-Phase Pressure Drops in Vertical Pipe," *J. Pet. Tech.* (June 1967) 829-838.
13. Chisholm, D.: "Pressure Gradients Due to Friction during the Flow of Evaporating Two-Phase Mixtures in Smooth Tubes and Channels," *Intl. J. Heat Mass Transfer* (1973) 16, 347.
14. Corey, A.T.: "The Interrelation Between Gas and Oil Relative Permeabilities," *Prod. Monthly* (1954) 19, 38-41.
15. Grant, M.A., and Sorey, M.L.: "The Compressibility and Hydraulic Diffusivity of a Water-System Flow," *Water Resources Research* (1979) 15, 684-686.
16. O'Sullivan, M.J.: "A Similarity Method for Geothermal Well Test Analysis," LBL Report 10968, Lawrence Berkeley Laboratory, Berkeley, CA.
17. Pritchett, J.W.: "Basic Characteristics of a Two-Phase System," Management Survey Course No. 4, Geothermal Resources Council, Sacramento, CA (Nov. 1980).
18. Ramey, H.J. Jr.: "Non-Darcy Flow and Wellbore Storage Effects in Pressure Buildup and Drawdown of Gas Wells," *J. Pet. Tech.* (Feb. 1965) 223-233.
19. McEdwards, D. and Benson, S.M.: "ANALYZE User's Manual," LBL Report 10907, Lawrence Berkeley Laboratory, Berkeley, CA (1980).
20. Grant, M.A.: "Permeability Reduction Factors at Wairakei," paper 77-HT-52 presented at AIChE/ASME Heat Transfer Conference, Salt Lake City, Aug. 15-17, 1977.
21. Bodvarsson, G.S., Vonder Haar, S., Wilt, M., and Tsang, C.S.: "Preliminary Estimation of the Reservoir Capacity and the Longevity of the Baca Geothermal Field, New Mexico," SPE paper 9273 presented at the SPE 55th Annual Technical Conference and Exhibition, Dallas, Sept. 21-24, 1980.
22. Counsil, J.R., and Ramey, H.J.: "Drainage Relative Permeabilities Obtained from Steam-Water Boiling Flow and External Gas Drive Experiments," Trans., Geothermal Resources Council (1979) 3, 141-143.

SI Metric Conversion Factors

cp	× 1.0*	E−03	=	Pa·s
cu ft	× 2.831 685	E−02	=	m^3
ft	× 3.048*	E−01	=	m
°F	(°F−32)/1.8		=	°C
°F	(°F+459.67)/1.8		=	K
lbm	× 4.535 924	E−01	=	kg
sq ft	× 9.290 304*	E−02	=	m^2
psi	× 6.894 757	E+00	=	kPa

*Conversion factor is exact

SPEJ

Original manuscript received in Society of Petroleum Engineers office Feb. 12, 1981. Paper accepted for publication Oct. 20, 1981. Revised manuscript received Feb. 26, 1982. Paper (SPE 9922) first presented at the SPE 1981 California Regional Meeting held in Bakersfield March 25-26.

CURSO: "INGENIERIA DE YACIMIENTOS GEOTERMICOS"

En colaboración con la OLADE, C.F.E., I.I.E.

del 13 marzo al 18 de mayo.

TEMA: "PRUEBAS DE PRESION"

6.- Mangold D.G. Tsang, C.F., Lippmann M.J. Witherspoon, P.A.:

"A study of a thermal discontinuity in well test analysis", J. Pet. Tech (Junio, 1981), 1095-1105

DR. FERNANDO SAMANIEGO
13-23 Marzo 1984

A Study of a Thermal Discontinuity in Well Test Analysis

Donald C. Mangold, Lawrence Berkeley Laboratory
Chin Fu Tsang, Lawrence Berkeley Laboratory
Marcelo J. Lippmann, Lawrence Berkeley Laboratory
Paul A. Witherspoon, SPE, Lawrence Berkeley Laboratory

Summary

The presence of zones of different temperatures in nonisothermal reservoirs may resemble permeability boundaries during well testing. This investigation employed numerical modeling to examine such effects in drawdown, buildup, and injection well tests. The results indicate that nonisothermal influence can be detected and accounted for by tests of sufficient duration with suitably placed observation wells.

Introduction

A challenge to the interpretation of well test results from nonisothermal reservoirs is the effect on the pressure response due to fluid and rock temperature-dependent properties. Since zones of different temperatures in the reservoir may resemble permeability boundaries, care in interpretation of results is required.[1] This study is an examination of these temperature effects on well test data where the producing well is completed in the center of a circular hot zone surrounded by a concentric cooler water region. The investigation was carried out with the intent of comparing the results of such tests with the classical Theis solution and discovering ways in which temperature differences can be accounted for in well test data analysis.

Only recently have there been discussions of nonisothermal well testing in the literature. An analytical study by Tsang and Tsang[2] motivated this study by giving semilog results to be expected from cold-water injection into a hot reservoir. By assuming a specific form for the variation of the permeability/viscosity ratio (k/μ) across the transition zone (from cold to hot water), they were able to derive solutions that follow the classic Theis curve for each region. From early- and later-time data, reservoir transmissivity (kh/μ) and storativity (ϕch) can be determined so that compressibility (c), reservoir permeability (k), porosity (ϕ), and thickness (h) can be evaluated. Their results prompted this numerical investigation of viscosity effects where production, buildup, and partial-penetration well tests are considered.

Background

The standard methods of well test data analysis in isothermal reservoirs have been documented thoroughly by Earlougher.[3] The problems of well testing in geothermal reservoirs have been discussed by only a few authors in the past decade. Recently, Narasimhan and Witherspoon[4] have reviewed the problems in carrying out and analyzing well tests in these systems. They mention that the conventional concept of transmissivity should be replaced by absolute permeability (k) or the product kh. In another recent study[5] of reinjection at the East Mesa geothermal area, pressure distributions based on viscosity ratios of 1:1.9 between hot and cold water were described. The semilog plots show a distinctive change in slope at the cold front. The approach used, however, was a series of steady-state runs with the cold front at varying distances from the production well and with energy and mass transport equations decoupled. Rice[6] used computer models to describe drawdown and buildup tests in single- and two-phase reservoirs under isothermal conditions. Earlier, Chappelear and Volek[7] modeled the injection of a hot liquid into a porous medium using temperature-dependent viscosity. They assumed that specific heat and density were independent of temperature, and they calculated temperature (not pressure) distributions within the reservoir, caprock, and bedrock. Their results show that the high viscosity of the colder water effectively controls the average

0149-2136/81/0006-8232$00.25

TABLE 1 – PROPERTIES OF THE AQUIFER USED IN THE SIMULATIONS

Thickness, h, ft (m)	164 (50)
Porosity ϕ, dimensionless	0.1
Intrinsic permeability k, md (10^{-15} m^2)	29 (29)
Specific storage coefficient S_s, ft^{-1} (m^{-1})	1.19×10^{-5} (3.9×10^{-5})
Rock density ρ_s, lbm/cu ft (kg/m^3)	165.4 (2650)
Rock specific heat C_s, Btu/lbm·°F (J/kg·K)	231.7 (970)
Thermal conductivity k_H, Btu·ft/h·sq ft·°F (W/m·K)	5.0079 (2.8935)

(2)

temperature and the temperature distribution within the system.

For composite reservoirs, Bixel *et al.*[8] gave results for the pressure response in isothermal reservoirs with linear discontinuities, for both drawdown and buildup tests. Later, Ramey[9] made an analytical study of well tests performed in cylindrical composite reservoirs showing permeability contrasts. Even though the systems analyzed were isothermal, their behavior may be similar to nonisothermal ones. These works suggest lines for extensions to this study.

Computational Approach

This study used a numerical model[10] developed at Lawrence Berkeley Laboratory (LBL) called CCC (conduction/convection/consolidation) to simulate a geothermal reservoir with a central hot cylindrical region surrounded by colder water. The program has coupled energy and mass transport equations to simulate single-phase nonisothermal saturated porous systems. Viscosity, specific heat, and density of water are taken properly as temperature-dependent properties (Tables 1 and 2). In a more recent version of CCC, the equation of state for the density of water has been made a function of both temperature and pressure. The program also has the ability to consider pressure- and temperature-dependent rock and fluid properties in general, but for this study only water properties were allowed to vary with temperature. In particular, intrinsic permeability was held constant throughout all cases to study variability due to viscosity alone. Pure liquid water was assumed; the effects of a salt solution of a 3-wt% brine in our problem are negligible (see section on additional factors). This model has been validated against a variety of analytical and semianalytical solutions as well as field data.[11-13]

The mesh design used for the majority of cases studied in this paper uses cylindrical symmetry with nodes at 3-ft (1-m) intervals to a distance of 984 ft (300 m). This fine mesh is necessary to simulate the temperature front movements properly. The nodal separation gradually increases after 984 ft (300 m) up to a constant-pressure and constant-temperature boundary node at 16,896 ft (5150 m) from the well. The caprock and bedrock are assumed to be insulated and impermeable (for the purposes of this study) to focus on the horizontal distribution of the temperature front. Two sizes of the hot spot were investigated: the case of a 328-ft (100-m) radius is discussed first, and then a hot spot with 164-ft (50-m) radius is analyzed in more detail. For simplicity, in most cases a single-layer model is assumed (i.e., effectively gravity is neglected). The effects of gravity and buoyancy of the hot water are considered in the case of partial penetration with a multilayer mesh design. The initial conditions assumed for the system are idealized for the sake of uniformity, with a sharp vertical thermal front boundary between the 482°F (250°C) inner region and the cooler 212°F (100°C) surrounding region. The same pattern in the pressure decline appears regardless of whether the front is initially sharp or diffuse (see section on effect of a diffuse thermal front). Since the degree of the dif-

TABLE 2 – PROPERTIES OF WATER USED IN THE SIMULATIONS

Compressibility κ, psi^{-1} (Pa^{-1})	4.4816×10^{-6} (6.5×10^{-10})
Density equation: $\rho = \rho_o [1 - \alpha(T - T_o) - \beta(T - T_o)^2]$	
Reference density ρ_o, lbm/cu ft (kg/m^3)	62.23 (996.9)
Reference temperature T_o, °F (°C)	77 (25)
First coefficient of thermal expansion α, °F^{-1} (°C^{-1})	5.706×10^{-4} (3.17×10^{-4})
Second coefficient of thermal expansion β, °F^{-2} (°C^{-2})	4.608×10^{-6} (2.56×10^{-6})

Temperature T (°F)	Temperature T (°C)	Viscosity μ, (cp)	Density ρ, (lbm/cu ft)	Heat Capacity C (Btu/lbm·°F)
122	50	0.5450	61.64	957.8
212	100	0.2800	59.86	900.4
257	125	0.2310	58.67	872.0
347	175	0.1585	55.69	820.2
482	250	0.1070	49.73	761.4

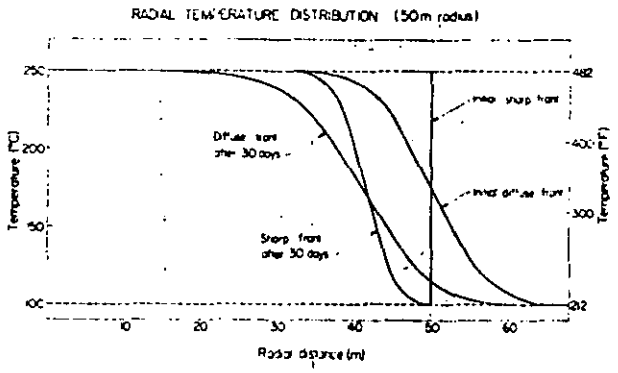

Fig. 3 – Temperature profiles for hot spots with initially diffuse and sharp fronts after 30 days of production.

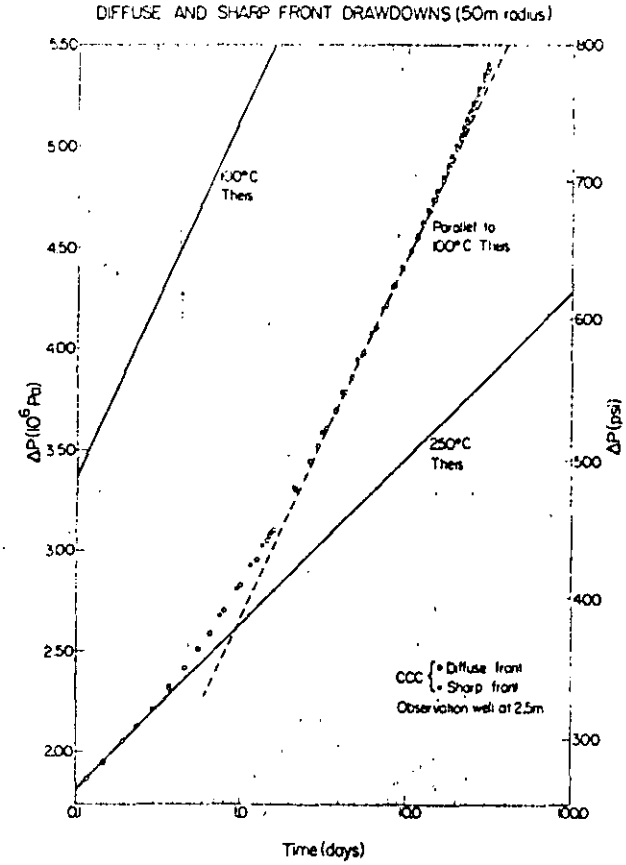

Fig. 4 – Drawdowns for hot spots with initially diffuse and sharp fronts during 30 days of production.

shaped curve. After 30 days of pumping, both the initially sharp and initially diffuse fronts show the effect of diffusion of the temperature front and there is less difference between the two fronts.

The drawdown curves for these two cases are shown in Fig. 4. It is clear that the pressure response for both cases follows the same general pattern. The pressure response of the diffuse thermal front is slightly less and slightly slower, as expected, due to its broader transition zone between the two temperature regions. The diffuse thermal zone produces a pressure behavior similar to a region of gradually decreasing permeability, whereas the sharp vertical thermal front produces a behavior that resembles a sudden permeability change, such as a barrier or fault. In either case, the general pattern of the drawdown is basically the same. This pattern is confirmed further by the buildup and falloff tests (see sections on buildup tests and on injection and production of hot water) and the partial-penetration case (see section on partial-penetration case). Therefore, the rest of the investigation was carried out using a sharp vertical thermal front as the initial condition for each case.

50-m Case: Production for 120 Days

In this case, production was continued for 120 days – i.e., until all the 482°F (250°C) water was extracted from the reservoir, which then was at 212°F (100°C) throughout. The progression in pressure change from the initial hot-spot condition to the end is shown in the semilog plot in Fig. 5, where there are several discernible periods of different response. During the earliest times (up to nearly 0.5 day) the pressure follows the 482°F (250°C) Theis behavior, as expected. There follows a transition time (from 0.5 to 2 days) where the curve shifts to run parallel to the 212°F (100°C) Theis curve but still below it in magnitude (from 2 to 20 days). Then the curve again shifts upward (20 to 60 days) until the temperature front begins to reach the observation well. At this point, the pressure changes drastically, sloping steeply upward to join the 212°F (100°C) Theis curve (for times greater than 60 days), as it should, since by the end of the 120 days the entire reservoir is at 212°F (100°C).

Two observations can be made on the basis of such a complete pressure history. First, as noted in the previous sections, the initial period of 482°F (250°C) Theis curve behavior is followed by a transition to a curve parallel to the colder-water Theis solution. Secondly, as the well continues to be produced, the curve shifts upward again as an indication of another boundary, in this case the moving boundary of the thermal front.

The practical application of this "second shift" is made by locating an observation well at some distance away from the produced well. As Fig. 6 shows, the effect of the moving thermal front occurs much earlier (at approximately 15 days) when observed at a distance of 64 ft (19.5 m) from the production well. Thus, the length of time for the moving boundary to be manifested can be minimized

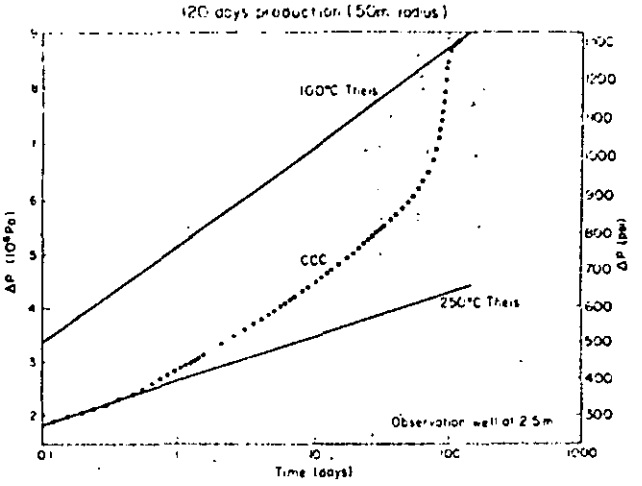

Fig. 5 – Drawdown history for 120 days of production from hot spot with 164-ft (50-m) radius; observation well at 8.2 ft (2.5 m).

by data taken at a suitably distant observation well.

However, if the observation well is too far away from the axis of the hot spot, it may be in the cold-water zone. Fig. 7 reveals that the same general shift of curves takes place but within a much shorter length of time (approximately 0.7 day). This well is 195 ft (59.5 m) from the producing well or 31 ft (9.5 m) outside the outer boundary of the hot spot. It is interesting to note that its early time behavior nevertheless follows a 482°F (250°C) Theis curve before shifting over to the 212°F (100°C) Theis curve. Clearly, employing one or more observation wells provides a ready check on the usual semilog direct analysis from a single well and increases the real possibility of detection of the moving thermal boundary.

As a further examination of these results, log Δp vs. log t/r^2 curves were plotted for r = 8.2, 64, 130, and 195 ft (2.5, 19.5, 39.5, and 59.5 m) [see Fig. 8 where the Theis curves for 212°F (100°C) and 482°F (250°C) are shown for reference]. The observations at 195 ft (59.5 m) and 130 ft (39.5 m) eventually merge into the 212°F (100°C) Theis curve. From all the t/r^2 curves, we can see that the departure from the 482°F (250°C) Theis behavior occurs at smaller values of t/r^2 for greater radial distances r from the well. Also, the merging of the pressure behavior with the 212°F (100°C) Theis solution happens at earlier values of t/r^2 for greater r. This confirms the use of more than one observation well at different radial distances from the producing well to monitor a well test to trace pressure behavior which may be related to a thermal boundary.

A usual type-curve matching procedure was applied to the log-log plot of r = 8.2 ft (2.5 m) data to estimate transmissivity (kh/μ) and storativity (ϕch). The results of the type-curve analysis are given in the Appendix. The match with the very early part of the curve yields a good estimate for kh/μ, as expected. But under such a direct analysis, if the analyst matched the later portion of the curve, he would be seriously mistaken. The estimated values for ϕch

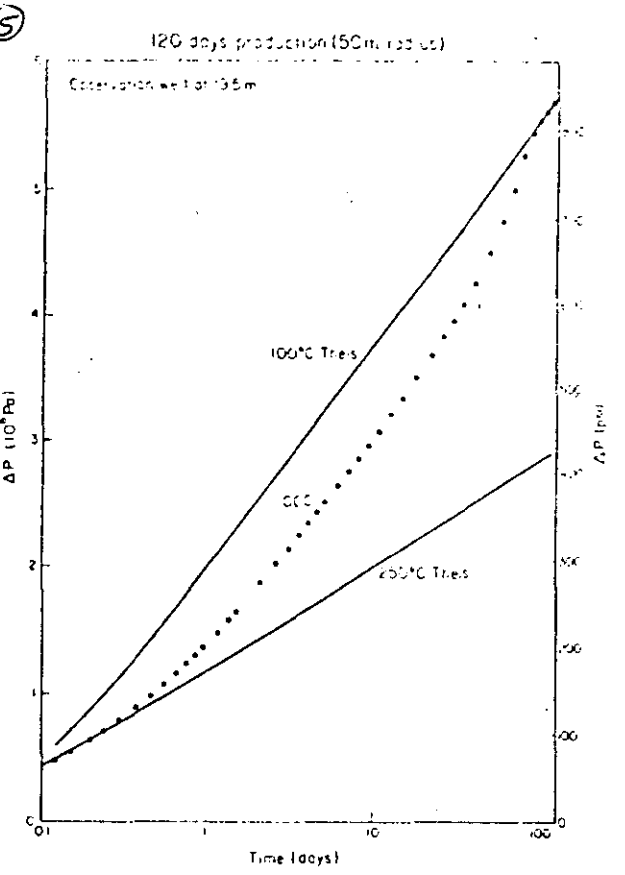

Fig. 6 – Drawdown history for 120 days of production from hot spot with 164-ft (50-m) radius; observation well at 64 ft (19.5 m).

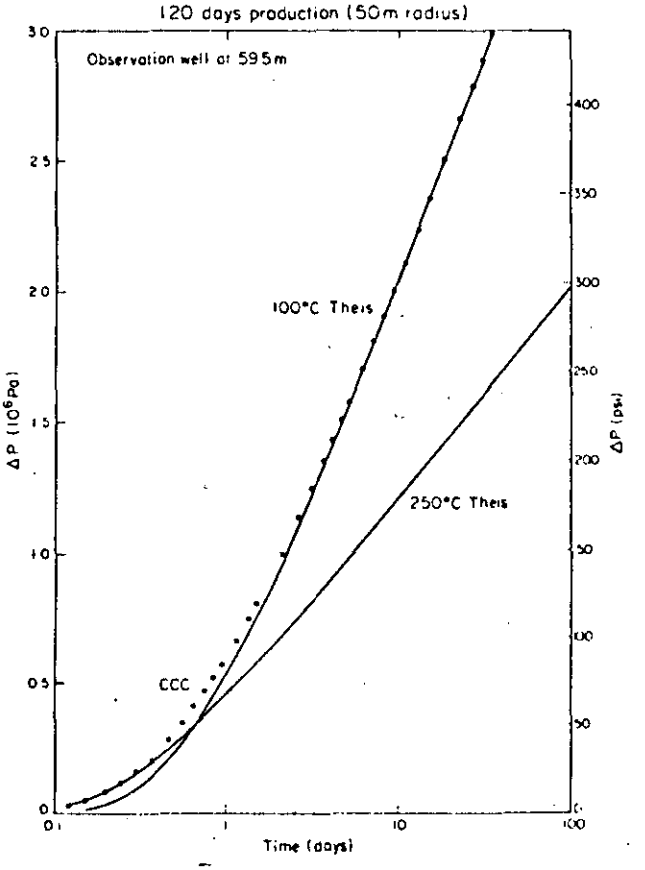

Fig. 7 – Drawdown history for 120 days of production from hot spot with 164-ft (50-m) radius; observation well at 195 ft (59.5 m).

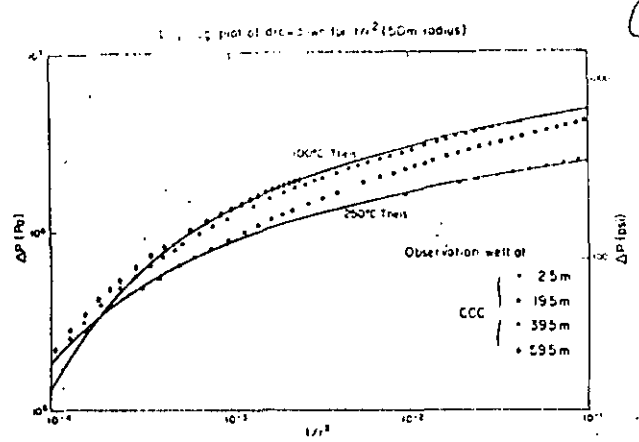

Fig. 8 – Log-log plot of drawdown vs. t/r^2 for hot spot with 164-ft (50-m) radius.

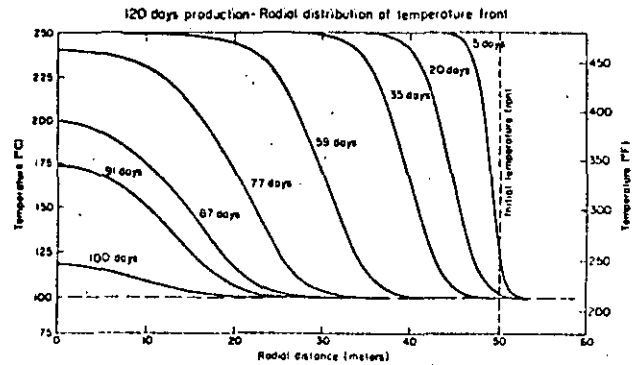

Fig. 9 – Radial distribution of temperature front at different times for production from hot spot with 164-ft (50-m) radius.

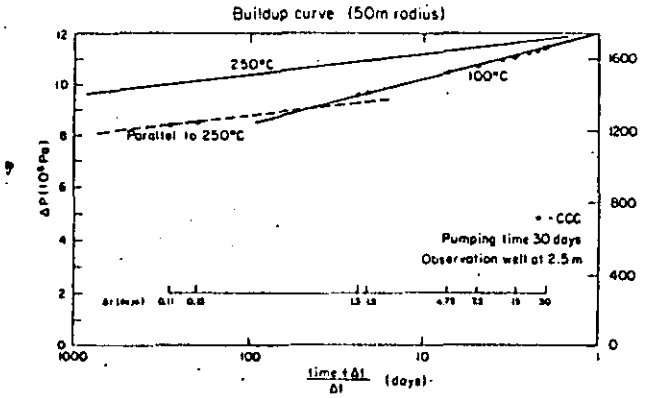

Fig. 10 – Buildup curve after 30 days of production for 482°F (250°C) hot spot with 164-ft (50-m) radius; surrounding region at 212°F (100°C); observation well at 8.2 ft (2.5 m).

reflect the sensitivity of type-curve matching in the determination of compressibility, even for the early-time data. Again, matching with the latest portion of the curve would lead to serious errors by direct analysis.

The progress of the temperature front is interesting to follow. In Fig. 9, a sequence of curves shows how the front moves slowly at first and quite rapidly at the end, reflecting differences in radial volume under a constant pumping rate. The diffusion of the front is very apparent; Table 3 gives values for the size of the front throughout its history and a comparison with a simple analytical conduction model.[14] This diffusion of the temperature front also may account for some of the shifting of the pressure change data curves over the period of production (see section on additional factors).

50-m Case: Buildup Tests

The buildup tests performed in this series of simulations confirm the same general behavior observed in the production tests, but the effects occur at earlier times. Fig. 10 shows a Horner plot of a buildup test after 30 days of production from the 164-ft (50-m) hot spot of the previous section. At the earliest times, the points are parallel to the 482°F (250°C) analytical curve, but after 1 day the points shift toward the 212°F (100°C) curve. By 5 days, the pressure is already following characteristic 212°F (100°C) buildup behavior.

The buildup test has several differences from a production well test. First, the response is generally faster than the drawdown test. Second, because there is only mass flow resulting from pressure equilibration, the thermal front moves very little during buildup. Of course, due to the convection and conduction affecting the thermal front during the preceding production period, there is already a diffuse zone when the buildup test begins. However, as a third contrast to drawdown tests, note that the small mass flow also means that the diffusion of the thermal front proceeds much more slowly because it is mainly by conduction. These latter two conditions do not permit the observation of a moving thermal boundary or a diffuse front as a means of discovering thermal effects, such as during drawdown tests. However, buildup tests should allow a better correlation to the proper analytical solution once a thermal front is suspected. Therefore, the best approach may be a combination of drawdown and

TABLE 3 – DIFFUSION OF THERMAL FRONT, 120-DAY PRODUCTION

Time (days)	Distance From Well (ft)	10% Limit, 239°F (ft)	Analytical Calculation (ft)	90% Limit 455°F (ft)	Analytical Calculation (ft)	Width of Thermal Front (ft)
0.15	164	–	–	–	–	0
5.00	162	167	–	156	–	11
20.00	148	159	151	133	144	26
35.00	131	144	138	115	125	29
59.00	98	117	108	79	89	38
77.00	66	89	80	30	49	59
87.00	33	69	48	0	16	69
91.00	Breakthrough	57	–	–	–	–

buildup tests. The production tests would provide an analyst with sufficient data to determine kh/μ, ϕch, and the presence of a moving thermal front. Then the data from buildup tests could be used to confirm the estimated values of the reservoir parameters and to match the pressure response to type curves to discover possible thermal effects.

Similar behavior on buildup tests was observed for other combinations of temperatures. In Fig. 11 there is a large temperature contrast between 482°F (250°C) and 122°F (50°C) waters, resulting in a fluid viscosity ratio of 1:5.1. Although this case is for a production time of only 15 days, by the end of another 15 days of shutting in the well, the pressures are responding according to the analytical solution for 122°F (50°C). This demonstrates the rapid adjustment of the system under different temperatures and confirms that buildup tests should prove to be a useful means for checking suspected thermal effects in well testing.

As noted earlier, the buildup tests necessarily begin with a diffuse front; nevertheless, the pressure response rapidly follows the general pattern observed in the drawdown tests. This is a further confirmation that whether the thermal front is sharp or diffuse, the pressure response follows the same pattern.

Injection and Production of Hot Water

The effect of hot-water injection for 30 days (same temperature as the hot spot) is shown in Fig. 12. It conforms to the same general pattern of pressure change described in the previous sections (but with an increase of pressure instead of a decline). After the end of the injection period, a falloff test was performed for 30 days with the results shown in Fig. 13. The behavior again follows a similar pattern to buildup tests after production, with a rapid response in the change of the semilog slope as the pressure of the system equilibrates.

In another simulation, the injected water was produced immediately after injection by pumping at the same rate as injection. The results are illustrated in Fig. 14. The initial semilog slope is twice the slope of the 482°F (250°C) Theis curve, as expected, but the following slope, although very clearly marked after just 2 days, does not follow the 212°F (100°C) slope or any integer multiple of it. However, this slope and, indeed, the entire plot of pressure changes may be obtained by superposition of two cases: (1) the falloff test of the previous paragraph and (2) production of the 30-day-injected hot spot where initially all pressures in the mesh were changed to one constant value but the temperature profile was kept exactly the same. The falloff test gives the correct variable pressure response pattern at early times, but it is necessary at later times to include the effect of the moving diffuse front due to production without the influence of the initial variable pressure distribution.

Reinjection and Production of Cold Water

An analytical solution has been found for geothermal reservoir pressure response to cold-water reinjection,[2] as mentioned earlier. The results in-

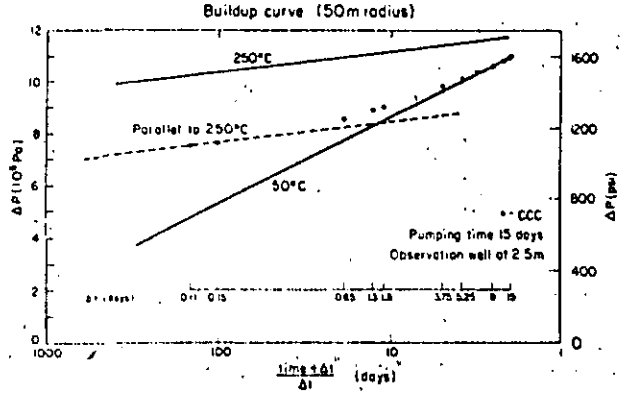

Fig. 11 – Buildup curve after 15 days of production for 482°F (250°C) hot spot with 164-ft (50-m) radius; surrounding region at 122°F (50°C); observation well at 8.2 ft (2.5 m).

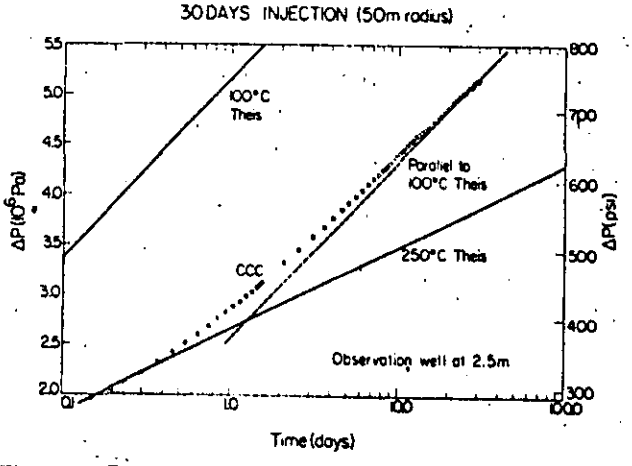

Fig. 12 – Pressure response of hot spot with 164-ft (50-m) radius during 30 days of 482°F (250°C) water injection; observation well at 8.2 ft (2.5 m).

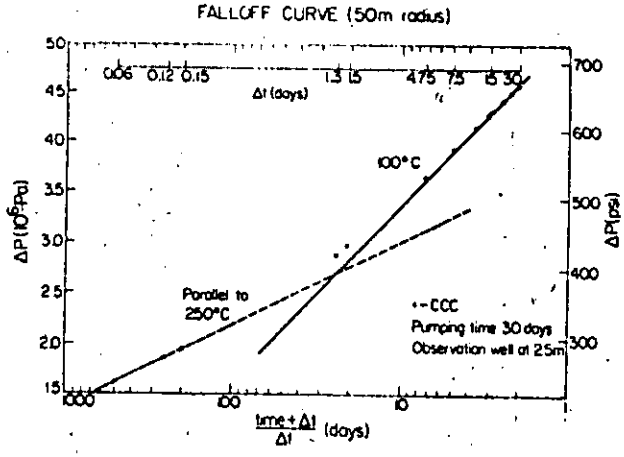

Fig. 13 – Falloff curve for hot spot with 164-ft (50-m) radius after 30 days of 482°F (250°C) water injection; observation well at 8.2 ft (2.5 m).

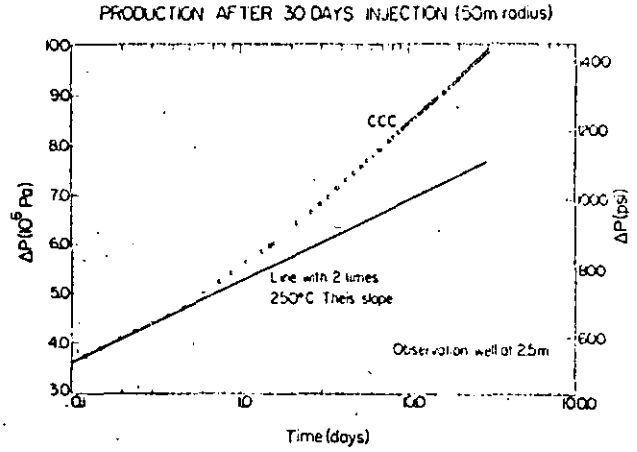

Fig. 14 – Pressure response of hot spot with 164-ft (50-m) radius during 30 days of production after 30 days of 482°F (250°C) water injection; observation well at 8.2 ft (2.5 m).

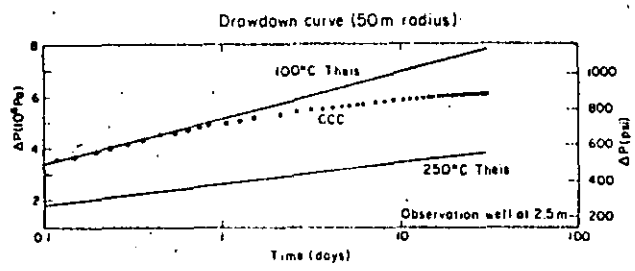

Fig. 15 – Drawdown curve for cold spot with 164-ft (50-m) radius; observation well at 8.2 ft (2.5 m).

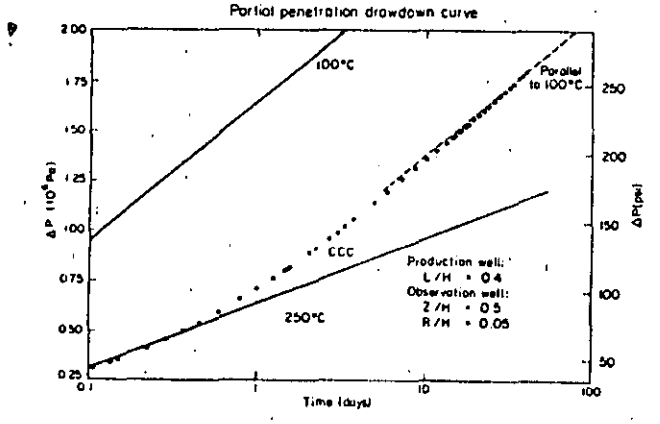

Fig. 16 – Drawdown curve for the case of 40% partial penetration in hot spot with 157.5-ft (48-m) radius.

(8) dicate that for small values of t/r^2, the pressure decline curve follows a Theis solution with parameters corresponding to those of the native hot water. For large t/r^2, it approaches a line parallel to a Theis curve with parameters corresponding to those of the injected water. The authors suggested that (1) from matching early data, kh and ϕch may be ascertained, and (2) after matching later data, the position of the front and, therefore, h may be estimated. Thus k, ϕc, and h are evaluated. However, this procedure has not been tested with field data.

The results of the analytical solution were checked against the numerical model CCC employed here. The characteristic pressure behavior noted in previous sections for drawdown and buildup tests was apparent and followed the behavior predicted by the analytical solution.

To corroborate these results, the behavior of a 212°F (100°C) cold spot of 164-ft (50-m) radius surrounded by a 482°F (250°C) region was studied. It was produced for 30 days in the same fashion as the previous hot-spot cases, with the results shown in Fig. 15. Again, the pattern is the same, but now in the opposite direction (from cold-water behavior toward hot-water behavior). After the data runs parallel to the 482°F (250°C) Theis solution, it shifts further toward that solution but runs nearly horizontal for the last 5 days. This is probably because the 482°F (250°C) water flows much more readily than the 212°F (100°C) water, so that the produced well appears to have a full recharge boundary at this point in time. As the cold spot is produced for longer times, tht data should turn further toward the 482°F (250°C) Theis solution and finally merge with it.

Thus, the effect of cold water injected or produced from hotter reservoirs conforms to the expected pattern due to fluid viscosity and density differences.

Partial-Penetration Case

The previous sections have assumed a single-layer model where there is necessarily full penetration and gravity is not an influence. To study thermal effects in the common situation of partial penetration, a multilayered cylindrical mesh (with gravity effects included) was used. There were five 32.8-ft (10-m) layers in the aquifer, with nodes at radial distances of 3 ft (1 m) out to a distance of 65.6 ft (20 m) from the well; beyond 65.6 ft (20 m), the size of the annular nodes gradually increased. The boundary between hot and cold regions was placed at 157.5 ft (48 m). The well was produced for 40 days from the top two layers at 40% of the former rate. The observation well is in the middle layer, 8.2 ft (2.5 m) from the axis of the system. The results are displayed in Fig. 16.

The same general pattern of the previous sections is apparent for partial penetration. The analytical solutions are taken from Witherspoon *et al.*[15] and are semilog straight lines for the times plotted and for the reservoir parameters used. This result confirms the effect of viscosity differences on the pressure response during a drawdown test, even when the well

TABLE 4 – COMPARISON OF PROPERTIES OF PURE WATER WITH 3-wt% BRINE
(3 wt% = 30,000 ppm TDS)

Property	Temperature (°F)	Temperature (°C)	Brine	Water	Percent Change
Density ρ, lbm/cu ft	482	250	51.10	49.73	2.75
	212	100	61.29	59.86	2.39
Heat capacity C, Btu/lbm·°F	482	250	738.5	761.4	−3.01
	212	100	873.5	900.4	−3.00
Viscosity μ, cp	482	250	0.1140	0.1070	6.54
	212	100	0.2983	0.2800	6.54
Density-capacity product ρC, 10^3 Btu/cu ft·°F	482	250	37.74	37.86	−0.34
	212	100	53.54	53.90	−0.67
Permeability/viscosity ratio k/μ, md/cp	482	250	254.4	271.0	−6.14
	212	100	97.22	103.6	−6.13

is partially penetrating and the influence of gravity is taken into account.

Three Additional Factors

There are three additional factors which have a possible influence on these results: the effect of natural convection, the effect of a brine solution, and the effect of a diffuse front. These possibilities are covered briefly in this section.

To study the effect of natural convection, a simulation was performed using the partial penetration mesh of five layers, with temperatures of 482°F (250°C) inside and 212°F (100°C) outside. There was no production at the well. After 27.5 days, the mass flow cycle in the simulation achieved quasisteady state and no further mass flow was computed; the heat flow calculations were continued to 38 days. The results were compared with analytical formulas recently derived by Hellstrom *et al.*[16] for buoyancy tilting of a thermal front in an aquifer, including the effect of a diffuse front. The numerically computed flow velocity at the front compared to within 0.76% of the analytical solution at 27.5 days. The maximum flow velocity due to natural convection was 4.774×10^{-7} ft/s (1.455×10^{-7} m/s) compared with the flow velocity from pumping, which was 1.406×10^{-5} ft/s (4.285×10^{-6} m/s) at 30 days, a factor of nearly 30:1. These results confirm that the use of a single-layer mesh for the major part of this investigation was acceptable, since natural convection has negligible effect on reservoir pressure for the time periods considered (up to approximately 40 days).

The effect of a brine solution instead of pure water was examined using estimation formulas from Wahl[17] for physical properties of geothermal brines. The results are displayed in Table 4. A 3-wt% brine (30,000 ppm TDS) was chosen for comparison, because many geothermal areas [New Zealand, Japan, Mexico, U.S. (except Salton Sea), and Iceland] have a smaller weight percent of total dissolved solids. The difference in properties between such a brine and water is negligible for ρC, and approximately 6% for μ or (k/μ). However, the error of 6% applies equally to the 482°F (250°C) and 212°F (100°C) waters, so that the viscosity ratio remains the same. Thus, encountering a brine solution in place of pure water in a field test should not affect the results reported here.

Finally, the diffuseness of the thermal front will have an effect on the slope of the semilog plot, as shown in Tsang and Tsang.[2] In their analytical formulas, the size of the diffuse zone (where the viscosity varies appreciably between the values for hot and cold water) depends on the aquifer diffusivity. The smaller the value of the diffusivity, the more the semilog straight line will turn to follow the Theis curve for the injected cold water. According to their numerical results, the value used for aquifer diffusivity in this investigation would lead to a curve which turns early to run parallel to the Theis curve for colder water. Thus, the present set of simulations does confirm their analytical results for the effect of the diffuse zone between hot and cold waters on pressure response in a well test.

Conclusions

This paper has shown that the effects of viscosity from regions of different temperature water can appear in well test data in a way that may be mistaken as permeability barriers in some cases. This effect can be recognized by a pumping test of sufficient duration with observation wells located at a suitable distance from the production well. The questions of identifying the moving thermal boundary, applications of the method to buildup tests, and partially penetrating wells have been discussed. The possible influences of gravity and buoyancy (i.e., natural convection), a brine solution, and the size of the diffuse zone also have been considered.

Future extensions of this investigation would include further work in deriving the analytical relationship between the time of departure from the Theis solution for the inner region and the distance to the boundary between the hot and cold waters, possibly along the line of Ramey.[9] With such a relationship, there is the potential that geothermal

well testing could point out the presence of different temperature regions.

Nomenclature

B = reservoir volumes per standard volume, dimensionless
c = fluid compressibility, psi^{-1} (Pa^{-1})
C = fluid specific heat, Btu/lbm·°F (J/kg·K)
C_a = aquifer rock specific heat, Btu/lbm·°F (J/kg·K)
h = aquifer thickness, ft (m)
k = intrinsic permeability, md (10^{-15}m^2)
k_H = thermal conductivity of solid/fluid mixture, Btu·ft/h·sq ft·°F (W/m·K)
m = slope of semilog straight line, psi/log cycle (Pa/log cycle)
p = fluid (pore) pressure, psi (Pa)
p_D = fluid pressure, dimensionless
q = volumetric flow rate, gal/min (dm^3/s)
q_{mass} = mass flow rate, lbm/s (kg/s)
r = radial distance, ft (m)
S_s = specific storage coefficient, ft^{-1} (m^{-1})
t = time
t_D = time, dimensionless
T = temperature, °F (°C)
T_o = reference water temperature, °F (°C)
α = first coefficient of thermal expansion for water, °F^{-1} (°C^{-1})
β = second coefficient of thermal expansion for water, °F^{-2} (°C^{-2})
κ = water compressibility, psi^{-1} (Pa^{-1})
μ = fluid viscosity (dynamic), cp (Pa·s)
ρ = fluid density, lbm/cu ft (kg/m^3)
ρ_a = aquifer rock density, lbm/cu ft (kg/m^3)
ρ_o = reference water density, lbm/cu ft (kg/m^3)
ϕ = porosity, dimensionless

Subscripts

a = aquifer
D = dimensionless quantity
e = Theis curve estimate
H = heat conductivity value
m = match value from type-curve analysis
o = reference quantity

Acknowledgments

This work was supported by the director of the Office of Energy Research, Office of Basic Energy Sciences, Material Sciences Div., and the assistant secretary for resource applications, Office of Industrial and Utility Applications and Operations, Geothermal Energy Div., of the U.S. DOE under Contract W-7405-ENG-48.

References

1. Tsang, C.F. *et al.*: "Numerical Modeling Studies in Well Test Analysis," *Proc.*, Second Invitational Well Testing Symposium, Lawrence Berkeley Laboratory, Berkeley, CA (1978) LBL Report 8883, 47-57.
2. Tsang, Y.W. and Tsang, C.F.: "An Analytic Study of Geothermal Reservoir Pressure Response to Cold Water Reinjection," *Proc.*, Fourth Stanford Workshop on Geothermal Reservoir Engineering, Stanford, CA (1978) 322-331.
3. Earlougher, Robert C. Jr.: *Advances in Well Test Analysis*, Monograph Series, SPE, Dallas (1977) 5.
4. Narasimhan, T.N. and Witherspoon, P.A.: "Geothermal Well Testing," LBL Report 8290, Lawrence Berkeley Laboratory, Berkeley, CA (Jan. 1979).
5. Howard, J. *et al.*: "Geothermal Resource and Reservoir Investigations of U.S. Bureau of Reclamation Leaseholds at East Mesa, Imperial Valley, California," LBL Report 7094, Lawrence Berkeley Laboratory, Berkeley, CA (Oct. 1978).
6. Rice, L.F.: "Pressure Drawdown and Buildup Analyses in Geothermal Reservoirs," *Proc.*, 11th Intersociety Energy Conversion Engineering Conf., State Line, NV (1976) 1.
7. Chappelear, J.E. and Volek, C.W.: "The Injection of a Hot Liquid into a Porous Medium," *Soc. Pet. Eng. J.* (March 1969) 100-114; *Trans.*, AIME, 246.
8. Bixel, H.C., Larkin, B.K., and van Poollen, H.K.: "Effect of Linear Discontinuities on Pressure Build-Up and Drawdown Behavior," *J. Pet. Tech.* (Aug. 1963) 885-895; *Trans.*, AIME, 228.
9. Ramey, H.J. Jr.: "Approximate Solutions for Unsteady Liquid Flow in Composite Reservoirs," *J. Cdn. Pet. Tech.* (Jan.-March 1970) 32-37.
10. Lippmann, M.J., Tsang, C.F. and Witherspoon, P.A.: "Analysis of the Response of Geothermal Reservoirs under Injection and Production Procedures," paper SPE 6537 presented at the SPE 47th Annual California Regional Meeting, Bakersfield, April 13-15, 1977.
11. Tsang, C.F., Lippmann, M.J., Goranson, C.B., and Witherspoon, P.A.: "Numerical Modeling of Cyclic Storage of Hot Water in Aquifers," LBL Report 5929, Lawrence Berkeley Laboratory, Berkeley, CA (Jan. 1977).
12. Mangold, D., Wollenberg, H., and Tsang, C.F.: "Thermal Effects in Overlying Sedimentary Rock from In-Situ Combustion of a Coal Seam," LBL Report 8172, Lawrence Berkeley Laboratory, Berkeley, CA (Sept. 1978).
13. Tsang, C.F., Busheck, T., and Doughty, C.: "A Numerical Simulation of the Auburn University Field Experiments," LBL Report 10210, Lawrence Berkeley Laboratory, Berkeley, CA (Jan. 1980).
14. Carslaw, H.S. and Jaeger, J.C.: *Conduction of Heat in Solids*, second edition, Oxford U. Press, Oxford, England (1959).
15. Witherspoon, P.A., Javandel, I., Neuman, S.P., and Freeze, R.A.: *Interpretation of Aquifer Gas Storage Conditions from Water Pumping Tests*, Monograph on Project NS-38, American Gas Assn., New York City (1967).
16. Hellstrom, G., Tsang, C.F., and Claesson, J.: "Heat Storage in Aquifers. Buoyancy Flow and Thermal Stratification Problems," Dept. of Mathematical Physics, Lund Inst. of Technology, Lund, Sweden (Oct. 1979).
17. Wahl, E.F.: *Geothermal Energy Utilization*, Wiley-Interscience, New York City (1977).

APPENDIX

Theis Curve Matching

These calculations are for the hot spot with 164-ft (50-m) radius, 482°F (250°C) inside, and 212°F (100°C) outside.

Early Times (up to 0.372 day)

At match point, for $t_D = 10.0$ there is $\Delta p = 58$ psi (400 kPa) at $t = 0.026$ day for flow rate $q = 960.56$ gal/min (60.602 dm^3/s).

$$\left(\frac{kh}{\mu}\right)_e = \frac{q}{4\pi}\left(\frac{p_D}{p}\right)_m$$

$$= 3.9555 \times 10^4 \text{ md·ft/cp}$$

CURSO ORGANIZADO A SOLICITUD DE LA ORGANIZACION LATINOAMERICANA DE ENERGIA, CON LA COLABORACION DE LA COMISION FEDERAL DE ELECTRICIDAD Y EL INSTITUTO DE INVESTIGACIONES ELECTRICAS.

CURSO: "INGENIERIA DE YACIMIENTOS GEOTERMICOS"
MATERIA: ASPECTOS PRACTICOS DE LA SIMULACION NUMERICA DE YACIMIENTOS.

TEMA: FINITE-DIFFERENCE MODEL OF TWO-DIMENSIONAL SINGLE- AND TWO-PHASE HEAR TRANSPORT IN A POROUS MEDIUM-VERSION 1

PROF. ING. VICTOR ARELLANO GOMEZ

MARZO, 1 9 8 4

CONTENTS

FIGURES

TABLES

Finite-Difference Model of Two-Dimensional, Single-, and Two-Phase Heat Transport in a Porous Medium——Version I

by

Charles R. Faust and James W. Mercer

ABSTRACT

Model documentation is presented for a two-dimensional (areal) heat-transport model capable of simulating both water- and vapor-dominated geothermal reservoirs that conform with the assumptions of the model. Finite-difference techniques are used to solve for the dependent variables pressure and enthalpy. The program is designed to simulate time-dependent problems such as those associated with geothermal reservoirs undergoing exploitation, and can treat the transition from compressed water to two-phase flow. In order to simulate more complicated field problems the present program is being extended, and therefore the model described in this report is referred to as VERSION I. A listing of the computer code is included.

INTRODUCTION

The continuity equations for steam and water are reduced to two nonlinear partial differential equations in which the dependent variables are fluid pressure and enthalpy. These equations are approximated using finite-difference techniques and are solved using a direct matrix technique. The nonlinear coefficients are calculated using Newton-Raphson iteration on the accumulation terms, and an option is provided for using either upstream or midpoint weighting on the mobility terms. The model can simulate flow of compressed water, two-phase mixtures, and super-heated steam over a temperature range of 10° to 300°C. In addition, it can handle the conversion from single-phase flow to two-phase flow.

The model described in this report is referred to as VERSION I and is considered to be a research tool; that is, this version is kept as simple as possible so that the program can be easily understood and modified. For this reason, many sophisticated changes and additions which are generally required to simulate complicated field problems are not included. Such changes are the subject of current research and will be described in subsequent reports.

Final Equations

Based on these assumptions the equations describing flow and heat transport in a geothermal reservoir are (Faust, 1976):

$$\nabla\cdot\left(\frac{b\rho_s kk_{rs}}{\mu_s}\nabla p\right)+\nabla\cdot\left(\frac{b\rho_w kk_{rw}}{\mu_w}\nabla p\right) \quad + bq_s'+bq_w' = b\frac{\partial(\phi\rho)}{\partial t} \tag{1}$$

and

$$\nabla\cdot\left(\frac{b\rho_s h_s kk_{rs}}{\mu_s}\nabla p\right) + \nabla\cdot\left(\frac{b\rho_w h_w kk_{rw}}{\mu_w}\nabla p\right) \quad + \nabla\cdot\left(K_m b\left[\left(\frac{\partial T}{\partial p}\right)_h\nabla p+\left(\frac{\partial T}{\partial h}\right)_p\nabla h\right]\right)$$

$$+ bq_s'h_s'+bq_w'h_w'+q'' \quad = b\frac{\partial}{\partial t}\left[\phi\rho h+(1-\phi)\rho_r h_r\right] \tag{2}$$

where the term, q", represents the conductive-heat gain (or loss) to the confining beds (overburden and underburden), and may be obtained from,

$$q''=K_r\frac{\partial T}{\partial z}\Big|_{\substack{\text{overburden}\\\text{contact}}} -K_r\frac{\partial T}{\partial z}\Big|_{\substack{\text{underburden}\\\text{contact}}} \tag{3}$$

Auxiliary Relationships

Additional assumptions and relationships include the following:

1) The fluid enthalpy, h, of the mixture is defined in the two-phase region by:

$$h = \frac{S_s\rho_s h_s + S_s\rho_w h_w}{\rho} \tag{4}$$

2) The density, ρ, of the mixture is defined by

$$\rho = S_s\rho_s + S_w\rho_w \ . \tag{5}$$

3) Phase saturations sum to one:

$$S_s + S_w = 1 \ . \tag{6}$$

4) Porosity is a function of pressure, and can be expanded about an initial porosity distribution by a truncated Taylor series with first order pressure terms:

$$\phi = \phi_i[1+\beta(p-p_i)], \tag{7}$$

where the subscript i indicates initial values.

5) Phase viscositites are functions of temperature (Meyer and others, 1967; modified for the cgs system),

$$\mu_r = 10^{-6}(0.407\cdot T + 80.4), \tag{8}$$

and,

$$\mu_w = 10^{-6} \left\{241.4 \cdot 10^{[247.8/(T+133.15)]}\right\} \quad (9)$$

where,

μ_s = dynamic viscosity of steam, g/cm-sec,

μ_w = dynamic viscosity of water, g/cm-sec,

T = temperature, °C.

Equation 8 is valid for superheated steam at 10^6 dynes per square centimeter pressure in the temperature range of 100 to 300 degrees Celsius, and is approximately valid for steam viscosity along the saturation line in that range. Equation 9 is valid for liquid water along the saturation line from 0 to 300 degrees Celsius.

6) The relative permeability expressions are functions of saturation and are a variation of those given by Corey (1954) for a drainage displacement process, that is, vaporization dominates condensation:

$$k_{rw} = \frac{(S_w - S_{wr} - S_{sr})^4}{(1 - S_{wr} - S_{sr})^4}, \quad (10)$$

and

$$k_{rs} = \left[1 - \frac{(S_w - S_{wr} - S_{sr})}{(1 - S_{wr} - S_{sr})}\right]^2 \cdot \left[1 - \frac{(S_w - S_{wr} - S_{sr})^2}{(1 - S_{wr} - S_{sr})^2}\right] \quad (11)$$

where S_{wr} and S_{sr} are specified residual water and steam saturations.

7) Reservoir thickness, rock density, rock specific heat and intrinsic permeability are functions of the spatial coordinates.

8) Rock enthalpy may be determined by the expression,

$$h_r = c_r T \quad (12)$$

where the rock enthalpy is in ergs per gram, the temperature is in degrees Celsius, and the formation heat capacity, c_r, is in ergs per gram per degree Celsius.

9) In the two-phase region, the amount of heat lost to the well is defined as

$$q_h = q'_s h'_s + q'_w h'_w , \quad (13)$$

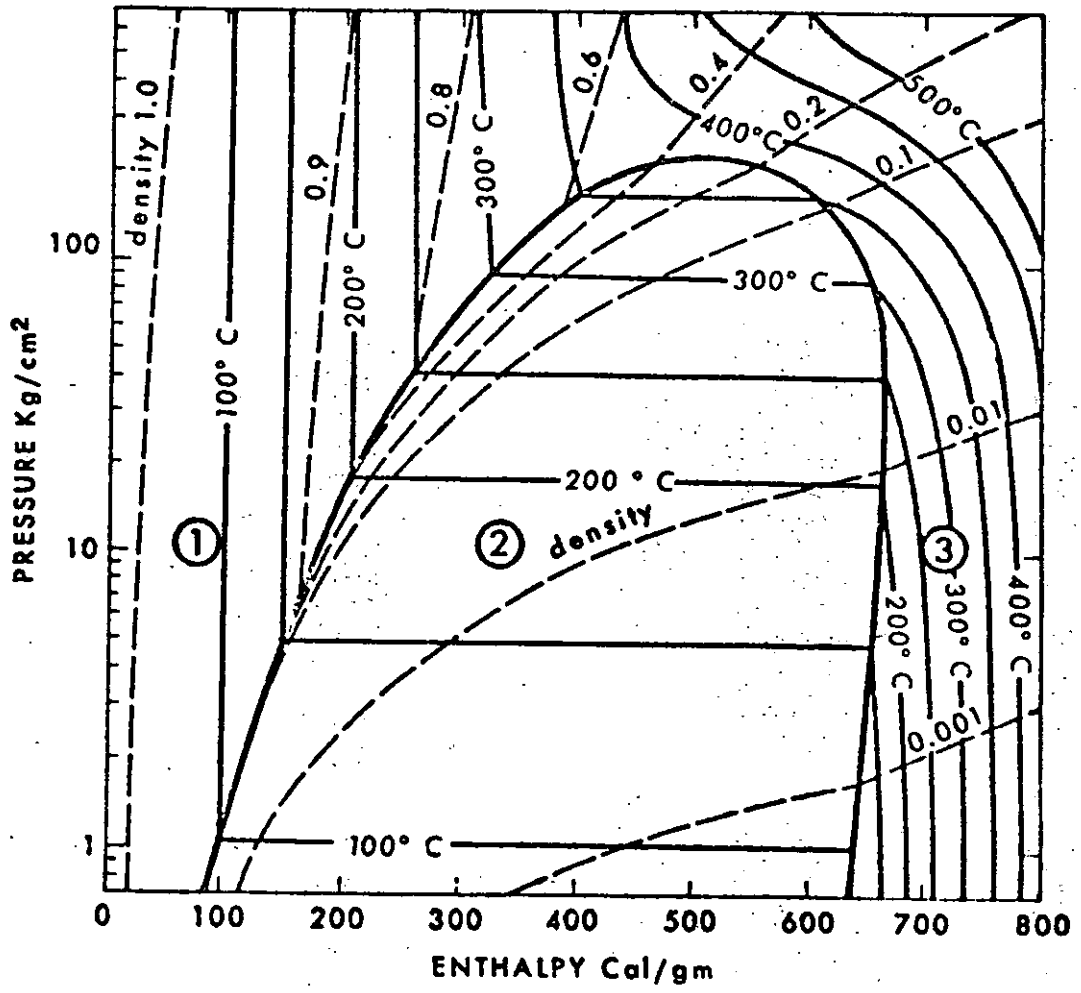

Figure 1. Pressure-enthalpy diagram for pure water and vapor showing three thermodynamic regions below the critical point: 1) compressed water, 2) two-phase steam and water and 3) superheated steam (modified from White, Muffler, and Truesdell, 1971).

and

$$h_w = 7.30984 \cdot 10^9 + 1.29239 \cdot 10^2\, p - 1.00333 \cdot 10^{-6} \cdot p^2 + 3.9881 \cdot 10^{-15} \cdot p^3 - 9.90697 \cdot 10^{15}/p + 1.29267 \cdot 10^{22}/p^2 - 6.28359 \cdot 10^{27}/p^3 , \quad (17)$$

where

p = pressure, dynes/cm^2

h = enthalpy, ergs/g

h_s = enthalpy of saturated steam, ergs/g

h_w = enthalpy of saturated water, ergs/g.

11) Temperature is treated as a function of pressure and enthalpy for the compressed-water and superheated-steam regions. For the compressed-water region,

$$T = -2.41231 + 2.56222 \cdot 10^{-8} \cdot h - 9.31415 \cdot 10^{-17} \cdot p^2 - 2.2568 \cdot 10^{-19} \cdot h^2 , \quad (18)$$

and for the superheated-steam region,

$$\begin{aligned} T = &- 374.669 + 4.79921 \cdot 10^{-6} \cdot p \\ &- 6.33606 \cdot 10^{-15} \cdot p^2 \\ &+ 7.39386 \cdot 10^{-19} \cdot h^2 \\ &- 3.3372 \cdot 10^{34}/h^2p^2 \\ &+ 3.57154 \cdot 10^{19}/p^3 \\ &- 1.1725 \cdot 10^{-37} \cdot h^3p \\ &- 2.26861 \cdot 10^{43}/h^4, \end{aligned} \tag{19}$$

where the temperature, T, is in degrees Celsius. For the two-phase (steam-water) region h_w is used in place of h in equation 18.

12) Total density, ρ, steam and water densities, ρ_s and ρ_w are considered functions of pressure and enthalpy. For the compressed-water region,

$$\begin{aligned} \rho = \rho_w = &\ 1.00207 + 4.42607 \cdot 10^{-11} \cdot p \\ &- 5.47456 \cdot 10^{-12} \cdot h \\ &+ 5.02875 \cdot 10^{-21} \cdot hp \\ &- 1.24791 \cdot 10^{-21} \cdot h^2, \end{aligned} \tag{20}$$

and for the superheated-steam region,

$$\rho = \rho_s = -2.26162 \cdot 10^{-5} + 4.38441 \cdot 10^{-9} \cdot p - 1.79088 \cdot 10^{-19} \cdot ph + 3.69276 \cdot 10^{-36} \cdot p^4 + 5.17644 \cdot 10^{-41} \cdot ph^3 , \quad (21)$$

where density is in grams per cubic centimeter. For the steam-water region, saturation pressures and enthalpies are used in equation 20 and 21 to obtain ρ_s and ρ_w .

Numerical Development

The technique used to solve equations 1 and 2 is based on the finite-difference method. For this method the areal extent of the reservoir is subdivided into rectangular grid blocks (see figure 2) in which the fluid and reservoir properties are assumed uniform. The continuous derivatives in equations 1 and 2 are approximated by finite-difference expressions at points (nodes) in the centers of the blocks. This results in a nonlinear system of 2n equations with 2n unknowns (the values of pressure and enthalpy at the nodes) where n is the number of nodes. The general finite-difference representation and solution procedure for this system of nonlinear equations are outlined below.

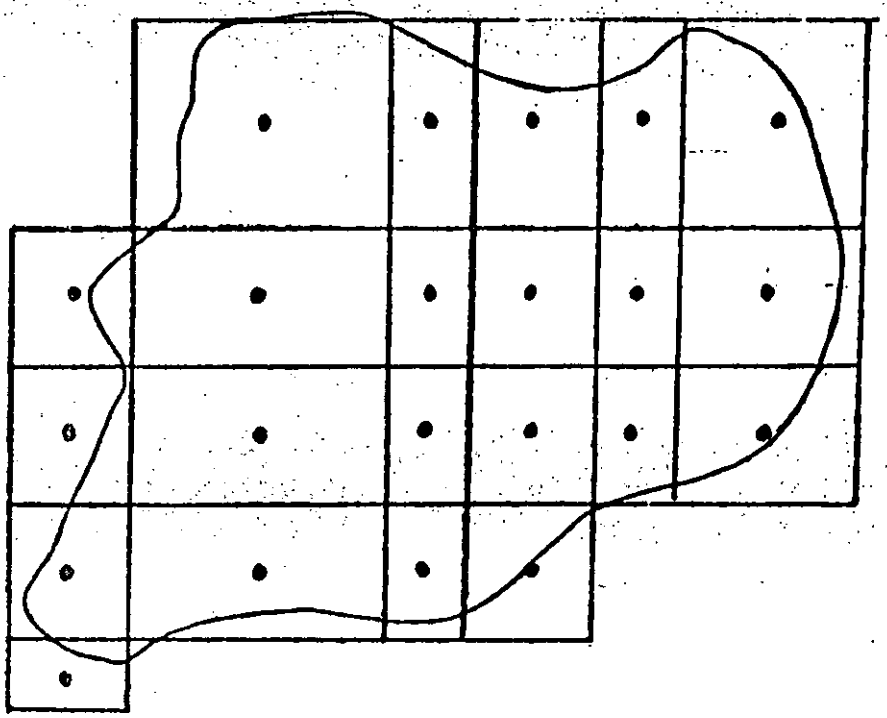

Figure 2. Finite-difference grid showing the locations of the reservoir, the grid blocks and nodes.

Finite-Difference Representation

Equations 1 and 2 may be written in compact, implicit finite-difference form as:

$$\Delta_x[(T_{wx}+T_{sx})\Delta_x p^{n+1}] + \Delta_y[(T_{wy}+T_{sy})\Delta_y p^{n+1}] + Vq'_m = \frac{1}{\Delta t}(M^{n+1}-M^n) , \tag{22}$$

and

$$\Delta_x(T_{hx}\Delta_x p^{n+1}) + \Delta_y(T_{hy}\Delta_y p^{n+1}) + \Delta_x(T_{cx}\Delta_x h^{n+1}) + \Delta_y(T_{cy}\Delta_y h^{n+1}) + Vq'_h + \frac{V}{b}q'' = \frac{1}{\Delta t}(E^{n+1}-E^n) , \tag{23}$$

where the right sides of equations 22 and 23 are the accumulation terms for mass and energy, respectively, and q'_m and q'_h are the total mass and heat lost to wells, respectively.

The transmissibility terms T_w , T_s , T_h , and T_c , are given by:

$$T_w = (kA/\ell)\rho_w k_{rw}/\mu_w \,, \tag{24a}$$

$$T_s = (kA/\ell)\rho_s k_{rs}/\mu_s \,, \tag{24b}$$

$$T_h = T_w h_w + T_s h_s + (AK_m/\ell)\left(\frac{\partial T}{\partial p}\right)_h \,, \tag{24c}$$

$$T_c = (AK_m/\ell)\left(\frac{\partial T}{\partial h}\right)_p \,, \tag{24d}$$

and the mass and energy terms M and E are:

$$M = V\phi\rho \,, \tag{25a}$$

$$E = V[\phi\rho h + (1-\phi)\rho_r h_r] \,, \tag{25b}$$

where V, A and ℓ are the grid block volume, cross-sectional area perpendicular to the flow direction, and the length increment in the flow direction, respectively. The difference operator acts as follows:

$$\Delta_x(T_{wx}\Delta_x p^{t+\Delta t}) = T_{wx_{i+\frac{1}{2},j}}\,(p^{t+\Delta t}_{i+1,j} - p^{t+\Delta t}_{i,j})$$

$$- T_{wx_{i-\frac{1}{2},j}}\,(p^{t+\Delta t}_{i,j} - p^{t+\Delta t}_{i-1,j}) \,, \tag{26}$$

where i and j are indices in the x- and y- directions, and t is the index for the time level.

The interblock transmissibility terms (values at $i + \frac{1}{2}$, $i - \frac{1}{2}$, $j + \frac{1}{2}$ and $j - \frac{1}{2}$) are composed of two parts: that which is a function of space only (for example, kA/ℓ) and that which is a nonlinear function of pressure and/or enthalpy (for example $\rho k_r/\mu$). To approximate these terms requires averaging or weighting of the various components over each grid block. For the space dependent part, this is accomplished by using a harmonic mean, for example,

$$(kA/\ell)_{i+\frac{1}{2}} = \frac{2k_{i+1}k_iA_{i+1}A_i}{k_{i+1}A_{i+1}\ell_i + k_iA_i\ell_{i+1}} \qquad (27)$$

The nonlinear part of the transmissibility terms are generally assigned the upstream value. The upstream node is determined by comparing the pressures at (i) and (i+1), and using the larger pressure to compute the nonlinear part. Alternatively this part may be determined by a length weighted arithmetic average, for example,

$$k_{rw_{i+\frac{1}{2}}} = \frac{k_{rw_{i+1}}\ell_{i+1} + k_{rw_i}\ell_i}{\ell_{i+1} + \ell_i} \qquad (28)$$

Of the two procedures, upstream weighting yields a lower order approximation of the spatial derivative but exhibits a more stable solution.

Solution Procedure

The difference equations 22 and 23 are solved simultaneously for the unknown pressure and enthalpy in each grid block for each time step. Since equations 22 and 23 are nonlinear, a provision is included to iterate on nonlinear coefficients. Newton-Raphson iteration is used on the accumulation terms and Picard iteration is used on the coefficients of the spatial derivatives. Two difference equations are obtained for each grid block, and the resulting system of 2n equation has the form,

$$[B]\ \{X^{t+\Delta t}\} - \{f(X^{t+\Delta t})\} + \{f(X^{t})\} + \{q\} = 0\ , \qquad (29)$$

where the superscript indicates the time level, the matrix [B] incorporates the transmissibility terms, the vector {X} contains the unknown pressure and enthalpy values, that is

$$\{X\} = \begin{Bmatrix} p_1 \\ h_1 \\ p_2 \\ h_2 \\ \vdots \\ p_n \\ h_n \end{Bmatrix}$$

and the vector {f(X)} is a non-linear function describing the accumulation terms.

To linearize 29, an iterative technique called the Newton-Raphson procedure is applied. The iteration level is indicated by a subscript, and in particular the first iteration (initial guess) is indicated by the subscript (o). Substitution of the initial guess into equation 29 yields a residual:

$$\left[B_o\right]\{X_o^{t+\Delta t}\} - \{f(X_o^{t+\Delta t})\} + \{f(X^t)\}$$

$$+ \{q_o\} = \{R(X_o^{t+\Delta t})\} . \qquad (30)$$

For the first time step, the initial conditions are used as the initial guess; for subsequent time steps, the results from the previous time step are used as the initial guess.

If the residual is expanded in a truncated first order Taylor series, one obtains,

$$\{R(X^{t+\Delta t})\} = \{R(X_o^{t+\Delta t})\} + \{\Delta X\}\left[\frac{\partial\{R(X_o^{t+\Delta t})\}}{\partial X_o^{t+\Delta t}}\right] \doteq 0 ,$$

or rearranging,

$$\left[\frac{\partial\{R(X_o^{t+\Delta t})\}}{\partial X_o^{t+\Delta t}}\right]\{\Delta X\} = - \{R(X_o^{t+\Delta t})\} . \qquad (31)$$

Taking the derivatives with respect to the unknown vector {X} equation 35 yields,

$$\left[\frac{\partial\{R(X_o^{t+\Delta t})\}}{\partial X_o^{t+\Delta t}}\right] = \left[B_o\right] - \left[\frac{\partial\{f(X_o^{t+\Delta t})\}}{\partial X_o^{t+\Delta t}}\right] , \qquad (32)$$

where $\left[\frac{\partial\{f(X_o^{t+\Delta t})\}}{\partial X_o^{t+\Delta t}}\right]$ is obtained by taking the partial derivatives of the accumulation terms with respect to pressure and enthalpy. Specifically, by use of the chain rule:

$$b\,\frac{\partial(\phi\rho)}{\partial p} = b\left[\rho\frac{d\phi}{dp} + \left(\frac{\partial\rho}{\partial p}\right)_h\right]$$

$$b\,\frac{\partial(\phi\rho)}{\partial h} = b\left(\frac{\partial\rho}{\partial h}\right)_p ,$$

$$b\,\frac{\partial}{\partial p}\left[\phi\rho h + (1-\phi)\rho_r h_r\right] = b\left[(\rho h - \rho_r h_r)\frac{d\phi}{dp} + h\left(\frac{\partial\rho}{\partial p}\right)_h + (1-\phi)\rho_r c_r\left(\frac{\partial T}{\partial p}\right)_h\right] ,$$

and

$$b\,\frac{\partial}{\partial h}\left[\phi\rho h + (1-\phi)\rho_r h_r\right] = b\left[\phi h\left(\frac{\partial\rho}{\partial h}\right)_p + (1-\phi)\rho_r c_r\left(\frac{\partial T}{\partial h}\right)_p + \phi\rho\right] .$$

Substituting 32 into equation 31 gives,

$$\left[\left[B_o\right] - \left[\frac{\partial\{f(X_o^{t+\Delta t})\}}{\partial X_o^{t+\Delta t}}\right]\right]\{\Delta X\} = -\{R(X_o^{t+\Delta t})\} , \qquad (33)$$

which is the matrix equation to be solved.

The new values of $X^{t+\Delta t}$ are determined from,

$$\{X_i^{t+\Delta t}\} = \{X_{i-1}^{t+\Delta t}\} + \{\Delta X\} \tag{34}$$

where $i = 1,2,\ldots,m$, m being the specified number of iterations. If $m = 1$, this procedure is equivalent to the residual formulation outlined by Weinstein, Stone, and Kwan (1969).

In most of the two-dimensional, areal simulations studied it was not necessary to use Newton-Raphson iteration on the nonlinear coefficients in [B] and {q} to obtain satisfactory solutions. For radial problems and vertical cross-sections this is not the case as pointed out by Toronyi and Farouq Ali (1975). As stated earlier, Picard iteration is used for [B] and {q}. In this process the nonlinear coefficients are simply updated on each iteration.

The solution of the linearized matrix equation 33 is solved using the Gauss-Doolittle method for banded, nonsymmetric matrices. The coefficient matrix is decomposed into the product of upper and lower triangular matrices, from which the solution may be determined by back substitution. Because the coefficient matrix is nonlinear, this solution procedure is required for each iteration of each time step. The general form of the coefficient matrix and the form in which it is stored in the program is shown in figure 3, where MDIM is the matrix bandwidth and NDIM is the number of rows.

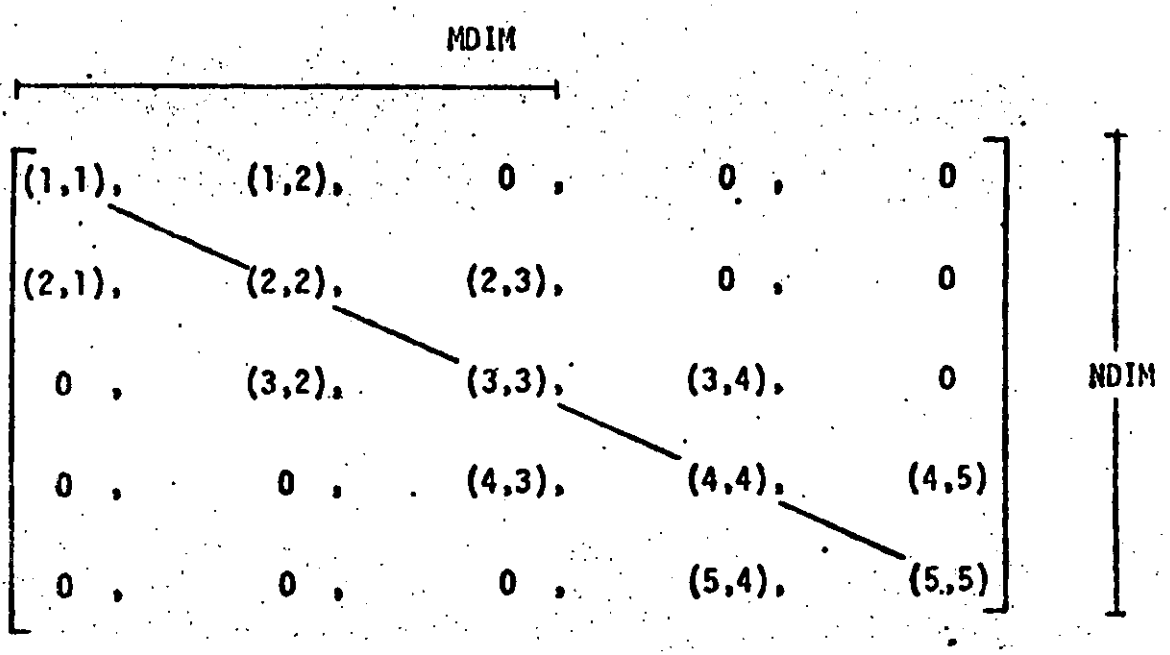

a. Normal storage of matrix where bold marks indicate the main diagonal.

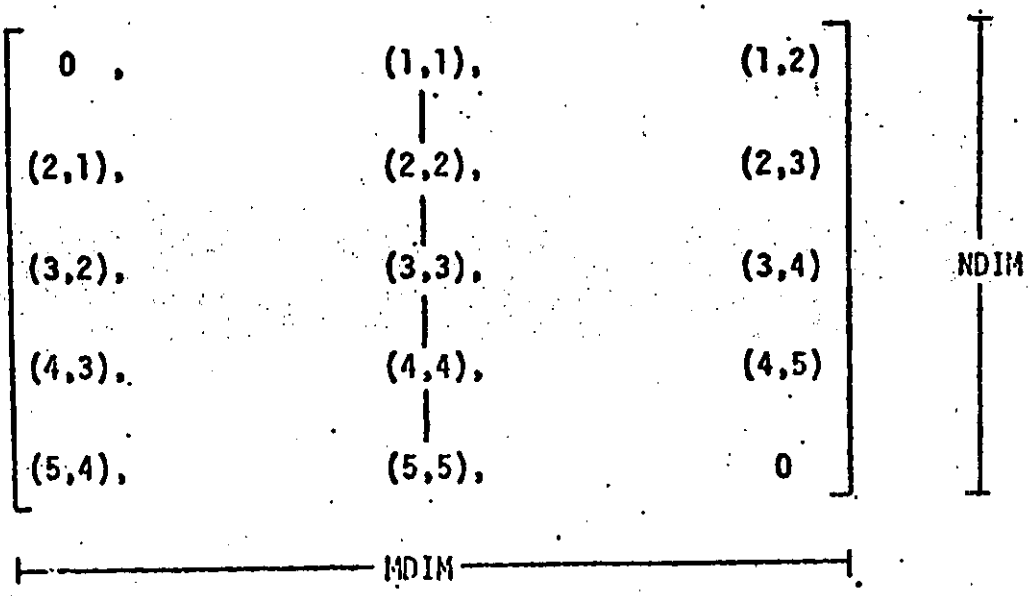

b. Banded storage of matrix showing new location of the main diagonal.

Figure 3. Normal storage of matrix and banded storage of matrix.

Heat Loss Calculations

Geothermal reservoirs occur in areas of anomalously high heat flow. The effects of the high geothermal gradient and the loss and gain of heat to the base and cap rock are important factors that are incorporated into the reservoir model. In a typical hydrothermal system, heat flows into the reservoir at the base and out at the top.

In order to obtain the heat flux through the confining beds three simplifying assumptions are made. First, the permeability in the confining bed is assumed to be low and convective flow may be neglected; thus, only the heat conduction equation needs to be solved. Further, the horizontal conduction terms in the confining beds are assumed to be small relative to the vertical terms, and may be neglected. For petroleum reservoirs undergoing thermal recovery, it has been demonstrated that the effect of horizontal conduction in the confining beds is small (Chase and O'Dell, 1973). This assumption leads to the one-dimensional, heat-conduction equation:

$$K_r \frac{\partial^2 T'}{\partial z^2} = (\rho c)_r \frac{\partial T'}{\partial t}$$

where the vertical thermal conductivity, density, and heat capacity of the confining bed are considered constant. The final assumption is that the geothermal reservoir, prior to exploitation, is at steady state; that is, the heat entering at the base equals that leaving at the top and the net heat gain of the reservoir is zero. This assumption allows consideration of only the "transient" heat flow caused by temporal temperature changes in the reservoir.

Therefore, the one-dimensional, conduction equation may be reformulated as follows:

$$K_r \frac{\partial^2 T^*}{\partial z^2} = (\rho c)_r \frac{\partial T^*}{\partial t} \qquad (35)$$

where $T^* = T' - T'_0$ (T' is the temperature in the confining bed and T'_0 is the initial temperature in the confining bed.)

Equation 35 is subject to initial and boundary conditions. The initial conditions are simply $T^*(z,0) = 0$. For the boundary condition at the top of the cap rock, the temperature change is assumed to be zero for all time. At the cap rock-reservoir boundary, a step function in temperature is used. It is determined using the difference between the initial reservoir temperature and the reservoir temperature at the last time step (that is, the step function is lagged by one time step). Once the T^* distribution through the cap rock is determined, Fourier's equation is used to compute the heat flux.

A similar set of boundary and initial conditions apply to the base rock; however, instead of solving equation 35 for both the top and bottom, it is assumed that the two fluxes are approximately equal and therefore the total heat leakage is obtained by multiplying the flux computed at the top by two. This assumption is valid since only the "transient" heat leakage is considered; however, this portion of the program could be modified if needed (for example, if steady state thermal gradients above and below the reservoir are significantly different).

In the numerical model, equation 35 is actually solved at each grid block for each iteration. It is solved using a Galerkin, finite-element approximation for the space derivative combined with an implicit difference approximation for the time derivative. Linear elements are used with a variable mesh generator that divides the confining bed thickness into ten elements that double in size with distance from the reservoir boundary. Therefore, the element adjacent to the reservoir is relatively small, and it is the temperature difference across this element that is used in Fourier's equation to compute the heat flux.

MODEL DOCUMENTATION

Notes on Use of Program

(1) This version of the finite-difference model is restricted to problems involving confined, horizontal reservoirs exhibiting two-dimensional flow. Futhermore, the reservoir is overlain and underlain by impermeable layers that allow only conduction of heat.

(2) To minimize core requirements, the dimensions of the arrays A(NBB,MBE) and R(NBB) must be specified for each problem, where

$$NBB = 2*NB$$

(NB - number of nonzero blocks, that is, blocks that have nonzero permeability) and MBE is the estimated matrix bandwidth given for two simultaneous unknowns at each grid block by

$$MBE = 2 * (2 * MM + 1) + 1$$

where,

$$MM = NY \text{ IF } NX > NY$$
$$MM = NX \text{ IF } NY > NX$$

and NX and NY are the number of columns and rows, respectively.

(3) The actual matrix bandwidth is computed internally and printed. If it differs from the estimated bandwidth, change MBE so that it is equal to the actual matrix bandwidth. Also, change the dimensions of array A.

(4) The regression equations used in this program are based on steam table data for a temperature range of 10° to 300°C.

(5) The units of the input data must be in the cgs system.

(6) At present most arrays are dimensioned to solve problems with a maximum of 20 columns and 10 rows.

(7) Relative permeability functions described in equations 10 and 11 are programmed in SUBROUTINE PRPTY statement numbers PRP1230 - PRP1300 where the residual water saturation, S_{wr} = 0.3 and the residual steam saturation, S_{sr} = 0.05. Other equations may be substituted for these; the only restriction is that relative permeability must be a smooth function of saturation. A non-smooth relationship (such as linear interpolation between data points) can result in an oscillatory, unstable solution.

(8) The two-dimensional treatment in this model assumes that the fluid properties are uniform with depth. This assumption is probably valid only for very thin reservoirs, but may be a suitable approximation for some applications.

(9) The program should be in double precision, except when using a computer having single precision accuracy to 10 significant digits, in which case remove the REAL*8 IMPLICIT cards.

(10) Although the unknown dependent variables are pressure and enthalpy, the user is given the option to read in either initial pressures and temperatures (KØD9 = 1) or initial pressures and enthalpies (KØD9 = 0). This option is provided since field temperatures are more readily available than enthalpies. If temperatures are read, they are converted in the program to enthalpies, and subsequent calculations are made using the enthalpy values. If the initial conditions of the reservoir are two phase, the user must read in enthalpies.

(11) To reduce the number of lines in the output, only the computed pressures and enthalpies are printed for each time step. The user may, however, also have the computed water saturations, temperatures, and fluid densities printed as often as desired by specifying the proper value for IPRT. This parameter allows the additional data to be printed every IPRT time step. For example, if IPRT = 10, saturations, temperatures and densities will be printed on time step 1, 10, 20, . . . until the end of the simulation.

(12) Minimum number of blocks required for a successful run are two in the x-direction and two in the y-direction.

Description of the Subroutines

The FØRTRAN IV code contains a main program and 12 subroutines, which are shown diagrammatically in Figure 4. The purpose of each subroutine is listed below.

MAIN Driving program for the subroutines. In addition, the large arrays, A and R, are dimensioned to minimize core requirements.

GDATA Reads and writes problem information according to the formats listed in the INPUT section of this report.

READ Reads the two dimensional arrays containing data for each finite-difference block.

TCALC Computes the interblock transmissibility terms. Intrinsic permeability is determined as a harmonic mean of the values in the two blocks.

MATR Computes and prints matrix bandwidth. The estimated bandwidth should equal the computed bandwidth. The bandwidth is used in dimensioning arrays, and if the estimated and computed bandwidths are not equal, computational errors could result. See the section on 'Notes on Use of Program' for details on how to calculate the estimated bandwidth.

PRPTY Computes thermodynamic properties based on regression equations determined using data from steam tables.

VERTCD Computes vertical conductive heat leakage through a confining bed. This is accomplished by solving the one-dimensional, heat-conduction equation at each finite-difference grid block. The numerical method used in this subroutine is the finite-element method.

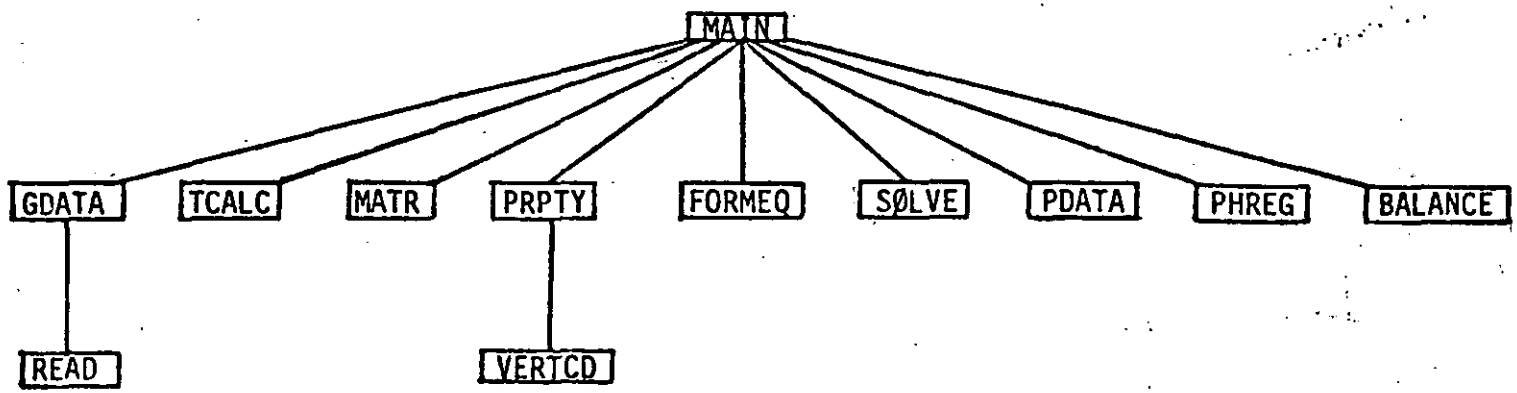

Figure 4. Program subroutines showing order and link of calling.

FØRMEQ Forms the final matrix equation. Note that the matrix is nonsymmetric and that the dependent variables, pressure and enthalpy are solved simultaneously.

SØLVE Solves the matrix equation using the Gauss-Doolittle method. It triangularizes a banded nonsymmetric matrix and then back substitutes.

PDATA Prints the computed pressures and enthalpies for each time step.

PHREG Determines the thermodynamic region for each finite-difference grid block.

BALNCE Computes a mass and energy balance for each time step.

A generalized flow chart showing the approximate order that the subroutines are used is shown in Figure 5.

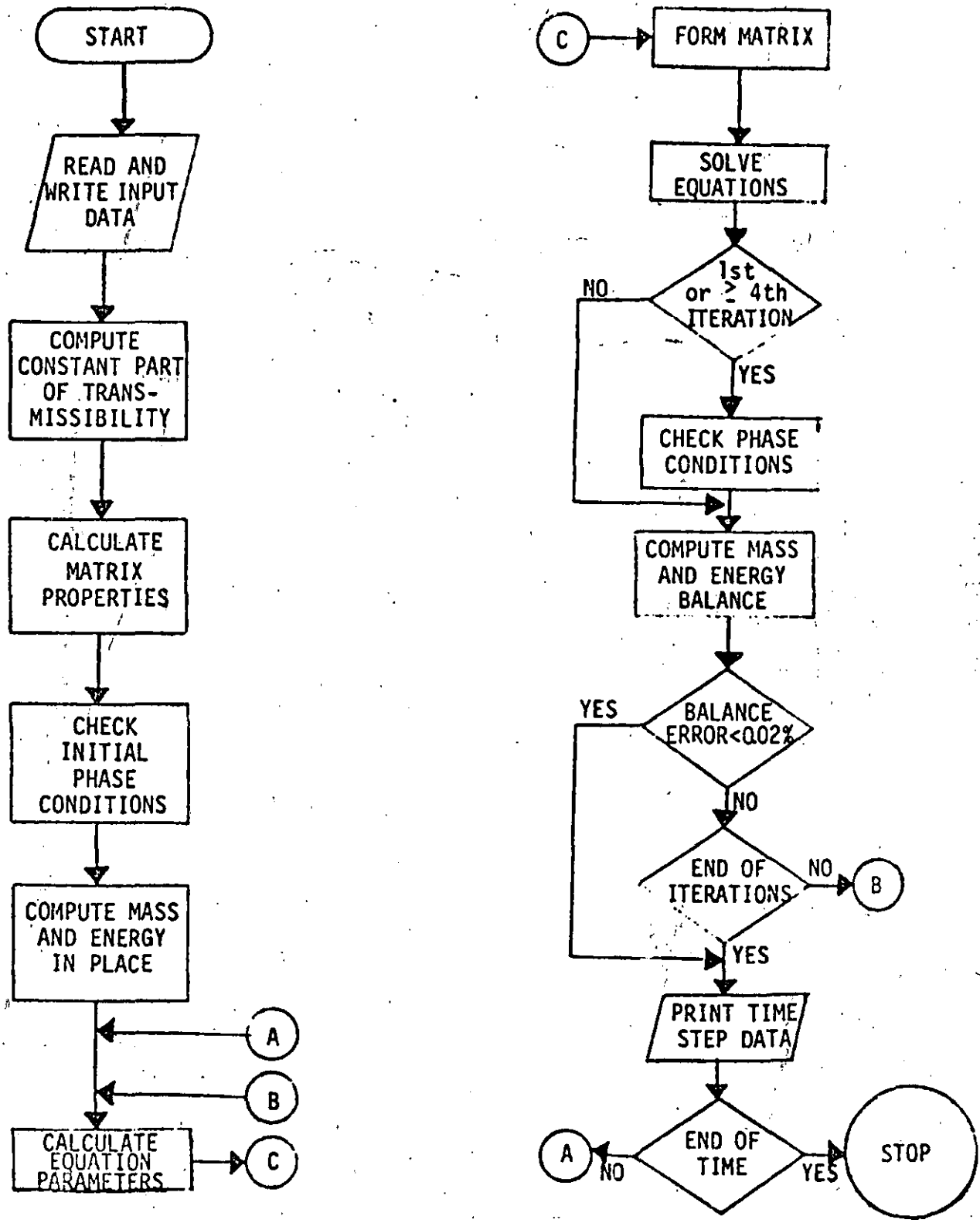

Figure 5. Generalized flow chart.

Input

Columns	Format	Name	Description
Card 1			
1-80	20A4	TITLE	Problem title
Card 2			
1-5	I5	NX	Number of columns (x-direction)
6-10	I5	NY	Number of rows (y-direction)
11-15	I5	NB	Number of non-zero blocks (those with non-zero permeability)
16-20	I5	NK	Maximum number of Newton iterations
21-25	I5	NT	Maximum number of time steps
26-30	I5	NS	Number of sources
31-35	I5	MBE	Estimated bandwidth (see text)
36-40	I5	IØPT	Read 1 for upstream weighting; 2 for midpoint weighting (See section on Finite-Difference Representation)
41-45	I5	PPRT	Number of time steps between printing thermodynamic data
Card 3			
1-10	G10.0	DELT	Time step (in seconds)

Columns	Format	Name	Description
Card 4			
1-5	I5	KØD1	Read 1 if x-spacing is constant (otherwise, leave blank)
6-10	I5	KØD2	Read 1 if y-spacing is constant
11-15	I5	KØD3	Read 1 if initial pressure is constant
16-20	I5	KØD4	Read 1 if initial enthalpy is constant
21-25	I5	KØD5	Read 1 if x-permeability is constant
26-30	I5	KØD6	Read 1 if y-permeability is constant
31-35	I5	KØD7	Read 1 if initial porosity is constant
36-40	I5	KØD8	Read 1 if reservoir thickness is constant
41-45	I5	KØD9	Read 1 if temperature is read in place of enthalpy
		Data Set 1 - X-spacing	
1-80	8G10.0	DX(I)	Spacing in the x-direction (NX values); if constant, KØD1 = 1 and only read one value (cm)
		Data Set 2 - Y-spacing	
1-80	8G10.0	DY(J)	Spacing in the y-direction (NY values); if constant, KØD2 = 1 and only read one value (cm)
		Data Set 3 - Initial pressure[4]	
1-80	8G10.0	P(I,J)	Initial pressure distribution in the reservoir; if constant, KOD3 = 1 and only read one value (dynes/cm^2)

[4]Start new card for the beginning of each new row (may start with the top row or bottom row, but be consistent) leaving blanks for missing blocks.

Columns	Format	Name	Description
		Data Set 4 - Initial enthalpy [4]+	
1-80	8G10.0	H(I,J)	Initial enthalpy distribution in the reservoir; if constant, KØD4 = 1 and only read one value (ergs/g)
		Data Set 5 - X-permeability [4]	
1-80	8G10.0	XK(I,J)	Reservoir permeability in x-direction; if constant, KØD5 = 1 and only read one value (cm^2)
		Data Set 6 - Y-permeability [4]	
1-80	8G10.0	YK(I,J)	Reservoir permeability in y-direction; if constant, KØD6 = 1 and only read one value (cm^2)
		Data Set 7 - Porosity [4]	
1-80	8G10.0	PHI(I,J)	Reservoir porosity; if constant, KØD7 = 1 and only read one value (dimensionless)
		Data Set 8 - Thickness [4]	
1-80	8G10.0	DZ(I,J)	Reservoir thickness; if constant, KØD8 = 1 and only read one value (cm)

[4] Start new card for the beginning of each new row (may start with the top row or bottom row, but be consistent) leaving blanks for missing blocks.

+ If KØD9 = 1, read initial temperature distribution (°C) instead.

Columns	Format	Name	Description
		Data Set 9 - Sources	
1-5	I5	I	Column number of well
6-10	I5	J	Row number of well
11-25	G15.0	Q(I,J)	Strength (g/s) of source/sink at block i,j

Note: 1-NS cards; if NS = 0 this data set is omitted.

Card 5

1-10	G10.0	XKC	Medium thermal conductivity of the reservoir (ergs/s-cm°C)
11-20	G10.0	CØND	Confining bed thermal conductivity (ergs/s-cm°C)
21-30	G10.0	PHFWT	Rock enthalpy derivative with respect to temperature (specific heat) (ergs/g°C)
31-40	G10.0	DF	Rock density (g/cm^3)
41-50	G10.0	BETA	Compressibility of reservoir (cm^2/dyne)

Output

To aid the user in detecting errors associated with data input, data that is read in is immediately printed; thus output appears in the following order:

- Title of Problem
- Finite-Difference Data
- Grid Numbers
- Time Parameters
- Codes
- Spacing in X-Direction
- Spacing in Y-Direction
- Initial Pressure
- Initial Enthalpy
- X-Permeability
- Y-Permeability
- Initial Porosity
- Reservoir Thickness
- Sources
- Rock Properties
- Maximum Bandwidth

In addition, every IPRT time step the following is also printed:

- Water Saturations
- Temperatures
- Density

} Printed at beginning of time step, but are based on pressure and enthalpy from previous time step.

Finally, on a successful run, the following is printed every time step:

Step Number

Time

Pressure Values

Enthalpy Values

Mass and Energy Balance

APPLICATIONS

Example 1

The linear flow of hot incompressible fluid through a confined aquifer may be described by the following equations:

$$K_r \frac{\partial^2 u}{\partial z^2} = \rho_r c_r \frac{\partial u}{\partial t}, \quad z > 0, \; t > 0 \tag{36a}$$

$$K_t \frac{\partial^2 u}{\partial x^2} - v_w \rho_w c_w \frac{\partial u}{\partial x} + \frac{2}{b} K_r \frac{\partial u}{\partial z} = \rho_t c_t \frac{\partial u}{\partial t}, \quad z = 0, \; x > 0, \; t > 0 \tag{36b}$$

subject to:

$$u(x,0) = 0, \; x > 0$$

$$u(0,t) = 1, \; z = 0, \; t \geq 0$$

$$\lim_{x^2 + z^2 \to \infty} u = 0$$

where $u = \frac{T-T_o}{T_1-T_o}$ is the normalized temperature; T_o is the overburden (underburden) temperature and the initial aquifer temperature; and T_1 is the temperature of the injection fluid. The subscripts refer to the rock, r, water, w, and total (rock and water), t.

Avdonin (1964) presents an analytical solution for equation (36):

$$u(\chi,\tau) = \frac{\chi}{\sqrt{\pi\tau}} \int_0^1 \left\{ \exp\left[- (s\gamma\sqrt{\tau} - \frac{\chi}{2s\sqrt{\tau}})^2 \right] \operatorname{erfc} \left(\frac{\alpha s^2\sqrt{\tau}}{2\sqrt{1-s^2}} \right) \right\} \frac{ds}{s^2} \cdots$$

where $\chi = \frac{2x}{b}$; $\tau = \frac{4K_t t}{c_t \rho_t b^2}$; $\gamma = \frac{Qc_w\rho_w}{4K_t}$;

$\alpha = \sqrt{\frac{K_r c_r \rho_r}{K_t c_t \rho_t}}$; and Q is the injection flow rate. (In the original reference, γ is defined with an 8 in the denominator; this appears to be a typographical error.)

To simulate this problem, the following assumptions were made:

1) Temperature is a function of enthalpy only, according to:

$$T = - 0.0208 + 2.39 \times 10^{-8} h \qquad (38)$$

2) Density is a function of pressure only, according to:

$$\rho = 0.989875 + 4.00894 \times 10^{11} p \qquad (39)$$

3) Porosity is constant.

These changes must be made in the program by appropriately changing the single-phase (water) statement functions for temperature and density, and by appropriately changing their respective pressure- and enthalpy-derivatives. For constant porosity, beta is read as zero. Other parameters and the initial conditions used in this example are given in table 1. A block-centered grid consisting of 20 blocks was used, and the time step was 6.25×10^6 sec. The total simulation time was 3.75×10^8 sec.

The results are presented in figure 6. This problem was chosen because it exhibits pronounced truncation error in the approximation of the spatial derivatives. Time steps were chosen to reduce time truncation errors. Both mid-point weighting and upstream weighting were used. It is clear that mid-point weighting approximates the temperature front better than upstream weighting, but exhibits oscillations at the base of the front. Upstream weighting smears the front out by numerical diffusion and does not exhibit oscillations.

TABLE 1 - DATA FOR AVDONIN LINEAR EXAMPLE

PARAMETER	SYMBOL	VALUE
velocity	v	1.28×10^{4} cm/sec
porosity	ϕ	0.20
reservoir thermal conductivity	K_m	3.20×10^{6} ergs/sec-cm °C
confining bed thermal conductivity	K'	3.20×10^{5} ergs/sec-cm °C
rock density	ρ_r	2.50 g/cm^3
rock specific heat	c_r	1.01×10^{7} ergs/g °C
aquifer thickness	b	2.00×10^{4} cm
initial pressure	p_i	1.38×10^{7} dynes/cm2
initial enthalpy	h_i	3.35×10^{9} ergs/g
initial fluid viscosity	u_i	3.58×10^{-3} g/cm-sec
initial temperature	T_i	80.19 °C
injection temperature	T'	40.01 °C
fluid density	ρ	0.99 g/cm^3
fluid specific heat	c_w	4.18×10^{7} ergs/g°C

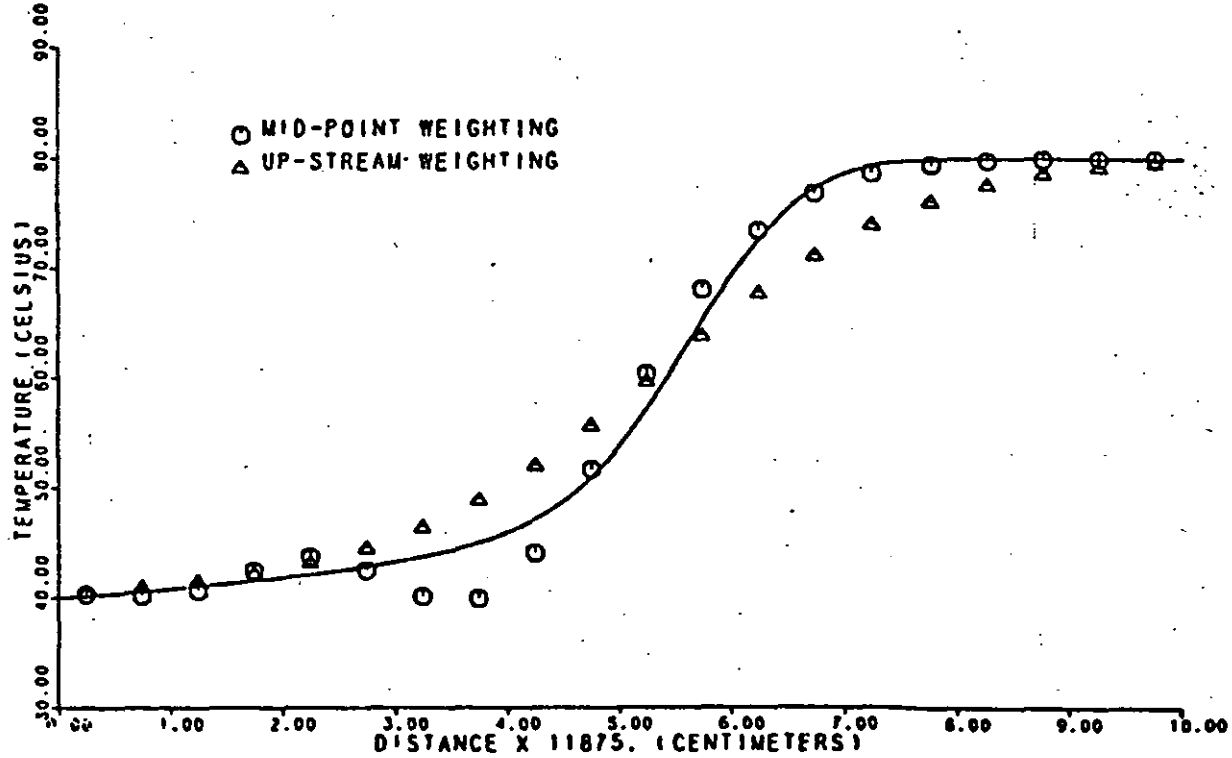

Figure 6. Finite-difference solution for the Avdonin linear example at time = 3.75×10^8 sec; analytical solution indicated by solid line.

NOTATION

Parameter	Coded Name	Description
b	DZ	reservoir thickness
c_r	PHFWT	rock specific heat
h	H	enthalpy
h_r	HROCK	rock enthalpy
h_s	HS	steam enthalpy
h_w	HW	water enthalpy
K_m	XKC	medium thermal conductivity
K_r	CØND	confining bed thermal conductivity
k	XK	x- permeability
	YK	y- permeability
k_r	XKW	water relative permeability
	XKS	steam relative permeability
p	P	pressure
q_m^*	Q	mass source term
q_h^*	QH	energy source term
q^{ll}	CQ	vertical conductive energy source term
S_w	SW1	water volume saturation
T	TEMP2	temperature
t	TIME	simulation time
β	BETA	rock compressibility
μ_s	VS	steam viscosity

Parameter	Coded Name	Description
μ_w	VW	water viscosity
ρ	DEN2	density
ρ_r	DF	rock density
ρ_s	DS	steam density
ρ_w	DW	water density
ϕ	PHI	porosity

REFERENCES CITED

Avdonin, N. A., 1964, Some formulas for calculating the temperature field of a stratum subject to thermal injection: Neft' i Gaz, v. 3, p. 37-41.

Chase, C. A., and O'Dell, P. M., 1973, Application of variational principles to cap and base rock heat losses: Soc. Petroleum Engineers Jour., v. 13. p. 200-210.

Corey, A. T., 1954, The interrelation between gas and oil relative permeabilities: Producers Monthly, v. 19, p. 38-41.

Faust, C. R., 1976, Numerical simulation of fluid flow and energy transport in liquid- and vapor-dominated hydrothermal systems: University Park, Pa., Pennsylvania State Univ., Ph.D. thesis, 163 p.

Faust, C. R., and Mercer, J. W., 1975, Mathematical modeling of geothermal systems, in Proceedings of the Second United Nations Symposium on the development and use of geothermal resources, San Francisco, Calif., May 20-29, 1975: United Nations, v. 3, p. 1635-1642.

Faust, C. R., and Mercer, J. W., 1976, An analysis of finite-difference and finite-element techniques for geothermal reservoir simulation, in Numerical simulation of reservoir performance, Society of Petroleum Engineers of AIME, 4th Symposium, Los Angeles, Calif., Feb. 19-20, 1976, Proc.: Soc. Petroleum Engineers, Paper SPE-5742, p. 337-354.

Keenan, J. H., Keys, F. G., Hill, P. G., and Moore, J. G., 1969, Steam tables: London, John Wiley & Son, Inc., 162 p.

Mercer, J. W., Faust, C. R., and Pinder, G. F., 1974, Geothermal reservoir simulation, in Conference on research for the development of geothermal energy resources, sponsored by National Science Foundation, Pasadena, Calif., Sept. 23-25, 1974, Proc.: Natl. Sci. Found. Rept. RA-N-74-159, p. 256-267.

Meyer, C. A., McClintock, R. B., Silvestri, G. J., and Spencer, R. C., 1967, ASME Steam Tables: New York, American Society of Mechanical Engineers, 2d ed., 328 p.

Toronyi, R. M., and Farouq Ali, S. M., 1975, Two-phase, two-dimensional simulation of a geothermal reservoir and the wellbore system, in Society of Petroleum Engineers of AIME, 50th Ann. Fall Mtg., Dallas, Tex., Sept. 28-Oct. 1, 1975, Proc.: Soc. Petroleum Engineers, Paper SPE-5521, 26 p.

Weinstein, H. G., Stone, J. L., and Kwan, T. V., 1969, Iterative procedure for solution of systems of parabolic and elliptic equations in three dimensions: I and EC Fund, v. 2, no. 2, p. 281-287.

White, D. E., Muffler, L. P. J., and Truesdell, A. H., 1971, Vapor-dominated hydrothermal systems compared with hot-water systems: Econ. Geology, v. 66, p. 75-97.

PROGRAM LISTING

```
C     MAIN PROGRAM                                                      MAP  10
C     ************                                                      MAP  20
      IMPLICIT REAL*8(A-H,O-Z)                                          MAP  30
C                                                                       MAP  40
C     PURPOSE:  TO SIMULATE VAPOR- AND LIQUID-DOMINATED GEOTHERMAL      MAP  50
C               RESERVOIRS USING FINITE DIFFERENCE TECHNIQUES           MAP  60
C     PROGRAMED BY CHARLES R. FAUST AND JAMES W. MERCER                 MAP  70
C                  U. S. GEOLOGICAL SURVEY                              MAP  80
C                  1975-1976                                            MAP  90
C     ----------------------------------------------------------------MAP 100
C                                                                       MAP 110
C     TO MINIMIZE CORE, DIMENSION A AND R FOR EACH PROBLEM:             MAP 120
C     A(NBH,MBE), R(NHB)                                                MAP 130
      DIMENSION A(300,43), R(300)                                       MAP 140
C                                                                       MAP 150
      COMMON /INPUT/ PHI(20,10),AK(20,10),YK(20,10),P(20,10),H(20,10),A(MAP 160
     1400),X1(400),NP(20,10),NPP(200,2),DX(20),DY(10),DZ(20,10),Q(20,10)MAP 170
      COMMON /CONTRO/ NK,NX,NXX,NY,NYY,NB,NBB,NT,DELT,TIME,PHF,T,DF,AKC,MAP 180
     1COND,COEF,BETA,IPHT                                               MAP 190
      COMMON /WORK/ AX(21,10),BX(21,10),EX(21,10),AY(20,11),BY(20,11),EYMAP 200
     1(20,11),TX(21,10),TXK(21,10),TY(20,11),TYK(20,11),XM(20,10),XMASS(MAP 210
     220,10),EN(20,10),ENERGY(20,10),C(20,10),D(20,10),F(20,10),G(20,10)MAP 220
     3,GF(20,10),XN(20,10),IP(20,10),DTP(20,10),DTH(20,10),PHIC(20,10),PMAP 230
     4OLD(20,10)                                                        MAP 240
      COMMON /EXTRA/ MBW,MBE                                            MAP 250
      COMMON /CHECK/ IND(200),INDOLD(200)                               MAP 260
C     ----------------------------------------------------------------MAP 270
C                                                                       MAP 280
C     GET DATA -                                                        MAP 290
      CALL GDATA(IOPT)                                                  MAP 300
C     ****************                                                  MAP 310
      NKK=NX                                                            MAP 320
C                                                                       MAP 330
C     FOR DIMENSIONING -                                                MAP 340
      NBBD=NBB                                                          MAP 350
      MBED=MBE                                                          MAP 360
C                                                                       MAP 370
C     CALCULATE TRANSMISSIBILITY TERMS -                                MAP 380
      CALL TCALC(DY,DX,DZ,AK,YK,TY,TYK,TX,TXK,AKC,NY,NX,NYY,NXX)        MAP 390
C     ************************************************************    MAP 400
C                                                                       MAP 410
C     CALCULATE BANDWIDTH -                                             MAP 420
      CALL MATR(NP,NY,NX,MBE,MBW)                                       MAP 430
C     ***************************                                       MAP 440
C                                                                       MAP 450
C     CHECK INITIAL PHASE CONDITIONS                                    MAP 460
C     COMPUTE THERMODYNAMIC REGION -                                    MAP 470
      CALL PHREG(IND)                                                   MAP 480
C     ***************                                                   MAP 490
      DO 10 K=1,NB                                                      MAP 500
   10 INDOLD(K)=IND(K)                                                  MAP 510
C                                                                       MAP 520
```

```
C     CALCULATE INITIAL BALANCE -                                       MAP  540
      CALL BALANCE(0,NKK,PCEE)                                          MAP  550
C     ************************                                          MAP  560
C                                                                       MAP  570
C                                                                       MAP  580
C  TIME LOOP -                                                          MAP  590
      DO 180 L=1,NT                                                     MAP  600
C                                                                       MAP  610
C  ITERATION LOOP -                                                     MAP  620
      DO 130 KKK=1,NK                                                   MAP  630
C                                                                       MAP  640
C     CALCULATE PROPERTY COEFFICIENTS -                                 MAP  650
      CALL PRPTY(L,KKK)                                                 MAP  660
C     ****************                                                  MAP  670
C                                                                       MAP  680
C     INITIALIZE BOUNDARY ARRAYS -                                      MAP  690
      DO 20 I=1,NX                                                      MAP  700
      AY(I,1)=0.D0                                                      MAP  710
      BY(I,1)=0.D0                                                      MAP  720
      EY(I,1)=0.D0                                                      MAP  730
      AY(I,NYY)=0.D0                                                    MAP  740
      BY(I,NYY)=0.D0                                                    MAP  750
   20 EY(I,NYY)=0.D0                                                    MAP  760
C                                                                       MAP  770
      DO 30 J=1,NY                                                      MAP  780
      AX(1,J)=0.D0                                                      MAP  790
      BX(1,J)=0.D0                                                      MAP  800
      EX(1,J)=0.D0                                                      MAP  810
      AX(NXX,J)=0.D0                                                    MAP  820
      BX(NXX,J)=0.D0                                                    MAP  830
   30 EX(NXX,J)=0.D0                                                    MAP  840
C                                                                       MAP  850
      DO 50 J=1,NY                                                      MAP  860
      DO 50 I=2,NX                                                      MAP  870
C     FOR UPSTREAM WEIGHTING -                                          MAP  880
      ALPHA=1.D0                                                        MAP  890
      IF (P(I-1,J).GT.P(I,J)) ALPHA=0.D0                                MAP  900
      IF (IOPT.EQ.1) GO TO 40                                           MAP  910
C     FOR MIDPOINT WEIGHTING -                                          MAP  920
      ALPHA=DX(I)/(DX(I)+DX(I-1))                                       MAP  930
   40 EX(I,J)=(ALPHA*XN(I,J)+(1.0-ALPHA)*XN(I-1,J))*TX(I,J)             MAP  940
      AX(I,J)=(ALPHA*DTP(I,J)+(1.0-ALPHA)*DTP(I-1,J))*TXK(I,J)+(ALPHA*TM
     1(I,J)+(1.0-ALPHA)*TM(I-1,J))*TX(I,J)                              MAP  950
   50 BX(I,J)=(ALPHA*DTM(I,J)+(1.0-ALPHA)*DTM(I-1,J))*TXK(I,J)          MAP  960
C                                                                       MAP  970
      DO 70 I=1,NX                                                      MAP  980
      DO 70 J=2,NY                                                      MAP  990
      ALPHA=1.D0                                                        MAP 1000
      IF (P(I,J-1).GT.P(I,J)) ALPHA=0.D0                                MAP 1010
      IF (IOPT.EQ.1) GO TO 60                                           MAP 1020
      ALPHA=DY(J)/(DY(J)+DY(J-1))                                       MAP 1030
   60 EY(I,J)=(ALPHA*XN(I,J)+(1.0-ALPHA)*XN(I,J-1))*TY(I,J)             MAP 1040
```

```
      AY(I,J)=(ALPHA*DTP(I,J)+(1.0-ALPHA)*DTP(I,J-1))*TYK(I,J)+(ALPHA*TMPNP1050
     1(I,J)+(1.0-ALPHA)*TM(I,J-1))*TY(I,J)                              PNP1060
   70 BY(I,J)=(ALPHA*DTH(I,J)+(1.0-ALPHA)*DTH(I,J-1))*TYK(I,J)          PNP1070
C                                                                       PNP1080
C     FORM FINAL MATRIX EQUATION -                                      PNP1090
      CALL FORMEQ(A,R,NBBD,MBED)                                        PNP1100
C     **************************                                        PNP1110
      IHALF=(MBW-1)/2                                                   PNP1120
C                                                                       PNP1130
C     TRIANGULARIZE -                                                   PNP1140
      CALL SOLVE(1,A,R,NBB,IHALF,NBBD,MBED)                             PNP1150
C     ************************************                              PNP1160
C                                                                       PNP1170
C     SOLVE -                                                           PNP1180
      CALL SOLVE(2,A,R,NBB,IHALF,NBBD,MBED)                             PNP1190
C     ************************************                              PNP1200
      DO 80 K=1,NB                                                      PNP1210
      X1(2*K-1)=X1(2*K-1)+R(2*K-1)                                      PNP1220
   80 X1(2*K)=X1(2*K)+R(2*K)                                            PNP1230
      IF (KKK.NE.1) GO TO 110                                           PNP1240
   85 CONTINUE                                                          PNP1245
      CALL PHREG(IND)                                                   PNP1250
C     ***************                                                   PNP1260
C                                                                       PNP1270
C     DID A CONVERSION OCCURE? -                                        PNP1280
      DO 100 K=1,NB                                                     PNP1290
```

```
  100 INDOLD(K)=IND(K)                                                  PNP1450
      GO TO 105                                                         PNP1455
  110 CONTINUE                                                          PNP1460
      IF (KKK.GE.4) GO TO 85                                            PNP1465
  105 CONTINUE                                                          PNP1467
      DO 120 K=1,NB                                                     PNP1470
      I=NPP(K,1)                                                        PNP1480
      J=NPP(K,2)                                                        PNP1490
      P(I,J)=X1(2*K-1)                                                  PNP1500
  120 H(I,J)=X1(2*K)                                                    PNP1510
      WRITE (6,190) KKK                                                 PNP1520
```

```
C                                                                       MAP1530
C     CALCULATE MASS AND HEAT BALANCE -                                 MAP1540
      CALL BALANCE(1,KKK,PCLE)                                          MAP1550
C     **************************                                        MAP1560
      ERR=DABS(PCLE)                                                    MAP1570
C     CHECK ERROR OF ENERGY BALANCE TO DETERMINE NUMBER OF ITERATIONS - MAP1580
      IF (ERR.LT.0.02) GO TO 140                                        MAP1590
  130 CONTINUE                                                          MAP1600
      GO TO 160                                                         MAP1610
  140 CONTINUE                                                          MAP1620
      DO 150 I=1,NX                                                     MAP1630
      DO 150 J=1,NY                                                     MAP1640
      XMASS(I,J)=XM(I,J)                                                MAP1650
  150 ENERGY(I,J)=EN(I,J)                                               MAP1660
  160 CONTINUE                                                          MAP1670
C                                                                       MAP1680
C  END ITERATION LOOP                                                   MAP1690
      DO 170 K=1,NBB                                                    MAP1700
  170 X(K)=X1(K)                                                        MAP1710
      TIME=TIME+DELT                                                    MAP1720
C                                                                       MAP1730
C     PRINT RESULTS -                                                   MAP1740
      CALL PDATA(P,H,TIME,L,NY,NX)                                      MAP1750
C     ****************************                                      MAP1760
  180 CONTINUE                                                          MAP1770
C                                                                       MAP1780
C  END TIME LOOP                                                        MAP1790
      STOP                                                              MAP1800
C                                                                       MAP1810
  190 FORMAT (//15X,16HITERATION NUMBER,I5)                             MAP1820
      END                                                               MAP1830
```

```
      SUBROUTINE GDATA(IOPT)                                                 DAT  10
C     **********************                                                 DAT  20
      IMPLICIT REAL*8(A-H,O-Z)                                               DAT  30
C                                                                            DAT  40
C     CALLED FROM MAIN                                                       DAT  50
C     PURPOSE:  TO READ AND WRITE PROBLEM INFORMATION                        DAT  60
C     ------------------------------------------------------------------CAT  70
      DIMENSION TITLE(20)                                                    DAT  80
C                                                                            DAT  90
      COMMON /INPUT/ PHI(20,10),AN(20,10),YN(20,10),P(20,10),H(20,10),X(DAT 100
     1400),X1(400),NP(20,10),NPP(200,2),DX(20),DY(10),DZ(20,10),G(20,10)DAT 110
      COMMON /CONTRO/ NK,NX,NXX,NY,NYY,NB,NBE,NT,DELT,TIME,PHFNT,UF,XRC,DAT 120
     1ICGAD,COEF,BETA,IPRT                                                  DAT 130
      COMMON /WORK/ AX(21,10),BX(21,10),EX(21,10),AY(20,11),BY(20,11),EYDAT 140
     1(20,11),TX(21,10),TAK(21,10),TY(20,11),TYK(20,11),AM(20,10),XMASSDAT 150
     220,10),EN(20,10),ENENGY(20,10),C(20,10),D(20,10),F(20,10),G(20,10)DAT 160
     3,QP(20,10),XN(20,10),IM(20,10),DIP(20,10),DIM(20,10),PHIC(20,10),PDAT 170
     40LD(20,10)                                                            DAT 180
      COMMON /EXTRA/ MBW,MBE                                                 DAT 190
C     ------------------------------------------------------------------CAT 200
C                                                                            DAT 210
C     READ AND WRITE UNITS -                                                 DAT 220
      NR=5                                                                   DAT 230
      NW=6                                                                   DAT 240
C                                                                            DAT 250
C     INITIALIZE SIMULATION TIME -                                           DAT 260
      TIME=0.D0                                                              DAT 270
C                                                                            DAT 280
C     READ AND WRITE TITLE OF PROBLEM -                                      DAT 290
      READ (NR,280) TITLE                                                    DAT 300
      WRITE (NW,290)                                                         DAT 310
      WRITE (NW,300) TITLE                                                   DAT 320
C                                                                            DAT 330
C     READ AND WRITE FINITE DIFFERENCE INFORMATION -                         DAT 340
      READ (NR,310) NX,NY,NB,NK,NT,NS,MBE,IOPT,IPRT                         DAT 350
C     NX - NUMBER OF COLUMNS (X-DIRECTION)                                   DAT 360
C     NY - NUMBER OF ROWS (Y-DIRECTION)                                      DAT 370
C     NB - NUMBER OF NON-ZERO BLOCKS                                         DAT 380
C     NK - MAXIMUM NUMBER OF NEWTON ITERATIONS                               DAT 390
C     NT - MAXIMUM NUMBER OF TIME STEPS                                      DAT 400
C     NS - NUMBER OF SOURCES                                                 DAT 410
C     MBE - ESTIMATED BANDWIDTH                                              DAT 420
C     IOPT - READ 1 FOR UPSTREAM WEIGHTING ON PRESSURES                      DAT 430
C            2 FOR MIDPOINT WEIGHTING                                        DAT 440
C     IPRT - NUMBER OF TIME STEPS BETWEEN PRINTING THERMO DATA               DAT 450
      WRITE (NW,320)                                                         DAT 460
      WRITE (NW,330) NX,NY,NB,NK,NT,NS,MBE,IOPT,IPRT                         DAT 470
C                                                                            DAT 480
      NXX=NX+1                                                               DAT 490
      NYY=NY+1                                                               DAT 500
      NBE=2*NB                                                               DAT 510
C     NBE - TOTAL NUMBER OF EQUATIONS                                        DAT 520
```

```
C                                                                       DAT 530
C     TIME PARAMETERS -                                                 DAT 540
      READ (NR,340) DELT                                                DAT 550
C     DELT - TIME STEP IN SECONDS                                       DAT 560
      WRITE (NW,370) DELT                                               DAT 570
C                                                                       DAT 580
C     DATA CODES -                                                      DAT 590
      READ (NR,310) KOD1,KOD2,KOD3,KOD4,KOD5,KOD6,KOD7,KOD8,KOD9       DAT 600
C     KOD1 - READ 1 IF X-SPACING IS CONSTANT                            DAT 610
C     KOD2 - READ 1 IF Y-SPACING IS CONSTANT                            DAT 620
C     KOD3 - READ 1 IF INITIAL PRESSURE IS CONSTANT                     DAT 630
C     KOD4 - READ 1 IF INITIAL ENTHALPY IS CONSTANT                     DAT 640
C     KOD5 - READ 1 IF X-PERMEABILITY IS CONSTANT                       DAT 650
C     KOD6 - READ 1 IF Y-PERMEABILITY IS CONSTANT                       DAT 660
C     KOD7 - READ 1 IF INITIAL POROSITY IS CONSTANT                     DAT 670
C     KOD8 - READ 1 IF RESERVOIR THICKNESS IS CONSTANT                  DAT 680
C     KOD9 - READ 1 IF TEMPERATURE IS READ IN PLACE OF ENTHALPY         DAT 690
      WRITE (NW,260) KOD1,KOD2,KOD3,KOD4,KOD5,KOD6,KOD7,KOD8,KOD9      DAT 700
C                                                                       DAT 710
C     SPACING -                                                         DAT 720
      IF (KOD1.EQ.1) GO TO 10                                           DAT 730
      READ (NR,340) (DX(I),I=1,NX)                                      DAT 740
      GO TO 30                                                          DAT 750
   10 READ (NR,340) DX1                                                 DAT 760
      DO 20 I=1,NX                                                      DAT 770
   20 DX(I)=DX1                                                         DAT 780
   30 WRITE (NW,350)                                                    DAT 790
      WRITE (NW,390) (DX(I),I=1,NX)                                     DAT 800
C                                                                       DAT 810
      IF (KOD2.EQ.1) GO TO 40                                           DAT 820
      READ (NR,340) (DY(J),J=1,NY)                                      DAT 830
      GO TO 60                                                          DAT 840
   40 READ (NR,340) DY1                                                 DAT 850
      DO 50 J=1,NY                                                      DAT 860
   50 DY(J)=DY1                                                         DAT 870
   60 WRITE (NW,360)                                                    DAT 880
      WRITE (NW,390) (DY(J),J=1,NY)                                     DAT 890
C                                                                       DAT 900
C     PRESSURE -                                                        DAT 910
      WRITE (NW,380)                                                    DAT 920
      CALL READ(P,KOD3,NY,NX)                                           DAT 930
C     ***********************                                           DAT 940
C                                                                       DAT 950
C     ENTHALPY -                                                        DAT 960
      IF (KOD9.EQ.1) WRITE (NW,270)                                     DAT 970
      IF (KOD9.NE.1) WRITE (NW,400)                                     DAT 980
      CALL READ(H,KOD4,NY,NX)                                           DAT 990
C     ***********************                                           DAT1000
      IF (KOD9.NE.1) GO TO 100                                          DAT1010
C                                                                       DAT1020
C     TEMPERATURES READ (COMPRESSED WATER REGION ASSUMED)               DAT1030
C     COMPUTE ENTHALPY BY NEWTON-RAPHSON METHOD                         DAT1040
```

```
      DO 80 J=1,NY                                                      DAT1050
      DO 80 I=1,NX                                                      DAT1060
      IF (H(I,J).EQ.0.) GO TO 80                                        DAT1070
      T=P(I,J)                                                          DAT1080
      H(I,J)=T*41841004.18                                              DAT1090
      PP=P(I,J)*0.1**7                                                  DAT1100
      HH=H(I,J)*0.1**7                                                  DAT1110
      DO 70 JJ=1,4                                                      DAT1120
      T1=-2.41231+2.562220-01*HH-9.31415D-03*PP*PP-2.2568D-05*HH*HH     DAT1130
      DT=2.562220-01-4.513600-05*HH                                     DAT1140
      DH=-(T1-T)/DT                                                     DAT1150
      HH=HH+DH                                                          DAT1160
   70 CONTINUE                                                          DAT1170
      H(I,J)=HH*10.**7                                                  DAT1180
   80 CONTINUE                                                          DAT1190
      WRITE (NW,400)                                                    DAT1200
      DO 90 J=1,NY                                                      DAT1210
   90 WRITE (NW,390) (H(I,J),I=1,NX)                                    DAT1220
  100 CONTINUE                                                          DAT1230
C                                                                       DAT1240
C     X- AND Y-PERMEABILITY -                                           DAT1250
      WRITE (NW,410)                                                    DAT1260
      CALL READ(XK,KOD5,NY,NX)                                          DAT1270
C     ************************                                          DAT1280
C                                                                       DAT1290
      WRITE (NW,420)                                                    DAT1300
      CALL READ(YK,KOD6,NY,NX)                                          DAT1310
C     ************************                                          DAT1320
C                                                                       DAT1330
C     POROSITY -                                                        DAT1340
      WRITE (NW,430)                                                    DAT1350
      CALL READ(PHI,KOD7,NY,NX)                                         DAT1360
C     ************************                                          DAT1370
C     SAVE PRESSURE AND INITIAL POROSITY -                              DAT1380
      DO 110 I=1,NX                                                     DAT1390
      DO 110 J=1,NY                                                     DAT1400
      POLD(I,J)=P(I,J)                                                  DAT1410
  110 PHIO(I,J)=PHI(I,J)                                                DAT1420
C                                                                       DAT1430
C     RESERVOIR THICKNESS (BY BLOCKS) -                                 DAT1440
      WRITE (NW,440)                                                    DAT1450
      CALL READ(DZ,KOD8,NY,NX)                                          DAT1460
C     ************************                                          DAT1470
C                                                                       DAT1480
C     SOURCE/SINK (G/SEC) -                                             DAT1490
      WRITE (NW,450)                                                    DAT1500
      DO 120 J=1,NY                                                     DAT1510
      DO 120 I=1,NX                                                     DAT1520
  120 Q(I,J)=0.D0                                                       DAT1530
      IF (NS.EQ.0) GO TO 140                                            DAT1540
      DO 130 K=1,NS                                                     DAT1550
      READ (NR,460) I,J,Q(I,J)                                          DAT1560
```

```
  130 WRITE (Nw,470) I,J,Q(I,J)                                          DAT1570
C                                                                        DAT1580
C     ROCK PROPERTIES -                                                  DAT1590
  140 READ (NR,340) XKC,COND,PHFWT,DF,BETA                               DAT1600
C     XKC - MEDIUM THERMAL CONDUCTIVITY                                  DAT1610
C     COND - CONFINING BED THERMAL CONDUCTIVITY                          DAT1620
C     PHFWT - ROCK ENTHALPY DERIVATIVE W.R.T. TEMPERATURE                DAT1630
C     DF - ROCK DENSITY                                                  DAT1640
C     BETA - ROCK COMPRESSIBILITY                                        DAT1650
      WRITE (Nw,480) XKC,COND,PHFWT,DF,BETA                              DAT1660
C                                                                        DAT1670
C     COMPUTE COEFFICIENT FOR CONDUCTIVE LEAKAGE -                       DAT1680
      IF (COND.LT.0.1) GO TO 150                                         DAT1690
      COEF=DF*PHFWT/COND                                                 DAT1700
      GO TO 160                                                          DAT1710
  150 COEF=0.D0                                                          DAT1720
  160 CONTINUE                                                           DAT1730
C                                                                        DAT1740
C     NUMBER GRID BLOCKS -                                               DAT1750
C     NP(I,J) - SEQUENCE NUMBERING OF BLOCKS I,J                         DAT1760
      IBN=0                                                              DAT1770
      DO 190 I=1,NX                                                      DAT1780
      DO 180 J=1,NY                                                      DAT1790
      IF (DZ(I,J).LT.0.001) GO TO 170                                    DAT1800
      IBN=IBN+1                                                          DAT1810
      NP(I,J)=IBN                                                        DAT1820
      GO TO 180                                                          DAT1830
  170 NP(I,J)=0                                                          DAT1840
  180 CONTINUE                                                           DAT1850
  190 CONTINUE                                                           DAT1860
      WRITE (Nw,240)                                                     DAT1870
      DO 200 J=1,NY                                                      DAT1880
  200 WRITE (Nw,250) (NP(I,J),I=1,NX)                                    DAT1890
C                                                                        DAT1900
C     COMPUTE I,J FOR EACH SEQUENTIAL BLOCK NUMBER -                     DAT1910
      DO 220 I=1,NX                                                      DAT1920
      DO 220 J=1,NY                                                      DAT1930
      IJ=NP(I,J)                                                         DAT1940
      IF (IJ.EQ.0) GO TO 220                                             DAT1950
      NPP(IJ,1)=I                                                        DAT1960
      NPP(IJ,2)=J                                                        DAT1970
      GO TO 220                                                          DAT1980
  220 CONTINUE                                                           DAT2000
C                                                                        DAT2010
C     INITIALIZE SOLUTION VECTOR -                                       DAT2020
      DO 230 K=1,N8                                                      DAT2030
      II=NPP(K,1)                                                        DAT2040
      JJ=NPP(K,2)                                                        DAT2050
      X(2*K-1)=P(II,JJ)                                                  DAT2060
      X1(2*K-1)=P(II,JJ)                                                 DAT2070
      X(2*K)=H(II,JJ)                                                    DAT2080
      X1(2*K)=H(II,JJ)                                                   DAT2090
```

```
  230 CONTINUE                                                          DAT2100
      RETURN                                                            DAT2110
C                                                                       DAT2120
  240 FORMAT (11X,12HGRID NUMBERS/11X,12(1H-))                          DAT2130
  250 FORMAT (11X,16I5)                                                 DAT2140
  260 FORMAT (/////11X,5HCODES/11X,5(1H-)/11X,9I5)                      DAT2150
  270 FORMAT (/////,11X,19HINITIAL TEMPERATURE/11X,19(1H-)/)            DAT2160
  280 FORMAT (20A4)                                                     DAT2170
  290 FORMAT (1H1,///35X,25HSTEAM-WATER FLOW ANALYSIS//)                DAT2180
  300 FORMAT (11X,70(1H*)//11X,20A4//11X,70(1H*)///)                    DAT2190
  310 FORMAT (16I5)                                                     DAT2200
  320 FORMAT (/11X,22HFINITE DIFFERENCE DATA/11X,22(1H-)/)              DAT2210
  330 FORMAT (1H ,10X,11HNUMBER OF -,2X,7HCOLUMNS,I23/21X,1H-,2X,4HROWS,DAT2220
     1I26/21X,1H-,2X,15HNON-ZERO BLOCKS,I15/21X,1H-,2X,18HMAXIMUM ITERATDAT2230
     2IONS,I12/21X,1H-,2X,18HMAXIMUM TIME STEPS,I12/21X,1H-,2X,7HSOURCESDAT2240
     3,I23/21X,1H-,2X,19HESTIMATED BANDWIDTH,I11/21X,1H-,2X,16HWEIGHTINGDAT2250
     4 OPTION,I14/21X,1H-,2X,15HPRINTING OPTION,I15///)                 DAT2260
  340 FORMAT (8G10.0)                                                   DAT2270
  350 FORMAT (/////,11X,22HSPACING IN X-DIRECTION/11X,22(1H-)/)         DAT2280
  360 FORMAT (/////,11X,22HSPACING IN Y-DIRECTION/11X,22(1H-)/)         DAT2290
  370 FORMAT (///,11X,15HTIME PARAMETERS/11X,15(1H-)//11X,28HINITIAL TIMDAT2300
     1E STEP IN SECONDS,G22.8/)                                         DAT2310
  380 FORMAT (/////,11X,16HINITIAL PRESSURE/11X,16(1H-)/)               DAT2320
  390 FORMAT (/(11X,8(G12.5,2X)))                                       DAT2330
  400 FORMAT (/////,11X,16HINITIAL ENTHALPY/11X,16(1H-)/)               DAT2340
  410 FORMAT (/////,11X,14HX-PERMEABILITY/11X,14(1H-)/)                 DAT2350
  420 FORMAT (/////,11X,14HY-PERMEABILITY/11X,14(1H-)/)                 DAT2360
  430 FORMAT (/////,11X,16HINITIAL POROSITY/11X,16(1H-)/)               DAT2370
  440 FORMAT (/////,11X,19HRESERVOIR THICKNESS/11X,19(1H-)/)            DAT2380
  450 FORMAT (/////,11X,7HSOURCES/11X,7(1H-)/)                          DAT2390
  460 FORMAT (2I5,G15.0)                                                DAT2400
  470 FORMAT (11X,2I5,G15.8)                                            DAT2410
  480 FORMAT (/11X,15HROCK PROPERTIES/11X,15(1H-)/11X,28HMEDIUM THERMAL DAT2420
     1CONDUCTIVITY-G17.5/11X,35HCONFINING BED THERMAL CONDUCTIVITY-G10.3DAT2430
     2/11X,25HROCK ENTHALPY DERIVATIVE-G20.5/11X,13HROCK DENSITY-G32.5/1DAT2440
     3X,'ROCK COMPRESSIBILITY=',G24.5/)                                 DAT2450
      END                                                               DAT2460-


      SUBROUTINE READ(DUM,KODE,NY,NX)                                   REC  10
      ******************************                                    REC  20
C     IMPLICIT REAL*8(A-H,O-Z)                                          REC  30
C                                                                       REC  40
C     CALLED FROM GDATA                                                 REC  50
C     PURPOSE:  TO READ TWO-DIMENSIONAL ARRAYS                          REC  60
C     ----------------------------------------------------------------  REC  70
C                                                                       REC  80
      DIMENSION DUM(20,10)                                              REC  90
C     ----------------------------------------------------------------  REC 100
      NR=5                                                              REC 110
      NW=6                                                              REC 120
      IF (KODE.EQ.1) GO TO 20                                           REC 130
      DO 10 J=1,NY                                                      REC 140
   10 READ (NR,70) (DUM(I,J),I=1,NX)                                    REC 150
      GO TO 40                                                          REC 160
   20 READ (NR,70) DUM1                                                 REC 170
      DO 30 J=1,NY                                                      REC 180
      DO 30 I=1,NX                                                      REC 190
   30 DUM(I,J)=DUM1                                                     REC 200
   40 DO 50 J=1,NY                                                      REC 210
   50 WRITE (NW,60) (DUM(I,J),I=1,NX)                                   REC 220
      RETURN                                                            REC 230
C                                                                       REC 240
   60 FORMAT (/(11X,8(G12.5,2X)))                                       REC 250
   70 FORMAT (8G10.0)                                                   REC 260-
      END
```

```
      SUBROUTINE TCALC(DY,DX,DZ,AK,YK,TY,TYK,TX,TXK,XKC,NY,NX,NYY,NXX)   TCA   10
C     ****************************************************************   TCA   20
      IMPLICIT REAL*8(A-H,O-Z)                                           TCA   30
C                                                                        TCA   40
C     CALLED FROM MAIN                                                   TCA   50
C     PURPOSE:  TO COMPUTE TRANSMISSIBILITY TERMS -                      TCA   60
C     ----------------------------------------------------------------   TCA   70
      DIMENSION DY(10), DX(20), DZ(20,10), AK(20,10), YK(20,10), TY(20,1TCA   80
     11), TYK(20,11), TX(21,10), TXK(21,10)                              TCA   90
C     ----------------------------------------------------------------   TCA  100
C                                                                        TCA  110
C     COMPUTE TRANSMISSIBILITY TERMS IN THE X-DIRECTION -                TCA  120
      DO 10 J=1,NY                                                       TCA  130
C     IF ONLY ONE COLUMN, SKIP CALCULATIONS -                            TCA  140
      IF (NX.EQ.1) GO TO 20                                              TCA  150
      DO 10 I=2,NX                                                       TCA  160
      TXC=DY(J)*DZ(I-1,J)/DX(I-1)                                        TCA  170
      TXD=DY(J)*DZ(I,J)/DX(I)                                            TCA  180
      TXA=TXC*AK(I-1,J)                                                  TCA  190
      TXB=TXD*AK(I,J)                                                    TCA  200
      TTT=TXA+TXB                                                        TCA  210
      IF (TTT.EQ.0.0) GO TO 10                                           TCA  220
C     PERMEABILITY TERM -                                                TCA  230
      TX(I,J)=2.0*TXA*TXB/TTT                                            TCA  240
C     HEAT CONDUCTION TERM -                                             TCA  250
      TXK(I,J)=2.0*TXC*TXD/(TXC+TXD)*XKC                                 TCA  260
   10 CONTINUE                                                           TCA  270
   20 CONTINUE                                                           TCA  280
C                                                                        TCA  290
C     COMPUTE TRANSMISSIBILITY TERMS IN THE Y-DIRECTION -                TCA  300
      DO 30 I=1,NX                                                       TCA  310
      IF (NY.EQ.1) GO TO 40                                              TCA  320
      DO 30 J=2,NY                                                       TCA  330
      TYC=DX(I)*DZ(I,J-1)/DY(J-1)                                        TCA  340
      TYD=DX(I)*DZ(I,J)/DY(J)                                            TCA  350
      TYA=TYC*YK(I,J-1)                                                  TCA  360
      TYB=TYD*YK(I,J)                                                    TCA  370
      TTT=TYA+TYB                                                        TCA  380
      IF (TTT.EQ.0.0) GO TO 30                                           TCA  390
      TY(I,J)=2.0*TYA*TYB/TTT                                            TCA  400
      TYK(I,J)=2.0*TYC*TYD/(TYC+TYD)*XKC                                 TCA  410
   30 CONTINUE                                                           TCA  420
   40 CONTINUE                                                           TCA  430
C                                                                        TCA  440
C     SET TRANSMISSIBILITY OF BOUNDARY BLOCKS (REGULAR RECTANGULAR MESH) TCA  450
C     TO ZERO (NO-FLOW) -                                                TCA  460
      DO 50 I=1,NX                                                       TCA  470
      TY(I,1)=0.00                                                       TCA  480
      TYK(I,1)=0.00                                                      TCA  490
      TY(I,NYY)=0.00                                                     TCA  500
   50 TYK(I,NYY)=0.00                                                    TCA  510
C                                                                        TCA  520
```

```
      DO 60 J=1,NY                                                      ICA 5
      TX(1,J)=0.D0                                                      ICA 5
      TXK(1,J)=0.D0                                                     ICA 5
      TX(NXX,J)=0.D0                                                    ICA 5
   60 TXK(NXX,J)=0.D0                                                   ICA 5
C                                                                       ICA 5
C     SET TRANSMISSIBILITY OF BOUNDARY BLOCKS (EXTERNAL AND INTERNAL,   ICA 5
C     IRREGULAR MESH) TO ZERO -                                         ICA 6
      DO 80 I=1,NX                                                      ICA 6
      DO 70 J=1,NY                                                      ICA 6
      IF (DZ(I,J).GT.0.D0) GO TO 70                                     ICA 6
      TX(I+1,J)=0.D0                                                    ICA 6
      TXK(I+1,J)=0.D0                                                   ICA 6
      TY(I,J+1)=0.D0                                                    ICA 6
      TYK(I,J+1)=0.D0                                                   ICA 6
      TXK(I,J)=0.D0                                                     ICA 6
      TX(I,J)=0.D0                                                      ICA 6
      TYK(I,J)=0.D0                                                     ICA 7
      TY(I,J)=0.D0                                                      ICA 7
   70 CONTINUE                                                          ICA 7
   80 CONTINUE                                                          ICA 7
      RETURN                                                            ICA 7
      END                                                               ICA 7
```

```
      SUBROUTINE MATH(NP,NY,NX,NEE,MBW)                                 MAT  10
C     ********************************                                  MAT  20
      IMPLICIT REAL*8(A-H,O-Z)                                          MAT  30
C                                                                       MAT  40
C     CALLED FROM MAIN                                                  MAT  50
C     PURPOSE:  COMPUTE MATRIX HANDWIDTH                                MAT  60
C     ----------------------------------------------------------------  MAT  70
      DIMENSION N(5), NP(20,10)                                         MAT  80
C     ----------------------------------------------------------------  MAT  90
C                                                                       MAT 100
C     COMPUTE MAXIMUM DIFFERENCE BETWEEN SEQUENTIAL BLOCK NUMBERS       MAT 110
C     OF ADJACENT BLOCKS -                                              MAT 120
      MM=0                                                              MAT 130
      DO 80 I=1,NX                                                      MAT 140
      DO 70 J=1,NY                                                      MAT 150
      DO 10 KK=1,4                                                      MAT 160
   10 N(KK)=0                                                           MAT 170
      I1=I-1                                                            MAT 180
      I2=I+1                                                            MAT 190
      J1=J-1                                                            MAT 200
      J2=J+1                                                            MAT 210
      IF (I1.EQ.0) GO TO 20                                             MAT 220
      N(1)=NP(I1,J)                                                     MAT 230
   20 CONTINUE                                                          MAT 240
      IF (I2.GT.NX) GO TO 30                                            MAT 250
      N(3)=NP(I2,J)                                                     MAT 260
   30 CONTINUE                                                          MAT 270
      IF (J1.EQ.0) GO TO 40                                             MAT 280
      N(2)=NP(I,J1)                                                     MAT 290
   40 CONTINUE                                                          MAT 300
      IF (J2.GT.NY) GO TO 50                                            MAT 310
      N(4)=NP(I,J2)                                                     MAT 320
   50 N(5)=NP(I,J)                                                      MAT 330
      IF (N(5).EQ.0) GO TO 70                                           MAT 340
      DO 60 K=1,4                                                       MAT 350
      IF (N(K).EQ.0) GO TO 60                                           MAT 360
C     COMPUTE DIFFERENCE -                                              MAT 370
      NN=N(5)-N(K)                                                      MAT 380
      IF (NN.LT.0) NN=-NN                                               MAT 390
C     COMPUTE MAXIMUM DIFFERENCE -                                      MAT 400
      IF (NN.GT.MM) MM=NN                                               MAT 410
   60 CONTINUE                                                          MAT 420
   70 CONTINUE                                                          MAT 430
   80 CONTINUE                                                          MAT 440
C     COMPUTE HANDWIDTH -                                               MAT 450
      MBW=2*(2*MM+1)+1                                                  MAT 460
      PRINT 90, NEE,MBW                                                 MAT 470
      RETURN                                                            MAT 480
C                                                                       MAT 490
   90 FORMAT (//11X,'MAXIMUM BANDWIDTH IS ',I4,2X,'COMPARED TO ESTIMATEDMAT 500
     1 BANDWIDTH OF ',I4///)                                            MAT 510
      END                                                               MAT 520
```

```
      SUBROUTINE PRPTY(L,KKK)                                          PRP   10
C     **********************                                           PRP   20
      IMPLICIT REAL*8(A-H,O-Z)                                         PRP   30
C                                                                      PRP   40
C     CALLED FROM MAIN                                                 PRP   50
C     PURPOSE:  TO COMPUTE THERMODYNAMIC PROPERTIES                    PRP   60
C     ---------------------------------------------------------------- PRP   70
      DIMENSION SW1(20,10), TEMP2(20,10), DEN2(20,10)                  PRP   80
      DIMENSION CQ(20,10)                                              PRP   90
C                                                                      PRP  100
      COMMON /INPUT/ PHI(20,10),XK(20,10),YK(20,10),P(20,10),H(20,10),X(PRP  110
     1400),X1(400),NP(20,10),NPP(200,2),DX(20),DY(10),CZ(20,10),G(20,10)PRP  120
      COMMON /CONTRO/ NK,NX,NXX,NY,NYY,NB,NBB,NT,DELT,TIME,PHFAT,UF,ARC,PRP  130
     1CONO,COEF,BETA,IPRT                                             PRP  140
      COMMON /WORK/ AX(21,10),BX(21,10),EX(21,10),AY(20,11),BY(20,11),EYPRP  150
     1(20,11),TX(21,10),TXK(21,10),TY(20,11),TYK(20,11),AM(20,10),AMASSPRP  160
     220,10),EN(20,10),ENERGY(20,10),C(20,10),D(20,10),F(20,10),G(20,10)PRP  170
     3,QH(20,10),XN(20,10),TM(20,10),DTP(20,10),DTM(20,10),PHIC(20,10),PRP  180
     4OLD(20,10)                                                      PRP  190
      COMMON /CHECK/ IND(200),INDOLD(200)                              PRP  200
C     ---------------------------------------------------------------- PRP  210
C                                                                      PRP  220
C     STATEMENT FUNCTIONS FOR THERMODYNAMIC PROPERTIES                 PRP  230
C                                                                      PRP  240
      F1(PX,HX)=1.00207+4.420070-4*PX-5.474500-5*HX+5.028750-7*HX*PX-1.2PRP  250
     147910-7*HX*HX                                                   PRP  260
      F2(PX,HX)=-2.41231+2.562220-1*HX-9.314150-3*PX*PX-2.256HD-5*HX*HX PRP  270
      F3(PX,HX)=-2.261620-5+0.043844100*PX-1.790880-5*PX*HX+3.692760-3*PPRP  280
     1X*PX*PX*PX+5.176440-13*HX*HX*HX*PX                              PRP  290
      F4(PX,HX)=-374.66900+47.992100*PX-0.633606000*PX*PX+7.393860-5*PX*HPRP  300
     1X-3.337206/HX/HX/PX/PX+0.035715400/PX/PX/PX-1.172500-9*HX*HX*HX*PX-PRP  310
     22.26861015/HX/HX/HX/HX                                          PRP  320
C                                                                      PRP  330
C     F1 - DENSITY, COMPRESSED WATER REGION                            PRP  340
C     F2 - TEMPERATURE, COMPRESSED WATER REGION                        PRP  350
C     F3 - DENSITY,  SUPER HEATED STEAM REGION                         PRP  360
C     F4 - TEMPERATURE, SUPER HEATED STEAM REGION                      PRP  370
      NKK=NK                                                           PRP  380
      IF (L.NE.1) GO TO 20                                             PRP  390
      IF (KKK.NE.1) GO TO 20                                           PRP  400
C                                                                      PRP  410
C     INITIALIZE ARRAYS -                                              PRP  420
      DO 10 I=1,NX                                                     PRP  430
      DO 10 J=1,NY                                                     PRP  440
      XN(I,J)=0.00                                                     PRP  450
      TM(I,J)=0.00                                                     PRP  460
      C(I,J)=0.00                                                      PRP  470
      D(I,J)=0.00                                                      PRP  480
      F(I,J)=0.00                                                      PRP  490
      G(I,J)=0.00                                                      PRP  500
      QH(I,J)=0.00                                                     PRP  510
      DTP(I,J)=0.00                                                    PRP  520
```

```
      DTF(I,J)=0.D0                                                     PHP 530
      SW1(I,J)=0.D0                                                     PHP 540
      DEN2(I,J)=0.D0                                                    PHP 550
      TEMP2(I,J)=0.D0                                                   PHP 560
   10 CONTINUE                                                          PHP 570
   20 CONTINUE                                                          PHP 580
      DO 80 I=1,NX                                                      PHP 590
      DO 80 J=1,NY                                                      PHP 600
      IF (DZ(I,J).EQ.0.D0) GO TO 80                                     PHP 610
      PP=P(I,J)                                                         PHP 620
      HH=H(I,J)                                                         PHP 630
      PP=PP*0.1**7                                                      PHP 640
      HH=HH*0.1**7                                                      PHP 650
C                                                                       PHP 660
      K=NP(I,J)                                                         PHP 670
      IF (IND(K)) 30,40,50                                              PHP 700
   30 CONTINUE                                                          PHP 710
C                                                                       PHP 720
C                                                                       PHP 730
C   COMPRESSED WATER REGION -                                           PHP 740
C                                                                       PHP 750
      DW=F1(PP,HH)                                                      PHP 760
      TEMP=F2(PP,HH)                                                    PHP 770
      PDWP=4.426070-11+5.026750-14*HH                                   PHP 780
      PDWH=-5.474560-12+5.026750-14*PP-2.495020-14*HH                   PHP 790
      PTWP=-1.862830-9*PP                                               PHP 800
      PTWH=2.562220-8-4.513G0-12*HH                                     PHP 810
C     WATER VISCOSITY -                                                 PHP 820
C     1967 ASME STEAM TABLES FORMULA (P. 74) -                          PHP 830
      VW=1.00-6*(241.4*10.**(247.8/(TEMP+133.15)))                      PHP 840
C                                                                       PHP 850
C     COMPUTE EQUATION COEFFICIENTS -                                   PHP 860
C     SPACE -                                                           PHP 870
      AN(I,J)=DW/VW                                                     PHP 880
      TM(I,J)=DW*HH/VW*10.**7                                           PHP 890
      UTF(I,J)=PTWH                                                     PHP 900
      UTF(I,J)=PTWP                                                     PHP 910
C     TIME -                                                            PHP 920
      C(I,J)=PDWP*PHI(I,J)*HH*10.**7+PHFWT*PIWP*DF*(1.0-PHI(I,J))       PHP 930
      C(I,J)=C(I,J)+DW*HH*1.07*BETA*PHIO(I,J)-PHIO(I,J)*BETA*DF*PHFWT*TEPHP 940
     1MP                                                                PHP 950
      D(I,J)=PDWH*PHI(I,J)*HH*10.**7+PHFWT*PIWH*DF*(1.0-PHI(I,J))+DW*PHIPHP 960
     1(I,J)                                                             PHP 970
      F(I,J)=PHI(I,J)*PDWP+DW*BETA*PHIO(I,J)                            PHP 980
      G(I,J)=PHI(I,J)*PDWH                                              PHP 990
C                                                                       PHP1000
      SW1(I,J)=1.00                                                     PHP1010
      TEMP2(I,J)=TEMP                                                   PHP1020
      DEN2(I,J)=DW                                                      PHP1030
C     HEAT DISCHARGE -                                                  PHP1040
      QH(I,J)=G(I,J)*HH*10.**7                                          PHP1050
      GO TO 60                                                          PHP1060
```

```
   40 CONTINUE                                                          PRP1070
C                                                                       PRP1080
C                                                                       PRP1090
C  TWO-PHASE REGION -                                                   PRP1100
      HW=730.984+129.239*PP-10.0333*PP*PP+0.39881*PP*PP*PP
     1   -99.0697/PP+12.9267/PP/PP-0.628359/PP/PP/PP
      HS=2822.82-39.952/PP+2.54342/PP/PP-0.938879*PP*PP                 PRP1110
      TEMP=F2(PP,HW)                                                    PRP1120
      DW=F1(PP,HW)                                                      PRP1130
      DS=F3(PP,HS)                                                      PRP1140
C     WATER SATURATION -                                                PRP1150
      SW=DS*(HS-HH)/(HH*(DW-DS)-(HW*DW-HS*DS))                          PRP1160
      SST=1.0-SW                                                        PRP1170
      SWC=SW                                                            PRP1180
C     VISCOSITIES -                                                     PRP1190
C     1967 ASME STEAM TABLES FORMULA (P. 74) -                          PRP1200
      VW=1.0E-06*(241.4*10.**(247.8/(TEMP+133.15)))                     PRP1210
      VS=1.0E-06*(.407*TEMP+80.4)                                       PRP1220
C     RELATIVE PERMEABILITY (WATER) -                                   PRP1230
      XKW=((SW-0.35)/0.65)**4                                           PRP1240
C     RELATIVE PERMEABILITY (STEAM) -                                   PRP1250
      XKS=(1.0-((SW-0.35)/0.65)**2)*(1.0-((SW-0.35)/0.65))**2           PRP1260
      IF (SW.LT.0.3) XKW=0.0                                            PRP1270
      IF (SW.LT.0.3) XKS=1.0                                            PRP1280
      IF (SW.GT.0.95) XKW=1.0                                           PRP1290
      IF (SW.GT.0.95) XKS=0.0                                           PRP1300
      DEN=DW*SW+SST*DS                                                  PRP1310
      HHH=HH*1.001D0                                                    PRP1320
      SW=DS*(HS-HHH)/(HHH*(DW-DS)-(HW*DW-HS*DS))                        PRP1330
      SST=1.0-SW                                                        PRP1340
      DEN1=DW*SW+DS*SST                                                 PRP1350
      PDWH=(DEN1-DEN)/(HHH-HH)*1.D-7                                    PRP1360
      PPP=PP*.999D0                                                     PRP1370
      HHW=730.984+129.239*PPP-10.0333*PPP*PPP+0.39881*PPP*PPP*PPP
     1   -99.0697/PPP+12.9267/PPP/PPP-0.628359/PPP/PPP/PPP
      HHS=2822.82-39.952/PPP+2.54342/PPP/PPP-0.938879*PPP*PPP           PRP1400
      T1=F2(PPP,HHW)                                                    PRP1410
      DDW=F1(PPP,HHW)                                                   PRP1420
      DDS=F3(PPP,HHS)                                                   PRP1430
      SW=DDS*(HHS-HH)/(HH*(DDW-DDS)-(HHW*DDW-HHS*DDS))                  PRP1440
      SST=1.0-SW                                                        PRP1450
      DEN1=DDW*SW+DDS*SST                                               PRP1460
      PDWP=(DEN1-DEN)/(PPP-PP)*1.D-7                                    PRP1470
      TEMP1=T1                                                          PRP1480
      PTWP=(TEMP1-TEMP)/(PPP-PP)*1.D-7                                  PRP1490
      SW=SWO                                                            PRP1500
C                                                                       PRP1510
C     SPACE -                                                           PRP1520
      XN(I,J)=XKW*DW/VW+XKS*DS/VS                                       PRP1530
      TM(I,J)=(XKW*DW*HW/VW+XKS*DS*HS/VS)*10.**7                        PRP1540
      DTP(I,J)=PTWP                                                     PRP1550
      DTH(I,J)=0.0                                                      PRP1560
```

```
C     TIME -                                                                    PRP1570
      C(I,J)=PDWP*PHI(I,J)*HH*10.**7+PHFWT*PIWP*DF*(1.0-PHI(I,J))               PRP1580
      C(I,J)=C(I,J)+DEN*HH*1.D7*BETA*PHIO(I,J)-PHIO(I,J)*BETA*DF*PHFWT*TPRP1590
     1EMP                                                                       PRP1600
      D(I,J)=PDWH*PHI(I,J)*HH*10.**7+DEN*PHI(I,J)                               PRP1610
      F(I,J)=PHI(I,J)*PDWP+DEN*BETA*PHIO(I,J)                                   PRP1620
      G(I,J)=PHI(I,J)*PDWH                                                      PRP1630
C                                                                               PRP1640
      SW1(I,J)=SW                                                               PRP1650
      TEMP2(I,J)=TEMP                                                           PRP1660
      DEN2(I,J)=DEN                                                             PRP1670
      QH(I,J)=Q(I,J)*(HW+(HS-HW)*XKS/(XKS+VS*XKW/VW*DW/DS))*10.**7              PRP1680
      GO TO 60                                                                  PRP1690
   50 CONTINUE                                                                  PRP1700
C                                                                               PRP1710
C                                                                               PRP1720
C  SUPER-HEATED STEAM REGION -                                                  PRP1730
      DS=F3(PP,HH)                                                              PRP1740
      PDWH=-1.79088D-12+PP+1.552932D-19*HH*HH*PP                                PRP1800
      PDWP=4.38441D-9-1.79088D-12*HH+1.47710+D-14*PP*PP*PP.5.17644D-20*HPRP1810
     1H*HH*HH                                                                   PRP1820
      HW=730.984+129.239*PP-10.0333*PP*PP+0.39881*PP*PP*PP
     1    -99.0697/PP+12.9267/PP/PP-0.628359/PP/PP/PP
      HS=2822.82-39.952/PP+2.54342/PP/PP-0.938879*PP*PP
      TT1=F4(PP,HH)
      TT2=F4(PP,HS)
      TT3=F2(PP,HW)
      TEMP=TT1-TT2+TT3
      HHH=HH*1.001D0
      TT1=F4(PP,HHH)
      TEMPH=TT1-TT2+TT3
      PPP=PP*0.999D0
      HW =730.984+129.239*PPP-10.0333*PPP*PPP+0.39881*PPP*PPP*PPP
     1    -99.0697/PPP+12.9267/PPP/PPP-0.6283-9/PPP/PPP/PPP
      HS=2822.82-39.952/PPP+2.54342/PPP/PPP-0.938879*PPP*PPP
      TT1=F4(PPP,HH)
      TT2=F4(PPP,HS)
      TT3=F2(PPP,HW)
      TEMPP=TT1-TT2+TT3
      PTWH=(TEMPH-TEMP)/(HHH-HH)*1.D-7
      PTWP=(TEMPP-TEMP)/(PPP-PP)*1.D-7
C     STEAM VISCOSITY -                                                         PRP1830
C     1967 ASME STEAM TABLES FORMULA (P. 74) -                                  PRP1840
      VS=1.0E-06*(.407*TEMP+80.4)                                               PRP1850
C                                                                               PRP1860
C     SPACE -                                                                   PRP1870
      XN(I,J)=DS/VS                                                             PRP1880
      TM(I,J)=DS*HH/VS*10.**7                                                   PRP1890.
      DTH(I,J)=PTWH                                                             PRP1900
      DTP(I,J)=PTWP                                                             PRP1910
C     TIME -                                                                    PRP1920
      C(I,J)=PDWP*PHI(I,J)*HH*10.**7+PHFWT*PIWP*DF*(1.0-PHI(I,J))               PRP1930
```

```
      C(I,J)=C(I,J)+DS*HH*1.D7*BETA*PHIO(I,J)-PHIO(I,J)*BETA*DF*PHFWT*TE  PHP1940
     1MP                                                                  PHP1950
      D(I,J)=PDWH*PHI(I,J)*HH*10.**7+PHFWT*PWH*DF*(1.0-PHI(I,J))+DS*PHI  PHP1960
     1(I,J)                                                               PHP1970
      F(I,J)=PHI(I,J)*PDWP+DS*BETA*PHIO(I,J)                              PHP1980
      G(I,J)=PHI(I,J)*PDWH                                                PHP1990
C                                                                         PHP2000
      SW1(I,J)=0.D0                                                       PHP2010
      TEMP2(I,J)=TEMP                                                     PHP2020
      DEN2(I,J)=DS                                                        PHP2030
      QH(I,J)=G(I,J)*HH*10.**7                                            PHP2040
   60 CONTINUE                                                            PHP2050
      IF (COEF.LT.0.1) GO TO 80                                           PHP2060
C                                                                         PHP2070
C     TRANSIENT CONDUCTIVE HEAT LEAKAGE ONLY -                            PHP2080
      IF (KKK.NE.1) GO TO 70                                              PHP2090
      IC=L+KKK                                                            PHP2100
      II=NP(I,J)                                                          PHP2110
      CALL VERTCO(DELT,TEMP,COEF,CONO,CQQ,II,IC)                          PHP2120
C     **********************************************                      PHP2130
      CQQ=CQQ*DX(I)*DY(J)                                                 PHP2140
      CQ(I,J)=CQQ                                                         PHP2150
   70 CONTINUE                                                            PHP2160
      QH(I,J)=QH(I,J)+CQ(I,J)                                             PHP2170
   80 CONTINUE                                                            PHP2180
      IF (KKK.NE.1) GO TO 120                                             PHP2190
C     PRINT THERMO DATA EVERY IPRT TIME STEP -                            PHP2200
      IF (MOD(L,IPRT).NE.0) GO TO 120                                     PHP2210
      PRINT 130                                                           PHP2220
      DO 90 J=1,NY                                                        PHP2230
      PRINT 140, (SW1(I,J),I=1,NX)                                        PHP2240
   90 CONTINUE                                                            PHP2250
      PRINT 150                                                           PHP2260
      DO 100 J=1,NY                                                       PHP2270
      PRINT 140, (TEMP2(I,J),I=1,NX)                                      PHP2280
  100 CONTINUE                                                            PHP2290
      PRINT 160                                                           PHP2300
      DO 110 J=1,NY                                                       PHP2310
      PRINT 140, (DEN2(I,J),I=1,NX)                                       PHP2320
  110 CONTINUE                                                            PHP2330
  120 CONTINUE                                                            PHP2340
      RETURN                                                              PHP2350
C                                                                         PHP2360
  130 FORMAT (//11X,'WATER SATURATIONS'/11X,17(1H-)//)                    PHP2370
  140 FORMAT (/(11X,8(G12.5,2X)))                                         PHP2380
  150 FORMAT (//11X,'TEMPERATURES'/11X,12(1H-)//)                         PHP2390
  160 FORMAT (//11X,'DENSITY'/11X,7(1H-)//)                               PHP2400
      END                                                                 PHP2410
```

```
      SUBROUTINE VERTCD(DELT,TT,COEF,COND,CW,II,IC)                      VRT  10
C     ********************************************                       VRT  20
      IMPLICIT REAL*8(A-H,O-Z)                                           VRT  30
C                                                                        VRT  40
C     CALLED FROM PRPTY                                                  VRT  50
C     PURPOSE:  TO COMPUTE VERTICAL CONDUCTIVE LEAKAGE THROUGH THE       VRT  60
C               CONFINING BED BY THE FINITE ELEMENT METHOD               VRT  70
C     ---------------------------------------------------------------    VRT  80
      DIMENSION A(9), B(9), C(9), G(9), F(9), DTEMP(200,11), DELZ(200,10VRT  90
     1), TI(200), DDTEMP(200,11)                                         VRT 100
C     ---------------------------------------------------------------    VRT 110
C                                                                        VRT 120
C     COMPUTE DELTA Z ( ON FIRST TIME STEP) -                            VRT 130
      CTHK1=102300.00                                                    VRT 140
      IF (IC.NE.2) GO TO 30                                              VRT 150
      NNZ=11                                                             VRT 160
C     NNZ = NUMBER OF NODES IN Z-DIRECTION                               VRT 170
C     COMPUTE DELZ (BASED ON TEN ELEMENTS AND DOUBLING THE SIZE OF EACH  VRT 180
C     ELEMENT) -                                                         VRT 190
      NNL=NNZ-1                                                          VRT 200
C     NNL = NUMBER OF ELEMENTS IN Z-DIRECTION                            VRT 210
      DELZ(II,NNL)=CTHK1/1023.00                                         VRT 220
      SUM=DELZ(II,NNL)                                                   VRT 230
      JSTOP=NNL-2                                                        VRT 240
      DO 10 JJ=1,JSTOP                                                   VRT 250
      DELZ(II,NNL-JJ)=2.*DELZ(II,NNL-JJ+1)                               VRT 260
   10 SUM=SUM+DELZ(II,NNL-JJ)                                            VRT 270
      DELZ(II,1)=CTHK1-SUM                                               VRT 280
C                                                                        VRT 290
C     INITIALIZE TI AND DDTEMP -                                         VRT 300
      TI(II)=TT                                                          VRT 310
      DO 20 J=1,NNZ                                                      VRT 320
   20 DDTEMP(II,J)=0.00                                                  VRT 330
   30 CONTINUE                                                           VRT 340
C                                                                        VRT 350
C     INITIALIZE DTEMP -                                                 VRT 360
      DO 40 J=1,NNZ                                                      VRT 370
   40 DTEMP(II,J)=DDTEMP(II,J)                                           VRT 380
C                                                                        VRT 390
C     FACTOR FOR TIME-DERIVATIVE -                                       VRT 400
      THETA=1.00                                                         VRT 410
C                                                                        VRT 420
C     SEE COATS,ET.AL., SPE J (DEC 1974) 590 FOR 1-DIM EQUATION.         VRT 430
C     BOUNDARY CONDITIONS -                                              VRT 440
C     UPPER -                                                            VRT 450
      DTEMP(II,1)=0.00                                                   VRT 460
C     LOWER -                                                            VRT 470
      DTEMP(II,NNZ)=TT-TI(II)                                            VRT 480
C                                                                        VRT 490
C                                                                        VRT 500
C     CALCULATE FINITE ELEMENT COEFFICIENTS FOR MATRIX EQUATION -        VRT 510
      J=0                                                                VRT 520
```

```
      DO 50 I=2,NNL                                                     V=1 530
      J=J+1                                                             V=1 540
      A1=DELZ(II,I-1)*COEF/(6.D0*DELT)                                  V=1 550
      C1=DELZ(II,I)*COEF/(6.D0*DELT)                                    V=1 560
C                                                                       V=1 570
      A(J)=A1-THETA/DELZ(II,I-1)                                        V=1 580
      B(J)=2.D0*A1+THETA/DELZ(II,I-1)+2.D0*C1+THETA/DELZ(II,I)          V=1 590
      C(J)=C1-THETA/DELZ(II,I)                                          V=1 600
C     RIGHT-HAND SIDE -                                                 V=1 610
C     USE DDTEMP FROM LAST SOLUTION AS INITIAL CONDITIONS               V=1 620
      D(J)=(A1+(1.D0-THETA)/DELZ(II,I-1))*DDTEMP(II,I-1)+(2.D0*A1-(1.D0-V=1 630
     1THETA)/DELZ(II,I-1)+2.D0*C1-(1.D0-THETA)/DELZ(II,I))*DDTEMP(II,I)+V=1 640
     2(C1+(1.D0-THETA)/DELZ(II,I))*DDTEMP(II,I+1)                       V=1 650
   50 CONTINUE                                                          V=1 660
C                                                                       V=1 670
C     SOLVE BY THOMAS METHOD (SEE CALIF BULL NC 63-4  SEPT, 1971 P 521) V=1 680
C     NOTE THAT THERE ARE NNZ-2*J EQUATIONS AND J UNKNOWNS              V=1 690
C                                                                       V=1 700
C     UPPER TRIANGULARIZE -                                             V=1 710
      F(1)=B(1)                                                         V=1 720
      D(1)=D(1)-A(1)*DTEMP(II,1)                                        V=1 730
      D(J)=D(J)-C(J)*DTEMP(II,NNZ)                                      V=1 740
      DO 60 I=2,J                                                       V=1 750
      F(I)=B(I)-C(I-1)*A(I)/F(I-1)                                      V=1 760
   60 D(I)=D(I)-A(I)*D(I-1)/F(I-1)                                      V=1 770
C                                                                       V=1 780
C     BACK SUBSTITUTE -                                                 V=1 790
      DTEMP(II,J+1)=D(J)/F(J)                                           V=1 800
      J1=J-1                                                            V=1 810
      DO 70 I=1,J1                                                      V=1 820
   70 DTEMP(II,J+1-I)=(D(J-1)-C(J-1)*DTEMP(II,J+2-I))/F(J-1)            V=1 830
C                                                                       V=1 840
C     DTEMP NOW CONTAINS NEW VALUES FOR TEMPERATURE DIFFERENCE          V=1 850
C                                                                       V=1 860
C     COMPUTE TRANSIENT CONDUCTIVE LEAKAGE                              V=1 870
      CQ=-2.D0*COND*(DTEMP(II,NNZ)-DTEMP(II,NNZ-1))/DELZ(II,NNL)        V=1 880
C                                                                       V=1 890
C     SAVE DTEMP                                                        V=1 900
      DO 80 J=1,NNZ                                                     V=1 910
   80 DDTEMP(II,J)=DTEMP(II,J)                                          V=1 920
      RETURN                                                            V=1 930
      END                                                               V=1 940
```

```
      SUBROUTINE FORMEQ(A,R,NBBD,MBEC)                                  FEC   10
C     **********************************                                FEC   20
      IMPLICIT REAL*8(A-H,O-Z)                                          FEC   30
C     CALLED FROM MAIN                                                  FEC   40
C     PURPOSE:  TO FORM THE FINAL MATRIX EQUATION                       FEC   50
C     ------------------------------------------------------------------FEC   60
      DIMENSION A(NBBD,MBEC), R(NBBD)                                   FEC   70
C                                                                       FEC   80
      COMMON /INPUT/ PHI(20,10),XK(20,10),YK(20,10),P(20,10),H(20,10),X FEC   90
     1400),X1(400),NP(20,10),NPP(200,2),DX(20),DY(10),DZ(20,10),G(20,10FEC  100
      COMMON /CONTRO/ NK,NX,NXX,NY,NYY,NB,NBB,NT,DELT,TIME,PHFAT,DF,XKC FEC  110
     1COND,COEF,BETA,IPRT                                               FEC  120
      COMMON /WORK/ AX(21,10),BX(21,10),EX(21,10),AY(20,11),BY(20,11),EYFEC  130
     1(20,11),TX(21,10),TXK(21,10),TY(20,11),TYK(20,11),XM(20,10),XMSSSFEC  140
     220,10),EN(20,10),ENERGY(20,10),C(20,10),D(20,10),F(20,10),G(20,10)FEC  150
     3,GR(20,10),XN(20,10),IM(20,10),DTP(20,10),DTM(20,10),PHIC(20,10),PFEC  160
     40LC(20,10)                                                        FEC  170
      COMMON /EXTRA/ MBW,MBE                                            FEC  180
C     ------------------------------------------------------------------FEC  190
      MP=(MBW+1)/2                                                      FEC  200
C     MP = MAIN DIAGONAL (STORED VERTICALLY)                            FEC  210
C                                                                       FEC  220
C     INITIALIZE ARRAYS -                                               FEC  230
      DO 10 K=1,NBB                                                     FEC  240
      DO 10 KK=1,MBW                                                    FEC  250
   10 A(K,KK)=0.D0                                                      FEC  260
C                                                                       FEC  270
C     COMPUTE MATRIX -                                                  FEC  280
      DO 50 K=1,NB                                                      FEC  290
      I=NPP(K,1)                                                        FEC  300
      J=NPP(K,2)                                                        FEC  310
C                                                                       FEC  320
C     MAIN DIAGONAL TERMS -                                             FEC  330
C     PRESSURE -                                                        FEC  340
      A(2*K-1,MP)=-EX(I,J)-EY(I,J)-EX(I+1,J)-EY(I,J+1)                  FEC  350
C     ENTHALPY -                                                        FEC  360
      A(2*K,MP-1)=-AX(I,J)-AY(I,J)-AX(I+1,J)-AY(I,J+1)                  FEC  370
      A(2*K,MP)=-BX(I,J)-BY(I,J)-BX(I+1,J)-BY(I,J+1)                    FEC  380
C                                                                       FEC  390
C     OFF DIAGONAL TERMS -                                              FEC  400
      II=I                                                              FEC  410
      IF (J.EQ.1) GO TO 20                                              FEC  420
      JJ=J-1                                                            FEC  430
      NN=NP(II,JJ)                                                      FEC  440
      IF (NN.EQ.0) GO TO 20                                             FEC  450
      NC=MP+(NN-K)*2                                                    FEC  460
      A(2*K-1,NC)=EY(I,J)                                               FEC  470
      A(2*K,NC-1)=AY(I,J)                                               FEC  480
      A(2*K,NC)=BY(I,J)                                                 FEC  490
   20 CONTINUE                                                          FEC  500
      IF (J.EQ.NY) GO TO 30                                             FEC  510
      JJ=J+1                                                            FEC  520
```

```
      NN=NP(II,JJ)                                                      FEG 530
      IF (NN.EQ.0) GO TO 30                                             FEG 540
      NC=MP+(NN-K)*2                                                    FEG 550
      A(2*K-1,NC)=EY(I,J+1)                                             FEG 560
      A(2*K,NC-1)=AY(I,J+1)                                             FEG 570
      A(2*K,NC)=BY(I,J+1)                                               FEG 580
   30 JJ=J                                                              FEG 590
      IF (I.EQ.1) GO TO 40                                              FEG 600
      II=I-1                                                            FEG 610
      NN=NP(II,JJ)                                                      FEG 620
      IF (NN.EQ.0) GO TO 40                                             FEG 630
      NC=MP+(NN-K)*2                                                    FEG 640
      A(2*K-1,NC)=EX(I,J)                                               FEG 650
      A(2*K,NC-1)=AX(I,J)                                               FEG 660
      A(2*K,NC)=BX(I,J)                                                 FEG 670
   40 IF (I.EQ.NX) GO TO 50                                             FEG 680
      II=I+1                                                            FEG 690
      NN=NP(II,JJ)                                                      FEG 700
      IF (NN.EQ.0) GO TO 50                                             FEG 710
      NC=MP+(NN-K)*2                                                    FEG 720
      A(2*K-1,NC)=EX(I+1,J)                                             FEG 730
      A(2*K,NC-1)=AX(I+1,J)                                             FEG 740
      A(2*K,NC)=BX(I+1,J)                                               FEG 750
   50 CONTINUE                                                          FEG 760
C                                                                       FEG 770
C     COMPUTE KNOWN VECTOR -                                            FEG 780
      DO 70 K=1,NBB                                                     FEG 790
      II=K-MP                                                           FEG 800
      R(K)=0.D0                                                         FEG 810
      DO 60 JJ=1,MBW                                                    FEG 820
      II=II+1                                                           FEG 830
      IF (II.LT.1) GO TO 60                                             FEG 840
      IF (II.GT.NBB) GO TO 70                                           FEG 850
      R(K)=R(K)+A(K,JJ)*X1(II)                                          FEG 860
   60 CONTINUE                                                          FEG 870
   70 CONTINUE                                                          FEG 880
C                                                                       FEG 890
      DO 80 K=1,NB                                                      FEG 900
      I=NPP(K,1)                                                        FEG 910
      J=NPP(K,2)                                                        FEG 920
C                                                                       FEG 930
C     NEWTON-RAPHSON RESIDUAL VECTOR -                                  FEG 940
      R(2*K-1)=-R(2*K-1)+XM(I,J)/DELT-XMASS(I,J)/DELT-C(I,J)            FEG 950
      R(2*K)=-R(2*K)+EN(I,J)/DELT-ENERGY(I,J)/DELT-DH(I,J)              FEG 960
C                                                                       FEG 970
C     LINEARIZED NEWTON-RAPHSON MATRIX -                                FEG 980
      A(2*K-1,MP)=A(2*K-1,MP)-F(I,J)*DX(I)*DZ(I,J)*DY(J)/DELT           FEG 990
      A(2*K-1,MP+1)=A(2*K-1,MP+1)-G(I,J)*DX(I)*DY(J)*DZ(I,J)/DELT       FEG1000
      A(2*K,MP-1)=A(2*K,MP-1)-C(I,J)*DX(I)*DY(J)*DZ(I,J)/DELT           FEG1010
      A(2*K,MP)=A(2*K,MP)-D(I,J)*DX(I)*DY(J)*DZ(I,J)/DELT               FEG1020
   80 CONTINUE                                                          FEG1030
      RETURN                                                            FEG1040

      END                                                               FEG1050
```

```
      SUBROUTINE SOLVE(KKK,B,R,NEQ,IHALFB,NDIM,MDIM)                    SOL   10
C     ************************************************                  SOL   20
      IMPLICIT REAL*8(A-H,O-Z)                                          SOL   30
C                                                                       SOL   40
C   ASYMMETRIC BAND MATRIX EQUATION SOLVER                              SOL   50
C     ORIGINALLY PROGRAMED BY JAMES C. DUGUID                           SOL   60
C                                                                       SOL   70
C   KKK=1 TRIANGULARIZES THE BAND MATRIX B                              SOL   80
C   KKK=2 SOLVES FOR RIGHT SIDE R, SOLUTION RETURNS IN R                SOL   90
C                                                                       SOL  100
      DIMENSION B(NDIM,MDIM), R(NDIM)                                   SOL  110
      NRS=NEQ+1                                                         SOL  120
      IHBP=IHALFB+1                                                     SOL  130
      IF (KKK.EQ.2) GO TO 30                                            SOL  140
C                                                                       SOL  150
C  TRIANGULARIZE MATRIX A USING DOOLITTLE METHOD                        SOL  160
C                                                                       SOL  170
      DO 20 K=1,NRS                                                     SOL  180
      PIVOT=B(K,IHBP)                                                   SOL  190
      KK=K+1                                                            SOL  200
      KC=IHBP                                                           SOL  210
      DO 10 I=KK,NEQ                                                    SOL  220
      KC=KC-1                                                           SOL  230
      IF (KC.LE.0) GO TO 20                                             SOL  240
      C=-B(I,KC)/PIVOT                                                  SOL  250
      B(I,KC)=C                                                         SOL  260
      KI=KC+1                                                           SOL  270
      LIM=KC+IHALFB                                                     SOL  280
      DO 10 J=KI,LIM                                                    SOL  290
      JC=IHBP+J-KC                                                      SOL  300
   10 B(I,J)=B(I,J)+C*B(K,JC)                                           SOL  310
   20 CONTINUE                                                          SOL  320
      GO TO 100                                                         SOL  330
C                                                                       SOL  340
C  MODIFY LOAD VECTOR R                                                 SOL  350
C                                                                       SOL  360
   30 NN=NEQ+1                                                          SOL  370
      IBAND=2*IHALFB+1                                                  SOL  380
      DO 70 I=2,NEQ                                                     SOL  390
      JC=IHBP-I+1                                                       SOL  400
      JI=1                                                              SOL  410
      IF (JC.LE.0) GO TO 40                                             SOL  420
      GO TO 50                                                          SOL  430
   40 JC=1                                                              SOL  440
      JI=I-IHBP+1                                                       SOL  450
   50 SUM=0.0                                                           SOL  460
      DO 60 J=JC,IHALFB                                                 SOL  470
      SUM=SUM+B(I,J)*R(JI)                                              SOL  480
   60 JI=JI+1                                                           SOL  490
   70 R(I)=R(I)+SUM                                                     SOL  500
C                                                                       SOL  510
C   BACK SOLUTION                                                       SOL  520
```

```
C                                                                       SOL 530
      R(NEQ)=R(NEQ)/B(NEQ,IMBP)                                         SOL 540
      DO 90 IBACK=2,NEQ                                                 SOL 550
      I=NN-IBACK                                                        SOL 560
      JP=I                                                              SOL 570
      KK=IMBP+1                                                         SOL 580
      MM=MIN0(IBAND,IMALFB+IBACK)                                       SOL 590
      SUM=0.0                                                           SOL 600
      DO 80 J=KK,MM                                                     SOL 610
      JP=JP+1                                                           SOL 620
   80 SUM=SUM+B(I,J)*R(JP)                                              SOL 630
   90 R(I)=(R(I)-SUM)/B(I,IMBP)                                         SOL 640
  100 RETURN                                                            SOL 650
      END                                                               SOL 660-
```

```
      SUBROUTINE PDATA(P,H,TIME,L,NY,NX)                                PDT  10
C     **********************************                                PDT  20
      IMPLICIT REAL*8(A-H,O-Z)                                          PDT  30
C                                                                       PDT  40
C     CALLED FROM MAIN                                                  PDT  50
C     PURPOSE:  TO PRINT COMPUTED PRESSURE AND ENTHALPY                 PDT  60
C     ------------------------------------------------------------------PDT  70
      DIMENSION P(20,10), H(20,10)                                      PDT  80
C     ------------------------------------------------------------------PDT  90
C                                                                       PDT 100
      PRINT 30, L,TIME                                                  PDT 110
      DO 10 J=1,NY                                                      PDT 120
   10 PRINT 40, (P(I,J),I=1,NX)                                         PDT 130
      PRINT 50                                                          PDT 140
      DO 20 J=1,NY                                                      PDT 150
   20 PRINT 40, (H(I,J),I=1,NX)                                         PDT 160
      RETURN                                                            PDT 170
C                                                                       PDT 180
   30 FORMAT (///11X,'STEP NUMBER',I4,10X,'TIME',E10.3/11X,15(1H*)///11XPDT 190
     1,'PRESSURE VALUES'/11X,15(1H-)//)                                 PDT 200
   40 FORMAT (/(11X,8(G12.5,2X)))                                       PDT 210
   50 FORMAT (//11X,'ENTHALPY VALUES'/11X,15(1H-)//)                    PDT 220
      END                                                               PDT 230-
```

```
      SUBROUTINE PHREG(INDEX)                                              PHR  05
C     **********************                                               PHR  10
      IMPLICIT REAL*8(A-H,O-Z)                                             PHR  20
C                                                                          PHR  25
C     CALLED FORM MAIN                                                     PHR  30
C     PURPOSE:  TO DETERMINE WHAT THERMODYNAMIC REGION A                   PHR  40
C               FINITE-DIFFERENCE BLOCK IS IN                              PHR  50
C     ---------------------------------------------------------------------PHR  60
      DIMENSION INDEX(200)                                                 PHR  70
C                                                                          PHR  80
      COMMON /INPUT/ PHI(20,10),XK(20,10),YK(20,10),P(20,10),H(20,10),X(PHR  90
     1400),X1(400),NP(20,10),NPP(200,2),DX(20),DY(10),DZ(20,10),Q(20,10)PHR 100
      COMMON /CONTRO/ NK,NX,NXX,NY,NYY,NB,NBB,NT,DELT,TIME,PHFWT,DF,XKC,PHR 110
     1COND,COEF,BETA,IPRT                                                 PHR 120
C     ---------------------------------------------------------------------PHR 130
C     INDEX=-1 FOR COMPRESSED WATER                                        PHR 140
C     INDEX=0  FOR TWO-PHASE                                               PHR 150
C     INDEX=1  FOR SUPERHEATED STEAM                                       PHR 160
      DO 10 K=1,NB                                                         PHR 170
      PP=X1(2*K-1)*0.1**7                                                  PHR 180
      HH=X1(2*K)*0.1**7                                                    PHR 190
C     COMPUTE SATURATED STEAM (HS) AND SATURATED WATER (HW) ENTHALPY -     PHR 200
      HS=2822.82-39.952/PP+2.54342/PP/PP-0.938879*PP*PP                    PHR 210
      HW=730.984+129.239*PP-10.0333*PP*PP+0.39881*PP*PP*PP
     1   -99.0697/PP+12.9267/PP/PP-0.628359/PP/PP/PP
      INDEX(K)=0                                                           PHR 240
      IF (HH.LT.HW) INDEX(K)=-1                                            PHR 250
      IF (HH.GT.HS) INDEX(K)=1                                             PHR 260
C     IF TEMPERATURE IS BELOW 50 DEG C (H=209.33) ASSUME IN COMP WATER     PHR 270
      IF (HH.LT.209.3300) INDEX(K)=-1                                      PHR 280
   10 CONTINUE                                                             PHR 290
      RETURN                                                               PHR 300
      END                                                                  PHR 310-
```

```
      SUBROUTINE BALNCE(ICX,KKK,PCEE)                                   BAL  05
C     ********************************                                  BAL  10
      IMPLICIT REAL*8(A-H,O-Z)                                          BAL  20
C                                                                       BAL  30
C     CALLED FROM MAIN                                                  BAL  40
C     PURPOSE:  TO COMPUTE MASS AND ENERGY BALANCE                      BAL  50
C     ------------------------------------------------------------------BAL  60
      COMMON /INPUT/ PHI(20,10),XK(20,10),YK(20,10),P(20,10),H(20,10),X(BAL  70
     1400),X1(400),NP(20,10),NPP(200,2),DX(20),DY(10),DZ(20,10),Q(20,10)BAL  80
      COMMON /CONTRO/ NK,NX,NXX,NY,NYY,NB,NBB,NT,DELT,TIME,PHFNT,DF,XKC,BAL  90
     1COND,COEF,BETA,IPRT                                               BAL 100
      COMMON /WORK/ AX(21,10),BX(21,10),EX(21,10),AY(20,11),BY(20,11),EYBAL 110
     1(20,11),TX(21,10),TXK(21,10),TY(20,11),TYK(20,11),XM(20,10),XMASS(BAL 120
     220,10),EN(20,10),ENERGY(20,10),C(20,10),D(20,10),F(20,10),G(20,10)BAL 130
     3,QH(20,10),XN(20,10),TM(20,10),DTP(20,10),DTH(20,10),PHIC(20,10),PBAL 140
     4OLD(20,10)                                                        BAL 150
      COMMON /CHECK/ IND(200),INDOLD(200)                               BAL 160
C     ------------------------------------------------------------------BAL 170
C                                                                       BAL 180
C     STATEMENT FUNCTIONS FOR THERMODYNAMIC PROPERTIES -                BAL 190
C                                                                       BAL 200
      F1(PX,HX)=1.00207+4.42607D-4*PX-5.47456D-5*HX+5.02875D-7*HX*PX-1.2BAL 210
     14791D-7*HX*HX                                                     BAL 220
      F2(PX,HX)=-2.41231+2.56222D-1*HX-9.31415D-3*PX*PX-2.2568D-5*HX*HX BAL 230
      F3(PX,HX)=-2.26162D-5+0.043844100*PX-1.79088D-5*PX*HX+3.69276D-8*PBAL 240
     1X*PX*PX*PX+5.17644D-13*HX*HX*HX*PX                                BAL 250
      F4(PX,HX)=-374.669D0+47.992100*PX-0.63360600*PX*PX+7.39386D-5*HX*HBAL 260
     1X-3.3372D6/HX/HX/PX/PX+0.0357154D0/PX/PX/PX-1.1725D-9*HX*HX*HX*PX-BAL 270
     22.26861D15/HX/HX/HX/HX                                            BAL 280
C                                                                       BAL 290
      DELM=0.D0                                                         BAL 300
      DELE=0.D0                                                         BAL 310
      DO 70 I=1,NX                                                      BAL 320
      DO 70 J=1,NY                                                      BAL 330
      IF (DZ(I,J).GT.0.D0) GO TO 10                                     BAL 340
      XM(I,J)=0.D0                                                      BAL 350
      EN(I,J)=0.D0                                                      BAL 360
      GO TO 70                                                          BAL 370
   10 CONTINUE                                                          BAL 380
      PP=P(I,J)                                                         BAL 390
      HH=H(I,J)                                                         BAL 400
      PP=PP*0.1**7                                                      BAL 410
      HH=HH*0.1**7                                                      BAL 420
      K=NP(I,J)                                                         BAL 430
      PHI(I,J)=PHIO(I,J)*(1.D0+(P(I,J)-POLD(I,J))*BETA)                 BAL 440
      HH=730.984+129.239*PP-10.0333*PP*PP+0.39881*PP*PP*PP
     A1    -99.0697/PP+12.9267/PP/PP-0.628359/PP/PP/PP
      IF (IND(K)) 20,30,40                                              BAL 470
   20 CONTINUE                                                          BAL 480
      DEN=F1(PP,HH)                                                     BAL 490
      TEMP=F2(PP,HH)                                                    BAL 500
      GO TO 50                                                          BAL 510
```

```
   30 CONTINUE                                                          BAL 520
      HS=2822.82-39.952/PP+2.54342/PP/PP-0.938879*PP*PP                 BAL 530
      TEMP=F2(PP,HW)                                                    BAL 540
      DW=F1(PP,HW)                                                      BAL 550
      DS=F3(PP,HS)                                                      BAL 560
      SW=DS*(HS-HH)/(HH*(DW-DS)-(HW*DW-HS*DS))                          BAL 570
      SST=1.0-SW                                                        BAL 580
      DEN=DW*SW+SST*DS                                                  BAL 590
      GO TO 50                                                          BAL 600
   40 CONTINUE                                                          BAL 610
      DEN=F3(PP,HH)                                                     BAL 620
      HW=730.984+129.239*PP-10.0333*PP*PP+0.39881*PP*PP*PP
     1   -99.0697/PP+12.9267/PP/PP-0.628359/PP/PP/PP
      HS=2822.82-39.952/PP+2.54342/PP/PP-0.938879*PP*PP
      TT1=F4(PP,HH)
      TT2=F4(PP,HS)
      TT3=F2(PP,HW)
      TEMP=TT1-TT2+TT3
   50 HROCK=TEMP*PHFWT                                                  BAL 640
      VOL=DY(J)*DX(I)*DZ(I,J)                                           BAL 650
      XMT=VOL*DEN*PHI(I,J)                                              BAL 660
      ENT=VOL*(PHI(I,J)*HH*DEN*10.**7+(1.0-PHI(I,J))*HROCK*DF)          BAL 670
      IF (ICX.EQ.0) GO TO 60                                            BAL 680
      DELM=DELM-XMASS(I,J)+XMT                                          BAL 690
      DELE=DELE-ENERGY(I,J)+ENT                                         BAL 700
   60 XM(I,J)=XMT                                                       BAL 710
      EN(I,J)=ENT                                                       BAL 720
   70 CONTINUE                                                          BAL 730
      IF (KKK.NE.NK) GO TO 90                                           BAL 740
      DO 80 I=1,NX                                                      BAL 750
      DO 80 J=1,NY                                                      BAL 760
      XMASS(I,J)=XM(I,J)                                                BAL 770
   80 ENERGY(I,J)=EN(I,J)                                               BAL 780
   90 CONTINUE                                                          BAL 790
      IF (ICX.EQ.0) GO TO 110                                           BAL 800
      QQQ=0.D0                                                          BAL 810
      EEE=0.D0                                                          BAL 820
      DO 100 I=1,NX                                                     BAL 830
      DO 100 J=1,NY                                                     BAL 840
      QQQ=QQQ+Q(I,J)*DELT                                               BAL 850
  100 EEE=EEE+QH(I,J)*DELT                                              BAL 860
      PCEM=(DELM-QQQ)*100.D0                                            BAL 870
      IF (QQQ.NE.0.D0) PCEM=PCEM/QQQ                                    BAL 880
      PCEE=(DELE-EEE)*100.D0                                            BAL 890
      IF (EEE.NE.0.D0) PCEE=PCEE/EEE                                    BAL 900
      WRITE (6,120) QQQ,EEE,DELM,DELE,PCEM,PCEE                         BAL 910
  110 CONTINUE                                                          BAL 920
      RETURN                                                            BAL 930
C                                                                       BAL 940
  120 FORMAT (//11X,23HMASS AND ENERGY BALANCE/11X,23(1H-)/32X,4HMASS,31BAL 950
     1X,4HHEAT/15X,12HDISCHARGE = ,G15.8,20X,G15.8/15X,12HSTORAGE =    ,GBAL 960
     215.8,20X,G15.8/15X,12H% ERROR =    ,G15.8,20X,G15.8)             BAL 970
      END                                                               BAL 980
```

ROUGH DRAFT

VERTICAL STEAM-WATER FLOW IN WELLS WITH HEAT TRANSFER VSTEAM

USER'S MANUAL

Release 2.0

SECTION 2
DATA INPUT REQUIREMENTS

2.1 INTRODUCTION

This section describes the required and optional input data for the program. Input data forms that illustrate the placement of the various input parameters on the data cards are described in the text below.

A single computer job can process as many different individual cases as desired. Each case requires five or more data cards as described in Section 2.2 for multicase runs, the data for each succeeding set is included immediately after that for the preceeding one. Also, preceeding the data for the first case are one or more cards for control parameters and fluid properties.

The required input data include a description of the flow string (total depth, lengths and diameters of component segments), mass flow rate, steam quality and the pressure at one end of the line. Fluid properties may be specified, or if unknown they can be determined from correlations and/or default values provided in the program. Detailed steam tables are included, but solution gas properties should be specified if known, rather than relying on generalized correlations.

2.2 INPUT DATA DESCRIPTION

The data input forms for the vertical steam-water flow model (VSTEAM) are included in this section. Card type 1 through 6 contain data that is used for all of the cases to be run; the temperature, pressure and steam property tables. These data are input only once, while cards 7 through 21 are input for each case. These cards, 7 through 21, describe in detail the wellbore and flowing conditions to be simulated, and includes control data for which flow equations are to be used, and data for transient heat flux effects between wellbore and formation.

Each card input uses either a right justified integer format or a real format which usually requires a decimal point. Each card will be exactly described in the following section, and a brief description of each variable on each card is included.

CARD TYPE 1	CONTROL PARAMETERS (1415)							
NC	NZ	IP	NTR	NPR	NST	NREG	IGAS	
5	10	15	20	25	30	35	40	45 50 55 60 65 70 75 80

NC - NUMBER OF CASES TO BE RUN (NOT CURRENTLY USED)

NZ - NUMBER OF INCREMENTS PER SEGMENT (DEFAULT = 5)

IP - OUTPUT CONTROL

- 0 - DO NOT PRINT INPUT DATA
- 1 - ECHO PRINT INPUT DATA
- 2 - PRINT INPUT DATA WITH DESCRIPTIVE TEST
- 3 - ECHO PRINT AND DESCRIPTIVE PRINT

NTR - NUMBER OF ENTRIES IN SUPERHEATED VAPOR TEMPERATURE TABLE (CARD TYPE 4A, $0 \leq NTR \leq 8$)

NPR - NUMBER OF ENTRIES IN SUPERHEATED VAPOR PRESSURE TABLE (CARD TYPE 4B, $0 \leq NPR \leq 20$)

NST - NUMBER OF ENTRIES IN STEAM TABLE (CARD TYPE 3). PROGRAM SUPPLIES OWN TABLE IF ENTERED AS ZERO OR BLANK (MAXIMUM OF 200).

NREG - FLOW REGIEME MAP CONTROL

- 0 - ROS/GRIFFITH MAP USED
- 1 - AZIZ MAP USED

IGAS - CONTROL OF SINGLE-PHASE STEAM

- 0 - TWO-PHASE SATURATED STEAM-WATER
- 1 - SINGLE-PHASE SUPERHEATED STEAM

NOTE: THIS CARD INPUT ONLY ONCE PER JOB

CARD TYPE 2	BASE CONDITIONS (2 F10.0)																			
PBASE		TBASE																		
5	10	15	20	25	30	35	40	45	50	55	60	65	70	75	80					

PBASE - BASE PRESSURE, PSIA. IF NOT SPECIFIED, ASSUMED AS 14.65 PSIA

TBASE - BASE TEMPERATURE, ^{o}F. IF NOT SECIFIED, ASSUMED AS 60^{o}F.

CARD TYPE 3	SATURATED STEAM TABLE (6F10.0)					
PST	TST	SVF	SVG	EHF	EHG	
5 10	15 20	25 30	35 40	45 50	55 60	65 70 75 80

INPUT NST TYPE 3 CARDS. IF NST = 0 ON CARD TYPE 1, THIS CARD TYPE IS NOT INPUT AND PROGRAM SUPPLIES ITS OWN TABLE.

PST - SATURATION PRESSURE, psia

TST - SATURATION TEMPERATURE, ^{o}F

SVF - SPECIFIC VOLUME OF LIQUID, cu.ft./lbm.

SVG - SPECIFIC VOLUME OF GAS, cu.ft./lbm.

EHF - SPECIFIC ENTHALPY OF LIQUID, BTU/lbm.

EHG - SPECIFIC ENTHALPY OF GAS, BTU/lbm.

NOTE 1.) SVF IS MODIFIED BY SGW ON CARD 9 TO ACCOUNT FOR GRAVITY OF BRINE.
2.) THIS CARD IS USUALLY NOT READ UNLESS ANOTHER FLUID SUCH AS CO_2 IS BEING CONSIDERED OR IMPURITIES CAUSE MEASURED DEVIATION FROM PURE WATER PROPERTIES.

CARD TYPE 4A	SUPERHEATED VAPOR TEMPERATURES (5F10.0)							
TRC (1)	TRC (2)	TRC (3)	TRC (4)	TRC (5)	TRC (6)	TRC (7)	TRC (8)
5 10	15 20	25 30	35 40	45 50	55 60	65 70	75 80

INPUT NTR VALUES (MAXIMUM OF 8) GIVING REFERENCE TEMPERATURES FOR TABLES SENTH AND SVOL, ^{o}F.

IF IGAS = 0 OR NTR = 0 ON CARD TYPE 1, THIS CARD IS NOT READ.

NOTE: IF SUPERHEATED VAPOR TABLES ARE NEEDED, SETTING IGAS = 1 AND NTR = 0 WILL CAUSE PROGRAM TO PROVIDE ITS OWN TABLES, AND CARD TYPES 4A, 4B, 5, AND 6 ARE NOT READ.

CARD TYPE 4B	SUPERHEATED VAPOR PRESSURES (8F10.0)							
NPR (I)	NPR (I)	NPR (I)	NPR (I)	NPR (I)	NPR (I)	NPR (I)	NPR (I)	
5 10	15 20	25 30	35 40	45 50	55 60	65 70	75 80	

INPUT NPR VALUES (MAXIMUM OF 20) GIVING REFERENCE PRESSURES FOR TABLES SENTH AND SVOL, PSIA.
IF IGAS = 0 OR NTR = 0 ON CARD TYPE 1, THIS CARD IS NOT READ.

CARD TYPE 5	SUPERHEATED VAPOR ENTHALPIES (8F10.0)							
SENTH (I,J)	SENTH (I,J)	SENTH (I,J)	SENTH (I,J)	SENTH (I,J)	SENTH (I,J)	SENTH (I,J)	SENTH (I,J)
5 10	15 20	25 30	35 40	45 50	55 60	65 70	75 80

INPUT NTR SETS OF TYPE 5 CARDS, EACH SET CONSISTING OF NPR VALUES OF SUPERHEATED VAPOR ENTHALPIES, BTU/lbm. (MAXIMUM OF 20 PER SET). FIRST SET OF NPR CARDS CORRESPONDS TO FIRST TEMPERATURE ON CARD TYPE 4A, AND ENTHALPY VALUES SHOULD MATCH PRESSURES ON CARD TYPE 4B.

IF IGAS = 0 OR NTR = 0 ON CARD TYPE 1, THIS CARD IS NOT READ.

CARD TYPE 6	SUPERHEATED VAPOR SPECIFIC VOLUMES (8F10.0)							
SVOL (I,J)	SVOL (I,J)	SVOL (I,J)	SVOL (I,J)	SVOL (I,J)	SVOL (I,J)	SVOL (I,J)	SVOL (I,J)
5 10	15 20	25 30	35 40	45 50	55 60	65 70	75 80

INPUT NTR SETS OF TYPE 6 CARDS, EACH SET CONSISTING OF NPR VALUES OF SUPERHEATED STEAM SPECIFIC VOLUMES, cu.ft./lbm. (MAXIMUM OF 20 PER SET). THE FIRST SET OF NPR CARDS CORRESPONDS TO THE FIRST TEMPERATURE ON CARD TYPE 4A, AND SPECIFIC VOLUME VALUES SHOULD MATCH PRESSURES ON CARD TYPE 4B.

IF IGAS = 0 OR NTR = 0 ON CARD TYPE 1, THIS CARD IS NOT READ.

NOTE: THIS CONCLUDES THE INITIAL DATA READ ONLY ONCE PER JOB

CARD TYPE 7 CASE IDENTIFICATION (18A4)

IDENT																
5	10	15	20	25	30	35	40	45	50	55	60	65	70	75	80	

IDENT IS AN ALPHANUMERIC TITLE CARD OF UP TO 72 CHARACTERS IDENTIFYING THE SPECIFIC CASE BEING RUN. THIS CARD SHOULD BE THE FIRST CARD OF EACH CASE RUN.

CARD TYPE 8 CONTROL PARAMETERS (10 I 5)

NDIA	NOUT	VOPT	IFLO	ITV	IHTX	NR	KE	MIX	LIFT							
5	10	15	20	25	30	35	40	45	50	55	60	65	70	75	80	

NDIA - NUMBER OF TUBING/CASING INPUT CARDS (TYPE 13) TO BE READ (MAXIMUM OF 15 - MINIMUM 1)

NOUT = 0 - INHIBIT PRINTING OF RESULTS OF INTERMEDIATE CALCULATIONS
= 1 - PRINT HEAT BALANCE SUMMARY TABLE
= 2 - PRINT INTERNAL VARIABLES USED
= 3 - OBTAIN PRINTOUT OF PHYSICAL PROPERTIES USED

VOPT = 1 - HAGEDORN AND BROWN = 3 - AZIZ AND GOVIER
= 2 - ORKISZEWSKI = 4 - BEGGS AND BRILL

IFLO = 0 - FLOW IN PIPE IS UPWARDS (ITV=1)
= 1 - FLOW IN PIPE IS DOWNWARDS (ITV=0)

ITV = 0 - PRESSURE TRAVERSE IS CALCULATED FROM TOP TO BOTTOM
= 1 - PRESSURE TRAVERSE IS CALCULATED FROM BOTTOM TO TOP

IHTX = 0 - ANALYTIC HEAT LOSS FROM WELLBORE TO ROCK AROUND WELLBORE
= 1 - WILLHITE WELLBORE HEAT LOSS CALCS
= 2 - TRANSIENT HEAT LOSS IN ROCK SURROUNDING WELLBORE (CARD TYPES 16 THROUGH 19 MUST BE INPUT)

NR = - NUMBER OF RADIAL RESERVOIR GRID BLOCKS (5 IS USUALLY SUFFICIENT)

KE = 0 - INCLUDE KINETIC ENERGY TERM IN CALCULATIONS
= 1 - EXCLUDE KINETIC ENERGY TERM IN CALCULATIONS (CAN BE USED ALMOST ALWAYS)

MIX = 0 - MIXTURE DENSITY WITH SLIPPAGE IS USED EVERYWHERE
= 1 - MIXTURE DENSITY WITHOUT SLIPPAGE IS USED EVERYWHERE

LIFT = 0 - CALCULATE PRESSURE PROFILE GIVEN RATE
= 1 - SET PRESSURE AND CALCULATE DELIVERABILITY

CARD TYPE 9	FLUID PROPERTIES (8F10.0)						
GLR	SGG	SGW	VGC	VWC	PC	TC	
5 10	15 20	25 30	35 40	45 50	55 60	65 70	75 80

GLR - SOLUTION GAS/WATER RATIO, SCF/STB

SGG - SOLUTION GAS GRAVITY

SGW - GRAVITY OF WATER W.R.T. PURE WATER. IF NOT SPECIFIED, ASSUMED AS 1.0

VGC - STEAM VISCOSITY FACTOR (DEFAULT = 1.0)

VWC - WATER VISCOSITY FACTOR (DEFAULT = 1.0)

TC - CRITICAL TEMPERATURE, ^{o}R, OF STEAM. IF BLANK, SUPPLIED BY PROGRAM.

PC - CRITICAL PRESSURE, PSIA, OF STEAM. IF BLANK, SUPPLIED BY PROGRAM.

CARD TYPE 10 CASE DESCRIPTION DATA (8F10.0)

DEPTH	EDI	TTOP	TBOT				
5 10	15 20	25 30	35 40	45 50	55 60	65 70	75 80

DEPTH - TOTAL LENGTH OF PIPE, FEET (MEASURED DEPTH

EDI - TUBING ROUGHNESS, INCHES. IF NOT SPECIFIED, ASSUMED AS 0.0006 INCHES.

TTOP - SURFACE ROCK TEMPERATURE, ^{o}F.

TBOT - BOTTOM HOLE ROCK TEMPERATURE, ^{o}F.

Victor M Arellano-Gomez

CARD TYPE 11	CASE DESCRIPTION (8F10.0)						
UWELL	DHOLE	TIME	URES	TDIS	RE		
5 10	15 20	25 30	35 40	45 50	55 60	65 70 75 80	

UWELL - OVERALL WELLBORE HEAT TRANSFER COEFF, BTU/(hr-^{o}F-ft^{2}) - APPLIES FROM FLUID TO OUTSIDE CEMENT.

DHOLE - HOLE DIAMETER USED AS BASIS FOR HEAT LOSS UNLESS DICAS IS SPECIFIED, INCHES

TIME - TOTAL TIME WELL HAS BEEN FLOWING, DAYS. USED FOR ANALYTIC HEAT LOSS CALCULATIONS.

URES - OVERALL RESERVOIR HEAT TRANSFER COEFFICIENT, BTU/(hr-^{o}F-ft^{2}). USED FOR ANALYTIC HEAT LOSS, THESE VALUES SHOULD RANGE FROM 1 TO 10, BUT CAN BE HIGHER IN A GEOTHERMAL WELL.

TDIS - THERMAL DIFFUSIVITY OF ROCK, BTU/(^{o}F-ft^{2}). IF NOT SPECIFIED, ASSUMED AT 0.04 BTU/(^{o}F-ft^{2})

RE - EXTERIOR RADIUS OF GRID, FEET (200 IS SUFFICENT)

NOTE: IF IHTX (CARD 8) IS ZERO, THEN THE OVERALL COEFFICIENT IS COMPUTED AS

$$\frac{1}{u} = \frac{1}{u_{well}} + \frac{f(t)}{u_{res}}$$

FOR MORE DETAILED WELLBORE HEAT TRANSFER TREATMENT, SET IHTX = 1 AND READ CARDS 12A, B, AND C.

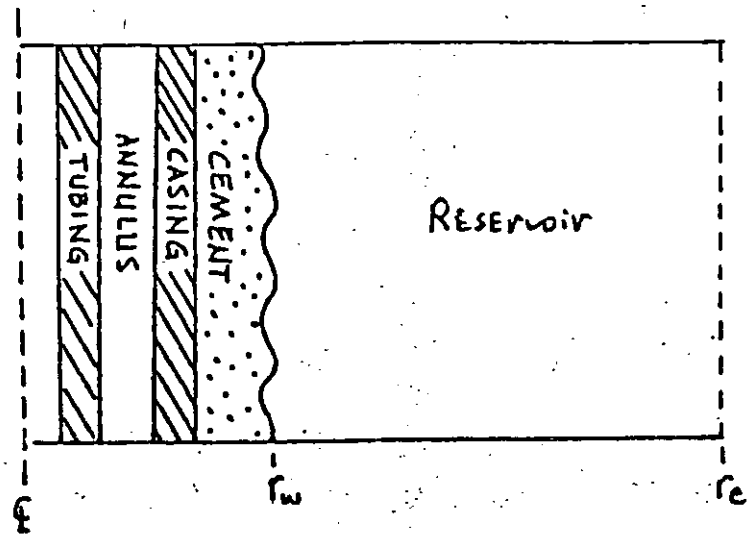

CARD TYPE 12	WELLBORE HEAT TRANSFER						(READ ONLY IF IHTX = 1)
AKINS	AKHA	AKCEM	AKE	EPSTO	EPSCI	UTOL	
5 10	15 20	25 30	35 40	45 50	55 60	65 70	75 80

AKINS = THERMAL CONDUCTIVITY OF TUBING INSULATION

AKHA = THERMAL CONDUCTIVITY OF ANNULUS FLUID

AKCEM = THERMAL CONDUCTIVITY OF THE CEMENT, BTU/HR/FT/DEG.F

AKE = THERMAL CONDUCTIVITY OF EXTERNAL RESERVOIR ROCK

EPSTO = EMISSIVITY OF TUBING (INSULATION) SURFACE

EPSCI = EMISSIVITY OF CASING INNER SURFACE

UTOL = CONVERGENCE TOLERENCE

CARD TYPE 12B	WELLBORE HEAT TRANSFER				(READ ONLY IF IHTX = 1)
RTI	RTO	RINS	RCI	RCO	
5 10	15 20	25 30	35 40	45 50	55 60 65 70 75 80

RTI = RADIUS INSIDE TUBING, FEET

RTO = RADIUS OUTSIDE TUBING, FEET

RINS = RADIUS OUTSIDE INSULATION, FEET

RCI = RADIUS INSIDE CASING, FEET

RCC = RADIUS OUTSIDE CASING, FEET

CARD TYPE 12C WELLBORE HEAT TRANSFER (READ ONLY IF IHTX = 1)

RHOAN	UMUAN	CAN	TEANN	
5 10	15 20	25 30	35 40	45 50 55 60 65 70 75 80

RHOAN - ANNULUS FLUID DENSITY, lb/ft^3

UMUAN - ANNULUS FLUID VISCOSITY, cp

CAN - ANNULUS FLUID HEAT CAPACITY, $BTU/lb.^oF$

TEANN - ANNULUS FLUID TEMPERATURE, deg.F

CARD TYPE 13 SOURCE DESCRIPTION DATA (5F10.0)

WT	XMAS	PREF	TREF	HREF									
5	10	15	20	25	30	35	40	45	50	55	60	65	70	75	80

WT - TOTAL MASS FLOW RATE, Klbm/hr. FOR DELIVERABILITY CALCULATIONS (LIFT $\neq$ 0), THIS IS THE INITIAL RATE GUESS.

XMAS - MASS FRACTION STEAM QUALITY AT PREF. NOT REQUIRED IF HREF SPECIFIED.

PREF - PRESSURE, PSIG, AT PIPE END WHERE CALCULATION OF TRAVERSE BEGINS AS SPECIFIED BY ITV
(IF ITV = 0, THEN PREF IS WELLHEAD)
(IF ITV = 1, THEN PREF IS BOTTOMHOLE)

TREF - TEMPERATURE, ^{o}F, AT LOCATION OF PREF. IF STEAM QUALITY IS GREATER THAN ZERO AND LESS THAN ONE, LEAVE BLANK AND TEMPERATURE IS AUTOMATICALLY SET TO THE SATURATION TEMPERATURE AT PREF. IF TREF SPECIFIED AS LESS THAN SATURATION TEMPERATURE, STEAM QUALITY IS SET TO ZERO AND PROGRAM CALCULATES A FLASH POINT INSIDE THE WELLBORE.

HREF - ENTHALPY, BTU/lbm. AT PREF AND TREF. IF LEFT BLANK, PROGRAM SUPPLIES CORRECT ENTHALPY CORRESPONDING TO PREF AND STEAM QUALITY.

CARD TYPE 14 DELIVERABILITY PARAMETERS (2I5,4F10.0)

NMAX	LBASE	PSET	EPS	DQ	QLMIN	
5	10	15 20	25 30	35 40	45 50	55 60 65 70 75 80

THIS CARD IS NOT READ IF LIFT = 0

IF LIFT = 1:

NMAX - MAXIMUM NUMBER OF ITERATIONS ALLOWED (10 to 30)

LBASE - NOT USED

PSET - SPECIFIED PRESSURE TO BE MATCHED, psia
- WELLHEAD PRESSURE IF IFLO = 0 (ITV = 1) ON CARD 08.
- BOTTOMHOLE PRESSURE IF IFLO = 1 (ITV = 0) ON CARD 08.

EPS - CONVERGENCE TOLERANCE FOR PRESSURE, FRACTION, DEFINED AS (TRUBHP-PCALC)/TRUBHP

DQ - LIQUID RATE DAMPING VALUE FOR INTERVAL SEARCH. IF NOT SPECIFIED, ASSUMED AS 2.0.

QLMIN - MINIMUM RATE BEFORE POTENTIAL ASSUMED TO BE ZERO, Klbm/hr.

CARD TYPE 15	FLOW CONDUIT DESCRIPTION (6F10.0, 15, 5X, F10.0)							
HTCH	DIA	DICAS	WTHIC	UHT	THETA	NTUBE		TRK
5 10	15 20	25 30	35 40	45 50	55 60	65	70	75 80

INPUT EXACTLY NDIA TYPE 15 CARDS

HTCH - DISTANCE FROM SURFACE TO DEPTH WHERE THIS SECTION BEGINS, FEET.

DIA - INSIDE DIAMETER OF TUBING, INCHES.

DICAS - INSIDE DIAMETER OF CASING, INCHES. NOT REQUIRED IF NTUBE = 0.

WTHIC - TUBING WALL THICKNESS, INCHES. NOT REQUIRED IF NTUBE = 0.

UHT - OVERALL HEAT TRANSFER COEFF, BTU/(HR SQ.FT ^{o}F), DEFAULT USES UWELL AND URES FROM CARD 11.

THETA - ANGLE OF CONDUIT INCLINATION FROM VERTICAL, DEGREES.

NTUBE - SPECIFIES WHETHER FLOW IS THROUGH TUBING OR ANNULUS

0 = TUBING FLOW
1 = ANNULAR FLOW

TRK - ROCK TEMPERATURE AT CORRESPONDING DEPTH, ^{o}F. CAN BE USED TO SPECIFY TEMPERATURE GRADIENT IN PLACE OF TTOP AND TBOT ON CARD TYPE 10. (USED FOR ANALYTIC HEAT TRANSFER CASE ONLY)

NOTE: IF IHTX (CARD 8) EQUALS ZERO OR ONE, THEN ANOTHER CASE MAY BE READ BY RETURNING TO CARD 7 FOR MORE INPUT.

CARD TYPE 16	RESERVOIR ROCK PROPEERTIES	(READ ONLY IF IHTX = 2)
RC	RK	
5 10	15 20	25 30 35 40 45 50 55 60 65 70 75 80

INPUT NDIA CARDS, BEGINNING WITH DATA FOR TOP LAYER

RC(I) - ROCK HEAT CAPACITY, BTU/(ft^3 - ^oF)

RK(I) - ROCK THERMAL CONDUCTIVITY, BTU/(DAY-ft-^oF)

NOTE: CARD TYPES 16 THROUGH 20 ARE READ ONLY IF TRANSIENT HEAT LOSS CALCULATIONS ARE TO BE MADE. IHTX ON CARD TYPE 8 MUST BE SPECIFIED AS 2. IF IHTX = 0, ANOTHER CASE CAN BE INPUT BY RETURNING TO INPUT STEAM AT CARD TYPE 7 AND BYPASSING CARDS 16 - 20.

CARD TYPE 17	THERMAL PROPERTY OVERREAD (415)			(READ ONLY IF IHTX = 2)
11	12	K1	K2	

5 10 15 20 25 30 35 40 45 50 55 60 65 70 75 80

11, 12 - BEGINNING AND ENDING RADIAL BLOCKS FOR WHICH NEW THERMAL PROPERTIES ARE TO BE ASSIGNED

K1, K2 - BEGINNING AND ENDING LAYERS FOR WHICH NEW THERMAL PROPERTIES ARE TO BE ASSIGNED

NOTE: IF NO OVERREADS ARE DESIRED, INPUT A BLANK CARD HERE AND SKIP TO CARD TYPE 18. FOR EACH CARD TYPE 17 INPUT, ONE CARD TYPE 17A MUST FOLLOW. FOLLOW CAST OF CARD TYPE 17 AND 17A PAIRS WITH A BLANK CARD.

CARD TYPE 17A THERMAL PROPERTY OVERREAD (2F10.0) (READ ONLY IF IHTX = 2)

URC	URK	
5 10	15 20	25 30 35 40 45 50 55 60 65 70 75 80

URC - ROCK HEAT CAPACITY, BTU/(ft^3 - ^oF), TO BE USED IN REGION DEFINED BY CARD TYPE 17

URK - ROCK THERMAL CONDUCTIVITY, BTU/(DAY-ft-^oF), TO BE USED IN REGION DEFINED BY CARD TYPE 17

CARD TYPE 18 RECURRENT CONTROL DATA (415) (READ ONLY IF IHTX = 2)

IGO	IFLO	NOUT	NMAP
5	10	15	20

THIS CARD IS READ ONCE FOR EACH TIME STEP DURING TRANSIENT HEAT LOSS CALCULATIONS

IGO = 0 QUIT, NO MORE CALCULATIONS TO BE MADE
= 1 CONTINUE CALCULATIONS

IFLO = 0 FLOW IN PIPE IS UPWARD (ITV=1)
= 1 FLOW IN PIPE IS DOWNWARD (ITV=0)

NOUT = 0 INHIBIT PRINTING OF INTERMEDIATE RESULTS
= 1 PRINTOUT WELLBORE HEAT BALANCE
= 2 PRINTOUT WELLBORE PROPERTIES AND INTERNAL VARIABLES

NMAP = 0 NO PRINTER MAP CONTROLS READ
= 1 READ CONTROLS FOR R-Z TEMPERATURE MAP TO BE OUTPUT

NOTE: RECURRENT DATA CONSISTS OF CARD TYPES 18, 19 AND 20. IF MORE CASES ARE TO BE RUN, INPUT IGO = 0 (BLANK CARD) AND RETURN TO INPUT STREAM AT CARD TYPE 7.

CARD TYPE 19	RECURRENT RATE DATA (5F10.0)				(READ ONLY IF IHTX = 2)			
DTC	WT	XMAS	PREFIX	TREFX	HREFX			
5 10	15 20	25 30	35 40	45 50	55 60	65 70	75 80	

DTC - TIME STEP USED FOR TRANSIENT CALCULATIONS, DAYS

WT - TOTAL MASS FLOW RATE, Klbm/hr

XMAS - MASS FRACTION STEAM QUALITY AT PREFX

PREFX - PRESSURE, psig, AT PIPE END WHERE CALCULATION OF TRAVERSE BEGINS

TREFX - TEMPERATURE, ^{o}F, AT PREFX (SEE CARD TYPE 10). IF VALUES OF PREFX AND TREFX ARE NOT SPECIFIED, VALUES FROM PREVIOUS TIME STEP ARE USED

HREFX - REFERENCE ENTHALPY

CARD TYPE 20 RECURRENT MAP CONTROLS (415, 4F10.0) (READ ONLY IF IHTX = 2)

IR1	IR2	KZ1	KZ2	XLGTH	YLGTH	TMIN	TMAX	
5 10	15	20	25 30	35 40	45 50	55 60	65 70 75 80	

READ ONLY IF NMAP = 1

IR1 - BEGINNING RADIAL BLOCKS TO BE MAPPED

IR2 - ENDING RADIAL BLOCKS TO BE MAPPED

KZ1 - BEGINNING LAYER TO BE MAPPED

KZ2 - ENDING LAYER TO BE MAPPED

XLGTH - HORIZONTAL MAP WIDTH, INCHES

YLGTH - VERTICAL MAP WIDTH, INCHES

TMIN - MINIMUM TEMPERATURE TO BE MAPPED, ^{o}F

TMAX - MAXIMUM TEMPERATURE TO BE MAPPED, ^{o}F

IF TMAX = 0, NO MAP PRINTED

DATA APPLIES TO LATER TIME STEPS UNTIL READ AGAIN

DIVISION DE EDUCACION CONTINUA
FACULTAD DE INGENIERIA U.N.A.M.

CURSO ORGANIZADO A SOLICITUD DE LA ORGANIZACION LATINOAMERICANA DE ENERGIA, CON LA COLABORACION DE LA COMISION FEDERAL DE ELECTRICIDAD Y EL INSTITUTO DE INVESTIGACIONES ELECTRICAS

CURSO: "INGENIERIA DE YACIMIENTOS GEOTERMICOS
MATERIA: MEDICION DE PROPIEDADES FISICAS DE ROCAS

TEMA: FINAL REPORT CAPABILITIES TO MEASURE GEOTHERMAL MATERIAL PROPERTIES AT SIMULATED IN SITU CONDICITIONS

PROF. ING. ENRIQUE CONTRERAS

MARZO, 1 9 8 4

DOE/ET/28301-1

FINAL REPORT

CAPABILITIES TO MEASURE GEOTHERMAL MATERIAL PROPERTIES AT SIMULATED *IN SITU* CONDITIONS

by

D. O. Enniss
S. W. Butters
R. Lingle
R. G. Van Buskirk
F. R. Prater

Submitted to:

Department of Energy
Division of Geothermal Energy
550 Second Street
Idaho Falls, Idaho 83401

Attn: Clay Nichols

Submitted by:

Terra Tek, Inc.
University Research Park
420 Wakara Way
Salt Lake City, Utah 84108

TR 79-49
July 1979

ABSTRACT

The lack of reservoir material property data has been identified as a major obstacle to geothermal development and commercialization. To meet this need a high pressure/high temperature test facility was designed and constructed at Terra Tek under Department of Energy funding. Testing capabilities include confining and pore fluid pressures to 200 MPa and temperatures to 535°C. Rock samples to 10.2 cm diameter can be accommodated.

The program summarized herein is the second year (October 1977-September 1978) effort (DOE Contract DE-AC07-77ET28301). Test techniques were developed to meet the geothermal community needs and tests were conducted to determine: mechanical properties, thermal conductivity, thermal diffusivity, thermal expansion, permeability, electrical resistivity and ultrasonic velocities. Sandstones, graywackes, granites, and basalts, from KGRA's in Baca, New Mexico; Milford, Utah; Geysers, California and Northern Nevada, respectively were characterized.

TABLE OF CONTENTS

LIST OF ILLUSTRATIONS

TABLE 1

Geothermal Core Testing Capabilities

Test Parameter	Maximum Confining Pressure MPa (ksi)	Maximum Pore Pressure MPa (ksi)	Maximum Temperature °C	Pore Fluid	Overall Accuracy	Application**
Mechanical Response	200 (30)	200 (30)	535	Gas Water Brine	±1%	Drilling Stimulation Subsidence
Thermal Conductivity	200 (30)	200 (30)	535	Gas Water Brine	±5%	Surface Exploration Subsurface Evaluation Reservoir Engineering
Thermal Diffusivity	200 (30)	200 (30)	535	Gas Water Brine	±5%	Surface Exploration Subsurface Evaluation Reservoir Engineering
Thermal Expansion	200 (30)	---*	535	Gas Water Brine	±5%	Reservoir Engineering Subsidence
Permeability	200 (30)	69 (10)	535	Gas Water Brine Acid Caustic	±10%	Reservoir Engineering Stimulation
Electrical Resistivity	200 (30)	200 (30)	300	Gas Water Brine	±2.5%	Surface Exploration Subsurface Evaluation
Ultrasonic Velocity	200 (30)	200 (30)	300	Gas Water Brine	±1%	Surface Exploration Subsurface Evaluation

* Not available at present.

** References 2-7

Contained within the appropriate individual description sections are data on sandstones, granites, graywackes, and basalts. The tests conducted include materials from KGRA's at Baca, New Mexico; Milford, Utah; Geysers, California and Northern Nevada. The data have been generated in support of the DOE/DGE supported programs in surface exploration, subsurface evaluation (logging), drilling, stimulation, reservoir engineering and subsidence, and in support of resource development activities by several industrial groups.

FACILITY DESCRIPTION

Capabilities

The geothermal material property test facility is shown in Figure 1. Data acquisition and associated control equipment are shown in the foreground separated from the load frame and pressure vessel (background) by a clear protective barrier. A schematic detailing major components of the load frame is contained in Figure 2. Capabilities of the high pressure-high temperature test facility are summarized:

- Confining pressure to 200 MPa (30,000 psi)
- Temperature to 535°C (1000°F)
- Axial load to 4.5×10^6 N (10^6 lbs)
- Sample size: 5.1 cm (2") diameter (to 535°C)
  10.2 cm (4") diameter (to 200°C)

While maintaining these previously described environments the following geothermal material properties can be determined:

- Mechanical properties: complete stress-strain response including longitudinal and lateral strains (volume response) and pore fluid pressure.
- Thermal properties: thermal conductivity, thermal diffusivity, thermal expansion coefficient
- Matrix and fracture permeability/conductivity to gases and liquids
- Electrical resistivity
- Ultrasonic velocities

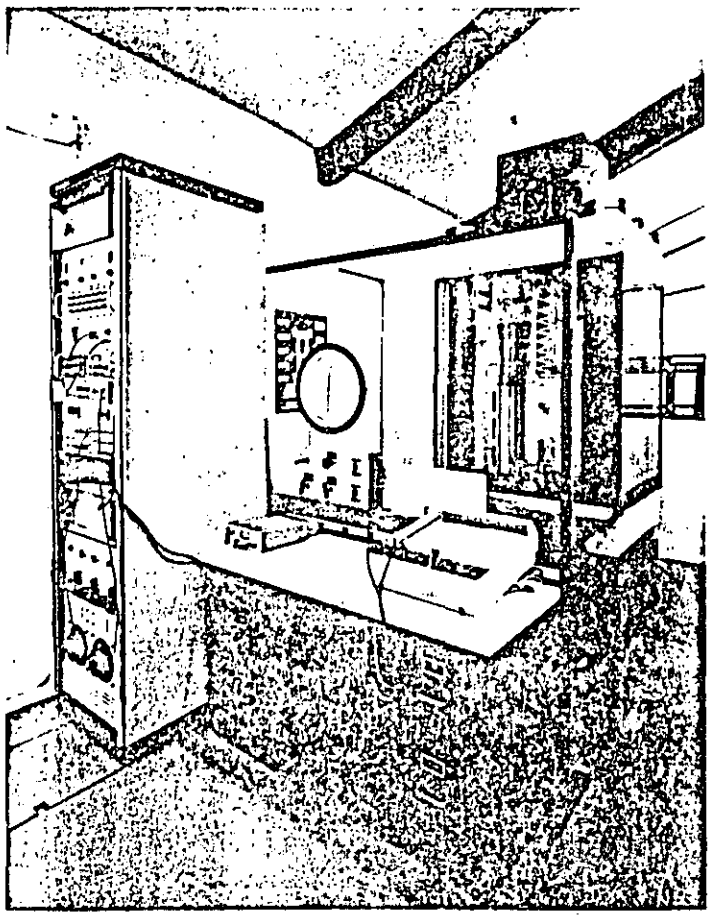

Figure 1. Geothermal material test system.

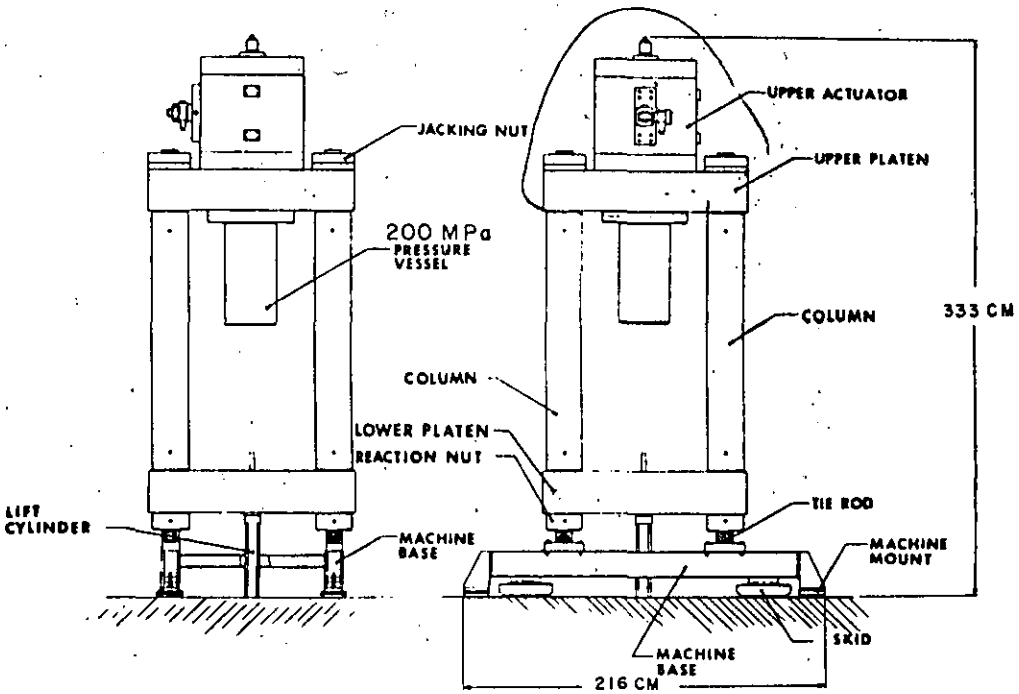

Figure 2. Geothermal material test system schematic.

Figure 3 contains a photograph of complementary equipment at Terra Tek including an identical vessel in a configuration designed specifically for long term consolidation (creep) tests, and a high temperature, high flow circulation system. This flow system is capable of pressures to 69 MPa (10,000 psi), temperatures to 312°C (600°F), and flow rates to 37 liters per minute (10 gal/min). As well as circulating fresh waters, it can transport mixed brines, light acids and light caustics.

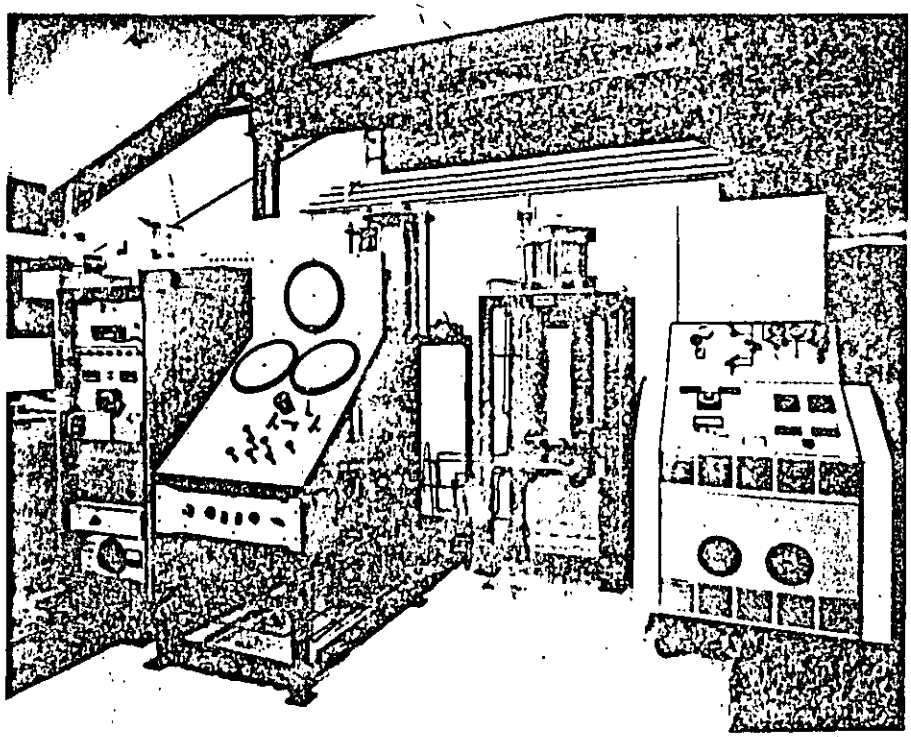

Figure 3. Complementary test equipment.

Pressure Vessel

The pressure vessel, in which the material property testing is conducted, is a 15.25 cm (6 inch) inside diameter hardened steel cylinder capable of internal pressures to 200 MPa (30,000 psi). A mild steel

cooling jacket/safety liner surrounds the vessel. Cooling water circulating in the jacket maintains a constant vessel wall temperature during extended duration testing. Elevated sample temperatures are achieved by internally mounted heaters (up to 9 kilowatts) which promote fast test times due to the avoidance of long heat up and cool down times associated with externally heated vessels.

Dowtherm A (liquid) was selected as a confined medium after testing determined that it remained electrically non-conductive at 200 MPa (30,000 psi) and 535°C(1000°F). Degradation begins in the fluid at approximately 400°C (750°F) but this does not prove to be a serious limitation since very little of the total fluid is exposed to the high temperature. Dowtherm A will not vaporize at atmospheric pressure until approximately 290°C (550°F). A pressure of 7 MPa (1000 psi) is sufficient to maintain the fluid phase to 535°C (1000°F)

All load, strain, temperature, and pore pressure measurements are made inside the pressure vessel. Pressure effect on each of these transducers is carefully documented. Samples ranging from 2.5 cm (1 inch) diameter x 5.1 cm (2 inch) length to 10.2 cm (4 inch) diameter x 20.3 cm (8 inch) length can be accommodated.

Load Frame and Control

The load frame is capable of applying an axial load of 4.5×10^6 newtons (1 million pounds) via the servo-controlled upper actuator. Column and rod design are used in the load frame. Prestressed rods and columns maintain a rigid frame. Pressure vessel to lower platen clearance allows for assembly of the test stack with heaters and multiple ceramic

shrouding prior to the insertion of the lower closure into the vessel. A reaction column is used to support the lower closure. This type of design allows for quick stack and vessel assembly thereby reducing test times and costs. The capacity is sufficient to provide loading to failure of all except the strongest rocks.

Load feedback and displacement feedback are available to provide constant load or actuator position operational modes. An electronic ramp generator is used to establish a constant displacement rate of the upper actuator and therefore allows accurate control of strain rate during triaxial compression testing.

TEST TECHNIQUES AND TEST DATA

Sample Preparation

When applying a confining stress to a rock sample it is necessary to isolate the internal pore fluid from the confining fluid. In low temperature rock mechanics tests, thin urethane jackets are used to seal the sample. At temperatures above 175°C (350°F) urethane degrades. For temperatures to 300°C (~600°F) a pre-molded silicone rubber (RTV) jacket is used. End sealing is accomplished by wiring the jacket to stainless steel endcaps. Testing at temperatures above 300°C (~600°F) requires the use of 0.025 cm (0.010 inch) thick annealed copper jackets. Sealing is accomplished by tapered endcaps; press-fit sealing rings allow quick assembly and reuse of the endcaps. Jacketing of this type has been used frequently in high temperature research and has been shown to have negligible influence on the measured strength of competent rock (granite, basalt)[8]. Jacketing effects of weaker, less competent materials (sandstone, shale) at large strains require documentation on a case by case basis.

For tests requiring no pore fluid between the sample and the inside of the jacket (electrical resistivity and permeability), RTV is applied directly to the sample surface. This provides a good adhesion plus an ideal jacket fit. The extent of silicone rubber infiltration is not significant.

The complete range of sample sizes, 2.54 cm (1.0 inch) diameter to 10.2 cm (4.0 inch) diameter can be accommodated by both sample preparation techniques.

No existe al Nº 8

Mechanical Response

The quasi-static stress-strain response of a material under simulated geothermal conditions is determined in the testing configuration of Figure 4. Both lateral and axial strains can be measured allowing the evaluation of failure characteristics, elastic properties and volumetric response characteristics. Pore pressure, confining pressure, and axial load are controlled by separate closed loop servocontrol systems allowing simulation of various pressure-load application "paths".

The test sample, prepared as discussed in a previous section, is located in the upper portion of the test vessel. Ceramic insulation is used on each end of the sample to minimize the longitudinal temperature

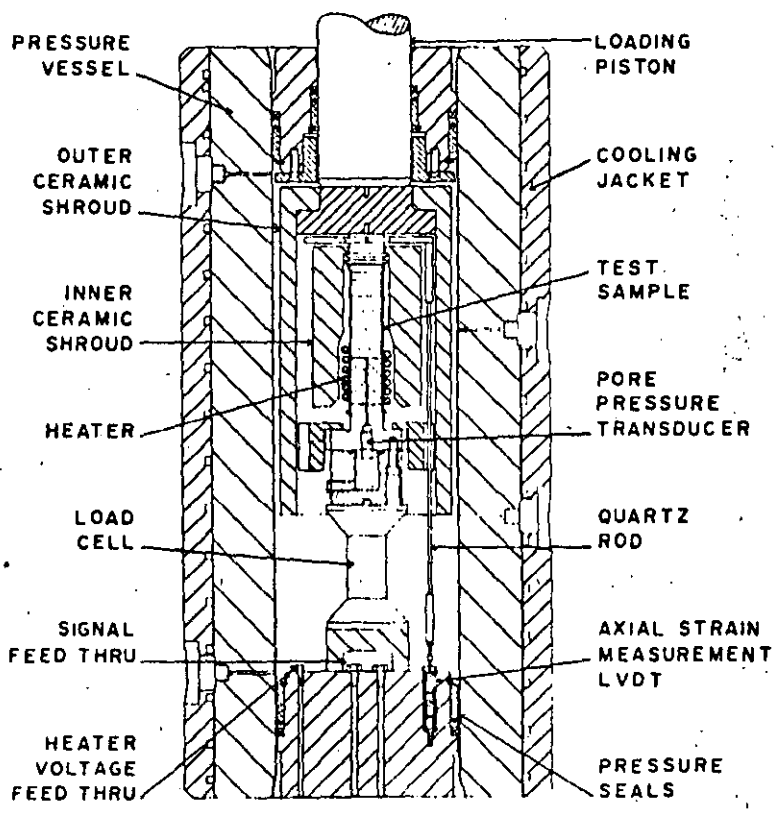

Figure 4. Mechanical response test configuration.

gradients. Heating elements are coiled about the lower aluminum insulator and the lower portion of the sample. A cylindrical ceramic shroud is placed over both the sample and the coiled heater to localize the fluid convection currents. Convection within the vessel is further minimized by a second all-encompassing ceramic shroud. These ceramic convection baffles enable temperatures of 535°C (1000°F) to be reached within the inner shroud while maintaining the fluid surrounding the exterior shroud to remain at less than ~100°C (200°F), well below the maximum allowable for the internal instrumentation and pressure seal.

Supporting this sample stack is a strain-gaged load cell selected to give optimum output for the anticipated load levels. Measurement of axial load in this manner eliminates the possibility of seal friction errors. Axial strain is measured by two LVDT's (linearly variable differential transformers) contained in the lower vessel closure. These transducers are attached to the top of the test sample by quartz rods. Quartz was selected because of its very low thermal expansion. Lateral strain measurement is made by a cantilever arrangement using long, stiff cantilever arms with strain-gaged sections near the bottom of the pressure vessel outside of the high temperature environment.

Axial strain measurements with appropriate calibration for temperature and pressure effects can be made over a range of ±1.27 cm (0.5 inches) and are accurate to 0.0013 cm (0.0005 inches). Lateral strains of ±0.64 cm (0.75 inches) can be measured and are accurate to 0.003 cm (0.001 inches). Confining pressure, pore pressure and axial load are accurate to within ±1 percent of the measured value.

During debugging of the mechanical response system, various unconfined and triaxial compression tests were conducted. Figures 5, 6, 7 and 8 contain typical mechanical response data. Figure 5 shows the stress-strain response of a granite material undergoing triaxial loading to failure. This sample was tested dry, without any pore fluid, at a temperature of 200°C (~400°F) and a confining pressure (σ_3) of 13.8 MPa (2000 psi). Both axial and lateral strains are shown versus axial stress difference (σ_1-σ_3). Figure 6 shows the volume response for the same test. Note the difference in behavior of the saturated and dry samples.

Figures 7 and 8 contain a failure envelope and failure stress versus temperature behavior respectively, of Westerly granite.

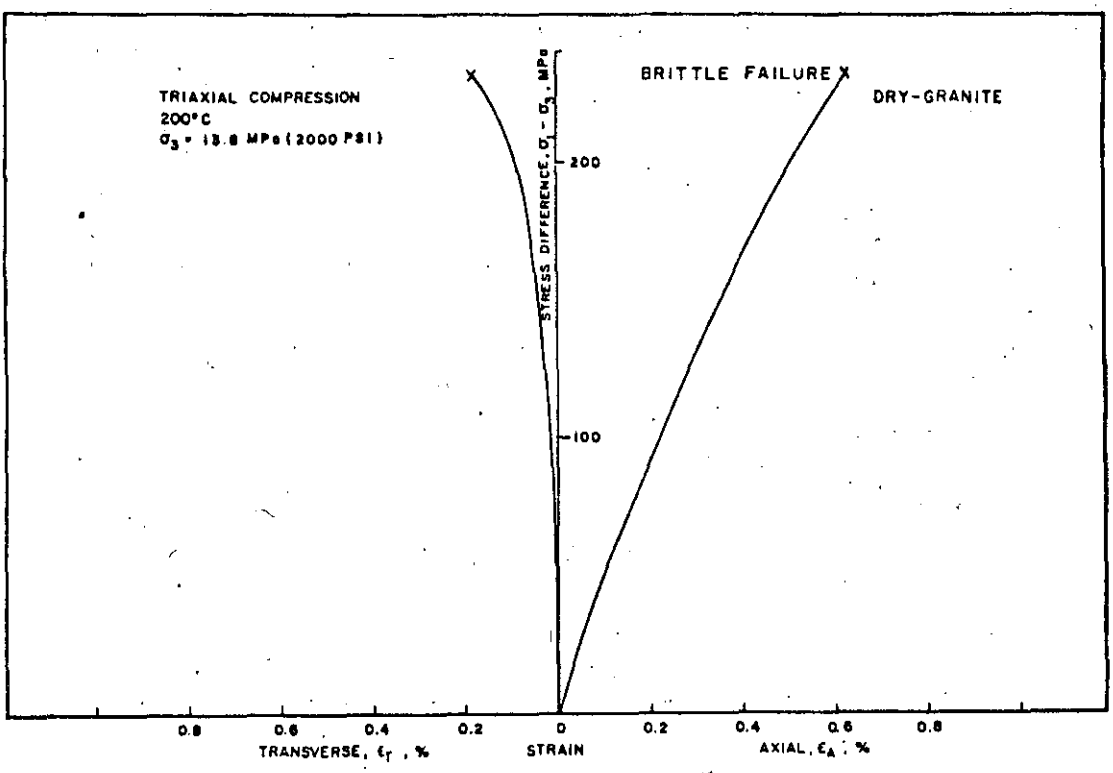

Figure 5. Mechanical response of a dry granite material at temperature.

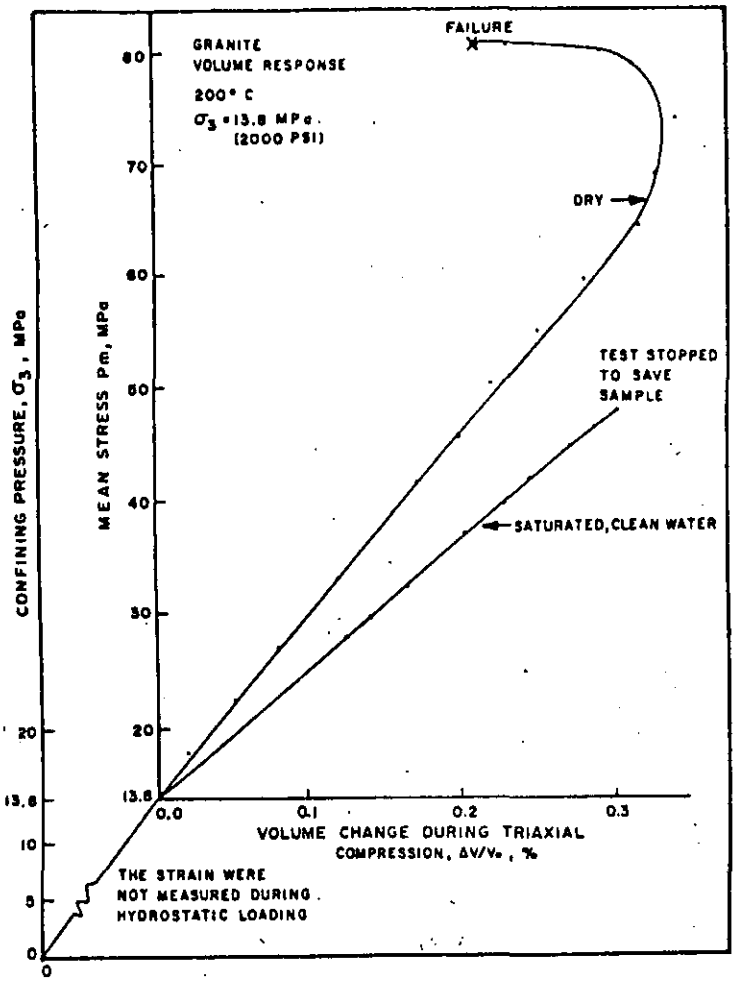

Figure 6. Volumetric response of a granite material at temperature.

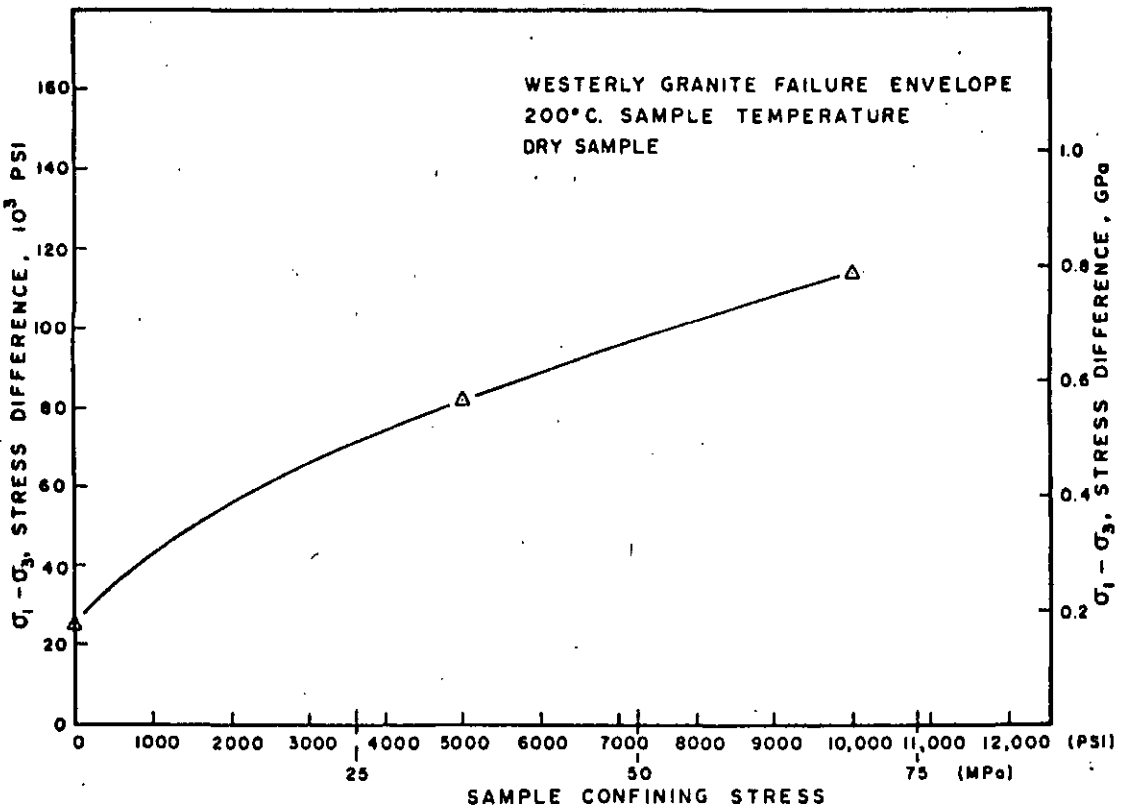

Figure 7. Failure envelope for Westerly granite.

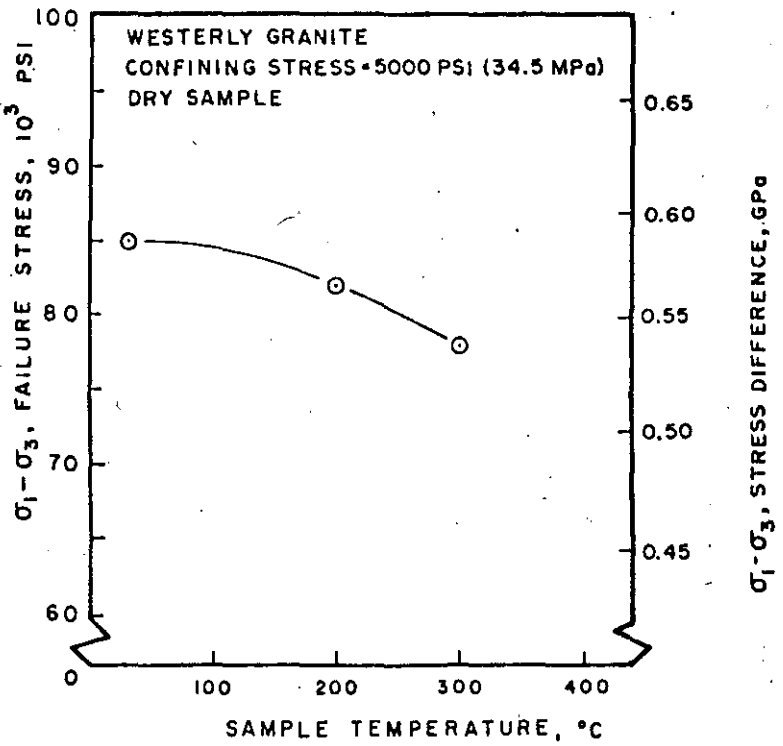

Figure 8. Failure stress as a function of temperature for Westerly granite confined at 34.5 MPa (5000 psi).

Thermal Conductivity

Thermal conductivity can be measured in the simulated temperature-pressure environment by the transient line heat source ("needle-probe") method as used by Woodside and Messmer[9]. A detailed discussion of the theory applicable to this testing is contained in Appendix A.

Basic sample heating and insulation are accomplished in the same manner as previously discussed in the mechanical response testing. A schematic of the thermal conductivity test set-up is contained in Figure 9. A 0.32 cm (0.125 inch) diameter heater approximating the behavior of an ideal line heat source is placed along the longitudinal axis of

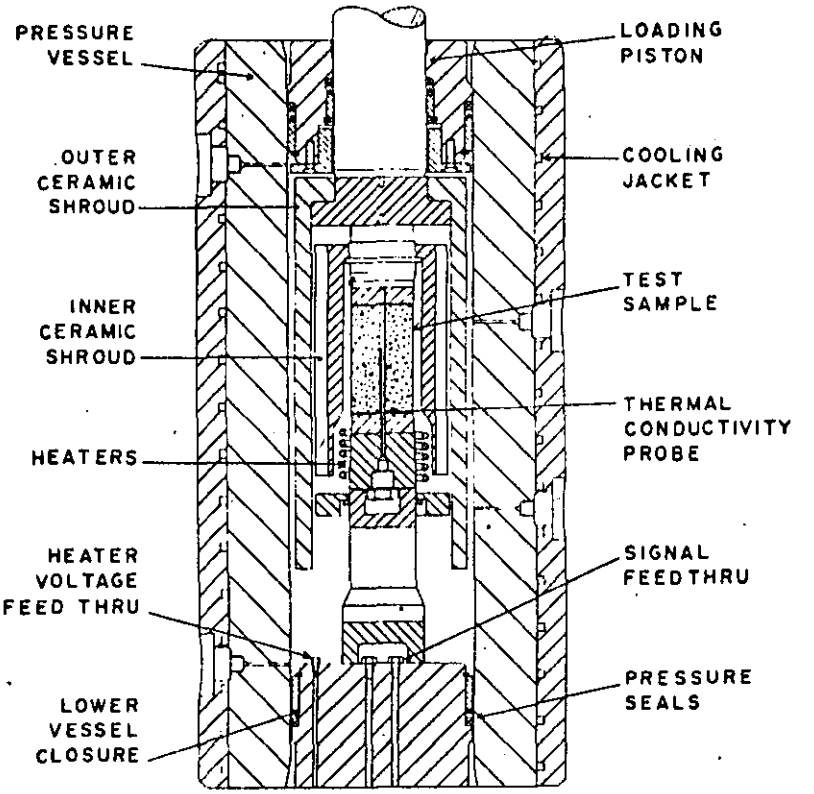

Figure 9. Thermal response test configuration.

a 5.1 cm (2.0 inch) diameter by 10.2 cm (4.0 inch) long test sample. A thermocouple is attached to the heater at the mid-sample location. The entire probe assembly is then "potted" in place with a mixture of ceramic cement and powdered copper to minimize the contact resistance between the probe and the sample. Ceramic insulators are used to minimize heat loss from the ends of the test sample. The overall internal heater length, 13.4 cm (5.25 inches), gives a heater length to heater diameter ratio of 42. Blackwell[10] has shown that a L/D ratio of 30 is minimum for an acceptable approximation of an infinite line source in this type of test.

Power, in the form of carefully monitored voltage and current, is applied to the probe heater (for periods less than one minute) while the test sample exterior is maintained at the desired temperature and pressure. Sample conductivity determines the probe heater temperature rise. The exterior temperature of the sample does not change; a sample of finite dimension can behave (as the theory requires) as though it were infinite in size. Thermal conductivity for the material is calculated from the internal heater temperature history and the power input. Due to the absence of thermal conductivity standards in this range, accuracy definition is uncertain. It is estimated that thermal conductivity values are accurate to within ±5 percent.

Thermal conductivity testing was performed following calibration with fused quartz (K @ 20°C = 1.36 W/m·K) at temperature and pressure. Major emphasis during debugging was placed on developing a standardized probe cementing procedure. Once this was established, consistent results were achieved.

An example of thermal conductivity testing performed on Westerly granite is contained in Figure 10. Comparison is made with published data contained in Clark's Handbook of Physical Constants[11]. The only significant deviation from the published values occur at 200°C. Also contained in this figure are thermal conductivity values for fused quartz. Confining pressure results in increased thermal conductivity as can also be seen from Figure 11. Even for a very low porosity rock the variation of thermal conductivity with pressure is significant.

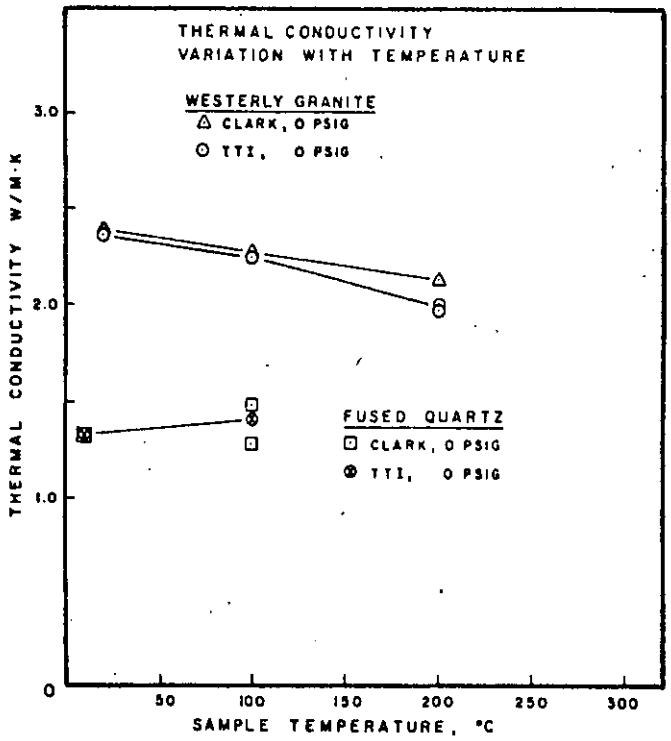

Figure 10. Thermal conductivity variation with temperature.

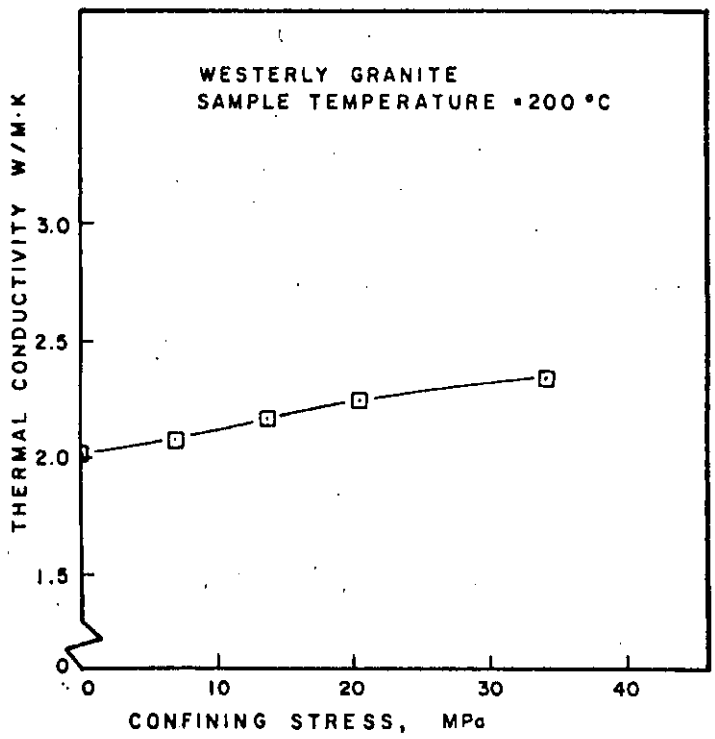

Figure 11. Thermal conductivity variation with confining pressure.

Thermal Diffusivity

Thermal diffusivity is the ratio of the system's ability to conduct heat to the system's ability to store heat. Thermal diffusivity (κ), thermal conductivity (K), density (ρ) and specific heat (c_p) are related by the following:

$$\kappa = \frac{K}{\rho c_p}$$

Thermal diffusivity measurement of core material under simulated *in situ* conditions is important: 1) for geothermal reservoir modeling and 2) as an alternate method of determining thermal conductivity (assuming the density and specific heat are adequately known).

Density can be measured and corrections for overburden pressures and temperature can be obtained from hydrostatic compression tests and thermal expansion tests, respectively. Because specific heat is a mass related phenomenon it can be accurately estimated for rock from mineralogical composition using Kopps Law (Figure 12) which averages the mass weighted specific heats of the individual mineralogical components. Somerton[12] has shown the changes in heat capacity with temperature for rock are similar for rocks of different mineralogical composition (Figure 13). Corrections must be included to account for the influence of pore fluid.

Several methods have been developed to experimentally determine thermal diffusivity of thermal systems[13]. Of these various approaches, the one best suited for determining thermal diffusivity in geologic materials under *in situ* conditions is based upon a classical heat transfer

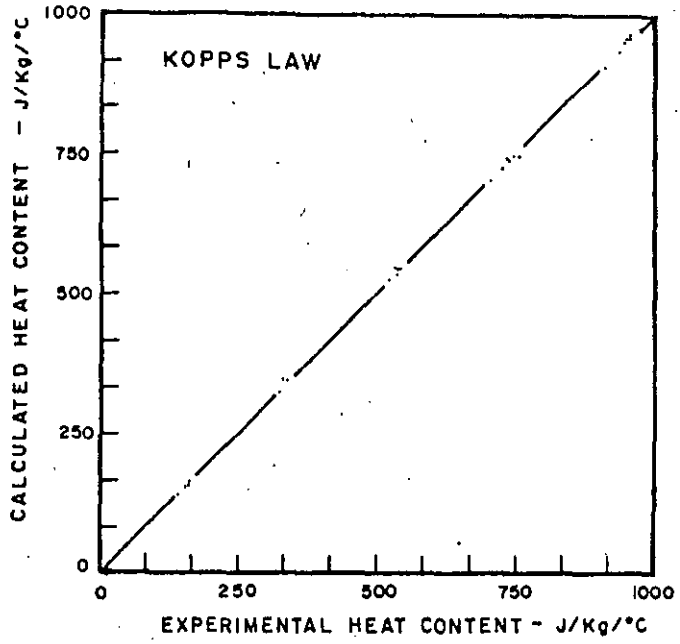

Figure 12. Comparison of calculated and measured heat contents.

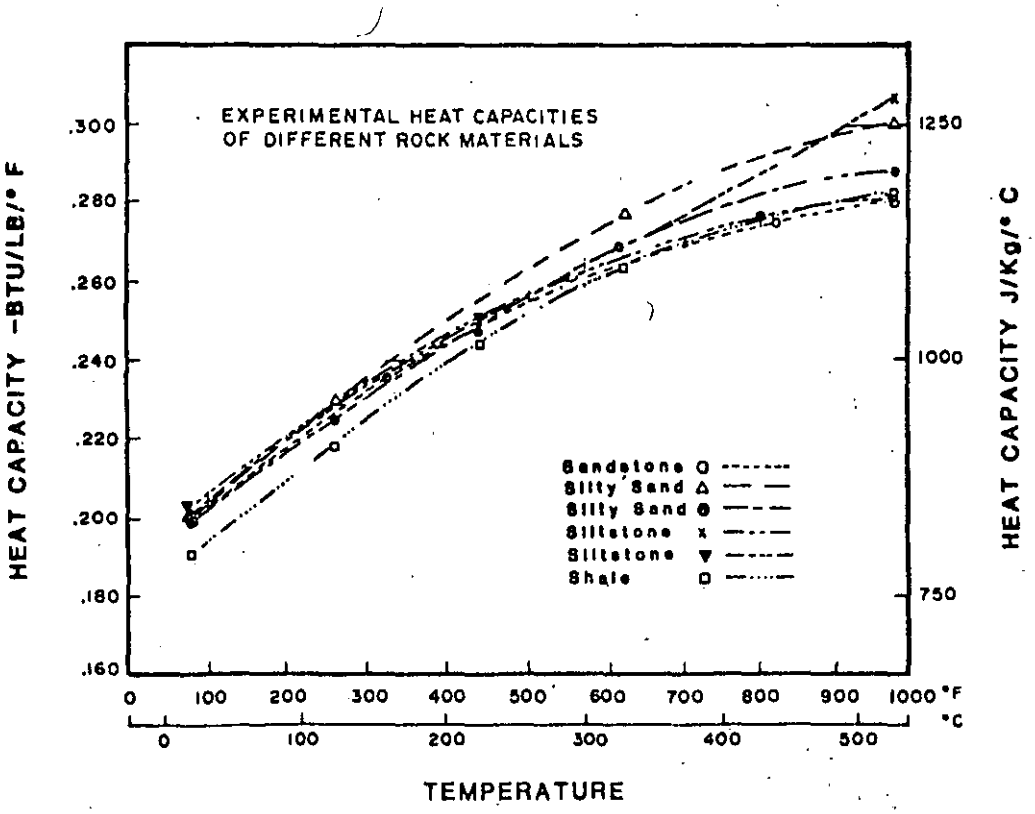

Figure 13. Experimental heat capacities of different rock materials.

model presented by Carslaw and Jaeger[14]. This model requires that a sinusoidal temperature oscillation be induced at the surface of a finite cylindrical sample while the internal temperature is monitored. Under such conditions the center temperature will lag the surface temperature by some time, t_1. This measured time lag, period of oscillation, and sample radius are then used to analytically determine diffusivity. A detailed presentation of the theory is contained in Appendix B.

The testing configuration is very similar to that of the thermal conductivity test set-up (see Figure 9). A thermocouple is plotted along the center axis of the sample cylinder using a potting mixture of ceramic cement and powdered copper. A second thermocouple is placed upon the outer surface of the sample and cemented to the rock surface. The sample is jacketed with material suitable for the anticipated temperature and pressure.

The sample is convectively heated with the temperature oscillation controlled by a programmable temperature controller. The insulating shroud minimizes the quantity of heated fluid and confines it to the region near the sample surface. Because of the simplicity of the measuring devices and the accuracy with which the radius of the sample, period of oscillation and time lag can be determined, diffusivity can be determined to within 5 percent.

Thermal diffusivity changes significantly with temperature, see Figure 14. This is to be expected due to the temperature dependence of both heat capacity and thermal conductivity (and to a much lesser extent, density). Figure 15 shows the comparison of thermal conductivity

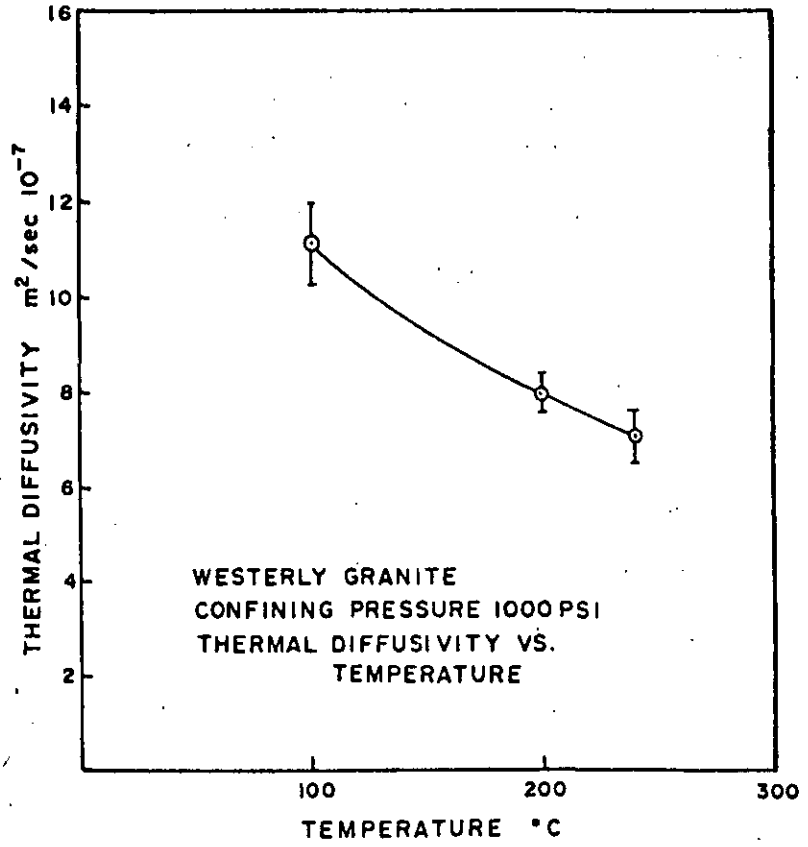

Figure 14. Thermal diffusivity response to temperature of Westerly granite.

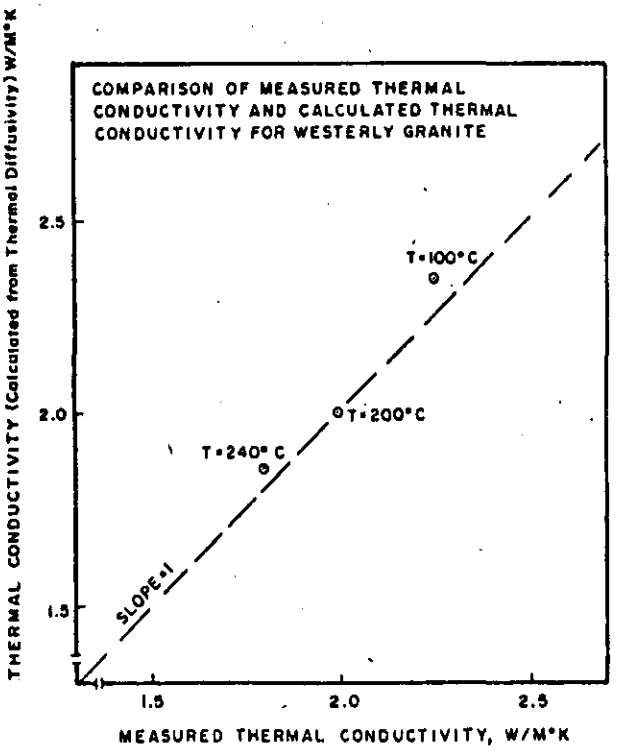

Figure 15. Calculated versus experimental thermal conductivities.

measured directly (needle-probe method) and values calculated from thermal diffusivity measurements with the appropriate density and heat capacity. Estimates are based upon published mineralogical compositions and density values.

Thermal Expansion

Thermal expansion characteristics of geologic materials have not been studied extensively at *in situ* conditions. Studies performed at elevated temperatures have shown the expansion coefficient to have considerable temperature dependence and significant nonrecoverable thermal strain, generally attributed to microcracking. During heating and cooling, fragmentation may occur within a rock sample as a result of anisotropy and thermoelastic property differences between adjacent grains. The magnitude of internal stresses will depend on the distribution and orientation of individual grains. The thermal fragmentation process depends, among other factors, on thermal gradients during heating and the reaction of rock material to induced thermal stresses[15]. Heating rates less than 2°C/min. have been found to cause significantly less fragmentation in small rock samples than higher heating rates[16].

Thermal expansion of geologic materials can be evaluated at *in situ* conditions in the configuration shown in Figure 16. Although the basic components, such as the ceramic shrouding and heater, are the same as previously presented, several unique aspects of this set-up are worth noting. All non-sample stack components exposed to the high temperature environment are fused quartz, with a thermal expansion

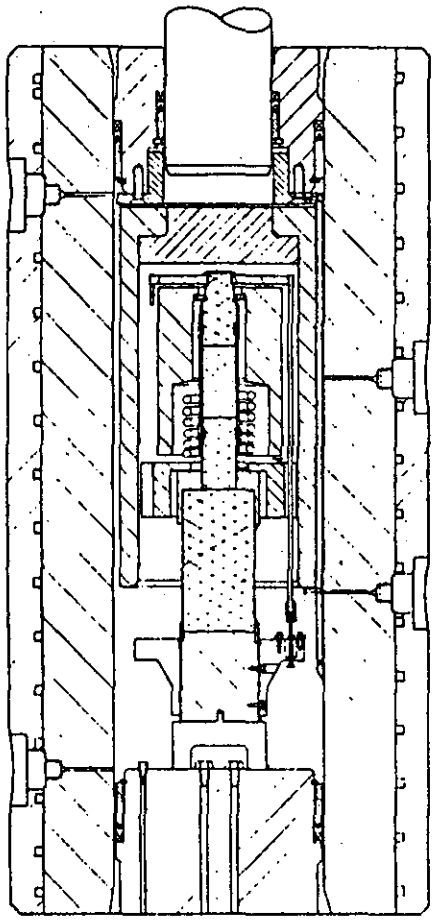

Figure 16. Thermal expansion test configuration.

coefficient of 0.5×10^{-6} cm/cm°C. Fused quartz endcaps and a fused quartz stack spacer support the sample. Quartz rods attached to the top of the test sample suspend the core elements of the LVDT transformers at the base. The expansion of the rods and stack components tend to offset one another except for the expansion of the sample. System expansion consists of the expansion of the fused quartz rods over a distance equal to the sample length. Compared to the anticipated range of rock expansion (~8-10 $\times 10^{-6}$ cm/cm°C), the expansion of the quartz is small.

High resolution LVDT's located near the base of the stack measure the axial strain induced by sample temperature change. Thermal strains of up to $\pm 2.5 \times 10^{-2}$ cm (0.010 inch) can be measured with an accuracy of $\pm 6.2 \times 10^{-5}$ cm (2.5×10^{-5} inch). Averaging the outputs of the two LVDT's removes any false strain due to tilting. Calibration was accomplished with three materials; fused quartz, steel, and aluminum. Using accepted expansion coefficients for these materials, the system expansion was determined as that amount of expansion in excess of published values for the calibration samples. The system expansion is typically 0.5×10^{-6} cm/cm°C, and is repeatable regardless of the sample material.

Sample temperature is monitored by a thermocouple placed at mid-point on the sample, continually in contact with the sample jacket. Sample temperature is increased at a predetermined rate depending on the test material. It is desirable that the sample temperature increase occur uniformly. Rates can be controlled from zero to 5°C/min., with rates of 0.5°C/min. generally being the most desirable. System accuracy can be strongly affected by the heating rate. Heating too rapidly produces increased hysteresis. With heating rates of less than 1°C/min., hysteresis is minimized and overall accuracy of ±5 percent is achieved.

Sample dimensions are; 2.54 cm (1.00 inch) diameter, 5.1 cm (2.00 inches) length, with the ends ground flat and parallel to within 2.5×10^{-3} cm (0.001 inch). Before jacketing, the sample is bonded to

the endcaps, with a minimum sized peripheral ring of adhesive along the interface line. A prestretched silicone jacket is sealed to the fused quartz endcaps by lock wire. Silicone jackets are preferred to copper in this type of testing because of the low Young's modulus of the silicone.

A typical test procedure includes stabilization at room temperature, followed by a programmed heating and cooling cycle. Stabilization at particular temperatures for up to 10 minutes assure uniform temperature distribution and increase the accuracy of strain measurements over a certain temperature range. However, best results over a broad temperature range are achieved by imposing a quasi-static temperature increase upon the sample and surrounding system. Results of such a test with a steel sample is shown in Figure 17. When scaled from the graph, the coefficient of expansion for the steel sample is $12.2 \times 10^{-6}\ °C^{-1}$; this includes system expansion. This compares well with published values for the thermal expansion coefficient of steel, which is approximately $11.6 \times 10^{-6}\ °C^{-1}$. An example of thermal strain versus temperature for a geologic material, welded ash fall tuff, is shown in Figure 18. Note the non-linear thermal strain.

Permeabilities

Permeability measurements at temperature, confining pressure and pore fluid pressure are accomplished in a test set-up similar to those previously described. Although both gas and liquid can be used as flow media, this discussion will focus on the liquid (principally water and brine) flow medium. Figure 19 shows a typical test configuration.

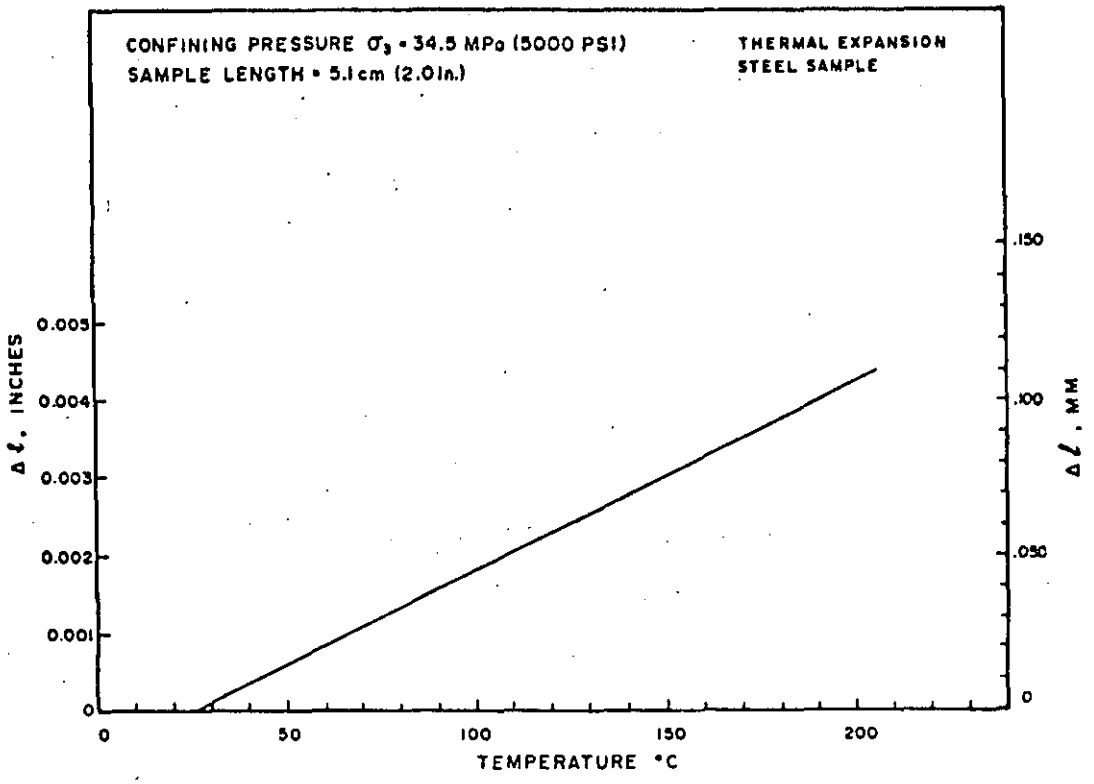

Figure 17. Thermal expansion of steel calibration sample.

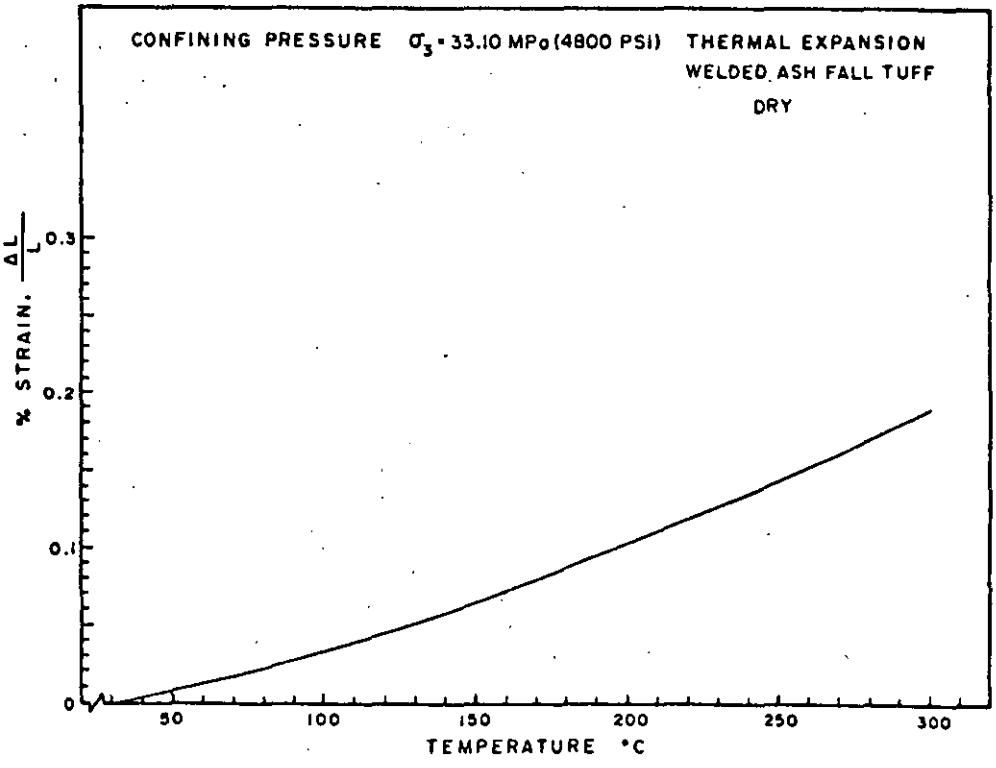

Figure 18. Thermal expansion of a welded ash fall tuff.

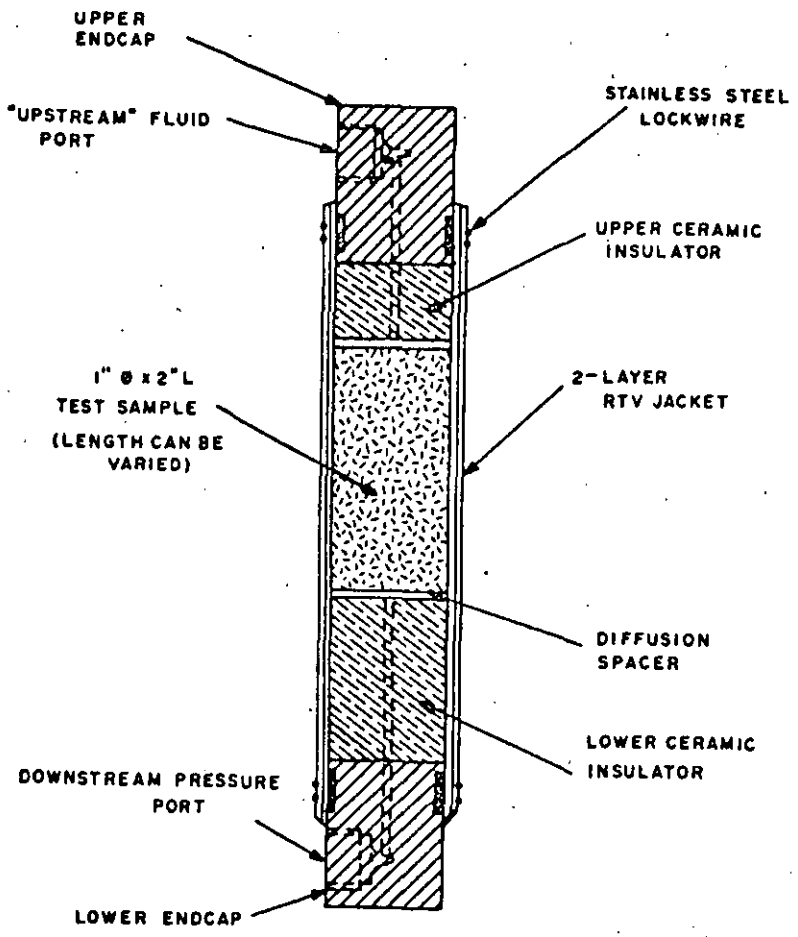

Figure 19. Permeability test sample schematic.

The test sample has two stainless steel diffusion discs placed at each end. These highly permeable, isotropic discs distribute the pore fluid over the sample end faces. Behind each disc is a ceramic insulator and stainless steel endcap. A coating of two component catalized silicone rubber (RTV) is applied to the test sample, adhering to the circumference of the sample and filling any irregularities. Flow is therefore prevented from occurring down the sides of the sample. Sealing is further enhanced by the application of confining pressure. An additional silicone rubber tube is placed over the sample and sealed by lock wire to the endcaps.

Flow lines are attached to the base discs. Inlet flow is introduced at the top of the test sample to allow preheating of the permeating fluid prior to entry into the top endcap. Confining pressure and pore fluid pressure are established and the sample is allowed to stabilize. Stabilization times vary based on porosity and estimated permeability. For the tests, flow across the sample can be controlled by two different means, constant flow rate or constant head pressure.

In the constant flow rate system, Figure 20, a constant displacement pump is used to establish flow. Differential pressure is measured between the upstream and downstream faces of the sample. The flow is several hundred times the total sample pore volume in order to achieve steady-state.

The other steady-state method currently being used is the constant head pressure technique. Schematically the system is shown in Figure 21. Gas pressure, held constant by precision regulators, is used to pressurize one side of a separation accumulator. This in turn pressurizes the fluid at the upstream end of the sample. After flowing through the test sample, the permeating fluid is collected in a downstream separation accumulator maintained at a lower constant pressure. Piston location in each accumulator is monitored electronically and is used to determine flow rate. Differential pressure across the sample is monitored by a transducer and recorded continually. Pressure and flow rate accuracy is better than ±1 percent. Provisions have been made to allow sampling or precision weighing of the circulated fluid.

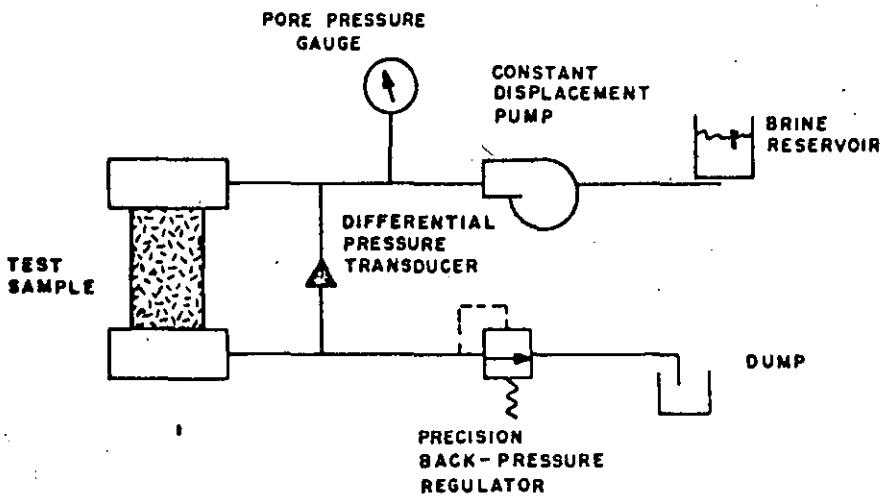

Figure 20. Constant flow permeability schematic.

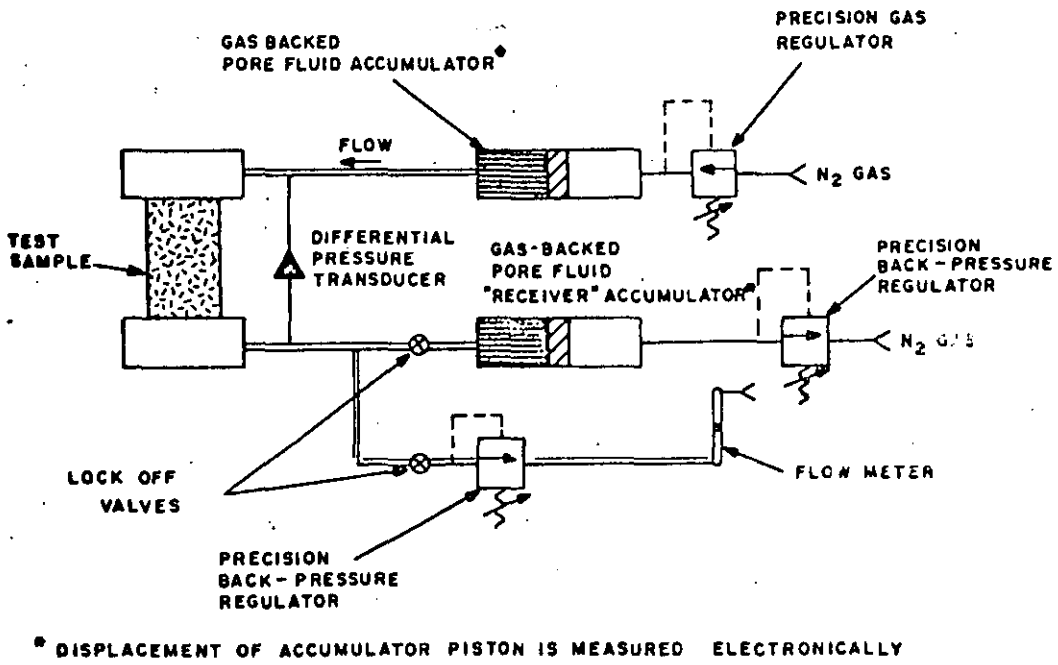

Figure 21. Constant head pressure permeability system schematic.

Permeability is calculated according to the Darcy law:

$$K = \frac{\nu_t}{\nu_r} \frac{Q_r \mu L}{A \Delta P}$$

where:

K = permeability, darcies

ν_t, ν_r = specific volume of fluid at temperature and at reference point, respectively, m^3/kg

Q_r = flow rate at reference point, ml/sec (measured at T = 23°C, constant)

μ = viscosity at flow temperature, c_p (temperature dependent)

L = sample length, cm

A = cross-sectional flow area, cm^2

ΔP = pressure differential, bars (absolute)

The specific volume ratio at the front of this equation constitutes a volumetric correction for fluid volume expansion at the flow temperature since flow rate measurements are made at a reference point with constant 23°C temperature. Pressure differential is maintained constant during the course of the test. All other parameters on the right side of this equation can be physically measured from the sample or determined from published data on the properties of water at temperature and pressure appropriately corrected for salinity[17].

The above techniques allow fluid permeability (brines, water, oils, or light acids) to be determined under simulated *in-situ* conditions for rocks ranging in permeability from 50 μdarcies to 1 darcy.

Special systems allowing permeating fluid preheat are available for high flow-high temperature circulations. Transient techniques can be employed for materials below this permeability range.

Permeability responses for two sandstones are shown in Figures 22 and 23. Test temperatures were limited to 200°C because pore fluid pressure was less than 2.07 MPa (300 psi) and flashing of the water to steam was not desired. In both cases, permeability declined significantly with temperature. This effect is discussed in detail by Casse and Ramey[18] and Danesh, *et. al.*[19] and is generally attributed to water-pore surface interactions.

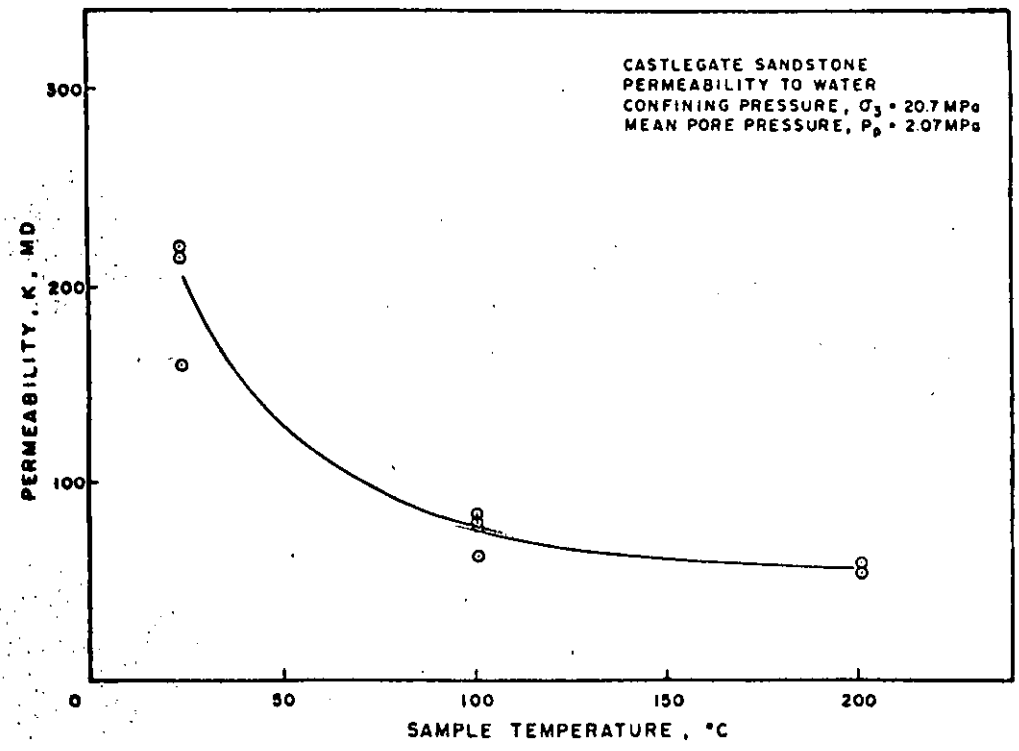

Figure 22. Castlegate sandstone permeability to water.

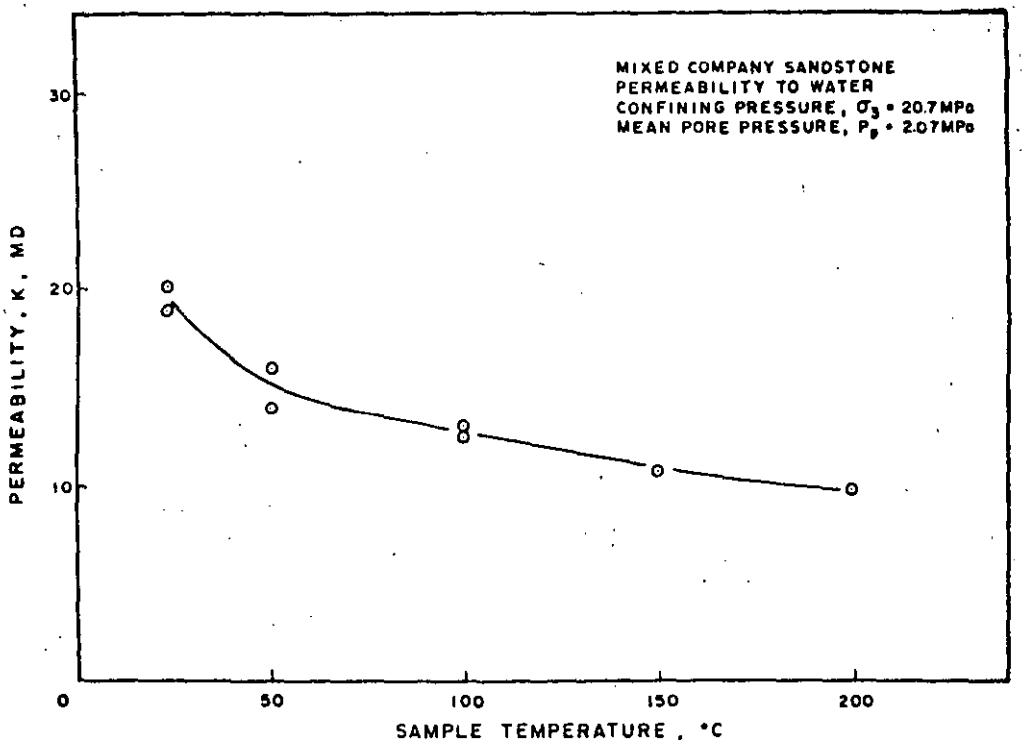

Figure 23. Mixed Company sandstone permeability to water.

Electrical Resistivity

Parameters relevant to the resistivity of geothermal rock are the temperature, pressure, pore fluid pressure, initial saturation, pore fluid chemistry and frequency. This particular area of study is somewhat complex and only a brief discussion will be given here. An expanded presentation is contained in Appendix C.

A detailed schematic of the test sample is shown in Figure 24. A four pole electrode arrangement is used; two current, two potential. A porous, 0.03 cm (0.010 inch) thick diameter ceramic disc is placed at each sample face, followed by a platinum mesh potential electrode. A porous ceramic spacer connects the titanium endcaps to the

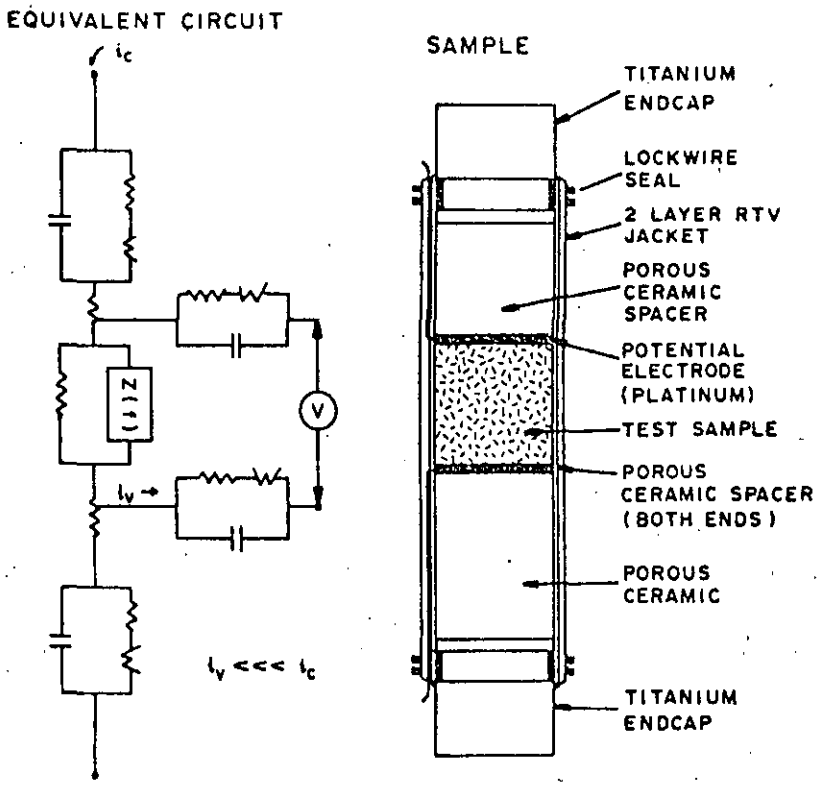

Figure 24. Electrical resistivity sample configuration and equivalent circuit.

sample. The entire assembly is then coated with high temperature silicone rubber for isolation from the confining medium. Samples of porous material are saturated for approximately 24 hours under vacuum with jacket material in place to prevent leakage paths due to jacketing wrinkles. Since the response of the test sample is electrically complex, impedance and phase angle measurements are made to determine the electrical response. Measurements are made using a Hewlett-Packard model 4274A Multi-Frequency LCR meter at approximately 2 volt alternating current (to prevent electrode polarization) and at frequencies ranging from 100 Hz to 10 Khz. The potential electrodes are isolated by

approximately 10^{12} ohms impedance improving the instrument's accuracy at high impedance values (10 KΩ and up). A schematic for the instrument and sample arrangement is shown in Figure 25.

Data obtained during the debugging of this test set-up is contained in Figure 26. As expected, the resistivity of the sandstone material declines with temperature, an effect that is primarily due to the increasing charge mobility caused by decreasing pore fluid viscosity. Pressure and temperature effects on the pore fluid also contribute to this effect*. In a material of this type, electrolyte effects tend to dominate, especially with heavy concentrations of ions.

Present capabilities allow measurement of electrical resistivity to 300°C and 207 MPa (30,000 psi) confining pressure. Accuracy of resistivity measurements are ±2.5 percent.

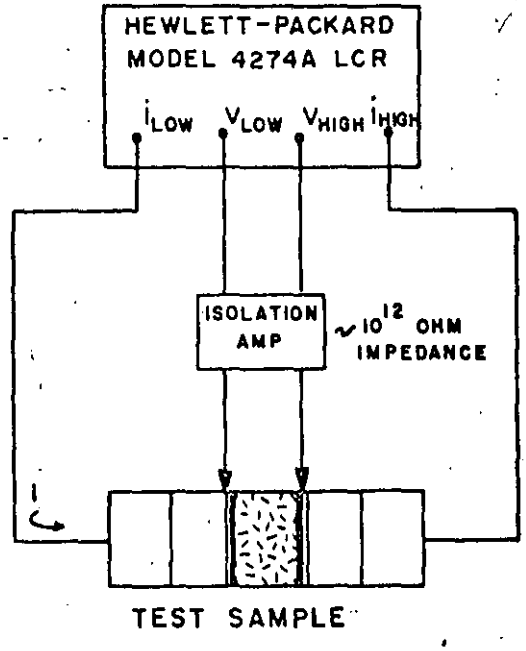

Figure 25. Electrical resistivity circuit configuration.

* See appendix for more complete discussion.

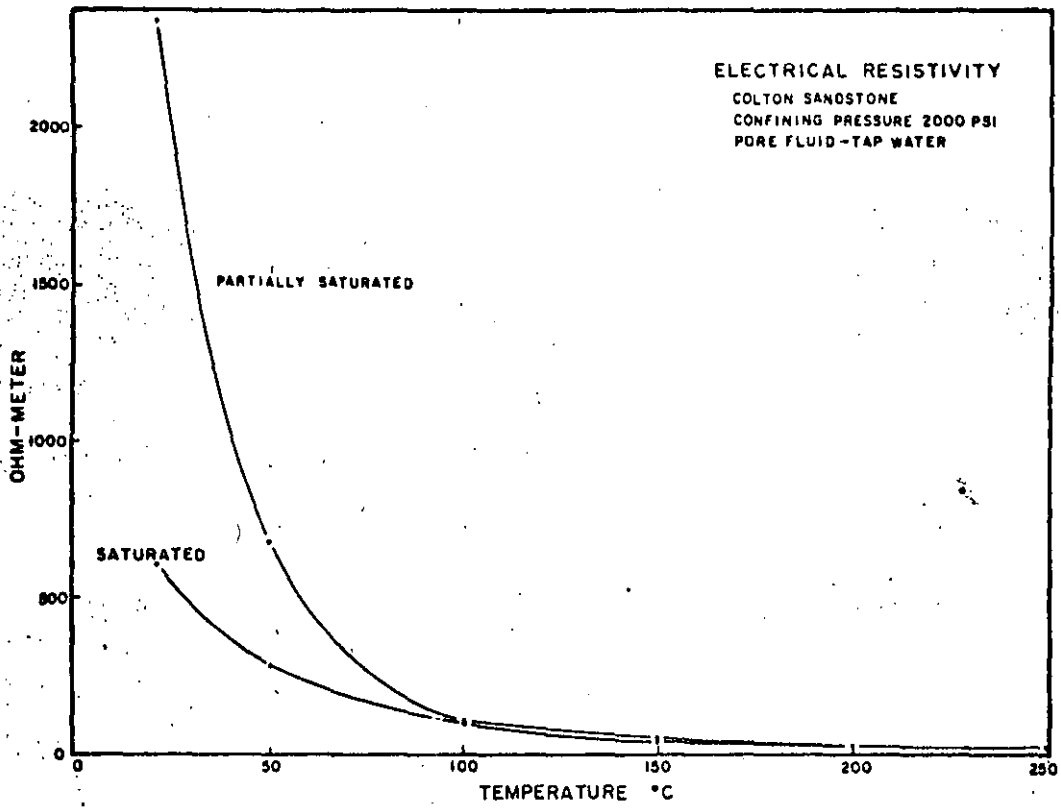

Figure 26. Electrical resistivity of partially and fully saturated Colton sandstone at temperature.

Ultrasonic Velocity Measurements

The longitudinal (p-wave) and shear (s-wave) velocities can be measured at elevated temperature, confining pressure and pore fluid pressure. These data, together with the bulk density of the material, are used to calculate dynamic elastic moduli.

The velocities are obtained using a "through transmission system" adapted from a technique introduced by Mattaboni[20]. The equipment configuration is shown in Figure 27. This method of measuring velocities in solids has been employed for some time at Terra Tek[21,22], and is not part of the development in this program.

Figure 28 shows the sample configuration that is presently being used. A ferroelectric ceramic material (lead titanate zerconate, PZT5)

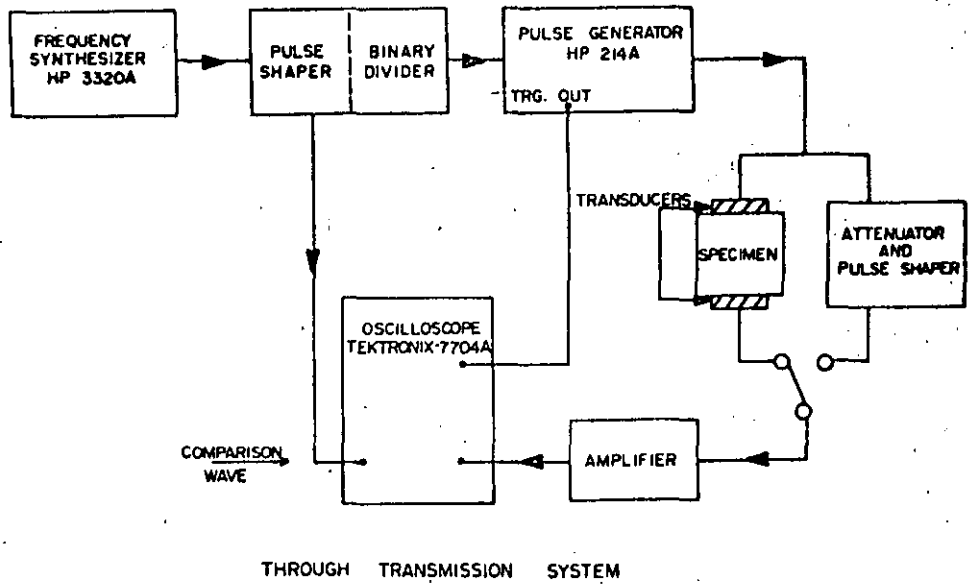

Figure 27. Ultrasonic measurement system schematic.

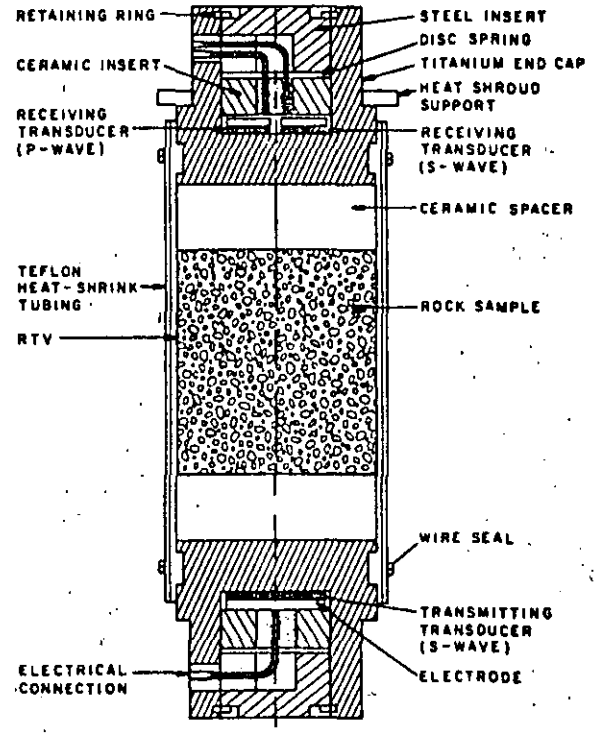

Figure 28. Ultrasonic velocity sample configuration.

was selected for use as the transducer elements. The desirable features of this material is its high Curie point (360°C) and piezoelectric coupling coefficient[23*]. A single transducer, cut to produce a shear wave is used as the emitter. It has been found from experience that this transducer produces sufficient p-wave energy to allow both shear and longitudinal velocity measurements if separate receivers are used to detect the respective signals. The electrical leads are ceramic insulated and all connections are either brazed or mechanically made with a positive contact force.

The temperature effect on the endcaps and ceramic spacers are determined by conducting a test without a sample. To date, successful measurements have been made to 250°C. No problems are foreseen in extending to 300°C in the near future.

Figure 29 shows the velocity data obtained on an aluminum reference sample and Westerly granite. The least squares fit of the aluminum data is well within 1 percent agreement with published data[24] as indicated in Table 2. The velocity data for aluminum and Westerly granite were obtained with the hydrostatic confining pressure held constant at 13.8 MPa (2000 psi) for all measurements. The slope of the least squares fit of the granite data is -4.65×10^{-3} per °C for the p-wave and -2.46×10^{-3} per °C for the s-wave. The RMS error is 3.75×10^{-2} (km/sec) for the p-wave and 1.88×10^{-2} (km/sec) for the s-wave. The measured velocities, calculated Young's moduli and Poisson's ratios are tabulated in Table 3.

---

* Approximately a factor of seven (7) larger than that of standard quartz transducers.

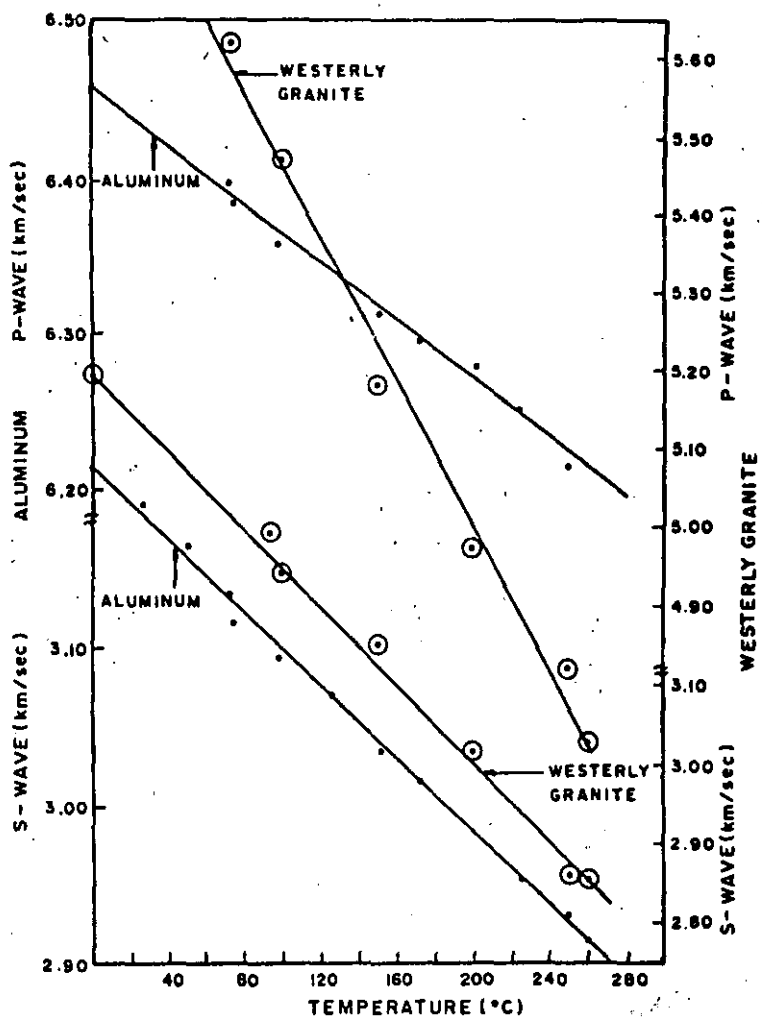

Figure 29. Ultrasonic velocity response of Westerly granite and aluminum.

TABLE 2

Comparison of Terra Tek and Published Data on 6061-T6 Aluminum

	ASAY[17]	TTI
Density (g/cc)	2.704	2.702
Longitudinal velocity (km/sec)	$6.428 - 9.1 \times 10^{-4}T^*$	$6.459 - 9.4 \times 10^{-4}T^*$
Shear velocity (km/sec)	$3.188 - 8.6 \times 10^{-4}T$	$3.217 - 1.16 \times 10^{-3}T$
Poisson's ratio	$0.336 + 1.1 \times 10^{-4}T$	$0.337 + 0.82 \times 10^{-4}T$
Young's modulus	$7.35 \times 10^4 - 41.6T$	$7.38 \times 10^4 - 43.49T$

*T = Temperature in ^{o}C

TABLE 3

Ultrasonic Velocities and Elastic Moduli as a Function of Temperature with the Confining Pressure at 13.8 MPa

Material	Density (gm/cc)	Sample Length (mm)	Temp. (^{o}C)	Velocities		Young's Modulus (GPa)	Poisson's Ratio
				P-Wave (km/sec)	S-Wave (km/sec)		
Al (6061-T6)	2.702	50.80	76	6.384	3.115	70.46	0.3438
Al (6061-T6)	2.702	50.80	99	6.358	3.094	69.57	0.3449
Al (6061-T6)	2.702	50.80	152	6.313	3.035	67.18	0.3497
Al (6061-T6)	2.702	50.80	173	6.295	3.021	66.00	0.3504
Al (6061-T6)	2.702	50.80	202	6.278	2.983	65.12	0.3542
Al (6061-T6)	2.702	50.80	225	6.252	2.954	63.96	0.3563
Al (6061-T6)	2.702	50.80	250	6.216	2.930	62.96	0.3572
Granite	2.631	48.97	75	5.624	3.297	70.82	0.2382
Granite	2.631	48.97	101	5.478	3.245	68.14	0.2297
Granite	2.631	48.97	151	5.184	3.154	63.14	0.2061
Granite	2.631	48.97	200	4.978	3.020	58.01	0.2088
Granite	2.631	48.97	250	4.822	2.860	52.88	0.2287

SUMMARY 40

The following geothermal material properties can be evaluated at simulated *in situ* conditions:

- Mechanical response
- Thermal conductivity
- Thermal diffusivity
- Thermal expansion
- Permeability
- Electrical resistivity
- Ultrasonic velocity

Major developments are now complete in each of these areas allowing basic testing capability in each. Sample configurations and testing procedures have been defined and verified through both "debugging" and actual testing experience.

Following is a general discussion of the data obtained in each testing area with references where appropriate to similar work in the literature. The data contained in the text of this report is representative of the data generated during testing development. Proprietary data is not included.

Mechanical Response

Data obtained on various materials have shown ultimate failure stress and failure mode (ductile or brittle) to be strongly pressure dependent. The nature of the pore fluid medium (liquid, gas, or two-phase

fluid) and its pressure state can also have considerable influence on the elastic modulus of the material. Temperature demonstrates a significant effect upon ultimate failure strength and may play an important role in determining the material compaction characteristics[25].

Thermal Conductivity

Thermal conductivities generally decline with increasing temperature in the granite and sandstone materials tested. This is consistent with published data[26]. The application of confining pressure can alter this decline and in some cases reverse it. Materials in which fractures and micro-cracks control the porosity seem more susceptible to the influence of pressure. The nature of the pore fluid can also significantly affect the thermal conductivity with water saturated rocks being more thermally conductive than dry or partially saturated rock[27].

Thermal Diffusivity

Thermal diffusivity of geologic materials tested decrease with increasing temperature. This effect is interrelated to the dependence of diffusivity upon thermal conductivity and specific heat. Specific heat has been shown to be strongly temperature dependent[12] and therefore has a significant influence on thermal diffusivity. Thermal conductivity is also temperature dependent and the two parameters act in such a way (see text for complete discussion) as to cause a decreasing thermal diffusivity with temperature.

Thermal Expansion

Data obtained under *in situ* pressure and temperature states have indicated considerable variation in expansion coefficients over the temperature ranges 23°C to 300°C. Due to the nature of rock (brittle, polycrystalline, heterogeneous and anisotropic mineral aggregates), microcracking can occur during temperature cycling as a result of dissimilar expansion and contraction[15].

Permeability

In general, permeabilities in porous materials (e.g. sandstone) demonstrate significant declines with increasing temperature. This phenomenon is believed to be due to rock-water interaction at the higher temperatures. Clay swelling and adsorption characteristics are believed to play a big role. Some very low permeability materials (granites in particular) have shown a somewhat different trend. Data obtained on a few such materials demonstrated permeabilities that increase with temperature[28,29,30].

Electrical Resistivity

Data generated in this test system have demonstrated trends and phenomenon that agree with published values. High porosity materials such as sandstones show dramatic resistivity decreases with temperature, an effect that is primarily due to increasing mobility caused by decreasing pore fluid viscosity[31,32].

Ultrasonic Velocity

To date successful testing has been conducted to 250°C and it is anticipated that testing capability can be extended to 300°C+ in the

near future. In general, velocities in very competent crystalline materials, such as granite, tend to decline with increasing temperature. Different tendencies have been observed in recent testing on saturated porous materials at elevated temperatures[33].

ACKNOWLEDGMENTS

The authors would like to express their appreciation for the guidance of the Department of Energy/Division of Geothermal Energy personnel -- Dr. Clay Nichols and Mr. Roy Mink (Idaho Falls Office) and Mr. C. B. McFarland, Jr. (Washington, D.C.).

Dr. Arfon Jones and Mr. Sidney Green provided considerable technical guidance and Mr. Charles Muller conducted the laboratory tests. Ms. J. Grant, Ms. Conchita Chan and Ms. Janie Ruff were responsible for manuscript preparation.

SECTION C-2

This section was originally Terra Tek report TR 75-13

"Methods for Determination of Physical Properties"

by

R. K. Dropek
S. W. Butters
A. H. Jones

ABSTRACT

Physical properties testing techniques have been evaluated, and, in particular, the applicability of these techniques to the determination of Nevada Test Site tuff properties. The physical properties include the as received bulk density, dry bulk density, grain density, effective and total porosity, permeability and microscopic analysis (grain size, grain spatial orientation and mineral content) for rocks. Multiple testing techniques are described with the use of the Ruska Mercury Porometer and Beckman Gas Pycnometer emphasized throughout the text. The Ruska Mercury Porometer is shown to increase bulk volume measuring accuracy. The Beckman Gas Pycnometer reduces test time for obtaining grain density values while improving accuracy. Water immersion methods are presently being used for grain densities where gas reactions with zeolitic materials may occur.

LIST OF ILLUSTRATIONS

LIST OF TABLES

INTRODUCTION

Physical properties data are a valuable aid in predicting and understanding the variations in the mechanical response of materials. In particular, the Nevada Test Site has used physical property data in estimating the stemming and containment potential of a site for nuclear testing. It is essential to accurately determine the densities for containment evaluation applications[38]. For instance, bulk and grain density accuracies of 0.001 gm/cm^3 when combined produce deviations in the calculated air void content* in excess of ±0.2% (not ±0.2% error but ±0.2% air voids). Thus new and presently used physical property techniques were calibrated and compared to evaluate accuracy. The new methods primarily involve improved volume determination.

Material volumes are usually determined by either direct measurement (calipers) or fluid displacement (immersion). Due to surface irregularities volume determination using direct caliper measurement usually results in high volumes, therefore low densities. Immersion techniques produce more accurate volume measurements on materials since they account for irregular surfaces. To improve volume determination accuracy, immersion techniques have been investigated. One method involves bulk volume determination using mercury or water while the other method determines grain volumes using helium.

A general understanding of rock structure and fabric is also helpful. Permeability, porosity and microstructure studies are used to determine structure and fabric. Effective porosity measures the volume of connected pores as opposed to the total porosity which measures the total pore volume.

---

*Equation 4, Table C-2-1

Microstructure analysis gives grain size distribution, orientation and mineral content analysis as well as pore size.

This report provides the testing techniques and present accuracy capabilities at Terra Tek for physical properties measurement. The physical properties test include as-received density*, dry bulk density, grain density, water content, effective and total porosity and gas or liquid permeability. Multiple test methods are given for most of the properties. Table C-2-1 lists the symbols and interrelations between the physical properties.

TABLE C-2-1

Physical Property Symbols and Equations

Symbols

K = permeability in darcy's

n_e = effective porosity in percent

n_t = total porosity in percent

ρ_w (gm/cm^3) = in situ bulk density (wet or "as-received" density)

ρ_d (gm/cm^3) = dry bulk density after oven drying

ρ_g (gm/cm^3) = grain density (density of solids)

S_r = degree of saturation in percent

V_{av} = air void content in percent

w = moisture content in percent of wet weight

Equations

$$w = 100 \times \frac{(\rho_w - \rho_d)}{\rho_w} \qquad (1)$$

$$n_t = 100 \times \left(1 - \frac{\rho_d}{\rho_g}\right) \qquad (2)$$

$$Sr = 100 \times \frac{(w \times \rho_w)}{n_t} \qquad (3)$$

$$V_{av} = 100 \times [1 + \rho_d (1 - 1/\rho_g) - \rho_w] \qquad (4)$$

*Wet and as-received density are used interchangeably in the text; wet does not infer that the material is fully saturated.

SUMMARY

Table C-2-2 summarizes the testing techniques and accuracies for the physical property methods. Accuracy was obtained from calibration tests. Error may be calculated using average Nevada Test Site tuff values (ρ_g = 2.40 gm/cm^3, ρ_w = 1.8 gm/cm^3, ρ_d = 1.45 gm/cm^3, and w = 19%).

Moisture content: The moisture content is determined by weighing a sample before and after oven drying with a resulting accuracy of 0.13% H_2O due to loss of water during crushing.

Bulk density: Dry or "as-received" bulk densities may be found from the volumes determined using 1) calipers, 2) the Ruska Mercury Porometer or 3) the water immersion method. If a precision machined sample is not available for caliper measurement, then for samples 30 cm^3 or larger the Ruska Mercury Porometer should be used, whereas the water immersion method is better for volumes less than 30 cm^3.

Grain density: The National Bureau of Standards powdered silicon (SRM 640) and the crystalline quartz tests indicate that the Beckman Gas Pycnometer technique is more accurate and precise than the water immersion method (0.001 gm/cm^3 as compared to 0.010 gm/cm^3 respectively). Materials containing zeolites may lead to volume drift in the gas pycnometer unless the sample is allowed to equilibrate with atmospheric moisture prior to testing.

Total porosity: The total porosity is calulated from the grain and dry bulk density values and consequently depends upon the techniques used in those determinations. Using the most accurate techniques the total porosity accuracy is within -0.35 percent n_t to 0.07 percent n_t.

Effective porosity: Effective porosity is determined using water immersion, mercury injection (Ruska Mercury Porometer) and gas pressurization

TABLE C-2-2

Accuracy and Error of Physical Property Methods

PHYSICAL PROPERTY	HOW DETERMINED	ACCURACY*	STRUCTURAL INTEGRITY ROCK NECESSARY FOR MEASUREMENT
Moisture Content (w)	Weight determined using electronic balance	0.13% w	poor to good
Wet Bulk Density (ρ_w)	Volume measured using 1) Calipers 2) Ruska Mercury Porometer 3) Water Immersion	1) -.014 to -.028 gm/cc 2) .001 gm/cc ±.002 gm/cc 3) -.002 gm/cc ±.004 gm/cc	1) fair to good 2) fair to good 3) poor to good
Dry Bulk Density† (ρ_d)	1) Calc. using w and ρ_w 2) Calipers 3) Ruska Mercury Porometer 4) Water Immersion	1) .004 gm/cc ± .002 gm/cc 2) -.017 to -.031 gm/cc 3) .004 gm/cc ±.002 gm/cc 4) .001 gm/cc ±.004 gm/cc	1) refer to w & ρ_w 2) fair to good 3) fair to good 4) poor to good
Grain Density (ρ_g)	Volume measured using 1) Water Immersion 2) Gas Pycnometer	1) .01 gm/cc ± .04 gm/cc 2) .001 gm/cc ± .005 gm/cc	1) poor to good 2) poor to good
Total Porosity** (n_t)	Calculated from ρ_g and ρ_d	-0.14%n_t ± .21%n_t	fair to good
Effective Porosity (n_e)	1) Ruska Mercury Porometer 2) Water Immersion 3) Gas Pycnometer	0.53% n_e	1) fair to good 2) poor to good 3) poor to good
Permeability (K)	Permeability equipment	Repeatable to within 20%	poor to good
Air Voids** (Av)	Calculated from ρ_g, ρ_d, ρ_w	.16% Av ± .44% Av	refer to densities
Saturation** (Sr)	Calculated from w, n_t & ρ_w	0.26% Sr ± .56% Sr	refer to e, n_t, ρ_w
Microscopic Analysis (Grain size, orientation and mineral content)	1) Large grain method using Bausch and Lomb Monocular 2) Medium grain method using Zeiss 3) Medium grain method using universal stage 4) Small grain method using scanning electron microscope	For all microscopic methods accuracy is dependent upon magnification level and smallest grain size.	1) poor to good 2) fair to good 3) fair to good 4) poor to good

* Errors may be calculated using average NTS tuff values (ρ_g = 2.40 gm/cm^3, ρ_w = 2.80 gm/cm^3, ρ_d = 1.45 gm/cm^3, and w = 19%)

** Accuracy calculated from Ruska Porometer and Beckman Pycnometer values.

† Dry bulk density accuracy includes moisture content error.

(Beckman Gas Pycnometer). The Ruska Mercury Porometer requires knowledge of the mean sample pore size for complete effective volume determination. While the gas pycnometer can determine effective pore volume, it cannot easily measure bulk volumes thus requiring another method to determine sample bulk volumes. Only the water immersion method is self-contained in that both bulk volume and effective pore volume may be determined using the same piece of equipment. No effective porosity standard exists, but method comparison showed the effective porosity to be repeatable to within 0.53 percent n_e.

Percent saturation and percent air voids: Enumeration of these properties is subject to accumulated error from density, porosity and percent moisture determinations. The accumulated accuracies for each property are shown in Table C-2-2. The percent saturation and percent air void accuracies are computed using the most accurate techniques for density, porosity and percent water.

Permeability: Permeability may be determined by either a transient or a steady-state method. No generally accepted permeability standards are available, but comparisons and variations in method suggest the values are repeatable to within 20%.

Microscopic analysis: Microscopic analysis consists of grain size, spatial orientation and mineral content determination. Four methods are available, each of which has its advantages. Mineral content analysis is not possible using the scanning electron microscope (Method IV). However, it provides means of testing low cohesion rock fabrics as does the "large grain method" (Method I). The "medium grain techniques" (Methods II and III) require fair to good cohesive rock fabrics because of thin-sectioning and handling. As stated in Table C-2-2, the determining factors deciding which method to use are the grain size and the structural integrity of the rock.

EQUIPMENT

Much of the equipment that is used is standard for all physical properties testing. Both the standard and specially developed equipment is described here according to the function performed.

Balances

The three balances used for measuring weight are the Mettler H 33 balance, Mettler Gram-Atic balance, and the Sartorius type 225-4So-400 balance. Both of the Mettler balances have an accuracy of $\pm 5 \times 10^{-5}$ gms and a maximum capacity of 160 gms, while the Sartorius is accurate to $\pm 5 \times 10^{-3}$ gms and has a 1.0 Kg capacity. The Mettler Gram-Atic Balance is used primarily for water immersion bulk density tests.

Oven

Oven drying is used to remove moisture. Samples are dried in a Blue M oven. The oven has a 300°C capacity but for physical properties testing purposes a setting of 105°C (ASTM standard) is maintained. The oven operates under forced air convection, thus promoting maximum drying. A Pyrex brand desiccator with calcium chloride drying agent is used to hold oven dried samples during cooling.

Ruska Mercury Porometer

The Ruska Mercury Porometer is used to measure volumes by mercury displacement. The porometer and its components are shown in Figures C-2-1 and C-2-2. It consists of a hand operated pump connected to a pycnometer, 2 1/4" x 3" in diameter, with an internal volume of 260 cm^3. A manometer, two pressure gauges and a volume pump are connected in series with the pycnometer. The manometer and volume pump are used for volume

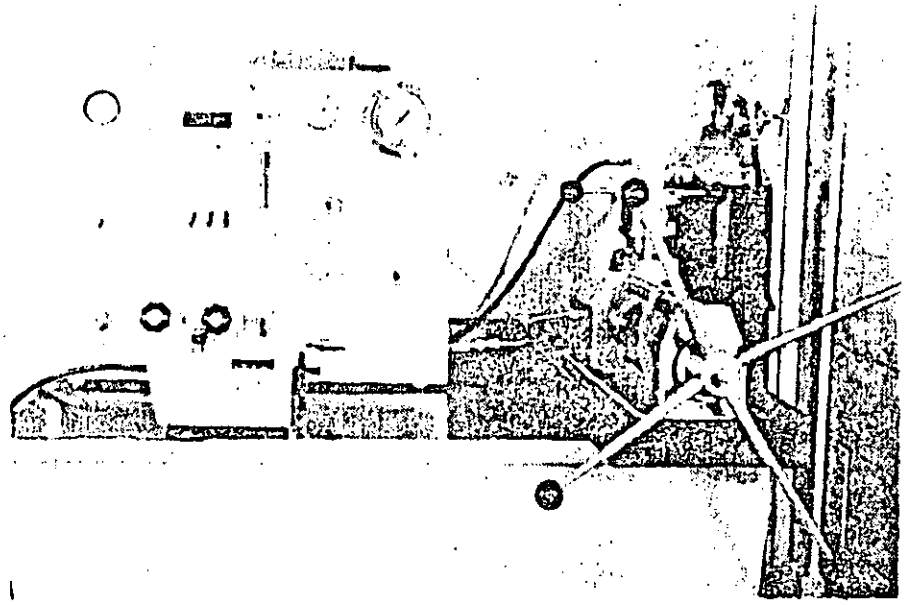

Figure C-2-1. Control panel with the Ruska Mercury Porometer (right) and the Beckman Gas Pycnometer (foreground).

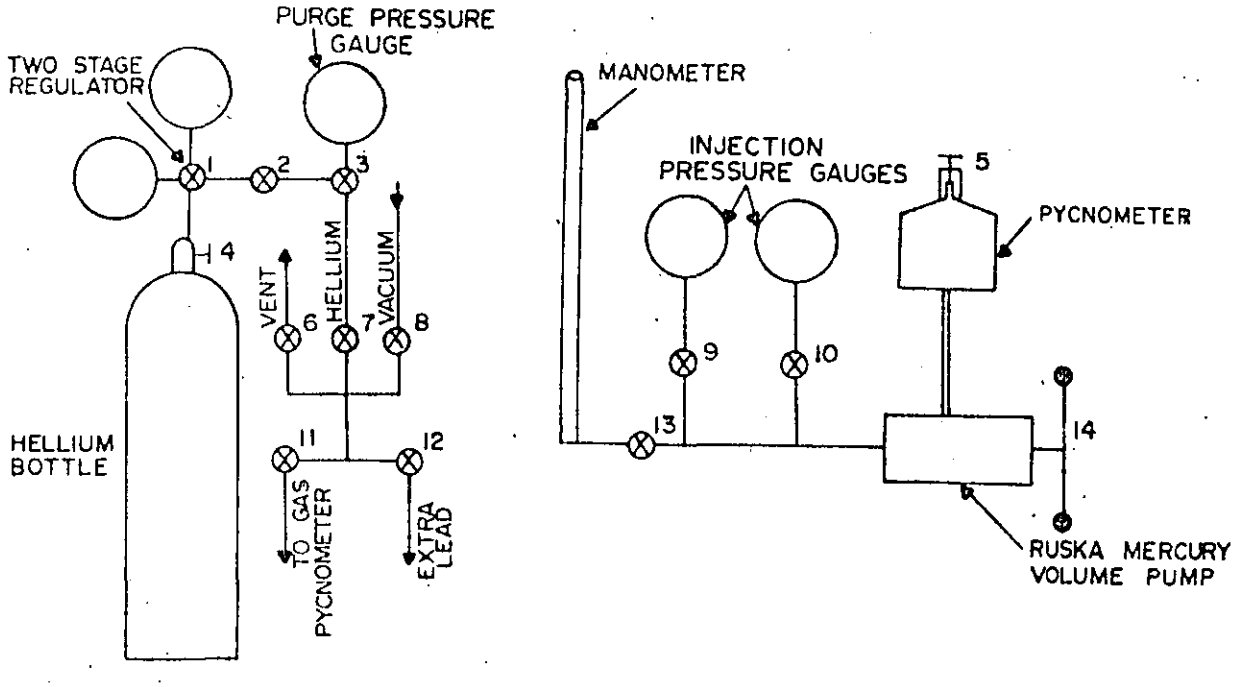

(a) Beckman Gas Pycnometer

(b) Ruska Mercury Porometer

Figure C-2-2. Control panel schematic.

determination while the pressure gauges are used for determining the injection pressures during effective porosity testing.

Beckman Gas Pycnometer

The Beckman 930 Air Comparison Pycnometer is used for determining grain volumes. This is a gas immersion technique (helium is used for the present application). Figure C-2-3 is a schematic of the pycnometer. The cup volume is 50 cm^3.

Permeability Equipment

Permeability is measured with Terra Tek designed equipment at atmospheric or confined pressure. This equipment uses either gas or liquid as a permeating fluid and is capable of performing the tests via either a transient method or a steady-state method. The transient method test can be run with a pore pressure regulated from 0 to 60 ksi. A differential pressure across the specimen can be regulated from 0 to 1 ksi, which is only limited by the range of the differential pressure transducer in present use. Steady-state tests can be performed also from 0 to 60 ksi pore pressure. Figure C-2-4 shows a schematic of the vessel configuration for permeability tests.

Microscopic Methods

Depending on the technique employed, there are three microscopes which may be used. The Bausch and Lomb model 31-33-61 monocular (0.7 to 3.0 x's magnification) is used for large grain size distribution tests. For medium grain size samples the Zeiss model RP-48 standard scope with binocular vision and photo attachment is used. For three dimensional studies, a universal stage is employed in conjunction with the Zeiss microscope. With the stage

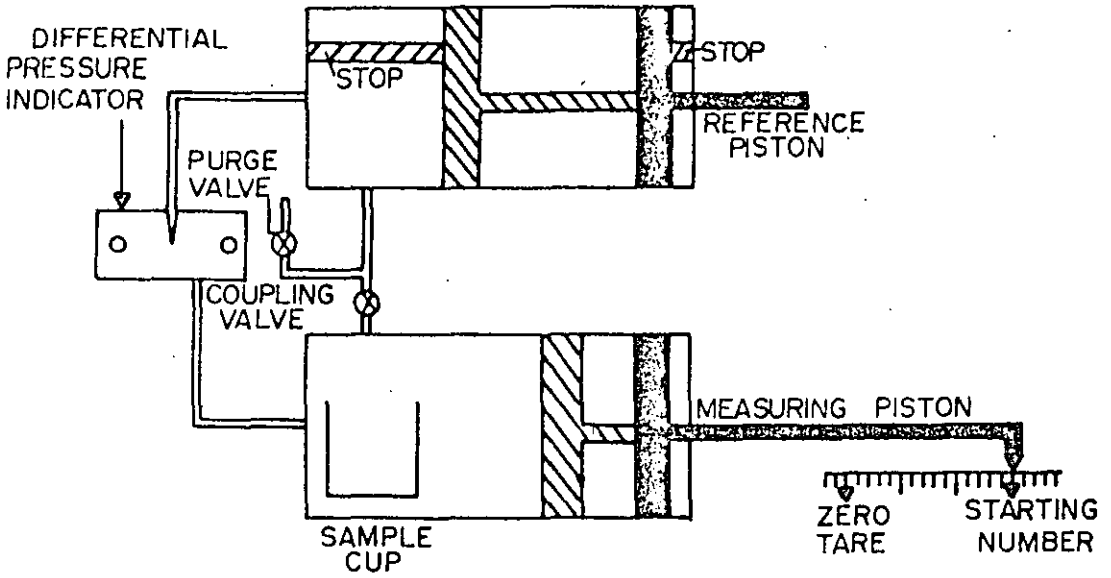

Figure C-2-3. Simplified Beckman Pycnometer Schematic.

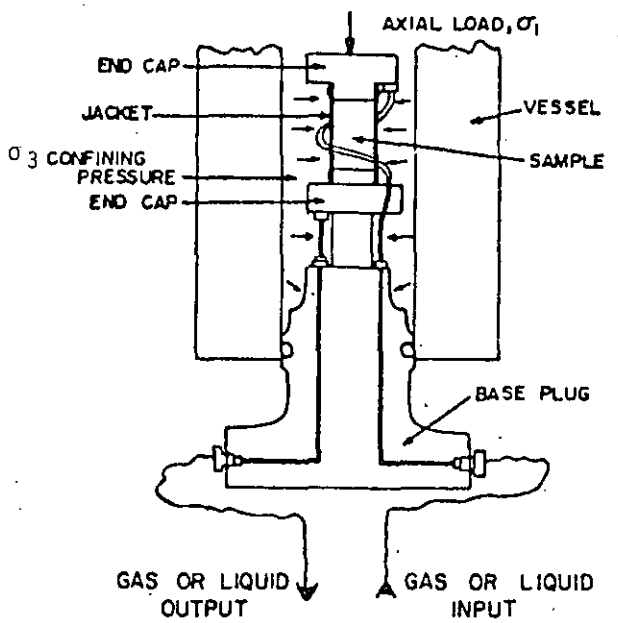

Figure C-2-4. Vessel Configuration for Permeability Tests.

preferred orientation of grains can be determined. Magnification of the Zeiss microscope ranges from 2.5 to 100 x's. For very fine grain samples the Scanning Electron Microscope (SEM) at the University of Utah Material Science Department is available.

This section discusses the measuring techniques and their relative accuracies using calibrated specimens. A brief explanation of the statistical methods and procedures used in this section may be found in Appendix A.[39] A 5 percent level of significance (α) was used in all statistical analysis except during effective porosity data comparison for which a 1 percent level of significance was used. Detailed machine operation, calculation procedures and data sheets are available upon request. REF 13.

Percent Moisture Content

The percent moisture content is expressed as the percentage by weight of the wet sample. To determine the moisture content a prepared sample is weighed immediately after removal from its hermetic container. The sample is then oven dried at 105°C for 24 hours, after which time it is removed from the oven, allowed to cool in the desiccator and again weighed.

The moisture content is:

$$w(\%\ H_2O) = \frac{W_{wet} - W_{dry}}{W_{wet}} \times 100 \qquad (5)$$

Tests have shown that crusing the samples beyond the bulk volume state results in eliminating additional water residing in occluded pores.[33] The measured moisture content has been shown to increase by as much as 1.5 percent upon crushing (i.e., from 15 percent water to 16.5 percent water). Samples are therefore broken off from the original core sample (to eliminate water cutting effects), crushed, and then oven dried. Tests have shown that at most an 0.13 percent water loss occurs during crushing, using Nevada Test Site tuff samples. Assuming all pore water to be eliminated. the error generated from crushing for a sample of 20 percent moisture content would be 0.65 percent. The moisture content error generates an error in dry

density of at most +0.003 gm/cm^3 when using average Nevada Test Site Tuff values.

Bulk Density

The term bulk density refers to the weight per unit volume of a material including all of its constituents: solid, liquid and gas. Both an "as received" and a dry bulk density may be found. The bulk densities may be determined by two different techniques. The weight is determined and then the volume measured by either direct measurement with calipers (for competent rocks) or fluid volume displacement. For the "as received density", caution must be taken to maintain the moisture content at its *in situ* level while for dry densities, it is necessary to eliminate all pore water from the sample. Thus measurement accuracy is a function of both volume and moisture content accuracy.

Method I: Direct Measurement

The direct measurement technique is best suited for competent rock samples that have easily calculated volumes, e.g., samples that may be readily cut into cylinders. Typically, a core sample is cut to a desired length from a wrapped NX size core (this core sample is usually the one used for mechanical testing). The cylinder is immediately weighed on the Sartorius balance and measured with calipers. The wet bulk density is determined using the weight and calculated volume while the dry bulk density is calculated using the sample moisture content as measured for a smaller piece of the same sample.

In using the direct measurement technique, preparation of the cylindrical samples requires saw cutting usually with the use of a liquid coolant. The error in weight resulting from the use of this coolant is less

than ±.03 percent for saturated ash-fall tuff. However, other materials which are less than "fully" saturated, have been shown to gain considerable amounts of water (10 percent to 20 percent of the rock samples weight) from being subjected to the coolant. Thus, the direct measurement method requires that caution be exercised when samples have irregular surfaces and/or less than "full" saturation. When errors caused by cutting water and surface irregularities are anticipated, the mercury immersion technique should be used with a sample chipped from the core rather than using a prepared specimen.

A prior Terra Tek investigation determined the "as received" density for selected tuff samples[3] using caliper measurement, mercury immersion and water immersion techniques.[38] The samples were 1 inch cylinders cut adjacent to each other from an NX core. The caliper method gave 1 percent to 2 percent lower densities than the immersion methods. This suggests that the immersion techniques may give more accurate volumes based on fluid conformity to irregular surfaces. More accurate volumes could be obtained with the caliper technique if the samples were machined to "perfect" cylinders. However, due to sample exposure to air, moisture loss would cause errors in the "as received" weight.

Method II: Mercury Immersion (using Ruska Mercury Porometer)

The mercury immersion technique may be used with materials which range in competency from poor to good. Soft, loose materials such as low grade shale, siltstone, etc., may be tested by first coating the sample with an 0.5 mm to 1.5 mm thick layer of beeswax to avoid sample breakup. Sample volumes are determined by immersing a sample into a calibrated volume of mercury and measuring the displaced volume.

The primary source of error for this method is air trapped on the sample surface. To determine the extent of the error, volume calibra-

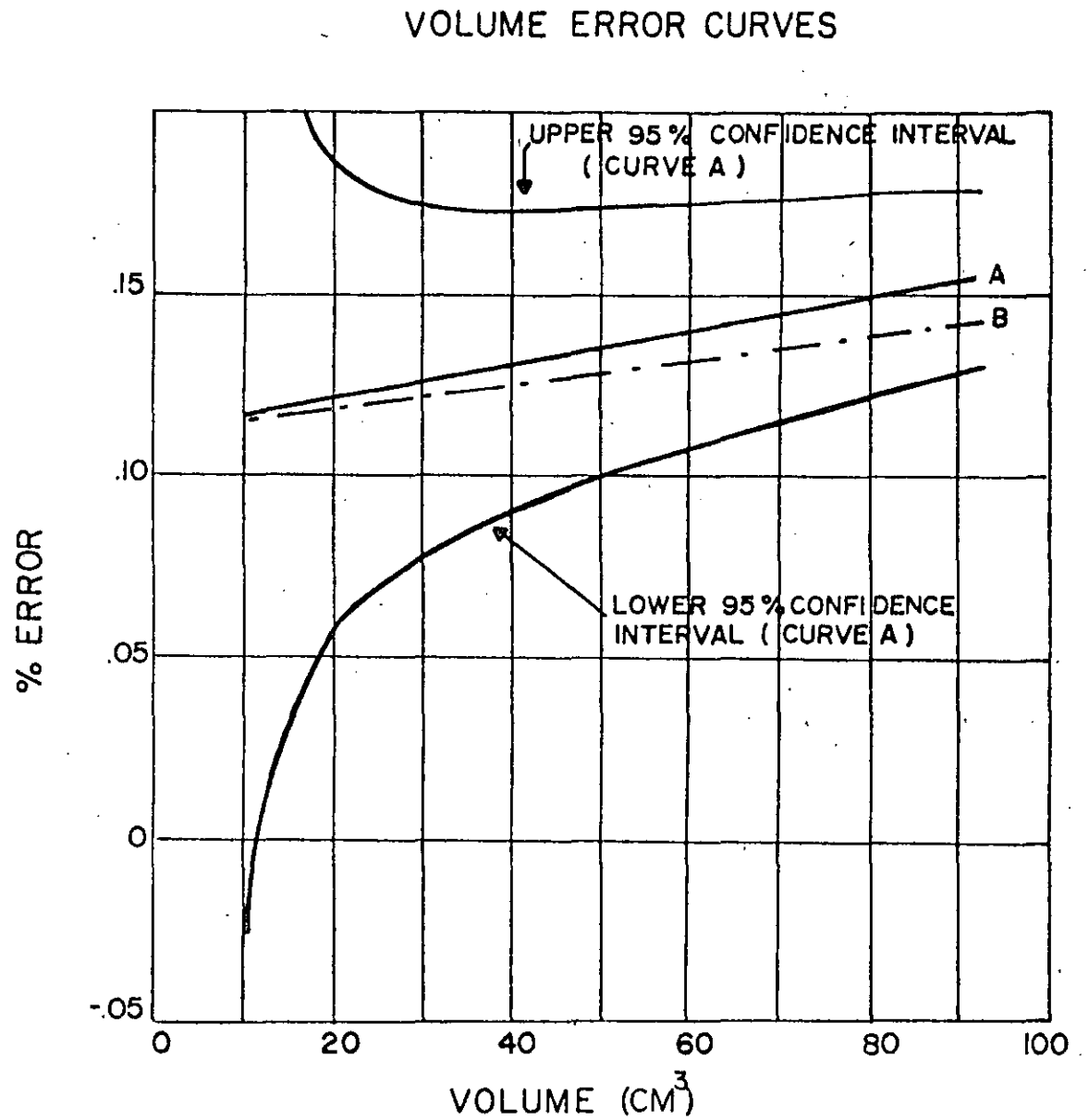

Figure C-2-5. Percent volume error -vs- sample volume (cm^3) in mercury porometer for linear least square fit of steel cylinder data. Curves A and B represent the uncoated and coated cylinder data respectively. "Zero" error is the micrometer measured volume.

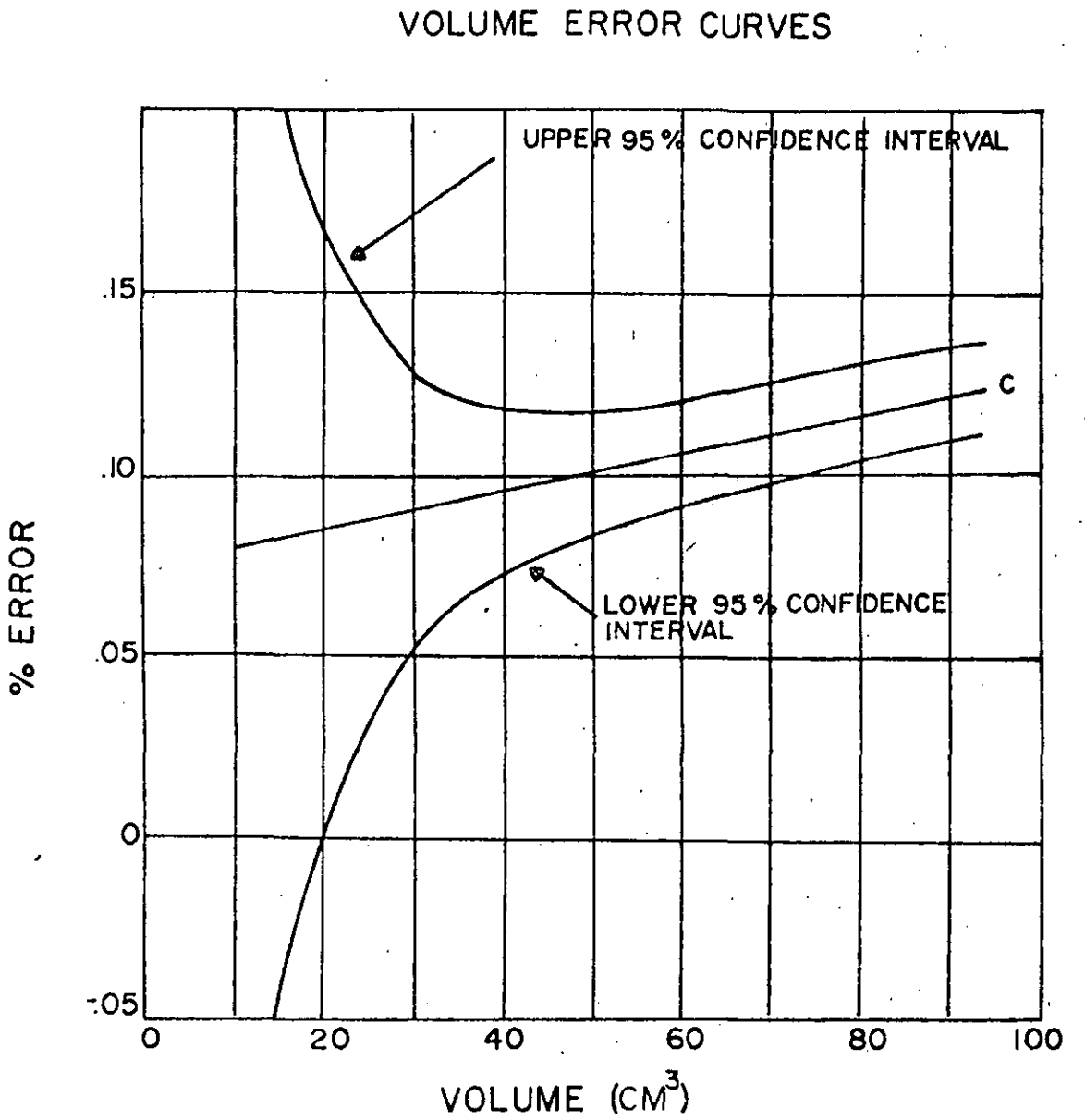

Figure C-2-6. Percent volume error -vs- sample volume (cm^3) in mercury porometer for linear least square fit of steel sphere calibration data. "Zero" error is the micrometer measured volume.

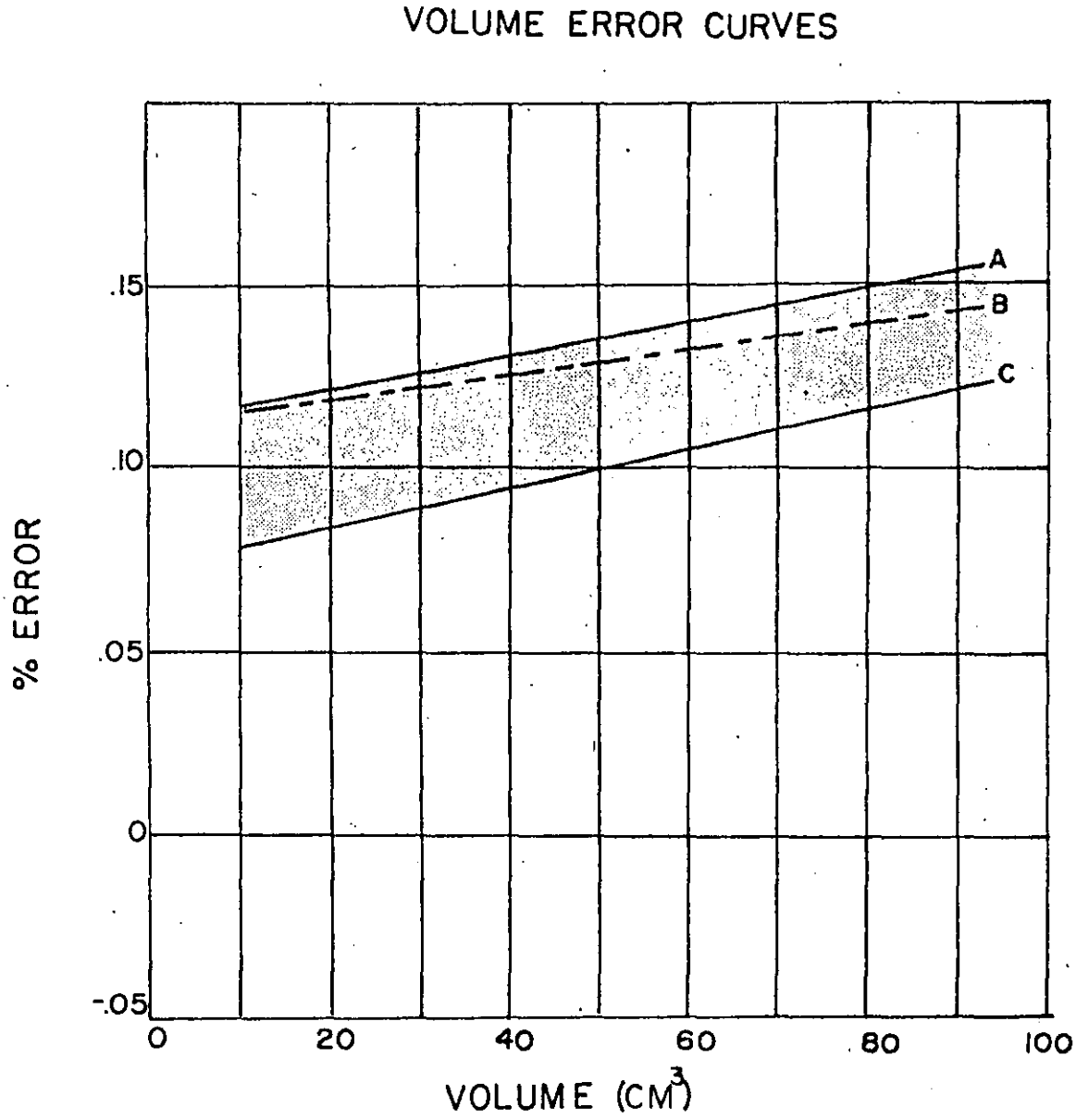

Figure C-2-7. Percent volume error -vs -sample volume (cm^3) in mercury porometer for linear least square fit of steel calibration data. "Zero" error is the micrometer measured volume. The shaded region represents the expected error band for sample measurement. Curves A and B are the uncoated and coated cylinder data respectively while curve C represents the uncoated sphere data.

tion tests were performed on metal cylinders and spheres with volumes ranging from 8.58 cm^3 to 93.07 cm^3. The "true" volume was considered to be the volume determined from micrometer measurement. The results indicated that 1) the porometer measured volumes are consistantly higher than the "true" volume with the absolute difference increasing with increasing sample volume, 2) the volume scatter from repeated measurements on any given calibration sample decreased as sample volume increased, 3) the steel spheres gave less scatter and volume error than the cylinders, and 4) the results from wax coating of the steel cylinders did not significantly vary from the uncoated steel cylinders after subtraction of the additional wax volume. Result 3) may be explained by considering the area to volume ratio of the cylinders and spheres. For equal volumes, a sphere has less surface area than a cylinder thus conceivably trapping less air and causing less error.

Figure C-2-5 shows the linear least square fit for the uncoated and "waxcoated" steel cylinder data (curves A and B respectively) including the 95% confident interval curves for "A". The shallower slope of curve B may be a result of the more "spherical" geometry of the wax coated cylinders. Figure C-2-6 shows the linear least square fit for the uncoated steel sphere data (curve C) including its 95% confidence interval curves. Figure C-2-7 shows curves A,B, and C where the shaded region represents an approximate range of mean volume error.

Because the error curves were reproducible and the cylinders and spheres approximate the full range of sample volumes and geometries of the rock samples to be tested, Figure C-2-5, C-2-6 and C-2-7 can be used for volume correction.

Wax coating the sample offers three distinct advantages: 1) it allows reuse of the sample for grain density determination, 2) it maintains

a constant surface between the mercury and the sample and 3) it does not allow mercury to penetrate the sample. A statistical (student t) comparison of the wax-coated and uncoated steel cylinder data showed that there was no significant difference in the volume errors thus indicating that the wax coating does not change the calibration curves. Microscopic examination of three rock samples (limestone, sandstone and tuff) after wax coating indicated no significant wax intrusion into surface pores. Tests on tuff and sandstone have shown moisture loss due to wax coating to be negligable (.03 percent or less moisture loss).

To check the use of the porometer having corrected for the volume based on curves A, B, and C in Figure C-2-7, Arkansas Quartz crystal densities were determined with sample volumes ranging from 13.39cm^3 to 28.86 cm^3. The mean quartz density determined from the mercury system was 2.649 gm/cm^3 with a standard deviation of 0.002 gm/cm^3. For ambient temperatures and pressures at the Terra Tek laboratory the most probable density value for a colorless natural α-quartz crystal is 2.651 gm/cm^3 according to Dana's Silica Volume[40] whereas x-ray powder diffraction measurements[41] give densities of 2.647 gm/cm^3. The porometer determined density did not significantly vary from the published values using a statistical (student t) analysis.

Figures C-2-5 and C-2-6 show that the scatter in volume measurement may be significantly reduced by using samples larger than about 30cm^3. A 30cm^3 volume is the suggested minimum sample volume for porometer testing since a corrected volume accuracy is obtained to within -0.015 cm^3 to +0.015 cm^3 with a resulting "as received" density to within -0.001 gm/cm^3 to +0.001 gm/cm^3 at a 95% confidence interval. The dry density includes the moisture content error (+.003 gm/cm^3) giving accuracy to within 0.004 gm/cm^3. Recall that the above accuracies are calculated from steel samples. Tests on uncoated ash-fall tuff samples suggest scatter to within -0.001 gm/cm^3 to +0.001 gm/cm^3.

Method III: Water Immersion

Volume determination by water immersion is suitable for materials ranging in competency from fair to good. The sample is first presoaked in distilled water so that no water absorption occurs during immersion. The specimen is then immersed in a distilled water bath and weighed, being sure that thermal equilibrium of sample water and bath water is maintained. The sample is removed from the bath, quickly surface dried and weighed in air. The resulting difference in sample weight submerged and in air gives the sample volume when the distilled water bath density for the ambient temperature and pressure is known.

Calibration of this method involved the volume determination of precision machined metal cylinders and spheres identical to those used for mercury immersion calibration. Volumes ranged from 8.58cm^3 to 28.94 cm^3. The metal samples indicated that all measured volumes were low by 0.06 percent when compared to the "true" (micrometer measured) volumes.

A calibration check was made using Arkansas quartz crystals. Using the 0.06 percent correction for the quartz crystal tests. a mean quartz denstiy of 2.649 gm/cm^3 was obtained from seven samples with a standard deviation of .002 gm/cm^3. Analysis (using the student t method) showed the water immersion quartz density to agree with both of the published α-quartz densities (2.651 gm/cm^3 from Dana's Silica Volume and 2.647 gm/cm^3 from powder diffraction measurement). The accuracy may then be stated to be within -0.006 gm/cm^3 to +0.002 gm/cm^3 at a 95% confidence interval using the 2.651 gm/cm^3 published quartz crystal density). Dry density accuracy would be within -0.003 gm/cm^3 to +0.005 gm/cm^3 when including the moisture content error (-.003 gm/cm^3). Wet and dry bulk density tests on ash-fall tuff samples have shown data scatter to be within the above stated bounds.

Grain Density

In general, geologic materials contain three distinct phases: solid, liquid, and gas. The term "grain density" deals with the density of only the solid phase. Thus it is necessary to eliminate the effects of the liquid and gas phases to obtain a true grain density. To measure the solid phase only, the material must be ground sufficiently small to eliminate the occluded pores, and a vacuum pulled on the sample to assist surface tension in assuring maximum saturation of the microscopic voids. The grain density accuracy on materials such as ash fall tuff is highly dependent on the pulverizing step and on the ability of water to penetrate the zeolites. It has been shown[42] that for maximum penetration of water into the zeolites, the sample powder should be soaked in distilled water for 3 to 4 days while a partial vacuum is pulled. There are also indications that different immersion fluids may cause density changes.

Standard laboratory procedure is to pulverize samples to -100 mesh (-0.149 millimeter) based on results investigating the effect of mesh size on grain density[43]. Studies on ash fall tuff[16] indicate that void sizes range from several millimeters to 10^{-7} millimeters with void shape ranging from spherical to limellar. The same study also suggested that some voids do remain intact after pulverizing and seem to be contained such that water molecules cannot access them. Thus, it would appear that the smallest occluded voids are not accessed by grinding to -100 mesh material. Grain density tests[43] showed an average 0.007 gm/cm^3 density increase when tuff samples were pulverized from -100 mesh material to -200 mesh material. This density increase causes a change in air void content of -.18% Vav. However, since the additional crushing time necessary to obtain -200 mesh material is considerable (5 minutes in pulverizer vs. 4 hours in ball mill)[44], obtaining this additional accuracy in density and air void content is not practical for Nevada Test Site applications. Nevertheless, a -200 mesh material is obtainable for special applications where maximum accuracy is required. With -325 mesh tuff Lawrence Livermore Laboratories[44]

derived inconsistent density results. This may be due to poor statistical sampling caused by grains of different density migrating in the ground mixture prior to testing or by the increased surface charge density on the grain boundaries further enhancing zeolitic reactions. Thus, even though accuracy for tuff is a function of the volume magnitude of the inaccessible voids, data indicates that grinding the tuff to a -100 mesh allows for maximum accuracy with minimal preparation.

Two techniques for determining grain densities are given in this section: a water pycnometer and gas pycnometer technique. The former method has been used as the standard grain density method at Terra Tek. However, because of improved techniques the gas pycnometer method is being implemented into standard laboratory usage.

Method I: Water Pycnometer Technique

This technique requires approximately 48 hours to obtain grain density values. A sample weighing approximately 50 gms is first ground to a -100 mesh particle size. The pulverized material is dried in the forced convection oven set at 105^{o}C for 24 hours. Approximately 25 gms of dried material are placed into a volume claibrated 50 ml. flask and immersed in distilled water. A vacuum is drawn on the flask and the subsequent water displacement volume in addition to the oven dried sample weight determines the grain density.

The accuracy of this method was determined using Standard Reference Material 640[45] obtained from the National Bureau of Standards. SRM 640 is a -200 mesh powder composed of high purity elemental silicon. The National Bureau of Standards has not yet determined the density of SRM 640. However, since SRM 640 is the powder form of solid SRM 990[46] the density stated for SRM 990 is used as the calibration density value, that being 2.329 gm/cm^3. In addition, both materials came from the same in-

dustrial source thus assuring uniformity in production technique. The mean density determined for SRM 640 using the water immersion technique was 2.319 gm/cm^3 with a standard deviation of .022 gm/cm^3. A statistical (student t) analysis showed that the water immersion mean density value for SRM 640 statistically agreed with the published value of 2.329 gm/cm^3. This result was due to the large standard deviation of .022 gm/cm^3. However, it is recommended that only three digit densities be given (e.g., 2.32 gm/cm^3) since uncertainty exists in the hundredths place and the accuracy stated as being within -0.05 gm/cm^3 to +0.03 gm/cm^3 at a 95 percent confidence interval.

Method II: Gas Pycnometer Technique

This method requires a test time of about 36 hours. Early investigation using the gas technique showed volume drift to be a problem presumably due to gas reactions with the zeolite in the ash-fall tuff. (Testing atmospheres included argon, helium and air.) This drift has been alleviated by not oven drying the pulverized sample prior to testing but instead allowing it to equilibreate with the atmospheric moisture. It is presumed that drift is avoided by the free water filling the small pores present in the zeolite, thus preventing a zeolitic reaction. The volume contribution of the free water is determined after testing and subtracted from the sample volume.

Arkansas quartz crystals and SRM 640 silicon powder were used for calibration of the gas pycnometer. Helium is used as the gas due to its small molecule. Using SRM 640, the Beckman Gas Pycnometer determined a density of 2.330 $\pm$ .005 gm/cm^3 at a 95 percent confidence interval for ten trials giving the maximum accuracy of the method as -0.004 gm/cm^3 to +0.006 gm/cm^3. For a 2.5 gm/cm^3 grain density sample the error is then -0.16 percent to 0.20 percent. The Arkansas quartz crystals were used as a calibration check

for which a mean density from seven trials was determined to be 2.647 gm/cm^3 with a standard deviation of 0.006 gm/cm^3. A statistical (student t) comparison showed no significant difference between the gas pycnometer mean quartz density and published α-quartz densities[40,41] determined from Dana's Silica Volume and x-ray powder diffraction measurements.

Grain Density Comparison (Water Immersion -vs- Gas Pycnometer)

In order to analyze differences between the water and gas pycnometer grain density techniques, the mean densities as determined for SRM 640 were statistically compared (using Aspen-Welch student t method). The result was that the two means, 2.31 gm/cm^3 and 2.330 gm/cm^3 for the water and gas pycnometer techniques respectively, were shown not to be statistically different. (This result was due primarily to the large standard deviation of the water immersion technique.) However, upon analyzing the standard deviations of the two techniques it was found (using the F statistic) that the gas pycnometer standard deviation was significantly less than the water immersion standard deviation. Thus for maximum accuracy and low data scatter the gas pycnometer should be used.

Porosity

Porosity of a material is the volume fraction of pores. The pore volume may be found by either measuring the solid volume (i.e., volume occupied by the solid grains) and subtracting that from the dry bulk volume thus obtaining the pore volume indirectly, or the pore volume may be measured directly by fluid impregnation. The latter technique measures the effective porosity, that is, those pores which are interconnected and thus accessible to measurement by an impregnating fluid. The total porosity measures all pore spaces whether they are occluded or interconnected. Consequently, the effective porosity is less than or equal to the total porosity.

Method I: Total Porosity (using dry and grain densities)

This method requires that both the grain density and the dry bulk density be determined for the material. Using ρ_d and ρ_g, the porosity is then calculated using equation (2), Table C-2-2.

The error in the total porosity value is a result of the errors in measuring the dry bulk density and grain density. Using the mercury porometer and gas pycnometer density accuracies, the calculated porosity accuracy is within -0.348 percent to +0.074 percent n_t using $\rho_g = 2.4$ gm/cm^3 and $\rho_d = 1.45$ gm/cm^3.

Method II: Effective Porosity

Effective porosity is the connected pore volume divided by the bulk volume. To determine the connected pore volume the sample may be impregnated with mercury, gas or water using for volume measurement the Ruska Mercury Porometer, Beckman Gas Pycnometer or Mettler Balance respectively. Using the Ruska Mercury Porometer, an oven dried bulk sample is placed into the pycnometer with mercury injected into the sample under pressure. The injected mercury volume is equivalent to the connected pore volume to a first approximation when using equation 6:

$$Vc = Vm \left(1 + \frac{P_1}{P_2' - P_1}\right) - Va + \Delta Vs \qquad (6)$$

where Vc is the connected pore volume, Vm is the injected mercury volume, P_1 is atmospheric pressure, P_2' is the internal trapped air pressure corrected for capillary forces[47], Va is the volume of air trapped on the sample surface and ΔVs is the volume change due to matrix shrinkage. The derivation for equation (6) may be found in Appendix B. The Beckman Gas Pycnometer requires standard volume measurment of an air dried bulk sample from which an apparent grain volume is determined after correcting for the

free water volume (recall the grain density technique). The sample bulk volume is then found from which the effective porosity can be calculated. The water immersion technique requires that a sample first be oven dried and weighed. The sample is saturated allowing distilled water to fill the connected pores and then immersed in a distilled water bath to determine its buoyant weight. The difference in buoyant weight to the oven dried weight gives an apparent grain volume. After bulk volume determination the effective porosity may be calculated.

A synthetic material, Tegraglas (3M product), was used to compare the effective porosity techniques. The material was selected because of its uniformity, availability in various pore sizes, and its comparibility to rock fabric. A comparison to an absolute value was not possible since no standard porous material exists. The three techniques determine the effective volume directly thus allowing direct calculation of the effective density. Table C-2-3 lists the obtained effective density means and standard deviations. To analyze the difference in the three methods, a statistical comparison (using an analysis of variance and Duncan's multiple range test) of the mean effective densities was conducted for each grade of material. The analysis showed that no significant difference in means was observed for grades 15 and 90 materials suggesting that the three methods were giving the same results. However, all three means were significantly different for the grade 40 material. The difference in the high and low mean effective density for the grade 40 material corresponds to an effective porosity difference of 0.53 percent porosity using equation 7. This would correspond to an error of 1.9 percent (% error not % porosity). For

many applications this size of error may not be critical. Consequently, any of the three methods could be used to determine effective porosities of granular materials (similar to Tegraglas in pore size) with a maximum uncertainty of about 0.53 percent porosity (% porosity not % error).

TABLE C-2-3

Mean Effective Densities (ρ_e) Using 3M Tegraglas

$$n_e = (1 - W/(\rho_e \times V_{bulk})) \times 100 \quad (7)$$

Material Grade (in microns)	Beckman Density gm/cm^3	Ruska Density gm/cm^3	Water Immersion Density gm/cm^3
15μ	ρ_e = 2.118 s = .006	ρ_e = 2.111 s = .002	ρ_e = 2.117 s = .006
40μ	ρ_e = 2.212 s = .003	ρ_e = 2.196 s = .002	ρ_e = 2.208 s = .001
90μ	ρ_e = 2.357 s = .003	ρ_e = 2.353 s = .003	ρ_e = 2.358 s = .001

Permeability

The Terra Tek permeability equipment allows determination of permeability at confining pressure, deviatoric stress, and pore fluid pressure. A difficult problem is that of determining when a sample has reached equilibrium at the pore pressure at which it is to be tested. If a pore pressure gradient is present in the sample, the peremability will be in error. This error can be avoided by monitoring the permeability until it is stable. The equipment is capable of gas or liquid permeabilities using either a transient method or a steady-state method. Appendix C outlines the equa-

tions in calculating the permeabilities.

The transient method[48], requires the application of a differential pressure pulse (≈ 1 percent of the confining pressure) across the sample. The resulting pressure decay vs. time, in addition to the properties of the permeating fluid, the sample geometry and the system volumes, enable calculation of the permeability. This method is more adapt to low porosity materials such as tight sandstones where permeabilities are in the tens of microdarcies. Consequently, accurate measurements are possible on very tight samples while easily accomodating high pore pressure (up to 4 kilobars). Figure C-2-8 shows a typical transient method plot.

A steady-state determination of permeability is made by measuring the steady-state flow of fluid through a sample for a small pressure differential across the sample. The permeability can be calculated if the flow rate, pressure drop, fluid viscosity and sample geometry are known.

Although there is no commonly accepted standard for permeability, several methods have been utilized to verify the accuracy of the measurements. For example, comparisons were made with sandstone samples obtained from the United States Bureau of Mines that had been tested over a range of confining pressures. Comparisons indicate values to be accurate and repeatable to within 20 percent depending upon sample permeability and testing conditions.

Microscopic Methods

The texture and fabric of a rock is often used to aid in explaining its anisotropic behavior.[16,17,49] Microstructure studies include analysis of particle size distribution, spatial orientation and mineral content. It is important that an unbiased sample population be obtained and that a statistically significant number of particles be counted. The sample size will depend upon the fabric complexity but studies[50] have shown that a minimum of 100 grains must be sampled to obtain a first approximation of

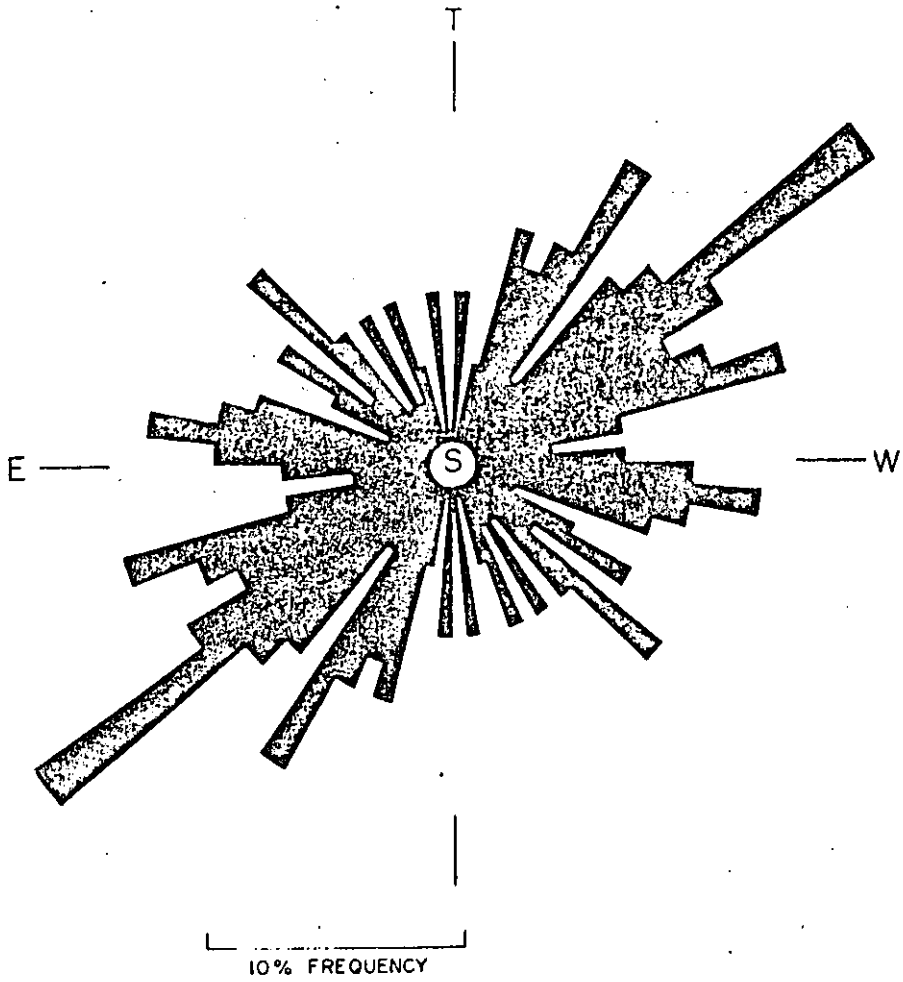

Figure C-2-10. Grain Orientation Frequency Histogram

Depending on the grain size and rock fabric three possible microscopic techniques may be employed:

1) An opaque, light reflection method for grain diameters greater than 10^{-3} in with fabric cohesion ranging from poor to good.

2) A thin section, light transmission method for fabrics having fair to good cohesion with grain diameters greater than 2×10^{-5} in., and

3) For grains smaller than 2×10^{-5} in., with poor to good fabric cohesion a scanning electron microscope (SEM).

The University of Utah SEM is available for the purpose.

The two sources of error which exist for the three techniques are 1) insufficient number of counted grains (discussed in proceeding paragraph) and 2) a biased estimate of the diameter caused by surface preparation. The surface plane may disect a particle at any diameter not necessary the average dia. Con-

sequently, grain size analysis yields an apparent diameter. Numerous correction factors have been proposed for converting from the apparent to the true diameter[51]. Reported coefficients range from 1.126 to 1.5 and may be used for true diameter estimates.

Method I: Large Grain Technique (dia. > 10^{-3} in.)

This technique utilizes the Bausch and Lomb monocular and follows all proceedures as outlined in the introduction. Random sampling consists of creating a grid on the sample and counting only those grains which lie under intersection points. Grain orientation cannot be measured using the Bausch and Lomb monocular.

Method II: Medium Grain Technique (dia. > 2 x 10^{-5} in.)

The Zeiss model RP-48 standard scope with binocular vision and photo attachment is the only equipment necessary for this test. Prepared samples require thin sectioning. Thin section work is done for Terra Tek by Western Petrographic of Tucson, Arizona. The thin section is made from a 1/4" cube with etching and dyes introduced during the sectioning process to highlight grains.

A random unbiased sample population of grain diameters, orientations and mineral contents is obtained by using a mechanical stage. Polar frequency diagrams may be constructed as shown in Figure C-2-10 with north-south, east- and west axis being established for the top thin section, east-west, top and bottom axis for one side and north-south, top-bottom axis for the other side.

Method III: Medium Grain Technique (alternate method using the universal stage)

An alternate technique is available for grain orientation studies. This involves the use of the universal stage which locates linear and planar features in three dimensional space. Subsequent diagrams of these grains involve the use of Wolf, Schmit or Lambert stereo nets. Sample preparation, sampling and measurement techniques follow Method II for grain size, orientation and mineral content studies; the only modification to the procedure being the additional two angles (strike and dip) recorded for each grain.

Method IV: Small Grain Technique (dia. < 2 x 10^{-5} in.)

For particle diameters which are less than 2 X 10^{-5} in. a scanning electron microscope (SEM) is available at the University of Utah. SEM photomicrographs can be used to measure grain size and grain dimensional orientation from photographs. Because of the lack of color, mineral content cannot be easily determined. The calculational procedures and error are similar as for those of Method II of this section. Measuring is different, however, in that grain size and angles are obtained from photographs.

CONCLUSION

The methods used for determining physical properties are highly dependent on the material structure, composition, and condition of the rock. Most of the properties are dependent on the pore structure. For example, the permeability and effective porosity are directly related to the interconnected pores while measurement of grain density and moisture content require the accessibility of all pores (occluded and interconnected) after crushing or pulverizing the sample. The composition of the rock is important when considering physical property techniques. For instance, the water immersion technique would disintegrate certain shales while care in sample preparation is required to prevent zeolitic reactions during grain density determination using the gas pycnometer method. Obviously, possible mineral interaction must be considered when selecting a measuring technique. The condition or competency of the rock also bears on the selection of a testing method. Examples of this would be a rock which is dry or less than fully saturated indicating that it should not be subjected to cutting water (water absorption) or the case of a highly fractured rock which requires a wax coating in order to prevent sample break-up during bulk volume determination.

With rock structure and composition known, the proper physical property tests may be selected. It is then desirable to construct a testing sequence to determine standard Nevada Test Site physical properties (ρ_w, ρ_g, w) which would give the most accurate results. The following test sequence is proposed:

1) Immediately upon unsealing a core, obtain a chip of material of approximately 50 cm^3 adjacent to the sample which will be mechanically tested. Clean the chip, weigh it and seal it in beeswax. Determine the combined weight of the sample plus wax.

2) Determine the sample bulk volume using the Ruska Mercury Porometer. The wax volume is eliminated by knowing its weight and density.

3) The bulk volume sample is stripped of wax, immediately passed through the jaw crusher and weighed. The crushed material is then oven dried.

4) After weighing the oven dried material, it is passed through the pulverizer and reduced to a -100 mesh material.

5) The grain density is then determined using the water immersion method. Grain density for many non-zeolitic materials can be done using the Beckman Gas Pycnometer to increase accuracy. Investigations are being conducted to evaluate its usefulness in determining grain densities for Nevada Test Site zeolitized ash-fall tuffs.

This procedure incorporates Terra Tek's most accurate techniques to date for determining the "as received" bulk density, moisture content and grain density on Nevada Test Site ash-fall tuffs. From these three values the dry bulk density, total porosity, percent saturation and percent air voids may be calculated.

APPENDIX A

Statistical Methods and Proceedures

Measurement accuracy and precision of a piece of equipment must be known prior to its use in a testing program. Accuracy is the ability to produce the true value while precision is concerned with data reproducibility. When dealing with normally disturbed-random observations, accuracy is best determined by comparing mean values ($\bar{x}$) while the best measure of precision is the sample standard deviation (s). Thus when analyzing a single machine or method, $\bar{x}$ and s usually suffice in describing its measurement characteristic. However, when numerous methods and equipment are being analyzed it is not always obvious now they statistically compare with each other using only the mean and standard deviation. For example, suppose two machines (A and B) were used to determine a density from seven samples with machine A giving $\bar{x}$ = 2.641 gm/cc, s = .009 gm/cc and machine B giving $\bar{x}$ = 2.649 gm/cc, s = .002 gm/cc. Using the proper statistical procedure (Aspen-Welch student t method, α = .05), it may be shown that the two means are <u>not</u> statistically different. This result is not obvious by simple examination of the sample mean and standard deviation. Hence, more refined statistical measures must be used to evaluate numerous performance characteristics.

Seven statistical measures are used in this report, namely 1) the sample <u>mean</u> ($\bar{x}$), 2) the sample standard deviation (s), 3) the student t test, 4) the Aspen-Welch formulation of the student t test, 5) the F test, 6) the analysis of variance and 7) Duncan's multiple range test. All the above tests requires normal sample distribution and random sampling. The meaning and use of each statistic is briefly given below. Detailed explanations may be obtained from reference (39).

The sample mean value ($\bar{x}$) commonly called the "average value", is the summation of all observations divided by the number of observations and it is used simply to give the central tendency of the data. Closely associated with the sample mean is the sample standard deviation (s) which measures the dispersion or scatter of the data about the mean value.

The student t statistic uses the values $\bar{x}$ and s as well as the number of observations (n) for analysis. Simply put, the student t test compares the sample mean $\bar{x}$ to the "true" mean (μ). The result is that statistically $\bar{x}$ is shown to either equal or not equal μ thus indicating whether the observations used in determining $\bar{x}$ are a subset of the observations which determine the value μ The Aspen-Welch formulation of the student t test is used mainly to compare the means of the two sets of independent observations. Typically this test involves the comparison of the sample means of two machines or methods. For example, a comparison of $\bar{x}_A$ and $\bar{x}_B$ is done from machines A and B with the result being either $\bar{x}_A = \bar{x}_B$ or $\bar{x}_A \neq \bar{x}_B$. (Tests for $\bar{x}_A < \bar{x}_B$ and $\bar{x}_A > \bar{x}_B$ may also be done.)

Once the equality of means has been statistically established using the student t methods, standard deviations may be compared using the F test. For example, the F test could determine whether the standard deviations (s_A and s_B) of two machines A and B were statistically either equal or if one was larger than the other. If it is concluded that $s_A = s_B$ then the two machines A and B are equally precise in measurement capabilities.

When comparing more than two means, an analysis of variance is used over the Aspen-Welch formulation. A typical analysis of variance would compare the mean values of many machines to determine if they could all

be from the same population, i.e., $\bar{x}_A = \bar{x}_B = \ldots \bar{x}_N$. If one or more means varies significantly from the other means, then the test says all means are not equal but not which mean (or means) are unequal. To determine the mean (or means) which are unequal requires the use of Duncan's multiple range test. Duncan's test examines each mean as to its equality to all of the other means with rejection of the mean occurring if equality is not realized.

In all of the statistical tests 3) through 7) use is made of $\bar{x}$, s and the sample size (n) as well as the level of significance term alpha (α). The level of significance term (α) is selected by the experimenter when using the published tables and charts during the statistical tests. The term (α) then indicates the probability the experimenter is willing to accept that the results of the statistical test are not occurring by chance. For example, when comparing a mean mineral density as determined from two machines A and B, ($\bar{x}_A = \bar{x}_B$), if the experimenter chooses an α = 5 percent it means that upon determining $\bar{x}_A \neq \bar{x}_B$ using one of the statistical methods, he can be 95 percent certain that the outcome of the test did not occur by chance. Likewise, if an α = 1 percent was chosen, a 99 percent probability that the outcome $\bar{x}_A \neq \bar{x}_B$ was not chance would be obtained. In the text an α = 5 percent was used except for the effective porosity data comparison for which an α = 1 was used.

APPENDIX B

Derivation for Ruska Porometer

Effective Pore Volume

Using the Ruska Porometer for effective porosity determination requires impregnation of the connected sample pores with mercury. Impregnation is accomplished by pressurizing the sample from atmospheric to 750 psig (manufactures suggested pressure). However, this injected volume is not the true effective pore volume. Errors result from the air trapped inside the sample, capillary forces acting within the pores and matrix shrinkage due to hydrostatic pressurization. Correction for these three errors may be accomplished through the following derivation.

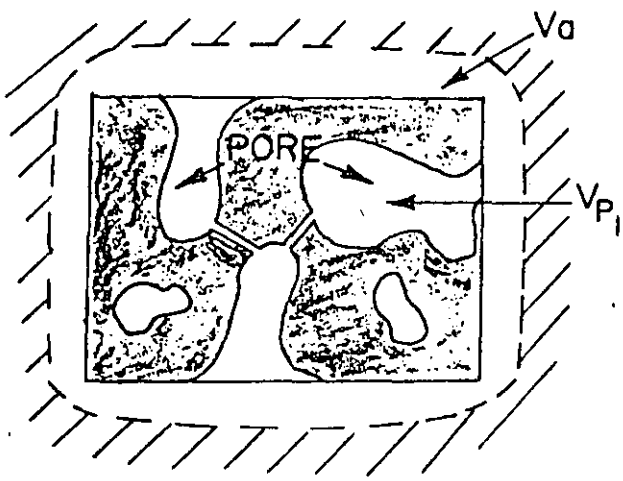

Figure C-2-11A: Porous sample prior to mercury injection.

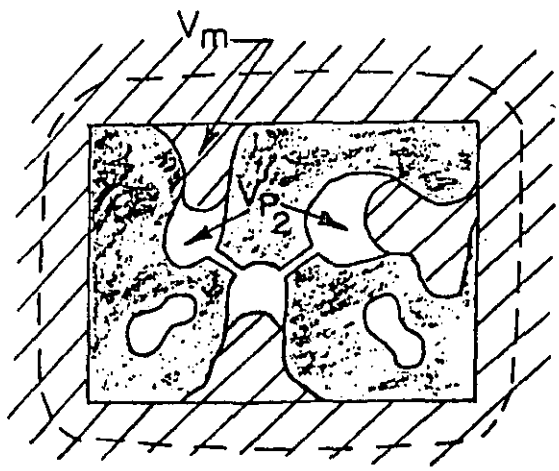

Figure C-2-11B: Porous sample after mercury injection.

Figure C-2-11: Porous material model before and after mercury injection. The shaded region represents the sample matrix while the crosshatched region represents the mercury.

Certain assumptions must first be made: (1) the mercury is in equilibrium and incompressible and (2) the perfect gas law may be applied to the trapped air. Figure C-2-11 shows a model of a porous material and shall be used to illustrate the problem.

Note the following variables:

Vp_1 = initial volume of air in pores

Va = initial volume of air trapped on sample surface

Vp_2 = final volume of air in pores

Vm = mercury impregnation volume

Vc = connected pore volume

It may be seen that the total volume of air before pressurization is equal to the volume of injected mercury plus the final air volume.

$$Vp_1 + Va = Vm + Vp_2 \qquad (1)$$

Furthermore, using the perfect gas law, the initial and final volumes of air may be related as being:

$$P_1 (Vp_1 + Va) = P_2 \times Vp_2 \qquad (2)$$

where P_1 and P_2 are the initial and final absolute pressures used during injection. Since the connected pore volume is equal to Vp_1, equation (1) may be rewritten as:

$$Vc = Vm + Vp_2 - Va \qquad (3)$$

Combining equations (1) and (2) and substituting into (3) gives:

$$Vc = Vm \left(1 + P_1 / (P_2 - P_1) \right) - Va \qquad (4)$$

If the present volume error is assumed to be caused by trapped air on the sample surface, then Figure C-2-7 may be used to calculate the trapped air volume Va if the bulk sample volume is known.

To account for the capillary forces within the pores a simple model of a circular capillary tube is used. By assuming circular pores a capillary pressure, Pc, may be derived as being:

$$Pc = \frac{4\ Fm \cos \alpha m}{d} \qquad \begin{aligned} Fm. &= -430 \text{ dynes/cm} \\ \alpha m &= 140^{o} \end{aligned} \qquad (5)$$

by solving a simple force balance problem. The term Fm is the surface tension of mercury while αm is the contact angle or angle of wetting and d is the mean pore diameter. The values of Fm and αm are from source 47. To a first approximation, the trapped air pressure is less than the gauge pressure by the value:

$$P_2' = P_2 - \frac{4Fm \cos \alpha m}{d} \qquad (6)$$

Since a hydrostatic pressure is being applied, a simple addition to the equation involving the matrix shrinkage may be included. Let ΔVs be the matrix shrinkage. Thus the basic form of the correction equation becomes:

$$Vc = Vm \left(1 + P_1/(P_2' - P_1) \right) - Va + \Delta Vs \qquad (7)$$

The matrix shrinkage is an additive correction since it represents a void shrinkage and thus reduces the amount of mercury which may be injected into the connected pores. The term ΔVs may be obtained if the bulk modulus and volume of the matrix is known for a given sample. The matrix volume may be obtained from the bulk volume minus the total porosity volume,

$$Vs = V_B - V_T \qquad (8)$$

where Vs is the matrix volume, V_B the bulk volume and V_T the total porosity volume as calculated from equation (2) in the text. In this instance the equation (7) modifies to:

$$V_c = Vm \left(1 + P_1/(P_2' - P_1) \right) - Va + (P_2 - P_1) \frac{Vs}{Ks} \qquad (9)$$

where Ks is the matrix bulk modulus. In samples where Ve $\simeq$ V_T equation (8) becomes:

$$\frac{V_c = Vm \left(1 + P_1/(P_2' - P_1)\right) - Va + (P_2 - P_1) \frac{V_B}{Ks}}{\left[1 + \frac{(P_2 - P_1)}{Ks}\right]} \qquad (10)$$

Equation 10 is a useful form of the correction equation when the total porosity volume is approximately equal to the effective volume because all of the terms except Ks and P_2' on the right hand side of the equation are determined during effective porosity testing. The bulk modulus Ks may easily be found by conducting hydrostatic loading tests on the sample matrix in a triaxial configuration. The term P_2' must be calculated using equation (6) thus requiring knowledge of the average pore diameter.

APPENDIX C

Permeability Equations for Transient and Steady State Methods

Transient Method

The transient method requires the reduction of the pressure drop vs. time plot, Figure C-2-8, to obtain the slope α. With α known along with the fluid constants, length and volume parameters, the permeability may be calculated.

A brief outline of the theory involved in measuring permeabilities using the transient technique is given below. A detailed treatment of this analysis is presented in reference 48.

The equation for compressible flow in a compressible media is:

$$\nabla^2 p = \frac{\mu\beta}{k} C \frac{\partial P}{\partial t} \qquad (1)$$

where

μ = fluid viscosity

β = fluid compressibility

k = permeability

C = a term which includes the compressibility of the rock matrix

and

P = pressure

If the following assumptions are made concerning fluid flow characteristics

1. Darcy's law is valid.
2. The fluid flow is laminar.
3. The change in fluid volume in the pores in the rock, due to the step pressure change, is negligible compared to the amount of fluid flowing through the sample during a test.

4. The pressure step is small compared to the absolute pore pressure so that the physical constants of the fluid (viscosity and compressibility) can be considered constant in all parts of the sample.

then the solution to Equation (1) is given by:

$$\Delta P = \overline{\Delta P}\left[\frac{V_2}{V_1+V_2}\right] e^{-xt} \qquad (2)$$

$\overline{\Delta P}$ = Initial step pressure added

ΔP = (Instantaneous pressure) - (Final pressure) i.e., $(P_i - P_f)$

V = Volume of reservoir at either end of the sample.

The permeability k is given from Equation (2) as :

$$k = \frac{\alpha\ \beta\ \mu\ \ell}{A(1/V_1 - 1/V_2)} \qquad (3)$$

$$\alpha = \text{Ln}\ \frac{P_i - P_f}{P_i} \div T \qquad (4)$$

where

α = the slope of the semilog plot of the natural log of the decaying pressure versus time.

ℓ = the sample length

A = the sample area

Thus, the permeability can be determined with no direct measurement of the flow rate. Clearly this is a major advantage for making measurements of the permeability at high pressure.

Steady State Method

The steady state method requires knowing only Q, the fluid flow rate in ml/sec and P_1 and P_2, the upstream and downstream pressures in atmospheres.

The permeability is then $K_{(darcies)} = \frac{Q\,L}{A(P_1 - P_2)}$ (5)

where L is the sample length in cm and A the sample area in cm^2.

Limitations of Rock Mechanics in Energy-Resource Recovery and Development

Panel on Rock Mechanics Problems That Limit Energy Resource Recovery and Development

U.S. National Committee for Rock Mechanics

Assembly of Mathematical and Physical Sciences

Limitations of Rock Mechanics in Energy-Resource Recovery and Development

Report of a
Study Conducted by the
Panel on Rock Mechanics Problems
That Limit Energy Resource
Recovery and Development

U.S. National Committee for Rock Mechanics
Assembly of Mathematical and Physical Sciences
National Research Council

NATIONAL ACADEMY OF SCIENCES
Washington, D.C. 1978

1

GEOTHERMAL ENERGY EXPLORATION AND PRODUCTION

T. William Thompson
Subpanel Chairman

INTRODUCTION

The exploitation of geothermal energy involves tapping the heat energy stored in the earth's crust. Hot rocks can always be found at some depth, but drilling and production costs and complexity limit the economic development of this energy source to areas where high temperatures are found near the surface. Localized upward displacement of isotherms can occur in areas of high-conductivity rocks, where near-surface rocks form an insulating blanket or where upward migration of molten rock, or hot waters, heats the upper strata. Many classical geothermal areas occur in areas of known volcanic or tectonic activity, where surface manifestations have led to the discovery of geothermal reservoirs.

In any geothermal area the mode of exploitation is dictated by the nature of the resource but always involves the removal of heat to the surface, where it may be used directly or converted to other forms of energy. Two major types of geothermal resource can be identified: resources where the rocks contain hot fluids in sufficient quantities to act as the heat-transfer medium (Figure 1.1), and those where the hot rock is essentially dry (Figure 1.2). The first type includes hot water (hydrothermal) and steam reservoirs. There is a gradation between these two kinds of reservoir and the type may change during fluid production, as pressure and temperature changes lead to phase changes of the reservoir fluid. By contrast the second type includes those resources where fluid is either absent or present in quantities too small to allow direct extraction of heat energy. This is the class of resource, commonly referred to as "hot dry" rock, from which heat must be extracted by injecting fluids. A third type of resource, allied closely to the first, is geopressured geothermal reservoirs in which the high-temperature fluid is at elevated pressure. These are less common, but are found in the sediments around the Gulf of Mexico, where they form a potentially important source of energy.

From the standpoint of rock mechanics, geothermal reservoirs may be divided into nonporous, which will always be hot-dry reservoirs, and porous, the latter class being further divided into reservoirs where the porosity is

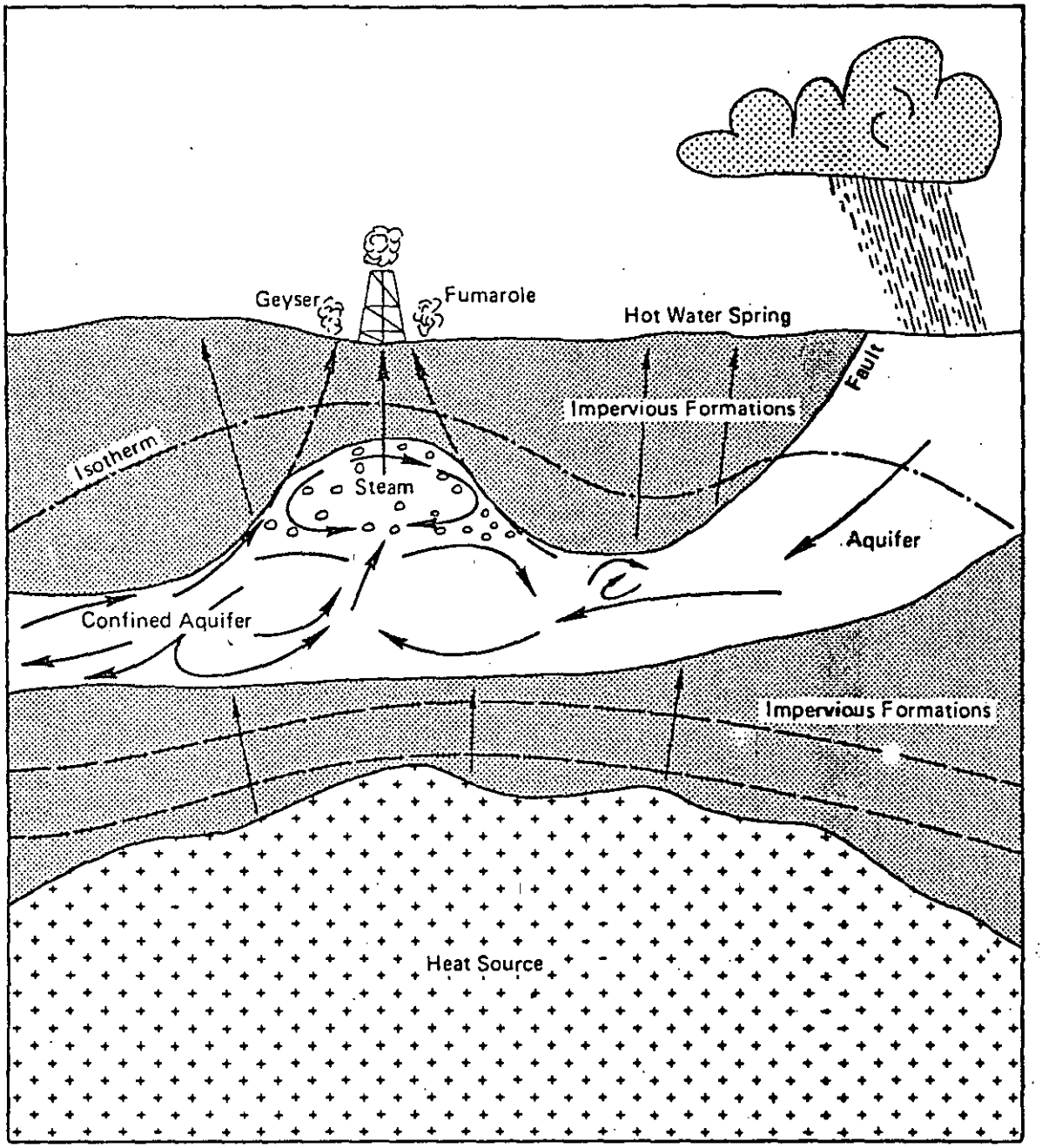

FIGURE 1.1 Schematic illustration of a steam-dominated hydrothermal geothermal system.

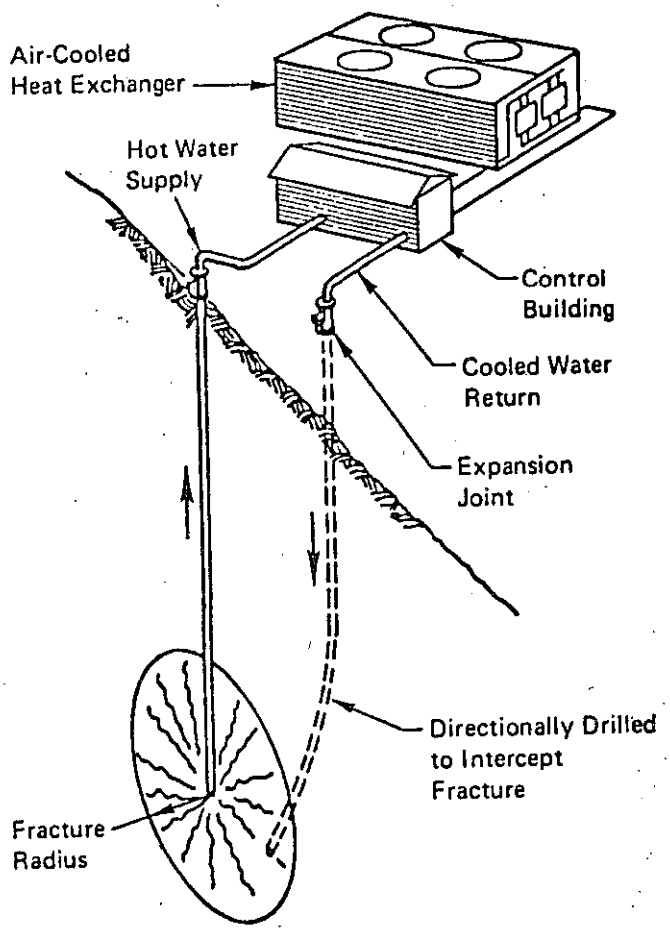

FIGURE 1.2 Schematic illustration of the hot-dry-rock geothermal energy-recovery method.

primarily due to fractures and those where the porosity is mainly intergranular. This report concentrates mainly on the fractured porous and the non-porous hot-dry-rock resources, because the problems associated with nonfractured porous resources are largely extensions of those associated with the exploitation of hydrocarbon reservoirs, which fall into the subject area of another subpanel. Nevertheless, many of the problems outlined in this section do apply to this class of resource.

Until recently, rock mechanics, in its restricted sense, has not been widely recognized as a major contributor to geothermal energy exploitation. However, continuing development has focused a need for better understanding of the mechanical behavior of producing fractured and nonfractured reservoirs. Specific knowledge is needed of the interaction of pore-pressure changes and compaction and of the potential effects of compacting reservoirs on subsurface subsidence. An understanding of fracture mechanics is integral to the development of non-porous, hot-dry-rock resources. In a broader sense, a

detailed knowledge of the physical and mechanical properties of rock masses, and their dependence on environment, is critical to the search for and evaluation and development of geothermal resources. Our present understanding of these areas is limited, particularly in the temperature and stress regimes applying in geothermal reservoirs.

In considering the recovery and development of geothermal resources the Subpanel concluded that the major overriding limitation caused by rock-mechanics problems was the basic lack of understanding of their geology, geophysics, and mechanics. All phases of recovery of these resources, from exploration and evaluation to production and environmental impact, require a suitable conceptual and theoretical model for the reservoir. Part of the problem in identifying and refining these models lies in the complexity of natural rock systems and the gross heterogeneity of fractured rocks; part is the inability to gather more than highly localized data in a system buried under thousands of feet of rock. Other limitations are due to the technological problems of manufacturing sensing and production equipment to operate under the hostile environment of a geothermal reservoir. Although not strictly rock mechanics, this area is related to rock mechanics and is of sufficient importance to warrant inclusion in this discussion. These limitations will be considered in greater detail later.

Although many of the basic limitations are currently subjects of research, this research is sporadic, deals with small areas, and is generally insufficient to produce the necessary large-scale resource development. The basic recommendation, therefore, is that a coordinated and expanded research effort should be initiated in this area. Although the major limitations on the development of known and proven resources lie in the areas of production and development technology, the lack of full understanding of the geology and mechanics of these systems will severely limit the timely identification and development of new geothermal resources in the future and the development of known sites to full potential. The complexity of these characteristics will dictate intermediate to long-term research programs, and it is recommended that these should be initiated as soon as practical.

Given the imperfect basic understanding of many aspects of the geology and mechanics of geothermal reservoirs, detailed projection into the intermediate and long term is a hazardous, but necessary, exercise. It is strongly recommended, therefore, that many of the major research and development areas should be the subject of preliminary feasibility studies. These feasibility studies could be of one- or two-year duration, and could be fairly low-budget items aimed at assembling all relevant current knowledge and pointing the way to the research necessary to remove the limitations.

Finally, the Subpanel strongly urges the continuation of interest and research effort into geothermal energy exploitation and development. Given sufficient effort to overcome the various problems, whether caused by geology, rock mechanics, or limitation in surface technology, geothermal resources form a potentially massive energy base whose exploitation would be environmentally acceptable.

ROCK MECHANICS LIMITATIONS IN GEOTHERMAL ENERGY EXPLORATION AND PRODUCTION

In view of the broad and diverse nature of the subject and the limited time available, it was thought to be neither possible, nor advisable, to detail completely the areas in which research is required. Thus the area of compaction mechanics, for example, has been identified as causing major limitations without detailing many of the problems and limitations that make up that area. To avoid inadvertent omissions the subject has been divided into six sections, each covering one phase of geothermal recovery, and each treated roughly in the same order as would be followed in resource development and exploitation: exploration, evaluation, drilling, stimulation, production, and environmental impact. These divisions are somewhat arbitrary and overlap in some areas, but they clarify the situation for the reader.

Exploration

Problems affecting exploration include the following:

- Imperfect characterization of geothermal resources in terms of exploration parameters
- Limited experience in applying deeper-sounding geophysical techniques such as deep-sounding magnetic and magnetotellurics to the identification of geothermal resources
- Lack of detailed knowledge of the effect of temperature on the physical, particularly electrical, properties of rocks
- Poor interpretive ability for detailed deep-sounding geophysical surveys

The search for commercial geothermal reservoirs depends mainly on the ability to recognize localities where high temperatures occur near the surface over an area sufficient for economical exploitation. Techniques exist, and are being perfected, that could be useful in obtaining this data on a regional basis. There is a growing understanding of the geological setting for potential geothermal sites, and existing geophysical techniques could be used for regional exploration. There remains, however, a need for better geological characterization of geothermal sites while potentially useful geophysical techniques are still in their infancy, particularly from the standpoint of interpretation.

For the regional identification of gross high spots, the use of deep magnetic techniques shows promise in identifying the depth of the Curie point, and hence in determining regional trends of this isotherm. In a more localized setting, magnetic, electrical, and particularly magnetotelluric techniques have a potentially significant role in exploration. These techniques suffer from imperfect knowledge of the dependence of rock properties on temperature and from poor characterization of geothermal sites. These shortcomings lead to limitations in interpreting data.

These techniques should be subjected to further research, and others should be sought and developed. This search should concentrate on techniques with a capability for deep surveying. Techniques that identify only surface abnormalities, or that identify only the first hot zone, are considered to be of limited application.

Evaluation

Barriers to successful evaluation of geothermal resources include the following:

- Inadequate down-hole techniques for characterizing the rock away from the boreholes
- Inadequate characterization of fractured formations
- Imperfect understanding of the mechanics of recharge and poorly developed techniques for identifying and tracing recharge in wet reservoirs
- Lack of down-hole instrumentation for heat-flux and conductivity measurements
- Absence of electronic components capable of sustaining high temperatures for reasonable periods
- Lack of high-temperature resistant synthetic materials for use in down-hole tools

The first stage in the evaluation of a geothermal resource would be intimately connected with the later stages of exploration, and many of the same techniques and limitations would apply. Improved early evaluation is a natural fallout from research into exploration techniques, particularly that research aimed at understanding the temperature dependence of rock physical properties and the measurement and interpretation of these properties at the surface.

In down-hole measurements, adequate techniques are not available for identifying and characterizing fractured rock systems or any rock systems away from the immediate vicinity of a borehole. Several techniques might help. These include passive seismic monitoring, precise down-hole gravimetric surveys, and hole-to-hole sonic and electrical methods. A study of the relation of surface or regional structures and the down-hole determination of the primitive-stress-field orientation could help significantly. Advances in these techniques would help to evaluate and manage sites now under development.

From the standpoint of down-hole technology, the main limitations are the poor high-temperature stability of electronic components and of synthetic materials used in down-hole tools. Many of the electronic problems can be and are being solved in the short term by the development of protected packages; eventually these problems will be overcome by the development of high-temperature stable components. Similarly the problems caused by synthetic material breakdown at high temperatures should be overcome with the continuing advance of this technology.

Further limitations were identified in the characterization of recharge for hydrothermal or steam reservoirs. Knowledge of recharge potential and areas will be essential in evaluating the availability of hot fluids and in the rational use of reinjection. Techniques currently under investigation to help in this characterization are based mainly on conventional hydrology and on the sophisticated analysis of water chemistry. These techniques, however, are not yet well understood, nor is their application to geothermal resources. This situation constitutes a major limitation to successful evaluation and management of existing reservoirs.

Drilling

The problems of successful drilling are as follows:

- Temperature limitations on drilling equipment
- Scarcity of high-temperature lubricant-mud additives for low-pressure high-loss zones
- Underdeveloped technology for temporary sealing of high-loss fracture zones

Drilling technology, in itself a wide field that continues to receive much attention, has been the subject of similar workshops. Many of the limitations identified in drilling geothermal reservoirs are not specific to geothermal energy, and most would be solved by an evolutionary rather than a revolutionary process; in any case, they are dealt with more competently in other forums. For these reasons, no limitations have been specifically identified other than those peculiar to geothermal energy.

Stimulation

Hydraulic Fracturing

Rock-mechanics limitations to hydraulic fracturing are as follows:

- Imperfect understanding of the detailed mechanisms and controls for hydraulic fracture propagation
- Lack of effective techniques for mapping fractures
- Lack of suitable high-temperature proppant-carrying fluid

Hydraulic fracturing is a critical component in the development of unfractured hot-dry-rock resources. In this development, fractures are used to establish a connection between two or more boreholes, which requires an ability to predict fracture orientation and geometry, and to determine these parameters after fracturing. It is known that fracture propagation will be controlled by the stress field and by lithology, but little is known of the interrelation of these controls, and propagation in complex natural lithologies cannot be predicted. Even if these factors were understood, the limits imposed by reservoir characterization and *in situ* stress measurement would hamper their application. So far, despite considerable research, no successful techniques are available for mapping these fractures after their production.

These factors form a major limitation on the economic development of impermeable geothermal resources. Several different approaches to the problem are needed, including a basic theoretical and experimental study of fracture mechanics in natural geological materials under various states of stress, a study of the relation between major structural trends, the *in situ* stress and artificially induced fracture geometry, and a continuation of the studies of various geophysical techniques for fracture mapping.

The whole area of defining fracture propagation and of mapping fractures is difficult and complex, and it is imperative that a considerable, long-lasting research effort be made to remove the major limitations imposed by the current state of the art.

Other less extensive problems are the lack of suitable high-temperature tools, such as impression packers and borehole televiewers, for mapping fractures at the borehole, and the absence of suitable high-temperature carrying fluids for proppants. These problems are being addressed, and the work will probably continue under the impetus of current site requirements.

Exotic Fracturing

Progress is affected in particular by the following:

- Poor understanding of thermal cracking in geological materials

A technique such as thermal cracking will be essential for full development of a hot-dry-rock resource, because it will increase the volume of rock contacted by the heat transfer fluid. A general lack of information and understanding of the detailed development of these fractures exists.

Other exotic fracturing techniques that may be applicable to geothermal development are the electrical and explosive methods. Electrical methods may be useful in the development of controlled-fracture initiation. Although these methods could be of use in geothermal developments and should be monitored, they must take low priority as far as research support in this area is concerned. Explosive fracturing has possible application in the development of extensive-volume fracturing and in connecting blind holes to natural fracture systems, but this technique is limited by the problems of developing explosives for use at the high geothermal temperatures and characterizing the fracturing produced. The desired results could probably be achieved in most cases by combinations of hydraulic and thermal fracturing, and for this reason explosive fracturing was assigned a low priority.

Chemical Stimulation

Although certain problems are identified in chemical stimulation, these are considered to be highly site-specific and to have limited overall impact. The limitations identified, therefore, are not considered to be applicable to the overall geothermal program, nor are they thought to be severe.

Production

The following are limitations to production of geothermal energy:

- Imperfect understanding of compaction mechanics of porous rocks and techniques to predict the behavior of these rocks when subject to varying pore pressures and temperatures
- Imperfect understanding of flow behavior in fractured reservoirs and the dependence of this on compaction and temperature
- Lack of monitoring instruments

The gross behavior of porous unfractured strata under varying pore pressures and temperatures is not completely understood. In fractured systems, even less is known, and flow characteristics are not well understood. The understanding available tends to be based on oversimple assumptions and to be restricted to isothermal and normal temperature conditions. The

solution of these problems is essential to the controlled operation of a geothermal reservoir and requires a major, long-term research effort in the theoretical area, in the laboratory, and in the field.

Durable instruments, capable of monitoring production, need to be developed. Some of these instruments will be used to monitor pressure, flow rate, and temperature. Current techniques and instruments need upgrading to withstand the hostile down-hole environment. Others should be developed for monitoring conditions within the reservoir, particularly changes in water/steam horizons and recharge areas. In this latter group, considerable research is needed in developing techniques to be applied to both down-hole and surface instruments.

Environmental Impact

Knowledge of the environmental impact of geothermal development is restricted by the following:

- Very limited understanding of subsurface- and surface-subsidence mechanisms
- Inadequate understanding of seismic-hazard potential resulting from production and reinjection
- Lack of understanding of the impact of reinjection on the environment and on production in terms of physical, chemical, and mechanical changes

The boundary condition for subsidence will be reservoir volume changes induced by production, reinjection, and temperature changes. An adequate understanding of the compaction mechanics of the reservoir rocks is therefore an essential prerequisite for subsidence evaluation. Even with this knowledge, little is known about the behavior of the rocks overlying a compacting reservoir, particularly in areas where fault activation may lead to discontinuous subsidence. These gaps in present knowledge constitute a serious environmental limitation to geothermal production.

In view of the tectonically active localities of many potential geothermal developments, the imperfect understanding of the relations of fluid pressures to earthquake activation creates a major limitation, particularly where reinjection is contemplated.

Summary

The limitations identified in the preceding subsections fall into two distinct groups: the strictly rock-mechanics or geoscience-based limitations and those that are esentially technological with a strong bearing on rock mechanics in the broad sense. The limiting areas, and their relevance to different types of geothermal reservoirs, are summarized in Figure 1.3.

RESEARCH PROGRAM

General Recommendations

Although many of the most urgent problems in geothermal development are not concerned with rock mechanics, timely and extensive future development will require a much better understanding of the mass behavior and properties of

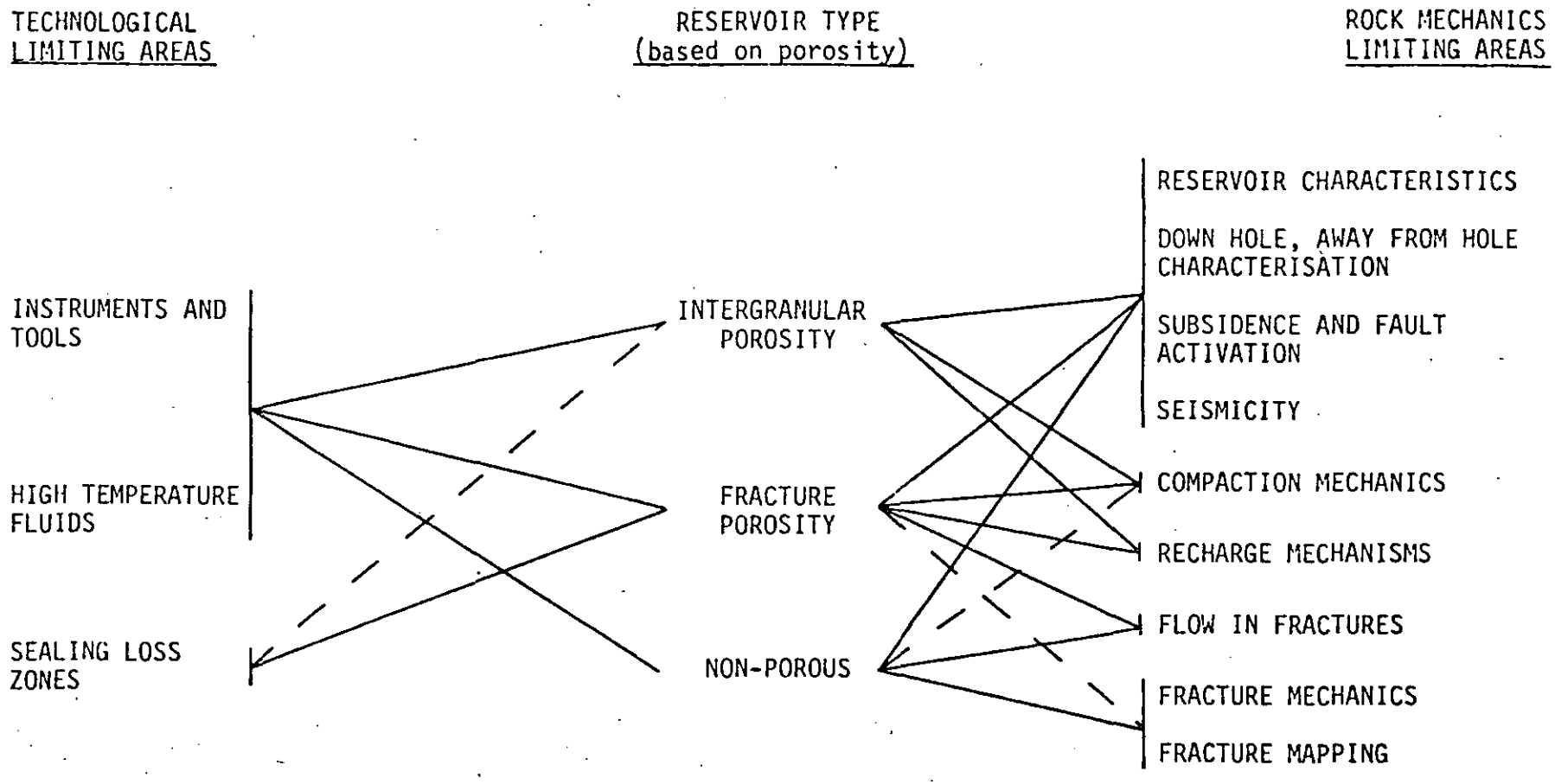

FIGURE 1.3 Relation of the various limitations to different classes of geothermal reservoirs.

geothermal reservoirs and the overlying rocks. The current level of knowledge in this area and the complexity of the problems involved demand a major research effort.

Assessing priorities for the various programs is difficult. Geothermal energy covers a wide range of rock types and production problems. Some programs are clearly most urgently needed in certain areas. In considering the limitations to the overall geothermal program, all rock mechanics research areas demand equal priority, whereas the various peripheral technological areas are of limited priority in the current study. They are undoubtedly important to the total geothermal effort but embrace research and development programs limited in nature, outside the area of the geosciences, and likely to be solved outside the geothermal program. These technological problems should, nevertheless, be kept in mind and their solution encouraged.

The Subpanel makes the following general recommendations:

- A comprehensive research program should be initiated immediately, for the purpose of removing the rock mechanics limitations to future geothermal development. This program should be initiated and continued with medium effort over a long period rather than with great effort for a short time.
- The program should be carried on in diverse research localities and by researchers with diverse backgrounds but with careful coordination by some central body.
- Adequate dissemination and interplay of the various research areas should be carried into other overlapping subject areas.
- Development in the various peripheral technological areas should be encouraged to improve down-hole techniques and equipment as soon as possible.

Specific Recommendations for Research

With these general purposes in mind the following specific research programs are recommended; the programs are divided into five major areas each containing several related programs. No priority is implied in the order of these programs. In certain programs an initial feasibility study is recommended. This study is envisaged as a one- or two-man-year, low-cost study, to define the state of the art in one particular area and to identify and evaluate the most promising lines of research.

Characterization, Identification, and Evaluation of Potential Geothermal Sites

- The characterization of the geological setting of commercial geothermal sites and the isolation of geological indicators that may help to identify future sites.
- An investigation of the influence of temperature on the physical properties of rocks from geothermal areas, particularly those properties that may apply to geophysical prospecting techniques.
- The development of geophysical techniques capable of identifying and characterizing geothermal sites, including development of both equipment and interpretation techniques. This program should be preceded by a feasibility study and should be closely related to the previous program.
- The application of existing and new geophysical techniques to geothermal sites, directed initially toward gaining experience in the use of

present techniques and later toward evaluating techniques developed in the preceding program.

- The identification and development of down-hole passive and active logging techniques for the characterization of formations away from the immediate vicinity of the borehole, particularly in fractured reservoirs.

Characterization of Recharge in Wet Geothermal Reservoirs

- The investigation of recharge mechanisms by hydrological and geological interpretation methods and by flow studies.
- The development of techniques for identifying recharge areas and geothermal fluid provenance. This development should be preceded by a feasibility study.

The Mechanics and Characterization of Artificial Fracturing

- An investigation of the influence of stress and lithology on fracture propagation and orientation and the development of mathematical techniques for predicting this influence.
- An investigation of known geological structures as possible indicators of preferred orientations or induced fractures.
- The development of techniques for determining the down-hole triaxial stress field.
- The development of techniques to be used for mapping fractures. This development should be preceded by a feasibility study.
- An investigation of thermal fracturing in stressed rocks and the development of mathematical techniques for predicting this.

Compaction, Thermal Mechanics, and Flow Studies

- The evaluation of existing theories for the behavior of porous rocks under elevated and varying pore pressures and temperatures, upgrading and extension of these theories, and development of new models where necessary.
- The development of theories and models for the behavior of naturally fractured rocks under elevated and varying pore pressures and temperatures.
- An investigation of fluid flow in natural fracture systems undergoing compaction and the development of theory and models to predict this flow.

Environmental Impact Studies

- The development of models for the behavior of rock masses above compacting reservoirs, including those where fault activation is possible. The models are to be based on data for rock properties and are to be evaluated against known areas of subsidence.
- An investigation of the effect of fluid pressures and of temperature on seismic activation in geothermal areas, with particular reference to reinjection.

CONCLUSIONS

Limitations imposed by rock mechanics on geothermal development have been identified in the areas of exploration, evaluation, drilling, stimulation, production, and environmental impact. These limitations arise from major

gaps in the present understanding of the nature and mechanics of geothermal reservoirs, together with some peripheral problems in technology caused by the hostile environment in a geothermal reservoir.

These limitations do not form absolute barriers to the current development of geothermal resources, but they will severely curtail future development. They form absolute limitations to the rapid, economic, and efficient development of a major, environmentally acceptable source of energy to its full potential.

The Subpanel recommends that a medium-level, long-term research program be initiated immediately to start to determine many of the unknowns in geothermal-resource exploration and production. Although this program should draw on diverse research talents, it should operate as an integrated unit by central coordination. The program should include concurrent efforts in the areas of site characterization and identification, recharge characterization, fracture propagation and orientation, compaction and thermal mechanics, fluid flow in fractured media, and subsidence and seismic hazards evaluation. Development of down-hole equipment and techniques capable of withstanding the harsh geothermal environment should also be encouraged.

In summary, geothermal energy forms a potentially massive resource for this nation, but the nature and mechanics of the reservoirs are poorly understood. It is imperative that this imperfect understanding be subjected to a large, well-coordinated research program now, if this resource is to reach its full potential in the future.

Suggested Methods for Determining Water Content, Porosity, Density, Absorption and Related Properties and Swelling and Slake-Durability Index Properties

PART 1: SUGGESTED METHODS FOR DETERMINING WATER CONTENT, POROSITY, DENSITY, ABSORPTION AND RELATED PROPERTIES

NOTES

(i) Mechanical significance of porosity and density data

The presence of pores in the fabric of a rock material decreases its strength, and increases its deformability. A small volume fraction of pores can produce an appreciable mechanical effect.

Information on the porous nature of rock materials is frequently omitted from petrological descriptions, but is required if these descriptions are to be used as a guide to mechanical performance. Sandstones and carbonate rocks in particular occur with a wide range of porosities and hence of mechanical character; igneous rocks that have been weakened by weathering processes also have typically high porosities.

Most rocks have similar grain densities and therefore have porosity and dry density values that are highly correlated (see note (v) equation 4). A low density rock is usually highly porous. It is often sufficient, therefore, to quote values for porosity alone, but a complete description requires values for both porosity and density.

Microscopic techniques used to determine volumetric content of mineral grains, do not provide a sufficiently accurate estimate of volumetric pore content, and experimental techniques are required. However, microscopy and also techniques such as mercury injection and permeability testing, can provide useful supplementary information on the shape and size of pores.

(ii) Nature of the rock sample

A representative sample for testing should generally comprise several rock lumps, each an order of magnitude larger than the largest grain or pore size. Microfissures of similar size to that of a rock will cause erratic results; their presence should be noted and if possible the lump size increased or reduced to specifically include or exclude the influence of such fissures.

The sample should if possible be large, to minimise the influence of experimental error. Alternative test methods are available calling for samples in different form; selection from among these should be based on the nature of rock to be tested.

(iii) Rock constituents

The following terms and symbols will be used to denote the masses and volumes of rock constituents when calculating physical properties such as porosity or density.

Grains (the solid component of the sample), mass M_s, volume V_s

Pore water, mass M_w, and volume V_w

Pore air, zero mass and volume V_a

Pores (voids), with volume $V_v = V_w + V_a$

Bulk sample mass $M = M_s + M_w$

Bulk sample volume $V = V_s + V_v$

Density of water ρ_w = mass of water per unit volume

(iv) Definitions, terminology and preferred S.I. units

Those physical properties pertinent to the methods of test about to be described may be defined in terms of the rock sample constituents listed above.

Water content w	$= \frac{M_w}{M_s} \times 100$	(%)
Degree of saturation S_r	$= \frac{V_w}{V_v} \times 100$	(%)
Porosity n	$= \frac{V_v}{V} \times 100$	(%)
Void ratio e	$= \frac{V_v}{V_s}$	(–)
Density = bulk density ρ (mass density)	$= \frac{M}{V} = \frac{M_s + M_v}{V}$	$\frac{(kg)}{(m^3)}$

Relative density d (specific gravity)	$= \frac{\rho}{\rho_w}$	(−)
Dry density ρ_d	$= \frac{M_s}{V}$	$\frac{(kg)}{(m^3)}$
Dry relative density (dry) d_d (specific gravity)	$= \frac{\rho_d}{\rho_w}$	(−)
Saturated density ρ_{sat}	$= \frac{M_s + V_v\rho_w}{V}$	$\frac{(kg)}{(m^3)}$
Saturated relative density d_{sat} (saturated specific gravity)	$= \frac{\rho_s}{\rho_w}$	(−)
Grain density ρ_s (density of solids)	$= \frac{M_s}{V_s}$	$\frac{(kg)}{(m^3)}$
Grain relative density d_s (grain specific gravity)	$= \frac{\rho_s}{\rho_s}$	(−)
Unit weight γ	$= \rho g$	$\frac{(N)}{(m^3)}$

(v) *Interdependence equations*

The physical properties defined above are interrelated, so that any one property may be calculated if others are known.

For simplicity only three properties will be referred to in the text, namely, water content, porosity and dry density of rock. The equations listed below may be used to calculate any of the remaining properties from these three.

Whereas water content, degree of saturation and porosity are usually expressed as percentages, the void ratio is usually expressed as a dimensionless ratio. The following interdependence equations have been given to conform to the above.

$$S_r = \frac{100w\rho_d}{n\rho_w} \quad (\%)$$

$$e = \frac{n}{100 - n} \quad (-)$$

$$\rho = \left(1 + \frac{w}{100}\right)\rho_d \quad \frac{(kg)}{(m^3)}$$

$$\rho_s = \frac{100\rho_d}{100 - n} \quad \frac{(kg)}{(m^3)}$$

(vi) *Determination of the grain mass* M_s

The grain mass M_s of the sample is defined as the equilibrium mass of the sample after oven drying at a temperature of 105°C.

A thermostatically controlled, ventilated drying oven capable of maintaining a temperature of 105°C accurate to 3°C for a period of at least 24 h is required.

The sample is regarded as 'oven dry' when successive mass determinations at intervals of 4 hr yield values differing by less than 0.1% of the sample mass.

The sample should not take up water in the interval between drying and mass determination. Where necessary the sample container should be covered with an airtight lid and stored in a desiccator during cooling.

(vii) *Determination of the bulk volume V*

Caliper method. The bulk volume of specimens in the form of regularly shaped prisms or cylinders may be calculated from vernier or micrometer caliper measurements. An average of several readings for each dimension, each accurate to 0.1 mm, should be used in the calculation of bulk volume.

Buoyancy method. The bulk volume of regular or irregular specimens may be calculated using Archimedes principle, from the difference between saturated-surface-dry and saturated-submerged sample weights. The method is not suited to friable, swelling or slaking rocks.

The sample is saturated by water immersion in a vacuum of less than 800 Pa (6 torr) for a period of at least one hour, with periodic agitation to remove trapped air.

The sample is then transferred underwater to a basket in an immersion bath. Its saturated-submerged mass M_{sub} is determined to an accuracy of 0.1 g from the difference between the saturated-submerged mass of the basket plus sample and that of the basket alone.

The sample is then removed from the immersion bath and surface dried with a moist cloth, care being taken to remove only surface water and to ensure that no rock fragments are lost. Its saturated-surface-dry mass M_{sat} is determined to an accuracy of 0.1 g.

The sample bulk volume is calculated as

$$V = \frac{M_{sat} - M_{sub}}{\rho_w}.$$

Mercury displacement method. High surface tension prevents mercury penetrating all but the largest pores in rock. The specimen is forced under mercury and its volume determined from the displaced fluid volume. A calibrated tube may be incorporated in the apparatus for this purpose, or the displacement may be measured by a micrometer screw gauge—electric contact technique. Alternatively a technique may be employed where the displaced mercury volume is obtained by mass determination. The apparatus should give results accurate to 0.5% of the specimen bulk volume, and should be periodically calibrated using a standard sphere or cylinder.

Water displacement method. The bulk volume of a saturated-surface-dry sample may be determined by water displacement using a technique similar to that for mercury displacement. Alternatively the dry or partially dry sample may be coated in wax or plastic and its bulk volume determined from the water volume displaced by the coated sample, corrected for the volume of coating material. The method requires accurate determination of coating volume and is best applied to large bulk samples where other techniques are impractical.

(viii) *Determination of pore volume (volume of voids)* V_v

Saturation method. The pore volume of a rock sample may be determined from the difference between saturated-surface-dry and oven-dry masses. The sample is saturated by water immersion in a vacuum and its saturated-surface-dry mass M_{ssd} is determined. It is then oven dried to determine the grain mass M_s.

The pore volume V_v is calculated as

$$V_v = \frac{M_{ssd} - M_s}{\rho_w}.$$

The Washburn–Bunting method (Washburn & Bunting, 1922). A rock specimen is oven-dried and immersed in mercury. The pressure on the mercury is reduced so that the pore air expands, leaves the rock and is trapped above the mercury column. The volume of pore air V_a is measured directly in a calibrated tube, after pressure has been equalised with that of the atmosphere. The method is rapid but is best suited to rocks with high porosity.

(ix) *Determination of grain volume* V_s

Boyle's law method. The pressure-volume relationship for a container filled with gas only is obtained, then for the same container filled with specimen plus gas. The difference in compressibility is due to the volume V_s of incompressible grains, and this volume may be calculated from the results. One type of Boyle's law single-cell porosimeter employs a graduated mercury pump to measure volume displacement, together with a Bourdon gauge to measure pressure change. Boyle's law double cell techniques employ pressure equalization between two containers at different initial pressures.

Pulverization method. After determination of bulk volume and grain mass, the oven-dry sample is pulverized and its grain volume G_v determined by displacement of an equivalent volume of liquid (e.g. toluene) in a volumetric flask.

Porosity calculated from bulk volume and grain volume using the pulverization method is termed *total* porosity, since the pore volume obtained includes that of 'closed' pores. Other techniques give *effective* porosity values since they measure the volume of interconnected pores only.

1. SUGGESTED METHOD FOR DETERMINATION OF THE WATER CONTENT OF A ROCK SAMPLE

1. SCOPE

This test is intended to measure the mass of water contained in a rock sample as a percentage of the oven-dry sample mass.

2. APPARATUS

(a) An oven capable of maintaining a temperature of 105°C to within 3°C for a period of at least 24 hr.

(b) A sample container of non-corrodible material, including an airtight lid.

(c) A desiccator to hold sample containers during cooling.

(d) A balance of adequate capacity, capable of weighing to an accuracy of 0.01% of the sample weight.

3. PROCEDURE

(a) The container with its lid is cleaned and dried, and its mass A determined.

(b) A representative sample comprised at least 10 lumps each having either a mass of at least 50 g or a minimum dimension of ten times the maximum grain size, whichever is the greater, is selected. For *in situ* water content determination sampling, storage and handling precautions should be such that water content remains within 1% of the *in situ* value.

(c) The sample is placed in the container, the lid replaced and the mass B of sample plus container determined.

(d) The lid is removed and the sample dried to constant mass at a temperature of 105°C.

(e) The lid is replaced and the sample allowed to cool in the desiccator for 30 min. The mass C of sample plus container is determined.

4. CALCULATION

$$\text{Water content } w = \frac{\text{pore water mass } M_w}{\text{grain mass } M_s} \times 100\%$$

$$= \frac{B - C}{C - A} \times 100\%.$$

5. REPORTING OF RESULTS

The water content should be reported to the nearest 0.1% stating whether this corresponds to *in situ* water content, in which case precautions taken to retain water during sampling and storage should be specified.

2. SUGGESTED METHOD FOR POROSITY/DENSITY DETERMINATION USING SATURATION AND CALIPER TECHNIQUES

1. SCOPE

(a) This test is intended to measure the porosity, the dry density and related properties of a rock sample in the form of specimens of regular geometry.

(b) The method should only be used for non-friable, coherent rocks that can be machined and do not appreciably swell or disintegrate when oven dried or immersed in water. The method is recommended when regularly shaped specimens are required for other test purposes.

2. APPARATUS

(a) An oven capable of maintaining a temperature of 105°C to within 3°C for a period of at least 24 hr.

(b) A desiccator to hold specimens during cooling.

(c) A measuring instrument such as vernier or micrometer caliper, capable of reading specimen dimensions to an accuracy of 0.1 mm.

(d) Vacuum saturation equipment such that the specimens can be immersed in water under a vacuum of less than 800 Pa (6 torr) for a period of at least one hour.

(e) A balance of adequate capacity, capable of determining the mass of a specimen to an accuracy of 0.01%.

3. PROCEDURE

(a) At least three specimens from a representative sample of a material are machined to conform closely to the geometry of a right cylinder or prism. The minimum size of each specimen should either be such that its mass is at least 50 g (for an average density rock a cube with sides of 27 mm will have sufficient mass) or such that its minimum dimension is at least ten times the maximum grain size, whichever is the greater.

(b) The specimen bulk volume V is calculated from an average of several caliper readings for each dimension. Each caliper reading should be accurate to 0.1 mm.

(c) The specimen is saturated by water immersion in a vacuum of less than 800 Pa (6 torr) for a period of at least 1 hr, with periodic agitation to remove trapped air.

(d) The specimen is removed and surface dried using a moist cloth, care being taken to remove only surface water and to ensure that no fragments are lost. Its saturated-surface-dry mass M_{sat} is determined.

(e) The specimen is dried to constant mass at a temperature of 105°C, allowed to cool for 30 min in a desiccator, and its mass is determined to give grain mass M_s. Specimens in this test are generally of sufficient coherence not to require containers, but these should be used if the rock is at all friable or fissile.

4. CALCULATIONS

Pore volume $$V_v = \frac{M_{sat} - M_s}{\rho_w}$$

Porosity $$n = \frac{100V_v}{V}\%$$

Dry density of rock $$\rho_d = \frac{M_s}{V}.$$

5. REPORTING OF RESULTS

(a) Individual results for at least three specimens per rock sample should be reported, together with average results for the sample.

(b) Density values should be given to the nearest 10 kg/m^3 and porosity values to the nearest 0.1%.

(c) The report should specify that bulk volume was obtained by caliper measurement and that pore volume was obtained by water saturation.

3. SUGGESTED METHOD FOR POROSITY/DENSITY DETERMINATION USING SATURATION AND BUOYANCY TECHNIQUES

1. SCOPE

(a) The test is intended to measure the porosity, the dry density and related properties of a rock sample in the form of lumps or aggregate of irregular geometry. It may also be applied to a sample in the form of specimens of regular geometry.

(b) The method should only be used for rocks that do not appreciably swell or disintegrate when oven-dried and immersed in water.

2. APPARATUS

(a) An oven capable of maintaining a temperature of 105°C to within 3°C for a period of at least 24 hr.

(b) A sample container of non-corrodible material, including an air-tight lid.

(c) A desiccator to hold sample containers during cooling.

(d) Vacuum saturation equipment such that the sample can be immersed in water under a vacuum of less than 800 Pa (6 torr) for a period of at least 1 hr.

(e) A balance of adequate capacity, capable of determining the mass of a specimen to an accuracy of 0.01%.

(f) An immersion bath and a wire basket or perforated container, such that the sample immersed in water can be freely suspended from the stirrup of the balance to determine the saturated-submerged mass. The basket should be suspended from the balance by a fine wire so that only the wire intersects the water surface in the immersion bath.

3. PROCEDURE

(a) A representative sample comprising at least 10 lumps of regular or irregular geometry, each having either a mass of at least 50 g or a minimum dimension of at least 10 times the maximum grain size, whichever is the greater, is selected. The sample is washed in water to remove dust.

(b) The sample is saturated by water immersion in a vacuum of less than 800 Pa (6 torr) for a period of at least one hour, with periodic agitation to remove trapped air.

(c) The sample is then transferred under water to the basket in the immersion bath. Its saturated-submerged mass M_{sub} is determined to an accuracy of 0.1 g from the difference between the saturated-submerged

mass of the basket plus sample and that of the basket alone.

(d) The sample container with its lid is cleaned and dried, and its mass A is determined.

(e) The sample is removed from the immersion bath and surface-dried with a moist cloth, care being taken to remove only surface water and to ensure that no rock fragments are lost. The sample is transferred to the sample container, the lid replaced, and the mass B of saturated-surface-dry sample plus container is determined.

(f) The lid is removed and the sample dried to constant mass at a temperature of 105°C, the lid replaced and the sample allowed to cool for 30 min in a dessicator. The mass C of oven-dry sample plus container is measured.

4. CALCULATIONS

4. Saturated-surface-dry mass $M_{sat} = B - A$

Grain weight $M_s = C - A$

Bulk volume $V = \dfrac{M_{sat} - M_{sub}}{\rho_w}$

Pore volume $V_v = \dfrac{M_{sat} - M_s}{\rho_w}$

Porosity $n = \dfrac{100V_v}{V}\ \%$

Dry density of rock $\rho_d = \dfrac{M_s}{V}$.

5. REPORTING OF RESULTS

(a) The report should include porosity and dry density values for the sample, and should specify that bulk volume was obtained by a buoyancy technique and that pore volume was obtained by water saturation.

(b) Density values should be given to the nearest 10 kg/m^3 and porosity values to the nearest 0.1%.

4. SUGGESTED METHOD FOR POROSITY/DENSITY DETERMINATION USING MERCURY DISPLACEMENT AND GRAIN SPECIFIC GRAVITY TECHNIQUES

1. SCOPE

(a) The test is intended to measure the porosity, the dry density and related properties of a rock sample in the form of lumps or aggregate of irregular geometry. It is particularly suitable if the rock material is liable to swell or disintegrate if immersed in water. The test may also be applied to regularly shaped rock specimens or to coherent rock materials, but other techniques are usually found more convenient in these cases.

2. APPARATUS

(a) An oven capable of maintaining a temperature of 105°C to within 3°C for a period of at least 24 hr. It should have forced ventilation exhausting to outside atmosphere.

(b) Specimen containers of non-corrodible material, including airtight lids.

(c) A dessicator to hold specimen containers during cooling.

(d) A balance of adequate capacity, capable of mass determination to 0.001 g.

(e) A mercury-displacement volume measuring apparatus capable of measuring specimen volume to 0.5%.

(f) Grinding equipment to reduce the sample to a pulverized powder less than 150 μm in grain size.

(g) A calibrated volumetric flask and stopper (conveniently 50 cm^3).

(h) A constant temperature water bath.

(i) A vacuum apparatus capable of maintaining a vacuum with a pressure of less than 800 Pa (6 torr).

(j) A soft brush of camel hair or of a similar softness.

3. PROCEDURE

(a) A representative sample is selected comprising at least ten rock lumps, the shape and size of lumps suiting the capabilities of the volume measuring apparatus. The minimum size of each lump should preferably be either such that its mass exceeds 50 g or such that its minimum dimension is at least ten times the maximum grain size, whichever is the greater. Specimens of swelling or fissile rock should be sampled and stored to retain water content to within 1% of its *in situ* value prior to testing.

(b) Each specimen is brushed to remove loose material and its volume V is measured by mercury displacement. Mercury adhering to the specimen is carefully removed, ensuring that no rock fragments are lost.

(c) The specimen container with its lid is cleaned, dried and its mass A is determined.

(d) The specimen is placed in the container, the lid replaced and mass B of container plus specimen at initial water content is determined.

(e) The lid is removed and the specimen oven dried to constant mass at a temperature of 105°C and allowed to cool for 30 min in a desiccator. The mass C of container plus oven-dry specimen is determined.

(f) Steps (b)–(e) are repeated for each specimen in the sample.

(g) Together the specimens are crushed and ground to a grain size not exceeding 150 μm. A number of representative sub samples of about 15 g of the pulverized material are selected and oven-dried.

(h) The mass D of a clean, dry volumetric flask plus stopper is determined to 0.001 g.

(i) The flask is filled with a fluid such as toluene that is non-reactive with the rock, is brought to equilibrium temperature in the constant temperature bath, and the

liquid level is adjusted accurately to the 50 cm³ graduation. The flask is removed, stoppered and its mass E determined to 0.001 g.

(j) The flask is emptied and dried, and the 15 g subsample of dry, pulverized rock added with the aid of a funnel. The mass F of flask, sample and stopper is measured to 0.001 g.

(k) The flask and subsample are evacuated for about 20 min and sufficient fluid added to thoroughly wet the sample. Further fluid is then added and the flask carefully evacuated to remove air. The flask is replaced in the constant temperature water bath and the liquid level adjusted accurately to the 50 cm³ graduation.

(l) The stoppered flask with its contents is allowed to cool and its mass G is determined to 0.001 g.

(m) Steps (j)–(l) are repeated for each subsample of pulverized material.

4. CALCULATIONS

(a) Water content $$w = \frac{B - C}{C - A} \times 100\%$$

(b) Grain density $$\rho_s = \frac{F - D}{V_f\left(1 - \frac{G - F}{E - D}\right)}$$

where V_f = calibrated volume of flask, usually 50 cm³

(c) Grain mass $$M_s = C - A$$

(d) Dry density of rock $$\rho_d = \frac{M_s}{V}$$

(e) Porosity $$n = \frac{100(\rho_s - \rho_d)}{\rho_s}\%.$$

5. REPORTING OF RESULTS

(a) Individual dry density values for each specimen in the sample should be reported, together with average values for the sample. Porosity values for each subsample should also be reported together with the average value.

(b) The report should specify that the bulk volume was obtained using a mercury displacement technique, and that the porosity was calculated from grain volume measurements using a pulverization technique.

(c) The grain density or grain specific gravity for the sample should be reported. The water content at which bulk volume measurement took place should be specified, stating whether this corresponds to *in situ* water content.

(d) Density values should be given to the nearest 10 kg/m³ and porosity values to the nearest 0.1 percent.

5. SUGGESTED METHOD FOR POROSITY/DENSITY DETERMINATION USING MERCURY DISPLACEMENT AND BOYLE'S LAW TECHNIQUES

1. SCOPE

(a) This test is intended to measure the porosity, the dry density and related properties of a rock sample. A sample in the form of specimens of a specific size and shape to suit the apparatus is usually required to ensure accurate results.

(b) The method should only be used for rocks that do not shrink appreciably during oven-drying.

2. APPARATUS

The procedure given below relates to a test using the Kobe type of single cell Boyle's Law porosimeter (Fig. 1). Any similar apparatus of equivalent accuracy may however be used. The apparatus consists essentially of the following:

Oven drying equipment:

(a) An oven capable of maintaining a temperature of 105°C to within 3°C for a period of at least 24 hr.

(b) A specimen container of non-corrodible material including an airtight lid.

(c) A desiccator to hold specimen containers during cooling.

(d) A balance of adequate capacity, capable of determining the mass of a specimen to an accuracy of 0.01%. A Boyle's law porosimeter such as a Kobe porosimeter having the following features:

(e) A mercury screw-piston pump with micrometer graduated to measure the volume of displaced mercury to an accuracy of 0.01 cm³. Conveniently one turn of the screw pump changes the volume of the specimen chamber by 1 cm³.

(f) A specimen chamber with removable cap to allow insertion of the specimen.

(g) A sight glass inscribed with a reference line, an electric indicator-contact or other means of registering a mercury datum level in the cap.

(h) A gas inlet and outlet, each with a shutoff valve, also a source of inert gas such as helium. Air may be used with some loss of accuracy, but must be adequately dried.

(i) A precision pressure gauge or pressure transducer with a range from 100 kPa to about 400 kPa, connected to measure the gas pressure in the specimen chamber.

3. PROCEDURE

(a) At least three specimens are selected from a representative sample of material and each specimen is tested separately to obtain an average result for the sample. The size and shape of a specimen should allow only a small clearance with the specimen chamber to

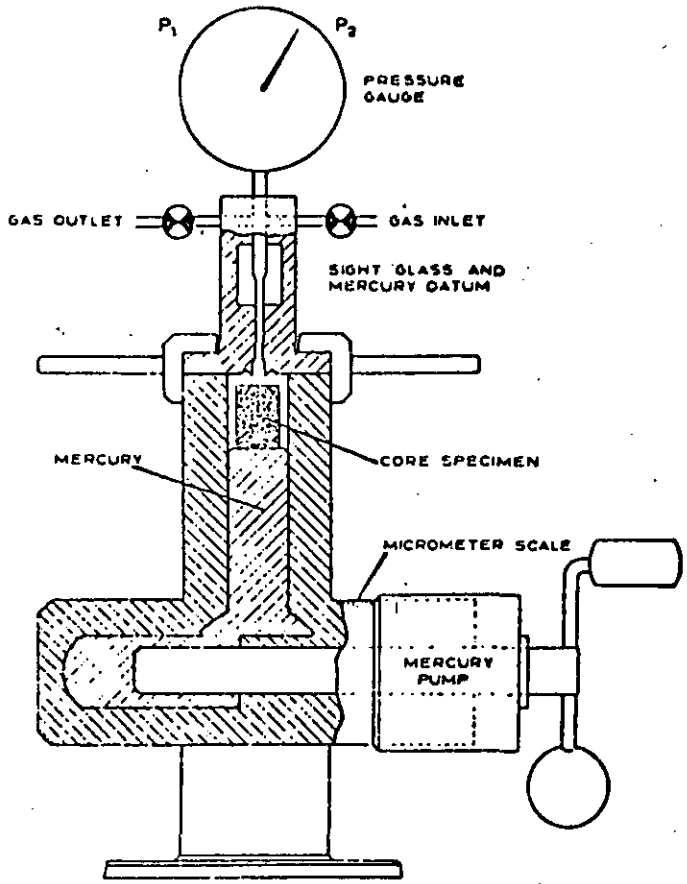

Fig. 1. Schematic diagram of a Kobe Boyle's law porosimeter.

ensure accurate results. The chamber is usually cylindrical and accepts a standard size of rock core. The size of each specimen should preferably be either such that its mass is a minimum of 50 g or that its minimum dimensions are at least ten times the maximum grain size, whichever is the greater.

(b) The specimen container with its lid is cleaned, dried and its mass A is determined.

(c) The specimen is placed in the container, dried to constant mass at a temperature of 105°C and the lid is replaced. It is allowed to cool for 30 min in a desiccator, and the mass B of oven-dry specimen plus container is determined.

(d) Use of the porosimeter: the mercury pump reading at the start of each compression or displacement cycle is termed the 'start point'. Inlet and outlet valves are closed at the start of a compression cycle so that the initial pressure P_1 is atmospheric. The start point and also the pressure P_2 at the end of a compression cycle are usually selected as standard for the apparatus, to ensure that the specimen still floats on mercury at the end of the cycle, hence avoiding imbibition that might occur if specimens became deeply immersed.

(e) To flush the specimen chamber with gas; inlet valve is closed, the outlet opened and the pump advanced until mercury reached the datum. The outlet is then half shut, the inlet opened and the pump retracted to beyond the start point. The inlet, then the outlet valve is closed.

(f) To determine the compression factor C_f for the cell: the specimen chamber is first flushed with gas, the outlet valve opened and the pump advanced to the start point. The outlet valve is shut with the specimen chamber at atmospheric pressure P_1. The pump is advanced and a micrometer reading C_0 taken when the pressure reaches P_2. The chamber is again flushed with gas, and with the outlet valve open the pump is advanced to a new start point 10 cm^3 beyond the original one. The outlet is closed with the chamber at atmospheric pressure P_1 and the pump advanced, a micrometer reading C_1 being taken when the pressure again reaches P_2.

The compression factor is computed from the formula:

$$C_f = \frac{10}{10 - (C_0 - C_1)}.$$

This factor is dependent on ambient pressure and should be periodically checked.

(g) Each test comprises a displacement stroke followed by a compression stroke with the specimen chamber empty (a blank run), then a displacement

stroke followed by a compression stroke with the specimen in the chamber. The procedure is as follows:

(h) With the inlet valve shut and the outlet open, the pump is advanced until the mercury reaches the datum. The micrometer reading R_1 is recorded.

(i) The chamber is flushed with gas, the pump advanced to the start point and the valves closed with the chamber at atmospheric pressure P_1. The pump is advanced and a micrometer reading R_2 recorded when the pressure reaches P_2.

(j) The specimen is removed from the desiccator and inserted in the chamber. The chamber is flushed with gas and step (h) repeated, recording the displacement stroke micrometer reading R_3 at which mercury reaches the datum.

(k) Step (i) is repeated, recording the compression stroke micrometer reading R_4 when the pressure again reaches P_2.

4. CALCULATIONS

Bulk volume $B_v = R_3 - R_1$

Grain volume $G_v = C_f(R_4 - R_2)$

Grain weight $G_w = B - A$

Porosity $n = \frac{B_v - G_v}{B_v} \times 100\%$

Dry density of rock $\rho_d = G_w/B_v$.

5. REPORTING OF RESULTS

(a) Individual dry density and porosity values for each specimen in the sample should be recorded, together with average values for the sample.

(b) The report should specify that the bulk volume was obtained using a mercury displacement technique, and that the porosity was calculated from grain volume measurements using a Boyle's law technique.

(c) Density values should be given to the nearest kg/m^3 and porosity values to the nearest 0.1 porosity percent.

6. SUGGESTED METHOD FOR VOID INDEX DETERMINATION USING THE QUICK ABSORPTION TECHNIQUE

1. SCOPE

(a) This test is intended to measure the void index, defined as the mass of water contained in a rock sample after a one hour period of immersion, as a percentage of its initial desiccator-dry-mass.

(b) The index is correlated with porosity, hence also with such properties as degree of weathering or alteration. The test is designed to call for a minimum of equipment. Where suitable equipment is available, however, the porosity and density of the rock material should be determined directly using techniques such as those proposed earlier (methods 2–5).

(c) The test should only be used for rocks that do not appreciably disintegrate when immersed in water.

2. APPARATUS

(a) A sample container of non-corrodible material, water tight and of sufficient capacity to contain the sample packed in dehydrated silica gel.

(b) A quantity of dehydrated silica gel.

(c) A balance of adequate capacity, accurate to 0.5 g.

3. PROCEDURE

(a) A representative sample is selected comprising at least ten rock lumps. The size of each lump should be such that its mass exceeds 50 g or such that its minimum dimension is at least ten times the maximum grain size, whichever is the greater.

(b) The sample in an air-dry condition is packed into the container, each lump separated from the next and surrounded by crystals of dehydrated silica gel. The container is left to stand for a period of 24 hr.

(c) The container is emptied, the sample removed, brushed clean of loose rock and silica gel crystals and its mass A determined to 0.5 g.

(d) The sample is replaced in the container and water is added until the sample is fully immersed. The container is agitated to remove bubbles of air and is left to stand for a period of one hour.

(e) The sample is removed and surface-dried using a moist cloth, care being taken to remove only surface water and to ensure that no fragments are lost. The mass B of the surface-dried sample is determined to 0.5 g.

4. CALCULATION

Void index $I_v = \frac{B - A}{A} \times 100\%$.

5. REPORTING OF RESULTS

(a) The void index for the sample should be reported to the nearest 1%.

(b) The report should specify that the void index is defined as the water content after desiccator drying followed by a one-hour period of immersion.

REFERENCES

1. American Petroleum Institute. API recommended practice for core-analysis procedure. Am. Petrol. Inst. Recommended Practice RP 40 (1960).
2. British Standards Institution. Methods for sampling and testing mineral aggregates, sands and fillers. British Standard 812 (1967).
3. British Standards Institution. Methods of testing soils for civil engineering purposes. British Standard 1377 (1967).
4. Buell A. W. Porosity and permeability analysis. In *Subsurface Geologic Methods*. Colorado Sch. Mines. pp. 168–179 (1949).

5. Duncan N. Rock mechanics and earthworks engineering part 5: quantitative classification of rock materials. *Muck Shifter*, October pp. 39-47 (1966).
6. Franklin J. A. Classification of rock according to its mechanical properties. Ph.D. Thesis, London University (1970).
7. Hamrol A. A quantitative classification of the weathering and weatherability of rocks. *5th Int. Conf. Soil Mech. Eng.* 2, 771, Paris (1961).
8. Hanes F. E. Determination of porosity, specific gravity, absorption and permeability, and details of sample preparation for various other rock studies Appendix II in Jet Piercing Research Project, Mines Branch Investigation Report. IB 62-27, Dept. Mines and Tech. Surveys, Ottawa. pp. 332-358 (1962).
9. Jenkins R. B. Accuracy of porosity determinations *Proc. 1st Ann. Meeting, Soc. Professional Well Log Analysts*, Tulsa, Oklahoma. 15 pp (1960).
10. Manger G. E. Method dependent values of bulk, grain and pore volume as related to observed porosity. U.S. Geol. Survey Bul. N 1203, 20 pp (1966).
11. Morgenstern N. R. & Phukan A. L. T. Non linear deformation of a sandstone. *Proc. 1st Int. Congress Rock Mech.* Lisbon 1, 543-548 (1966).
12. Obert L., Windes S. L., Duvall W. I. Standardised tests for determining the physical properties of mine rock. U.S. Bur. Mines Report of Investigations 3891 (1946).
13. Washburn E. W. & Bunting E. N. Determination of porosity by the method of gas expansion. American Ceramic Soc. 5, No. 48, 112 (1922).

PART 2: SUGGESTED METHODS FOR DETERMINING SWELLING AND SLAKE-DURABILITY INDEX PROPERTIES

NOTES

(i) Mechanical significance of swelling and slake-durability data

An abundant class of rock materials, notably those with high clay content, are prone to swelling, weakening or disintegration when exposed to short term weathering processes of a wetting and drying nature. Special tests are necessary to predict this aspect of mechanical performance. These tests are index tests; they are best used in classifying and comparing one rock with another. The swelling strain index should not, for example, be taken as the actual swelling strain that would develop *in situ*, even under similar conditions of loading and of water content.

These tests simulate natural wetting and drying processes. Other types of test are better suited to estimating resistance to such weathering agencies as frost, salt crystallization or attrition (De Puy, 1965).

(ii) Nature of the rock sample

Where possible undisturbed rock specimens should be tested, since rock fabric has an important effect on the other properties to be measured. Where the sample is too weak or too broken to allow preparation of undisturbed specimens, as is usually the case with joint-filling materials for example, the swelling tests may be carried out on remoulded specimens. Remoulding should be according to standard procedures for soil compaction, and the procedure followed should be described when reporting the test results.

(iii) Application of the tests to hard and soft rocks

These tests are commonly required for classification or characterization of the softer rock materials. They may also be used, however, for characterization of harder rocks where the rock condition, its advanced state of weathering for example, indicates that they are appropriate.

Rocks that disintegrate during the tests should be further characterized using soil classification tests such as determination of the liquid and plastic limits, the grain size distribution, or the content and type of clay minerals present.

1. SUGGESTED METHOD FOR DETERMINATION OF THE SWELLING PRESSURE INDEX UNDER CONDITIONS OF ZERO VOLUME CHANGE

1. SCOPE

This test is intended to measure the pressure necessary to constrain an undisturbed rock specimen at constant volume when it is immersed in water.

2. APPARATUS

The apparatus may be adapted from that used for soil consolidation testing, and consists essentially of the following:

(a) A metal ring for rigid radial restraint of the specimen, polished and lubricated to reduce side friction and of depth at least sufficient to accommodate the specimen.

(b) Porous plates to allow water access at top and bottom of the specimen, the top plate of such a diameter to slide freely in the ring. Filter papers may be inserted between specimen and plates.

(c) A cell to contain the specimen assembly, capable of being filled with water to a level above the top porous plate. The principal features of the cell and specimen assembly are illustrated in Fig. 2.

(d) A micrometer dial gauge or other device reading to 0.0025 mm, mounted to measure the swelling displacement at the central axis of the specimen.

(e) A load measuring device capable of measuring to an accuracy of 1%, the force required to resist swelling.

DARCY'S LAW and the FIELD EQUATIONS of the FLOW of UNDERGROUND FLUIDS

M. KING HUBBERT
MEMBER AIME

SHELL DEVELOPMENT CO.
HOUSTON, TEXAS

T. P. 4352

ABSTRACT

In 1856 Henry Darcy described in an appendix to his book, Les Fontaines Publiques de la Ville de Dijon, a series of experiments on the downward flow of water through filter sands, whereby it was established that the rate of flow is given by the equation:

$$q = -K(h_2 - h_1)/l,$$

in which q is the volume of water crossing unit area in unit time, l is the thickness of the sand, h_1 and h_2 the heights above a reference level of the water in manometers terminated above and below the sand, respectively, and K a factor of proportionality.

This relationship, appropriately, soon became known as Darcy's law. Subsequently many separate attempts have been made to give Darcy's empirical expression a more general physical formulation, with the result that so many mutually inconsistent expressions of what is purported to be Darcy's law have appeared in published literature that sight has often been lost of Darcy's own work and of its significance.

In the present paper, therefore, it shall be our purpose to reinform ourselves upon what Darcy himself did, and then to determine the meaning of his results when expressed explicitly in terms of the pertinent physical variables involved. This will be done first by the empirical method used by Darcy himself, and then by direct derivation from the Navier-Stokes equation of motion of viscous fluids. We find in this manner that:

$$\mathbf{q} = (Nd^2)(\rho/\mu)[\mathbf{g} - (1/\rho)\ \text{grad}\ p] = \sigma\mathbf{E},$$

is a physical expression for Darcy's law, which is valid for liquids generally, and for gases at pressures higher than about 20 atmospheres. Here N is a shape factor and d a characteristic length of the pore structure of the solid, ρ and μ are the density and viscosity of the fluid, $\sigma = (Nd^2)(\rho/\mu)$ is the volume conductivity of the system, and $\mathbf{E} = [\mathbf{g} - (1/\rho)\ \text{grad}\ p]$ is the impelling force per unit mass acting upon the fluid. It is found also that Darcy's law is valid only for flow velocities such that the inertial forces are negligible as compared with those arising from viscosity.

In general, three-dimensional space there exist two superposed physical fields: a field of force of characteristic vector **E**, *and a field of flow of vector* **q**. *The force field is more general than the flow field since it has values in all space capable of being occupied by the fluid.*

So long as the fluid density is constant or is a function of the pressure only,

$$curl\ \mathbf{E} = 0,\ \mathbf{E} = -\ \text{grad}\ \Phi$$

where

$$\Phi = gz + \int \frac{dp}{\rho}.$$

The field of flow, independently of the force field, must satisfy the conservation of mass, leading to the equation of continuity

$$div\ \rho\mathbf{q} = -\ f\ \partial\rho/\partial t,$$

where f is the porosity, and t is the time. For steady motion $\partial\rho/\partial t = 0$, and

$$div\ \rho\mathbf{q} = 0.$$

Manuscript received in Petroleum Branch office on Sept. 12, 1956. Paper prepared for presentation before Darcy Centennial Hydrology Symposium of the International Association of Hydrology held in Dijon, France, Sept. 20-26, 1956, and for dual publication as part of the Dijon Symposium and in the Darcy Centennial Issue of *Journal of Petroleum Technology*.

Discussion of this paper is invited. Discussion in writing (3 copies) may be sent to the office of the *Journal of Petroleum Technology*. Any discussion offered after Dec. 31, 1956, should be in the form of a new paper.

If the fluid is also of constant density,

$$\text{div } \mathbf{q} = 0 .$$

The two fields are linked together by Darcy's law,

$$\mathbf{q} = \sigma \mathbf{E} ,$$

which is physically analogous to Ohm's law in electricity.

Then, when $\mathbf{E} = -\text{grad } \Phi$,

$$\mathbf{q} = -\sigma \text{ grad } \Phi .$$

By means of the foregoing equations the flow of both homogeneous and heterogeneous fluids through porous solids becomes amenable to the same kind of analytical treatment as is already familiar in electrical and thermal conduction.

The relation of Darcy's work to the development of a valid theory of the flow of fluids through porous solids is somewhat analogous to that of Faraday to the Maxwellian equations of electromagnetism. It forms a solid experimental foundation for such a field theory, and the errors attributed by various recent authors to Darcy appear upon closer inspection to have been those committed by the authors themselves.

INTRODUCTION

In Paris in the year 1856 there was published by Victor Dalmont as a part of the *Libraire des Corps Impériaux des Ponts et Chaussées et des Mines* a monograph by the French engineer Henry Darcy,[1] Inspector General of Bridges and Roads, bearing the title:

"LES
FONTAINES PUBLIQUES
DE LA VILLE DE DIJON
Exposition et Application
DES PRINCIPES A SUIVRE ET DES
FORMULES A EMPLOYER
Dans les Questions
de
DISTRIBUTION D'EAU
Ouvrage Terminé
Par un Appendice Relatif aux Fournitures
d'Eau de Plusieurs Villes
AU FILTRAGE DES EAUX
et
A la Fabrication des Tuyaux de Fonte,
de Plomb, de Tole et de Bitume."

For several years previously M. Henry Darcy had been engaged in modernizing and enlarging the public water works of the town of Dijon, and this treatise, comprising a 647-page volume of text and an accompanying *Atlas* of illustrations, constitutes an engineering report on that enterprise.

The item of present interest represents only a detail of the general work and appears in an appendix on pages 590 to 594 under the heading "Determination of the Law of Flow of Water Through Sand," and pertains to a problem encountered by Darcy in designing a suitable filter for the system. Darcy needed to know how large a filter would be required for a given quantity of water per day and, unable to find the desired information in the published literature, he proceeded to obtain it experimentally.

A drawing of the apparatus used is given as Fig. 3 in the *Atlas* and is here reproduced in facsimile as Fig. 1. This consisted of a vertical iron pipe, 0.35 m in diameter and 3.50 m in length (the figure shows 3.50 m but the text says 2.50), flanged at both ends. At a height of 0.20 m above the base of the column, there was placed a horizontal screen supported by an iron grillwork upon which rested a column, a meter or so in length, of loose sand. Water could be admitted into the system by means of a pipe, tapped into the column near its top, from the building water supply, and could be discharged through a faucet from the open chamber near its bottom. The faucet discharged into a measuring tank 1 m square and 0.50 m deep, and the flow rate could be controlled by means of adjustable valves in both the inlet pipe and the outlet faucet.

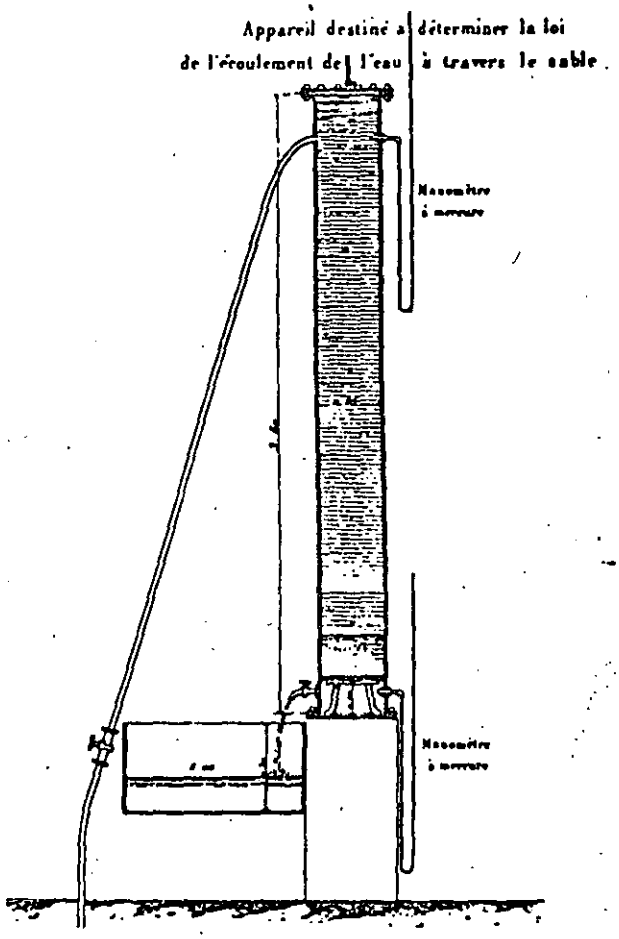

FIG. 1—FACSIMILE OF DARCY'S ILLUSTRATION OF HIS EXPERIMENTAL APPARATUS. (FROM *Les Fontaines Publiques de la Ville de Dijon, Atlas*, FIG. 3).

For measuring the pressures mercury manometers were used, one tapped into each of the open chambers above and below the sand column. The unit of pressure employed was the *meter of water* and all manometer readings were reported in meters of water measured above the bottom of the sand which was taken as an elevation datum. The observations of the mercury manometers were accordingly expressed directly in terms of the heights of the water columns of equivalent water manometers above a standard datum.

The experiments comprised several *series* of observations made between Oct. 29 and Nov. 2, 1855, and some additional experiments made during Feb. 17 to 18, 1856. For each series the system was charged with a different sand and completely filled with water.

[1]References given at end of paper.

By adjustment of the inlet and outlet valves the water was made to flow downward through the sand at a series of successively increasing rates. For each rate a reading of the manometers was taken and recorded as a pressure difference in meters of water above the bottom of the sand. The results of two of these series, using different sands, are shown graphically in Fig. 2. In each instance it will be seen that the total rate of discharge increases linearly with the drop in head across the sand of the two equivalent water manometers.

Darcy's own summary of the results of his experiments is given in the following passage (p. 594):

"Ainsi, en appelant e l'épaisseur de la couche de sable, s sa superficie, P la pression atmosphérique, h la hauteur de l'eau sur cette couche, on aura $P + h$ pour la pression à laquelle sera soumise la base supérieure; soient, de plus, $P \pm h_n$ la pression supportée par la surface inférieure, k un coefficient dépendant de la perméabilité de la couche, q le volume débité, on a

$$q = k \frac{s}{e} [h + e \mp h_n]$$

qui se réduit à

$$q = k \frac{s}{e}(h + e)$$

quand $h_n = 0$, ou lorsque la pression sous le filtre est égale à la pression atmosphérique.

"Il est facile de déterminer la loi de décroissance de la hauteur d'eau h sur le filtre; en effet, soit dh la quantité dont cette hauteur s'abaisse pendant un temps dt, sa vitesse d'abaissement sera $-\frac{dh}{dt}$; mais l'équation ci-dessus donne encore pour cette vitesse l'expression

$$\frac{q}{s} = v = \frac{k}{e}(h + e).$$

"On aura donc

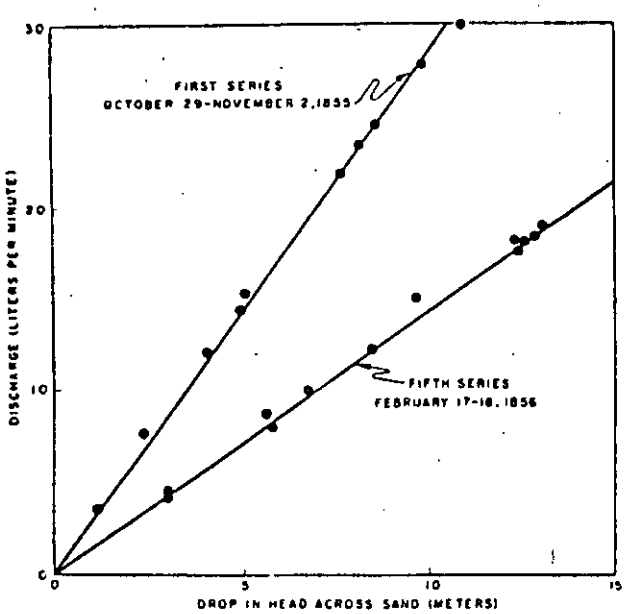

FIG. 2—GRAPHS COMPILED FROM DARCY'S TABULAR DATA ON HIS EXPERIMENTS OF OCT. 29 TO NOV. 2, 1855, AND OF FEB. 17-18, 1856, SHOWING LINEAR RELATION BETWEEN FLOW RATE AND DIFFERENCES IN HEIGHTS OF EQUIVALENT WATER MANOMETERS.

$$-\frac{dh}{dt} = \frac{k}{e}(h + e); \text{ d'où } \frac{dh}{(h + e)} = -\frac{k}{e}dt,$$

et

$$l(h + e) = C - \frac{k}{e}t.$$

[l is the logarithm to the base e.]

"Si la valeur h_n correspond au temps t_n et h à un temps quelconque t, il viendra

$$l(h + e) = l(h_n + e) - \frac{k}{e}[t - t_n] \quad . \quad . \quad . \quad . \quad (1)$$

"Si on remplace maintenant $h + e$ et $h_n + e$ par $\frac{qe}{sk}$ et $\frac{q_n e}{sk}$, il viendra

$$lq = lq_n - \frac{k}{e}(t - t_n) \quad . \quad . \quad . \quad . \quad . \quad . \quad . \quad (2)$$

et les deux équations (1) et (2) donnent, soit la loi d'abaissement de la hauteur sur le filtre, soit la loi de variation des volumes débités à partir du temps t_n.

"Si k et e étaient inconnus, on voit qu'il faudrait deux expériences préliminaires pour faire disparaître de la seconde le rapport inconnu $\frac{k}{e}$."

Translating Darcy's statements into the notation which will subsequently be used in the present paper, what Darcy found and stated was that, when water flows vertically downward through a sand, the volume of water Q passing through the system in unit time is given by

$$Q = KA\frac{h_1 - h_2}{l}, \text{ or by } -KA\frac{h_2 - h_1}{l}; \quad . \quad (1)$$

and the volume crossing unit area in unit time by

$$Q/A = q = K\frac{h_1 - h_2}{l}, \text{ or by } -K\frac{h_2 - h_1}{l},$$

. . . . . (2)

where K is a factor of proportionality, A the area of cross section and l the thickness of the sand, and h_1 and h_2 the heights above a standard reference elevation of water in equivalent water manometers terminated above and below the sand, respectively.

Writing Eq. 2 in differential form gives

$$q = -K(dh/dl) \quad . \quad . \quad . \quad . \quad . \quad . \quad . \quad . \quad (3)$$

Soon after the publication of Darcy's account of these experiments, the relationship expressed by Eqs. 1 to 3 became known, appropriately, as Darcy's law.

It has subsequently come to be universally acknowledged that Darcy's law plays the same role in the theory of the conduction of fluids through porous solids as Ohm's law in the conduction of electricity, or of Fourier's law in the conduction of heat. On the other hand, Darcy's own statement of the law was in an empirical form which conveys no insight into the physics of the phenomenon. Consequently, during the succeeding century many separate attempts were made to give the statement of the law a more general and physically satisfactory form, with the result that there appeared in the technical literature a great variety of expressions, many mutually contradictory, but all credited directly or indirectly to Henry Darcy.

It has accordingly become recently the fashion, when some of these expressions have been found to be physically untenable, to attribute the error to Darcy himself. In fact one recent author, in discussing a supposed statement of Darcy's law which is valid for horizontal flow only, has gone so far as to explain that

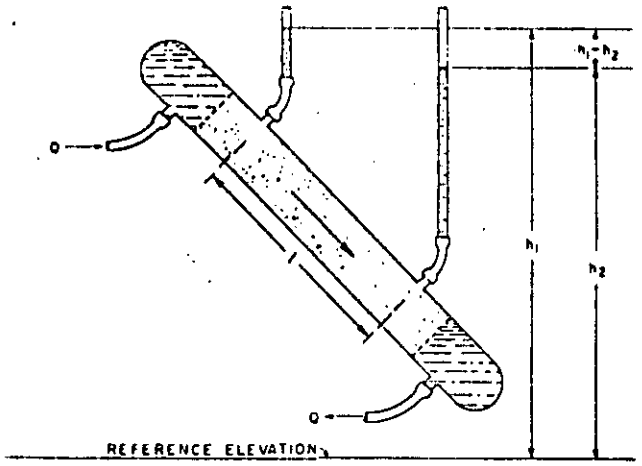

FIG. 3—APPARATUS FOR VERIFYING DARCY'S LAW FOR FLOW IN VARIOUS DIRECTIONS.

Darcy was led to the commission of this error by restricting his experiments to flow in a horizontal direction.

On this centennial occasion of Darcy's original publication, it would appear to be fitting, therefore, instead of merely paying our respects to Darcy in the form of an empty homage, that we first establish unequivocally what Darcy himself did and said with respect to the relationship which bears his name; second, try to ascertain the generality and physical content of the relationship and to give it a proper physical expression; and third, attempt to see how this fits into a general field theory of the flow of fluids through porous solids in three-dimensional space.

The first of these objectives has already been accomplished; the second and third will now be given our attention.

THE PHYSICAL CONTENT OF DARCY'S LAW

As we have seen heretofore, what Darcy determined was that, when water flows vertically downward through a sand, the relation of the volume of water crossing unit area normal to the flow direction in unit time, to the thickness of the sand, and to the difference in heights of equivalent water manometers terminated above and below the sand, is given by the following equation:

$$q = K\frac{h_1 - h_2}{l} \quad \text{or} \quad q = -K\frac{h_2 - h_1}{l}, \quad . \quad . \quad (2)$$

where K is "a coefficient depending upon the permeability of the sand."

Questions immediately arise regarding the generality of this result. Would it still be true if the water flowed upward through the sand? or horizontally? What changes would be effected in the relationship if some different liquid characterized by a different density and viscosity were used? In what manner does K depend upon the permeability of the sand, or upon its measurable statistical parameters such as coarseness and shape? And finally, what physical expression can be found which properly embodies all of these variables?

The answer to most of these questions can be determined empirically by an extension of Darcy's original experiment. If, for example, we construct an apparatus such as that shown in Fig. 3, consisting of a movable cylinder with a rigid sand pack into which two manometers, at an axial distance l apart, are connected by flexible rubber tubing, we can determine the validity of Darcy's law with respect to the direction of flow. With the apparatus vertical and the flow downward at a total rate Q, the manometer difference $h_2 - h_1$ will have some fixed value Δh. Now, keeping Q constant and inverting the column so that the flow will be vertically upward, it will be found that Δh also remains constant. Next, setting the column horizontal, Δh still remains constant. In this manner we easily establish that Darcy's law is invariant with respect to the direction of the flow in the earth's gravity field, and that for a given Δh the flow rate Q remains constant whether the flow be in the direction of gravity or opposed to it, or in any other direction in three-dimensional space.

This leads immediately to a generalization for flow in three-dimensional space. At each point in such space there must exist a particular value of a scalar quantity h, defined as the height above a standard elevation datum of the water column in a manometer terminated at the given point. The ensemble of such values then gives rise to a scalar field in the quantity h with its attendant family of surfaces, h = constant. In such a scalar field water will flow in the direction perpendicular to the surfaces, h = constant, and at a rate given by

$$\mathbf{q} = -K \operatorname{grad} h \, . \quad . \quad . \quad . \quad . \quad . \quad . \quad . \quad . \quad . \quad (4)$$

Continuing our empirical experimentation, we find that when we change either of the fluid properties, density or viscosity, or the geometrical properties of the sand, Eq. 4 still remains valid but the value of K changes. In particular, by varying one factor at a time, we find

$$\left.\begin{aligned} K &\propto \rho \quad , \\ K &\propto 1/\mu \, , \end{aligned}\right\} \quad . \quad . \quad . \quad . \quad . \quad . \quad . \quad . \quad . \quad . \quad (5)$$

where ρ is the density and μ is the viscosity of the fluid. Likewise, if we use a number of geometrically similar sands which differ only in grain size, we find that

$$K \propto d^2 , \quad . \quad . \quad . \quad . \quad . \quad . \quad . \quad . \quad . \quad . \quad . \quad (6)$$

where d is a length such as the mean grain diameter, which characterizes the size scale of the pore structure of the sand.

Introducing the results of Eqs. 5 and 6 into Eq. 4 then gives

$$\mathbf{q} = K' d^2 (\rho/\mu)(-\operatorname{grad} h), \quad . \quad . \quad . \quad . \quad . \quad (7)$$

in which K' is a new factor of proportionality containing all other variables not hitherto explicitly evaluated. This remains, however, an empirical equation devoid of dynamical significance since there is no obvious reason why the flow of a viscous fluid through a porous solid should be proportional to a dimensionless quantity, $-\operatorname{grad} h$.

This deficiency can be eliminated when we introduce the equation relating the manometer height h to the dynamical quantities, gravity and pressure. At any point P within the flow system, characterized by elevation z and manometer height h, the pressure is given by the hydrostatic equation

$$p = \rho g \, (h - z),$$

from which

$$h = (p/\rho g) + z \, , \quad . \quad . \quad . \quad . \quad . \quad . \quad . \quad . \quad . \quad (8)$$

and

$$-\operatorname{grad} h = -(1/\rho g) \operatorname{grad} p - \operatorname{grad} z \quad . \quad (9)$$

Multiplying both sides of Eq. 9 by g then gives

$$-g \text{ grad } h = -(1/\rho) \text{ grad } p - g \text{ grad } z . \quad . \quad . \quad . \quad . \quad . \quad . \quad . \quad . \quad . \quad (10)$$

With the z-axis vertical and positive upward, then grad z is a unit vector directed upward, so that $-g$ grad z is a vector of magnitude g directed downward. Designating this by g, Eq. 10 becomes

$$-g \text{ grad } h = \mathbf{g} - (1/\rho) \text{ grad } p, \quad . \quad . \quad . \quad (11)$$

in which each of the terms to the right represents, both in direction and magnitude, the force exerted upon unit mass of the fluid by gravity and by the gradient of the fluid pressure respectively; the fluid flows in the direction of, and at a rate proportional to, their resultant, $-g$ grad h. Hence the dynamical factor g has evidently been concealed in the original factor K and must still be present in the residual factor K'. Introducing this explicitly, we may now write

$$\mathbf{q} = (Nd^2)(\rho/\mu)(-g \text{ grad } h), \quad . \quad . \quad . \quad (12)$$

in which N is a final factor of proportionality. Dimensional inspection shows that N is dimensionless, and a physical review indicates that no dynamical variables have been omitted, so that N must be related to the only remaining variable, namely the shape of the passages through which the flow occurs. Since shape is expressed by angular measurement and angles are dimensionless, $[L/L]$, then N must be a dimensionless shape factor whose value is constant for systems which are either identically, or statistically, similar geometrically. By identical similarity is meant similarity in the strict Euclidean sense: all corresponding angles equal, and all corresponding lengths proportional. By statistical similarity is meant that two complex geometrical systems which may not be identically similar on a microscopic scale are still indistinguishable as to shape on a macroscopic scale—for example, two sets of randomly packed uniform spheres.

The term $(-g \text{ grad } h)$ can also be written in the form

$$-g \text{ grad } h = -\text{grad } (gh), \quad . \quad . \quad . \quad . \quad . \quad . \quad (13)$$

where gh represents the amount of work required to lift a unit mass of water from the standard datum of elevation outside the system to the height h of the water in the manometer. Then, since the additional work required to transport the water down the water-filled tube of the manometer to its terminus is zero, it follows that

$$gh = \Phi \quad . \quad . \quad . \quad . \quad . \quad . \quad . \quad . \quad . \quad . \quad . \quad (14)$$

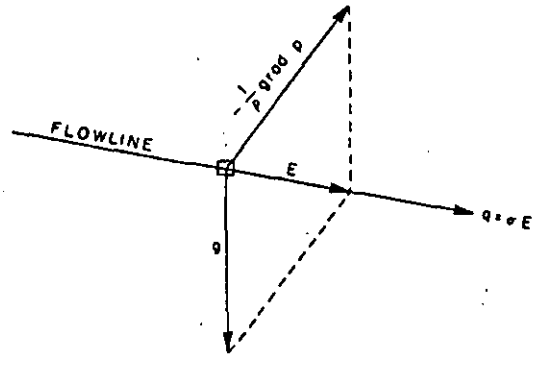

FIG. 4—RELATION OF FORCE PER UNIT MASS, E, TO THE PRIMARY FORCES g AND $-(1/\rho)$ GRAD p; AND OF THE FLOW VECTOR q TO E.

is a measure of the energy per unit mass, or the *potential*, of the water in the system at the point at which the manometer is terminated. A manometer is thus seen to be a fluid potentiometer, the potential at every point being linearly related to the manometer height h by Eq. 14. Then, if we let E be the force per unit mass, or the intensity of the force field acting upon the fluid, we have

$$\mathbf{E} = -\text{grad } \Phi = -g \text{ grad } h = \mathbf{g} - (1/\rho) \text{ grad } p, \quad (15)$$

and, by substitution into Eq. 12, Darcy's law may be expressed in any of the following equivalent forms (Fig. 4):

$$\left.\begin{aligned} \mathbf{q} &= -(Nd^2)(\rho/\mu) \text{ grad } \Phi = \sigma\mathbf{E}, \\ \mathbf{q} &= -(Nd^2)(\rho/\mu)\, g \text{ grad } h = \sigma[\mathbf{g} - (1/\rho) \text{ grad } p], \\ \mathbf{q} &= -(Nd^2)(\rho/\mu)\, g \text{ grad } h = (\sigma/\rho)[\rho\mathbf{g} - \text{grad } p], \end{aligned}\right\} \quad . \quad . \quad . \quad . \quad . \quad . \quad . \quad . \quad . \quad . \quad . \quad (16)$$

where

$$\sigma = [(Nd^2)(\rho/\mu)]$$

is the volume conductivity of the system. In the last of Eqs. 16, the bracketed term

$$[\rho\mathbf{g} - \text{grad } p] = \rho\mathbf{E} = \mathbf{H} . \quad . \quad . \quad . \quad . \quad . \quad . \quad (17)$$

represents the force H per unit volume.

When we compare Darcy's law in the form:

$$\mathbf{q} = \sigma\mathbf{E} = -\sigma \text{ grad } \Phi ,$$

with Ohm's law:

$$\mathbf{i} = \sigma_e \mathbf{E}_e = -\sigma_e \text{ grad } V ,$$

where i is the current density, σ_e the electrical conductivity, $\mathbf{E}_e$ the electrical force-field intensity, and V the electrical potential, the physical as well as the mathematical analogy between Darcy's law and Ohm's law becomes immediately apparent.

THE PROBLEM OF PERMEABILITY

Now that we have achieved a complete physical statement of Darcy's law, it remains for us to define what shall be meant by the permeability of the system.

It will be recalled that Darcy stated that the factor K is "a coefficient depending upon the permeability of the sand." Following this it has often been the custom, especially among ground-water hydrologists, to define the permeability of a system to be synonymous with K. But, as we have seen, the factor K is the lumped parameter,

$$K = (Nd^2)(\rho/\mu)\, g,$$

comprising the geometrical properties of the sand, the dynamical properties of the fluid, and even the acceleration of gravity. Consequently, if K is taken as a measure of the permeability, it will be seen that the same sand will have different permeabilities to different fluids.

During recent years there has been a convergence of opinion toward the conclusion that permeability should be a constant of the solid independently of the fluids involved. If we accept this view, then it is seen that the only property of the solid affecting the rate of flow is the geometrical factor,

$$k = Nd^2 ,$$

which we may accordingly define to be its permeability. Then since N is dimensionless and d is a length, it follows that the dimensions of permeability are $[L^2]$; and

in any consistent system of units, the unit of permeability is the square of the unit of length.

In practice the magnitude of this quantity, for a given porous solid, is determined hydrodynamically by flowing a liquid through the solid, and measuring all variables except k, and then solving Darcy's law for k:

$$k = Nd^2 = \frac{q\mu}{\rho g - \text{grad } p},$$

which, when the vector quantities are resolved into their components in the flow direction s, becomes

$$k = \frac{q\mu}{\rho g_s - \partial p/\partial s}. \quad . \quad . \quad . \quad . \quad . \quad . \quad . \quad . \quad . \quad (18)$$

It is found in this manner that for randomly packed, uniform spheres of diameter d, the value of the shape-factor N is approximately 6×10^{-4}. Then, for a pack of uniform spheres of any size, the permeability will be approximately

$$k = (6 \times 10^{-4})\, d^2.$$

If d, for different packs, is allowed to vary from about 10^{-4} to 10^{-1} cm, corresponding to the approximate range of grain sizes from fine silts to coarse sands, the permeability will vary from about 10^{-12} to 10^{-6} cm^2, which is also approximately the range of the permeabilities of the corresponding clastic sediments.

In view of the fact that magnitudes of permeabilities of rocks are remote from that of the square of any unit of length in common use, there is some advantage in having a practical unit such that most measured values fall within the range 1 – 10,000 practical units. If such a practical unit is to fit into a consistent system of measurement without awkward conversion factors, then it must also be a submultiple of the fundamental unit of the form:

$$1 \text{ practical unit} = 10^{-n} \text{ fundamental units.}$$

In the cgs system with the fundamental unit the (centimeter)^2, the optimum value of the exponent n would be about 12, or

$$1 \text{ practical unit} = 10^{-12} \text{ cm}^2.$$

Regrettably the unit of permeability used almost universally in the petroleum industry, for which the name "darcy" has been pre-empted, was defined originally in terms both of an incomplete statement of Darcy's law:[2,3]

$$k = -\frac{q\mu}{\partial p/\partial s}, \quad . \quad . \quad . \quad . \quad . \quad . \quad . \quad . \quad . \quad (19)$$

and an inconsistent system of measurement. The permeability k is defined to be 1 darcy when $q = 1$ (cm^3/cm^2)/sec, $\mu = 1$ cp, and $\partial p/\partial s = 1$ *atmosphere*/cm.

In the complete Darcy's law of Eq. 18, the factor ρg_s, except when the motion is horizontal, is of comparable magnitude to $\partial p/\partial s$, and so cannot be ignored. Consequently, since it is not practical to measure ρg_s in atmospheres/cm, it follows that permeabilities, expressed in darcys, cannot be used in a proper statement of Darcy's law without the insertion of a numerical factor to convert ρg_s from cgs units into atmospheres/cm.

The only alternative is to convert permeabilities expressed in darcys into the cgs unit, the cm^2. For this conversion

$$1 \text{ darcy} = 0.987 \times 10^{-8} \text{ cm}^2,$$

which is within 1.3 per cent of the submultiple, 10^{-8} cm^2.

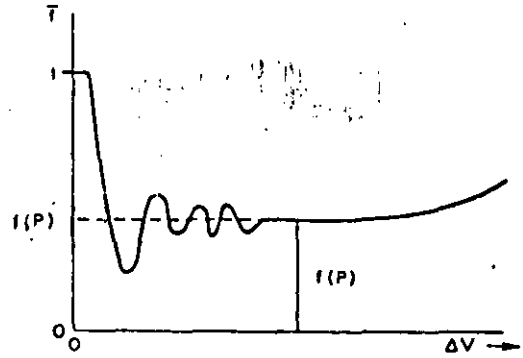

FIG. 5—METHOD OF DEFINING POINT VALUES OF MACROSCOPIC QUANTITIES ILLUSTRATED WITH THE POROSITY f.

Few permeability measurements are accurate to within 1.3 per cent and, when several specimens from the same formation are measured, the scatter is much greater than this. Consequently, for all ordinary computations, the approximate conversions:

$$1 \text{ darcy} \cong 10^{-8} \text{ cm}^2,$$

$$1 \text{ md} \cong 10^{-11} \text{ cm}^2,$$

are more accurate than the permeability data available; though if the data warrant it, the more precise conversion can of course be used.

DERIVATION OF DARCY'S LAW FROM NAVIER-STOKES EQUATION

Having thus achieved the desired generalization and a proper physical statement of Darcy's law by an extension of the empirical method which Darcy himself employed, let us now see if the same result can be derived directly from the fundamental equation of Navier and Stokes for the motion of a viscous fluid.

MACROSCOPIC AND MICROSCOPIC SCALES

In order to do this we must first distinguish between the two size scales, the macroscopic and the microscopic, on which the phenomena considered are to be viewed.

The macroscopic scale, which is the one we have been using thus far, is a scale that is large as compared with the grain or pore size of the porous solid. On this scale the flow of a fluid through a porous solid is seen as a continuous phenomenon in space. However, when we are dealing with macroscopic quantities which have particular values at each point in space, but which may vary with position, it is necessary for us to define more clearly what is meant by the value of a macroscopic quantity at a given point.

This can be illustrated with the concept of porosity. Suppose that we are interested in the porosity at a particular point. About this point we take a finite volume element ΔV, which is large as compared with the grain or pore size of the rock. Within this volume element the average porosity is defined to be

$$\bar{f} = \frac{\Delta V_f}{\Delta V}, \quad . \quad . \quad . \quad . \quad . \quad . \quad . \quad . \quad . \quad . \quad . \quad (20)$$

where ΔV_f is the pore volume within ΔV. We then allow ΔV to contract about the point P and note the value of $\bar{f}$ as ΔV diminishes. If we plot $\bar{f}$ as a function of ΔV (Fig. 5), it will approach smoothly a limiting value as ΔV diminishes until ΔV approaches the grain

or pore size of the solid. At this stage $\bar{f}$ will begin to vary erratically and will ultimately attain the value of either 1 or 0, depending upon whether P falls within the void or the solid space.

However, if we extrapolate the smooth part of the curve of $\bar{f}$ vs ΔV to its limit as ΔV tends to zero, we shall obtain an unambiguous value of f at the point P. We thus define the value of the porosity f at the point P to be

$$f(P) = \underset{\Delta V \to 0}{\text{extrap lim}} \frac{\Delta V_f}{\Delta V}, \quad . \quad . \quad . \quad . \quad . \quad (21)$$

where "extrap lim" signifies the extrapolated limit as obtained in the manner just described.

By an analogous operation the point value of any other macroscopic quantity may be obtained, so that hereafter, when such quantities are being considered, their values will be understood to be defined in the foregoing manner, and we may state more simply:

$$\left.\begin{aligned} Q(P) &= \lim_{\Delta V \to 0} \bar{Q}(\Delta V), \\ \text{or} \\ Q(P) &= \lim_{\Delta S \to 0} \bar{Q}(\Delta S), \\ \text{or} \\ Q(P) &= \lim_{\Delta s \to 0} \bar{Q}(\Delta s), \end{aligned}\right\} \quad . \quad . \quad . \quad . \quad (22)$$

where the quantity of interest is a function of a volume, an area, or a length, respectively.

The microscopic scale, on the contrary, is a scale commensurate with the grain or pore size of the solid, but still large as compared with molecular dimensions or of the motional irregularities due to Brownian or molecular movements.

Microscopic Equations of Motion

Let us next consider the steady, macroscopically rectilinear flow of an incompressible fluid through a porous solid which is macroscopically homogeneous and isotropic with respect to porosity and permeability. We shall then have the fluid flowing with a constant macroscopic flow rate $\mathbf{q}$ under a constant impelling force per unit of mass $\mathbf{E}$, and in virtue of the isotropy of the system, we shall have

$$\mathbf{q} = \sigma \mathbf{E}, \quad . \quad . \quad . \quad . \quad . \quad . \quad . \quad . \quad . \quad . \quad . \quad (23)$$

where σ is an unknown scalar whose value we shall seek to determine.

Then, choosing x-, y-, and z-axes,

$$\left.\begin{aligned} \mathbf{q} &= \mathbf{i}\, q_x + \mathbf{j}\, q_y + \mathbf{k}\, q_z, \\ \mathbf{E} &= \mathbf{i}\, E_x + \mathbf{j}\, E_y + \mathbf{k}\, E_z, \end{aligned}\right\} \quad . \quad . \quad . \quad . \quad . \quad (24)$$

and

$$\left.\begin{aligned} q_x &= \sigma E_x, \\ q_y &= \sigma E_y, \\ q_z &= \sigma E_z, \end{aligned}\right\} \quad . \quad . \quad . \quad . \quad . \quad . \quad . \quad . \quad . \quad . \quad (25)$$

where $\mathbf{i}$, $\mathbf{j}$, and $\mathbf{k}$ are unit vectors parallel to the x-, y-, and z-axes, respectively, and the subscripts signify the corresponding scalar components of the vectors.

Further, there will be no loss of generality, and our analysis will be somewhat simplified, if we choose the x-axis in the macroscopic direction of flow. Then

$$\left.\begin{aligned} &\mathbf{q} = \mathbf{i}\, q_x\,; \mathbf{E} = \mathbf{i}\, E_x, \\ \text{and} \\ &q_y = q_z = 0\,; E_y = E_z = 0. \end{aligned}\right\} \quad . \quad . \quad . \quad . \quad (26)$$

Next, consider the microscopic flow through a macroscopic volume element ΔV of sides Δx, Δy, and Δz. The void space in such an element will be seen to be an intricately branching, three-dimensional network of flow channels, each of continuously varying cross section. A fluid particle passing through such a system will follow a continuously curving tortuous path. Moreover, the speed of the particle will alternately increase and decrease as the cross section of the channel through which it flows becomes larger or smaller. Such a particle will accordingly be seen to be in a continuous state of acceleration with the acceleration vector free to assume any possible direction in space.

Consider now the forces which act upon a small volume element dV of this fluid. By Newton's second law of motion

$$dm\, \mathbf{a} = \Sigma d\mathbf{F}, \quad . \quad . \quad . \quad . \quad . \quad . \quad . \quad . \quad . \quad . \quad . \quad (27)$$

where dm is the mass of the fluid, a the acceleration, and $\Sigma d\mathbf{F}$ is the sum of all the forces acting upon the fluid contained within dV. There are many ways in which these forces may be resolved, but for present purposes it will be convenient to resolve them into a driving or impelling force $d\mathbf{F}_d$ and a resistive force arising from the viscous resistance of the fluid element to deformation, $d\mathbf{F}_v$. Eq. 27 then becomes

$$dm\, \mathbf{a} = d\mathbf{F}_d + d\mathbf{F}_v. \quad . \quad . \quad . \quad . \quad . \quad . \quad . \quad . \quad . \quad . \quad (28)$$

By the principle of D'Alembert we may also introduce a force $d\mathbf{F}_a = -\, dm\, \mathbf{a}$, which is the inertial reaction of the mass dm to the acceleration a, and with this substitution Eq. 28 becomes

$$d\mathbf{F}_d + d\mathbf{F}_a + d\mathbf{F}_v = 0. \quad . \quad . \quad . \quad . \quad . \quad . \quad . \quad . \quad . \quad (29)$$

Of these forces, $d\mathbf{F}_d$, which is imposed from without and does not depend primarily upon the motion of the fluid, may be regarded as the independent variable. The forces $d\mathbf{F}_a$ and $d\mathbf{F}_v$ both owe their existences to the fluid motion, and their effect is to impede that motion.

The relation of the separate terms of Eq. 29 to the externally applied forces and the fluid motion are given by the equation of Navier and Stokes, which in vector form may be written as follows:

$$\rho\,[\mathbf{g} - (1/\rho)\ \text{grad}\ p]\, dV = \rho\, (D\mathbf{v}/Dt)\, dV - \mu\,[\nabla^2 \mathbf{v} + (1/3)\ \nabla\nabla\cdot\mathbf{v}]\, dV, \quad . \quad . \quad . \quad (30)$$

in which $\mathbf{v}$ is the microscopic velocity, and $p = -\,(1/3)\,(\sigma_x + \sigma_y + \sigma_z)$ is the microscopic pressure at a point. The σ's are normal components of microscopic stress.

The expression $D\mathbf{v}/Dt$ is the total derivative with respect to time of the velocity $\mathbf{v}$, and is equal to the acceleration a. This can be expanded into

$$D\mathbf{v}/Dt = \frac{\partial \mathbf{v}}{\partial t} + \mathbf{v}\cdot\nabla\mathbf{v},$$

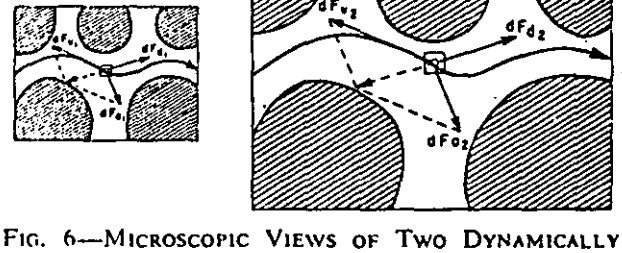

Fig. 6—Microscopic Views of Two Dynamically Similar Flow Systems.

in which the term $\partial \mathbf{v}/\partial t$ signifying the rate of change of the velocity at a particular point is zero for steady motion. The expression $\nabla \cdot \mathbf{v}$, in the last term of Eq. 30, is the divergence of the velocity; and for an incompressible fluid this also is zero.

Since the flow being considered is the steady motion of an incompressible fluid, Eq. 30 simplifies to

$$\rho [\mathbf{g} - (1/\rho) \text{ grad } p] \, dV = \rho (\mathbf{v} \cdot \nabla \mathbf{v}) \, dV - \mu (\nabla^2 \mathbf{v}) \, dV \quad . \quad . \quad . \quad . \quad . \quad . \quad . \quad . \quad (31)$$

Transformation from Microscopic to Macroscopic Equations of Motion

Eq. 31 expresses the relation of the fluid velocity and its derivatives in a small microscopic volume element to the applied force $d\mathbf{F}_a$ acting upon that element. If we could integrate the three terms of this equation with respect to the volume, over the macroscopic volume ΔV, and then convert the results into equivalent macroscopic variables, our problem would be solved. In fact the integration of the first two terms presents no difficulty. The total driving force on the fluid content of the volume ΔV, as obtained by integrating the microscopic forces $d\mathbf{F}_a$, is:

$$\mathbf{F}_a = \int_{f\Delta V} d\mathbf{F}_a = \int_{f\Delta V} (\rho \mathbf{g} - \text{grad } p) \, dV = (\rho \mathbf{g} - \overline{\text{grad } p}) \, f\Delta V \quad . \quad . \quad . \quad . \quad . \quad . \quad (32)$$

where $\overline{\text{grad } p}$ is the volumetric average of the microscopic grad p over the fluid volume $f\Delta V$.

From the macroscopic equations, the driving force $\mathbf{F}_a$ is given by:

$$\mathbf{F}_a = \rho f\Delta V \, \mathbf{E} = \rho [\mathbf{g} - (1/\rho) \text{ grad } p] f\Delta V. \quad (33)$$

Then by combining Eqs. 32 and 33,

$$\int_{f\Delta V} (\rho \mathbf{g} - \text{grad } p) \, dV = (\rho \mathbf{g} - \overline{\text{grad } p}) \, f\Delta V = \rho f\Delta V [\mathbf{g} - (1/\rho) \text{ grad } p], \quad (34)$$

from which it is seen that the macroscopic grad p is equal to the volumetric average, $\overline{\text{grad } p}$, of the microscopic grad p.

Integrating the inertial term:

$$\left.\begin{aligned} \mathbf{F}_v &= \int_{f\Delta V} d\mathbf{F}_v = \rho \int_{f\Delta V} \mathbf{v} \cdot \nabla \mathbf{v} \, dV \\ &= \mathbf{i} \, \rho \int_{f\Delta V} (u \, \partial u/\partial x + v \, \partial u/\partial y + w \, \partial u/\partial z) \, dx \, dy \, dz \\ &+ \mathbf{j} \, \rho \int_{f\Delta V} (u \, \partial v/\partial x + v \, \partial v/\partial y + w \, \partial v/\partial z) \, dx \, dy \, dz \\ &+ \mathbf{k} \, \rho \int_{f\Delta V} (u \, \partial w/\partial x + v \, \partial w/\partial y + w \, \partial w/\partial z) \, dx \, dy \, dz . \end{aligned}\right\} \quad . \quad (35)$$

Since there is no net gain in velocity with macroscopic distance, each separate integral of the expanded form of Eq. 35 is equal to zero, and we obtain for the volume element ΔV,

$$\mathbf{F}_v = \int_{f\Delta V} d\mathbf{F}_v = 0 \quad . \quad . \quad . \quad . \quad . \quad . \quad . \quad . \quad . \quad (36)$$

Then, in virtue of Eq. 36,

$$\int_{f\Delta V} d\mathbf{F}_v = \mu \int_{f\Delta V} \nabla^2 \mathbf{v} \, dV = - \mathbf{F}_a \quad . \quad . \quad . \quad . \quad (37)$$

Ordinarily the evaluation of

$$\int_{f\Delta V} \nabla^2 \mathbf{v} \, dV$$

would require a detailed consideration of the geometry of the void space through which the flow occurs and of the flow field within that space. This difficulty can be circumvented, however, and the integral evaluated except for a dimensionless factor of proportionality, *provided the flow field is kinematically similar for different rates of flow.*

Criteria of Similarity

Consider two flow systems consisting of two geometrically similar porous solids through which two different fluids are flowing. The criterion of geometrical similarity is that if l_1 and l_2 are any corresponding lengths of the two systems, then for every pair of such lengths

$$l_2/l_1 = l_r = \text{const} \, . \quad . \quad . \quad . \quad . \quad . \quad . \quad . \quad (38)$$

The criterion of kinematic similarity is that if $\mathbf{v}_1$ and $\mathbf{v}_2$ are the velocities at corresponding points in the two systems, the two velocities must have the same direction and their magnitudes the ratio

$$v_2/v_1 = v_r = \text{const} \, .$$

Then, since the forces $d\mathbf{F}_a$ and $d\mathbf{F}_v$ acting upon a fluid element are each determined by the velocities and the fluid density, or viscosity, and $d\mathbf{F}_a$ is determined by $d\mathbf{F}_v$ and $d\mathbf{F}_v$, if the fluid motions of the two systems are kinematically similar, all corresponding forces will have the same directions and their magnitudes the same ratio (Fig. 6).

Thus

$$\frac{(dF_a)_2}{(dF_a)_1} = \frac{(dF_v)_2}{(dF_v)_1} = \frac{(dF_d)_2}{(dF_d)_1} \quad . \quad . \quad . \quad . \quad . \quad . \quad (39)$$

Since only two of the three forces are independent, we need to consider the ratios of only the first two, and, by reciprocation,

$$\left(\frac{dF_a}{dF_v}\right)_2 = \left(\frac{dF_a}{dF_v}\right)_1 \quad . \quad . \quad . \quad . \quad . \quad . \quad . \quad . \quad (40)$$

indicating that for each system the ratio of the inertial to the viscous force must be the same.

From Eq. 31

$$\frac{(dF_a)_2}{(dF_a)_1} = \frac{\rho_2}{\rho_1} \frac{(\mathbf{v} \cdot \nabla \mathbf{v})_2}{(\mathbf{v} \cdot \nabla \mathbf{v})_1} \frac{dV_2}{dV_1} \quad . \quad . \quad . \quad . \quad . \quad . \quad (41)$$

$$\frac{(dF_v)_2}{(dF_v)_1} = \frac{\mu_2}{\mu_1} \frac{(\nabla^2 \mathbf{v})_2}{(\nabla^2 \mathbf{v})_1} \frac{dV_2}{dV_1} \quad . \quad . \quad . \quad . \quad . \quad . \quad (42)$$

In Eq. 41 $\mathbf{v} \cdot \nabla \mathbf{v}$ expands into the sum of a series of terms, each of the form $u \, \partial u/\partial x$, which is a velocity squared divided by a length. In Eq. 42 $\nabla^2 \mathbf{v}$ expands into a series of terms, each of the form $\partial^2 u/\partial x^2$, which is a velocity divided by the square of a length. Then, since the ratios of all corresponding velocities and of all corresponding lengths of the two systems are constant, we may choose any suitable velocity and any convenient length. We accordingly choose for the velocity the macroscopic flow rate q whose dimensions are $[L^3 \, L^{-2} \, T^{-1}]$, or $[LT^{-1}]$. For the characteristic length we choose d, which must be some convenient statistical length parameter of the microscopic geometry of the system. With these substitutions the first two terms of Eq. 39 become

$$\frac{\rho_2 q_2^2 d_2^2}{\rho_1 q_1^2 d_1^2} = \frac{\mu_2 q_2 d_2}{\mu_1 q_1 d_1} \quad . \quad . \quad . \quad . \quad . \quad . \quad . \quad . \quad (43)$$

and, by reciprocation, Eq. 40 becomes

$$\frac{\rho_2 q_2^2 d_2^2}{\mu_2 q_2 d_2} = \frac{\rho_1 q_1^2 d_1^2}{\mu_1 q_1 d_1},$$

or

$$\frac{q_2 d_2}{\mu_2/\rho_2} = \frac{q_1 d_1}{\mu_1/\rho_1} \quad . \quad . \quad . \quad . \quad . \quad . \quad . \quad . \quad . \quad (44)$$

The dimensionless quantity $(qd)/(\mu/\rho)$ is the Reynolds number R of the system, which, as seen from its derivation, is a measure of the ratio of the inertial to the viscous forces of the system. Our criterion for kinematic similarity between the two systems thus reduces to the requirement that

$$R_2 = R_1 . \quad . \quad . \quad . \quad . \quad . \quad . \quad . \quad . \quad . \quad . \quad (45)$$

Now let us specialize the two systems by making

$$d_2 = d_1, \rho_2 = \rho_1, \mu_2 = \mu_1 ,$$

which is equivalent to requiring the same fluid to flow through the same porous solid at velocities, q_2 and q_1. However, when these values are substituted into Eq. 44, we obtain

$$q_2 = q_1 ,$$

indicating that, in general, when the same fluid flows through a given porous solid at two different rates, the resulting flow fields cannot be kinematically similar.

However, since dF_v is proportional to q^2 and dF_v to q, then as q is decreased dF_i diminishes much more rapidly than dF_v. Consequently there must be some limiting value of $q = q^*$, or of $R = R^*$, at and below which the inertial force dF_i is so much less than the viscous force dF_v that the effect of the former is negligible as compared with the latter. For flow in this domain we may then write

$$d\mathbf{F}_v = -d\mathbf{F}_d ;$$

and the force ratios become

$$\frac{(dF_v)_2}{(dF_v)_1} = \frac{(dF_d)_2}{(dF_d)_1} , \quad . \quad . \quad . \quad . \quad . \quad . \quad . \quad . \quad (46)$$

whereby kinematical similarity is maintained for all rates of flow $q < q^*$.

Integration of Viscous Forces

With this result established let us now return to the integration of $d\mathbf{F}_v$ over the volume element $f\Delta V$.

$$\int_{f\Delta V} d\mathbf{F}_v = \mu \left[\mathbf{i} \int_{f\Delta V} \nabla^2 u \, dV + \mathbf{j} \int_{f\Delta V} \nabla^2 v \, dV + \mathbf{k} \int_{f\Delta V} \nabla^2 w \, dV \right] . \quad . \quad . \quad . \quad . \quad . \quad . \quad . \quad (47)$$

In virtue of the fact that, by our choice of axes, q_y and q_z are both zero and there is no net flow in the y- or z-direction, the last two integrals to the right are both zero, and Eq. 47 simplifies to

$$\int_{f\Delta V} d\mathbf{F}_v = \mathbf{i}\, \mu \int_{f\Delta V} \nabla^2 u \, dV . \quad . \quad . \quad . \quad . \quad . \quad . \quad . \quad (48)$$

From our earlier discussion, so long as the flow remains kinematically similar for different rates, the quantity $\nabla^2 u$, which is a velocity divided by the square of a length, is related to the macroscopic parameters by

$$\nabla^2 u = -\alpha \, (q/d^2) , \quad . \quad . \quad . \quad . \quad . \quad . \quad . \quad . \quad (49)$$

where α is a dimensionless constant of proportionality for the element dV but has a different value for each different element of volume.

Substituting Eq. 49 into Eq. 48 then gives

$$\int_{f\Delta V} d\mathbf{F}_v = -\mathbf{i}\, \mu \, (q/d^2) \int_{f\Delta V} \alpha \, dV = -\frac{\mu \mathbf{q}}{Nd^2} f\Delta V , \quad . \quad . \quad . \quad . \quad . \quad . \quad . \quad . \quad (50)$$

where $1/N$ is the average value of α over $f\Delta V$.

Substituting this result into Eq. 37, we obtain

$$\rho[\mathbf{g} - (1/\rho) \operatorname{grad} p] f\Delta V = -\int d\mathbf{F}_v = \frac{\mu \mathbf{q}}{Nd^2} f\Delta V ,$$

or

$$\mathbf{q} = Nd^2 \, (\rho/\mu) [\mathbf{g} - (1/\rho) \operatorname{grad} p] , \quad . \quad . \quad (51)$$

which is the derived Darcy's law in the same form as Eq. 16 deduced earlier from empirical data.

Discussion of Darcy's Law

The direct derivation of Darcy's law from fundamental mechanics affords a further insight into the physics of the phenomena involved over what was obtainable from the earlier method of empirical experimentation. It has long been known empirically, for example, that Darcy's law fails at sufficiently high rates of flow, or at a Reynolds number, based on the mean grain diameter as the characteristic length, of the order of $R = 1$.[4]

At the same time one of the most common statements made about Darcy's law has been that it is a special case of Poiseuille's law; and most efforts at its derivation have been based upon various models of capillary tubes or of pipes. It also has been known since the classical studies of Osborne Reynolds[5] in 1883 that Poiseuille's law fails when the flow makes the transition from laminar to turbulent motion, so the conclusion most often reached as to the cause of the failure of Darcy's law has been that the motion has become turbulent.

From what we have seen, this represents a serious misinterpretation and lack of understanding of Darcy's law. In the Darcy flow each particle moves along a continuously curvilinear path at a continuously varying speed, and hence with a continuously varying acceleration; in the Poiseuille flow each particle moves along a rectilinear path at constant velocity and zero acceleration. Therefore, instead of Darcy's law being a special case of Poiseuille's law, the converse is true; Poiseuille's law is in fact a very special case of Darcy's law. Another special case of Darcy's law is the rectilinear flow between parallel plates.

Consequently deductions concerning the Darcy-type flow made from the simpler Poiseuille flow are likely to be seriously misleading. The deduction that the Reynolds number at which Darcy's law fails is also the one at which turbulence begins is a case in point. We have seen that the cause of the failure of Darcy's law is the distortion that results in the flowlines when the velocity is great enough that the inertial force becomes significant. This occurs at a very slow creeping rate of flow which, for water, has the approximate value of

$$q^* \cong \frac{\mu}{\rho d} \cong (1 \times 10^{-2} \text{ cm}^2 \text{ sec}^{-1}) \, (1/d) ,$$

corresponding to $R^* = 1$, when d is the mean grain diameter.

Thus when $d = 10^{-2}$ cm Darcy's law fails at a flow rate $q \cong 1$ cm/sec.

Since this represents the threshold at which the effects of inertial forces first become perceptible, and since turbulence is the result of inertial forces becoming predominant with respect to resistive forces, it would be inferred that the incidence of turbulence in the Darcy flow would occur at very much higher velocities or at very much higher Reynolds numbers than those for which linearity between the flow rate and the driving force ceases. That this is in fact the case has been verified by visual observations of the flow of water containing a dilute suspension of colloidal bentonite through a transparent cell containing cylindrical obstacles. This system, when observed in

polarized light, exhibits flow birefringence which is stationary for steady laminar flow but highly oscillatory when the motion is turbulent. Observations of only moderate precision indicate that the incidence of turbulence occurs at a Reynolds number of the order of 600 or 700, or at a flow velocity of the order of several hundred times that at which Darcy's law fails.

Examination of the Shape-Factor N

In both procedures used thus far, the factor N has emerged simply as a dimensionless factor of proportionality whose magnitude is a function of the statistical geometrical shape of the void space through which the flow occurs. For systems which are either identically or statistically similar geometrically, N has the same value. Beyond this we have little idea of the manner in which N is related to the shape or of what its numerical magnitude should be, except as may be determined by experiment. Let us now see if the value of N, at least to within an order of magnitude, can be determined theoretically.

Since we have already seen in Eq. 50 that $1/N = \overline{\alpha}$, where α is the factor of proportionality between the macroscopic quantity q/d^2 and the microscopic quantity $\nabla^2 u$, it follows that in order to determine the magnitude of N we must first determine that of the average value of $\nabla^2 u$. For this purpose, with the fluid incompressible, the macroscopic flow parallel to the x-axis, and the inertial forces negligible, only the x-component of the Navier-Stokes Eq. 31,

$$\rho g_x - \partial p/\partial x = -\mu\left(\frac{\partial^2 u}{\partial x^2} + \frac{\partial^2 u}{\partial y^2} + \frac{\partial^2 u}{\partial z^2}\right), \quad (52)$$

needs to be considered. When this is integrated with respect to the volume over the fluid space $f\Delta V$, it becomes

$$\overline{(\rho g_x - \partial p/\partial x)}\, f\Delta V = -\mu\left[\int_{f\Delta V} \frac{\partial^2 u}{\partial x^2}\, dV + \int_{f\Delta V} \frac{\partial^2 u}{\partial y^2}\, dV + \int_{f\Delta V} \frac{\partial^2 u}{\partial z^2}\, dV\right]. \quad (53)$$

Of the three integrals to the right, the first, which represents the expansion of the fluid in the x-direction, is zero; and from symmetry, the last two, both being the integrals of derivatives with respect to axes at right angles to the flow, are equal to each other. In consequence, Eq. 53 is reduced to the simpler form:

$$\overline{(\rho g_x - \partial p/\partial x)}\, f\Delta V = -2\mu \int (\partial^2 u/\partial y^2)\, dV = -2\mu\, \overline{(\partial^2 u/\partial y^2)}\, f\Delta V,$$

in which $\overline{\partial^2 u/\partial y^2}$ is the average value of $\partial^2 u/\partial y^2$ throughout the macroscopic volume element. Solving this for $\overline{\partial^2 u/\partial y^2}$ then gives

$$\overline{(\partial^2 u/\partial y^2)} = -(1/2\mu)\,\overline{(\rho g_x - \partial p/\partial x)}. \quad (54)$$

Our problem now reduces to one of attempting to determine the average value of $\partial^2 u/\partial y^2$ for the system in terms of the kinematics of the flow itself. If we extend any line through the system parallel to the y-axis, this line will pass alternately through solid and fluid spaces. At each point on the line in the fluid space, there will be a particular value of the x-component u of the velocity, which will be zero at each fluid-solid contact, but elsewhere will have finite, and usually positive, values giving some kind of a velocity profile across each fluid gap. If this profile for each gap could be determined, then we could also compute $\partial^2 u/\partial y^2$ at each point on the line and thereby determine $\overline{\partial^2 u/\partial y^2}$ for the line, which, in a homogeneous and isotropic system, would also be the average value for a volume.

To attempt to do this in detail would be a statistical undertaking beyond the scope of the present paper. As a first approximation, however, we may simplify the problem by assuming:

1. That all the gaps are equal and of width $2\overline{\lambda}$, where $\overline{\lambda}$ is the average half-width of the actual gaps.
2. That through each gap the velocity profile satisfies the differential equation
$$\partial^2 u/\partial y^2 = \overline{\partial^2 u/\partial y^2} = -C \quad (55)$$
3. That the total discharge through the averaged gaps is the same as that through the actual gaps.

The velocity profile for the averaged gaps can then be obtained by integrating Eq. 55 with respect to y. Taking a local origin of coordinates at the middle of the gap, and integrating Eq. 55 twice with respect to y, we obtain

$$u = -Cy^2/2 + Ay + B, \quad (56)$$

in which A and B are constants of integration. Then, supplying the boundary conditions, $u = 0$ when $y = \pm\overline{\lambda}$, gives

$$0 = -C\overline{\lambda}^2/2 \pm A\overline{\lambda} + B$$

from which

$$A = 0\,;\, B = C\overline{\lambda}^2/2.$$

Substituting these into Eq. 56, we obtain

$$u = (C/2)\,(\overline{\lambda}^2 - y^2) \quad (57)$$

as the equation of the parabolic profile of the averaged velocity across the averaged gap.

The mean value, $\overline{u}$, of u across this gap is given by

$$\overline{u} = (1/\overline{\lambda})\int_0^{\overline{\lambda}} u\, dy = \frac{C}{2\overline{\lambda}}\int_0^{\overline{\lambda}} (\overline{\lambda}^2 - y^2)\, dy = C\overline{\lambda}^2/3. \quad (58)$$

Then, replacing C by $(1/2\mu)\,(\rho g_x - \partial p/\partial x)$ from Eqs. 55 and 54, we obtain

$$\overline{u} = \frac{\overline{\lambda}^2}{6}\frac{\rho}{\mu}\,\overline{[g_x - (1/\rho)\,\partial p/\partial x]} \quad (59)$$

This can be converted into terms of the macroscopic velocity, q_x, by noting that for a macroscopic length of line l normal to the flow direction

$$q_x\, l = 2\overline{u}\,\Sigma\lambda,$$

or

$$q_x = 2\overline{u}\,(\Sigma\lambda/l) = \overline{u}\, f, \quad (60)$$

where f is the porosity.

With this substitution Eq. 59 becomes

$$q_x = \frac{f\overline{\lambda}^2}{6}\cdot\frac{\rho}{\mu}\cdot[g_x - (1/\rho)\,\partial p/\partial x], \quad (61)$$

or, more generally,

$$q = \frac{f\overline{\lambda}^2}{6}\cdot\frac{\rho}{\mu}\cdot[g - (1/\rho)\,\text{grad}\,p], \quad (62)$$

which is a statement of Darcy's law that is valid to the extent of the validity of the averaging approximation used in its derivation.

In this, it will be noted that the geometrical factor $(f/6)\ \overline{\lambda}^2$ represents the permeability, so that

$$k \cong (f/6)\,\overline{\lambda}^2 = N_{\overline{\lambda}}\,\overline{\lambda}^2 \ ,$$

or

$$N_{\overline{\lambda}} \cong f/6 \quad . \quad . \quad . \quad . \quad . \quad . \quad . \quad . \quad . \quad . \quad (63)$$

where $N_{\overline{\lambda}}$ is the shape factor corresponding to $\overline{\lambda}$ as the characteristic length of the system.

Determination of $\overline{\lambda}$

The mean half gap-width $\overline{\lambda}$ along a linear traverse can be determined in either of two ways. The most obvious way is by direct observation by means of micrometer measurements along rectilinear traverses across a plane section of the porous solid.

Of greater theoretical interest, however, is an indirect method due to Corrsin.[6] Instead of a line, let a rectangular prism of cross-sectional area δ^2, where δ can be made arbitrarily small, be passed through a porous solid which is macroscopically homogeneous and isotropic. This prism will pass alternately through solid segments and void segments. Let n be the number of each which is traversed per unit length. Then the number of intersections with the solid surface per unit length will be $2n$, and if $\overline{a}$ is the average area of the solid surface cut out by the prism at each intersection, the total area per unit length, $d\beta$, will be

$$d\beta = 2n\,\overline{a} \ . \quad . \quad . \quad . \quad . \quad . \quad . \quad . \quad . \quad . \quad (64)$$

If a parallel family of such prisms is made to fill all space, the number per unit area perpendicular to the axis of the prisms will be $1/\delta^2$, and the solid surface intersected per unit volume will be

$$\beta = 2n\ (\overline{a}/\delta^2) \quad . \quad . \quad . \quad . \quad . \quad . \quad . \quad . \quad . \quad (65)$$

In addition, the total length of the void spaces per unit length of line will be

$$2n\,\overline{\lambda} = f \ ,$$

or

$$n = f/(2\overline{\lambda}) \quad . \quad . \quad . \quad . \quad . \quad . \quad . \quad . \quad . \quad . \quad (66)$$

Substituting the value of n from Eq. 66 into 65 and solving for $\overline{\lambda}$ then gives

$$\overline{\lambda} = \frac{f}{\beta} \cdot \frac{\overline{a}}{\delta^2} \quad . \quad . \quad . \quad . \quad . \quad . \quad . \quad . \quad . \quad . \quad (67)$$

Since f and β can be measured, the value of $\overline{\lambda}$ could be determined if $\overline{a}/\delta^2$ were known.

The latter can be determined in the following manner: A homogeneous and isotropic distribution of the internal surface S, inside a macroscopic space, implies that if all equal elements dS of the surface were placed without rotation at the center of a reference sphere, their normals would intersect the sphere with a uniform surface density. Then, with the normals fixed in direction, if the surface elements were all moved equal radial distances outward, at some fixed radius they would coalesce to form the surface of a sphere. If the prisms of cross-sectional area δ^2, parallel to a given line, were then passed through this sphere, the average value of a/δ^2 would be

$$\overline{a/\delta^2} = \frac{\Sigma a}{\Sigma \delta^2} \ ; \quad . \quad . \quad . \quad . \quad . \quad . \quad . \quad . \quad . \quad . \quad (68)$$

and, when the summation includes one whole hemisphere,

$$\overline{a/\delta^2} = \overline{a}/\delta^2 = \frac{\text{area of hemisphere}}{\text{area of diametral plane}} = \frac{2\pi r^2}{\pi r^2} = 2 \ .$$

. . . . . (69)

Introducing this result into Eq. 67 then gives

$$\overline{\lambda} = 2f/\beta \ . \quad . \quad . \quad . \quad . \quad . \quad . \quad . \quad . \quad . \quad . \quad (70)$$

A method for measuring β has been described by Brooks and Purcell,[7] but for present purposes the data on randomly packed uniform spheres, for which β can be computed, will suffice. For such a system, with n spheres per unit volume,

$$\beta = \frac{\text{area of spheres}}{\text{total volume}} = \frac{n \,.\, 4\pi r^2}{\frac{n}{1-f} \cdot \frac{4\pi r^3}{3}} = \frac{3(1-f)}{r}$$

$$= \frac{6(1-f)}{d} \ , \quad . \quad . \quad . \quad . \quad (71)$$

where d is the sphere diameter.

Then, introducing this result into Eq. 70, we obtain for packs of uniform spheres

$$\overline{\lambda} = \frac{f}{3(1-f)} \ . \ d \quad . \quad . \quad . \quad . \quad . \quad . \quad . \quad (72)$$

and

$$\overline{\lambda}^2 = \frac{f^2}{9(1-f)^2} \ . \ d^2 \quad . \quad . \quad . \quad . \quad . \quad . \quad . \quad (73)$$

Comparison with Experimental Data

In order to compare the value of $N_{\overline{\lambda}}$ corresponding to the characteristic length $\overline{\lambda}$, with N_d, corresponding to the sphere diameter d, we must first establish the relation between $N_{\overline{\lambda}}$ and N_d. This can be done by noting that, by definition,

$$N_{\overline{\lambda}}\,\overline{\lambda}^2 = N_d\,d^2 = k \ ,$$

where k is the permeability of the system. Consequently

$$N_{\overline{\lambda}} = N_d\,(d^2/\overline{\lambda}^2) \quad . \quad . \quad . \quad . \quad . \quad . \quad . \quad . \quad (74)$$

Then, introducing the value of $d^2/\overline{\lambda}^2$ from Eq. 73 into Eq. 74, gives for a pack of uniform spheres

$$N_{\overline{\lambda}} = \frac{9(1-f)^2}{f^2} \cdot N_d \quad . \quad . \quad . \quad . \quad . \quad . \quad . \quad (75)$$

The value of N_d for well-rounded quartz sands, screened to nearly uniform sizes, has been determined by the author's former research assistant, Jerry Conner. Using packs of different uniform sands with mean grain diameters ranging from 1.37×10^{-2} to 7.15×10^{-2} cm, Conner made seven independent determinations of N_d. The average value obtained was

$$\overline{N}_d = 6.0 \times 10^{-4} \ , \quad . \quad . \quad . \quad . \quad . \quad . \quad . \quad . \quad . \quad (76)$$

with individual values falling within the range between 5.3×10^{-4} and 6.7×10^{-4}.

Conner did not determine the porosity, but the average value of the porosity of randomly packed, uniform spherical glass beads found by Brooks and Purcell[7] was 0.37. Inserting this value of f, and Conner's value of N_d, into Eq. 75 then gives for the equivalent experimental value of $N_{\overline{\lambda}}$:

$$N_{\overline{\lambda}} = 26.2\,N_d = 1.57 \times 10^{-2} \quad . \quad . \quad . \quad . \quad (77)$$

Comparing this experimental result with the approximate theoretical result of Eq. 63, it will be seen that

$$\frac{N_{\overline{\lambda}}\ (\text{theoretical})}{N_{\overline{\lambda}}\ (\text{observed})} = \frac{f/6}{1.57 \times 10^{-2}} = 4 \ . \quad . \quad (78)$$

Since our object at the outset was merely to gain some insight into the nature of the shape-factor N occurring in Darcy's law, no particular concern is to be felt over the discrepancy in Eq. 78 between the observed and the theoretical values. All that this really indicates is that the system of averaging required should be better than the oversimplified one actually used. For a more complete analysis, account needs to be taken of the frequency distribution of the half gap-width λ, and also of the functional relation between $\bar{u}$ and λ. The fact that our approximate analysis yields a result in error by only a factor of 4 makes it appear promising that if account is taken of the variability of λ and of $\bar{u}$ as a function of λ, much better approximations may be obtainable.

Darcy's Law for Compressible Fluids

Our analysis thus far has been restricted to the flow of incompressible fluids for which the divergence term, $-(1/3)\,\mu\,\nabla\nabla\cdot\mathbf{v}$, could be eliminated from the Navier-Stokes equation. For the flow of a compressible fluid, this term must be retained, and with the flow parallel to the x-axis,

$$F_d = -\mu\int_{\Delta V}\left[\frac{4}{3}\frac{\partial^2 u}{\partial x^2}+\frac{\partial^2 u}{\partial y^2}+\frac{\partial^2 u}{\partial z^2}+\frac{1}{3}\left(\frac{\partial^2 v}{\partial x\partial y}+\frac{\partial^2 w}{\partial x\partial w}\right)\right]dV \quad . \quad . \quad . \quad . \quad . \quad . \quad . \quad . \quad . \quad . \quad . \quad . \quad (79)$$

of which the last two terms are equal to zero, leaving

$$F_d = -\mu\int_{\Delta V}\left(\frac{4}{3}\frac{\partial^2 u}{\partial x^2}+\frac{\partial^2 u}{\partial y^2}+\frac{\partial^2 u}{\partial z^2}\right)dV \quad ,$$

or

$$F_d = -2\mu\,[(2/3)\,(\overline{\partial^2 u/\partial x^2})+(\overline{\partial^2 u/\partial y^2})]/\Delta V. \quad . \quad . \quad . \quad . \quad . \quad . \quad . \quad . \quad . \quad . \quad . \quad . \quad . \quad . \quad . \quad . \quad . \quad . \quad (80)$$

Here, $\overline{\partial^2 u/\partial x^2}$ represents the gradient of the divergence of the velocity in the x-direction, or the rate of the fluid expansion. Should this term be of the same order of magnitude as $\overline{\partial^2 u/\partial y^2}$, and if the flow of a gas through the porous system is otherwise similar to that of a liquid, then the viscous resistance to a gas should be greater than that for a liquid of the same viscosity.

To compare the two terms $\overline{\partial^2 u/\partial x^2}$ and $\overline{\partial^2 u/\partial y^2}$, it will be noted that each is of the form: velocity/(length)^2. We have already seen that

$$\overline{\partial^2 u/\partial y^2} \cong -3\,\overline{u}/\overline{\lambda^2} \cong -q/\overline{\lambda^2},$$

indicating that the magnitude of this term is determined by the fact that large variations of u in the y-direction take place within the width of a single pore. Comparable variations of u in the x-direction, however, due to the expansion of the fluid, occur only in fairly large macroscopic distances. Consequently, we may write

$$\overline{\partial^2 u/\partial x^2} \cong \partial^2 q/\partial x^2 \cong q/l^2,$$

where l is a macroscopic distance. The ratio of the two terms is accordingly

$$\frac{\overline{\partial^2 u/\partial x^2}}{\overline{\partial^2 u/\partial y^2}} \approx \frac{\overline{\lambda^2}}{l^2} \quad . \quad . \quad . \quad . \quad . \quad . \quad . \quad . \quad . \quad . \quad . \quad . \quad (81)$$

Then, since $l^2 >> \overline{\lambda^2}$, it follows that the additional frictional drag caused by the divergence term is negligible, and this term may be deleted from the equation.

We conclude, therefore, from this approximate analysis, that Darcy's law in its differential form is the same for a gas as for a liquid, *provided that the flow behavior of a gas in small pore spaces, other than expansion, is similar to that of a liquid.*

It has been conclusively shown, however, by L. J. Klinkenberg[9] that the two flows are not similar, and that, in general, k_g, the permeability to gas based on the assumed validity of Darcy's law for gases, is not equal to k_l, the permeability to liquids; and, in fact, is not even a constant.

In the case of the flow of a liquid through small pores, the microscopic velocity v becomes zero at the fluid-solid boundary; for gas flow, on the contrary, there exists along the boundary a zone of slippage of thickness δ, which is proportional to the length of the mean-free path of the molecules. Consequently the gas velocity does not become zero at the boundaries, and the frictional resistance to the flow of gas is less than that for a liquid of the same viscosity and macroscopic velocity.

Since δ is proportional to the mean-free path, it is also approximately proportional to $1/p$. Consequently when the gas permeability, k_g, of a given porous solid is determined with the same gas at a number of different mean pressures, the resulting values of k_g, when plotted as a function of $1/p$, give a curve which is approximately linear with $1/p$. Moreover, different gases, having different mean-free paths, give curves of different slopes. The limiting value of k_g *as* $1/p \to 0$, or as p becomes very large, is also equal to k_l, the permeability obtained by means of a liquid (Fig. 7).

In view of this fact it is clear that, in general, the flow of gases through porous solids is not in accordance with Darcy's law. However, from Klinkenberg's data, at pressures greater than about 20 atmospheres (2×10^7 dynes/cm^2, or 300 psi), the value of k_g differs from k_l by less than 1 per cent. Therefore, since most oil and gas reservoir pressures are much higher than this, it can be assumed that gases do obey Darcy's law under most reservoir conditions.

FIELD EQUATIONS OF THE FLOW OF FLUIDS THROUGH POROUS SOLIDS

The establishment of Darcy's law provides a basis upon which we may now consider the field equations that must be satisfied by the flow of fluids through porous solids in general, three-dimensional space. This

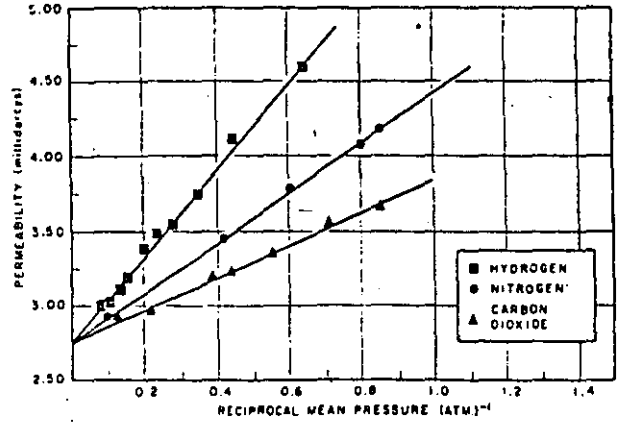

FIG. 7—VARIATION AS A FUNCTION OF $1/p$ OF THE APPARENT PERMEABILITY OF A GIVEN SOLID AS DETERMINED BY THE DIFFERENT GASES. THE VALUE OF 2.75 MD, AS $(1/p)$ TENDS TO 0, DIFFERS BUT SLIGHTLY FROM THAT OF 2.55 MD OBTAINED USING A LIQUID (AFTER L. J. KLINKENBERG, *API Drill. and Prod. Prac.*, 1941).

problem is complicated, however, by the fact that the fluids considered may be either of constant or of variable density; that one or several different fluids, either intermixed or segregated into separate macroscopic spaces, may be present simultaneously; and that all degrees of saturation of the space considered are possible.

The problem of dealing with such cases becomes tractable when we recognize that the behavior of each different fluid can be treated separately. Thus, for a specified fluid, there will exist at each point in space capable of being occupied by that fluid a macroscopic force intensity vector **E**, defined as the force per unit mass that would act upon a macroscopic element of the fluid if placed at that point. In addition, if the fluid does occupy the space, its macroscopic flow rate at the given point will be indicated by the velocity vector **q**, the volume of the fluid crossing unit area normal to the flow direction in unit time.

We shall thus have for each fluid two superposed fields, a field of force and a field of flow, each independently determinable. The equations describing the properties of each of these fields, and their mutual interrelations, comprise the field equations of the system; these in turn, in conjunction with the boundary conditions, determine the nature of the flow.

The Field of Force

We have seen already that the force per unit mass is given by

$$\mathbf{E} = \mathbf{g} - (1/\rho)\ \text{grad}\ p \quad . \quad . \quad . \quad . \quad . \quad . \quad (15)$$

and the force per unit volume by

$$\mathbf{H} = \rho\mathbf{E} = \rho\mathbf{g} - \text{grad}\ p \quad . \quad . \quad . \quad . \quad . \quad . \quad (17)$$

Either of these force vectors could be used, and either is determinable from the other, but before choosing one in preference to the other, let us first consider the properties of their respective fields, of which the most important for present purposes is whether or not the field has a potential. To simplify our analysis we will make the approximations that

$$\mathbf{g} = \text{const}\ , \quad . \quad . \quad . \quad . \quad . \quad . \quad . \quad . \quad . \quad . \quad (82)$$

and for chemically homogeneous liquids under the range of temperatures and pressures normally encountered in the earth to drillable depths,

$$\rho = \text{const}. \quad . \quad . \quad . \quad . \quad . \quad . \quad . \quad . \quad . \quad . \quad (83)$$

For gases, on the other hand, we shall have an equation of state

$$\rho = f(p, T) \quad . \quad . \quad . \quad . \quad . \quad . \quad . \quad . \quad . \quad . \quad (84)$$

where T is the absolute temperature.

The vector **E** has a particular value at each point in space and the ensemble of such values comprises its vector field. The criterion of whether this field has a potential, that is to say, of whether

$$\mathbf{E} = -\ \text{grad}\ \Phi\ ,$$

where Φ is a scalar field, is whether the field **E** is irrotational, which can be determined from its curl. From Eq. 15,

$$\begin{aligned} \text{curl}\ \mathbf{E} &= \text{curl}\ [\mathbf{g} - (1/\rho)\ \text{grad}\ p] \\ &= \nabla \times \mathbf{g} - \nabla \times [(1/\rho)\ \nabla p]. \end{aligned}$$

As is well known, the gravity field is irrotational even without the assumption that $\mathbf{g} = \text{const}$, so that $\nabla \times \mathbf{g} = 0$. Also

$$\begin{aligned} &-\nabla \times [(1/\rho)\ \nabla p] = -\nabla(1/\rho) \times \nabla p \\ &-(1/\rho)\ \nabla \times \nabla p \\ &= -\nabla(1/\rho) \times \nabla p\ . \end{aligned}$$

Consequently

$$\text{curl}\ \mathbf{E} = -\nabla(1/\rho) \times \nabla p = \nabla p \times \nabla(1/\rho)\ , \quad . \quad . \quad . \quad . \quad . \quad . \quad . \quad . \quad . \quad . \quad . \quad (85)$$

so that

$$\text{curl}\ \mathbf{E} = 0 \ \text{when}\ \nabla p \times \nabla(1/\rho) = 0 \quad . \quad (86)$$

Therefore, in order for the field to be irrotational, and hence derivable from a scalar potential, it is necessary either that $\nabla p = 0$, corresponding to constant pressure, or $\nabla(1/\rho) = 0$, corresponding to constant density, or else that the vectors ∇p and $\nabla(1/\rho)$ be collinear, corresponding to a coincidence of the surfaces of equal density and equal pressure.

The second of these three cases is satisfied by a liquid of constant density, and the third by a gas whose density is a function of the pressure only, such as occurs under either isothermal or adiabatic conditions. For the general case, however, of a gas for which $\rho = f(p, T)$, and the surfaces of equal temperature do not coincide with those of equal pressure, then the surfaces $\rho = \text{const}$ will also not coincide with the surfaces $p = \text{const}$ and we shall have two intersecting families of surfaces, $(1/\rho) = \text{const}$, and $p = \text{const}$, for which Eq. 85 applies.

This is the condition corresponding to thermal convection, and the fluid will have a convective circulation in the direction that will tend to bring the surfaces of equal density into coincidence with those of equal pressure, with the less dense fluid uppermost.

Hence, subject to the condition that either $\rho = \text{const}$, or $\rho = f(p)$,

$$\text{curl}\ \mathbf{E} = 0 \ \text{and}\ \mathbf{E} = -\ \text{grad}\ \Phi\ . \quad . \quad . \quad . \quad (87)$$

The value of Φ at any arbitrary point P in space (Fig. 8) is then obtained by

$$\left.\begin{aligned} \Phi(P) &= \Phi(P_o) - \int_{P_o}^{P} E_s\, ds \\ &= \Phi(P_o) - \int_{P_o}^{P} \left[g_s - (1/\rho)\frac{\partial p}{\partial s} \right] ds \\ &= \Phi(P_o) + \int_{o}^{z} g\, dz + \int_{p_o}^{p} \frac{dp}{\rho} \\ &= \Phi(P_o) + gz + \int_{p_o}^{p} \frac{dp}{\rho}\ , \end{aligned}\right\} \quad . \quad . \quad . \quad . \quad . \quad . \quad . \quad . \quad . \quad . \quad . \quad (88)$$

where the integral from P_o to P is taken along any path s. Then by setting $\Phi(P_o) = 0$ when $z = 0$ and $p_o = 1$ atmosphere, we obtain

$$\Phi(P) = gz + \int_{o}^{p} \frac{dp}{\rho}\ , \quad . \quad . \quad . \quad . \quad . \quad . \quad . \quad (89)$$

where p is now the gauge pressure, or the absolute pressure less 1 atmosphere.

If the fluid is incompressible and chemically homogeneous, this reduces to the simpler form

$$\Phi(P) = gz + p/\rho\ . \quad . \quad . \quad . \quad . \quad . \quad . \quad . \quad . \quad (90)$$

For this case, if a manometer is tapped into the system at the point P, the height h above the level $z = 0$, to which the liquid will rise, will be

$$h = z + p/\rho g \quad , \quad . \quad . \quad . \quad . \quad . \quad . \quad . \quad . \quad (91)$$

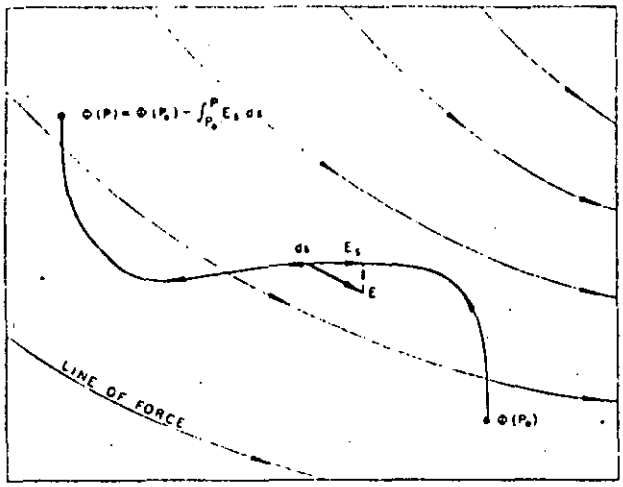

FIG. 8—THE POTENTIAL Φ AS A LINE INTEGRAL OF THE FIELD OF FORCE E.

from which it follows that

$$gh = gz + p/\rho = \Phi \quad . \quad . \quad . \quad . \quad . \quad . \quad . \quad . \quad (92)$$

in agreement with our earlier definition of Φ in Eq. 14.

If the fluid is incompressible and chemically inhomogeneous, as in the case of water of variable salinity, the density ρ will not be a function of pressure only, and, in general, surfaces of constant density will not be parallel to surfaces of constant pressure. For such a system curl $\mathbf{E} \neq 0$, and no potential exists.

We thus see that, with the exception of cases of thermal convection, and of inhomogeneous liquids of variable density, the fields E for both liquids and gases are irrotational and are derivable from a potential Φ. Since E is a force per unit of mass, then Φ is an energy per unit of mass, and represents the work required to transport the given fluid by a frictionless process along a prescribed (p, T)-path from a standard position and state to that of the point considered. Surfaces $\Phi = \text{const}$ are accordingly equipotential surfaces, or surfaces of constant energy of position, and the fluid will tend to flow from higher to lower potentials or energy levels.

The field of force per unit volume, H, can be disposed of summarily. Since

$$\mathbf{H} = \rho\mathbf{g} - \text{grad } p ,$$

then

$$\begin{aligned} \text{curl } \mathbf{H} &= \nabla \times (\rho\mathbf{g}) - \nabla \times \nabla p \\ &= \nabla\rho \times \mathbf{g} + \rho\nabla \times \mathbf{g} - \nabla \times \nabla p . \end{aligned}$$

But, since $\nabla \times \nabla p$ and $\nabla \times \mathbf{g}$ are each zero, then

$$\text{curl } \mathbf{H} = \nabla\rho \times \mathbf{g} \quad . \quad . \quad . \quad . \quad . \quad . \quad . \quad . \quad (93)$$

This is zero only when ρ is constant or when the surfaces of constant density are horizontal. The last condition never occurs except when the fluid is at rest or when the motion is vertical. Hence, for motion in any direction other than vertical, the field of the vector H does not have a potential except when the density of the fluid is constant. For the special case of constant density,

$$\mathbf{H} = - \text{grad } \Pi , \quad . \quad . \quad . \quad . \quad . \quad . \quad . \quad . \quad (94)$$

where

$$\Pi = \rho\Phi = \rho gz + p . \quad . \quad . \quad . \quad . \quad . \quad . \quad . \quad . \quad (95)$$

is the energy per unit volume of the fluid at any given point.

In view of the fact that the field E has a potential for both liquids and gases under the conditions specified above, whereas, in general, the field H has a potential only for the special case of liquids of constant density, then there is no advantage in using the latter in preference to the former, and henceforth it shall be dropped from further consideration.

The generality of the field of force, as herein defined, merits attention. The force vector E for any given fluid not only has values in space occupied by that fluid, but also in any space capable of being occupied by the fluid. At a point in air, for example, the force $\mathbf{E}_w$ for water would be

$$\mathbf{E}_w = \mathbf{g} - (1/\rho_w) \text{ grad } p,$$

and since, in air, grad p is $\rho_{air}\,\mathbf{g}$, then

$$\mathbf{E}_w = \frac{\rho_w - \rho_{air}}{\rho_w}\,\mathbf{g} \cong \mathbf{g} . \quad . \quad . \quad . \quad . \quad . \quad . \quad . \quad (96)$$

The field E for a given fluid thus extends throughout all space of continuous permeability. When several fluids are to be considered, then at each point in space there will be a different value of E, for each separate fluid, given by:

$$\left.\begin{aligned} \mathbf{E}_1 &= \mathbf{g} - (1/\rho_1) \text{ grad } p , \\ \mathbf{E}_2 &= \mathbf{g} - (1/\rho_2) \text{ grad } p , \\ &\cdots\cdots\cdots\cdots \\ \mathbf{E}_n &= \mathbf{g} - (1/\rho_n) \text{ grad } p . \end{aligned}\right\} \quad . \quad . \quad . \quad . \quad . \quad . \quad (97)$$

The vectors E for the separate fluids of different densities will differ among themselves, both in magnitude and direction, but will all fall in the same vertical plane, that defined by g and − grad p (Fig. 9).

Similarly the potentials of different fluids at the same point will be:

$$\left.\begin{aligned} \Phi_1 &= gz + \int (dp/\rho_1) , \\ \Phi_2 &= gz + \int (dp/\rho_2) , \\ &\cdots\cdots\cdots\cdots \\ \Phi_n &= gz + \int (dp/\rho_n) , \end{aligned}\right\} \quad . \quad . \quad . \quad . \quad . \quad . \quad (98)$$

where $\rho_1, \rho_2, \ldots \rho_n$ are the variable densities of the separate fluids.

Since the equipotential surfaces for the separate fluids must be normal to the respective vectors E, then it follows that the equipotential surfaces of different fluids passing through a given point will not be parallel to one another, although they will all intersect along a line normal to the (g, − grad p)-plane.

THE FIELD OF FLOW

We have already defined the flow vector q for a space which is entirely filled with a single fluid. For a space which is incompletely filled with a single fluid, or is occupied by two or more intermixed fluids, then there will be two or more superposed flow fields, not in general in the same direction, and a separate value of q for each separate fluid.

The principal condition which must be satisfied by the field of flow independently of the field of force is that it must be in accord with the principle of the conservation of mass. Thus, if a closed surface, S, fixed with respect to the porous solid, is inscribed within the field of flow, then the total net outward mass flux of any given fluid in unit time will be equal to the diminution of the mass of that fluid enclosed by S, assuming that processes which create or consume the given fluid are forbidden.

This condition is expressed by

$$\int\!\!\int_S \rho q_n \, dS = - \partial m/\partial t \quad . \quad . \quad . \quad . \quad . \quad . \quad . \quad (99)$$

where q_n is the outward-directed normal component of $\mathbf{q}$, and m the mass enclosed (Fig. 10).

In the case of a space completely saturated with the given fluid, by dividing the integral (Eq. 99) by the volume V and then letting V tend to zero, we obtain

$$\text{div } \rho\mathbf{q} = \lim_{V \to 0} \frac{1}{V} \iint_S \rho q_n \, dS = -\frac{1}{V}\frac{\partial m}{\partial t} , \quad . . . . . (100)$$

which is the rate of loss of mass per unit macroscopic volume at a given point. Then, since

$$\partial m/\partial t = fV \, (\partial \rho/\partial t) ,$$

Eq. 100 becomes

$$\text{div } \rho\mathbf{q} = -f(\partial \rho/\partial t) , \quad . . . . . (101)$$

which is the so-called "equation of continuity" of the flow. If the motion is steady, then $\partial \rho/\partial t$ is zero, and the equation simplifies to

$$\text{div } \rho\mathbf{q} = 0 . \quad . . . . . (102)$$

When this is expanded it becomes

$$\text{div } \rho\mathbf{q} = \nabla \cdot \rho\mathbf{q} = \nabla\rho \cdot \mathbf{q} + \rho \nabla \cdot \mathbf{q} = 0 ,$$

and when ρ is constant over space, corresponding to the flow of a homogeneous liquid, $\nabla\rho = 0$, and

$$\text{div } \mathbf{q} = 0 . \quad . . . . . (103)$$

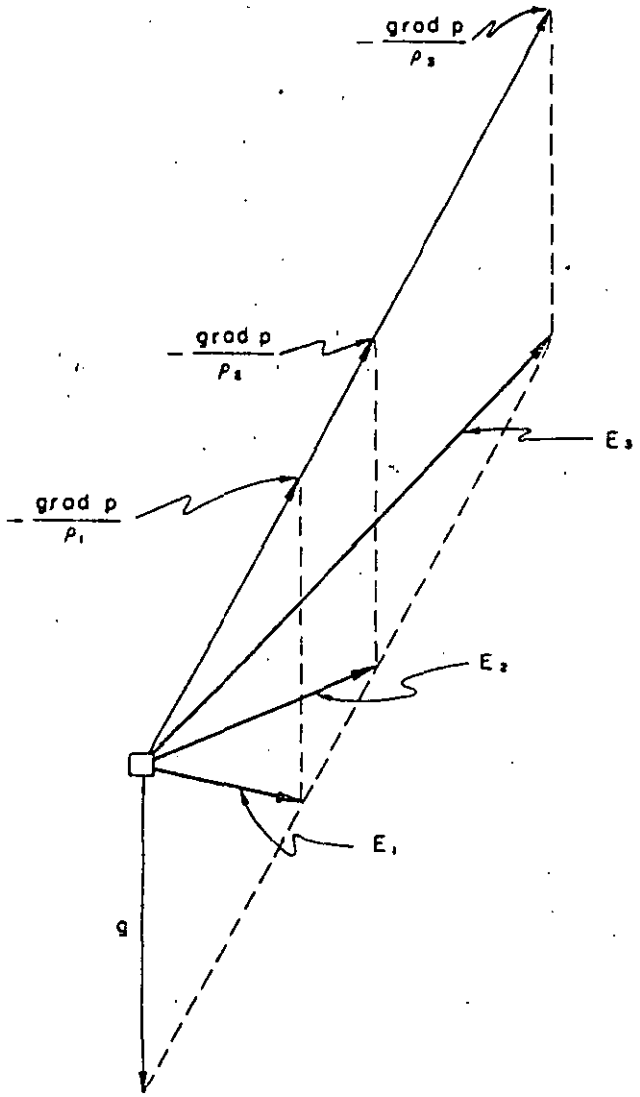

FIG. 9—FORCE VECTORS E AT THE SAME POINT CORRESPONDING TO FLUIDS OF DIFFERENT DENSITIES.

RELATION BETWEEN FIELD OF FORCE AND FIELD OF FLOW

In a space completely saturated by a single fluid, the field of flow and the field of force are linked together by Darcy's law

$$\mathbf{q} = \sigma\mathbf{E} , \quad . . . . . (104)$$

which, in those cases for which curl $\mathbf{E} = 0$, becomes

$$\mathbf{q} = -\sigma \text{ grad } \Phi . \quad . . . . . (105)$$

If the solid is isotropic with respect to permeability, the conductivity σ is a scalar and the flowlines and the lines of force will coincide; if the solid is anisotropic, σ will be a tensor and $\mathbf{E}$ and $\mathbf{q}$ will then differ somewhat in direction except when parallel to the principal axes of the tensor.

Limiting our discussion to isotropic systems, by taking the curl of Eq. 105, we obtain

$$\text{curl } \mathbf{q} = -\nabla \times \sigma\nabla\Phi = -\nabla\sigma \times \nabla\Phi - \sigma\nabla \times \nabla\Phi .$$

Then, since the last term to the right is zero, this becomes

$$\text{curl } \mathbf{q} = -\nabla\sigma \times \nabla\Phi , \quad . . . . . (106)$$

which is zero only when σ is constant throughout the field of flow. Therefore, in general,

$$\text{curl } \mathbf{q} \neq 0 , \quad . . . . . (107)$$

and this circumstance precludes the derivation of the flow field from an assumed velocity potential, for, with the exception of the flow of a fluid of constant density and viscosity in a space of constant permeability, no such function exists.

The flow of a given fluid through a porous solid incompletely saturated with that fluid is equivalent to flow through a solid of reduced permeability, because the space available to the flow diminishes as the saturation decreases. For saturations greater than some critical minimum value, the flow obeys Darcy's law subject to the permeability having this reduced, or so-called, "relative-permeability" value. Thus, with two interspersed but immiscible fluids in the same macroscopic space,

$$\left.\begin{aligned} \mathbf{q}_1 &= \sigma_{r1}\mathbf{E}_1 = \sigma_{r1}[\mathbf{g} - (1/\rho_1) \text{ grad } p] , \\ \mathbf{q}_2 &= \sigma_{r2}\mathbf{E}_2 = \sigma_{r2}[\mathbf{g} - (1/\rho_2) \text{ grad } p] , \end{aligned}\right\} . . (108)$$

where σ_{r1} and σ_{r2} are the relative conductivities of the two fluids.

It will be noted that, except for vertical motion, $\mathbf{E}_1$ and $\mathbf{E}_2$ are not parallel. Consequently the two force fields and flow fields will be, in general, transverse to one another.

Pioneer work on relative permeability as a function of saturation was done on the single fluid, water, by L. A. Richards[9] in 1931. Subsequently studies of the simultaneous flow of two or more fluids were initiated by Wyckoff and Botset,[10] and by Hassler, Rice, and Leeman[11] in 1936. Since that time many other such studies for the systems water-oil-gas have been published.

One flaw which has been common to most of these multifluid experiments has been that the experimental arrangements and their interpretation were usually based upon the premise that the flowlines of the various components are all parallel and in the direction

REFERENCES

1. Darcy, Henry: *Les Fontaines Publiques de la Ville de Dijon*, Victor Dalmont, Paris (1856).

2. Wyckoff, R. D., Botset, H. G., Muskat, M., and Reed, D. W.: "The Measurement of the Permeability of Porous Media for Homogeneous Fluids," *Rev. Sci. Instruments* (1933), 4, 394.

3. A.P.I. Code No. 27, "Standard Procedure for Determining Permeability of Porous Media" (Tentative), 1st Edition (Oct., 1935), American Petroleum Institute.

4. Fancher, G. H., Lewis, J. A., and Barnes, K. B.: "Some Physical Characteristics of Oil Sands," Pennsylvania State College Mineral Industries Experiment Station Bulletin 12 (1933), 65.

5. Reynolds, Osborne: "An Experimental Investigation of the Circumstances Which Determine Whether the Motion of Water Shall Be Direct or Sinuous and of the Law of Resistance in Parallel Channels," *Philos. Trans. Royal Soc. London* (1883), 174, 935; or *Papers on Mechanical and Physical Subjects*, University Press, Cambridge (1901), Vol. II, 51.

6. Corrsin, Stanley: "A Measure of the Area of a Homogeneous Random Surface in Space," *Quart. Appl. Math.* (1954-1955), 12, 404.

7. Brooks, C. S., and Purcell, W. R.: "Surface Area Measurements on Sedimentary Rocks," *Trans.* AIME (1952), 195, 289.

8. Klinkenberg, L. J.: "The Permeability of Porous Media to Liquids and Gases," *API Drill. and Prod. Prac.* 1941 (1942), 200.

9. Richards, L. A.: "Capillary Conduction of Liquids Through Porous Mediums," *Physics* (1931), 1, 318.

10. Wyckoff, R. D., and Botset, H. G.: "The Flow of Gas-Liquid Mixtures Through Unconsolidated Sands," *Physics* (1936), 7, 325.

11. Hassler, Gerald L., Rice, Raymond R., and Leeman, Erwin H.: "Investigations on the Recovery of Oil from Sandstones by Gas Drive," *Trans.* AIME (1936), 118, 116.

12. Hubbert, M. King: "The Theory of Ground-Water Motion," *Jour. Geol.* (1940), 48, 785.

13. Hubbert, M. King: "Entrapment of Petroleum Under Hydrodynamic Conditions," *Bull.* AAPG (1953), 37, 1954.

★★★

OPERATING MANUAL

UNIVERSAL POROMETER

MODEL NO. 1053-801

SERIAL NO. 27669

RUSKA INSTRUMENT CORPORATION

REGISTRATION CARDS

You have just joined the growing group of discriminating technicians, engineers, and scientists who have chosen Ruska Instruments.

To insure the best possible after-the-sale service, please fill in the postage paid registration card below and mail it as soon as possible.

After putting your instrument or system in service, the second "follow-up" card should be completed and mailed. This will assist Ruska in its continuing effort to provide the best instruments and service to our valued customers.

Thank you again for choosing Ruska.

FOLLOW-UP CARD

DATE: _____

COMPANY NAME AND ADDRESS _____

_____

_____

YOUR NAME AND TITLE _____

INSTRUMENT OR SYSTEM NUMBER _____ SERIAL NO. _____

WHAT IS YOUR APPLICATION? _____

WHY DID YOU CHOOSE RUSKA? _____

_____

IS YOUR INSTRUMENT PERFORMING AS EXPECTED? YES ☐ NO ☐

IF NO, PLEASE DESCRIBE _____

_____

ARE YOU INTERESTED IN OTHER RUSKA PRODUCTS? YES ☐ NO ☐

PLEASE DESCRIBE REQUIREMENT _____

_____

THANK YOU!

MAIL TODAY

WARRANTY REGISTRATION CARD

COMPLETE COMPANY NAME AND ADDRESS _____

_____

_____

INSTRUMENT OR SYSTEM MODEL NUMBER _____

SERIAL NUMBER _____

DATE RECEIVED _____

NAME AND TITLE OF PERSON FILLING OUT CARD

RUSKA INSTRUMENT CORPORATION • HOUSTON, TEXAS

TEST REPORT

PRESSURE TEST

Description of Apparatus Tested UNIVERSAL POROMETER

Model 1053-801 Serial Number 27669 Mfr. RUSKA

FOR

INSTITUTO DE INVESTIGACIONES ELECTRICAS

MEXICO

Customer's Order No. 0736 Job No. M068480
E-00048

PRESSURE TEST SPECIFICATION NO. ER-171

	SPECIFIED	TESTED
Working Pressure	1,000 psi	
Test Pressure	2,000 psi	2,000 psi
Working Temperature	Ambient	Ambient
Duration of Test	10 minutes	10 min.
Number of Cycles	One	1
Test Fluid	Nitrogen	GN_2
Test Gage	Bourdon Tube	PG-137
Accuracy of Gage	2%	2%
NBS Traceability Test No.		194533

Description of Test Before the gage was attached, the unit was proof-pressure tested in the Ruska blockhouse.

Test Completed, Date 10-July-80 Observer H. J. Baldwin

Responsible Officer E Z Hicks

Title V. P. Technical Services

RUSKA *reservoir engineering instrumentation*

UNIVERSAL POROMETER

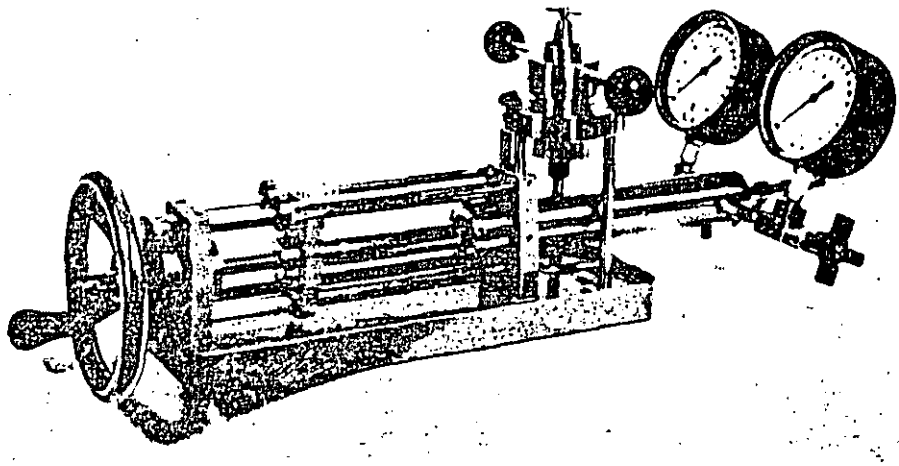

UNIVERSAL POROMETER

The RUSKA Universal Porometer is a versatile, accurate apparatus for determining porosity of consolidated porous bodies such as cores from subsurface geologic strata. The porometer lends itself to use by two methods: the Kobe, or Boyle's Law, method and the mercury injection method, each having its particular advantages. The ease of operation makes this instrument especially suitable for use in core analysis laboratories which process large number of cores. Rugged construction makes it equally suitable for use in the field.

The porometer consists of a 100 cc volumetric mercury pump, to which a pycnometer is attached. The pump has a precision ground and honed, hard-chrome plated plunger and a precision measuring screw. The chamber of the pycnometer admits cores to 1¼" long and 1½" in diameter. The porometer is furnished with one or two test-quality pressure gages, with ranges dependent on the method of operation.

A rapid acting breech-lock closure with O-ring seal is provided for the pycnometer. A needle valve in the pycnometer lid opens the chamber to atmosphere. Displacement of the pump metering plunger is indicated on scales and a micrometer dial. The easily read graduations of the scales and dial provide direct readings of volumes to 0.01 cc. The base, which is functionally designed, has mounting holes at the corners and an elevated rim to trap spilled mercury.

For porosity measurements where accuracy is the prime factor, the Boyle's Law method is commonly used. In this method, a fixed volume of air at atmospheric pressure is compressed to an indicated volume at a reference pressure, usually 30 psi or 2 kg/cm^2. This procedure is then repeated with the core specimen in the pycnometer, providing data from which the core grain volume is readily calculated. The bulk volume of the core is measured by mercury displacement in the pycnometer and read directly on the volume scale. From the grain and bulk volume measurements, the porosity is calculated. Since the sample has been penetrated only by

air, it can be used for additional core analysis tests.

In those situations where accuracy must be sacrificed for speed, and it is immaterial that the specimen cannot be tested further, the mercury injection method can be used. The bulk volume similarly is obtained by mercury displacement; the pore volume is obtained by measuring the volume of mercury forced into the pore spaces at high pressure, usually 750 psi or 50 kg/cm^2. The ratio of these volumes gives the fractional porosity of the sample. Although this is undoubtedly the faster of the two methods, it may be subject to considerable error due to capillary effects. Additionally, a correction must be applied to the volume of mercury injected to compensate for air entrapped in the pore spaces at the reference pressure. Therefore, in view of the considerable shortcomings of the mercury injection method, caution should be exercised during its application.

The instrument can also be furnished equipped with two gages, thus becoming a universal porometer which can be operated as a Boyle's Law porometer and as a mercury injection porometer. A cut-off valve is then provided for the low range pressure gage so this this gage will not be damaged when the higher pressures necessary for mercury injection are applied.

ORDERING INFORMATION

PRODUCT NO.	DESCRIPTION
1051-801-00	BOYLE'S LAW POROMETER, with 60 psi gage, complete with tools, 5 spare pycnometer gaskets, and operating instructions, evacuated and filled with mercury. DIMENSIONS: 10" x 8" x 29" WEIGHT: 50 pounds
1051-805-00	BOYLE'S LAW POROMETER, with 4 kg/cm^2 gage, complete with tools, 5 spare pycnometer gaskets, and operating instructions, evacuated and filled with mercury. DIMENSIONS: 10" x 8" x 29" WEIGHT: 50 pounds
1052-801-00	MERCURY INJECTION POROMETER, with 1000 psi gage, complete with tools, 5 spare pycnometer gaskets, and operating instructions, evacuated and filled with mercury. DIMENSIONS: 10" x 8" x 29" WEIGHT: 50 pounds
1052-805-00	MERCURY INJECTION POROMETER, with 60 kg/cm^2 gage, complete with tools, 5 spare pycnometer gaskets, and operating instructions, evacuated and filled with mercury. DIMENSIONS: 10" x 8" x 29" WEIGHT: 50 pounds
1053-801-00	UNIVERSAL POROMETER, with one each 60 psi and 1000 psi gage and with cut-off valve for the 60 psi gage, complete with tools, 5 spare pycnometer gaskets, and operating instructions, evacuated and filled with mercury. DIMENSIONS: 10" x 10" x 29" WEIGHT: 54 pounds
1053-805-00	UNIVERSAL POROMETER, with one each 4 kg/cm^2 and 60 kg/cm^2 gage and with cut-off valve for the 4 kg/cm^2 gage, complete with tools, 5 spare pycnometer gaskets, and operating instructions, evacuated and filled with mercury. DIMENSIONS: 10" x 10" x 29" WEIGHT: 54 pounds

ORDER BY PRODUCT NUMBER

OPERATING INSTRUCTIONS

RUSKA UNIVERSAL POROMETER

I. DESCRIPTION OF THE INSTRUMENT

The Ruska Universal Porometer is a versatile, accurate apparatus for determining porosity of consolidated porous bodies such as cores from subsurface geologic strata. The porometer lends itself to use by two methods: the Kobe or Boyle's Law method and the mercury injection method, each having its particular advantages. The ease of operation makes this instrument especially suitable for use in core analysis laboratories which process large number of cores. Rugged construction makes it equally suitable for use in the field.

The porometer consists of a 100 cc volumetric mercury pump, to which a pycnometer is attached. The pump has a precision ground and honed, hard-chrome plated, stainless steel plunger and an alloy steel measuring screw. The chamber of the stainless steel pycnometer has a volume of approximately 50 cc and admits cores up to 1¼" long and 1½" in diameter. The porometer is furnished with one or two test quality pressure gages, with ranges dependent on the method of operation.

The pycnometer lid has a rapid acting breach-lock closure with an "O" ring seal. A needle valve in the lid opens the chamber to atmosphere. The movement of the pump metering plunger is indicated on two scales. The right and left hand scales provide, respectively, decreasing and increasing readings with the forward stroke of the plunger. Both scales are graduated to read the plunger displacement in cubic centimeters. The handwheel dial is graduated in 0.01 cc subdivisions and permits estimation of plunger displacement to 0.001 cc. The right hand scale, which has decreasing graduations, is used for all volume measurements during determination of porosity by the Kobe method. Additionally, the right hand scale is used to provide

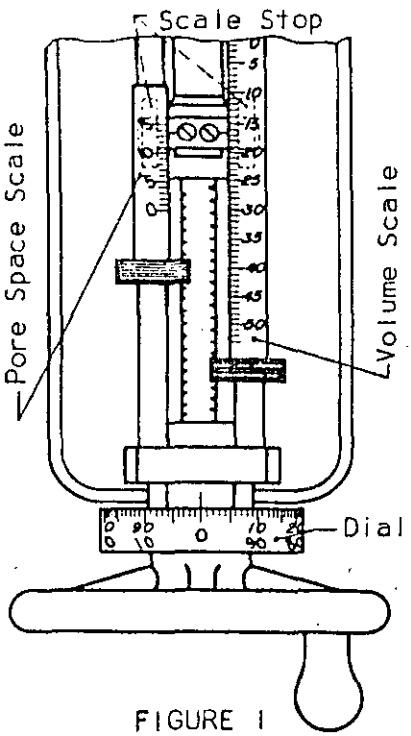

FIGURE 1

bulk volume readings when the mercury injection method of porosity measurement is used. The sole function of the left hand scale, which has increasing graduations, is to indicate the pore space volume when the mercury injection method is used. The right hand and left hand scales are respectively referred to as the VOLUME SCALE AND PORE SPACE SCALE. The numbers on the volume scale slant right and those on the pore space scale slant left, facilitating selection of the corresponding numbers on the handwheel dial: those slanting right supplement volume scale readings and those slanting left supplement pore space scale readings.

To avoid reading errors due to backlash between measuring screw and nut, all readings must be taken on the in-stroke. If a volume measurement has been overshot, the operator should back off at least one handwheel turn and take a new reading.

2. PREPARATION OF THE INSTRUMENT FOR SERVICE

The pycnometer is readied for service by thorough evacuation and subsequent filling with mercury, using the arrangement shown on Page 3. Approximately four pounds of mercury constitute a proper charge.

The pycnometer lid is locked in position and its valve closed. The pump plunger is withdrawn so as to create a void space in the pump cylinder of 45-50 cc. After opening the pinch clamp on the vacuum tubing and the fill valve in the cylinder end, the porometer system and mercury-filled flask are evacuated for one to two hours. The manometer is used for leak detection and measurement of vacuum efficiency.

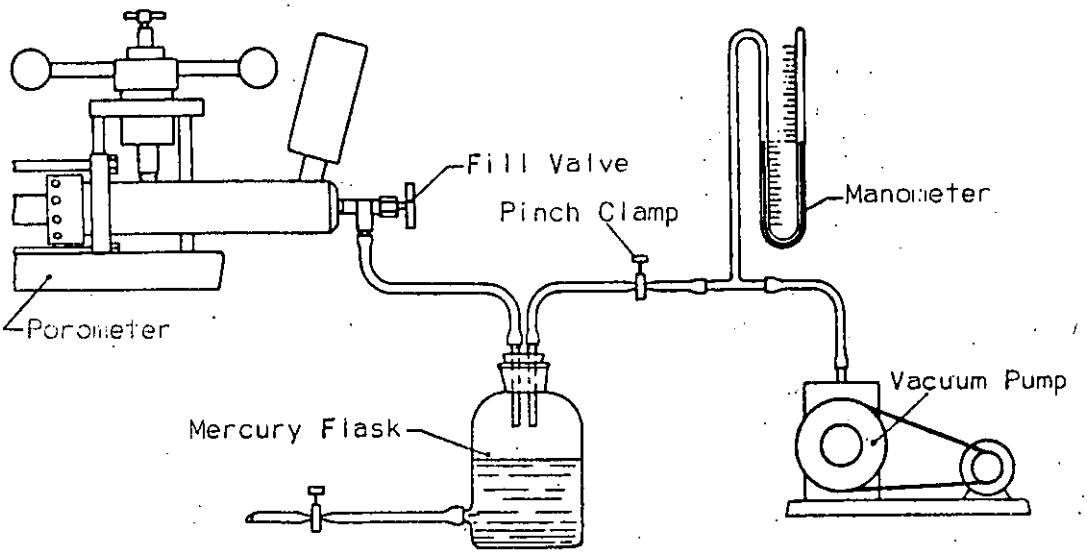

FIGURE 2

When a satisfactory vacuum (i.e. no manometer-detectable pressure exists in system) has been maintained for the prescribed period, the pinch clamp is closed. The mercury flask is then inverted and raised above the porometer. If evacuation has been complete, mercury will gravitate into and fill the void space in the entire porometer system. The fill valve is closed and the pycnometer valve opened, thereby relieving the system vacuum without allowing air to enter the pump cylinder.

The plunger is withdrawn a short distance and the pycnometer lid removed. Foreign matter which may have collected on the mercury surface in the pycnometer should be removed. The pycnometer is now ready for the operation discussed in Sections 3, 4, and 5.

If in the course of operations, air is inadvertently admitted into the pump cylinder, the system must be evacuated essentially as described. However, at the outset, the pycnometer valve is left open with the vacuum pump operating. Air will then displace mercury from the system until the mercury level drops below the fill valve. Subsequently, when the pycnometer valve is closed, mercury blocks in the porometer or connecting tubing will have been precluded, and total vacuum will be attained in the entire system.

Only in the event a vacuum source is not available should the porometer be charged other than in the previously described manner. When such is the case, it is filled with approximately four pounds of mercury through the pycnometer. The mercury is drawn into the pump cylinder by withdrawal of the plunger with mercury present in the pycnometer. After charging the requisite amount of mercury, the pycnometer lid is locked in position, mercury brought up to the pycnometer valve seat, and the valve closed. To remove the trapped air, the porometer is tilted backwards until the face of the pressure gage is horizontal. By alternately moving the plunger in and out of the cylinder, first pressure and then suction is applied in the gage and system. Air trapped in the gage, as well as other parts of the system, is displaced by mercury and collects in a recess behind the packing gland. By bringing the instrument into its correct position, this air can be expelled into the pycnometer and subsequently released. It will be necessary to repeat this procedure several times to reduce the volume of trapped air to an acceptable level.

At the first opportunity, the porometer should be vacuum charged in the prescribed manner so that maximum accuracy in experimental results will be obtained.

3. DETERMINATION OF BULK VOLUME

The volume scale and handwheel dial provide direct readings in cubic centimeters of the bulk volume of a solid body, porous object, or core enclosed in the pycnometer. The bulk volume can be measured rapidly and accurately because of the design features and factory adjustments of the porometer. In particular, the presetting of the traveling yoke stop facilitates measurements. If the volume scale is engaged with the stop when the pycnometer is empty and the handwheel dial is correctly set, a volume scale reading of zero will be obtained when the pycnometer is full of mercury. That is, the scale reading will be zero when the forward movement of the pump plunger has displaced mercury into the empty pycnometer up to the seat of the pycnometer valve. The pycnometer is considered to be empty when

mercury is just visible in the bottom and full when the first droplet of mercury appears in the valve seat.

The void volume of a closed, empty pycnometer is approximately 50 cc. The exact volume is determined by factory calibration, and the yoke stop is set accordingly. For example, if the calibrated volume is 49.15 cc, the yoke stop is preset with the pycnometer empty so that a volume scale reading slightly more than 49 cc is obtained when the scale is engaged with the stop. The instrument is then readied for operation by simply adjusting the handwheel dial to read 15, using the dial numbers slanting to the right.

The determination of bulk volume, using a pycnometer with a volume of 49.15 cc, consists of the following procedural sequence:

a. With the pycnometer open to permit visual observation, mercury is withdrawn until the pycnometer is empty.

b. The volume scale is engaged with the yoke stop and the handwheel dial set to read graduation 15, slanted right.

c. The core or body is placed in the pycnometer and the pycnometer lid is locked in position, leaving the valve open.

d. Mercury is injected into the pycnometer until a bead of mercury appears in the pycnometer valve seat. (The appearance of the bead indicates the pycnometer is full, the void space being completely occupied by mercury and body.)

e. The volume of the body is read directly on the volume scale and handwheel dial numbers slanting right. For example, if the volume scale reading is somewhat greater than 12 cc and the dial indicates 32½, the bulk volume of the body is exactly 12.325 cc.

4. DETERMINATION OF POROSITY BY MERCURY INJECTION

Following the determination of bulk volume, the pore space, and consequently the porosity of a core, can be evaluated by mercury injection with-

out removing the core from the pycnometer. In essence, the method consists of a measured, high pressure injection of mercury into the pore spaces of the core, utilizing the left hand or pore space scale and handwheel dial for exact metering of the volume of mercury thus injected. The volume injected is considered to be equivalent to the pore volume, subject to correction for the air trapped and compressed in the core. Since the recommended injection or reference pressure is 750 psig, or approximately 50 atmospheres, an additive two per cent correction of the pore space reading is necessary.

When the porometer is employed for pore space measurements, compensation must be made for the volumetric expansion of the porometer system between atmospheric and reference pressures. This magnitude of this compensation is called the "correction factor"; it is equal to the volume of of mercury displaced by the plunger when the pressure in the mercury-filled instrument is raised from zero to reference pressure. The factor will remain constant as long as air is not permitted to enter the pump cylinder or attached gages. Careless operation of the porometer can result in air being drawn through the pycnometer into the pump cylinder.

The traveling yoke stop for the pore space scale also has been preset at the factory. If the handwheel dial is properly adjusted, the correction factor automatically will be compensated for during pore volume measurements, and direct readings of pore volume will be provided.

The correction factor is determined in the following manner:

a. The lid is locked in position on the empty pycnometer with the valve open, and the mercury level is brought up to the valve seat.

b. The pycnometer valve is closed, the pore space scale is engaged with the traveling yoke stop, and the handwheel dial is zeroed.

c. The system pressure is increased to the 750 psig reference pressure. The dial reading of the figures slanting left will be a direct measure

of the correction factor, which is noted. The correction factor should not exceed 0.50 cc; if it is larger, air is trapped in the system and must be removed in accordance with the servicing instructions.

d. With the system at 750 psig, the yoke stop is readjusted, if necessary, to provide a pore space scale reading of zero.

If, for example, the correction factor was measured as 0.27 cc, the accuracy of the correction factor is checked as follows:

e. Pressure is reduced in the system to atmospheric or less, and the pycnometer valve opened.

f. The mercury level is brought up to the valve seat. The pore scale is engaged with the traveling yoke stop, and using the figures slanting right, the handwheel dial is set at 27 for the correction factor.

g. The valve is closed and pressure increased to reference pressure. If the indicated pore space is 0.00, the accuracy of correction factor and the index mark setting are verified.

Assuming a pycnometer volume of 49.15 cc, a correction factor of 0.27 cc, and a measured core bulk volume of 12.325 cc (see Section 3, procedure for bulk volume measurements), the porosity of the core is determined by mercury injection as follows:

a. Immediately following bulk volume measurement, the pycnometer valve is closed on the bead of mercury visible in the valve seat.

b. The pore space scale is engaged with the traveling yoke stop, and using the figures slanting right, the handwheel dial is set at 27 for the correction factor.

c. The system pressure is raised to 750 psig.

d. The pore volume of the core is read directly on the pore space scale and the handwheel dial numbers slanting left. For example, if the pore space scale reading is somewhat greater than 3 cc and the dial indicates 21½, the pore volume of the core is exactly 3.215 cc.

e. The fractional porosity of the core can be calculated from the formula,

$$\text{Porosity} = \frac{\text{Pore Volume}}{\text{Bulk Volume}}$$

and, for the above example,

$$\text{Porosity} = \frac{3.215 \text{ cc}}{12.325 \text{ cc}} = 0.261$$

5. DETERMINATION OF POROSITY BY THE KOBE METHOD

The Kobe, or Boyle's Law, method is used for porosity measurements where accuracy rather than speed is the prime consideration. In contrast to the mercury injection method of direct measurement of pore space, the Kobe method determines the grain or solids volume of a porous mass. If the bulk volume is known, the porosity is readily calculated from the grain volume measurement, since the difference between bulk and grain volumes is equal to the pore space.

The Kobe method is based on Boyle's Law, which states that in a gaseous system the product of absolute pressure and volume is a constant at a given temperature. Through the application of Boyle's Law to porometer data, equations for the calculation of grain volume are derived. While an understanding of the derivation is not necessary for routine porometer operation, it is essential if, for example, modifications are to be made in standard procedures. For this reason, the derivation is described in the attached appendix.

CALIBRATION OF POROMETER FOR GRAIN VOLUME MEASUREMENTS

Where rapidity of operation is desired and a slight reduction in accuracy is acceptable, the response of the porometer to various grain volumes is determined initially. That is, by means of a preliminary calibration, a graphical relationship is obtained which facilitates future grain volume

measurements. Derivation of the relationship is effected in the following manner:

a. The porometer volume scale and dial are set in accordance with the instructions in Section 3, so that readings obtained equal the pycnometer volume less the volume of mercury in the pycnometer.

b. A 40.00 cc reference volume (V_R) of air at atmospheric pressure is enclosed in the pycnometer and compressed to the 30 psig reference pressure. The final volume scale and dial reading (V_F') is noted.

c. Step (b) is repeated until V_F' stabilizes, which indicates operating thermal equilibrium has been established. This stabilized V_F' value is recorded.

d. Assuming operating thermal equilibrium exists, a 38.00 cc reference volume of air at atmospheric pressure is enclosed in the pycnometer and compressed to the 30 psig reference pressure. The final volume scale and dial reading (V_F') is recorded.

e. Step (d) is repeated using a reference volume of 36.00 cc. With respect to Step (b), Steps (d) and (e) simulate the presence of grain volumes of 2.00 and 4.00 cc in the pycnometer prior to compression. Step (b) simulates zero grain volume.

f. The operations of Step (d) are repeated using successive 2.00 cc reference volume decrements until sufficient data are available to define the relationship between simulated grain volumes and the corresponding values of V_F' over the full range of the porometer. All data must be obtained under <u>constant</u> atmospheric pressure.

The experimental data are accumulated as shown in the table below, in Columns 1 and 3. The data show that when 40.00 cc of air are compressed to the reference pressure, a V_F' of 13.04 cc is obtained. The data also show that when 38.00 cc of air are compressed, a V_F' of 12.38 cc will result.

However, if the volume scale and dial initially indicated 40.00 cc (reference pycnometer volume) and a core with 2.00 cc grain volume was enclosed in the pycnometer together with 38.00 cc of air, a V_F' of 14.38 cc would have been obtained (sum of Columns 2 and 3). In a like manner, the true V_F' values can be calculated from data obtained with simulated grain volumes.

IDEALIZED DATA FOR THE
DEVIATION OF THE GRAPHICAL RELATIONSHIP
BETWEEN GRAIN VOLUME (V_G) AND COMPRESSION VOLUME (V_F')

Ref. Press: 30 psig Atm. Press: 750 mm Hg Ref. Pycn. Vol: 40.00 cc

(V_R) Reference Air Volume	(V_G) Simulated Grain Volume	V_F' Final Volume Reading	True V_F' Col. 2 + Col. 3
40.00 cc	0.00 cc	13.04 cc	13.04 cc
38.00	2.00	12.38	14.38
36.00	4.00	11.73	15.73
34.00	6.00	11.08	17.08
32.00	8.00	10.43	18.43
30.00	10.00	9.78	19.78
28.00	12.00	9.13	21.13
26.00	14.00	8.47	22.47
24.00	16.00	7.82	23.82
22.00	18.00	7.17	25.17
20.00	20.00	6.52	26.52
18.00	22.00	5.87	27.87
16.00	24.00	5.21	29.21

The data in Columns 2 and 4 are then graphically related, as illustrated in Figure 3. Therefore, if a core of unknown grain volume provides a V_F' of 17.20 cc, the grain volume is indicated by the graph to be 6.20 cc.

Although the data in the table are idealized, data obtained in actual practice will be similar. Each instrument, however, should be individually calibrated to avoid errors due to the entrapment of very small volumes of air or to the volumetric expansion of the porometer systems between atmospheric and reference pressure.

RELATIONSHIP BETWEEN GRAIN VOLUME (V_G)
AND COMPRESSION VOLUME (V_F')

Ref. Press: 30 psig Atm. Press: 750 mm Hg Ref. Pycn. Vol: 40.00 cc

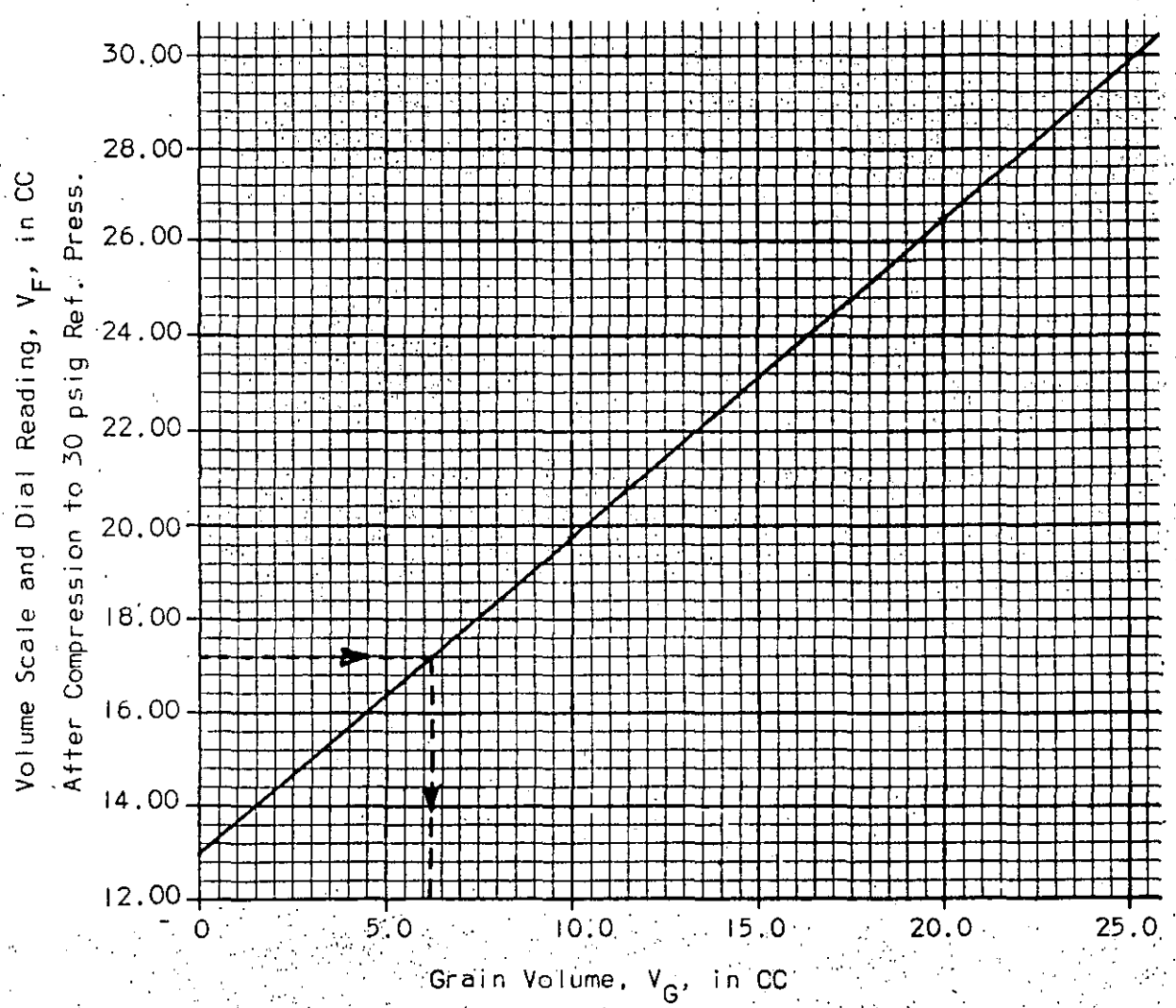

FIGURE 3

As mentioned above, all calibration work must be performed under constant atmospheric pressure. A correction factor is applied to grain volume data obtained under different atmospheric pressures. Figure 4 provides a simple method for determining the applicable correction factors.

CORRECTION FACTORS FOR VARIOUS ATMOSPHERIC PRESSURES
BASED ON 750 mm Hg CALIBRATION PRESSURE

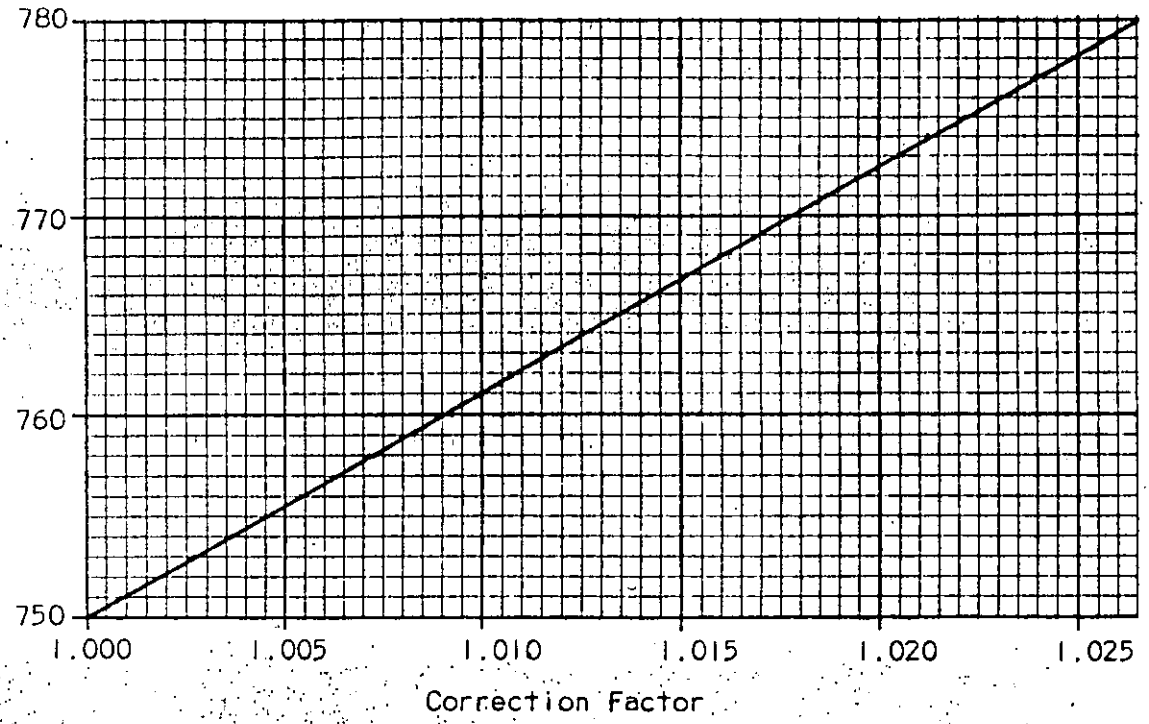

FIGURE 4

If, however, the porometer was calibrated at 757 mm Hg atmospheric pressure, the correction factors in Figure 4 are not applicable. The correct curve is obtained by dividing the abscissa values shown in Figure 4 by 1.0063 (value given for 757 mm Hg pressure) while retaining the same ordinate values. This correction factor curve will properly supplement the 757 mm calibration curve. The example below illustrates the procedure of the use of Figures 3 and 4.

EXAMPLE OF POROSITY DETERMINATION

Assuming the porometer scale and dial are set as prescribed in Section 3, the porosity of a core can be determined by the above modification of the Kobe method as follows:

a. Using a reference pycnometer volume of 40.00 cc, a core is enclosed in the pycnometer, the reference volume being indicated by the volume scale and dial.

b. Assuming operating thermal equilibrium exists, the system pressure is increased to 30 psig and the V_F' value is obtained from the volume scale and dial reading.

c. If atmospheric pressure differs from 750 mm Hg (pressure at which calibration curve was derived), a correction in the indicated V_F' value should be made. If atmospheric pressure is 770 mm Hg and the indicated V_F' was 26.52 cc, then by use of Figure 4,

$$\text{True } V_F' = \frac{\text{Indicated } V_F'}{\text{Correction Factor}} = \frac{26.52}{1.0178} = 26.06$$

d. Using the graphical relationship in Figure 3, the grain volume corresponding to the true V_F' value obtained is determined. A true V_F' of 26.06 cc corresponds to 19.10 cc grain volume.

e. The fractional porosity can be calculated, assuming the bulk volume, V_B, has been determined as outlined in Section 3:

$$\text{Porosity} = 1 - \frac{V_G}{V_B}$$

A P P E N D I X

I. DERIVATION OF EQUATIONS FOR CALCULATION OF GRAIN VOLUMES USING THE KOBE METHOD

Assume a reference volume of air at atmospheric pressure is enclosed in the pycnometer and subsequently compressed to some reference pressure. If the reference volume of air was equal, for example, to 40.00 cc and the volume scale and handwheel dial were set accordingly prior to compression, then in accordance with Boyle's Law;

$$P_A V_R = P_R V_F \qquad (1)$$

where

P_A = Atmospheric pressure

V_R = Reference air volume; equal to initial reading on volume scale and dial (40.00 cc)

P_R = Reference pressure, absolute; equal to test gage reading plus atmospheric pressure

V_F = Volume of V_R ater compression to P_R; equal to final reading on volume scale and dial.

Assume the pressure in the system is released and the pump plunger withdrawn until the volume V_R is indicated on the volume scale and dial as before. If a core of grain volume V_G is then enclosed in the pycnometer along with air at atmospheric pressure, the total volume of air in the pycnometer is given by:

$$\text{Volume Atmospheric Air} = V_R - V_G \qquad (2)$$

When the system is compressed to the reference pressure, P_R, the final reading on the volume scale and dial will equal the volume of compressed air in the pycnometer, plus the grain volume of the core.
That is,

$$\text{Volume of Compressed Air} = V_F - V_G \qquad (3)$$

where

V_F' = Compressed volume of $(V_R - V_G)$ plus grain volume of core; equal to final reading on volume scale and dial.

Therefore, using (2) and (3) above, the application of Boyle's Law provides the following relationship between the initial and final pycnometer conditions:

$$P_A (V_R - V_G) = P_R (V_F' - V_G) \quad (4)$$

where all terms have been defined previously. Clearing parentheses,

$$P_A V_R - P_A V_G = P_R V_F' - P_R V_G \quad (5)$$

Substitution of (1) in (5) gives,

$$P_R V_F - P_A V_G = P_R V_F' - P_R V_G \quad (6)$$

which, when solved for V_G, yields:

$$V_G = \frac{P_R}{P_R - P_A} (V_F' - V_F) \quad (7)$$

Equation (7) is the basic equation of the Kobe method of porosity determination. Although it can be used in such form, calculations would be comparatively tedious. Additionally, the accuracy of results would be dependent on the accuracy of gage and barometric pressure measurements. These objections can be circumvented by evaluating the ratio $\frac{P_R}{P_R - P_A}$ solely by pump manipulation and using the value so obtained for a series of grain volume measurements.

The ratio $\frac{P_R}{P_R - P_A}$ also called the pressure factor, F_P, likewise is derived by the application of Boyle's Law to porometer data. Referring to the method of Equation (1), if two successive compression runs are made using reference volumes (V_R) of 40.00 and 30.00 cc, the following relationships are obtained.

$$40.00\ P_A = V_F\ P_R \qquad (8)$$

$$30.00\ P_A = V_F'\ P_R \qquad (9)$$

where

V_F' = Volume of 30.00 cc air after compression to P_R.

Subtracting (8) from (9),

$$-10\ P_A = P_R\ (V_F' - V_F) \qquad (10)$$

Suitable algebraic treatment of (10) provides the following:

$$-\frac{P_A}{P_R} = \frac{V_F' - V_F}{10}$$

$$1 - \frac{P_A}{P_R} = 1 + \frac{V_F' - V_F}{10}$$

$$\frac{P_R - P_A}{P_R} \quad \frac{10 + V_F' - V_F}{10}$$

or

$$\frac{P_R}{P_R - P_A} = \frac{10}{10 + V_F' - V_F} \qquad (11)$$

Since the pressure factor, F_P, by definition is the ratio $\frac{P_R}{P_R - P_A}$ then from (11),

$$F_P = \frac{10}{10 + V_F' - V_F} \qquad (12)$$

When F_P is known and substituted in (7), the working equation for calculation of grain volumes by the Kobe method is obtained:

$$V_G = F_P\ (V_F' - V_F) \qquad (13)$$

Where all terms have been defined previously.

2. POROMETER OPERATION BY KOBE METHOD, OPTIONAL METHOD

The porometer volume scale and dial are set in accordance with the instructions in Section 3, so that readings obtained equal the pycnometer volume less the volume of mercury present in the pycnometer.

a. The 40.00 cc reference volume of air at atmospheric pressure is enclosed in the pycnometer and compressed to the 30 psig reference pressure. The final volume scale and dial reading, V_F, is noted.

b. Step (a) is repeated until V_F stabilizes, which indicates operating thermal equilibrium has been established. V_F is recorded, providing a numerical value indicated by the volume scale and dial for the V_F term in (13).

c. A volume of 30 cc of air, as indicated by the volume scale and dial, is compressed to 30 psig. The compressed volume, V_F', is recorded immediately since thermal equilibrium exists. The pressure correction, F_P, can now be calculated from (12) for use in (13).

d. The pump plunger is withdrawn until the volume scale and dial indicate 40.00 cc, and the core to be tested is enclosed in the pycnometer.

e. Pressure in the system is increased to the 30 psig reference pressure. The final volume scale and dial reading are recorded, providing a numerical value for the V_F' term (13).

Since V_F, F_P, and V_F' are now known, the fractional porosity can be calculated, assuming the bulk volume V_B has been determined as outlined in Section 3:

$$\text{Porosity} = 1 - \frac{F_P (V_F' - V_F)}{V_B} \qquad (14)$$

Steps (a), (b), and (c) are used for the evaluation of F_P, and, incidental to the evaluation, the numerical value of V_F is obtained also. These values will remain constant as long as barometric pressure does not

change, and the operating thermal equilibrium does not shift appreciably. As a precaution against such changes, the F_P should be re-evaluated frequently. Extensive experience indicates that the determination F_P after every 8-10 grain volume measurements provides accurate data. As the operator acquires experience in his particular environment, he will be able to ascertain readily the frequency with which F_P evaluation is required. The simplest check in the need for redetermination of F_P is repetition of Step (b) above, which would reveal any change which had occurred in V_F since the previous determination.

UNIVERSAL POROMETER CATALOG NO: 1053-801

INSTRUMENT NO. 27669

The pycnometer volume of this porometer was established as 47.40 cc.

Evacuated, filled, and tested at 1,000 psi ~~kg/cm²~~

Correction factor when inspected (see Pages 3 and 7) 0.39 cc.

Inspected by: S. Bedenbaugh

Date: 14 July, 1980

SERVICE PARTS LIST

Part No.	Req.	Description
54-700-220	5	Pycnometer Gasket
99540	1	Pump Packing, Set
58-110	4	Fill Valve Packing
1050-034	1	Pycnometer Valve
26-516	1	Pressure Gage, 1000 psi
26-518	1	Pressure Gage, 60 psi
26-520	1	Pressure Gage, 60 kg/cm^2
26-519	1	Pressure Gage, 4 kg/cm^2
94-617	1	Spanner Wrench
94-618	1	Spanner Wrench
99545-001	1	Packing Booster

RUSKA INSTRUMENT CORPORATION

P. O. BOX 36010 · HOUSTON, TEXAS 77036

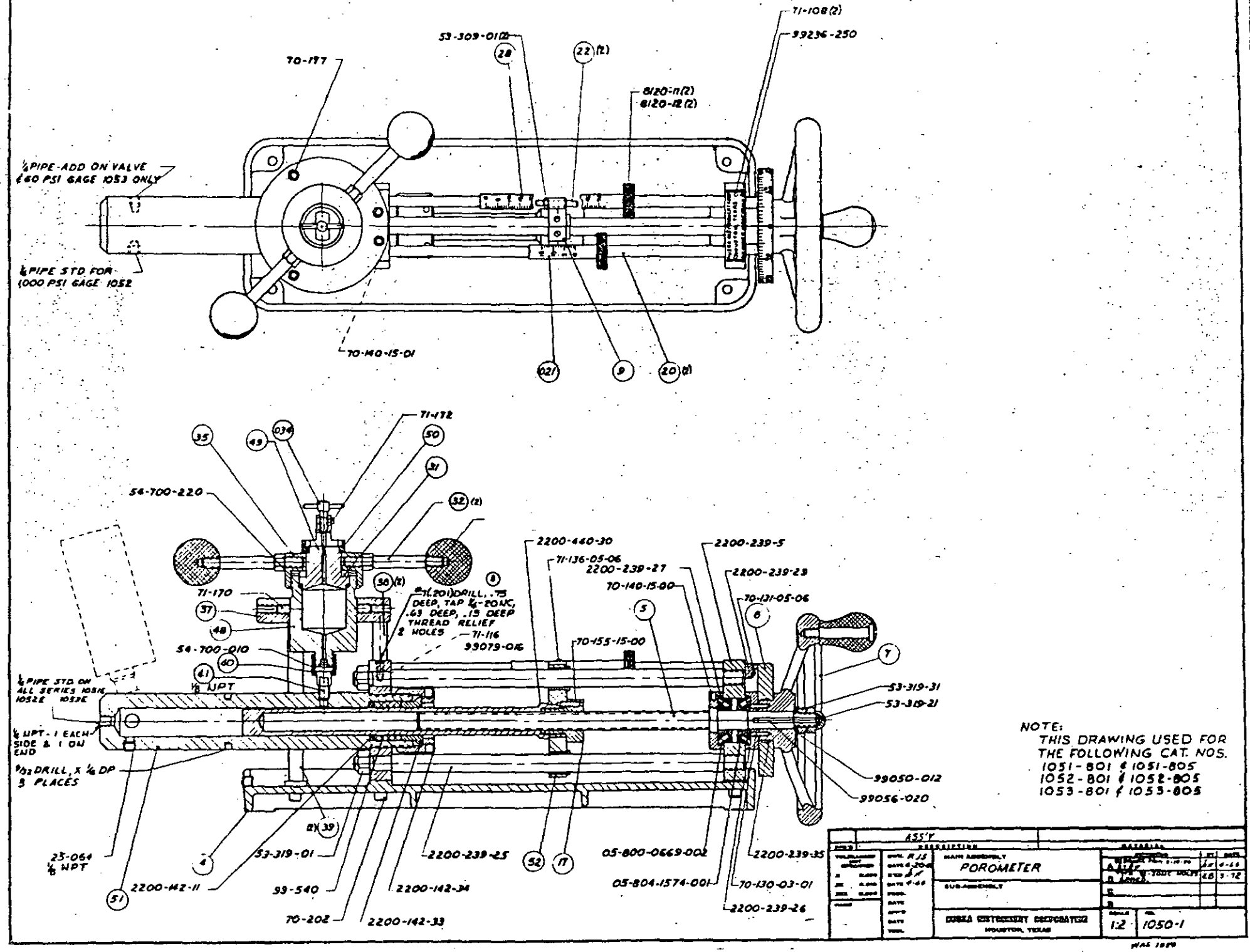

NOTE:
THIS DRAWING USED FOR THE FOLLOWING CAT. NOS.
1051-801 & 1051-805
1052-801 & 1052-805
1053-801 & 1053-805

ASS'Y				
MAIN ASSEMBLY	POROMETER			
SUB-ASSEMBLY				
CORE LABORATORY INCORPORATED HOUSTON, TEXAS		SCALE 1:2	DWG. 1050-1	

RUSKA UNIVERSAL POROMETER AND CAPILLARY PRESSURE APPARATUS

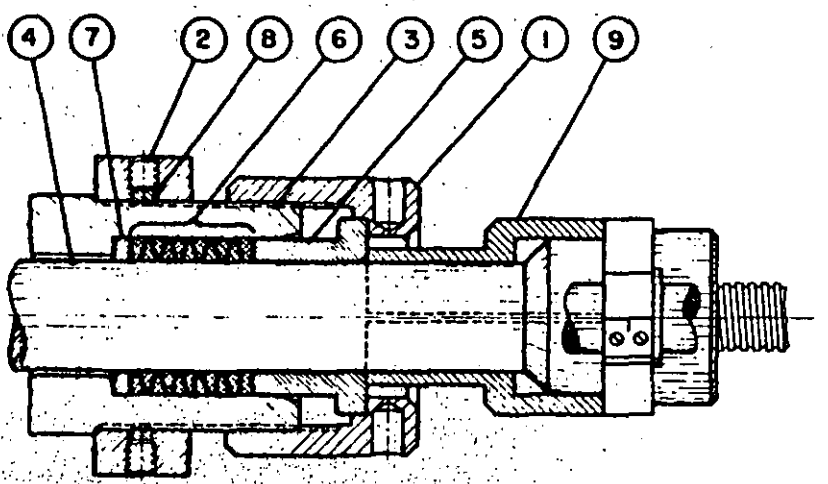

PACKING:

Ruska Volumetric Pump Units used in connection with the Universal Porometer and the Mercury Injection Capillary Pressure Apparatus are furnished with removable cylinders to facilitate packing and to make it unnecessary to use split packing rings. Wedge-shaped machined Teflon rings with alternately opposing wedge profiles are used to pack the pumps.

Teflon packing is impervious to the attack of all fluids that may be present in the pump. It will stand up under the most severe service, but is somewhat difficult to install. A special packing booster is required to compress the Teflon packing when the packing gland is tightened.

To repack the volumetric pump units of the Universal Porometer and the Capillary Pressure Apparatus, the pycnometer assembly must be disconnected from the pump cylinder by unscrewing the pycnometer bottom connection. The packing nut (1) must then be removed, and the set screws (2) on the rear yoke taken out, so that the cylinder (3) can be unscrewed. The packing space and the plunger (4) should be cleaned. The packing nut (1), follow ring (5), and the packing (6), in the order shown, are then slipped on the plunger and the cylinder is replaced, being sure that it is well locked in place. The junk ring (7) may remain in the cylinder. The serrated brass lock plugs (8) under the set screws on the rear yoke must be aligned with the threads on the cylinder. The plunger and packing should be slightly lubricated (see Lubrication). The packing is pushed in the packing space with the follow

[illegible]
AND
[illegible]

SUPPLEMENT TO MODELS 1050, 1051, 1052, AND 1053 OPERATING MANUAL

PROCEDURE FOR FILLING RUSKA POROMETER WITHOUT THE USE OF A VACUUM PUMP

GENERAL

To properly fill the Ruska Porometer with mercury, it is necessary to remove all air from the system, and replace it with mercury.

This process can be achieved in approximately one hour of carefully following the procedure outlined below. The achievement of a good solid system is evidenced by a correction factor of less than 0.35.

It is usually necessary to repeat the following total procedure at least four times to remove all of the air.

1. Open the gage cut-off valve if there are two gages on the pump.

2. With the pump in the normal attitude on the bench, approximately 4 pounds of mercury are drawn into the cylinder through the open pycnometer by withdrawing the plunger.

3. When all mercury is in the pump, the pycnometer lid is replaced and tightened.

4. Open the bleed valve on the pycnometer cap and advance the plunger until mercury appears at the valve opening.

5. Close the bleed valve.

6. Placing the front edge of the pump base casting (at the cylinder end) on the edge of a work bench, tilt the pump forward such that the cylinder points down. The gages must be slanted down such that the internal Bourdon tube is below the level of the gage connection to the pump.

7. With the pump in this position, advance and retract the plunger approximately 10 times. Each advance should be sufficient to create a reading of approximately 50 psi on the low pressure gage. When it appears that the low pressure gage is free of air, it is valved off and the pressurizing process is repeated to about 700 psi with the high pressure gage. If the pump has just one gage, this process is modified accordingly.

   Each withdrawal should be taken beyond the starting point sufficiently to create a suction.

8. After the 10 cycles are achieved, rock the pump from side to side while it is still in the tilted position, such that any air trapped in the side of the Bourdon tube will work its way to the connection of the gage.

9. Return the pump to its normal position flat on the bench while it is still pressurized.

10. Withdraw the plunger until the gage reads zero and no pressure exists.

11. Open pycnometer valve and bleed to atmosphere.

12. Remove pycnometer cap and reduce level of mercury slightly by retracting the plunger.

13. Tilt pump back, with the cylinder pointing up slightly (approximately 5 to 10°).

    Observe air bubbles at the mercury surface in the pycnometer.

14. When all bubbles cease, replace the cap and repeat the entire procedure several times until no bubbles appear at the surface of the mercury.

15. Upon completion, the correction factor should be 0.35 or less.

    If it appears to be slightly higher and it is impossible to expel any more bubbles, it is possible to dissolve the small amount of air remaining by pressurizing the pump and letting it remain in this state overnight.

CAUTION: ONCE A HARD SYSTEM IS ACHIEVED, NEVER WITHDRAW THE PLUNGER TO THE POINT WHERE MERCURY GOES BELOW THE BOTTOM OF THE PYCNOMETER.

ring. The packing space will be filled so that the follow ring enters the packing gland after the packing nut is tightened, and leaves sufficient space for further tightening. After the new packing has been installed, the pycnometer is reassembled with the volumetric pump unit.

A packing booster (9) must be used to pull the packing tight. The booster consists of two half shells which are inserted into the bore of the packing nut between the follow ring and pump traveling yoke. By using the normal hand drive of the pump plunger, the booster forces the follow ring into the packing gland, thus compressing the Teflon rings. After the packing has been sufficiently compressed, the packing nut is pulled tight. Full pressure should be applied, then released, and the procedure repeated. If there should be any leakage, the packing may be tightened further in the same manner. The Teflon packing cannot be injured by excessive tightening. The pump packing must never be tightened while the pump is under pressure.

LUBRICATION:

The main bearings of the pump are packed at the factory with bearing grease and should require little additional attention. If necessary, they may be lubricated by removing the bearing shield behind the front yoke. The spindle and plunger should occasionally be cleaned, and painted with a heavy lubricant such as Esso XP-90 compound or its equivalent. They should then be run in and out of the packing gland a few times while the instrument is not under pressure.

SERVICE PARTS LIST

Part No.	Req.	Description
99540	1	Pump Packing, Set
94-617	1	Spanner Wrench
94-618	1	Spanner Wrench
99545-001	1	Packing Booster

NOTE: PLEASE GIVE SERIAL NUMBER IN ANY CORRESPONDENCE CONCERNING THIS PUMP.

OPERATING MANUAL

LIQUID PERMEAMETER

MODEL NO. 1013-801

SERIAL NO. 26486

RUSKA INSTRUMENT CORPORATION

W A R N I N G

PRESSURIZED VESSELS AND ASSOCIATED EQUIPMENT ARE POTENTIALLY DANGEROUS. THE APPARATUS DESCRIBED IN THIS MANUAL SHOULD BE OPERATED ONLY BY PERSONNEL TRAINED IN PROCEDURES THAT WILL ASSURE SAFETY TO THEMSELVES, TO INNOCENT SPECTATORS, AND TO THE EQUIPMENT.

L I Q U I D P E R M E A M E T E R

MODEL 1013-801

L I Q U I D P E R M E A M E T E R (No. 1013-801-00)

The Ruska Liquid Permeameter permits determining the permeability of consolidated core sections with liquid. Permeability measurements are made by determining the time necessary for a fixed amount of liquid at a given temperature to pass through the core under a given pressure gradient.

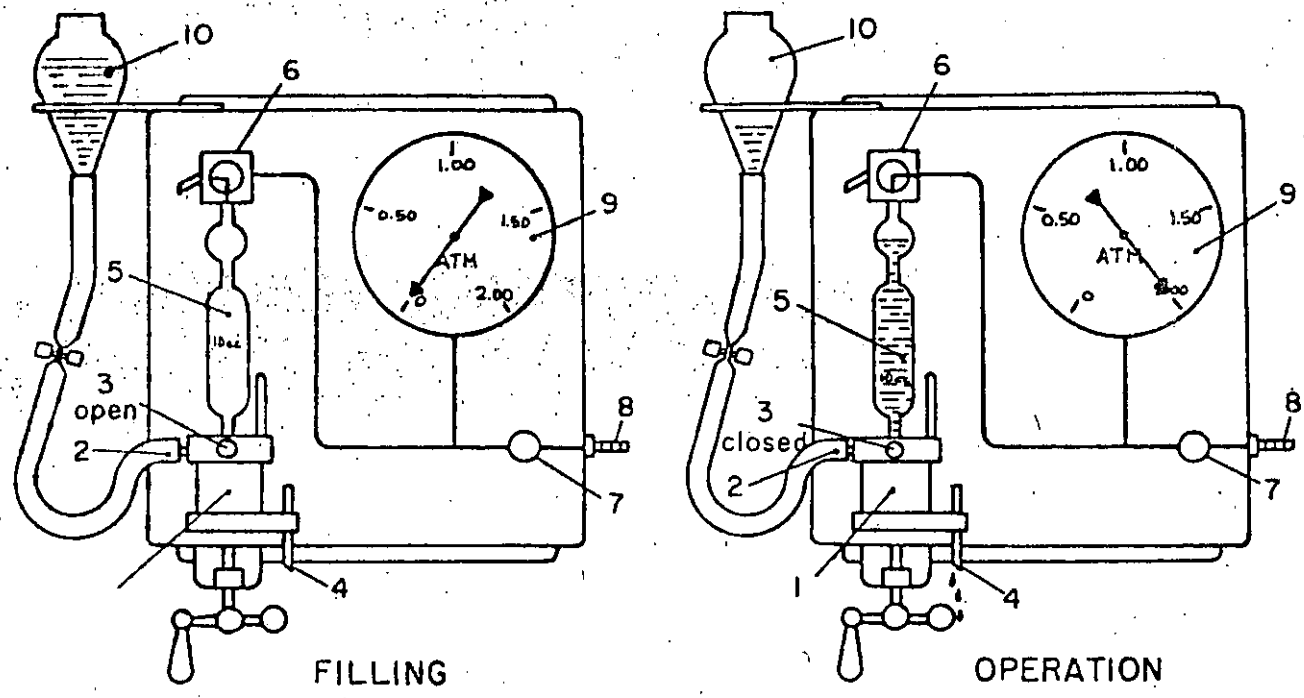

LIQUID PERMEAMETER

The instrument has a coreholder (1), with built-in thermometer and fill connection (2), with cutoff valve (3), with a special lid and overflow tube (4). A burette (5), is supported by its lower end in the coreholder and its upper end in the discharge-fill valve assembly (6), to which the gas pressure line from the pressure regulator (7) connects. The upstream pressure is indicated on a calibrated Bourdon tube pressure gage(9). Burettes

of various sizes may be used and are available with volumes of 50, 10, and 5 cc. They are interchanged by unscrewing the knurled nuts which hold them in their supports.

Preparation of Core Samples

Core samples are cut to size and extracted in the same way as for the Gas Permeameter (see Pages 2 and 3).

Prior to making liquid permeability measurements, the core sample, however, must first be saturated with the test fluid. Failure to achieve complete saturation will result in erroneously low measured permeability values; therefore, the core should be evacuated for one-half to one hour prior to immersion in the previously evacuated test fluid.

In making the selection of the test fluid, cognizance should be taken of the possibility of chemical interaction between the core material and the test fluid. Use of an inert hydrocarbon test fluid such as Soltrol-50 (low viscosity) and Soltrol-100 (high viscosity), . core test fluids manufactured by Phillips Petroleum Company (Exxon equivalent solvents are Isopar E and Isopar G respectively), will preclude chemical interaction. When aqueous base test fluids are employed, chemical equilibrium between the core material and the fluid must exist before accurate permeability data can be obtained. The simplest criterion for evaluating equilibrium conditions is the precision or repeatability of test data.

Operational Procedure

Following saturation, the core is inserted into the coreholder. A separatory funnel (10), filled with the test liquid, is connected with a piece of rubber tubing to the fill nipple on the coreholder. The coreholder valve is opened and the discharge-fill valve is turned to "Fill". After the pinch cock on the tubing has been opened, the liquid will flood the coreholder and fill the burette. The coreholder valve is closed when the liquid level in the burette is well above its upper index mark. After the pressure on the gage has been adjusted with the pressure control valve,

the discharge-fill valve is turned to "Discharge". The time necessary for the liquid level in the burette to drop from the upper to the lower index mark is determined. When changing from one liquid to another, the liquid lines should be flushed with a solvent or water and then vented.

Calculations:

The formula for calculating liquid permeability is: $K = \frac{\mu V L}{A P t}$

Where:

K = Permeability in darcys of the sample.

μ = Viscosity in centipoises of the liquid used in making the measurements at the observed temperature.

V = Volume in cubic centimeters of liquid flowed through sample during time interval.

t = Time in seconds for the fixed volume (50 cc, 10 cc, or 5 cc) of liquid to flow through sample under a given pressure gradient.

P = Pressure gradient in atmospheres, read on the pressure gage.

L = Length of the sample in centimeters.

A = Cross-sectional area of the sample in square centimeters.

Sample Calculation

Observed:
(1) Volume of liquid flowed through sample = 10.0 cc
(2) Time to flow 10 cc through core = 30.0 seconds
(3) Pressure gradient = 2.00 atmospheres
(4) Diameter of core = 1.90 centimeters
(5) Length of core = 1.90 centimeters
(6) Temperature = 25°C.

Installation

Before the Ruska permeameter is put in operation, it should be checked for leaks and mounted in its permanent location in the laboratory. The following routine is suggested:

1. CHECK THE PERMEAMETER FOR AIR LEAKS. Connect the supply pressure line to the instrument. Plug the coreholder with a stopper into which has been mounted a piece of metal of suitable size to make it air-tight. Apply pressure to the instrument up to the maximum pressure capacity of the gage and close the regulating valve. Do not disconnect the supply pressure line when pressure testing. If there is no pressure drop indicated on the gage in approximately ten minutes, the instrument does not leak.

   If the pressure drops, check all joints with soap water for possible leaks. Any leaking connection must be made air-tight. All instruments leaving our plant are checked thoroughly before the flowmeter is calibrated; however, to insure a perfect performance, it is best to check it again since the jarring in transit may have loosened some fittings. Gas leaks in the instrument lines to the flowmeter selector valve have no influence on permeability measurements.

2. SELECT A PLACE FOR THE PERMANENT INSTALLATION of your permeameter. Drill three holes in a supporting wall so that the instrument can be fastened by the hangers on the back of the frame. Care should be taken to see that the instrument is plumb.

It is advisable to check the permeameter periodically for air-tightness.

SERVICE PARTS LIST

See Catalog Section 401.2-4

Cat. No.	
	For Nos. 1011-801 and 1013-801
26-615	Pressure Gage
1011-901	Thermometer, Mounted, with O-Ring Gasket
	Accessories for No. 1011 Only
86-723	Small Flowmeter Tube, Calibrated, with Gaskets and Float
86-724	Medium Flowmeter Tube, Calibrated, with Gaskets and Float
86-725	Large Flowmeter Tube, Calibrated, with Gaskets and Float
1011-1-8	Lucite Shield for Flowmeter
	Accessories for No. 1013 Only
1013-1-44	Burette, 5 cc
1013-1-43	Burette, 10 cc
1013-1-42	Burette, 50 cc
08-000	Leveling Bulb
1013-800-100	Set of Burette Packing Nuts & all Gaskets, Consisting of: 2 Each No. 1013-1-21 2 Each No. 54-700-010
	Set (5) O-Ring Gaskets for Discharge-Fill Valve, Consisting of: 2 Each No. 54-700-012 1 Each No. 54-700-008 2 Each No. 54-700-006
1013-1-3	Lucite Shield for Burette

NOTE: PLEASE GIVE SERIAL NUMBER OF INSTRUMENT WHEN ORDERING PARTS.

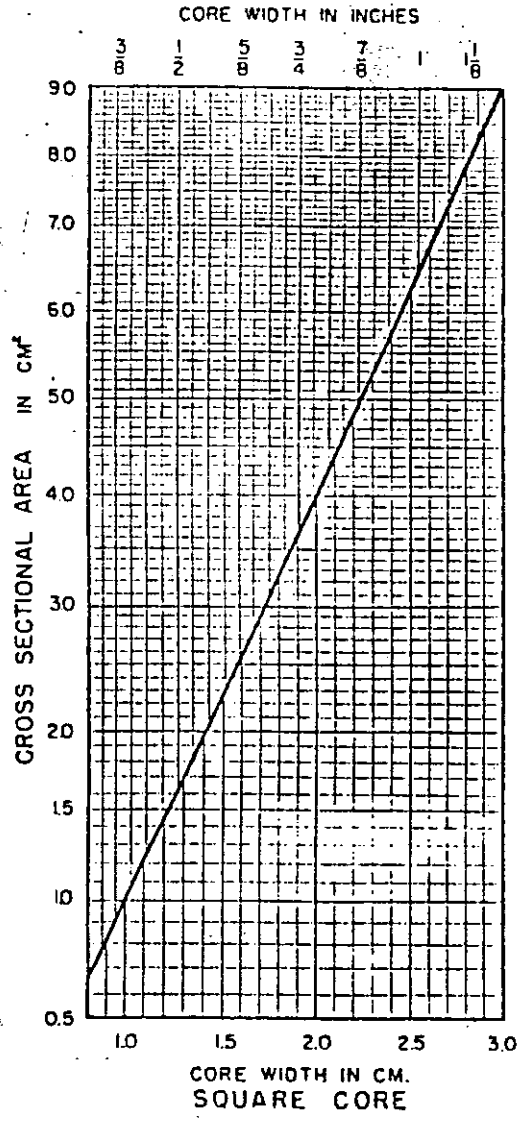

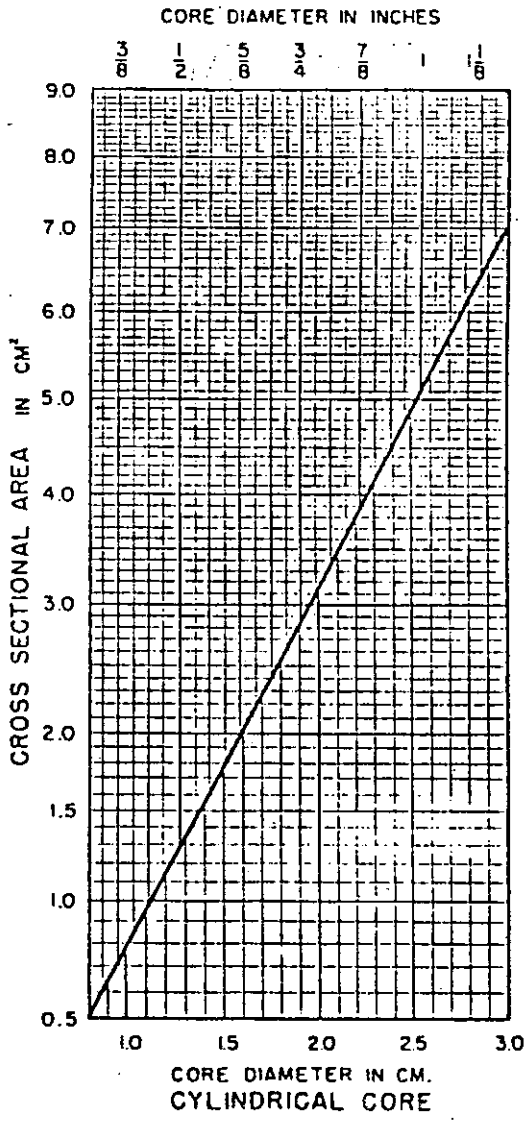

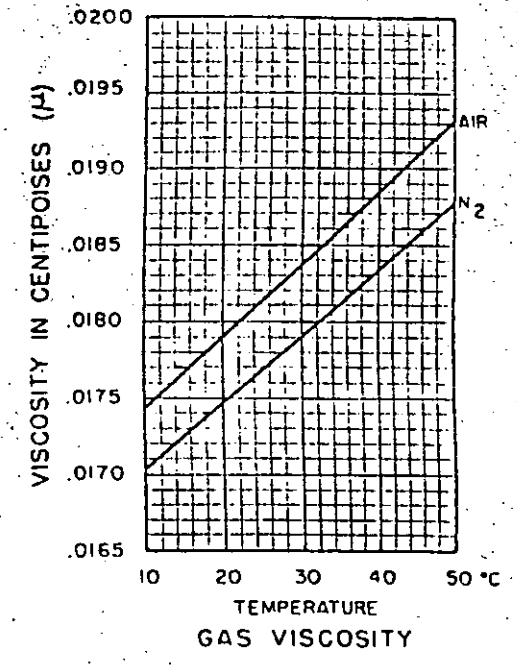

DIAMETER-AREA CURVES
FOR
PERMEABILITY PLUGS

RUSKA INSTRUMENT CORPORATION
HOUSTON TEXAS U.S.A.

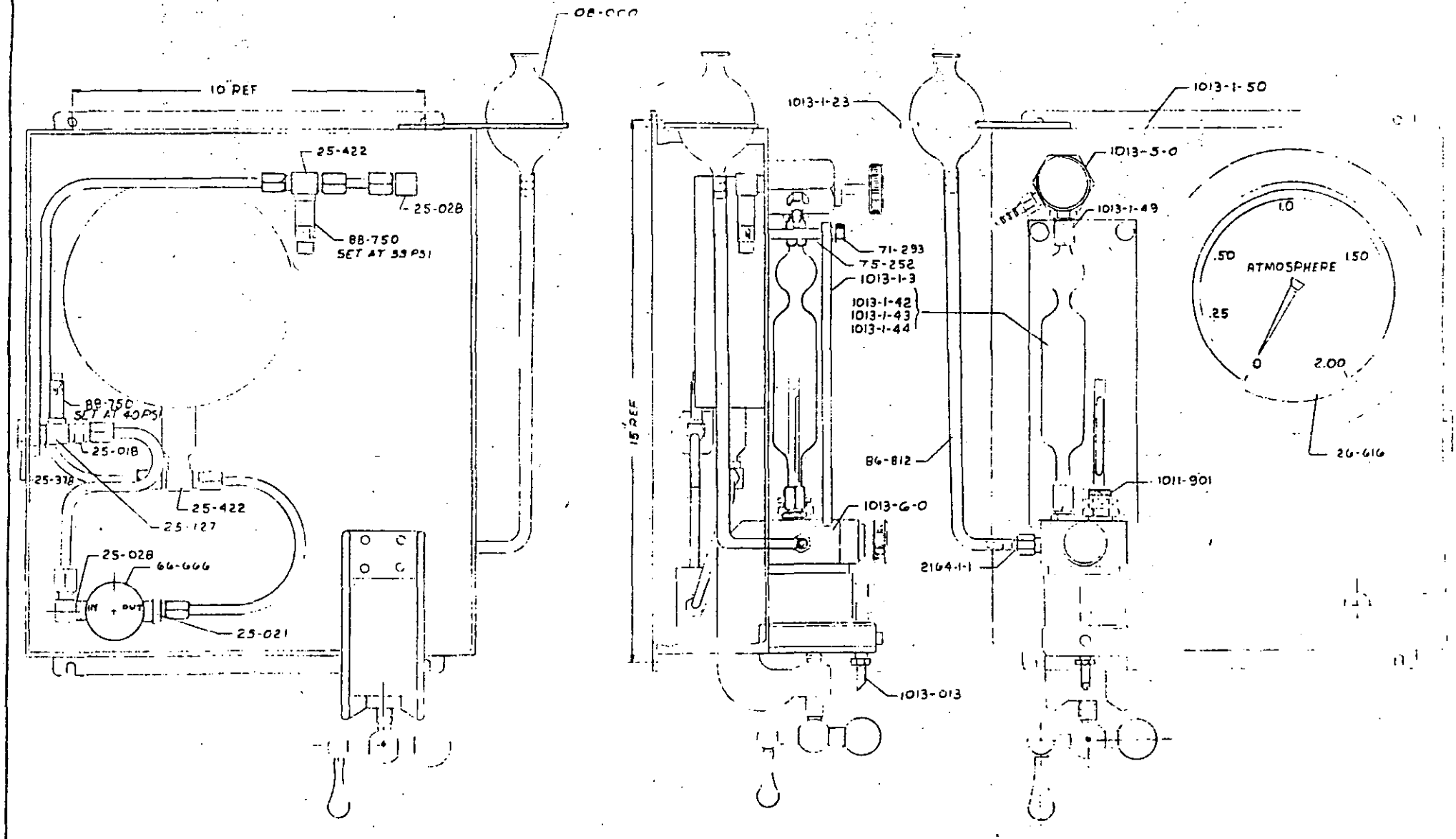

ASSEMBLY	SEE LIST		
DESCRIPTION		MATERIAL	
DRWN JC 3/7/86	MAIN ASSEMBLY LIQUID PERMEAMETER		
	SUB-ASSEMBLY		
	CORE LABORATORIES INCORPORATED HOUSTON, TEXAS	SCALE 1:2	NO. 1013-801-0

CORE LABORATORIES, INC.

GAS PERMEAMETER OPERATING INSTRUCTIONS

TABLE OF CONTENTS

Page No.

SECTION FIVE: MAINTENANCE AND TESTING (Continued)

LIST OF FIGURES

LIST OF TABLES

GAS PERMEAMETER OPERATING INSTRUCTIONS

SECTION ONE: GENERAL

1.1 Permeability

As related to earth formations, permeability is a property of the formation and is a measure of the formation's capacity to conduct fluids (oil, gas and water). The permeameter is an instrument designed to determine this property of fluid transmissibility. Permeability values, as determined by the correct operation of this instrument, should be within 5% of the actual permeability.

The specific permeability of a core may be experimentally determined by subjecting a prepared sample to an elevated gas pressure and measuring the volume flow rate of the gas; dry air is specified by API (See API RP-40, "API Recommended Practice for Core Analysis Procedure"). The dimension of permeability is defined as the "Darcy". A sample is described as having one Darcy permeability when an incompressible liquid of one centipoise viscosity will flow at a rate of 1 cm^3/sec., through a cross-sectional area of one sq. cm. (perpendicular to the direction of flow), along a one cm. length with a flowing pressure differential of one atmosphere. Laminar (viscous, nonturbulent) flow conditions are assumed. This definition is shown in Figure 1-1.

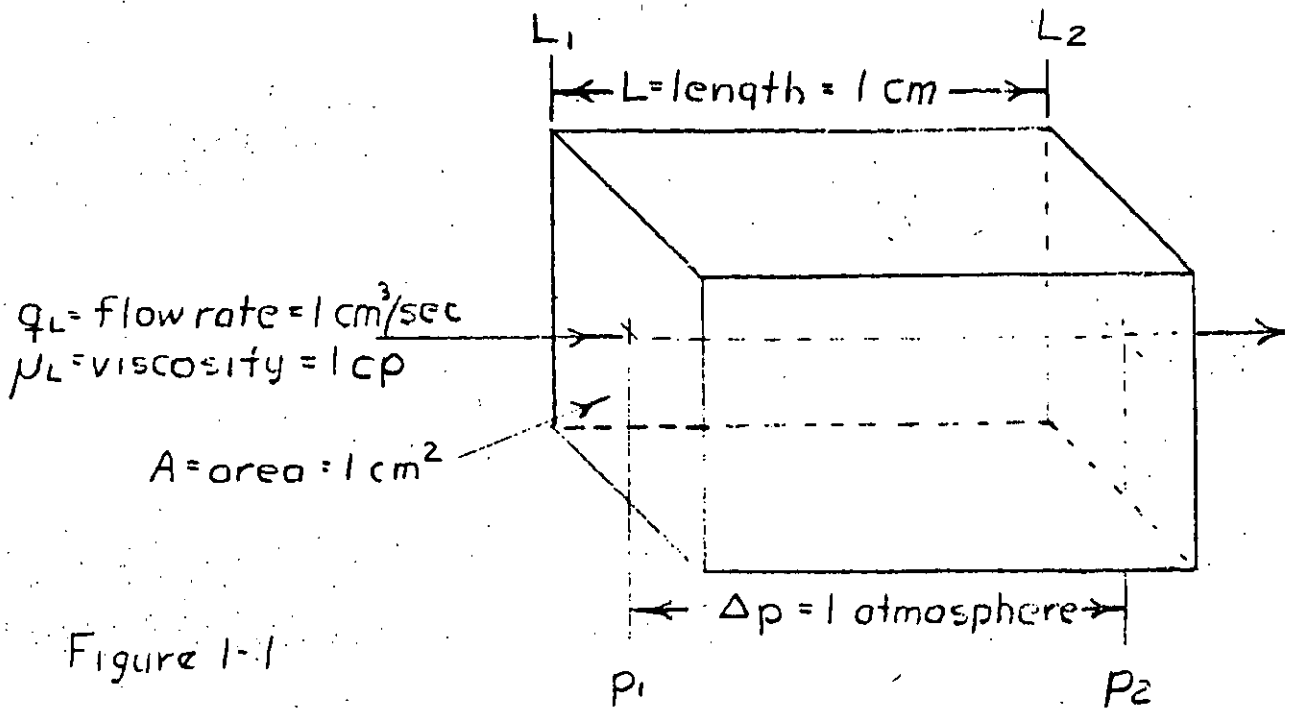

Figure 1-1

1.2 Darcy's Law

Permeabilities may be calculated for other conditions and fluids by the application of the equation describing Darcy's Law. For an incompressible liquid, Darcy's Law states:

$$k_L = \frac{\mu_L q_L L}{A(p_1 - p_2)}$$

k_L = Permeability (darcies)

μ_L = Liquid viscosity (centipoise)

q_L = Incompressible liquid volume flow rate (cm^3/sec.)

L = Length of core sample (cm)

A = Cross-sectional area (cm^2)

$p_1 - p_2$ = Δp, pressure difference from inflow to outflow face of sample (standard atmospheres absolute)

The Darcy equation relating to compressible fluids (gas) is as follows:

$$k_g = \frac{2\mu_g (q_g)(L)(p_a)}{A(p_1+p_2)(p_1-p_2)}$$

k_g = Permeability (darcies)

μ_g = Gas viscosity (cp) at the mean pressure and temperature of the sample

q_g = Gas volume flow rate at atmospheric pressure & temperature* (cm^3/sec.)

p_1 = Inflow or upstream pressure (standard atmospheres absolute)

p_2 = Outflow or downstream pressure (standard atmospheres absolute)

p_a = Atmospheric pressure (standard atmospheres)

* It is assumed that the sample is at room (atmospheric) temperature.

The foregoing equations are known as the linear form of Darcy's Law. They are used when flow occurs in essentially one direction, as in the determination of permeability of a test plug. This form is used throughout these instructions. Another form of Darcy's Law, known as the radial flow form, is used when analyzing a radial flow system, such as the flow of fluids from a reservoir into a wellbore. The radial flow equations are not pertinent to these instructions and are therefore not cited.

SECTION TWO: OPERATING PRINCIPLE

2.1 Core Holders

The permeameter permits the core sample to be partially enclosed (sealed), such that two opposite faces of the sample are exposed. This is accomplished through the use of either (1) a Hassler-type core holder for cylindrical core plugs or (2) a Fancher-type compressed rubber stopper core holder designed for small cylindrical, cube, or irregularly shaped samples. Irregularly shaped samples must be wax-mounted or plastic-mounted in a cylindrical metal sleeve.

1. The Hassler-type holder uses compressed air or nitrogen to squeeze (seal) the core sample in a rubber sleeve (boot) as shown in Figure 2-1 on Page 4. A vacuum is usually applied to expand the sleeve so that the sample can be inserted into or removed from the holder. The 200 psi air forces the sleeve tightly against the sample, preventing the inlet air from flowing between the sample and the sleeve. The vent valve is used to remove the sleeve pressure prior to opening the vacuum valve. This prevents overloading of the vacuum pump.

2. The Fancher-type holder shown in Figure 2-2 on Page 5, utilizes a compressed, soft rubber stopper to seal the core sample. A screw-clamp arrangement is used to squeeze (compress) the soft rubber stopper, which seals the outer surface of the core sample. Air should not leak or bypass the sample.

2.2 Permeameter Flow System

The path of air flow through the permeameter is shown in Figure 2-3 on Page 6. Air is introduced through the Source valve to

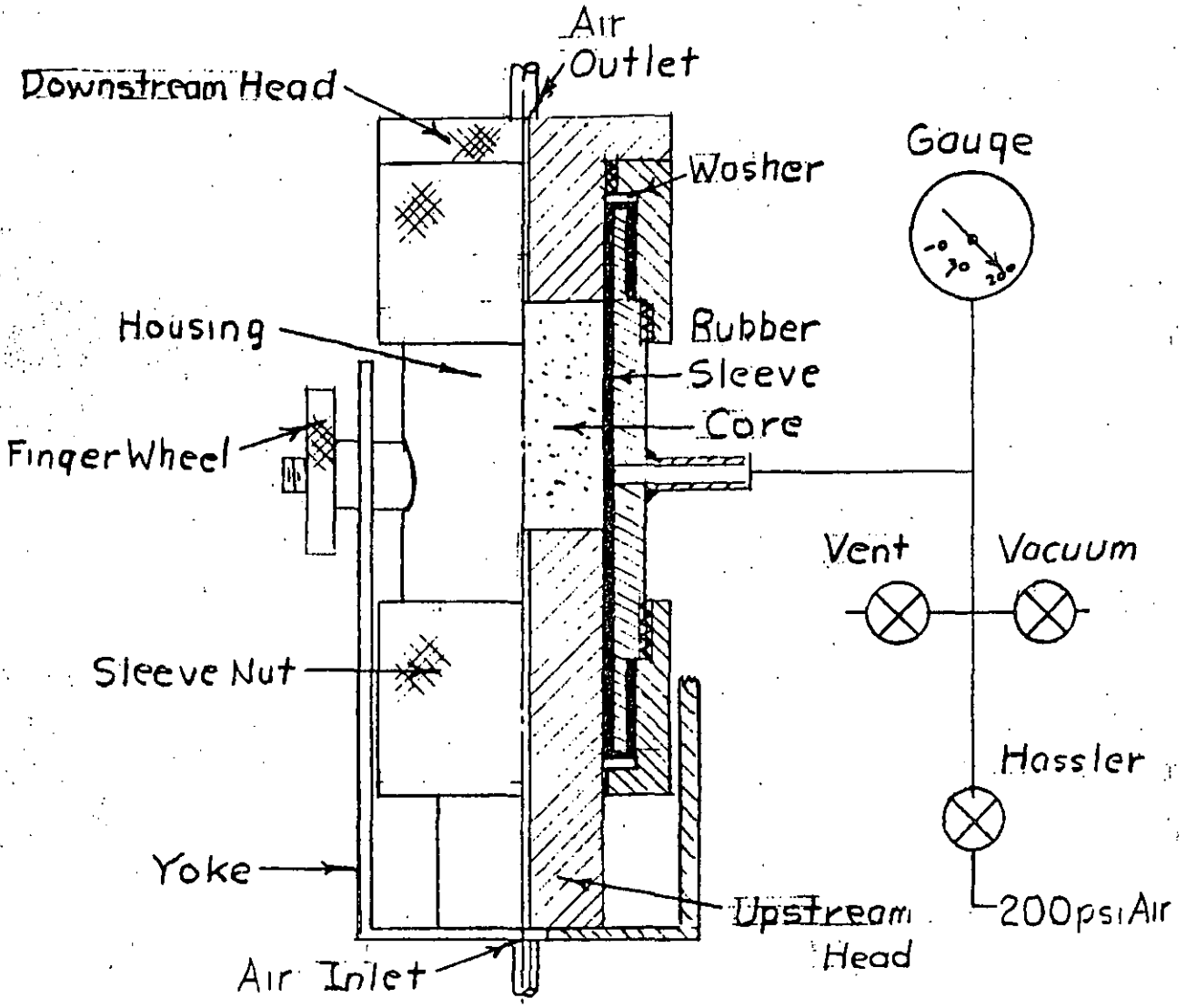

Figure 2-1
Hassler-Type Core Plug Holder

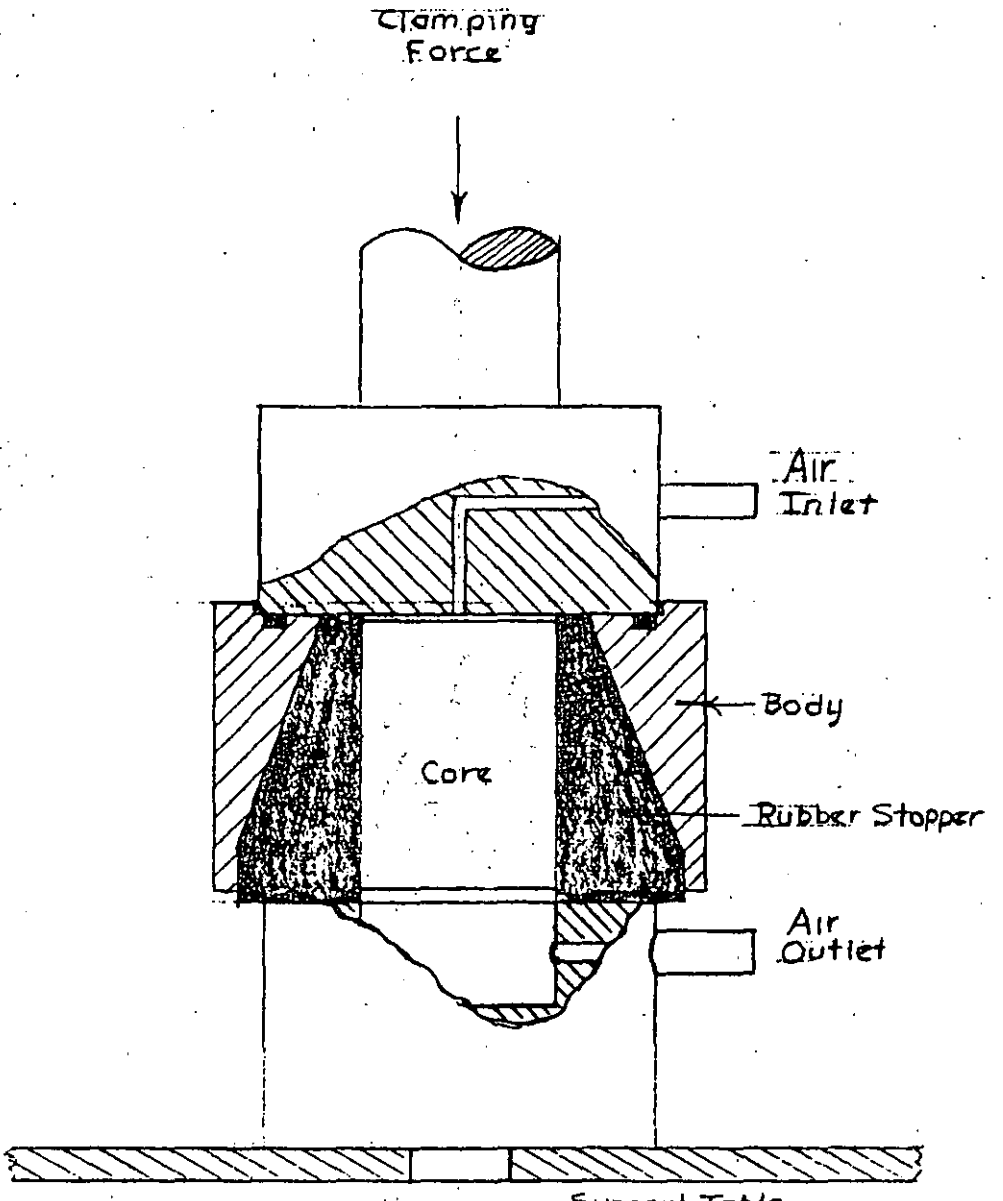

Figure 2-2
Fancher-Type Core Holder

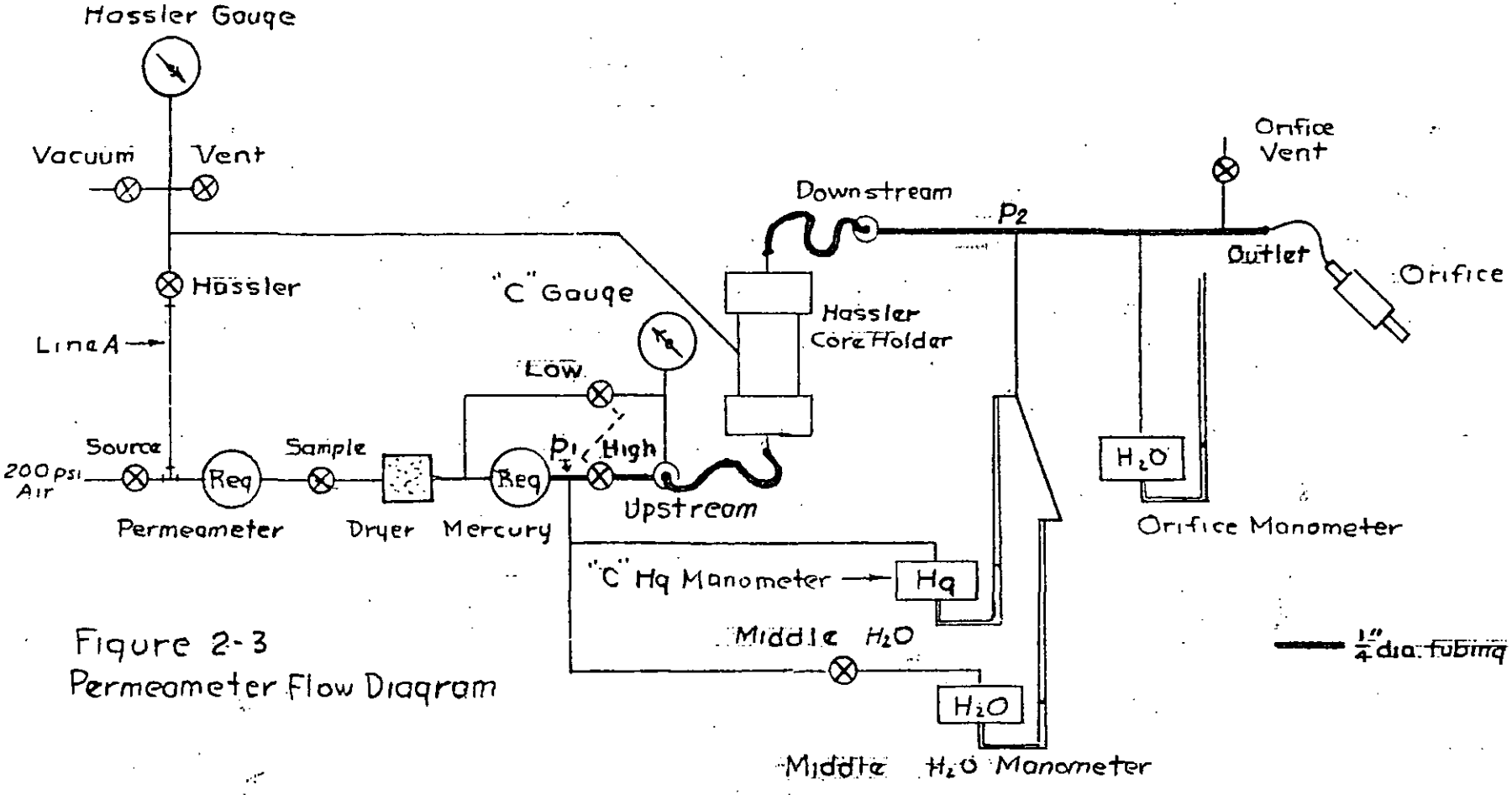

Figure 2-3
Permeameter Flow Diagram

the Permeameter regulator. With the Sample and Low valves open, the regulator may be adjusted to give a "C" Gauge reading that is proportional to a gauge pressure of the upstream face of the core. When analyzing low permeability samples, the Low valve is opened and the High valve is closed. For medium and high permeability core samples, the Low valve is closed and the High valve is opened. With the High valve open, the Mercury regulator may be adjusted to produce any selected differential (p_1-p_2) pressure indication either (1) on the "C" H_g manometer for medium permeability core samples, or (2) with the middle water valve open on the Middle Water manometer for high permeability core. The air flows through the core sample and Orifice in proportion to the applied differential air pressure. The differential pressure developed across the calibrated Orifice is used to determine the air volume flow rate.

2.3 Permeability Calculations

The equation for calculating permeability from Darcy's Law is given in Paragraph 1.2. In order to simplify the equation to a slide-rule calculation, the equation has been reduced to the following:

$$k_g = \frac{C\, q_a\, L}{A}$$

k_g = Gas permeability (millidarcies)

q_a = Volume flow rate of air (cm^3/sec. at atmospheric conditions)

WHERE: $$C = \frac{(1000)(2)(\mu_a)(p_a)}{(p_1+p_2)(p_1-p_2)} = \frac{(1000)\ 2\ (\mu_a)(p_a)}{(p_1+p_2)\ (\Delta_p)}$$

μ_a = Dry air viscosity (0.0186 centipoise)

1. "C" Values

The "C" gauge psig dial is graduated in values of "C" equivalent to selected p_1's; the Mercury manometer scale is graduated in values of "C" calculated for selected millimeter of mercury equivalent Δ_p's. When the Middle Water manometer is used, "C" value may be taken from Table 2-I for the developed water column height indication of Δ_p.

For the scaled values of "C" on the gauge and mercury manometer, p_2 was assumed to be 0.019 atmospheres (equivalent to a gauge pressure of 200 mm. of water). This assumption results in a negligible error, because an orifice generally can be selected which will produce an orifice pressure very near the 200 mm. of H_2O value.

Table 2-I permits the selection of "C" for even 10 mm. increments of Middle Water manometer readings and to the nearest 25 mm. increment of Orifice manometer reading. The 50 mm. incremented pressure at p_2 has been included in these calculated "C" values. Selecting the "C" for the nearest 25 mm. of Orifice manometer reading improves the accuracy of the permeability measurement.

2. "q_a" Values

The air flow rate "q_a" is numerically equal to:

$$q_a = \frac{(\text{Orifice Q})(h_w)}{200}$$

Orifice Q = Orifice constant; volume flow rate of air through the orifice when a flowing pressure drop of 200 mm. of water is imposed across the orifice (cm^3/sec)

hw = Orifice water manometer reading (mm)

SECTION THREE: INSTALLATION

3.1 Location

The permeameter is self-contained except for an air supply of approximately 200 psig and a vacuum source if a Hassler core holder is to be used. The instrument may be set on any lab bench top, in an area that is 28 inches wide and 12 inches deep. Preferably, the laboratory area should be vibration free, heated (75° F.) and away from outside doors which could cause abrupt temperature changes. Additional bench space will be required if a Fancher-type core holder is to be used.

If the permeameter is equipped with a Hassler-type core holder, the core holder can be used with the porosimeter for determining pore volumes. If pore volumes are to be measured, the porosimeter and the permeameter should be adjacent to one another in order to minimize connecting line volume.

TABLE 2-I

"C" Value vs. Middle Water Manometer Readings
For Selected Orifice Manometer Readings

Middle H_2O Manometer	Orifice Manometer (mm. H_2O)			
	50	100	150	200
(mm. H_2O)	"C" Values			
200	949	945	940	936
190	1000	995	990	985
180	1060	1050	1050	1040
170	1120	1110	1110	1100
160	1190	1180	1180	1170
150	1270	1260	1260	1250
140	1360	1350	1350	1340
130	1470	1460	1450	1450
120	1590	1580	1570	1570
110	1730	1730	1720	1710
100	1910	1900	1890	1880
90	2120	2110	2100	2090
80	2380	2380	2370	2350
70	2730	2720	2700	2690
60	3190	3170	3160	3140
50	3830	3810	3790	3770
40	4780	4760	4740	4720
30	6380	6350	6320	6290
20	9580	9530	9490	9440
10	19160	19070	18980	18890

3.2 Air (Gas) Supply

A compressed gas supply in the pressure range of 200 psig is required for the Hassler-type core holder sleeve pressure. In the event a 200 psig air compressor is not available, the permeameter must be modified to disconnect the sleeve pressure portion of the plumbing. This will permit inexpensive bottled nitrogen, equipped with a 200 psig regulator, to be connected to the core holder portion where the volume requirements are minimal. A minimum 40 psig air source may be connected to the remaining portion of the permeameter.

Referring to Figure 2-3, Line A may be removed. Connect the 200 psi nitrogen source to the Hassler valve connection. The connection, from which Line A was removed at its lower end, must be plugged. This will permit the separation of the sleeve pressure and the air flow systems.

The Permeameter and Mercury regulators are of a constant-bleed design. For this reason, it is generally economically impractical to use bottled air, regulated at 200 psig, as an air source.

A length of 1/4" I.D. X 3/16" wall thickness rubber hose is adequate for connecting the vacuum source to the Hassler Vacuum valve. The valve is fitted with a hose bib that will accept the rubber tubing. A small Dynapump will serve as the vacuum source in the event it is impractical to run a vacuum line to the permeameter.

3.3 Initial Instrument Set-Up

After the instrument has been uncrated, check for any damage that may have occurred in transit. Give careful attention to the top and bottom of the glass manometer tubes.

The permeameter is shipped with the water and mercury drained from the manometers. Plastic bottles filled with mercury and water are supplied; the fluids must be transferred into the manometer wells. Referring to Figure 3-1, the mercury manometer is identifiable by the "C" scale of 60 through 2200. The other two manometers are water manometers. All manometers should be filled through the threaded hole in the manometer well cover. The operating liquid level is approximately 3/16" below the top of the reservoir. Do not overfill. Teflon tape or thread dope should be used when the threaded plugs are replaced; do not over-tighten or the lucite covers will be damaged. The Middle Water manometer should be vented by opening the Middle Water valve, before water is added to that well.

After the manometer wells have been filled to the proper level, the manometer scales, on the front of the panel, should be loosened and adjusted slightly up or down so that the liquid meniscus and the zero scale graduation marks are at the same elevation.

The instrument was tested for leaks and proper operation prior to crating and shipping. However, an additional check should be made before the permeameter is used to develop data for a client. Section Five describes maintenance procedures designed to check the permeameter.

SECTION FOUR: OPERATING INSTRUCTIONS

4.1 Controls and Indicators

Figure 3-1 is a drawing of the permeameter panel; the panel contains all of the controls and indicators necessary for the operation of the permeameter.

Referring to Figure 2-3 also, it may be seen that the controls have the following functions:

1. Hassler Core Holder - Contains the core sample during the permeability determination. It can also be used in conjunction with a porosimeter to determine the pore volume of a core sample.

2. Hassler (Sleeve Pressure) Gauge - Is a compound gauge which indicates either the pressure or the vacuum that is being applied to the Hassler rubber sleeve.

3. Vacuum Valve - Permits the vacuum to expand the internal diameter of the Hassler rubber sleeve, such that a core sample may be easily inserted or removed.

4. Vent Valve - Vents the Hassler sleeve pressure to atmospheric pressure.

5. Hassler Valve - Permits 200 psig air (nitrogen) pressure to be applied to the Hassler holder, forcing the rubber sleeve against the sample and holder heads.

6. Source Valve - Permits the source air pressure to be applied to either the permeameter regulator and Hassler valve or only to the regulator, depending upon the instrument construction.

7. Permeameter Regulator - Controls the sample air supply pressure at an adjusted, reduced operating level. This reduced air pressure is connected to the Sample valve.

8. Sample Valve - Permits the air to flow through the Dryer, to the Low valve and Mercury regulator.

9. Mercury Regulator - Reduces the Permeameter regulated air pressure to an adjustable, lower operating level. This lower pressure air flows to the High valve, to the high pressure well of the Mercury manometer and to the Middle Water valve.

10. High and Low Valves - Permits air, at either of two pressure levels, to flow to the "C" Gauge and Upstream tubing connection. These two valves have a common actuator so that when one valve is open, the other is closed. With the Low valve open, a higher air pressure is applied to the upstream face of the core; it is used when the core samples have low permeability. The High valve permits a lower air pressure to be applied to the upstream face of the core sample; it is to be used when the core samples have medium to high permeabilities.

11. "C" Gauge - Indicates "C" values, equivalent to higher differential pressures imposed across the core. This gauge is used when core samples in the low permeability range are being tested. The Permeameter regulator is adjusted in order to obtain a specific desired "C" value indication on this gauge.

12. "C" Mercury Manometer - Indicates "C" values, equivalent to lower differential pressures imposed across the sample. This manometer is used when core samples in the medium permeability range are being tested. The Mercury regulator may be adjusted to obtain either a specific "C" value on the manometer or a specific Orifice manometer reading.

13. Middle Water Valve - Permits air from the Mercury regulator to flow into the Middle Water manometer well. This valve must not be opened unless the Mercury regulator has been backed off to a Mercury manometer "C" value indication that is greater than 700 (<1" of mercury equivalent pressure).

14. Middle Water Manometer - Indicates millimeters of water equivalent to the differential pressure across the sample. This manometer is used when core samples in the high permeability range are being tested. The "C" value equivalent must be taken from Table 2-I. The Mercury regulator may be adjusted in order to obtain either a specific Middle Water manometer reading or a specific Orifice manometer reading.

15. Orifice Manometer - Indicates millimeters of water equivalent to the flowing air pressure differential being developed across the calibrated orifice.

16. Calibrated Orifice - Is a restriction to the flow of air through the permeameter. This restriction creates a measurable differential pressure that is proportional to the air volume flow rate. One of several orifices may be selected; the one selected for use with a particular core sample should have a calibrated orifice constant (air volume flow rate) such that reading accuracy of the "C" device and the Orifice manometer will be high.

17. Orifice Vent Valve - Bypasses (vents) the flow of sample air around the calibrated orifice.

18. Upstream & Downstream Connections - Permits the permeameter to be used with a choice of core holders, such as the Hassler, Fancher or whole-core.

4.2 Hassler Core Holder

Two standard Hassler core plug holders are available, a 1" and a 1½" diameter model. Core samples between one and 3 inches in length may be handled. Referring to Figure 2-1, insertion of a core sample may be accomplished as follows:

1. Close the Hassler and Vent valves; open the Vacuum valve.
2. Loosen the finger-wheel nuts that hold the yoke; lower the yoke and upstream head clear of the sleeve.
3. Insert the core sample into the sleeve and follow with the upstream head until the core is held solid between the heads. Close the Vacuum valve.
4. Hold the yoke and open the Vent valve, permitting the sleeve to grip the sample and heads; release the yoke to permit the rubber sleeve to align the sample and heads.

5. Press the yoke firmly upward and tighten the finger wheels securely.
6. Close the Vent, open the Hassler, putting 200 psig against the sleeve. To reduce the risk of a "blown sleeve", close the Hassler, locking the 200 psi in the system.
7. Attach the upstream and downstream lines to the respective heads and proceed with the permeability determination.

The core sample may be removed as follows:

1. Terminate the air flow through the sample.
2. Open Vent and bleed sleeve pressure to zero.
3. Close Vent and open Vacuum.
4. Loosen yoke-finger wheels and slide upstream head and core down and out of core holder.

Precautions to be observed:

1. The ends of the core samples must be reasonably square to the axis of the sample and parallel to one another. Irregular ends on the sample may result in the rubber sleeve being pinched or cut.
2. The upstream head is secured by the frictional forces exerted by the rubber sleeve and by the yoke-finger wheels. Failure to tighten the finger wheels may result in the head being expelled from the holder. If this occurs, the 200 psi sleeve pressure gas will expand against an unsupported rubber sleeve.
3. If the cylindrical-shaped sample is a consolidated, coarse-grained sandstone or has a rough exterior surface, a test should be made to establish that the 200 psi sleeve pressure is an adequate sealing force. Measure the permeability of the sample with sleeve pressures of 150, 175 and 200 psi. If the permeability suffers an apparent decrease with each increase in sleeve pressure, it is evident that some air flow is occurring between the rubber sleeve and the surface of the sample. The sleeve pressure system will need to be modified with a higher pressure gauge if 200 psig is found to be inadequate. Establish the highest pressure at which a good seal is established; determine the permeabilities at this sleeve pressure. The Hassler gauge is a 200 psi gauge; pressures slightly higher than 200 will not harm the gauge.
4. Unconsolidated sand, that must be secured in lead tubes, is a special problem.

4.3 Fancher Core Holder

The Fancher core holder is designed to contain drilled or sawed core samples that are approximately two centimeters long. Referring to Figure 2-2, the core plug may be mounted in the Fancher core holder as follows:

1. Select the tapered rubber stopper which has a concentrically bored (molded) hole that is equivalent to the sample dimension.
2. Insert the sample into the hole such that the sample end is flush with the small end of the stopper.
3. Place the tapered stopper into the matching internal taper of the body.
4. Center the core holder between the clamp ends. Tighten the clamp screw until the sample is sealed within the stopper and holder.
5. Attach the Upstream and Downstream lines to their respective points on the Fancher holder.
6. Proceed with the permeability determination.
7. The sample is removed from the Fancher holder in the reverse order of the above steps.
8. Cube-shaped samples may be formed by the diamond sawing of an irregular-shaped portion of the core and when horizontal and vertical permeabilities are to be obtained. Normally 2 cm. cubes are formed with a saw equipped with two parallel-mounted blades, 2 cm. apart. A standard tapered rubber stopper is available to fit these shapes. Greater care and squeeze pressure are required to assure that the sample cube is sealed within the stopper, especially if the sample is cut slightly under-size or has slightly rounded corners. Possible leak (bypass) paths exist at the corners.

4.4 Wax (Plastic) Mounted Samples

In some instances, the formation samples may be too friable (poorly consolidated) or too small from which to cut either a cylindrical or cubical shaped sample. When this occurs, a small sample may be shaped by sawing, grinding or paring in order to get a dimensional form. The shaped core sample may then be cemented into a standard size cylindrical tube in the following manner:

1. Cover the bottom of a shallow pan with an even layer of clean sand. Set the cylindrical tube upright on the sand surface.
2. Set the sample inside the upright tube; slightly embed both into the sand.

3. With a propane torch, heat the end of a stick of sealing wax and channel the melted wax into the annular space between the sample and the tube; fill this annular volume to a level just below the top of the core sample.
4. Generally, a seal between the wax and tube will be attained if the tubing is preheated to the melting point of the wax. If the permeability of the mounted sample is determined while the wax is slightly warm, there is less chance that the seal will leak.
5. Some Fancher core holder apparati are designed such that the wax-core and the wax-tubing seals may be tested. After the permeability has been measured, connect the upstream permeameter line to the test plate connection; place a few drops of alcohol on one end of the mounted sample. Press the opposite end of the tubing firmly against the test plate rubber washer and adjust Permeameter regulator with the Source, Sample and Low valves open. Air bubbles must not appear between the wax and tubing; the bubbles formed at the sample face should be uniformly distributed across the sample. A disproportionate number of bubbles forming along the core-wax junction indicates a poor seal between the wax and sample. The core must be resealed if the above test indicates that air is flowing around, rather than through, the core sample.

4.5 Routine Operation

For the purposes of this section, it will be assumed that (1) the core sample is in a core holder, (2) the core holder is properly connected to the Upstream and Downstream connections on the permeameter panel, (3) an adequate air supply (40 psig if the Hassler valve is connected to a nitrogen regulator set to 200 psig or 200 psig if the Hassler valve is connected between the Source valve and the Permeameter regulator), and (4) the Source and Sample valves are closed.

1. Close the Middle Water valve; open the Low and Orifice Vent valves.
2. Back-off (screw counterclockwise) on the Permeameter and Mercury regulators.
3. Open the Source and Sample valves and adjust (clockwise) the Permeameter regulator for a "C" reading of 10 on the "C" gauge.

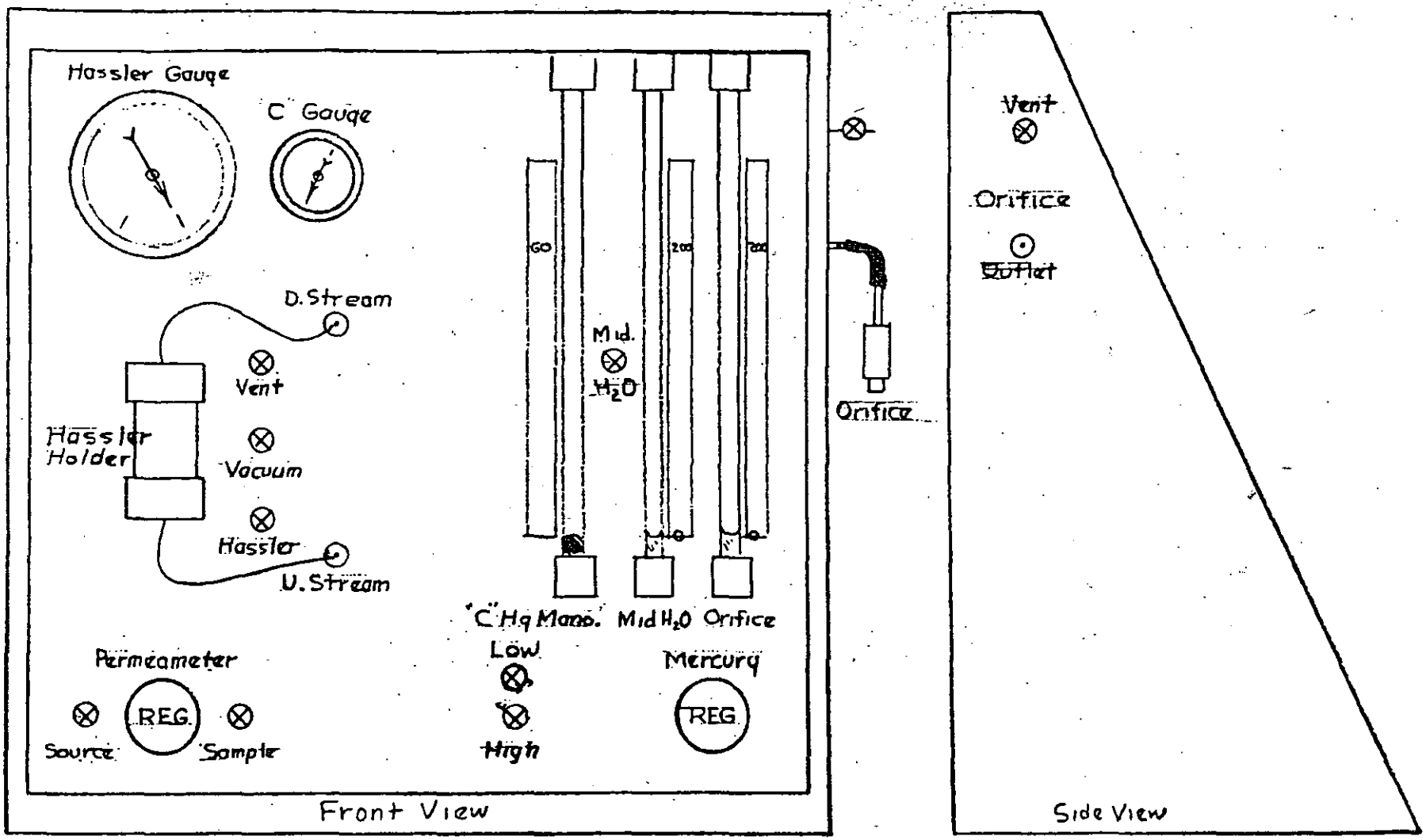

Figure 3-1
Permeameter Panel

4. From a visual inspection or past experience, estimate the permeability of the core sample.
   a. If the permeability is estimated to be less than 1 md., select an orifice with an Orifice Q value in the range of 0.1 or less.
   b. If the permeability is estimated to be between 1 and 100 md., an orifice should be selected with an Orifice Q value in the range of 0.1 to 10.
   c. If the permeability is to be higher than 100 md., an orifice with an Orifice Q value in the range of 10 or greater should be selected.

   If whole core diametric (parallel to bedding planes) permeabilities are being determined, the above Orifice Q values should be increased by a factor of 10.

5. Connect the orifice selected to the Orifice outlet with a short section of rubber tubing.
6. If the orifice selected has an Orifice Q that is:
   a. Greater than 1, open the High valve (this automatically closes the Low valve). Adjust the Mercury regulator until the "C" H_g manometer indicates a value of 60.
   b. Less than 1, open the Low valve. This automatically closes the High valve.
7. Slowly (carefully) start closing the Orifice Vent and observe the water rise in the Orifice manometer. If the air flow rate is too high for the orifice selected, when the Vent valve is closed, water will be expelled from the manometer. Do not allow this to happen; select a larger orifice or adjust the Permeameter or Mercury regulator to establish a higher "C" value (lower differential pressure). Higher Orifice manometer readings will provide better manometer reading accuracy for the determination of q_a. Preferably, do not use a manometer reading of less than 20 mm. of water.
8. Based on this first trial, with the orifice selected, it may be advantageous to select another orifice for improved manometer reading accuracy. The best overall accuracy will be obtained when the gas flow rate is adjusted to obtain gauge and manometer readings on the upper end of the scales. Upper end of the scales will be low "C" values and high water manometer readings. Experience will be the best guide for a particular (geographical area) laboratory. An orifice may be changed by first opening the Vent valve, replacing the orifice and then slowly closing the Vent valve as before.

9. When stabilized flow (steady manometer indications) is established, record the following data:
   a. "C" value or Middle Water column height in millimeters (convertible to "C" from Table 2-I).
   b. Orifice Q value.
   c. Orifice Manometer reading (hw) in millimeters.
   d. Length (L) of the sample in centimeters.
   e. Diameter of the sample in centimeters, from which the cross-sectional area (A) in square centimeters may be calculated.
10. Calculations are shown below:

$$k_g \text{ in millidarices} = C \text{ (Orifice Q)} \frac{hw}{200} \frac{L}{A}$$

11. Precautions to be observed:
   a. Keep the Orifice Vent open except during those times that Orifice manometer readings are being made. This will minimize the possibilities of expelling the water from the Orifice manometer.
   b. Do not pressurize the Hassler sleeve unless a core sample is securely clamped in the holder. The 1/16" thick rubber sleeve will be ruptured if 200 psi air pressure is introduced into an empty or unsecured Hassler holder.
   c. Samples that are 1/16" smaller than the Hassler diameter may be held in the Hassler holder without damage to the sleeve. Cores with smaller diameters than this may be effectively enlarged by inserting the sample into another rubber sleeve of the proper thickness to make the combined diameter of the core and sleeve equal to the Hassler diameter. Spacer rings will be required if the enlarging rubber sleeve is longer than the core sample.
   d. The air or nitrogen pressure level required for proper sealing of the Hassler rubber sleeve and the core sample will be dependent upon sand grain size, thickness and hardness of the rubber sleeve and smoothness of the cut on the core's outer surfaces. Normally, 200 psig sleeve pressure will give satisfactory sealing. A technique for determining an adequate sealing pressure was discussed in Paragraph 4.2.
   e. Do not open the Middle Water valve unless the Mercury regulator is adjusted to a "C" Hg manometer value greater than 700.

SECTION FIVE: MAINTENANCE AND TESTING

Under normal operating conditions, maintenance will be minimal. With compressed air being supplied to the permeameter, the following items

should be considered during normal maintenance:

5.1 Dryer

When the silica gel in the dryer becomes pink to white in color, it should be replaced with new or rejuvenated silica gel. Water vapor in the sample air can react with water-sensitive materials in the core samples and unstable flow conditions will result. If this occurs, time and accuracy will be lost. In some instances, moisture may affect the orifice such that the calibrated Orifice Q value is incorrect.

5.2 Manometers

1. The liquid meniscus must be level with the zero scale graduation when the permeameter is at atmospheric pressure throughout. The manometer scales may be loosened and adjusted as required. Add make-up liquid (see Installation) for severe level discrepancies; find the cause for the loss of liquid.
2. If the Mercury manometer glass tubes become dirty, remove the dirty mercury and clean (wash) the sight glass. The sight glass may be removed as follows:
   a. Withdraw (siphon) the mercury from the manometer well through the threaded fill-hole.
   b. Remove the top cross-member from panel.
   c. Loosen the Swagelok (with Zytel plastic ferrules) nuts at top and bottom of the sight glass.
   d. Disconnect the tubing connection at rear of the top manometer tube bracket.
   e. Remove the top bracket using a No. 8 Allen wrench; gently lift the glass from the bottom tubing connection.
   f. Clean the glass bore with soap and water; dry completely.
   g. Reverse the above steps to install the glass tube.
   h. Fill the manometer well with clean mercury, to the proper level.
   i. Test for leaks after all the Swagelok nuts have been properly tightened. (See "Instrument Leaks" below).
   j. The Water manometer glass tubes may be removed and cleaned in the same manner.

5.3 Sand Grains

Dust and fine sand grains may be seen collecting in the section of plastic tubing that connects the downstream core holder outlet with the Downstream connection located on the permeameter panel. If this line is kept clean, it will minimize the quantity of fine rock particles that reach the orifice. The orifice must be clean; the Orifice Q calibration constant was determined when the orifice was new, clean and dry.

5.4 Instrument Leaks

1. Upstream Leaks

Minor leaks upstream of the core sample are not generally considered to be detrimental to permeability measurements. However, in some instances, a leak may contribute to an erroneously low p_1. Most leaks can be detected with the bubble solution technique which involves saturating each suspected tubing connection with a soap solution (such as Snoop) and observing the growth of bubbles if a leak is present. Lines and connections leading from the downstream ends of both the Mercury regulator and Low valve to the upstream face of the core holder should be tested. This includes lines and connections leading to the Mercury manometer and Middle Water valve. Copper lines may have been damaged by mercury, if the mercury has ever been accidentally expelled from the Mercury manometer.

A critical area for upstream leaks is in the lines leading to the Middle Water manometer well. These lines (connections) may be easily tested by adjusting the Mercury regulator (with the Middle Water valve open) to obtain a 200 mm Middle Water manometer pressure reading; open the Orifice Vent and close the Middle Water valve. A no-leak manometer system will hold the pressure level at 200 mm of H_2O pressure. A decreasing manometer level indicates a leak and it must be corrected.

2. Downstream Leaks

Leaks downstream of the core sample cannot be tolerated. The flow system downstream of the core sample may be easily and quickly tested in the following manner:

a. Place a solid steel or aluminum plug in the core holder.
b. Pressure the Middle Water manometer to 200 mm. of water and close the Middle Water valve.
c. Remove the Orifice and close the Orifice Vent.
d. With a squeeze bulb connected to the orifice rubber hose, pressurize the downstream lines to a pressure of 200 mm. of H_2O as indicated by the Orifice manometer. Seal the hose with a screw-pinch clamp.
e. A decreasing Orifice manometer reading represents a downstream leak which MUST BE FOUND and corrected. Be certain to check the upper end of the H_g and Middle Water manometer sight glasses.

5.5 Hassler Core Holder

1. A leak in the Hassler core holder system may be found in the following manner:

   a. Pressurize the Hassler rubber sleeve to 200 psig with a very porous and permeable core sample in the holder. This core sample should be equal in length to the longest core samples that are analyzed.
   b. Close the Hassler valve; a drop in sleeve pressure, as indicated by the Hassler gauge, represents a leak which must be found and corrected. The following steps should isolate the location of the leak:

      1) Seal the upstream plastic line leading to the core holder with a pinch clamp; also pinch clamp the orifice-rubber tubing. Close the Orifice Vent valve. An increasing pressure, as indicated by the Orifice manometer, is indicative of a pin-hole leak in the Hassler rubber sleeve and the sleeve must be replaced.
      2) If the Hassler core holder leak is not in the rubber sleeve, tighten the upper and lower sleeve nuts. If this does not correct the leak, use bubble solution to determine the location of the leak. Make the appropriate repairs.

2. A defective Hassler sleeve may be replaced in the following manner, referring to Figure 2-1:

   a. Remove both the upstream and downstream heads. The downstream head is threaded into the downstream (top) knurled sleeve nut.
   b. Remove both knurled sleeve nuts.
   c. Remove the defective rubber sleeve and select a replacement (1/16" thick rubber tube) of the proper length and diameter dimensions. Insert the new sleeve into the housing.
   d. With ½" of sleeve extending out the bottom of the housing, stretch the sleeve outward and up, over the housing end. The sleeve should cover the housing end, below the threaded portion.
   e. Lightly lubricate the threads and washer; replace the knurled sleeve nut and hand-tighten.

f. Repeat Steps d and e for the upper end. Use the vacuum as an aid in holding the sleeve in place, once the sleeve has been stretched back and down over the housing. A properly installed sleeve must be stretched smooth, free of any twists or wrinkles.
g. Do not overtighten the knurled sleeve nuts or the rubber sleeve may be damaged (pinch-cut between the housing end and the inner surface of the washers).
h. Recheck for leaks as previously described.

5.6 Flow System Correction for High Permeability Core Samples

The theory of Darcy's Law states that p_1 and p_2 are the upstream and downstream pressures at the respective faces of the core sample. As can be seen from Figure 2-3, by the design of this permeameter, the points at which p_1 and p_2 are measured are not directly at the core faces. At very high air flow rates, the pressure drop between the p_1 point and the inflow core face and the pressure drop between the outflow core face and the p_2 point may represent an appreciable portion of the total pressure drop between p_1 and p_2. The consequence of this pressure drop is that the "C" value, converted from the Middle Water manometer reading, will be erroneously small and the computed permeability of the sample will be less than the true permeability.

Each permeameter should be tested at several flow rates, in order to determine the magnitude of this pressure drop across the flow system. A test of the permeameter may be performed in the following manner:

1. Insert one-inch length of plastic tubing, of the proper diameter, into the Hassler core holder. Connect an orifice, with a large Orifice Q, to the outlet.
2. Open the High valve, back out the Mercury regulator and open the Middle Water valve.
3. Open the Supply valve; close the Orifice Vent valve.
4. Adjust the Mercury regulator to produce a 200 mm of water pressure differential on the Orifice manometer.
5. The Middle Water manometer will indicate the flowing pressure drop across the system, at an air flow rate that is equivalent to the Orifice Q value.
6. Repeat Step 4 for 150 and 100 mm. Orifice manometer readings.
7. Prepare a graph of q_a Air Flow Rate ($cm^3/sec.$) versus Middle Water Manometer reading (mm H_2O) for the three air flow rates. More than one orifice may be required to cover the range of air flow rates normally used. Figure 5-1 is an example graph.

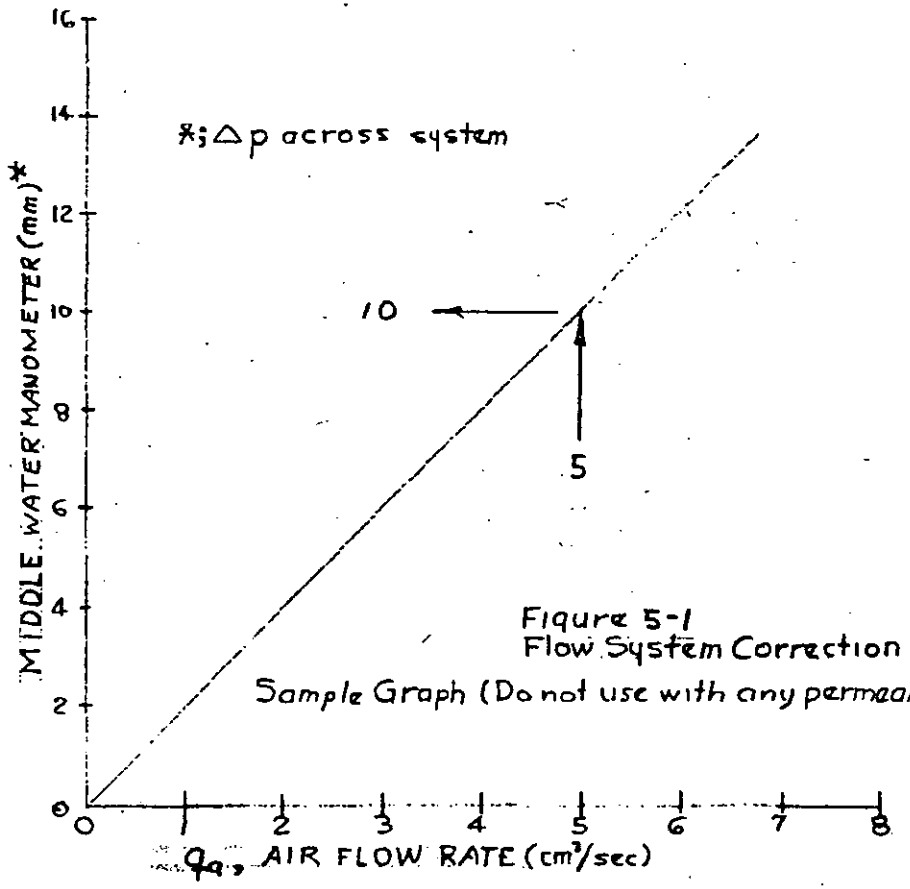

Figure 5-1
Flow System Correction
Sample Graph (Do not use with any permeameter)

8. Your prepared graph may then be used to correct the measured pressure differential from the Middle Water manometer (p_1-p_2) to the true differential pressure across the core sample. Preserve and post this graph where it will be readily available.

It follows that:

[Apparent (p_1-p_2)] = (Δp across system) + [True (p_1-p_2) across core sample]

[True (p_1-p_2) across core sample] = [Apparent (p_1-p_2)] - (Δp across system)

EXAMPLE: For a high permeability core sample, 200 mm of H_2O was developed across a 5.00 orifice with the attendant Middle Water manometer reading shown below:

Middle Water Manometer reading is the [Apparent (p_1-p_2)] = 160 mm H_2O

Δp across system: 10 mm H_2O (From example graph q_a = 5.00 cm^3/sec)

[True (p_1-p_2)] across core sample: 160 - 10.0 = 150 mm H_2O

"C" from Table 2-I: 1250 @ 150 mm H_2O Middle Water and 200 mm H_2O Orifice manometer reading.

For this example, an uncorrected Middle Water manometer reading of 160 mm would have yielded a "C" of 1170, representing an erroneously low permeability, in error by 6.3 percent. This error would have been in excess of the API established standard of 5% for permeability measurements.

5.7 Klinkenberg (Gas Slippage) Effects and Corrections

It has been determined that a gas will move through a core sample at a disproportionately higher rate than will a liquid; this higher gas rate is a function of the mean free path in which the gas molecule may move. The mean free path of the gas molecule is affected by the molecule size and temperature, the gas pressure and the pore size. As pore pressure is elevated, the mean free path is restricted, the gas flow rate decreases and approaches the proportionate liquid flow rate; the measured gas permeability approaches the permeability that would be measured if liquid were the flowing medium.

Mathematical Relationship:

$$k_l = 0.68(k_a)^{1.06}$$

TABLE S-II

KLINKENBERG (GAS SLIPPAGE) EMPIRICAL CORRECTION

PERMEABILITY BY AIR (k_a) VS. PERMEABILITY BY LIQUID (k_l)

0 - 0.158		0.159 -0.39		0.40 - 0.69		0.70 - 0.99		1.00 - 2.9		3.0 - 5.9		6.0 - 8.9		9.0 - 11.9		12 - 39		40 - 69		70 - 99		100 - 129		130 - 159		160 - 175	
k_a	k_l	k_a	k_l	k_a	k_l	k_a	k_l	k_a	k_l	k_a	k_l	k_a	k_l	k_a	k_l	k_a	k_l	k_a	k_l	k_a	k_l	k_a	k_l	k_a	k_l	k_a	k_l
0.01		0.159		0.40	0.26	0.70	0.46	1.00	0.68	3.0	2.2	6.0	4.5	9.0	7.0			40	34	70	61	100	88	130	116	160	144
or		to	0.10	0.41	0.26	0.71	0.47	1.01	0.69	3.1	2.2	6.1	4.6	9.1	7.0			41	35	71	62	101	89	131	117	161	145
Less	<0.01	0.174		0.42	0.27	0.72	0.48	1.02	0.69	3.2	2.3	6.2	4.7	9.2	7.1	12	10	42	35	72	63	102	90	132	118	162	146
0.011		0.175		0.43	0.28	0.73	0.48	1.03	0.70	3.3	2.4	6.3	4.8	9.3	7.2	13	10	43	36	73	63	103	91	133	119	163	147
to	0.01	to	0.11	0.44	0.28	0.74	0.49	1.04	0.71	3.4	2.5	6.4	4.8	9.4	7.3	14	11	44	37	74	64	104	93	134	120	164	148
0.028		0.188		0.45	0.29	0.75	0.50	1.05	0.71	3.5	2.5	6.5	4.9	9.5	7.4	15	12	45	38	75	65	105	93	135	121	165	149
0.029		0.189		0.46	0.29	0.76	0.51	1.06	0.72	3.6	2.6	6.6	5.0	9.6	7.4	16	13	46	39	76	66	106	94	136	122	166	150
to	0.02	to	0.12	0.47	0.30	0.77	0.52	1.07	0.73	3.7	2.7	6.7	5.1	9.7	7.5	17	14	47	40	77	67	107	95	137	123	167	151
0.046		0.204		0.48	0.31	0.78	0.52	1.08	0.73	3.8	2.8	6.8	5.2	9.8	7.6	18	15	48	41	78	69	108	96	138	123	168	152
0.047		0.205		0.49	0.32	0.79	0.53	1.09	0.74	3.9	2.9	6.9	5.2	9.9	7.7	19	15	49	42	79	69	109	97	139	124	169	153
to	0.03	to	0.13	0.50	0.32	0.80	0.54	1.10	0.75	4.0	2.9	7.0	5.3	10.0	7.8	20	16	50	43	80	70	110	98	140	125	170	154
0.062		0.22		0.51	0.33	0.81	0.54	1.11	0.8	4.1	3.0	7.1	5.4	10.1	7.9	21	17	51	43	81	71	111	98	141	126	171	154
0.063		0.23	0.14	0.52	0.34	0.82	0.55	1.2	0.83	4.2	3.1	7.2	5.5	10.2	8.0	22	18	52	44	82	72	112	99	142	127	172	155
to	0.04	0.24	0.15	0.53	0.34	0.83	0.56	1.3	0.91	4.3	3.2	7.3	5.6	10.3	8.0	23	19	53	45	83	73	113	100	143	128	173	156
0.078				0.54	0.35	0.84	0.56	1.4	1.0	4.4	3.3	7.4	5.7	10.4	8.1	24	20	54	46	84	74	114	101	144	129	174	157
0.079		0.25	0.16	0.55	0.36	0.85	0.57	1.5	1.0	4.5	3.3	7.5	5.7	10.5	8.2	25	21	55	47	85	74	115	102	145	130	From:	Minus
to	0.05	0.26	0.16	0.56	0.36	0.86	0.58	1.6	1.1	4.6	3.4	7.6	5.8	10.6	8.3	26	21	56	48	86	75	116	103	146	131	175	
0.095		0.27	0.17	0.57	0.37	0.87	0.58	1.7	1.2	4.7	3.5	7.7	5.9	10.7	8.4	27	22	57	49	87	76	117	104	147	132	299	-20
0.096		0.28	0.17	0.58	0.38	0.88	0.59	1.8	1.3	4.8	3.6	7.8	6.0	10.8	8.4	28	23	58	50	88	77	118	105	148	133	300	-30
to	0.06	0.29	0.18	0.59	0.38	0.89	0.60	1.9	1.3	4.9	3.7	7.9	6.1	10.9	8.5	29	24	59	51	89	78	119	106	149	134	699	
0.110		0.30	0.19	0.60	0.39	0.90	0.60	2.0	1.4	5.0	3.7	8.0	6.1	11.0	8.6	30	25	60	52	90	79	120	107	150	135	700	-40
0.111		0.31	0.19	0.61	0.40	0.91	0.61	2.1	1.5	5.1	3.8	8.1	6.2	11.1	8.7	31	26	61	53	91	80	121	108	151	136	999	
to	0.07	0.32	0.20	0.62	0.41	0.92	0.62	2.2	1.6	5.2	3.9	8.2	6.3	11.2	8.8	32	27	62	53	92	81	122	109	152	137	1000	-50
0.127		0.33	0.21	0.63	0.42	0.93	0.63	2.3	1.6	5.3	4.0	8.3	6.4	11.3	8.8	33	28	63	54	93	82	123	110	153	138	1699	
0.128		0.34	0.21	0.64	0.42	0.94	0.64	2.4	1.7	5.4	4.0	8.4	6.5	11.4	8.9	34	28	64	55	94	83	124	111	154	139	1700	-60
to	0.08	0.35	0.22	0.65	0.43	0.95	0.65	2.5	1.8	5.5	4.1	8.5	6.5	11.5	9.0	35	29	65	56	95	84	125	112	155	140	2299	
0.144		0.36	0.23	0.66	0.44	0.96	0.65	2.6	1.9	5.6	4.2	8.6	6.6	11.6	9.1	36	30	66	57	96	85	126	112	156	140	2300	-80
0.145		0.37	0.23	0.67	0.44	0.97	0.66	2.7	1.9	5.7	4.3	8.7	6.7	11.7	9.2	37	31	67	58	97	86	127	113	157	141	5799	
to	0.09	0.38	0.24	0.68	0.45	0.98	0.67	2.8	2.0	5.8	4.4	8.8	6.8	11.8	9.3	38	32	68	59	98	87	128	114	158	142	5800	-100
0.158		0.39	0.25	0.69	0.45	0.99	0.67	2.9	2.1	5.9	4.4	8.9	6.9	11.9	9.3	39	33	69	60	99	88	129	115	159	143	7500	

The gas slippage effect is essentially a laboratory phenomenon, because permeability is determined with low pressure air. The laboratory determined gas permeabilities will be higher than the true permeability because hydrocarbon-bearing formations contain liquids and/or gas at high pressures. The Klinkenberg effect is very significant on low permeability core samples. For those clients who request it, Core Laboratories can apply an empirical correction to the measured gas permeabilities which will result in better agreement between liquid and gas permeabilities. These empirical corrections are shown on Table 5-II. The measured gas permeability (k_a) bracket is found on the table; the approximate liquid permeability (k_l) is shown. The mathematical relationship between k_a and k_l is: $k_l = 0.68(k_a)^{1.06}$

As an example, a permeability determination made on a sample at 32 psig (C=4) upstream pressure may be found to be lower than a permeability determination made at 7 psig (C=30) upstream pressure. A natural tendency, on the part of the core analyst, may be to assume that this difference is the result of either turbulence or system restrictions at the higher flow rate (lower "C"), when actually the difference is the Klinkenberg effect at two different mean pressure levels. Generally speaking, turbulence and system flow restrictions will occur with high permeability core samples and the Klinkenberg effect will be more pronounced on low permeability samples.

SECTION SIX: REPLACEMENT PARTS

Item	Description
6.1	1. Regulator, permeameter Moore Products, Nullmatic Model 40-50 2. Regulator, mercury Moore Products, Nullimatic Model 40-7
6.2	Valves, source, sample, upstream water, orifice vent, Hassler vent, Hassler, vacuum, High and Low permeability with dual toggle handle -- Hoke, 1511F2B
6.3	Manometers; mercury, upstream water, orifice a. Sight glasses 3/8" OD X 5/64" wall X 14-3/8" long, pyrex -- CLI (special made)
6.4	1. Gauge; Hassler sleeve (30"-0-200 psi) 2. Gauge; "C" valve, with modified dial face (0-60 psig) -- CLI (special made)
6.5	Dryer, complete a. Silica gel desiccant -- CLI (special made)

Item	Description
6.6	Upstream and downstream tygon plastic tubing - 5/16" OD X 1/16" wall X 10"
6.7	Orifice rubber hose - 1/2" OD X 1/8" wall
6.8	Hassler Core Holder complete 1. Rubber sleeve 2. Upstream head 3. Downstream head 4. Upstream nut 5. Downstream nut 6. Housing 7. End washers -- CLI (special made)
6.9	Orifices, calibrated with orifice constant -- CLI (special made and calibrated)
6.10	1. Cabinet, complete Premier; TR-2119 2. Front Panel; CLI (special made)

SECTION SEVEN: AUXILIARY EQUIPMENT

7.1 Permeameter Test Kit

1. General

The permeameter test kit contains all the necessary equipment to test the permeameter as discussed in SECTION FIVE: Maintenance. In addition, Orifice Q constants may be checked or determined. An Orifice Q can change; normally the Orifice Q will decrease with use due to very fine-sized particles plugging the orifice capillaries. An appreciable increase in an orifice constant suggests that the orifice may have been fractured and it should be discarded. Leaks downstream of the orifice are not permitted during the test.

An orifice may be calibrated if an accurate gas flow meter is available. The test kit has three in the form of bubble flow meters. A bubble flow meter is a calibrated length of glass tubing, through which a soap film (bubble) may be displaced. The volume of the tube divided by the time required for the displacement, equals the volume flow rate.

2. Orifice Calibration Instructions

An orifice may be calibrated in the following manner:

a. A core sample of medium permeability (50-100 md.) is placed into the core holder.
b. The porcelain orifice stem is connected to the Orifice outlet with the rubber hose. The orifice must be clean, dry and at room temperature. The aluminum outer tubing must be epoxy-sealed to the porcelain.
c. Source, Sample, and High valves are opened; Orifice Vent is carefully closed, and the Mercury regulator is adjusted to produce a 200 mm of water column on the Orifice manometer.
d. A drilled rubber stopper is used to connect a length of plastic tube to the aluminum orifice discharge. The other end of the plastic tube is connected to a bubble flow meter. The bubble flow meter selected should be large enough to require at least 20 seconds for the soap film bubble to be displaced from the bottom graduation (zero mark) of the bubble meter to the top graduation (full scale of 10, 100 or 500 ml.)
e. Squeezing the rubber bulb, at the lower end of the flow meter, will cause the soap solution (SNOOP) to rise and contact the lower edge of the calibrated tube. The incoming gas, from the orifice, will displace a soap film bubble into the tube.
f. When the bubble, being displaced upward, reaches the Zero mark, the electric timer is started; when the bubble reaches the Full-Scale mark, the electric timer is stopped. Several moving bubbles will be required to wet the inside wall of the flow meter before a bubble will successfully traverse the entire calibrated length of the tube.
g. The "Orifice Q" will be:

$$\text{Orifice Q in } cm^3/\text{sec.} = \frac{\text{Full Scale volume in } cm^3}{\text{Time of traverse in seconds}}$$

h. Several traverse "times" should be accumulated in order to arrive at an average time. During the timed intervals there must always be 200 mm of water indicated on the Orifice manometer. Timed intervals should agree within $\pm 1\%$.
i. The calibrated volume between the zero and the full-scale graduations is specified to be within $\pm 1\%$. If the measured Orifice Q is within 1% of the original value, continue to use the original; if the new Orifice Q is different by an amount greater than 1%, use the newly determined Orifice Q. Relabel the orifice.

3. Miscellaneous Equipment Included and Their Uses

Item	Quantity	Use
Screw-pinch Clamps	2	To close the orifice rubber hose during downstream leak test. To close upstream and orifice hose during Hassler boot leak test.
SNOOP	2	Bubble solution for filling bubble flow meters. Bubble solution for location of leaks
Core Plugs (1" & 1½" dia.)	4	Test plugs during orifice calibration. Test plugs during Hassler sleeve leak test.
Solid Lucite Plugs (1" & 1½" dia.)	2	Test plug for downstream leak test.
Lucite Tubing (1" & 1½" dia.)	2	Test plug for "Δp across system" test
Bulb Aspirator	1	To pressurize downstream lines for leak test.
Test Gauge	1	Optional, for laboratories that routinely use the "C" gauge that is mounted on the permeameter panel
Charts & Tables	3	"C" Values vs. mm H_g "C" Values vs. mm H_2O

7.2 Hassler Core Holder's Use with a Porosimeter

The Hassler core holder may be used with a porosimeter, in order to directly determine the pore volume of a core sample. This can be accomplished with a simple 1/8" Saran Y-tubing connection. The porosimeter instructions include the details of this procedure.

7.3 Whole Core Permeameter Core Holder

The permeameter test panel can be utilized with any of the whole core type core holders for measuring vertical or horizontal permeabilities. Whole core horizontal permeabilities are run on cylindrical-shaped samples with two stainless steel screens mounted diametrically opposite one another, each covering a 90^{o} surface quadrant. Generally, the screen spans the entire length of the sample.

Where 90^{o} screens are used, which span the length of core, the calculation of permeability, using Darcy's equation, is as follows:

$$k_g = \frac{(C)(\text{Orifice Q})}{L}$$ All factors are previously defined.

The equation above is applicable where the length of screen spans the entire length of the core sample. In the event a sufficiently long screen is not available to span the entire length (L) of a sample, the value of L must be altered to an apparent length (L_a) as follows:

$$L_a = \sqrt{(L)(L_{screen})}$$

L = Length of core sample, cm
L_{screen} = Length of screen, cm

Refer to the individual core holder instructions for the mechanical details of securing a whole-core sample in a specific piece of equipment. Generally, the previously mentioned conditions must be met:

1. Adequate sleeve pressure must be maintained, to seal the sample, to prevent leakage between the sample and the sleeve.
2. The ends of the samples must also be sealed when the gas flow path is diametrically across the sample.
3. The flow system Δp must be small relative to the total Δp across the system and core sample. This is especially important for samples with high permeability. Special screens may be required in some instances and larger lines connected between the core holder and permeameter panel.

JES:pm